Exploring the role of exosomes in the metabolic regulations of metastatic ovarian cancer

Thesis Submitted for the Degree of

Doctor of Philosophy (Science)

in the Faculty of Science

of Jadavpur University

By

SRADDHYA ROY

University Registration No.: SLSBT1112321

Under the supervision of

Dr. Nabanita Chatterjee

Department of Receptor Biology and Tumor Metastasis

Chittaranjan National Cancer Institute

37, S. P. Mukherjee Road,

Kolkata-700 026

India

2025

Chittaranjan National Cancer Institute
(An Autonomous Body under Ministry of Health & Family Welfare, Govt. of India)
37, S. P. Mukherjee Road, Kolkata 700 026, INDIA
Tel: 2476 5101/02/04/20/22; Fax: 91-33-2475 7606
E-mail: cncinst@gmail.com
Web site: www.cnci.ac.in

CERTIFICATE FROM THE SUPERVISOR

This is to certify that the thesis entitled **"Exploring the role of exosomes in the metabolic regulations of metastatic ovarian cancer"** Submitted by **Smt. Sraddhya Roy** who got her name registered on 29th November, 2021 for the award of Ph. D. (Science) Degree of Jadavpur University, is absolutely based upon her own research work under the supervision of **Dr. Nabanita Chatterjee, Senior Scientific Officer at Department of Receptor Biology and Tumor Metastasis, Chittaranjan National Cancer Institute, Kolkata-700026** and that neither this thesis nor any part of it has been submitted for either any degree / diploma or any other academic award anywhere before**.**

12/03/2025

(Signature of the Supervisor date with official seal)

Dr. Nabanita Chatterjee, Ph.D
Senior Scientific Officer (SSO II)
Chittaranjan National Cancer Institute
Ministry of Health & Family Welfare (An Autonomous Body)
37, S.P. Mukherjee Road, Kolkata - 700 026, INDIA

Declaration

I do hereby declare that the work embodied in this thesis entitled **"Exploring the role of exosomes in the metabolic regulations of metastatic ovarian cancer"** submitted for the award of Doctor of Philosophy (Ph. D.) in Science is the completion of the studies conducted by me under the supervision of Dr. Nabanita Chatterjee, Senior Scientific Officer at Department of Receptor Biology and Tumor Metastasis in Chittaranjan National Institute. The work is original and has not been submitted in part or full for either any equivalent degree/ diploma or any other academic award elsewhere.

I confirm that all the proper acknowledgments have been mentioned in the thesis.

Sraddhya Roy
Senior Research Fellow
Department of Receptor Biology and Tumor Metastasis
Chittaranjan National Cancer Institute
37, S. P. Mukherjee Road
Kolkata-700026

Acknowledgments

First and foremost, I would like to convey my heartfelt gratitude to my supervisor, ***Dr. Nabanita Chatterjee****, for her continuous encouragement, consistent guidance and unflinching support, taking me hand in hand in shaping my research work. Her expertise and dedication as a supervisor have paved the way toward the completion of my work by pushing me through my fear and always being there by my side in difficult times. I am thankful for her invaluable mentorship which has been an inspiring and enriching experience, and I am profoundly grateful for her belief in my abilities. I am out of words to explain her contribution to bringing out the best in me, making me acquainted with the world of research and staying steadfast in my efforts.*

I extend my gratitude to ***Dr. Jayanta Chakrabarti****, Director of Chittaranjan National Cancer Institute, for providing me with the platform to perform my research work with the necessary support in many ways for the completion of my research. On the same note, I am thankful to* ***Dr. Dona Sinha****, HOD, Dept. Receptor Biology and Tumor Metastasis for allowing me to pursue my research in the laboratory. I sincerely acknowledge all the respected faculty members of CNCI who enriched my knowledge with their valuable lectures during the course work, as well as the entire academics, research and hospital facilities for providing me with the necessary guidelines throughout my tenure. I am thankful to the* ***Central Research Instrumentation Facility (CRIF)*** *of CNCI for technically supporting my experiments. I am also thankful to our Flow cytometer technicians,* ***Mrs. Shalini Upadhyay*** *and* ***Mr. Rupankar Ghosh*** *for the acquisition of flow cytometry data. I extend my sincere gratitude to* ***Dr. Rathindranath Baral****, former HOD of the Department of Immunoregulations and Immunodiagnostics, and his entire research team for assisting me with support during experiments. I would also sincerely acknowledge* ***Dr. Abhijit Rakshit****, HOD of Animal care and Maintenance Department of CNCI and his entire team for supporting the animal studies. I am thankful to the* ***University Grants Commission (UGC)*** *for providing me with a fellowship for 5 years. The constant support from administration and security has made a smoother and protective environment towards the completion of my course.*

I am thankful to one of my mentors, ***Dr. Manisha Vernekar,*** *as a clinician of CNCI for providing me with samples to conduct my research. I am also extremely thankful to all the volunteers who willingly participated in this study, without whom the implementation of the study would have been impossible.*

I am extremely indebted to Jadavpur University for permitting me to register for Ph.D. degree. My heartfelt gratitude extends to ***Prof. Parimal Karmakar****, Ex-HOD of the Department of Life Science and Biotechnology,* ***Prof. Tarum Jha****, Ex-HOD of the Department of Pharmacy and* ***Prof. Biswadip Das****, present HOD of the Department of Life Science and Biotechnology for nurturing me with*

valuable suggestions as panel members of Research Advisory Committee (RAC), Jadavpur University.

I am blessed to have such beautiful lab mates and colleagues ***Ms Ananya Das, Ms. Aparajita Bairagi, Ms. Arundhati Roy, Mrs Sukanya Ghosh, Ms Priyanka Saha*** *and* ***Ms Anurima Samanta*** *for their constant support and friendship during my PhD journey. Special thanks to Ananya Das, Aparajita Bairagi, and Arundhati Roy for making my challenging days enjoyable with love and humor. Working with such talented and dedicated colleagues has been a privilege, and I will always cherish the memories and lessons we shared. I also admire* ***Dr. Suchisnigdha Dutta*** *for helping me in my search for a lab to pursue my Ph.D. I am thankful to all the interns of our laboratory, especially our present intern,* ***Mr. Koustav Maiti****, who actively participated in the experiments. I extend my regards to former lab technician* ***Mr. Srikanta Barua*** *and present lab technician* ***Mr. Ganga Rauth*** *for their cooperation in maintaining the laboratory.*

My words fail to express my deepest gratitude to my parents, ***Mr. Goutam Roy*** *and* ***Mrs. Sathi Roy****. Their unwavering belief in me and their love are the pillars of all my achievements. Baba and Maa have always bestowed me with strength and constant backing through their words of encouragement and care during the most challenging times. Throughout this journey, the lessons and moral values inculcated in me by them have supported me unconditionally. This work is a tribute to their endless sacrifices and inspiration. My grandmother,* ***Late. Abha Rani Roy****, whom I lost recently, would have been very happy to see me complete my degree. My stressbuster,* ***Bruno****, who left me back in 2020, will be equally missed in the days of happiness in achieving this milestone.*

I also extend my appreciation and gratitude to my husband, ***Mr. Somnath Chakraborty****, for his unconditional love and patience during the ups and downs I faced on this journey. His unseen care from such a long distance and his belief in me have encouraged me during moments of self-doubt. I am also profoundly thankful to my in-laws,* ***Mr. Paritosh Chakraborty*** *and* ***Mrs. Kalyani Chakraborty*** *for creating a nurturing environment with their kindness and understanding to concentrate on my work.*

Finally, I dedicate this thesis to the Almighty for blessing me with the opportunity to prove myself. The perseverance and wisdom granted me confidence in completing this journey.

Date:
Place:

Sraddhya Roy
Senior Research Fellow
Department of Receptor Biology and Tumor Metastasis
Chittaranjan National Cancer Institute
37, S.P. Mukherjee Road
Kolkata-700026

Contents

Abstract

Ovarian cancer (OvCa) turns as the alarming condition across the globe governed by its metastasizing capacity and disease-associated inflammation leading to increased mortality rate. The dreadful disease might be recognised as altered metabolically programed environment in which the cancer associated metastasis is controlled by several factors, among them, the extracellular vesicles i.e. exosomes, have been in the limelight in current research. Thus, this study aims to understand the molecular mechanisms that adversely influence the metastasis of the disease, leading to poor outcomes in the survival of the patients.

Metastasis involves a plethora of biomolecules actively participating in devising the tumor microenvironment (TME) for proliferation and survival of cancer cells. An extensive database mining revealed higher SIRT1 status, disorients numerous biological processes, expressing with its genomic abnormalities in OvCa, which instigated us to investigate the molecular crosstalk augmenting the process of metastasis. Further, we identified SIRT1 associated hub genes played a significant role epithelial-mesenchymal transition (EMT) and cellular signalling cascade PI3K/AKT, thereby illustrating SIRT1 as a notable target in OvCa therapy. Additionally, a comparative analysis of a small molecule inhibitor (SMI) and a phytochemical named Hyperforin by Molecular docking confirmed SIRT1 Inh III as a potent inhibitor of SIRT1 whose potency was further validated by *in-vitro* and *in-vivo* analysis.

A clinicopathological analysis of OvCa was conducted to depict the risk factors for the development of OvCa, revealing that Body Mass Index (BMI), metastasis, degree of dissemination were significantly correlated with increasing levels of the diagnostic marker, CA-125, which negatively impacted the survival of the patients. Furthermore, the expression of SIRT1 was found to be regulated by elevated expression of HIF-1α, establishing a hypoxic TME under the effect of increased release of exosomes from the tumor tissues as compared to the adjacent normal tissue, thereby driving the proliferation of cancer cells as denoted by heightened Ki-67 expression. This phenomenon is supported by the continuous supply of energy from elevated glycolytic pathway as indicated by increased deposition of glycogen in the cancer tissues. All these findings underscored the intricate interplay between all these molecules in the TME of OvCa with the idea that increasing levels of exosomes and SIRT1 expression can precise the staging of OvCa and aid clinicians in planning respective therapeutic strategies for the patients.

Upon further analyzing the sociodemographic parameters, we deduced that pain is a major symptom that prevailed in the OvCa patients, with its severity escalating significantly with tumor differentiation. Thus, in-depth analysis of the molecular circuitry revealed COX-2 to be significantly upregulated in the poorly differentiated OvCa tissues. Additionally, SIRT1/COX-2 colocalization was also strikingly higher in the tumor tissues that reinforced the metastatic process by increasing the colocalized expression of MMP2/MMP9 and VEGF/ANGPT2. Alternatively, decreasing colocalized SIRT1/PTEN expression indicated a compromised tumor suppressive function of PTEN under the effect of increased cytokines levels. Further investigation revealed that under the interference of exosomes in reprogramming the TME, the levels of SIRT1/COX-2/IL-6 increased, but the inhibition of SIRT1 decreased their expression. Positive results were also observed with EMT markers, E-cad and Vim. Apoptotic markers, Bax and Bcl-2, along with reactive oxygen species (ROS) generation, also revealed significant differences in their expression under the impact of exogenous exosomes, which eventually got mitigated under the effect of SIRT1 Inhibitor.

The exosomal orchestration was not only limited to the cancer cells but also induced oncogenic transformation into normal cells, which was confirmed by heightened expression of SIRT1/COX-2/IL-6 axis, as well as the alterations in EMT markers (E-cad and Vim), in presence and absence of SIRT1 Inhibitor. A deeper investigation identified PI3K/AKT signaling cascade to be elevated under the effect of exosomes that diminished under the effect of SIRT1 Inhibitor. *In-vivo* analysis validated that blocking exosomal secretion in combination with metabolic inhibition could also remarkably reduce the metabolic markers (SIRT1), metastatic and EMT markers (MMP2/MMP9, VEGF/ANGPT2, E-cad/Vim/Snail, Ki-67), and glycolytic markers (GLUT1/HKII/PKM). Additionally, the mitigation of increased glycogen deposition and greater glucose uptake accompanied by increased pyruvate content, lessened lactate generation and ATP levels under the decreased activity of SIRT1 enzyme also confirmed that metabolism and metastasis are strongly intertwined in OvCa. Concisely, targeting exosome-mediated signaling by selectively inhibiting SIRT1 grants a promising therapeutic strategy to treat the disrupted metabolic-metastatic axis and improve patient survival outcomes.

List of Abbreviations

3D	:	Three dimensional
ADME	:	Absorption, distribution, metabolism, excretion
ADSCs	:	Adipose-derived stem cells
Akt	:	Protein Kinase B
ALDH3A1	:	Aldehyde Dehydrogenase 3 Family Member A1
ALDOA	:	Aldolase A
ANGPT2	:	Angiopoietin 2
ANXA2	:	Annexin A2
AUC	:	Area under curve
BBB	:	Blood-brain barrier
BC	:	Breast cancer
BMI	:	Body mass index
BMP	:	Bone morphogenic protein
CA 19.9	:	Cancer antigen 19.9
CA-125	:	Cancer/carbohydrate antigen-125
CAFs	:	Cancer-associated fibroblasts
CDX	:	Caudal-related homeobox
CEA	:	Carcinoembryonic antigen
CFDA-SE (CFSE)	:	5-(and-6)-Carboxyfluorescein Diacetate Succinimidyl Ester
CI	:	Confidence interval
CML	:	Chronic myeloid leukemia
CNS	:	Central nervous system
CNV	:	Copy number variation
Con	:	Control
COX-2	:	Cyclooxygenase-2
CPTAC	:	Clinical Proteomic Tumor Analysis Consortium
CRC	:	Colorectal cancer
CXCL	:	Chemokine (C-X-C motif) ligand
CXCR	:	C-X-C chemokine receptor
DAB	:	3, 3’-diami-nobenzidine tetrahydrochloride

DAPI	:	4-6-diamidino-2-phenylin
DCFDA	:	5(6)-Carboxy-2′,7′-dichlorofluorescein diacetate
DLS	:	Dynamic light scattering
DM	:	Distant metastasis
DMSO	:	Dimethyl sulphoxide
EBV	:	Epstein-Barr Virus
E-cad	:	E-cadherin
ECM	:	Extracellular matrix
EGFR	:	Epidermal growth factor receptor
ELISA	:	Enzyme-linked immunosorbent assay
EMT	:	Epithelial–mesenchymal transition
EOC	:	Epithelial ovarian cancer
EpCAM	:	Epithelial cellular adhesion molecule
Er-α	:	Estrogen receptor-alpha
FAO	:	Fatty acid oxidation
FOXQ1	:	Forkhead Box Q1
Fu	:	Fraction unbound
GAPDH	:	Glyceraldehyde 3-phosphate dehydrogenase
GC	:	Gastric cancer
GLUT	:	Glucose transporter
GO	:	Gene Ontology
GSCA	:	Gene set cancer analysis
GSVA	:	Gene set variation analysis
HBA	:	Hydrogen bond acceptor
HBD	:	Hydrogen bond donor
HCC	:	Hepatocellular carcinoma
HDACs	:	Histones deacetylases
hERG	:	Human ether-a-go-go-related gene
HG	:	High glucose
HIA	:	Human intestinal absorption
HIF-1α	:	Hypoxia-inducible factor-1 alpha
HINT1	:	Histidine triad nucleotide-binding protein 1

HOXA5	:	Homeobox-A5
HR	:	Hazard ratio
HSP90α	:	Heat shock protein 90 alpha
HUVECs	:	Human umbilical vein endothelial cells
i.p.	:	Intraperitoneal injection
IF	:	Immunofluorescence
IHC	:	Immunohistochemistry
IL	:	Interleukin
IMPPAT	:	Indian Medicinal Plants, Phytochemistry And Therapeutics
KEGG	:	Kyoto Encyclopedia of Genes and Genomes
KSHV	:	Kaposi's sarcoma-associated herpesvirus
LDH	:	Lactate dehydrogenase
LMP1	:	Latent membrane protein 1
MBD1	:	Methyl-CpG binding domain protein 1
MCODE	:	Molecular complex detection
MET	:	Mesenchymal-epithelial transition
MFI	:	Mean fluorescence intensity
miRNAs	:	MicroRNAs
MITF	:	Microphthalmia transcription factor
MMP2	:	Matrix Metalloprotease 2
MMP9	:	Matrix Metalloprotease 9
MMT	:	Mesothelial-mesenchymal transition
MSCs	:	Mesenchymal stem cells
mTORC1	:	Mammalian target of rapamycin complex 1
MTT	:	3-(4,5-dimethylthiazol-2-yl)-2,5 diphenyltetrazolium bromide
MW	:	Molecular weight
NA	:	Not applicable
NAD	:	Nicotinamide adenine dinucleotide
Nampt	:	Nicotinamide phosphoribosyltransferase
nROTB	:	Number of rotatable bonds
NRS	:	Numerical rating scale
NSCLC	:	Non-small cell lung carcinoma

nSMase2	:	Neutral sphingomyelinase 2
NTA	:	Nanoparticle tracking analysis
NTExos	:	Non-treated + Exosomes
OCT2	:	Organic cation transporter 2
OD	:	Optical density
OS	:	Overall survival
OvCa	:	Ovarian cancer
OXPHOS	:	Oxidative phosphorylation
PAS	:	Periodic acid and Schiff
PBS	:	Phosphate buffer saline
PC	:	Prostate cancer
PD	:	Pelvic dissemination
PDB	:	Protein data bank
PGE2	:	Prostaglandin E2
PI3K	:	Phosphatidylinositol 3-kinase
PK	:	Pyruvate kinase
PMCs	:	Peritoneal mesothelial cells
PMN	:	Pre-metastatic niche
PPI	:	Protein–protein interaction
PTEN	:	Phosphatase and tensin homolog
Rg	:	Radius of gyration
RISC	:	RNA-induced silencing complex
RMSD	:	Root mean square deviation
RMSF	:	Root mean square fluctuation
ROC	:	Receiver-operating characteristic curve
ROS	:	Reactive oxygen species
RT	:	Room temperature
RTKs	:	Receptor tyrosine kinases
SASA	:	Solvent accessible surface area
SEM	:	Scanning electron microscopy
SIRT1 Inh	:	SIRT1 Inhibitor
SIRT1	:	Silent information regulator 1

SIRT1 Inh+Exos	:	SIRT1 Inhibitor + Exosomes
SIRTs	:	Sirtuins
α-SMA	:	Alpha-smooth muscle actin
SMIs	:	Small molecule inhibitors
SNV	:	Single nucleotide variation
STRING	:	Search Tool for the Retrieval of Interacting Genes/Proteins
TCA	:	Tricarboxylic acid cycle
TCGA	:	The Cancer Genome Atlas
TFs	:	Transcription factors
TGF- β	:	Transforming growth factor-beta
TILs	:	Tumor infiltrating lymphocytes
TIMP2	:	Tissue inhibitor of metalloproteinase 2
TME	:	Tumor microenvironment
TNBC	:	Triple negative breast cancer
TNF-α	:	Tumor necrosis factor-alpha
TPSA	:	Total polar surface area
UALCAN	:	University of Alabama Cancer Database
VDss	:	Volume of distribution at steady state
VEGFs	:	Vascular endothelial growth factors
Vim	:	Vimentin
WHO	:	World Health Organization

Introduction

1. Background:

The third most common and fatal gynaecological malignancy is ovarian cancer (OvCa) ranked after cervical and uterine cancer. However, The Global Cancer Observatory reported 324,603 new OvCa cases around the globe in 2022. Consequently, due to the commonality of late-stage onset when it is typically more aggressive and resistant to standard therapies, OvCa is among the most challenging cancer types to treat, with a cumulative risk of incidence being 0.73 [1].The increased mortality rate and poor survival are the result of late diagnosis [2]. The symptomless progression of the disease restrains the disease to be detected early-stage. The symptoms are mostly neglected due to their non-specificity and inappropriate nature leading to the late diagnosis resulting in poor survival of the patients. Furthermore, multiple risk factors like age, body mass index (BMI), family history, menopausal status etc. alarm the onset of the disease [3]. As per World Health Organization (WHO) classification, OvCa is classified into three prime categories namely, primary OvCa of epithelial origin which accounts for 60% of the cases, germ cell tumor (30%) and sex cord stromal tumor (8%). Since the occurrence rate of epithelial cancer is highest among all other subtypes, it is subcategorized depending on its histological types and proliferation rate of the cancer cells [4]. The heterogeneous group of epithelial OvCa is categorized under various histological subtypes namely serous, mucinous, endometrioid, clear cell, transitional cell tumors (Brenner tumors), carcinosarcoma, mixed epithelial tumor, undifferentiated carcinoma [5]. Among the Asian countries, India ranks highest in mortality, whereas the occurrence rate has decreased in young patients in Europe and North America [6]. The age-adjusted OvCa occurrence rates in India account for 5.4 to 8.0 per 100,000 population distributed in different parts of the country [7]. Early, estimation revealed that by 2020 approximately 59, 276 new incidences would be reported in India, which would increase by 55% by 2035 resulting in an increase in mortality rate by 67%, creating an alarming situation in the country [8]. As per GLOBOCAN 2022, 47,333 (6.6%) new OvCa cases were reported and ranks third in number among all other cancers in females (Figure 1). As per recent data published by the National Cancer Registry Programme, OvCa rates are increasing in various geographical areas, including the North Eastern region of India, with 41.9% locally advanced/locoregional cases and 29% both distant metastasis (DM) and localized cases [9]. Thus, this alarming situation demands an absolute necessity of early-stage diagnosis with a proper treatment regime for the patients to improve the survival rate of the patients.

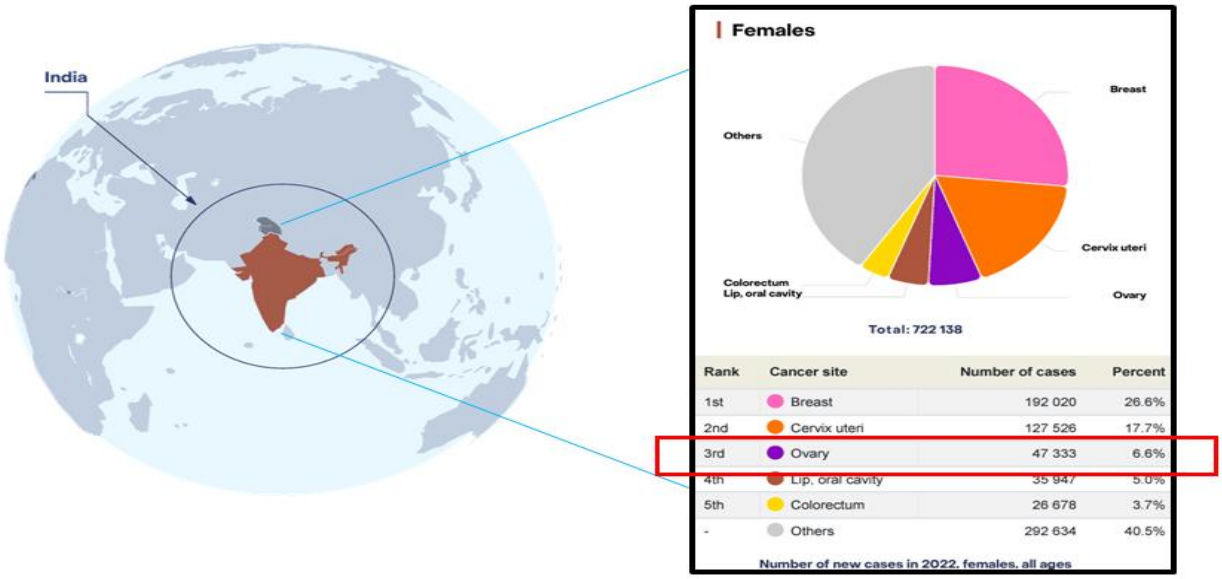

Figure 1. Prevalence of OvCa cases in India (GLOBOCAN, 2022)

2. Ovarian cancer metastasis

The OvCa cells metastasize by two distinct mechanisms, firstly through passive dissemination and secondly through the hematogenous pathway. Passive dissemination involves direct implantation of the clustered cancer cells after a relatively simpler process of migration through the ascitic fluid followed by adhesion and invasion into the abdominopelvic organs, mostly in the omentum. On the contrary, the hematogenous route involves a series of crucial interconnected phenomena. Firstly, the cells intravasate where the cells reprogram the basal membrane and enter into the bloodstream or lymphatic vessels. The cells then migrate and extravasate from the blood and the lymph vessels after they find a suitable microenvironment for their homing and proliferation at the target sites. The formation of a suitable tumor microenvironment (TME) involves complex intermolecular interactions between the cancer cells and the extracellular matrix (ECM), that allow the cancer cells to escape the immunosurveillance and form colonies at the secondary sites. Alternatively, in the ascites-driven pathway, tumor cells disseminate within the peritoneal fluid, a process closely linked to the accumulation of ascites in advanced ovarian cancer cases. These circulating tumor cells attach to and infiltrate the mesothelial layer that lines the peritoneal surfaces. The presence of ascitic fluid provides a supportive environment for tumor cell survival and transport, facilitating their adhesion to mesothelial cells. This infiltration is often aided by alterations in the mesothelial barrier, such as changes in the ECM composition and signaling pathways that enhance tumor cell motility and invasiveness [10].

3. Role of exosomes in OvCa metastasis

There are a lot of evidence to suggest that exosomes are critically involved in the OvCa metastasis by promoting adhesion, invasion, angiogenesis, immune evasion, chemoresistance and serving as the key mediators of tumor-stroma crosstalk by regulating the survival of the cancer cells, reprogramming and educating other cells to promote metastasis [11]. OvCa metastasis is often mediated by the interaction of exosomes with the TME [12][13]. Exosome content release can alter the fate of target cells by regulating the recipient cells by transferring microRNAs (miRNAs), non-coding RNAs, mRNA, rRNA and tRNA which are reported to be carried as exosomal cargoes [14]. The formation of a pre-metastatic niche (PMN) is an essential phenomenon for the occurrence of secondary metastasis creating an atmosphere at distant sites for the migrating tumor cells to colonize and proliferate [15]. Additionally, exosomes also participate in the mesothelial-mesenchymal transition (MMT) by acting as an intercellular communicator between mesothelial cells and tumor cells and facilitating co-invasion of tumor cells and peritoneal mesothelial cells derived cancer associated fibroblasts (CAFs) into the peritoneal matrix [16]. Exosomes are also reported to perform crucial roles in angiogenesis by transferring proangiogenic molecules angiogenin, vascular endothelial growth factors (VEGF), interleukin-6 (IL-6), IL-8 to endothelial cells [17][18]. Exosomes dependent transfer of miR-205 from cancer cells to endothelial cells thereby activating the phosphatase and tensin homolog (PTEN)/protein kinase B (Akt) signaling cascade and promoting angiogenesis [19]. Moreover, the hypoxic TME is responsible for the elevated secretion of exosomes from the cancer cells and leads to the transformation of cancer cells to a more aggressive phenotype leading to chemoresistance via activation of STAT3/Rab proteins [20]. Exosomes derived from hypoxic epithelial OvCa cells are reported to promote the phenotypic alteration of M1 macrophage to aggressive M2 phenotype and thus promoting proliferation and migration of the cancer cells [21]. Understanding the specific mechanisms of peritoneal dissemination and the interactions between tumor cells and exosomes with the investigation of baseline molecular mechanisms remains critical for developing targeted treatments and improving prognosis. An overall schematic of roles played by exosomes is represented in Figure 2.

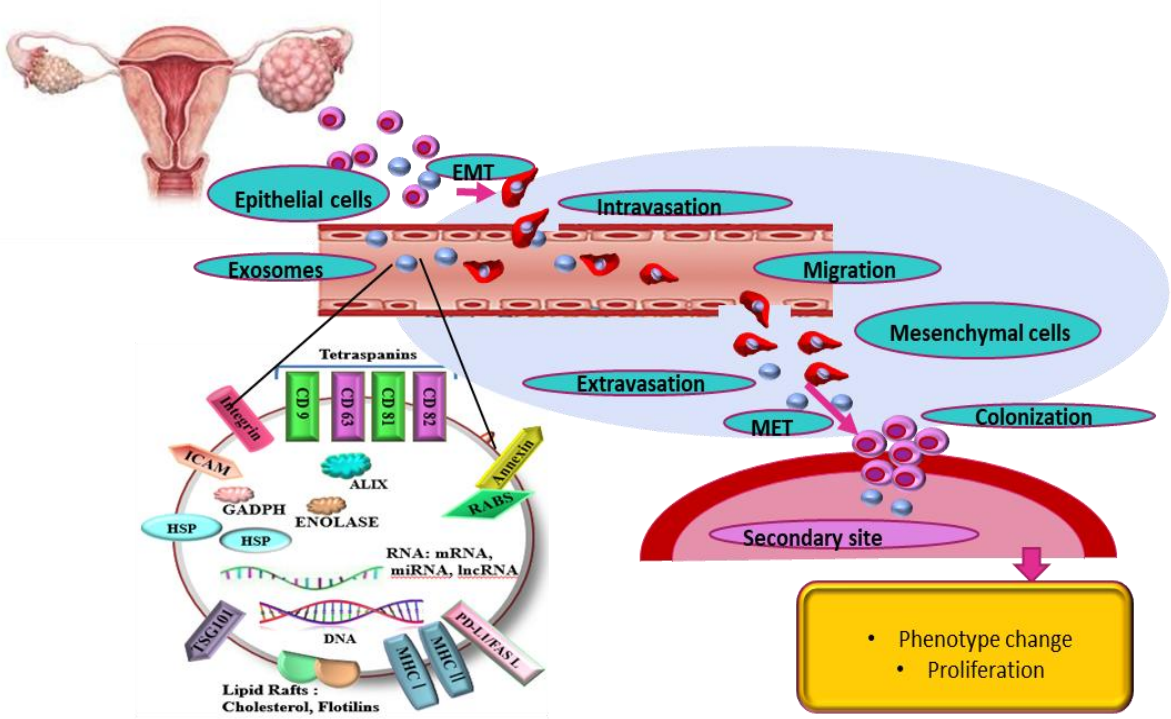

Figure 2. Role of exosomes in OvCa metastasis

4. Metabolism in Ovarian Cancer: A Focus on Glycolysis

A characteristic feature of the metabolism in malignant tumor cells is their altered use of glucose compared to normal cells. Cellular energy is mainly produced through glycolysis and oxidative phosphorylation (OXPHOS). When oxygen levels are typically high, cells depend on OXPHOS for energy. However, under oxygen-deprived state, they shift to glycolysis. Conversely, tumor cells uptake the glycolytic pathway even in abundant oxygen levels, referred to as the Warburg effect or aerobic glycolysis. These metabolic alterations aid the cancer cells to survive even in the hypoxic tumor microenvironment that protects them from oxidative damage and apoptosis [22].

In epithelial OvCa cells, heightened glycolysis and increased glucose uptake are notable metabolic changes [23]. In normal cells, receptor tyrosine kinases (RTKs) trigger the Phosphatidylinositol 3-kinase (PI3K)/ Akt signaling pathway, which boosts glucose transporter (GLUT) 1 expression. In cancer cells, oncogene activation allows glucose uptake to occur autonomously, without the need for external growth factors. One of the most common mutations in OvCa is the mutated PIK3CA gene which is responsible for enhancing PI3K/Akt pathway impact. Glucose metabolism is often affected by hypoxia-inducible factor 1-alpha (HIF1α) as it regulates the VEGF-RTK signaling cascade and drives the metabolic

shift toward glycolysis [24]. However, the loss of function due to mutation negatively regulates PI3K signaling that intensifies Akt pathway activation and strengthens the glycolytic profile in OvCa. In this context, the roles performed by exosomes in influencing the regulatory pathways in metabolism need to be explored.

Nicotinamide adenine dinucleotide (NAD) is a molecule that acts as a coenzyme participating in redox reactions in multiple metabolic processes such as glycolysis, the tricarboxylic acid (TCA) cycle, oxidative phosphorylation and serine biosynthesis [25]. NAD is an absolute requirement by the cancer cells to maintain the growth and survival of the highly proliferating cells and thus NAD needs to be replenished. Several glycolytic enzymes like including glyceraldehyde 3-phosphate dehydrogenase (GAPDH) and lactate dehydrogenase (LDH), which are required for glycolysis are modulated by the increased levels of NAD by acting as a coenzyme [26]. In addition, increased levels of the rate-limiting NAD biosynthetic enzyme, Nicotinamide phosphoribosyltransferase (Nampt), maintain elevated NAD levels thereby promoting growth and anticancer drug resistance in cancer cells [27]. Tumor cells preferentially utilize glycolysis under hypoxic conditions to generate pyruvate, though it is reduced into lactic acid instead of further oxidizing to the mitochondrial acetyl-CoA to generate ATP [28]. Then, this metabolic switch, which is associated with elevated concentrations of lactate and reduced pH, hypoxia, and increased reactive oxygen species (ROS) within the tumor microenvironment (TME), induces cancer progression and immune escape [29]. A probable mechanism of metabolic state in OvCa cells is unveiled in Figure 3. Images were prepared using https://www.biorender.com/.

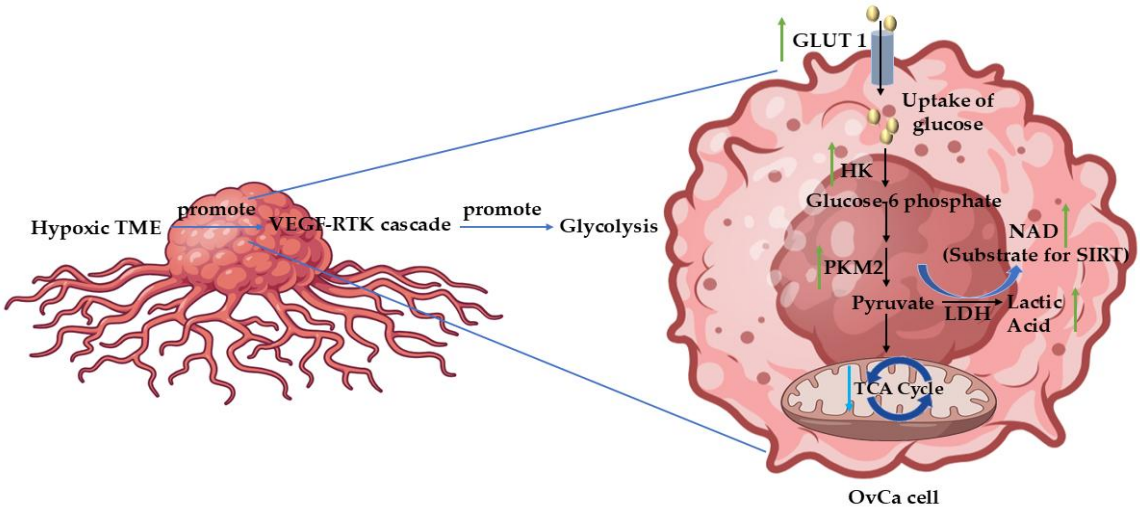

Figure 3. Schematic of a probable mechanism in OvCa metabolism

5. Regulation of metabolism with SIRTs

Numerous studies have established a strong correlation between cellular glucose metabolism and tumorigenesis, emphasizing that cancer cells must reprogram their metabolic pathways to meet the heightened energy demands of rapid and uncontrolled proliferation [30]. In this context, over the last decade, mammalian sirtuin family has gained tremendous attention for their roles as stress adaptors and post-translational modifiers. They actively participate in various cellular phenomenon that includes DNA repair, energy metabolism, and tumorigenesis. Surprisingly, genomic instability and metabolic reprogramming are identified as two hallmarks of cancer.

SIRT1-SIRT7 are the seven proteins that constitute the sirtuin family. They have a catalytic domain for binding NAD+ which varies in their N- and C-termini. Their localization in the cells, enzymatic activity and their respective binding targets are due to their diverse terminal extensions. SIRT1, SIRT6, and SIRT7 are located in the nucleus whereas SIRT3, SIRT4 and SIRT5 dwell in mitochondria and SIRT2 is mostly localized in the cytosol of the cells. However, they can translocate from their respective compartments to perform their roles [31]. Sirtuins (SIRTs) operate in diverse cell compartments: they deacetylate histones and various transcription regulators in the nucleus, but additionally particular proteins in alternative cell compartments, like within the cytoplasm and the mitochondria. Consequently, SIRTs respond to physiological changes in energy status to control fat and glucose metabolism and are critical regulators of the circuitry that dictates energy homeostasis [32]. The reaction of the amide with deacetylation cleavage by NAD+ generates nicotinamide and O-ADP-ribose, an intermediate during the reaction. This intermediate is required for the deacetylation reaction conducted by SIRT for transferring a single acetyl group from lysine to O-ADP-ribose moiety to produce O-acetyl-ADP-ribose and deacetylated lysine product. This reaction uses up an equivalent mole of NAD+ per acetyl group removed while governed by the cellular [NAD]/[NADH] ratio [33][34]. Recent developments have emphasized the contribution of SIRTs in epithelial-mesenchymal transition (EMT), a process that enables cancer cell invasion and spread, and in the modulation of energy metabolism programs. Moreover, an increased understanding of the key implication of epigenetic changes in the initiation, promotion and progression of cancer has shed new light on the role of SIRTs as prominent epi-enzymes implicated in these steps [35]. Thus, investigation of the regulatory roles of SIRT in cancer progression is required for identifying potential therapeutic targets.

SIRT1 drives the oncogenic signaling in BC cells by modulating the transduction network mediated by estrogen receptor-α (ERα) [36]. Furthermore, SIRT1 overexpression activates c-Myc protein in thyroid cancer which is an outcome of PTEN deficiency [37]. SIRT2 mostly acts as a tumor suppressor, however, its expression negatively impacts acute myeloid leukemia, pancreatic cancer, neuroblastoma, high-grade human HCC [38][39][40]. SIRT3 also negatively regulates the progression of cancer in oral squamous cell carcinoma by decreasing the ROS levels [41]. In pancreatic cancer, SIRT3 is reported to deacetylate glutamate oxaloacetate transaminase and thus arrests malate-aspartate NADH shuttle required for the growth of the cancer cells [42]. A pilot study reveals that lower expression of SIRT4 is associated with a lower survival rate in lung cancer patients [43]. Inhibition of SIRT4 is reported to activate mammalian target of rapamycin complex 1 (mTORC1) that increases glutamine metabolism [44]. SIRT5 acts as a tumor suppressor in squamous cell carcinoma [45] and endometrial cancer [46]. SIRT6 is also reported to regulate tumorigenesis, for instance, SIRT6 represses glutamine metabolism, ribosomal gene expression and glycolysis and its loss increases the metabolic cascades that in turn contribute to the development of tumor [47]. However, SIRT7 acts as a tumor promoter by enhancing the genomic integrity in the cancer cells. In colorectal cancer (CRC), SIRT7 regulates the EMT by increasing vimentin (Vim) and fibronectin and downregulating E-cadherin (E-cad) and β-catenin expression [48]. Under this doctrine, *Zeng et al*. demonstrated that SIRT1 is associated with poor survival in OvCa [49]. Thus, assisted by multiple evidence, although SIRTs perform their respective roles in distinct cancer types but SIRT1 being upregulated in OvCa forms a central attraction for study.

6. Relevance of SIRT1 in OvCa

Women with germline pathogenic variants in BRCA1 or BRCA2 exhibit a higher prevalence of serous adenocarcinomas compared to mucinous or borderline tumors [50]. Inactivation of BRCA1 by mutations and promoter methylation are linked with increased levels of NAD which in turn reveals that Nampt plays a pivotal role in BRCA1 related NAD synthesis. Furthermore, in OvCa, there exists an inverse correlation between BRCA1 expression and NAD level an inverse correlation has been observed between BRCA1 expression and NAD levels. However, an increase in BRCA1 levels in a concentration-dependent manner was observed when incubated with NAD. Additionally, NAD levels increase with overexpression of Nampt which in turn increases the expression of BRCA1 in primary OvCa cells as well as OvCa cancer cell lines including A2780, HO-8910, and ES2. These observations focus on the intricate relation between BRCA, NAD metabolism, Nampt activity in OvCa. In this context,

investigating the roles of SIRT1 in OvCa is very relevant and crucial to understand the altered metabolic reprogramming [51].

7. Role of SIRT1 in other malignancies

Cancer-associated phenomena like chemo-resistance, hyperproliferation, pro-survival properties within cancer cells are often influenced by overexpression of SIRT1. Interestingly, SIRT1 has a dual impact on tumorigenesis. Although it possesses context-dependent tumor-suppressive functions, extensive literature supports its large contribution to metastasis in a wide range of cancer types. SIRT1 stimulates tumorigenesis through deacetylation of tumor-suppressive and DNA damage-repairing proteins, resulting in the inactivation of important signaling pathways that protect the cell from tumorigenesis. Multiple malignancies, including PC [52], BC [53], non-small cell lung carcinoma (NSCLC) [54], colon [55], and gastric cancers (GC) [54], as well as melanoma [56], leukemia [57], and OvCa [58] are influenced, promoted, and progressed by SIRT1 modulations. Some small-molecule inhibitors of SIRT1 have been developed based on experimental evidence demonstrating that they downregulate cancer cell growth, proliferation, and viability in vitro. SIRT1 is shown to deacetylate STAT3 which acts as an inhibitor of gluconeogenesis [59,60] through the interaction between SIRT1 and STAT3 in GC. This cross-talk is a driver of malignant progression by promoting cell survival signaling, down-regulating tumor suppressor genes, and stimulating drug resistance that exacerbates patient suffering. This interaction accelerates malignant progression by activating proteins associated with cell survival, downregulating tumor suppressor genes, and promoting drug resistance, contributing to poor patient outcomes.

Additionally, SIRT1 overexpression has been reported in hematological malignancies, such as T-cell acute lymphoblastic leukemia, chronic lymphocytic leukemia, diffuse large B-cell lymphoma, and chronic myeloid leukemia (CML) [61–63]. SIRT1 is thus identified as a key tumor promoter and as a potential therapeutic target in cancer, as summarized in these findings.

8. Role of SIRT1 in EMT

EMT in cancer is significantly modulated by Transforming growth factor (TGF)-β which in turn also upregulates SIRT1. SIRT1 interacts with several transcription factors (TFs) to downregulate or degrade E-cad, thereby promoting resistance to cell death and migration and invasion of cancer cells. The involvement of SIRT1 in triggering EMT has been illustrated by multiple studies, mainly through the repression of E-cad [64]. The synergistic role of miR-217 and SIRT1 in EMT is evident in chronic pancreatitis and PC [65]. TGF-β1 initiates EMT

via SIRT1-induced E-cad degradation by down-regulating miR-217. Therefore, miR-217 is a tumor suppressor in pancreatic ductal adenocarcinoma through KRAS targeting [66] and reduces significantly in cancers such as clear cell renal cell carcinoma [67] and GC [68], wherein loss of miR-217 is associated with poor survival. In PC, SIRT1 modulates EMT by binding to ZEB1, an EMT-related TFs, and bringing SIRT1 to the E-cad promoter which in turn downregulates the E-cad expression [69]. In this phenomenon, E-cad is translationally inhibited because of its deacetylation at the histone H3 and reduced attachment of RNA polymerase II.

Transcriptional inhibition of E-cad occurs due to deacetylation of histone H3 and decreased attachment of RNA polymerase II. In line with this, in pancreatic cancer, upregulated methyl-CpG binding domain protein 1 (MBD1) indicates lymph node metastasis, accounting for poor survival [70] and is linked to SIRT1 to promote EMT. SIRT1 is also overexpressed in most hepatocellular carcinoma (HCC) tissues, where it promotes invasion and metastasis through increasing the expression of EMT markers, including SNAIL, twist, and Vim, and decreasing E-cad expression. Moreover, poor survival in HCC is associated with overexpression in HCC, thus the importance and therapeutic value of selective SIRT1 inhibitors is reflected [71,72]. The SIRT1-mediated downregulation of miR-204 inactivates LKB1, which promotes the invasion of GC. miR-204 expression restoration and SIRT1 knockdown promote mesenchymal-epithelial transition (MET) phenotype to inhibit GC metastasis by upregulating E-cad and downregulating Vim levels [73]. SIRT1 also promotes EMT in melanoma by downregulating E-cad expression and deacetylating Beclin-1, it facilitates the degradation via autophagy [74]. These results emphasize the versatile actions of SIRT1 in promoting EMT and positioning itself as a crucial target for further therapeutic interventions in combatting cancer progression and migration.

9. Exosomal role in regulating metabolism in cancer

TME is a heterogeneous atmosphere, with different groups of cells, alterations in the ECM numerous observations on how exosomes can effectively remould metabolism on different carcinogenic pathways and sustain tumor growth. Both the cancer and stromal cells are metabolically reprogrammed by the exosomes in a manner that permits the tumor access to metabolic resources [75]. In CRC, exosomes downregulate the Cav-1 expression and upregulate the expression of GLUT1 which increases the rate of glycolysis in the CAFs. Furthermore, exosomes induce normal fibroblasts to differentiate into CAFs by upregulating α-smooth muscle actin (SMA) expression [76]. In addition, exosomes control the crosstalk between cancer cells and cancer-associated adipocytes. Upon uptake of adipocyte-derived

exosomes by the malignant melanoma cells, the proliferation rate increases, and proteomics study of those exosomes indicated the exosomes carried fatty acid oxidation-associated proteins which in turn modulated the metabolism in the cancer cells [77]. Simultaneously, exosomes are also reported to modulate the endothelial cells in the TME that primarily depend on glycolysis as their energy source. For instance, *Wang et al.* evaluated that the AML-derived exosomes when internalized by the endothelial cells the glycolytic pathway increases due to the transfer of VEGF/VEGFR [78]. Although little is known about the mode of intercellular communication between cancer cells and mesenchymal stem cells (MSCs), but evidence reveals that exosomes play a role in their conversion into the tumor-like phenotype. For example, exosomes derived from prostate cancer (PC) cells are found to carry pyruvate kinase (PK) M2 which when transferred to the MSCs through exosomes, enhances the aggressiveness of the cancer cells and metastasizes to bones [79]. Exosomes derived from a Kaposi's sarcoma-associated herpesvirus (KSHV)-infected cell contained virus-encoded mRNAs that were integrated by surrounding non-infected cells, resulting in a shift in glycolysis and the suppression of mitochondrial biogenesis. It was observed that the exosomes modulated the metabolic reprogramming of adjacent cells, which mediated the proliferation of infected cells and promoted the malignant angiogenesis of Kaposi's sarcoma [80]. Exosomes from chemo-resistant CRC were found to be capable of imparting drug resistance to chemosensitive cells by inducing upregulation of glycolysis [81]. Thus, multiple evidence illustrates that exosomes perform a significant role in metabolic reprogramming facilitating cancer growth, progression, immunosuppression and drug resistance.

10. Role of exosomes in EMT

EMT is the result of the loss of epithelial characteristics and gain of mesenchymal attributes by the cancer cells required for their migration to the distant secondary sites leading to metastasis [82]. The transformed cells secrete greater loads of exosomes as compared to the untransformed cells and are rich in oncogenic mesenchymal markers like Vim, N-cad, fibronectin and decreased epithelial markers E-cad, epithelial cellular adhesion molecule (EpCAM), occludins, etc. along with an increase in the levels of EMT inducing TFs like ZEB1, SIP1/ZEB2, Twist1/2, Snai1/2/3 (Snail/Slug/Smuc). These TFs suppress the epithelial gene expression and enhance the mesenchymal markers thereby reprogramming the gene expression associated with EMT/MET plasticity [82]. The release of exosomes is modulated by the hypoxic conditions which elevate their secretory levels as compared to the normoxic state of the cells [83]. In BC, the loss of tumor suppressor, p85α, the stromal cells convert

into CAFs thereby releasing exosomes carrying Wnt10b which augment metastasis by Wnt pathway-mediated EMT [84]. Exosomes derived from CAFs derived exosomes carry miRNA-181d-5p that initiate the EMT in BC by downregulating caudal-related homeobox-2 (CDX2)/homeobox-A5 (HOXA5) axis [85]. Moreover, CAFs derived exosomal miRNA-21, -378e, -143 elevate the stem cells concentration thereby promoting EMT BC cells [86]. In CRC, the polarization of macrophages from M1 phenotype to M2 occurs due to exosomal transfer of miR-25-3p, miR-130b-3p, miR-425-5pmiRNA which in turn activate the PI3K/Akt signaling and promote EMT by secretion of VEGF [87]. In airway epithelial cells, the Mast cell derived exosomes promote TGFβ1-induced EMT cascade by increasing gene expression of *Twist1, Matrix metalloproteinase (MMP)9, TGF-β1*, bone morphogenic protein-7 (*BMP-7*), *Snail/Slug* and decreased expression of E-cad [88]. However, adipose-derived stem cells (ADSCs) derived exosomal miRNA-215-5p inhibited the high glucose (HG)-induced EMT process of podocytes by targeting the transcription of ZEB2 [89]. Exosomal TGFβ also participates in inducing EMT by activating the Smad dependent pathway resulting in overexpression of nuclear Snail, thereby downregulating E-cad [90]. *Roy et al.* demonstrated that exosomes remain high in OvCa under hypoxic conditions by modulating SIRT1, thereby increasing the Ki-67 expression in ovarian tumor tissues [91][92]. Figure 4 schematically represents the role of exosomes in mediating EMT.

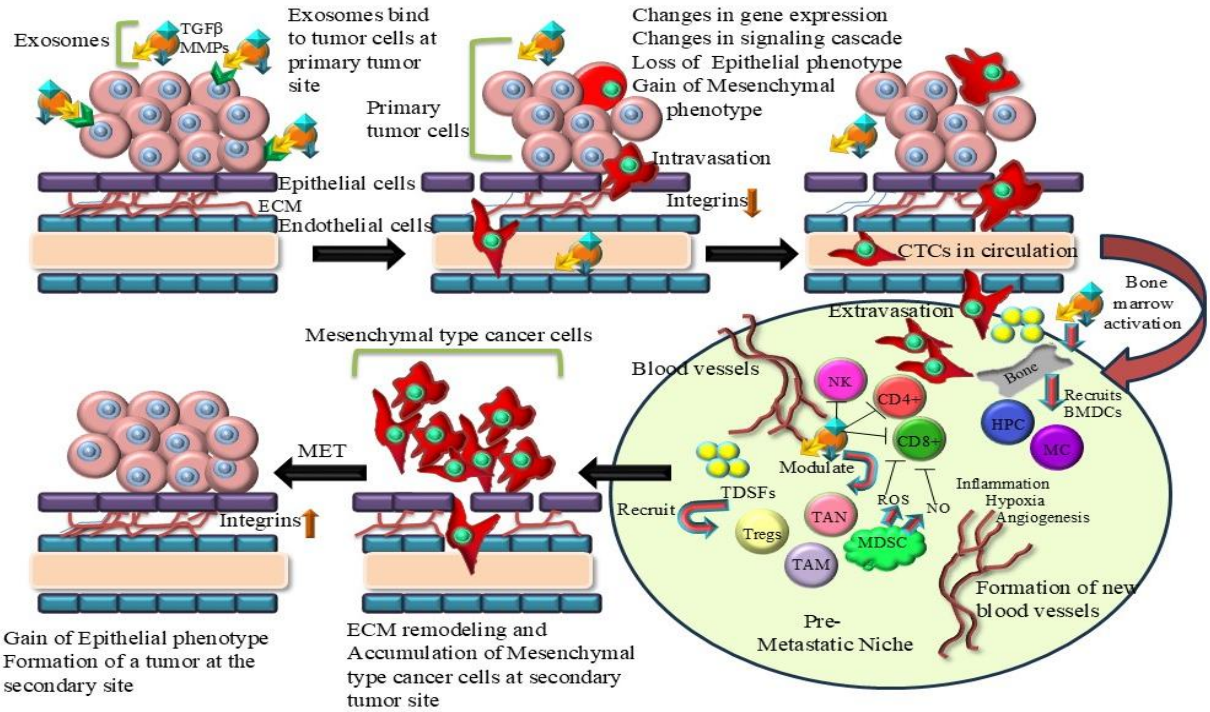

Figure 4. Role of exosomes in mediating EMT

Rationale of the study

The significant global health impact imposed by the higher incidences of OvCa leading to the highest mortality rate in women throws a challenge to the clinicians creating a critical arena of research. Despite technological advancements, the lack of screening techniques and the non-symptomatic nature of the disease primarily drive late-stage diagnosis. This menace demands diagnosis at a treatable stage so that the survival rate increases. Moreover, the Late-stage diagnosis and complex disease mechanisms due to the highly heterogeneous nature with distinct subtypes limit the therapeutic approaches. This demands insights into underlying mechanisms driving the tumorigenesis, progression. Although there exist conventional treatment strategies like surgery, chemotherapy but the alarming situations demand the identification of potential targets to combat the disease and design personalized treatment regimens. The importance of adapting Westernized lifestyle, sociodemographic and economic attributes, gynaecological factors should be taken under consideration upon noticing the increasing number of OvCa incidences across the globe. Thereby, proper awareness among the people and efficient treatment strategies must be designed to improve the healthcare systems to control the rapid prevalence of the disease. Under this doctrine, we aimed to investigate the interplay between exosomes and cells in the TME which regulates the metastasis in OvCa. The following objectives are hypothesized to perform the study.

Objectives

- To identify and characterize different metabolic markers in correlation with exosomes status in metastatic ovarian cancer
- To establish the altered signaling cascade involving the different metabolic regulators in exosome mediated metastasis
- To study the metastasizing ability of exosomes and cancer cells in mice xenograft model and also evaluate the metabolic and metastatic markers in the tumor microenvironment.

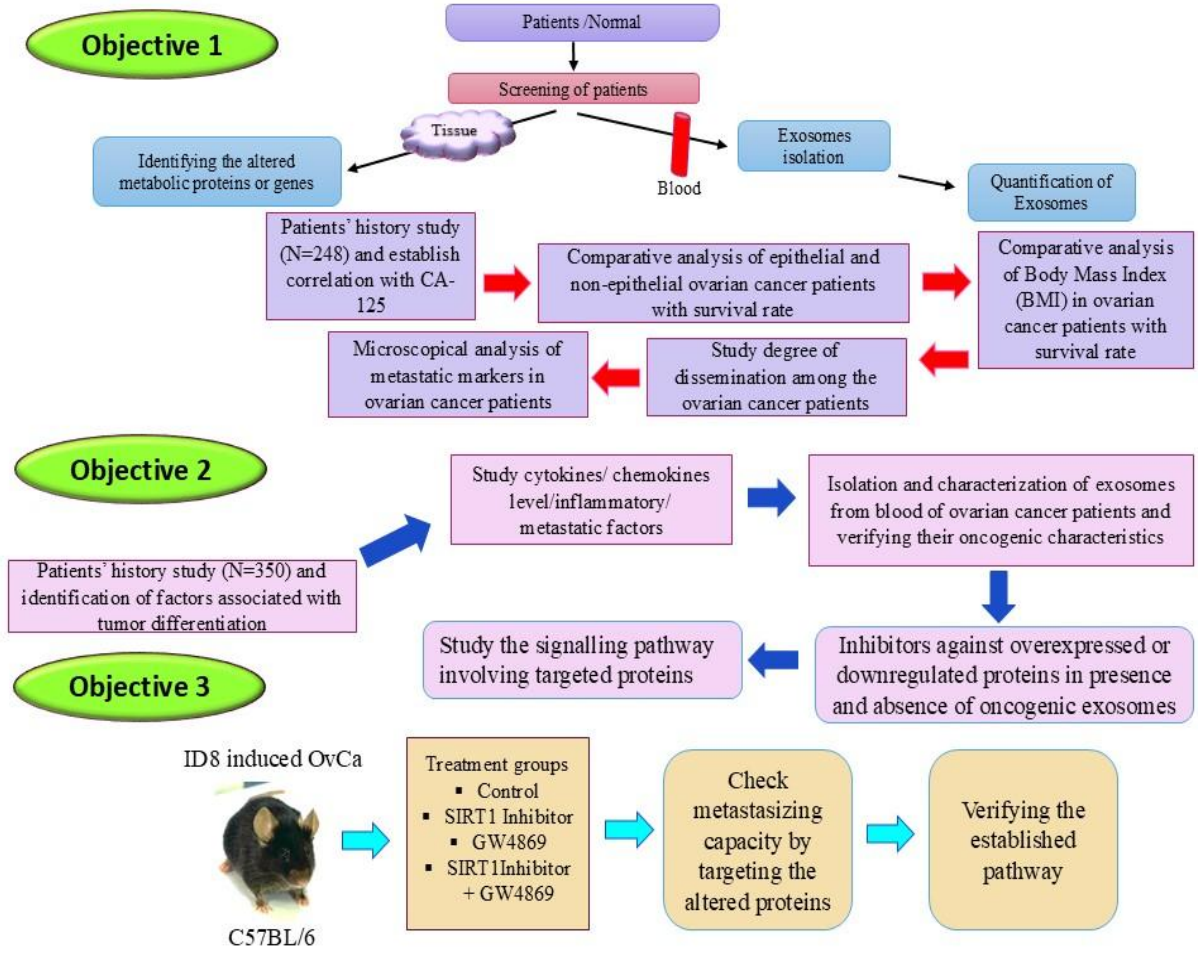

Figure 5: Schematic of strategy of work

References

[1] A.M. Filho, M. Laversanne, J. Ferlay, M. Colombet, M. Piñeros, A. Znaor, D.M. Parkin, I. Soerjomataram, F. Bray, The GLOBOCAN 2022 cancer estimates: Data sources, methods, and a snapshot of the cancer burden worldwide, Int. J. Cancer. (2024). https://doi.org/10.1002/IJC.35278.

[2] S. Narod, Can advanced-stage ovarian cancer be cured?, Nat. Rev. Clin. Oncol. 13 (2016) 255–261. https://doi.org/10.1038/nrclinonc.2015.224.

[3] C. Stewart, C. Ralyea, S. Lockwood, Ovarian Cancer: An Integrated Review, Semin. Oncol. Nurs. 35 (2019) 151–156. https://doi.org/10.1016/j.soncn.2019.02.001.

[4] M. Devouassoux-Shisheboran, C. Genestie, Pathobiology of ovarian carcinomas, Chin. J. Cancer. 34 (2015) 50–55. https://doi.org/10.5732/cjc.014.10273.

[5] T. Kaku, S. Ogawa, Y. Kawano, Y. Ohishi, H. Kobayashi, T. Hirakawa, H. Nakano, Histological classification of ovarian cancer, Med. Electron Microsc. 36 (2003) 9–17. https://doi.org/10.1007/s007950300002.

[6] M. Malvezzi, G. Carioli, T. Rodriguez, E. Negri, C. La Vecchia, Global trends and predictions in ovarian cancer mortality, Ann. Oncol. 27 (2016) 2017–2025. https://doi.org/10.1093/annonc/mdw306.

[7] National Centre For Disease Informatics and Research National Cancer Registry Programme Indian Council of Medical Research Three-Year Report of Population Based Cancer Registries Incidence and Distribution of Cancer (Report of 25 PBCRs in India), 2016.

[8] N.S. Murthy, S. Shalini, G. Suman, S. Pruthvish, A. Mathew, Changing trends in incidence of ovarian cancer - The Indian Scenario, Asian Pacific J. Cancer Prev. 10 (2009) 1025–1030.

[9] M. Chaturvedi, S. Krishnan, P. Das, K.L. Sudarshan, S. Stephen, V. Monesh, P. Mathur, Descriptive Epidemiology of Ovarian Cancers in India: A Report from National Cancer Registry Programme, Indian J. Gynecol. Oncol. 21 (2023) 1–9. https://doi.org/10.1007/S40944-022-00694-1/METRICS.

[10] G. Si, X. Chen, Y. Li, X. Yuan, Exosomes promote pre-metastatic niche formation in colorectal cancer, Heliyon. 10 (2024) 124. https://doi.org/10.1016/j.heliyon.2024.e27572.

[11] Y. Zhu, C. Wang, Z. Ma, F. Li, C. Xu, W. Pan, A. Liu, Role of Exosomes in the Invasion and Metastasis of Ovarian Cancer and Application Potential of Clinical Diagnosis and Treatment, J. Cancer. 14 (2023) 1141–1150. https://doi.org/10.7150/jca.83663.

[12] K. Nakamura, K. Sawada, Y. Kinose, A. Yoshimura, A. Toda, E. Nakatsuka, K. Hashimoto, S. Mabuchi, K.I. Morishige, H. Kurachi, E. Lengyel, T. Kimura, Exosomes promote ovarian cancer cell invasion through transfer of CD44 to peritoneal mesothelial cells, Mol. Cancer Res. 15 (2017) 78–92. https://doi.org/10.1158/1541-7786.MCR-16-0191.

[13] X. Guan, Z. hong Zong, Y. Liu, S. Chen, L. li Wang, Y. Zhao, circPUM1 Promotes Tumorigenesis and Progression of Ovarian Cancer by Sponging miR-615-5p and miR-6753-5p, Mol. Ther. Nucleic Acids. 18 (2019) 882–892. https://doi.org/10.1016/j.omtn.2019.09.032.

[14] D.K. Jeppesen, A.M. Fenix, J.L. Franklin, J.N. Higginbotham, Q. Zhang, L.J. Zimmerman, D.C. Liebler, J. Ping, Q. Liu, R. Evans, W.H. Fissell, J.G. Patton, L.H. Rome, D.T. Burnette, R.J. Coffey, Reassessment of Exosome Composition, Cell. 177 (2019) 428-445.e18. https://doi.org/10.1016/j.cell.2019.02.029.

[15] W. Feng, D.C. Dean, F.J. Hornicek, H. Shi, Z. Duan, Exosomes promote pre-metastatic niche formation in ovarian cancer, Mol. Cancer. 18 (2019) 124. https://doi.org/10.1186/s12943-019-1049-4.

[16] L. Pascual-Antón, B. Cardeñes, R. Sainz de la Cuesta, L. González-Cortijo, M. López-Cabrera, C. Cabañas, P. Sandoval, Mesothelial-to-Mesenchymal Transition and Exosomes in Peritoneal Metastasis of Ovarian Cancer, Int. J. Mol. Sci. 22 (2021) 11496. https://doi.org/10.3390/ijms222111496.

[17] Y. Han, J. Ren, Y. Bai, X. Pei, Y. Han, Exosomes from hypoxia-treated human adipose-derived mesenchymal stem cells enhance angiogenesis through VEGF/VEGF-R, Int. J. Biochem. Cell Biol. 109 (2019) 59–68. https://doi.org/10.1016/j.biocel.2019.01.017.

[18] Z. Li, W. Yan-qing, Y. Xiao, L. Shi-yi, Y. Meng-qin, X. Shu, Y. Dong-yong, Z. Ya-jing, C. Yan-xiang, Exosomes secreted by chemoresistant ovarian cancer cells promote angiogenesis, J. Ovarian Res. 14 (2021) 7. https://doi.org/10.1186/s13048-020-00758-w.

[19] L. He, W. Zhu, Q. Chen, Y. Yuan, Y. Wang, J. Wang, X. Wu, Ovarian cancer cell-secreted exosomal miR-205 promotes metastasis by inducing angiogenesis, Theranostics. 9 (2019) 8206–8220. https://doi.org/10.7150/thno.37455.

[20] K.D.P. Dorayappan, R. Wanner, J.J. Wallbillich, U. Saini, R. Zingarelli, A.A. Suarez, D.E. Cohn, K. Selvendiran, Hypoxia-induced exosomes contribute to a more aggressive and chemoresistant ovarian cancer phenotype: a novel mechanism linking STAT3/Rab proteins, Oncogene. 37 (2018) 3806–3821. https://doi.org/10.1038/s41388-018-0189-0.

[21] X. Chen, J. Zhou, X. Li, X. Wang, Y. Lin, X. Wang, Exosomes derived from hypoxic epithelial ovarian cancer cells deliver microRNAs to macrophages and elicit a tumor-promoted phenotype, Cancer Lett. 435 (2018) 80–91. https://doi.org/10.1016/j.canlet.2018.08.001.

[22] O. WARBURG, On the origin of cancer cells., Science. 123 (1956) 309–14. https://doi.org/10.1126/science.123.3191.309.

[23] Y. Ma, W. Wang, M.O. Idowu, U. Oh, X.-Y. Wang, S.M. Temkin, X. Fang, Ovarian Cancer Relies on Glucose Transporter 1 to Fuel Glycolysis and Growth: Anti-Tumor Activity of BAY-876., Cancers (Basel). 11 (2018) 33. https://doi.org/10.3390/cancers11010033.

[24] M.K.Y. Siu, Y.-X. Jiang, J.-J. Wang, T.H.Y. Leung, S.F. Ngu, A.N.Y. Cheung, H.Y.S. Ngan, K.K.L. Chan, PDK1 promotes ovarian cancer metastasis by modulating tumor-mesothelial adhesion, invasion, and angiogenesis via α5β1 integrin and JNK/IL-8 signaling., Oncogenesis. 9 (2020) 24. https://doi.org/10.1038/s41389-020-0209-0.

[25] K. Yaku, K. Okabe, T. Nakagawa, NAD metabolism: Implications in aging and longevity., Ageing Res. Rev. 47 (2018) 1–17. https://doi.org/10.1016/j.arr.2018.05.006.

[26] K. Yaku, K. Okabe, K. Hikosaka, T. Nakagawa, NAD Metabolism in Cancer Therapeutics., Front. Oncol. 8 (2018) 622. https://doi.org/10.3389/fonc.2018.00622.

[27] B. Tan, S. Dong, R.L. Shepard, L. Kays, K.D. Roth, S. Geeganage, M.-S. Kuo, G. Zhao, Inhibition of Nicotinamide Phosphoribosyltransferase (NAMPT), an Enzyme Essential for NAD+ Biosynthesis, Leads to Altered Carbohydrate Metabolism in Cancer Cells., J. Biol. Chem. 290 (2015) 15812–15824. https://doi.org/10.1074/jbc.M114.632141.

[28] C. Rodríguez, N. Puente-Moncada, R.J. Reiter, A.M. Sánchez-Sánchez, F. Herrera, J. Rodríguez-Blanco, C. Duarte-Olivenza, M. Turos-Cabal, I. Antolín, V. Martín, Regulation of cancer cell glucose metabolism is determinant for cancer cell fate after melatonin administration., J. Cell. Physiol. 236 (2021) 27–40. https://doi.org/10.1002/jcp.29886.

[29] C. Harmon, C. O'Farrelly, M.W. Robinson, The Immune Consequences of Lactate in the Tumor Microenvironment., Adv. Exp. Med. Biol. 1259 (2020) 113–124. https://doi.org/10.1007/978-3-030-43093-1_7.

[30] C. Sebastián, R. Mostoslavsky, The role of mammalian sirtuins in cancer metabolism., Semin. Cell Dev. Biol. 43 (2015) 33–42. https://doi.org/10.1016/j.semcdb.2015.07.008.

[31] Z. Mei, X. Zhang, J. Yi, J. Huang, J. He, Y. Tao, Sirtuins in metabolism, DNA repair and cancer, J. Exp. Clin. Cancer Res. 35 (2016) 182. https://doi.org/10.1186/s13046-016-0461-5.

[32] R.H. Houtkooper, E. Pirinen, J. Auwerx, Sirtuins as regulators of metabolism and healthspan, Nat. Rev. Mol. Cell Biol. 13 (2012) 225–238. https://doi.org/10.1038/nrm3293.

[33] A.A. Sauve, Sirtuin chemical mechanisms, Biochim. Biophys. Acta - Proteins Proteomics. 1804 (2010) 1591–1603. https://doi.org/10.1016/j.bbapap.2010.01.021.

[34] Y. Shi, Y. Zhou, S. Wang, Y. Zhang, Sirtuin Deacetylation Mechanism and Catalytic Role of the Dynamic Cofactor Binding Loop, J. Phys. Chem. Lett. 4 (2013) 491–495. https://doi.org/10.1021/jz302015s.

[35] V. Carafa, L. Altucci, A. Nebbioso, Dual tumor suppressor and tumor promoter action of sirtuins in determining malignant phenotype, Front. Pharmacol. 9 (2019) 38. https://doi.org/10.3389/fphar.2019.00038.

[36] M.F. Santolla, S. Avino, M. Pellegrino, E.M. De Francesco, P. De Marco, R. Lappano, A. Vivacqua, F. Cirillo, D.C. Rigiracciolo, A. Scarpelli, S. Abonante, M. Maggiolini, SIRT1 is involved in oncogenic signaling mediated by GPER in breast cancer, Cell Death Dis. 6 (2015) e1834–e1834. https://doi.org/10.1038/cddis.2015.201.

[37] D. Herranz, A. Maraver, M. Cañamero, G. Gómez-López, L. Inglada-Pérez, M. Robledo, E. Castelblanco, X. Matias-Guiu, M. Serrano, SIRT1 promotes thyroid carcinogenesis driven by PTEN deficiency, Oncogene. 32 (2013) 4052–4056. https://doi.org/10.1038/ONC.2012.407.

[38] L. Dan, O. Klimenkova, M. Klimiankou, J.-H. Klusman, M.M. van den Heuvel-Eibrink, D. Reinhardt, K. Welte, J. Skokowa, The role of sirtuin 2 activation by nicotinamide phosphoribosyltransferase in the aberrant proliferation and survival of myeloid leukemia cells, Haematologica. 97 (2012) 551–559. https://doi.org/10.3324/haematol.2011.055236.

[39] P.Y. Liu, N. Xu, A. Malyukova, C.J. Scarlett, Y.T. Sun, X.D. Zhang, D. Ling, S.-P. Su, C. Nelson, D.K. Chang, J. Koach, A.E. Tee, M. Haber, M.D. Norris, C. Toon, I. Rooman, C. Xue, B.B. Cheung, S. Kumar, G.M. Marshall, A. V Biankin, T. Liu, The histone deacetylase SIRT2 stabilizes Myc oncoproteins, Cell Death Differ. 20 (2013) 503–514. https://doi.org/10.1038/cdd.2012.147.

[40] J. Chen, A.W.H. Chan, K.-F. To, W. Chen, Z. Zhang, J. Ren, C. Song, Y.-S. Cheung, P.B.S. Lai, S.-H. Cheng, M.H.L. Ng, A. Huang, B.C.B. Ko, SIRT2 overexpression in hepatocellular carcinoma mediates epithelial to mesenchymal transition by protein kinase B/glycogen synthase kinase-3β/β-catenin signaling, Hepatology. 57 (2013) 2287–2298. https://doi.org/10.1002/hep.26278.

[41] I.-C. Chen, W.-F. Chiang, S.-Y. Liu, P.-F. Chen, H.-C. Chiang, Role of SIRT3 in the regulation of redox balance during oral carcinogenesis, Mol. Cancer. 12 (2013) 68. https://doi.org/10.1186/1476-4598-12-68.

[42] H. Yang, L. Zhou, Q. Shi, Y. Zhao, H. Lin, M. Zhang, S. Zhao, Y. Yang, Z. Ling, K. Guan, Y. Xiong, D. Ye, SIRT3-dependent GOT2 acetylation status affects the malate–

aspartate NADH shuttle activity and pancreatic tumor growth, EMBO J. 34 (2015) 1110–1125. https://doi.org/10.15252/embj.201591041.

[43] K. Shedden, J.M.G. Taylor, S.A. Enkemann, M.S. Tsao, T.J. Yeatman, W.L. Gerald, S. Eschrich, I. Jurisica, T.J. Giordano, D.E. Misek, A.C. Chang, C.Q. Zhu, D. Strumpf, S. Hanash, F.A. Shepherd, K. Ding, L. Seymour, K. Naoki, N. Pennell, B. Weir, R. Verhaak, C. Ladd-Acosta, T. Golub, M. Gruidl, A. Sharma, J. Szoke, M. Zakowski, V. Rusch, M. Kris, A. Viale, N. Motoi, W. Travis, B. Conley, V.E. Seshan, M. Meyerson, R. Kuick, K.K. Dobbin, T. Lively, J.W. Jacobson, D.G. Beer, Gene expression-based survival prediction in lung adenocarcinoma: a multi-site, blinded validation study, Nat. Med. 14 (2008) 822–827. https://doi.org/10.1038/NM.1790.

[44] A. Csibi, S.M. Fendt, C. Li, G. Poulogiannis, A.Y. Choo, D.J. Chapski, S.M. Jeong, J.M. Dempsey, A. Parkhitko, T. Morrison, E.P. Henske, M.C. Haigis, L.C. Cantley, G. Stephanopoulos, J. Yu, J. Blenis, The mTORC1 pathway stimulates glutamine metabolism and cell proliferation by repressing SIRT4, Cell. 153 (2013) 840–854. https://doi.org/10.1016/J.CELL.2013.04.023.

[45] C.C. Lai, P.M. Lin, S.F. Lin, C.H. Hsu, H.C. Lin, M.L. Hu, C.M. Hsu, M.Y. Yang, Altered expression of SIRT gene family in head and neck squamous cell carcinoma, Tumour Biol. 34 (2013) 1847–1854. https://doi.org/10.1007/S13277-013-0726-Y.

[46] C. Bartosch, S. Monteiro-Reis, D. Almeida-Rios, R. Vieira, A. Castro, M. Moutinho, M. Rodrigues, I. Graça, J.M. Lopes, C. Jerónimo, Assessing sirtuin expression in endometrial carcinoma and non-neoplastic endometrium, Oncotarget. 7 (2016) 1144–1154. https://doi.org/10.18632/ONCOTARGET.6691.

[47] C. Sebastián, B.M.M. Zwaans, D.M. Silberman, M. Gymrek, A. Goren, L. Zhong, O. Ram, J. Truelove, A.R. Guimaraes, D. Toiber, C. Cosentino, J.K. Greenson, A.I. MacDonald, L. McGlynn, F. Maxwell, J. Edwards, S. Giacosa, E. Guccione, R. Weissleder, B.E. Bernstein, A. Regev, P.G. Shiels, D.B. Lombard, R. Mostoslavsky, The histone deacetylase SIRT6 is a tumor suppressor that controls cancer metabolism, Cell. 151 (2012) 1185–1199. https://doi.org/10.1016/J.CELL.2012.10.047.

[48] H. Yu, W. Ye, J. Wu, X. Meng, R.Y. Liu, X. Ying, Y. Zhou, H. Wang, C. Pan, W. Huang, Overexpression of sirt7 exhibits oncogenic property and serves as a prognostic

factor in colorectal cancer, Clin. Cancer Res. 20 (2014) 3434–3445. https://doi.org/10.1158/1078-0432.CCR-13-2952.

[49] Q. He, K. Chen, R. Ye, N. Dai, P. Guo, L. Wang, Associations of sirtuins with clinicopathological variables and prognosis in human ovarian cancer, Oncol. Lett. 19 (2020) 3278. https://doi.org/10.3892/OL.2020.11432.

[50] N. Petrucelli, M.B. Daly, T. Pal, BRCA1- and BRCA2 -Associated Hereditary Breast and Ovarian Cancer Summary Genetic counseling Suggestive Findings, Gene Rev. (1998) 1–37. https://www.ncbi.nlm.nih.gov/books/NBK1247/.

[51] D. Li, N.-N. Chen, J.-M. Cao, W.-P. Sun, Y.-M. Zhou, C.-Y. Li, X.-X. Wang, BRCA1 as a nicotinamide adenine dinucleotide (NAD)-dependent metabolic switch in ovarian cancer., Cell Cycle. 13 (2014) 2564–71. https://doi.org/10.4161/15384101.2015.942208.

[52] B. Jung-Hynes, M. Nihal, W. Zhong, N. Ahmad, Role of sirtuin histone deacetylase SIRT1 in prostate cancer. A target for prostate cancer management via its inhibition?, J. Biol. Chem. 284 (2009) 3823–32. https://doi.org/10.1074/jbc.M807869200.

[53] X. Jin, Y. Wei, F. Xu, M. Zhao, K. Dai, R. Shen, S. Yang, N. Zhang, SIRT1 promotes formation of breast cancer through modulating Akt activity, J. Cancer. 9 (2018) 2012–2023. https://doi.org/10.7150/jca.24275.

[54] L. Han, X.-H. Liang, L.-X. Chen, S.-M. Bao, Z.-Q. Yan, SIRT1 is highly expressed in brain metastasis tissues of non-small cell lung cancer (NSCLC) and in positive regulation of NSCLC cell migration., Int. J. Clin. Exp. Pathol. 6 (2013) 2357–65.

[55] Z. Lin, D. Fang, The Roles of SIRT1 in Cancer, Genes Cancer. 4 (2013) 97–104. https://doi.org/10.1177/1947601912475079.

[56] M. Ohanna, C. Bonet, K. Bille, M. Allegra, I. Davidson, P. Bahadoran, J.-P. Lacour, R. Ballotti, C. Bertolotto, SIRT1 promotes proliferation and inhibits the senescence-like phenotype in human melanoma cells., Oncotarget. 5 (2014) 2085–95. https://doi.org/10.18632/oncotarget.1791.

[57] W. Chen, R. Bhatia, Roles of SIRT1 in leukemogenesis., Curr. Opin. Hematol. 20 (2013) 308–13. https://doi.org/10.1097/MOH.0b013e328360ab64.

[58] T. Shuang, M. Wang, Y. Zhou, C. Shi, Over-expression of Sirt1 contributes to chemoresistance and indicates poor prognosis in serous epithelial ovarian cancer (EOC), Med. Oncol. 32 (2015) 260. https://doi.org/10.1007/s12032-015-0706-8.

[59] Y. Nie, D.M. Erion, Z. Yuan, M. Dietrich, G.I. Shulman, T.L. Horvath, Q. Gao, STAT3 inhibition of gluconeogenesis is downregulated by SirT1, Nat. Cell Biol. 11 (2009) 492–500. https://doi.org/10.1038/ncb1857.

[60] S. Zhang, S. Huang, C. Deng, Y. Cao, J. Yang, G. Chen, B. Zhang, C. Duan, J. Shi, B. Kong, H. Friess, N. Zhao, C. Huang, X. Huang, L. Wang, X. Zou, Co-ordinated overexpression of SIRT1 and STAT3 is associated with poor survival outcome in gastric cancer patients., Oncotarget. 8 (2017) 18848–18860. https://doi.org/10.18632/oncotarget.14473.

[61] K.Y. Jang, S.H. Hwang, K.S. Kwon, K.R. Kim, H.N. Choi, N.-R. Lee, J.-Y. Kwak, B.-H. Park, H.S. Park, M.J. Chung, M.J. Kang, D.G. Lee, H.S. Kim, H. Shim, W.S. Moon, SIRT1 expression is associated with poor prognosis of diffuse large B-cell lymphoma., Am. J. Surg. Pathol. 32 (2008) 1523–31. https://doi.org/10.1097/PAS.0b013e31816b6478.

[62] J.C. Wang, M.I. Kafeel, B. Avezbakiyev, C. Chen, Y. Sun, C. Rathnasabapathy, M. Kalavar, Z. He, J. Burton, S. Lichter, Histone Deacetylase in Chronic Lymphocytic Leukemia, Oncology. 81 (2011) 325–329. https://doi.org/10.1159/000334577.

[63] T. Kozako, A. Aikawa, T. Shoji, T. Fujimoto, M. Yoshimitsu, S. Shirasawa, H. Tanaka, S. Honda, H. Shimeno, N. Arima, S. Soeda, High expression of the longevity gene product SIRT1 and apoptosis induction by sirtinol in adult T-cell leukemia cells, Int. J. Cancer. 131 (2012) 2044–2055. https://doi.org/10.1002/ijc.27481.

[64] R. Palmirotta, M. Cives, D. Della-Morte, B. Capuani, D. Lauro, F. Guadagni, F. Silvestris, Sirtuins and Cancer: Role in the Epithelial-Mesenchymal Transition., Oxid. Med. Cell. Longev. 2016 (2016) 3031459. https://doi.org/10.1155/2016/3031459.

[65] S. Deng, S. Zhu, B. Wang, X. Li, Y. Liu, Q. Qin, Q. Gong, Y. Niu, C. Xiang, J. Chen, J. Yan, S. Deng, T. Yin, M. Yang, H. Wu, C. Wang, G. Zhao, Chronic pancreatitis and pancreatic cancer demonstrate active epithelial–mesenchymal transition profile, regulated by miR-217-SIRT1 pathway, Cancer Lett. 355 (2014) 184–191. https://doi.org/10.1016/j.canlet.2014.08.007.

[66] W.-G. Zhao, S.-N. Yu, Z.-H. Lu, Y.-H. Ma, Y.-M. Gu, J. Chen, The miR-217 microRNA functions as a potential tumor suppressor in pancreatic ductal adenocarcinoma by targeting KRAS, Carcinogenesis. 31 (2010) 1726–1733. https://doi.org/10.1093/carcin/bgq160.

[67] H. Li, J. Zhao, J.W. Zhang, Q.Y. Huang, J.Z. Huang, L.S. Chi, H.J. Tang, G.Q. Liu, D.J. Zhu, W.M. Ma, MicroRNA-217, down-regulated in clear cell renal cell carcinoma and associated with lower survival, suppresses cell proliferation and migration., Neoplasma. 60 (2013) 511–5. https://doi.org/10.4149/neo_2013_066.

[68] D. Chen, D. Zhang, Y. Lu, L. Chen, Z. Zeng, M. He, F. Wang, Y. Li, H. Zhang, H. Pelicano, W. Zhang, R. Xu, microRNA-217 inhibits tumor progression and metastasis by downregulating EZH2 and predicts favorable prognosis in gastric cancer., Oncotarget. 6 (2015) 10868–79. https://doi.org/10.18632/oncotarget.3451.

[69] V. Byles, L. Zhu, J.D. Lovaas, L.K. Chmilewski, J. Wang, D. V Faller, Y. Dai, SIRT1 induces EMT by cooperating with EMT transcription factors and enhances prostate cancer cell migration and metastasis, Oncogene. 31 (2012) 4619–4629. https://doi.org/10.1038/onc.2011.612.

[70] J. Xu, W. Zhu, W. Xu, W. Yao, B. Zhang, Y. Xu, S. Ji, C. Liu, J. Long, Q. Ni, X. Yu, Up-regulation of MBD1 promotes pancreatic cancer cell epithelial-mesenchymal transition and invasion by epigenetic down-regulation of E-cadherin., Curr. Mol. Med. 13 (2013) 387–400.

[71] C. Hao, P.-X. Zhu, X. Yang, Z.-P. Han, J.-H. Jiang, C. Zong, X.-G. Zhang, W.-T. Liu, Q.-D. Zhao, T.-T. Fan, L. Zhang, L.-X. Wei, Overexpression of SIRT1 promotes metastasis through epithelial-mesenchymal transition in hepatocellular carcinoma., BMC Cancer. 14 (2014) 978. https://doi.org/10.1186/1471-2407-14-978.

[72] S.J. Serrano-Gomez, M. Maziveyi, S.K. Alahari, Regulation of epithelial-mesenchymal transition through epigenetic and post-translational modifications, Mol. Cancer. 15 (2016) 18. https://doi.org/10.1186/s12943-016-0502-x.

[73] L. Zhang, X. Wang, P. Chen, MiR-204 down regulates SIRT1 and reverts SIRT1-induced epithelial-mesenchymal transition, anoikis resistance and invasion in gastric cancer cells., BMC Cancer. 13 (2013) 290. https://doi.org/10.1186/1471-2407-13-290.

[74] T. Sun, L. Jiao, Y. Wang, Y. Yu, L. Ming, SIRT1 induces epithelial-mesenchymal transition by promoting autophagic degradation of E-cadherin in melanoma cells, Cell Death Dis. 9 (2018) 136. https://doi.org/10.1038/s41419-017-0167-4.

[75] S. Tan, L. Xia, P. Yi, Y. Han, L. Tang, Q. Pan, Y. Tian, S. Rao, L. Oyang, J. Liang, J. Lin, M. Su, Y. Shi, D. Cao, Y. Zhou, Q. Liao, Exosomal miRNAs in tumor microenvironment, J. Exp. Clin. Cancer Res. 39 (2020) 67. https://doi.org/10.1186/s13046-020-01570-6.

[76] A. Rai, D.W. Greening, M. Chen, R. Xu, H. Ji, R.J. Simpson, Exosomes Derived from Human Primary and Metastatic Colorectal Cancer Cells Contribute to Functional Heterogeneity of Activated Fibroblasts by Reprogramming Their Proteome, Proteomics. 19 (2019) e1800148. https://doi.org/10.1002/pmic.201800148.

[77] I. Lazar, E. Clement, S. Dauvillier, D. Milhas, M. Ducoux-Petit, S. LeGonidec, C. Moro, V. Soldan, S. Dalle, S. Balor, M. Golzio, O. Burlet-Schiltz, P. Valet, C. Muller, L. Nieto, Adipocyte Exosomes Promote Melanoma Aggressiveness through Fatty Acid Oxidation: A Novel Mechanism Linking Obesity and Cancer, Cancer Res. 76 (2016) 4051–4057. https://doi.org/10.1158/0008-5472.CAN-16-0651.

[78] K. Rohlenova, K. Veys, I. Miranda-Santos, K. De Bock, P. Carmeliet, Endothelial Cell Metabolism in Health and Disease, Trends Cell Biol. 28 (2018) 224–236. https://doi.org/10.1016/j.tcb.2017.10.010.

[79] J. Dai, J. Escara-Wilke, J.M. Keller, Y. Jung, R.S. Taichman, K.J. Pienta, E.T. Keller, Primary prostate cancer educates bone stroma through exosomal pyruvate kinase M2 to promote bone metastasis, J. Exp. Med. 216 (2019) 2883–2899. https://doi.org/10.1084/jem.20190158.

[80] O. Yogev, S. Henderson, M.J. Hayes, S.S. Marelli, Y. Ofir-Birin, N. Regev-Rudzki, J. Herrero, T. Enver, Herpesviruses shape tumour microenvironment through exosomal transfer of viral microRNAs, PLoS Pathog. 13 (2017) 1–24. https://doi.org/10.1371/journal.ppat.1006524.

[81] X. Wang, H. Zhang, H. Yang, M. Bai, T. Ning, T. Deng, R. Liu, Q. Fan, K. Zhu, J. Li, Y. Zhan, G. Ying, Y. Ba, Exosome-delivered circRNA promotes glycolysis to induce chemoresistance through the miR-122-PKM2 axis in colorectal cancer, Mol. Oncol. 14 (2020) 539–555. https://doi.org/10.1002/1878-0261.12629.

[82] A. Conigliaro, C. Cicchini, Exosome-Mediated Signaling in Epithelial to Mesenchymal Transition and Tumor Progression, J. Clin. Med. 8 (2018) 26. https://doi.org/10.3390/jcm8010026.

[83] N. Syn, L. Wang, G. Sethi, J.P. Thiery, B.C. Goh, Exosome-Mediated Metastasis: From Epithelial-Mesenchymal Transition to Escape from Immunosurveillance, Trends Pharmacol. Sci. 37 (2016) 606–617. https://doi.org/10.1016/j.tips.2016.04.006.

[84] Y. Chen, C. Zeng, Y. Zhan, H. Wang, X. Jiang, W. Li, Aberrant low expression of p85α in stromal fibroblasts promotes breast cancer cell metastasis through exosome-mediated paracrine Wnt10b, Oncogene. 36 (2017) 4692–4705. https://doi.org/10.1038/onc.2017.100.

[85] N.W. Mian He , Hao Qin , Terence C W Poon , Siu-Ching Sze , Xiaofan Ding , Ngai Na Co , Sai-Ming Ngai , Ting-Fung Chan, Hepatocellular carcinoma-derived exosomes promote motility of immortalized hepatocyte through transfer of oncogenic proteins and RNAs, Rev. Financ. Stud. 36 (2015) 1008–1018. https://doi.org/10.1093/carcin/bgv081.

[86] E. Donnarumma, D. Fiore, M. Nappa, G. Roscigno, A. Adamo, M. Iaboni, V. Russo, A. Affinito, I. Puoti, C. Quintavalle, A. Rienzo, S. Piscuoglio, R. Thomas, G. Condorelli, Cancer-associated fibroblasts release exosomal microRNAs that dictate an aggressive phenotype in breast cancer, Oncotarget. 8 (2017) 19592–19608. https://doi.org/10.18632/oncotarget.14752.

[87] D. Wang, X. Wang, M. Si, J. Yang, S. Sun, H. Wu, S. Cui, X. Qu, X. Yu, Exosome-encapsulated miRNAs contribute to CXCL12/CXCR4-induced liver metastasis of colorectal cancer by enhancing M2 polarization of macrophages, Cancer Lett. 474 (2020) 36–52. https://doi.org/10.1016/j.canlet.2020.01.005.

[88] Y. Yin, G.V. Shelke, C. Lässer, H. Brismar, J. Lötvall, Extracellular vesicles from mast cells induce mesenchymal transition in airway epithelial cells, Respir. Res. 21 (2020) 101. https://doi.org/10.1186/s12931-020-01346-8.

[89] J. Jin, Y. Wang, L. Zhao, W. Zou, M. Tan, Q. He, Exosomal miRNA-215-5p Derived from Adipose-Derived Stem Cells Attenuates Epithelial-Mesenchymal Transition of Podocytes by Inhibiting ZEB2, Biomed Res. Int. 2020 (2020) 2685305. https://doi.org/10.1155/2020/2685305.

[90] S. Heerboth, G. Housman, M. Leary, M. Longacre, S. Byler, K. Lapinska, A. Willbanks, S. Sarkar, EMT and tumor metastasis, Clin. Transl. Med. 4 (2015) 6. https://doi.org/10.1186/s40169-015-0048-3.

[91] S. Roy, A. Das, M. Vernekar, S. Mandal, N. Chatterjee, Understanding the Correlation between Metabolic Regulator SIRT1 and Exosomes with CA-125 in Ovarian Cancer: A Clinicopathological Study, Biomed Res. Int. 2022 (2022) 5346091. https://doi.org/10.1155/2022/5346091.

[92] S. Roy, A. Das, M. Vernekar, S. Das, N. Chatterjee, Abstract 2461: SIRT1 regulates ovarian cancer metastasis via altering the exosome release and glycogen deposition, Cancer Res. 81 (2021) 2461. https://doi.org/10.1158/1538-7445.AM2021-2461.

Chapter 1

"Database mining identifies SIRT1 as a regulatory molecule driving metastasis in ovarian cancer"

1.1. Introduction

The deacetylating potential of upregulated SIRT1 has driven the attention of researchers to investigate the abnormal functionality of the various deacetylated proteins that affect the metabolic state, DNA repair and survivability of OvCa cells [1]. Additionally, activated SIRT1 in OvCa cells enhances proliferation and promotes tumor growth by inhibiting the apoptotic process by deacetylating the pro-apoptotic factors [2].The poor survival outcomes of the OvCa patients are due to the higher SIRT1 expression that induces the malignant transformation of the cancer cells [3]. Parallelly, another vital factor that participates in controlling several cellular mechanisms like controlling angiogenesis, instigating the apoptotic cascade, promoting DNA repair mechanisms is the tumor suppressor p53 [4]. However, it has been observed in advanced malignancies that the p53 gene is often mutated with a gain of function as an oncogene and loses its tumor suppressing ability which eventually augments the aggressiveness of the disease [5].

The effect of SIRT1 is dependent on the tumor type and the genomic state of the cell along with the p53 status in the cells. However, in cells in which p53 and other tumor suppressors are lost, and their repressive activity is restrained, the expression level of SIRT1 goes high. There exist several cancer cell lines that lack p53 expression, exhibit overexpressed SIRT1 and upon knockdown of SIRT1 they undergo apoptosis [6], which signifies the continued proliferation of the cancer cells in a p53-independent manner. For instance, tumor cells overcome the apoptotic pathway upon FOXO deacetylation by SIRT1. Furthermore, the Lys16 on histone H4 is deacetylated which is a crucial marker for oncogenesis [7][8]. Thus, continued cell proliferation occurs when overexpressed SIRT1 maintains the histones in the deacetylated state for greater access to transcription factor complexes. However, SIRT1 is noted to inhibit P53 by deacetylating C-terminal Lys382 residue and disabling their transcriptional activity which promotes tumorigenesis [9]. In this regard, SIRT1 and p53 both emerge as recognizable targets for improving the treatment strategy towards OvCa.

Since phytochemicals are often implanted as alternative treatment strategies for the disease natural products [10] and small molecule inhibitors (SMIs) like Inauhzin [11] can inhibit SIRT1 mitigating its oncogenic effects. However, due to the paucity of technical

support in their processing since ancient days, natural products cannot be established as potent drugs for cancer. Thus, establishing and designing chemical compounds have gained pharmacological importance as treatment regimens. EX527, a potent and selective SIRT1 inhibitor (Inh) is implemented in treating cancer like EC [12], HCC [13], PC [14] that works well in the presence of NAD. Simultaneously, implementing natural SIRT1 inhibitors due to their effective pharmacological effects has gained interest. For instance, a phloroglucinol derivative, Hyperforin derived from the aerial part of *Hypericum perforatum* (St. JohnC swort) is established as a potent inhibitor of SIRT1 [15]. In this background, we investigated the effectiveness of both Hyperforin and SIRT1 Inh III to understand their efficacy in mitigating OvCa.

SIRT1 has been reported to deacetylate multiple factors that cause dysregulation in several signaling cascades which augments the oncogenesis [16]. Among the several dysregulated signaling pathways, the PI3K/Akt pathway in BC is highly dysregulated under the modulatory effect of increased SIRT1 which in turn promotes the growth of BC cells by deacetylating AKT [17]. Additionally, in several malignancies, AKT is observed to be overexpressed which causes abnormalities in the PI3K/AKT pathway and restrains the apoptotic cascade thereby promoting the growth and proliferation of cancer cells [18]. Furthermore, PC cells gain their proliferative potential under the effect of SIRT1 deregulated PI3K molecule [19]. Additionally, in this research work, we have also investigated the pathways dysregulated by SIRT1 associated molecules on an *in-silico* basis which might promote OvCa cell growth and proliferation.

1.2. Specific objectives

- Database mining and identifying SIRT1 as an upregulated biomolecule in OvCa.
- Identifying the SIRT1 associated factors and oncogenic signaling cascades.
- Identifying a potent inhibitor of SIRT1 in OvCa.
- *In-vitro* and *in-vivo* validation of the identified SIRT1 Inh in OvCa.

1.3. Materials and Methods

1.3.1. Materials

The reagents used for conducting the experiments are listed in Table 1.

Table 1. List of reagents

Serial No.	Product	Company	Catalogue No.
1.	Rabbit polyclonal anti-human SIRT1 antibody	Cell Signalling Technology	D739
2.	HRP-linked anti-rabbit Antibody	Cell Signalling Technology	7074P2
3.	DKXRB FITC AFFINITY	Invitrogen	A16024
4.	p53 Monoclonal Antibody (DO-1)	Invitrogen	AHO0152
5.	Goat anti-Mouse IgG (H+L) Cross-Adsorbed Secondary Antibody, PE	Invitrogen	P-852
6.	eBioscience™ 1X RBC Lysis Buffer	Invitrogen	00-4333-57
7.	Annexin V Conjugates for Apoptosis Detection	Invitrogen	A13199
8.	4-6-DIAMIDINO-2-PHENYLIN (DAPI)	Invitrogen	D1306
9.	PENICILLIN STREPTOMYCIN SOL	Invitrogen	15140148
10.	α-SMA Rabbit pAb	Abclonal	A7248
11.	Fibronectin Rabbit pAb	Abclonal	A23830
12.	Collagen Rabbit pAb	Abclonal	A1352
13.	DAB Substrate	Sigma Aldrich	11718096001
14.	Collagenase Type IV	Sigma Aldrich	C4-22
15.	o-Xylene solution	Sigma Aldrich	40201
16.	RPMI	Gibco ™	A10491-01
17.	Fetal Bovine Serum (FBS)	Gibco ™	10270-106
18.	Hematoxylin Solution (Mayer's, Modified)	ABCAM	ab220365
19.	Eosin Y-solution 0.5% Aqueous	MERCK	109844
20.	5(6)-Carboxy-2′,7′-dichlorofluorescein diacetate (DCFDA)	MERCK	21884
21.	Hydrogen peroxide solution	MERCK	88597
22.	Dibutylphthalate polystyrene xylene (DPX) Mountant for histology	Sisco Research Laboratories Pvt. Ltd.	88147

Serial No.	Product	Company	Catalogue No.
23.	Dimethyl Sulphoxide (DMSO) extrapure, 99%	Sisco Research Laboratories Pvt. Ltd.	43404
24.	Methanol extrapure AR, 99.8%	Sisco Research Laboratories Pvt. Ltd.	65524
25.	Albumin Bovine (pH 7) fraction V (Bovine Serum Albumin, BSA), 98%	Sisco Research Laboratories Pvt. Ltd.	83803
26.	3-(4,5-dimethylthiazol-2-yl)-2,5 diphenyltetrazolium bromide (MTT) tetrazolium	HIMEDIA	MB186
Buffer Composition			
27.	Phosphate buffer saline (PBS) 1X	8g NaCl; 0.2g KCl; 1.44g Na_2HPO_4.7H2O; 0.24g KH_2PO_4; H_2O to 1L; pH-7.4	
28.	Citrate Buffer	12.044g Sodium Citrate Dihydrate; 11.341g Citric acid; H_2O to 1000mL; pH-6	

1.3.2. Methods

1.3.2A. Understanding genetic alterations of SIRT1 and TP53 among all cancer types

The assessment of alteration frequency and mutations of *SIRT1* and *TP53* were investigated using CBioportal server (https://www.cbioportal.org) for all cancers to understand their status in the cancer genomics data set. University of Alabama Cancer Database (UALCAN) server (http://ualcan.path.edu/index.html) was used to analyze the protein and RNA levels of SIRT1 and TP53 in OvCa. Both *SIRT1* and *TP53* gene expression and protein expression were examined using The Cancer Genome Atlas (TCGA) and Clinical Proteomic Tumor Analysis Consortium (CPTAC) OMICS, respectively. Additionally, the PrognoScan database (http://dna00.bio.kyutech.ac.jp/PrognoScan-cgi/PrognoScan.cgi) was used (adjusted Cox $P<0.05$) to determine the impact of both SIRT1 and TP53 on the OS and disease-free survival (DFS) in OvCa.

1.3.2B. Immunofluorescence

The tissue slides, both tumor and adjacent normal (N=21), were deparaffinized using xylene followed by a rehydration using alcohol gradient (100%, 90%, 70% and 50%). The slides were then fixed with methanol/H_2O_2 and then immersed in citrate buffer at an optimum temperature of 95°C-100°C for antigen retrieval, followed by blocking with 5% BSA. Primary antibodies of p53 and SIRT1 were added to the slides and incubated overnight at 4°C for Immunofluorescence (IF). The next day, after adding the secondary antibodies FITC and

Texas Red tagged (1:1000), followed by staining the nucleus with 4',6-diamidino-2-phenylindole (DAPI), images were captured after mounting using Dibutylphthalate polystyrene xylene (DPX) under an OLYMPUS BX53 fluorescence microscope [20].

1.3.2C. Cell culture and Cell viability analysis

ID8, murine OvCa cells and SKOV3, ovarian adenocarcinoma cells were grown in DMEM and RPMI media, respectively, supplemented with 10% FBS and 1% Pen/Strep. The cells were cultured until 80% confluency. Following trypsinization, the cells were seeded in 96 well plates to determine drug dose SIRT1 Inh III at different drug concentrations (0.01µM, 0.1µM, 1µM, 10µM). After 24 hrs treatment, MTT tetrazolium was added to evaluate the viable cells followed by the addition of 150µl Dimethyl Sulphoxide (DMSO) in each well and optical density (OD) value was obtained by an ELISA plate reader (Infinite 200PRO-TECAN, 30050303) at 595nm [21].

1.3.2D. Immunohistochemistry

Adjacent normal tissue and primary OvCa tissues were obtained from OvCa patients. Control (Con) and treated tissue sections were obtained from mice for protein expression analysis. Immunohistochemistry (IHC) staining was conducted as described by *Roy et al*. with SIRT1, p53, α-SMA, collagen, and fibronectin as primary antibodies (1:500) and the addition of an anti-rabbit secondary antibody (1:1000) on the following day. The reaction was determined by adding 3, 3'-diaminobenzidine tetrahydrochloride (DAB) in the dark at room temperature (RT) and hematoxylin as counterstain followed by DPX mounting and imaging was carried out under a bright field compound microscope (OLYMPUS CX40) [22]. H-score = [(0 X % negative cells) + (1 X % weak positive cells) + (2 X % moderate positive cells) + (3 x % strong positive cells)] where 0 = no staining visible, 1 = weak staining, 2 = moderate staining and 3 = strong staining and the H-score ranges from 0 (negative) to 300 (100% strong staining) [23].

1.3.2E. Analysis of protein-protein interaction, identification of hub genes and functional enrichment analysis

Search Tool for the Retrieval of Interacting Genes/Proteins (STRING) v11.0 database (http://string-db.org) was used to derive protein-protein interaction (PPI) of differentially expressed genes (DEGs) with a confidence score of 0.7. PPI network was demonstrated by the Cytoscape software. The highly connected clusters within the network (based on

connectivity degree) were derived by the molecular complex detection (MCODE) plugin of the Cytoscape software. biological information associated with the top-ranked interconnected MCODE cluster was deduced by an online gene functional annotation and analysis application, Metascape (http://metascape.org/). The MCODE gene cluster was further investigated for Gene Ontology (GO), Reactome pathway analyses and the Kyoto Encyclopedia of Genes and Genomes (KEGG) analyses.

1.3.2F. Investigation of SIRT1 associated genes

To investigate the differential expression deduced from MCODE analysis, Gene Set Cancer Analysis (GSCA) server (https://guolab.wchscu.cn/GSCA/#/). the cancer-associated pathways and their interconnection with the immune cells' infiltration was observed by this analysis. Copy number variation (CNV) and single nucleotide variation (SNV) of the interested gene set and their relationship with miRNA expression were also studied by this online tool [24].

1.3.2G. Tertiary structures of PI3K and AKT target proteins

Three-dimensional (3D) structures of the target proteins PI3K (PDB ID: 5DXT) and AKT (PDB ID: 3QKK) were obtained from Protein data bank (PDB) (https://www.rcsb.org) database.

1.3.2H. Homology modeling of SIRT1 target protein

Since the stereochemical quality of 3D structure of SIRT1 was not available in the PDB, the target sequence of the SIRT1 protein of *Homo sapiens* with a length of 555 residues (ID: AAH12499) was retrieved from NCBI database. The crystal structure of SIRT1 (PDB ID: 5BTR) was analyzed by a basic local alignment search tool (BLAST) and was chosen as a template for further study. Further, structural modeling was done using SWISS-MODEL web-based server (https://swissmodel.expasy.org/). PROCHECK at the SAVESv6.1 server (https://saves.mbi.ucla.edu/) was used for stereochemical quality check and model validation.

1.3.2I. Identification of natural product and ligand Preparation

A rigorous literature review and the Indian Medicinal Plants, Phytochemistry And Therapeutics (IMPPAT 2.0) database identified Hyperforin, obtained from *Hypericum perforatum* [25]. PubChem database (https://pubchem.ncbi.nlm.nih.gov/) was accessed for the 3D structure of selected ligands SIRT1 Inh III (CID: 5113032) and Hyperforin (CID:

441298). The PDB format of the ligands was obtained from Open Babel [26]. The properties of the ligands can be found in Table 2.

Table 2: Properties of SIRT1 Inh III and Hyperforin curated from PubChem database

Compound	Source	PubChem CID	2D Structure
SIRT1 Inh III	Synthetic	5113032	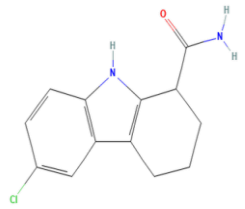
Hyperforin	Aerial part, flower of *Hypericum perforatum*	441298	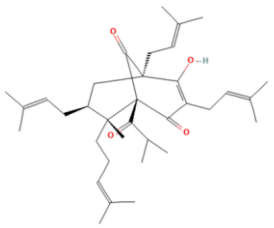

1.3.2J. Molecular docking and visualization

A combination of different software namely Open Babel, AutoDock, and AutoDock Vina under PyRx v0.8 tool was used to perform molecular docking [27]. Discovery Studio software and Protein-Ligand Interaction Profiler (PLIP) web server (https://plip-tool.biotec.tu-dresden.de/plip-web/plip/index) was used to understand the non-covalent interactions between protein-ligand complexes. The entire protein-ligand complex was accommodated within the Vina grid box [28]. The visualization of the molecular interactions was performed by PyMolv2.6.0 tool.

1.3.2K. Drug likeness studies

Molinspiration cheminformatics server (http://www.molinspiration.com/) was used to understand the physiochemical properties of SIRT1 Inh III and Hyperforin. Lipinski's rule of five: molecular weight <500g/mol, H-bond acceptors <10, H-bond donors <5, logP <5, and compounds violating more than one rule are less likely to be orally bioavailable was used to understand the Drug likeness agenda [29].

1.3.2L. Investigation of pharmacokinetic profile of ligands

To investigate the pharmacokinetic and physiochemical properties and toxicity profile of the ligands, PubChem database was used to deduce the SMILES structure of the ligands. pkCSM server (https://biosig.lab.uq.edu.au/pkcsm/prediction) was used to understand the pharmacokinetic properties such as absorption, distribution, metabolism, excretion, (ADME) and toxicity profile of the ligands [30].

1.3.2M. Molecular dynamics simulation and trajectory analysis

GROMACS 2024.3 was used to conduct the Molecular dynamics (MD) simulation of the protein–ligand complex using the CHARMM27 force field to establish the protein topologies [31]. TIP3 water model was used to solvate the protein and complexes 1.0nm in a dodecahedron box under the neutralizing effect of sodium (Na+) ions in the solvated system. Linc's constraint algorithm and steepest descent technique were used to reduce the energy consumption of the system. To create the conditions of a general experiment, the temperature and pressure of the system were set to 300K and one atmospheric pressure [32]. Velocity-rescale thermostat with a reference temperature of 300K was implemented to perform the canonical ensemble of the complexes (NVT thermal equilibration) as well as the isobaric-isothermal ensemble (NPT pressure equilibration) for 100ps. 100ps time steps were used to conduct the final MD production run for 50ns. The MD trajectories of the protein-ligand complexes were examined to assess the structural stability using root mean square deviation (RMSD), root mean square fluctuation (RMSF), and radius of gyration (RG). Solvent accessibility and strength of interactions were assessed by Solvent-accessible surface area (SASA), hydrogen bond interactions, and hydrogen bond pair lengths analysis. The resulting plots were visualised under the XMGrace software [33][34].

1.3.2N. Haematoxylin and Eosin staining

Deparaffinization of the mice tissue slides was done by xylene treatment and rehydrated using alcohol gradient, followed by addition of Mayer's hematoxylin for 30s. To remove the excess stain, the slides were subjected to washing with distilled water, followed by addition of 1% eosin Y solution to the slides for 10-30s and then washed again using distilled water. The slides were again dehydrated using an alcohol gradient followed by xylene treatment and DPX mount. The images of H&E staining were captured under a brightfield compound microscope (OLYMPUS CX40) [35].

1.3.2O. Scratch assay

SKOV3 cells were seeded and allowed to grow in 35mm dish for 24hrs. A scratch was drawn using 200µl micropipette tip and treated with the drug for 24 hrs. Nikon ECLIPSE Ts2 inverted microscope was used to take the images of the control and treated plates after completion of the treatment [36].

1.3.2P. Establishment of in-vivo OvCa mice model

Intraperitoneal injection (i.p.) of 7×10^6 ID8 cells suspended in 700µl 1X PBS was executed in 6 to 8 weeks old C57BL/6 mice (N=8) were taken for the experimental study (Proposal No. IAEC-1774/NC-4/2022/16). After 8 weeks of inoculation, animals were monitored and treated with EX527 (10 mg/kg) diluted in sterile 1X PBS, intraperitoneally every week. After treatment for 4 weeks, the mice were monitored for survival and sacrificed for further experiments [37][12].

1.3.2Q. Flow cytometry

2×10^5 primary cells of mice ovarian tumor and normal ovary obtained after collagenase IV processing were inoculated in a 60mm petri dish under non-treated (Con) and treated condition (SIRT1 Inh III) categories. To analyze the apoptotic rate as well as the ROS generation under the treatment conditions mentioned above, AnnexinV and 5(6)-Carboxy-2′,7′-dichlorofluorescein diacetate (DCFDA), under individual experimental conditions, were added and incubated for 2hrs and 30min at RT in the dark, respectively. BD LSRFortessa flow cytometer was used to analyze the data [38] and FlowJo software was used to analyze the data.

1.3.2R. Statistical analysis

The colocalization and mean fluorescence intensity (MFI) of the fluorescent images were analyzed using the Fiji-ImageJ software (https://imagej.net/Fiji). FlowJo software was used to analyze the flow cytometric data. GraphPad Prism (v8.0) was used for Two-way ANOVA and Student's t-test and prepare respective graphs wherever applicable. $P<0.0001$ and $P\leq0.05$ were considered to be statistically significant. [22].

1.4. Results

1.4.1. SIRT1 and TP53 are genomically altered in OvCa showing higher protein expression in tumor samples with a grade-wise increase

TCGA database in Cbioportal revealed that the gene alteration frequency of *SIRT1* is highest in OvCa (20%) (Figure 1A). However, gene alteration frequency and mutation of tumor suppressor *TP53* was more than *SIRT1* in OvCA (100%) (Figure 1B). 0.7% somatic mutation frequency of *SIRT1* was observed having no driver mutation. However, variant of uncertain significance (VUS) was recorded to be 25 which includes missense (21), truncating (3), inframe (1) (Figure 1C). Simultaneously, the somatic mutation frequency of *TP53* was 33.8% along with 746 missense, 326 truncating, 31 inframe, 94 splice, 11 fusion (driver mutations) and 7 VUS (5 missense, 1 truncating, 1 inframe) (Figure 1D). Despite *TP53* mutation frequency being higher, *SIRT1* mutations report an alarming threat in 20% of cases, making it a potent target to be investigated. Upon analyzing the protein level from the CPTAC database, it was revealed that the protein level of both SIRT1 and TP53 was significantly higher in the tumor than in normal (Figure 1E), along with their increase in level with advanced grades of the disease (Figure 1F). Furthermore, the SIRT1 expression was found to be elevated in the TP53 mutant samples than in the non-mutant ones, as revealed by TCGA analysis (Figure 1G).

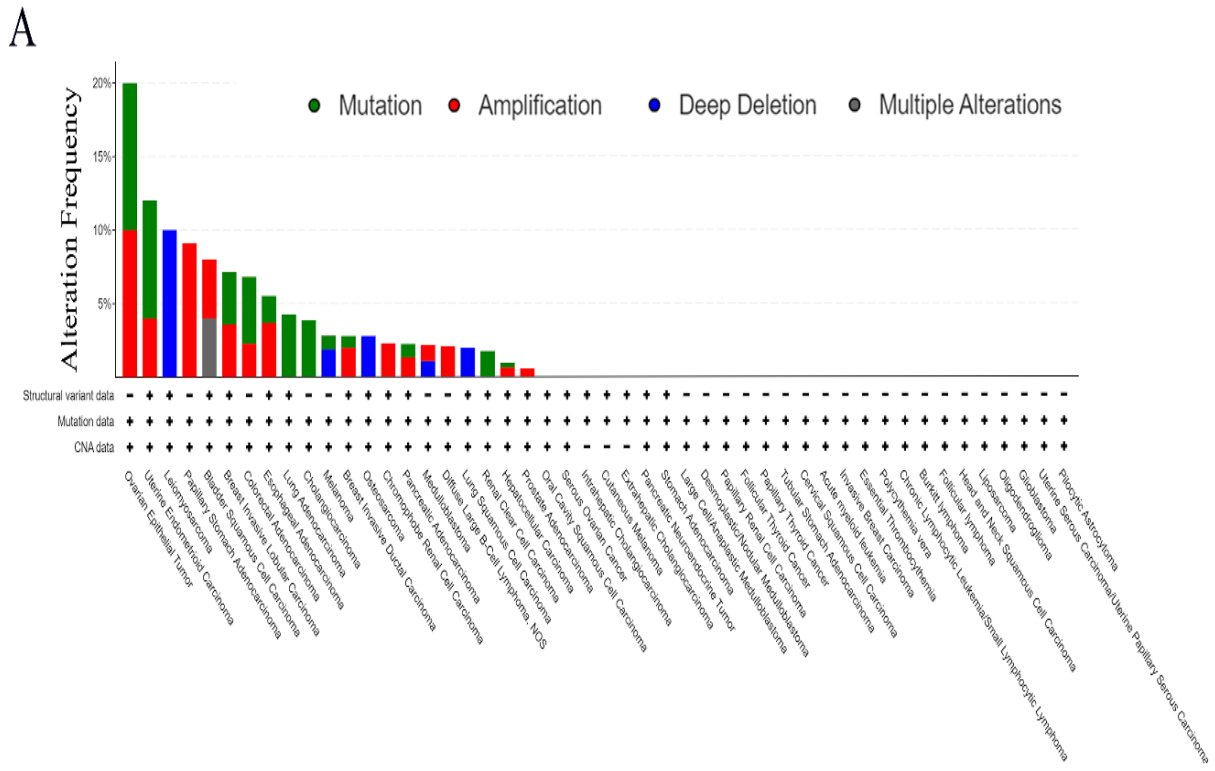

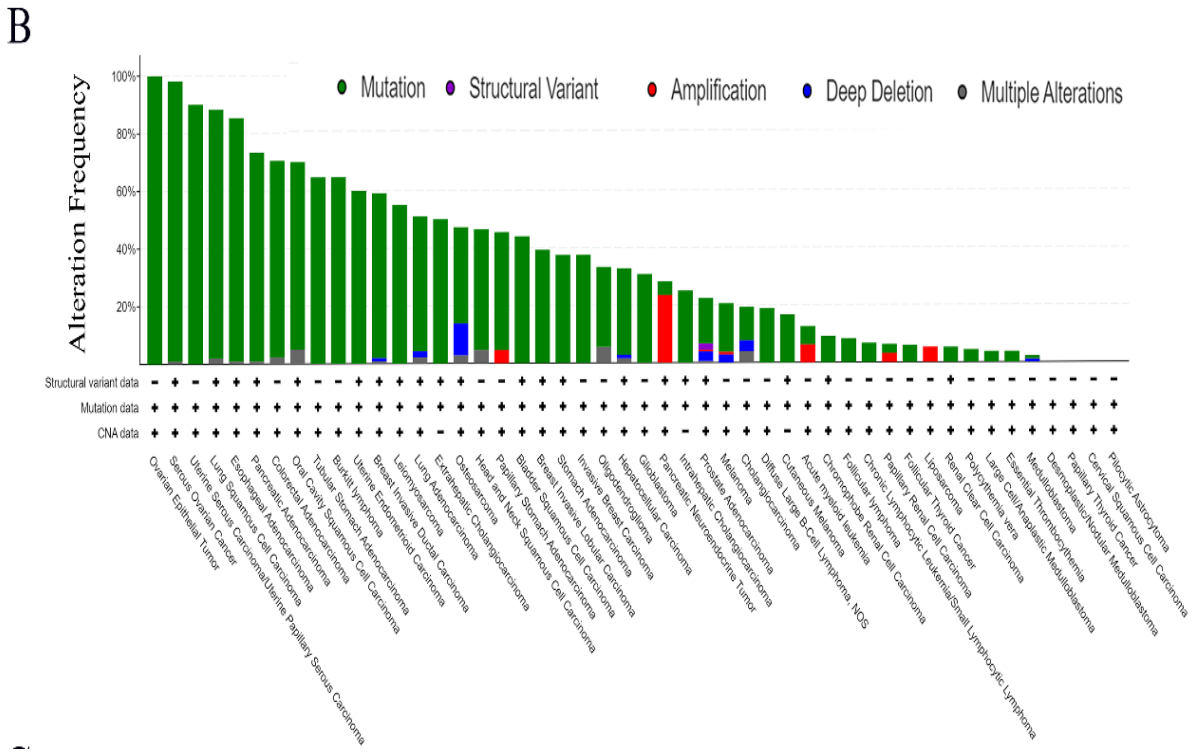
B
Alteration Frequency
100%
80%
60%
40%
20%
Mutation
Structural Variant
Amplification
Deep Deletion
Multiple Alterations
Structural variant data
Mutation data
CNA data
Ovarian Epithelial Tumor
Serous Ovarian Cancer
Uterine Serous Carcinoma/Uterine Papillary Serous Carcinoma
Lung Squamous Cell Carcinoma
Esophageal Adenocarcinoma
Pancreatic Adenocarcinoma
Colorectal Adenocarcinoma
Oral Cavity Squamous Cell Carcinoma
Tubular Stomach Adenocarcinoma
Burkitt Lymphoma
Uterine Endometrioid Carcinoma
Breast Invasive Ductal Carcinoma
Leiomyosarcoma
Lung Adenocarcinoma
Extrahepatic Cholangiocarcinoma
Osteosarcoma
Head and Neck Squamous Cell Carcinoma
Papillary Stomach Adenocarcinoma
Bladder Squamous Cell Carcinoma
Breast Invasive Lobular Carcinoma
Stomach Adenocarcinoma
Invasive Breast Carcinoma
Oligodendroglioma
Hepatocellular Carcinoma
Glioblastoma
Pancreatic Neuroendocrine Tumor
Intrahepatic Cholangiocarcinoma
Prostate Adenocarcinoma
Melanoma
Cholangiocarcinoma
Diffuse Large B-Cell Lymphoma
Cutaneous Melanoma
Acute myeloid leukemia
Chromophobe Renal Cell Carcinoma
Follicular lymphoma
Chronic Lymphocytic Leukemia/Small Lymphocytic Lymphoma
Papillary Renal Cell Carcinoma
Follicular Thyroid Cancer
Liposarcoma
Renal Clear Cell Carcinoma
Polycythemia vera
Large Cell/Anaplastic Medulloblastoma
Essential Thrombocythemia
Medulloblastoma
Desmoplastic/Nodular Medulloblastoma
Papillary Thyroid Cancer
Cervical Squamous Cell Carcinoma
Pilocytic Astrocytoma

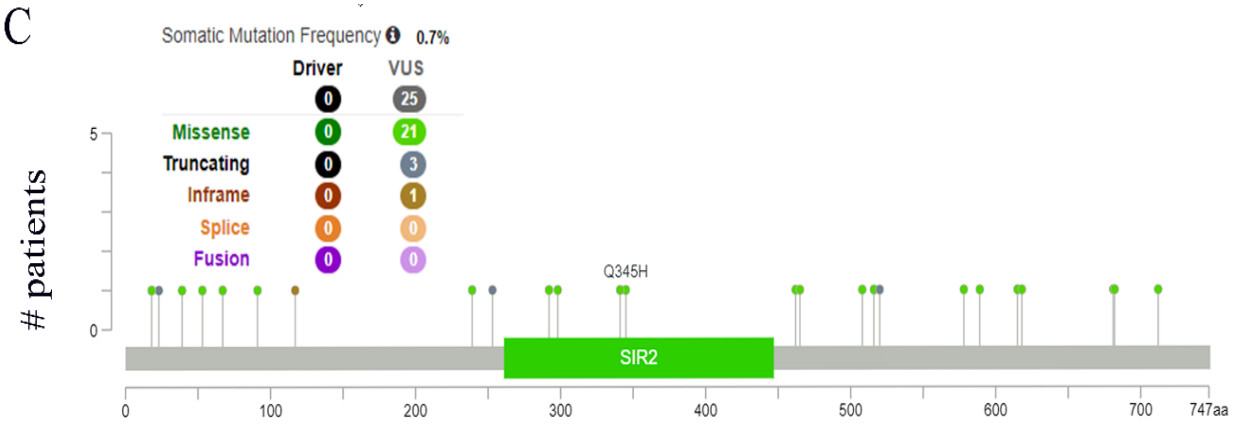
C
Somatic Mutation Frequency 0.7%
Driver
VUS
Missense 0 21
Truncating 0 3
Inframe 0 1
Splice 0 0
Fusion 0 0
patients
5
0
Q345H
SIR2
0
100
200
300
400
500
600
700
747aa

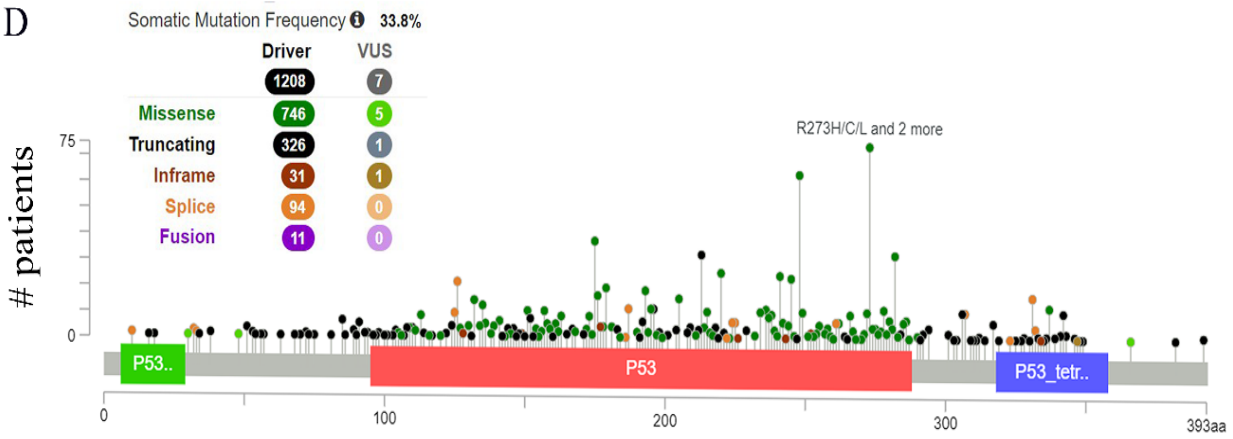
D
Somatic Mutation Frequency 33.8%
Driver
VUS
Missense 746 5
Truncating 326 1
Inframe 31 1
Splice 94 0
Fusion 11 0
patients
75
0
R273H/C/L and 2 more
P53..
P53
P53_tetr..
0
100
200
300
393aa

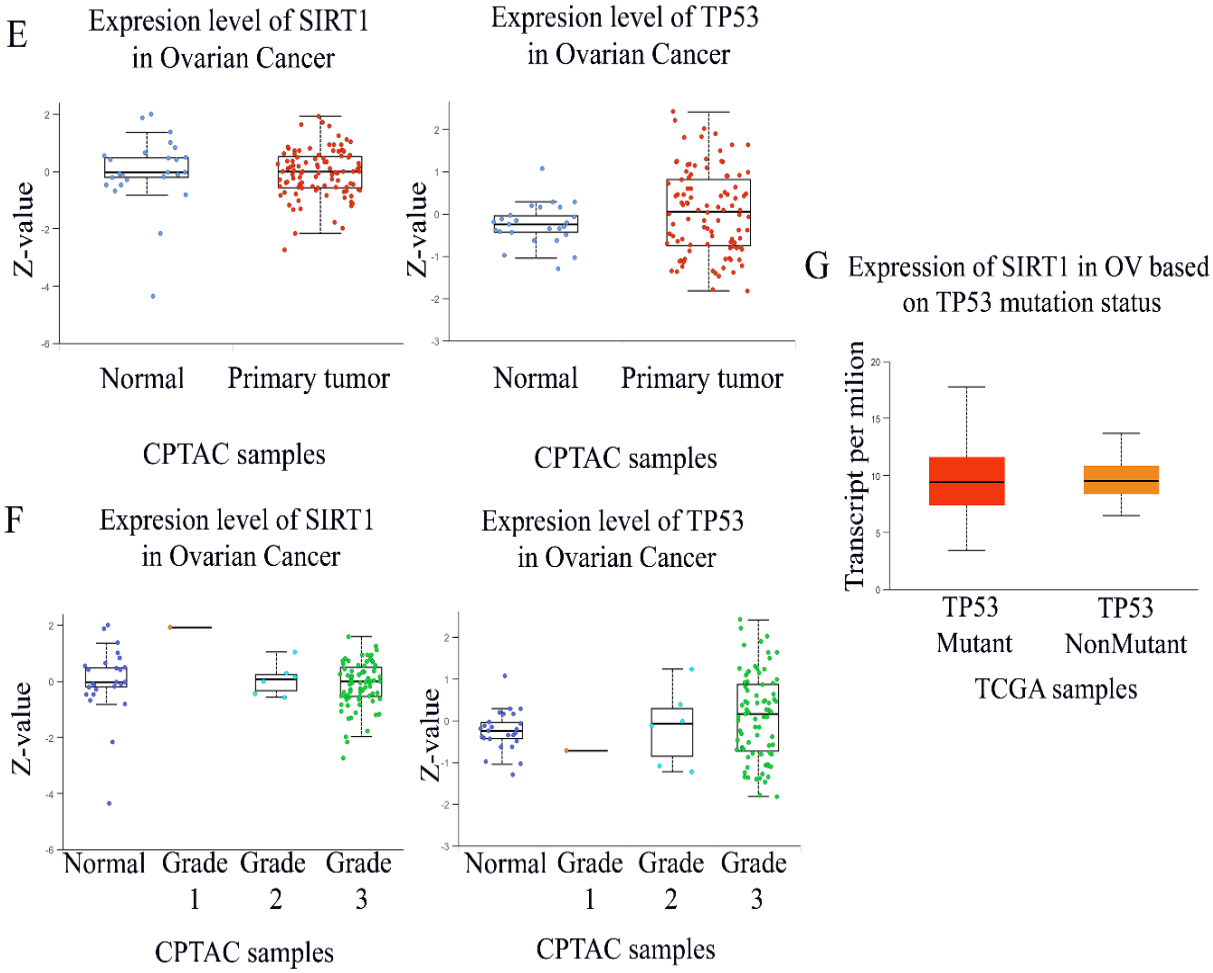

Figure 1. A. Frequency of genetic variation of *SIRT1* in different TCGA cancer types from the CBioportal; B. Frequency of genetic variation of *TP53* in different TCGA cancer types from the CBioportal; C. Types of mutations in *SIRT1* and the mutation sites; D. Types of mutations in *TP53* and the mutation sites; E. Protein expression of SIRT1 and TP53 in normal and primary tumor from CPTAC database; F. Protein level expression of SIRT1 and TP53 in tumor grade from CPTAC database; G. Expression of SIRT1 in TP53 mutant and non-mutant samples in the mRNA level from TCGA database.

1.4.2. Expression of SIRT1 and p53 increased in OvCa tumor tissues as compared to normal

The colocalized expression of SIRT1 and p53 increased in the tumor as compared to the adjacent normal tissues. However, the expression of SIRT1 and p53 exhibited a non-significant relation in the tumor, however, their individual expression was higher in the tumor as compared to the normal (Figure 2A). SIRT1 and p53 expression was higher in the tumor as compared to the normal tissue, as revealed by IHC analysis. It was observed that SIRT1 expression increased with an increase in H-score for p53 (Figure 2B).

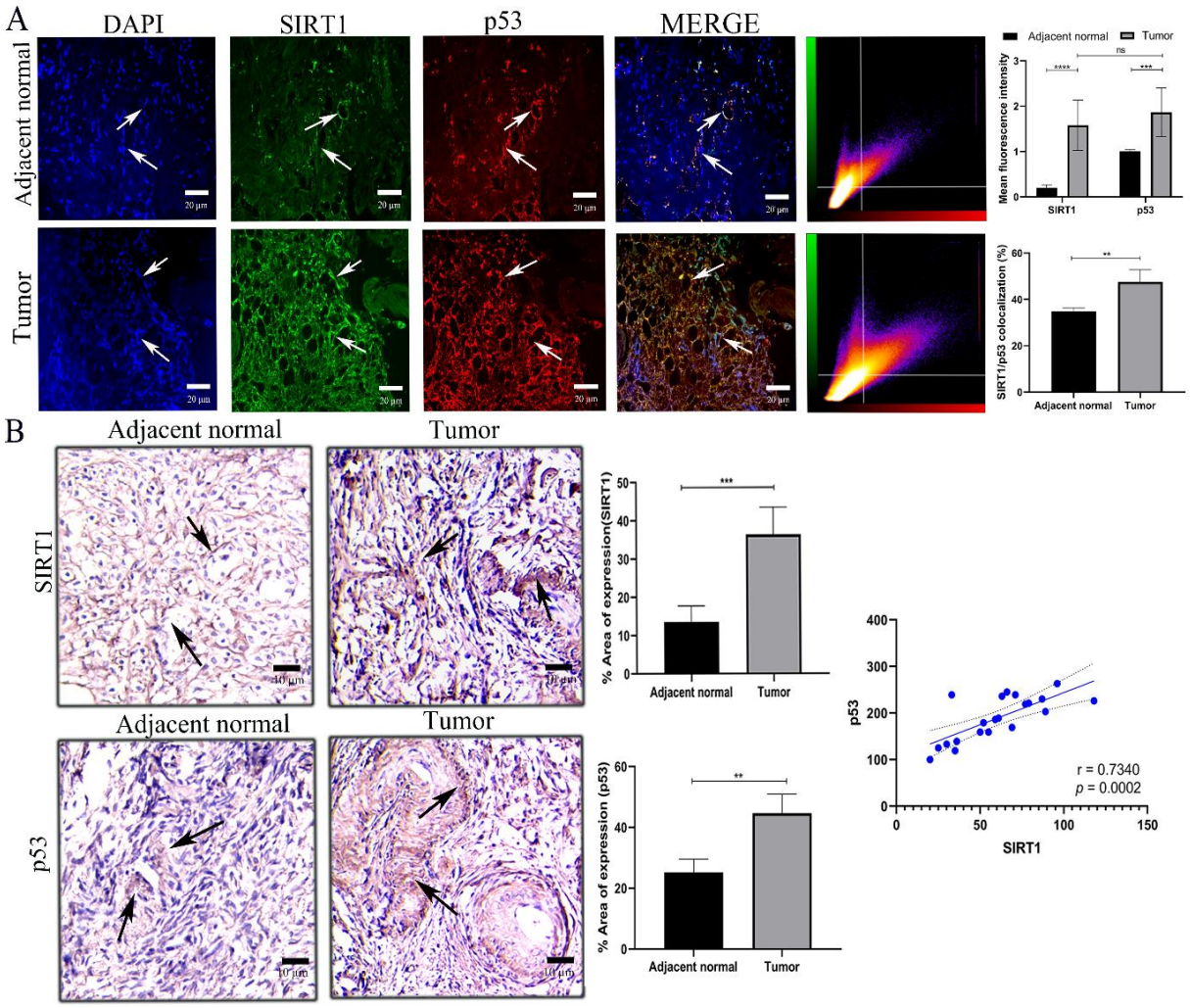

Figure 2. A. MFI and colocalized expression of SIRT1 and p53 in adjacent normal and tumor tissues by IF analysis; B. Area of expression of SIRT1 and p53 in adjacent normal and tumor tissues by IHC analysis. (*P<0.05, **P<0.01, ***P<0.001, ****P<0.0001)

1.4.3. OS and DFS of SIRT1 and p53 in OvCa patients

Surprisingly, the PrognoScan database (OS/DFS) for SIRT1 and p53 revealed that high SIRT1 levels affected the OS/DFS of the OvCa patients as compared to the increased expression of p53 (Figure 3A-B). Thus, we proceeded with SIRT1 for further investigation.

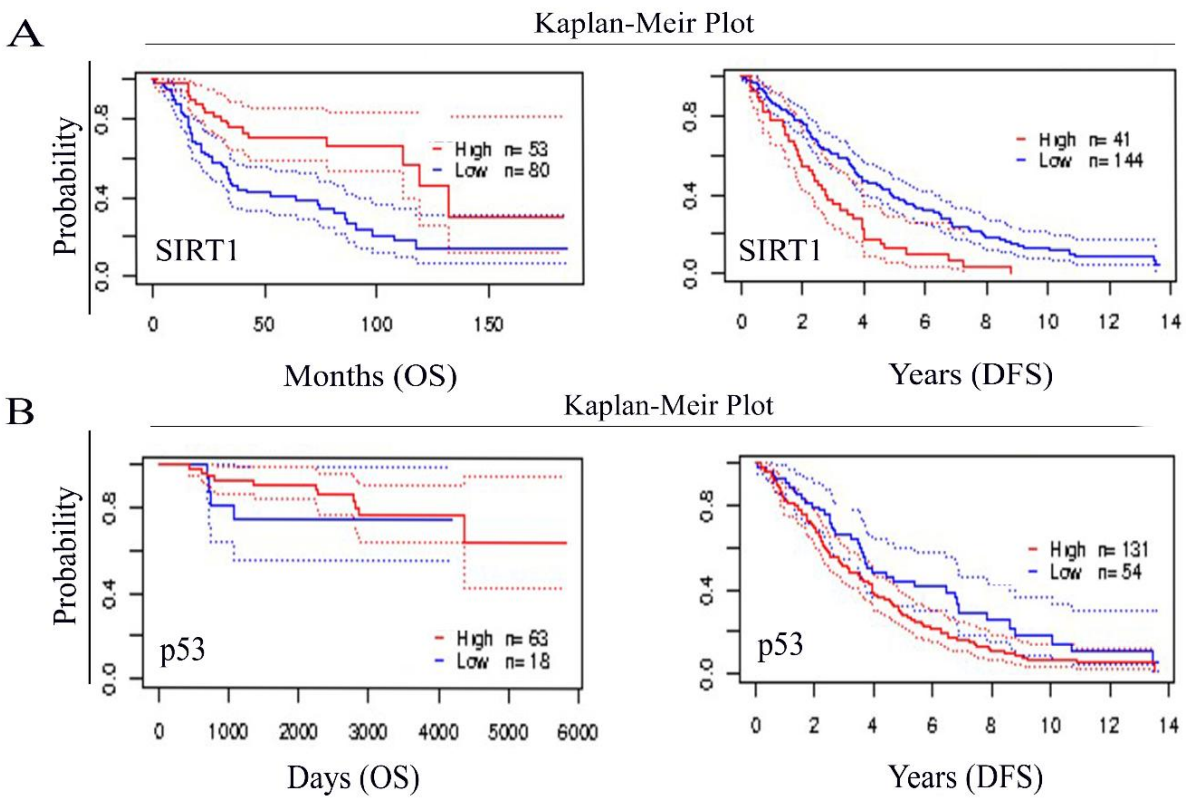

Figure 3. A. OS and DFS of SIRT1 from PrognoScan database; B. OS and DFS of p53 from PrognoScan database. (*P<0.05, **P<0.01, ***P<0.001, ****P<0.0001)

1.4.4. Identification of SIRT1 with other associated genes in OvCa

SIRT1 is linked with 45 nodes and 459 edges of associated interacting genes (Figure 4A). Hub genes analysis revealed 3 clusters by haircut cluster finding method (*k*-core=2). 27 nodes and 246 edges with a score of 18.923 comprised Cluster 1 (Figure 4B). The Maximal Clique Centrality (MCC) method revealed EGFR, PTEN, MYC, CDK2, AKT1, IL-6, FOXO3, IL-1β, TP53 and SIRT1 as core genes to be targeted (Figure 4B). GO analysis of the targetable proteins multiple regulatory processes in OvCa (Figure 4C) including positive regulation of cell migration pathways. Cytokines involvement and modulation of AKT signaling along with TP53 degradation were evaluated by Reactome analysis (Figure 4D). KEGG analysis demonstrated that pathways in cancer (hsa05200), PI3K-AKT signaling pathway (hsa04151) are altered under the regulatory effect of MCODE analyzed gene set (Figure 4E).

A

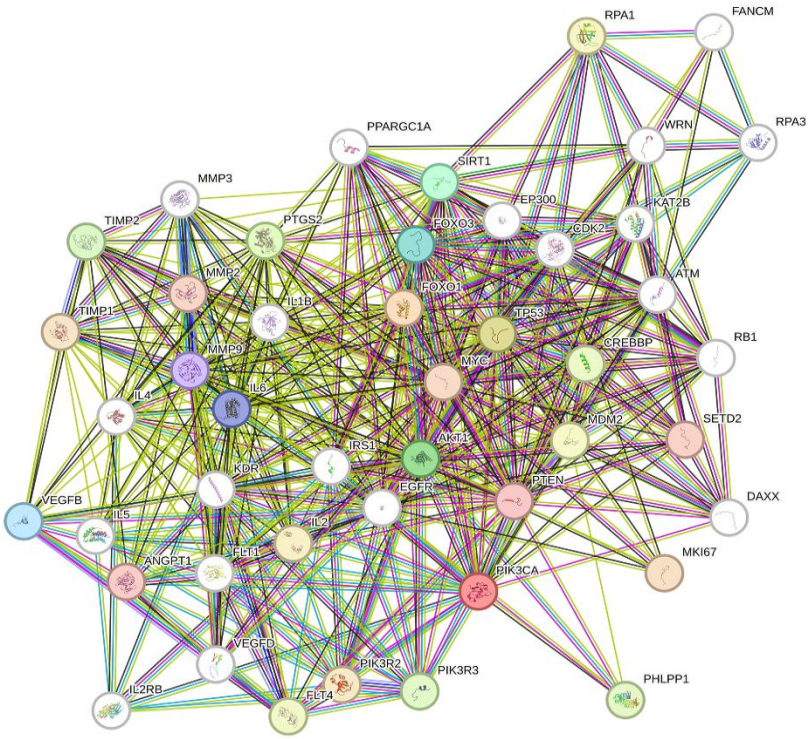
RPA1
FANCM
PPARGC1A
WRN
RPA3
SIRT1
MMP3
EP300
KAT2B
TIMP2
PTGS2
FOXO3
CDK2
MMP2
ATM
FOXO1
IL1B
TIMP1
TP53
RB1
MMP9
CREBBP
MYC
IL4
IL6
MDM2
SETD2
IRS1
AKT1
KDR
EGFR
PTEN
VEGFB
DAXX
IL5
IL2
FLT1
MKI67
ANGPT1
PIK3CA
VEGFD
PIK3R2
PIK3R3
PHLPP1
IL2RB
FLT4

B

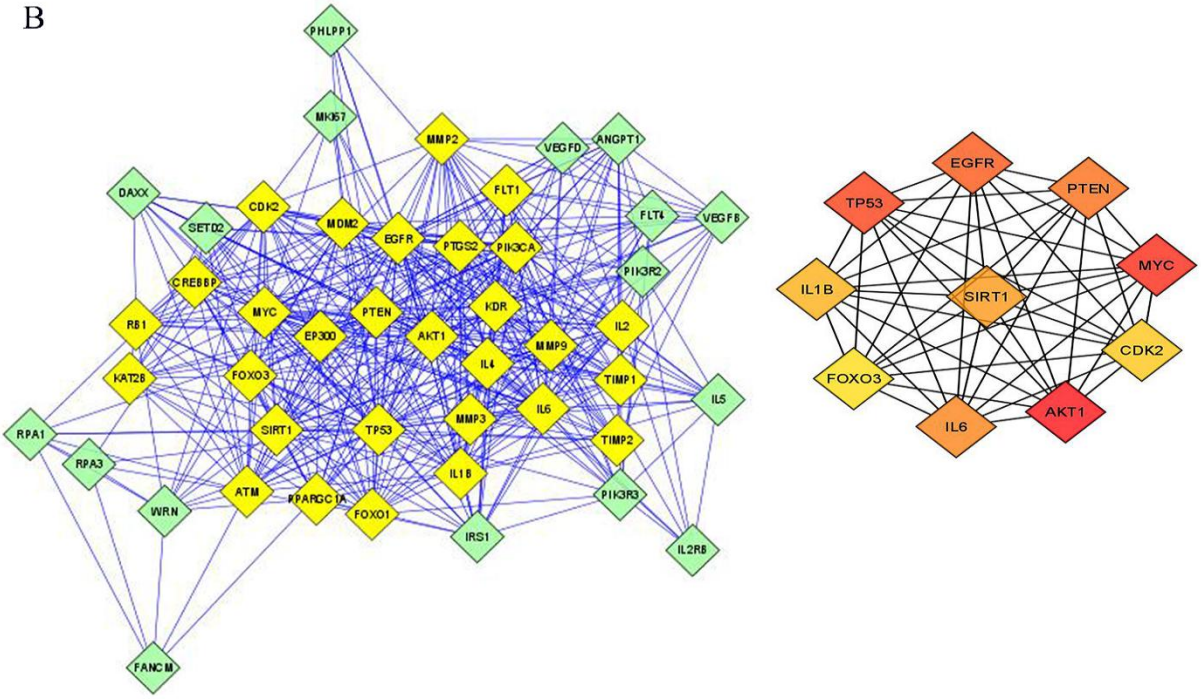
PHLPP1
MKI67
MMP2
VEGFD
ANGPT1
DAXX
FLT1
CDK2
SETD2
MDM2
FLT4
VEGFB
EGFR
PTGS2
PIK3CA
PIK3R2
CREBBP
MYC
PTEN
KDR
IL2
RB1
EP300
AKT1
MMP9
IL4
KAT2B
FOXO3
TIMP1
IL5
IL6
RPA1
SIRT1
TP53
MMP3
TIMP2
RPA3
IL1B
ATM
PPARGC1A
PIK3R3
WRN
FOXO1
IRS1
IL2RB
FANCM
EGFR
PTEN
TP53
MYC
IL1B
SIRT1
CDK2
FOXO3
AKT1
IL6

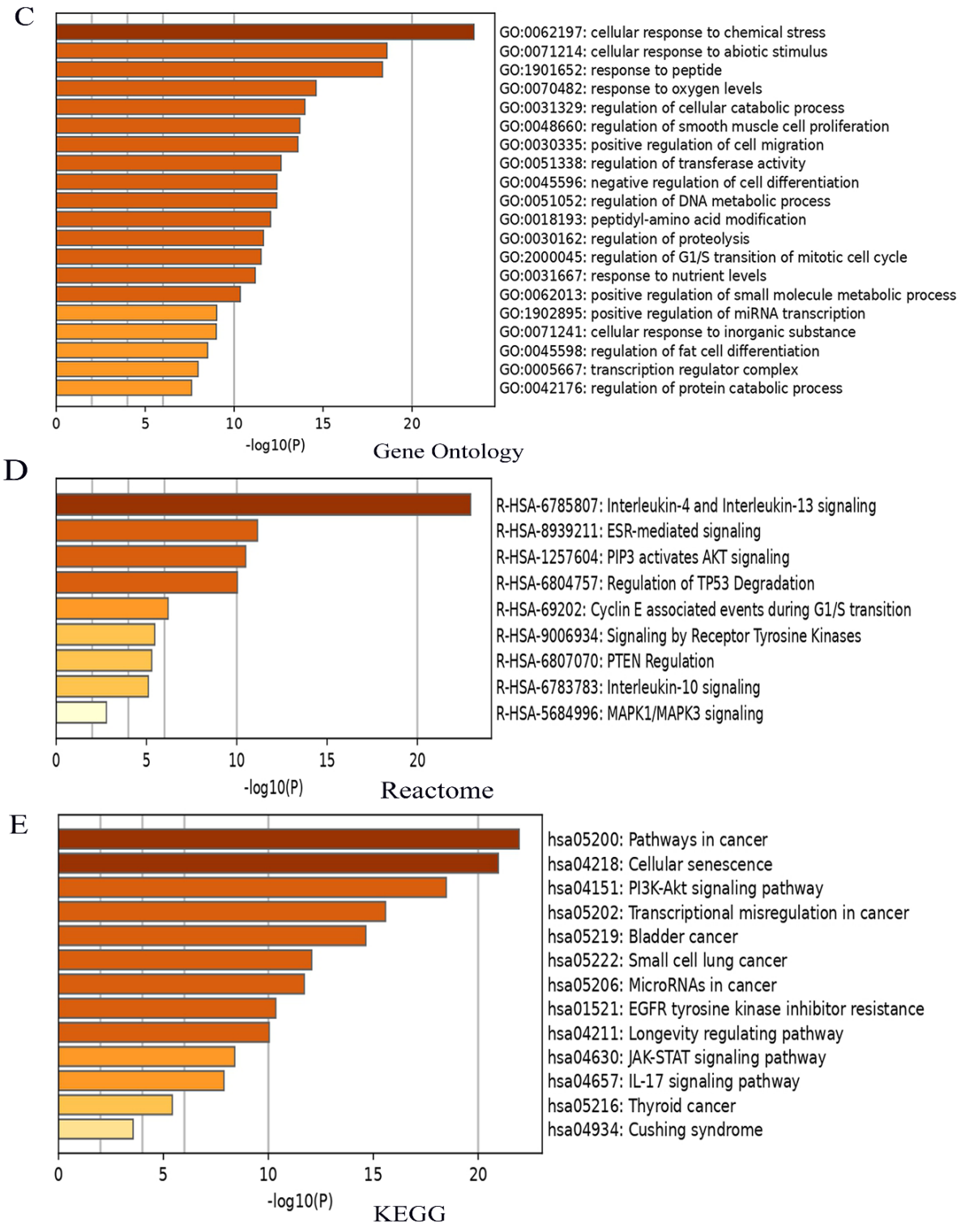

Figure 4. A. PPI network of SIRT1 by the STRING database; B. Top MCODE cluster in the Cytoscape with the top 10 hub genes within the network (EGFR, PTEN, MYC, CDK2, AKT1, IL-6; C. GO analysis of the MCODE genes; D. Reactome analysis of the MCODE genes; E. KEGG pathway enrichment analysis of the MCODE genes.

1.4.5. Analysis of signaling cascade modulated by SIRT1 and its associated molecules

GSVA score of the MCODE set of genes revealed EMT and immune cells infiltration to be associated with the genes in OvCa (P ≤0.05; *# FDR≤0.05) (Figure 5A). Th17, cytotoxic T cells, B cells, Th1 cells are significantly mutant regulated by the MCODE set of genes (Figure 5B). Amplification (homozygous: 1.55%; heterozygous: 21.76%) and deletion (homozygous: 0.35%; heterozygous: 26.08%) occurred in SIRT1 and associated genes in OvCa were assessed by CNV analysis (Figure 5C). The CNV of these genes is significantly associated with mRNA expression (FDR≤0.05) that incorporates multiple genes (Figure 5D). Additionally, TP53 has the highest SNV frequency (90.53%) in OvCa (Figure 5E).

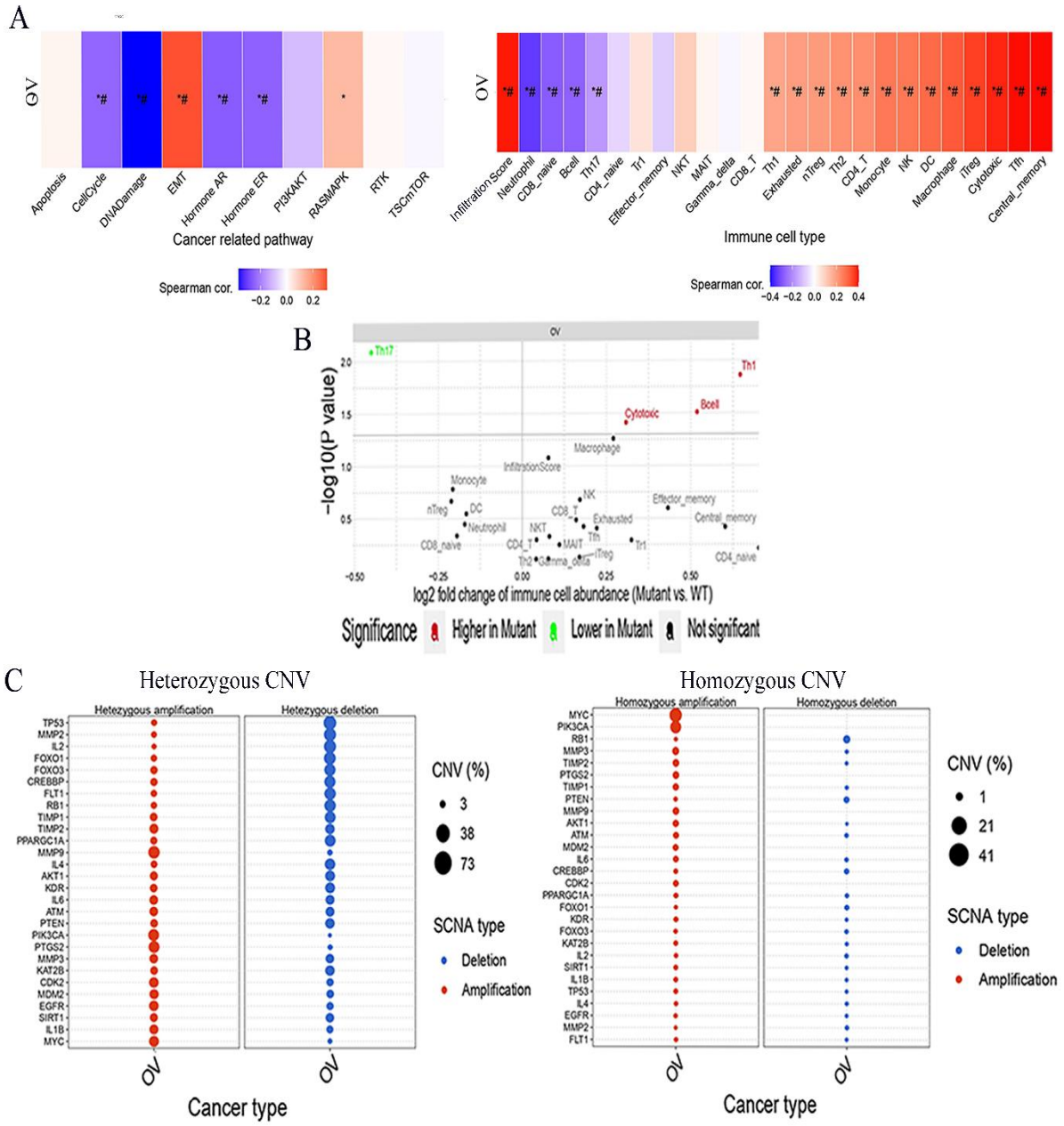

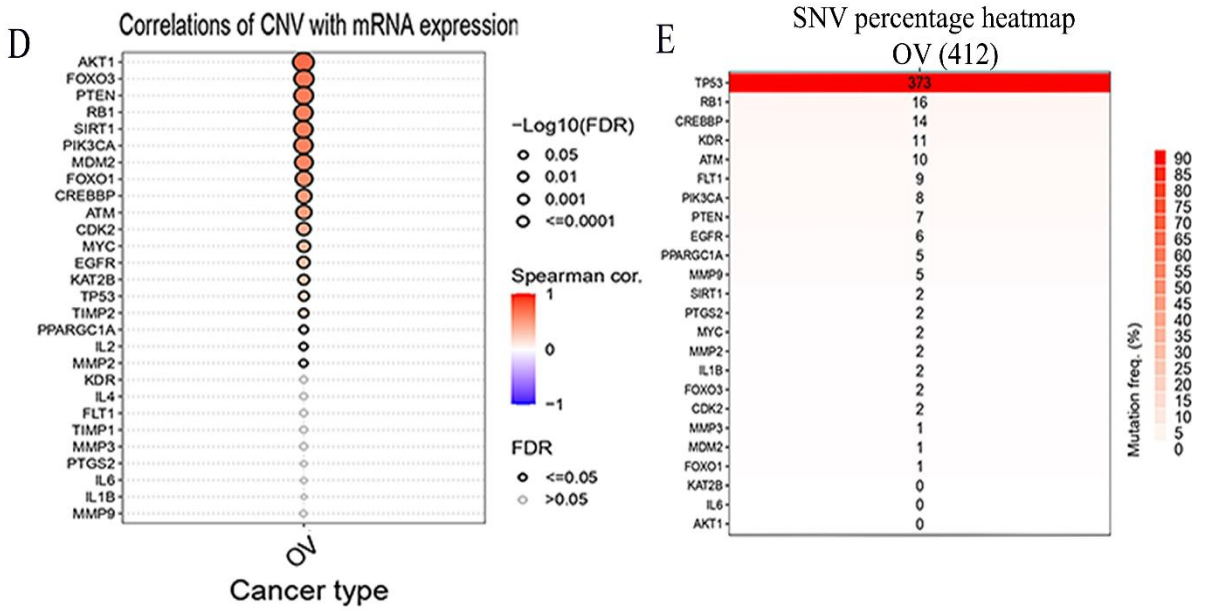

Figure 5. A. MCODE gene set effect on various OvCa related pathways and immune cells' infiltrates; B. Immune cells (Mutant vs. Wild type) associated with OvCa; C. Heterozygous and homozygous CNVs of the gene set in OvCa; D. Correlations between CNVs of the gene set with the mRNA expression in OvCa; E. SNV percentage heatmap of the gene set in OvCa.

1.4.6. Molecular Docking Study

Molecular docking analysis revealed SIRT1 Inh III to be more potent than Hyperforin in inhibiting SIRT1, PI3K, and AKT. Non-covalent bonds (Hydrogen bonds, hydrophobic bonds, salt bridges, and π-cation interactions) were determined (Table 3) and the schematic of the molecular docking study is reflected in Figure 6A-F.

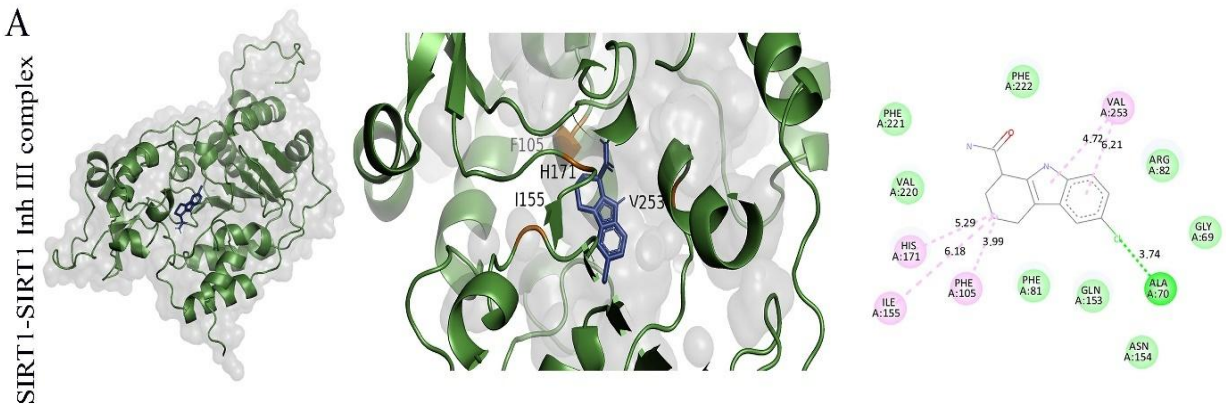

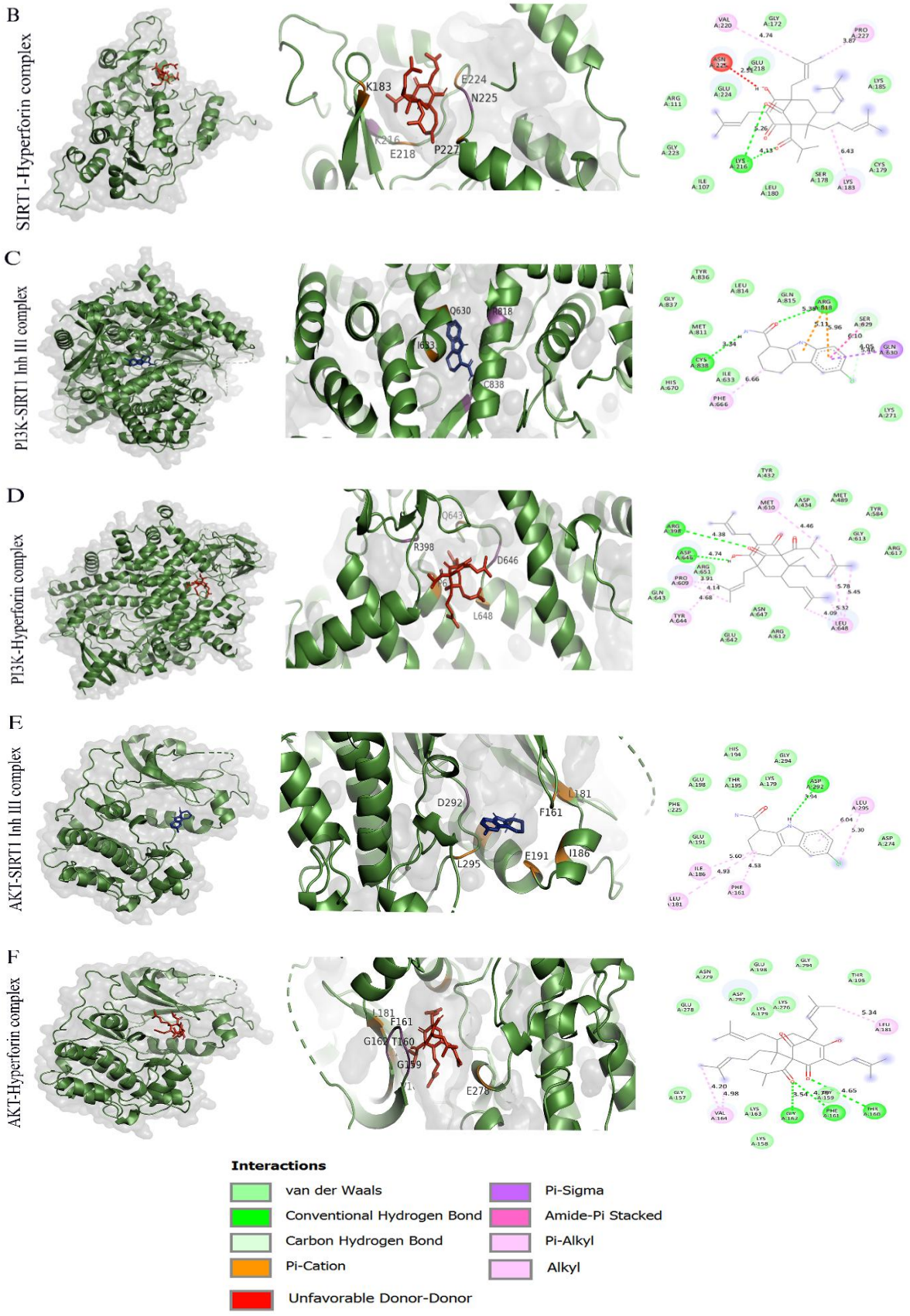

Figure 6. 3D Interaction and 2D Interaction representation of A. SIRT1-SIRT1 Inh III; B. SIRT1-Hyperforin; C. PI3K-SIRT1 Inh III; D. PI3K-Hyperforin; E. AKT-SIRT1 Inh III; and F. AKT-Hyperforin complex.

SIRT1 Inh III and Hyperforin showed free binding energy -8.6 and -6.9 kcal/mol with SIRT1, respectively. SIRT1 Inh III and Hyperforin with PI3K revealed that free binding energy -7.2 and -7 kcal/mol, respectively. Additionally, SIRT1 Inh III and Hyperforin have a binding energy of -7.4 and -6.8 kcal/mol, respectively with AKT (Table 3).

Table 3. Summary of molecular docking analysis results of SIRT1 Inh III and Hyperforin with target proteins

Target with PDB ID	Ligand	Binding energy (kcal/mol)	No. of H-bonds	H-bond forming residues	No. of non-covalent interactions	Non-covalent bond forming residues
SIRT 1	SIRT1 Inh III	-8.6	-	-	4	F105, I155, H171, V253
	Hyperforin	-6.9	2	K216, N225	5	K183, K216, E218, E224, P227
PI3K (5DXT)	SIRT1 Inh III	-7.2	2	R818, C838	3	Q630, I633, R818
	Hyperforin	-7	2	R398, D646	4	R398, P609, Q643, L648
AKT (3QKK)	SIRT1 Inh III	-7.4	1	D292	6	F161, L181, I186, E191, L295, E198
	Hyperforin	-6.8	4	G159, T160, F161, G162	6	F161, V164, K179, L181, E198, E278

1.4.7. Drug likeness property analysis

In comparison to Hyperforin (miLogP value 8.39 > 5), SIRT1 Inh III (miLogP value 2.51 < 5) indicated that SIRT1 Inh III can be absorbed efficiently. TPSA (total polar surface area) of both Hyperforin and SIRT1 Inh III were less than 140 Å, suggesting the good absorption capacity of both the ligands. nROTB (number of rotatable bonds), a topological characteristic that measures molecular flexibility and drug's oral bioavailability, was investigated as well [39]. SIRT1 has 1 ROTB and Hyperforin has 11 ROTB, suggesting that the ligands were flexible enough. SIRT1 Inh III followed 'Lipinski's Rule of 5' without any violations, while Hyperforin showed 2 violations (Table 4).

Table 4. Drug-likeness property analysis of SIRT1 Inh III and Hyperforin through Molinspiration sever

Compound Name	MW (g/mol) (<500g/mol)	miLogP (≤5)	HBA (<10)	HBD (<5)	nROTB (≤10)	TPSA (Å2)	Lipinski Violation
SIRT1 Inh III	248.71	2.51	3	3	1	58.88	0
Hyperforin	536.8	8.39	4	1	11	71.44	2

1.4.8. ADME/T Profiling

1.4.8A. Absorption property analysis

The crucial parameters for drug bioavailability prediction are the Caco2 permeability and Human intestinal absorption (HIA). Both SIRT1 Inh III and Hyperforin could be easily absorbed through the human intestine as they have good HIA values (predicted HIA value > 30%) [30]. SIRT1 Inh III serves as the substrate of permeability P-glycoprotein which is abundantly present in epithelial cells. SIRT1 Inh III and Hyperforin could modulate the physiological roles of P-glycoprotein, as both were predicted to be P-glycoprotein I and P-glycoprotein II inhibitors, respectively. The detailed profiling is reflected in Table 5.

Table 5. Predicted absorption properties of compounds

Ligands	SIRT1 Inh III	Hyperforin
Water solubility (log mol/L)	-3.823	-3.893
Caco2 permeability (log Papp in 10-6 cm/s)	1.219	1.055
Human intestinal absorption (%)	91.742	98.386
Skin permeability (log Kp)	-3.183	-2.715
P-glycoprotein substrate	Yes	No
P-glycoprotein I inhibitor	No	Yes
P-glycoprotein II inhibitor	No	Yes

1.4.8B. Distribution property analysis

SIRT1 Inh III showed a higher value of Volume of distribution at steady-state (VDss), illustrating that it can be easily distributed in plasma or tissue. The central nervous system (CNS) permeability also revealed that they can't harm the central nervous system as they have little brain access (Table 6).

Table 6. Predicted distribution properties of compounds

Ligands	VDss (log L/kg)	Fraction unbound (human) (Fu)	BBB permeability (log BB)	CNS permeability (log PS)
SIRT1 Inh III	0.455	0.208	0.003	-1.957
Hyperforin	-0.64	0	-0.237	-1.304

1.4.8C. Determination of metabolic fates

The primary detoxification enzyme in the body is cytochrome P450 (CYP) isozymes, primarily found in the liver. CYP enzyme inhibition or activation is important for drug interaction and can lead to unexpected side effects or even treatment failures, thereby making these findings important in the study [40]. The details are illustrated in Table 7.

Table 7. Predicted metabolic fates of compounds

Ligands	CYP2D6 substrate	CYP3A4 substrate	CYP1A2 inhibitor	CYP2C19 inhibitor	CYP2C9 inhibitor	CYP2D6 inhibitor	CYP3A4 inhibitor
SIRT1 Inh III	No	No	Yes	Yes	No	No	No
Hyperforin	No	Yes	No	No	No	No	No

1.4.8D. Excretion property analysis

The chemicals may be eliminated through alternative paths, such as faeces, bile, or sweat to prevent interactions with other medications as both the compounds serve as substrates of the renal organic cation transporter-2 (OCT2), (Table 8).

Table 8. Predicted excretion properties of compounds

Ligands	Total clearance (log ml/min/kg)	Renal OCT2 substrate
SIRT1 Inh III	-0.127	No
Hyperforin	0.664	No

1.4.8E. Toxicological property determination

AMES toxicity test showed non-carcinogenic nature of both the compounds along with no hepatotoxic properties. The human ether-a-go-go-related gene (hERG), responsible for translating a subunit of the voltage-gated potassium ion channel Kv11.1 [41] was not inhibited by either of the compounds. Additionally, both the compounds were not linked to skin sensitivity, (Table 9).

Table 9. Predicted toxicological profile of compounds

Ligands	AMES toxicity	hERG I inhibitor	hERG II inhibitor	Hepatotoxicity	Skin sensitivity
SIRT1 Inh III	No	No	No	No	No
Hyperforin	No	No	No	No	No

1.4.9. MD simulation of complexes

The study involved the following protein-ligand complexes: i) SIRT1 with SIRT1 Inh III, ii) SIRT1 with Hyperforin, iii) PI3K with SIRT1 Inh III, iv) PI3K with Hyperforin, v) AKT with SIRT1 Inh III, and vi) AKT with Hyperforin. These complexes were analyzed to examine their interactions and stability in a simulated biological environment.

1.4.9A. RMSD and RMSF analysis

SIRT1 Inh III displayed lower RMSD (0.252 ± 0.042nm) for AKT protein, indicating it maintained a relatively stable conformation during the simulation with very little fluctuations whereas higher RMSD in the case of SIRT1 (0.842 ± 0.301nm) and PI3K (0.509 ± 0.113nm) was observed, that demonstrate more deviation from the initial conformation than Hyperforin (Table 10). During simulation, both SIRT1 Inh III and Hyperforin were stabilized between 30ns and 45ns for SIRT1. However, between 0ns and 10ns, the backbone of PI3K-Hyperforin complex was deviating. However, a deviation of PI3K-SIRT1 Inh III complex was observed between 0ns and 12ns and also between 37ns and 40ns. All the complexes were stabilized after 15ns except SIRT1- SIRT1 Inh III complex and AKT-Hyperforin. A lower RMSF for SIRT1 (0.122 ± 0.11nm) and AKT (0.087 ± 0.042nm) was observed in case of SIRT1 Inh III revealing that its residues are less flexible and exhibit less fluctuations than Hyperforin. However, the complexes revealed higher RMSF in case of PI3K (0.135 ± 0.05nm), indicating the effect on binding stability of greater flexibility in some regions (Table 10) and represented in Figure 7A-B.

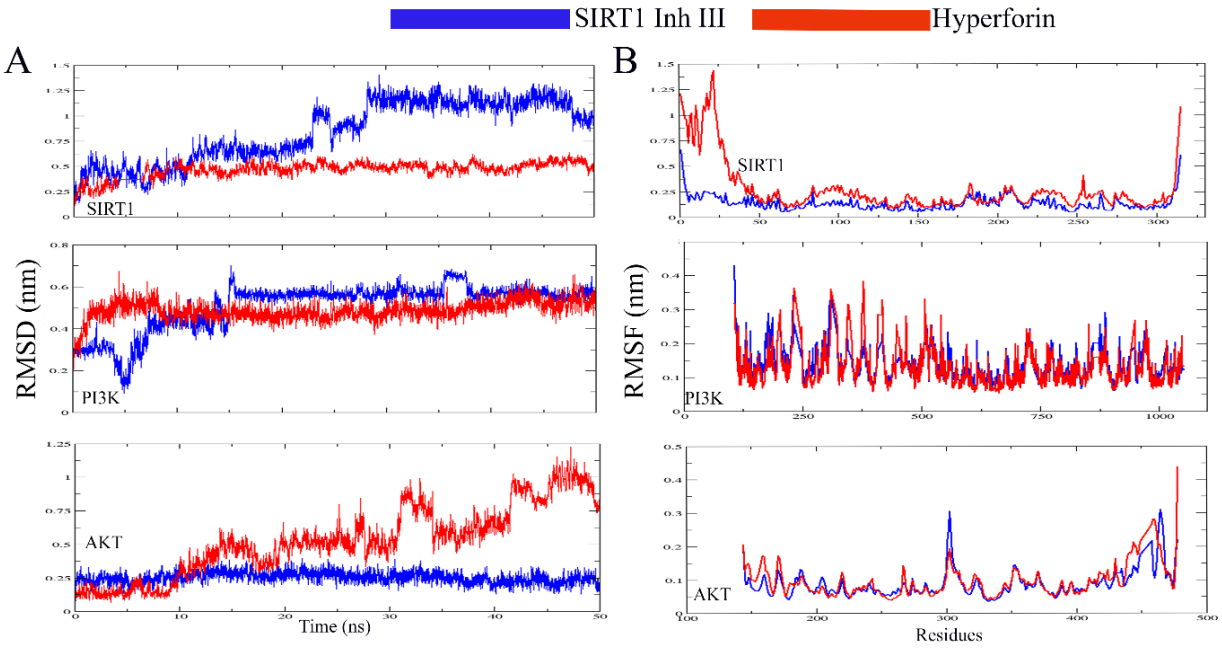

Figure 7. A. RMSD of the backbone of protein-ligand complexes; B. RMSF of protein-ligand complexes at the residual level. The colour code for the respective protein-ligand complexes is shown at the top of the figure.

1.4.9B. Rg and SASA determination

A compact protein-ligand complex was observed in case of SIRT1 Inh III by revealing a better Rg for SIRT1 (2.138 ± 0.026nm) and AKT (2.071 ± 0.008nm). However, Hyperforin displayed better Rg for PI3K (3.063 ± 0.011nm) (Table 10). A relatively lower solvent exposure suggested a more buried binding pose for SIRT1 Inh III with a lower SASA for SIRT1 (176.725 ± 4.695nm²) and AKT (166.511 ± 2.95nm²) whereas, Hyperforin displayed a lower SASA for PI3K (404.217 ± 4.457nm²) (Table 10). A variation in H-bond formed between target proteins and inhibitor was observed between 0 to 5 during 50ns simulation (Figure 8A-B).

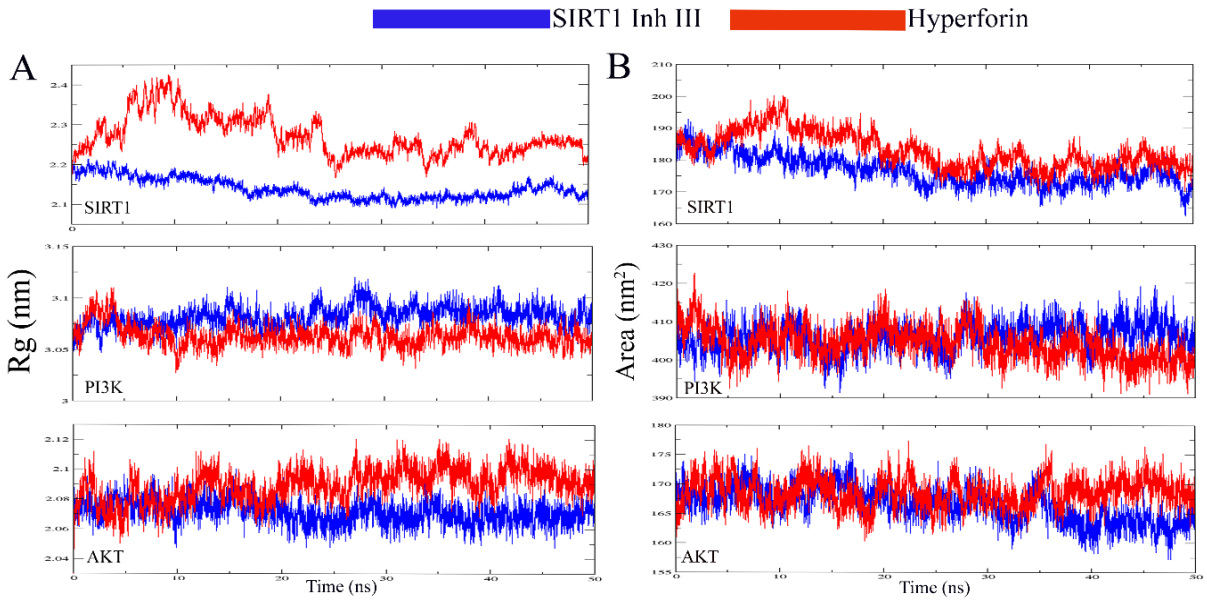

Figure 8. A. Rg upon binding with ligands; B. SASA upon binding with ligands; B. Inter-molecular hydrogen bonds between ligands and target proteins. The colour code for the respective protein-ligand complexes is shown at the top of the figure.

1.4.9C. Number of H-bonds and relative distance measurement

A greater number of H-Bonds for PI3K (1.06) and AKT (1.118) was high in case of SIRT1 Inh III, indicating consistent and strong interactions with the target protein (Table 10). To assess the H-bond strength, the pair distance between the donor and the acceptor was also analyzed. The average pair distance for all three proteins was lesser for SIRT1 Inh III than Hyperforin, suggesting increased binding strength (Figure 9A-B).

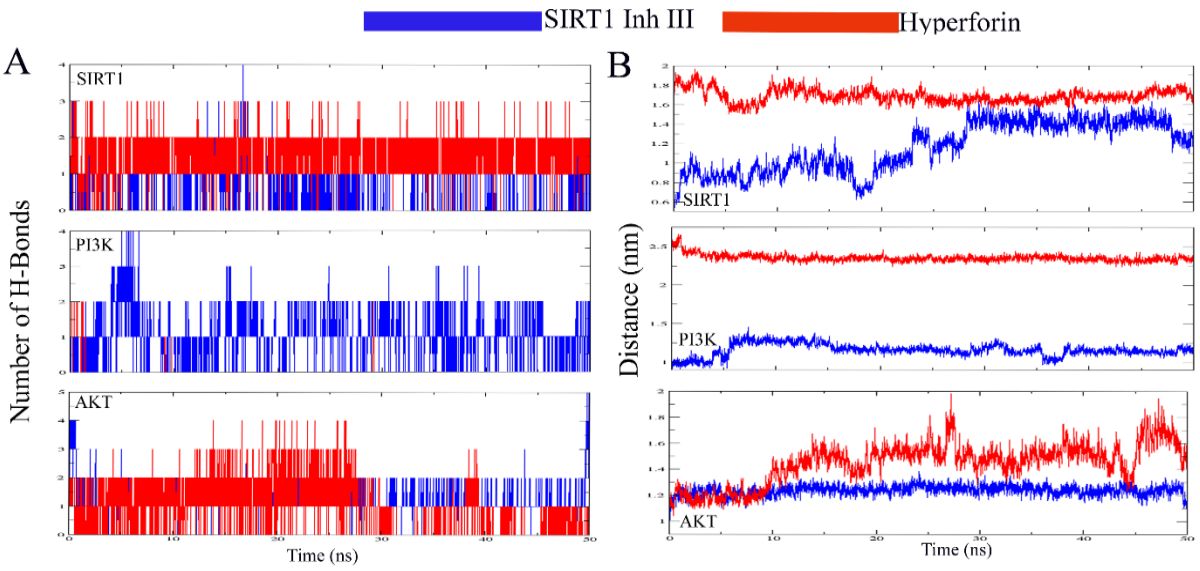

Figure 9. A. Number of H-bonds determination; B. Hydrogen bond pair distance between acceptor and donor of protein-ligand complexes. All MD simulation trajectory analysis was done over 50ns for SIRT1, PI3K, and AKT, respectively. The colour code for the respective protein-ligand complexes is shown at the top of the figure.

Table 10. Average values of RMSD, RMSF, Rg, SASA, and distance between acceptor and donor, and no. of H-bonds in protein-ligand complexes

Target with PDB ID		**SIRT 1**		**PI3K (5DXT)**		**AKT (3QKK)**	
Ligand		**SIRT1 Inh III**	**Hyperforin**	**SIRT1 Inh III**	**Hyperforin**	**SIRT1 Inh III**	**Hyperforin**
RMSD (nm)	**Mean**	0.842	0.489	0.509	0.486	0.252	0.525
	SD	0.301	0.37	0.113	0.047	0.042	0.263
RMSF (nm)	**Mean**	0.122	0.285	0.135	0.126	0.087	0.094
	SD	0.11	0.292	0.05	0.054	0.042	0.047
Rg (nm)	**Mean**	2.138	2.271	3.082	3.063	2.071	2.089
	SD	0.026	0.05	0.011	0.011	0.008	0.011
SASA (nm2)	**Mean**	176.725	182.877	405.936	404.217	166.511	168.586
	SD	4.695	5.621	3.738	4.457	2.95	2.573
Mean H-bonds		0.419	1.618	1.06	0.032	1.118	0.952
Pair distance (nm)	**Mean**	1.161	1.69	1.16	2.354	1.237	1.447
	SD	0.257	0.07	0.082	0.046	0.039	0.158

1.4.10. In-vitro analysis of SIRT1 Inh III potential

Since SIRT1 Inh III has a better binding affinity than Hyperforin for all target proteins, we conducted *in-vitro* analysis to evaluate its efficacy. It showed a lower IC_{50} value on SKOV3 (0.1606µM) as represented in Figure 10A. The wound healing assay revealed positive results for SIRT1 Inh III with a decrease in migratory potential of the SKOV3 cells where percentage confluency decreased under the treated conditions after 24hrs whereas the percentage inhibition increased after the 24hrs treatment with SIRT1 Inh III as compared to the control (Figure 10B).

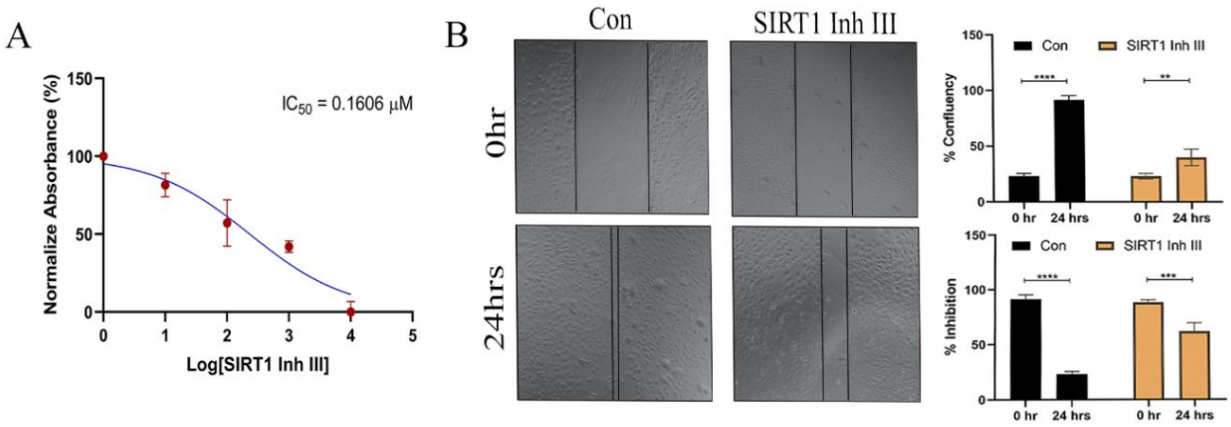

Figure 10. A. MTT analysis of SIRT1 Inh III in SKOV3 cells; B. Analysis of migration of SKOV3 cells by scratch assay in control and treated groups. (*P<0.05, **P<0.01, ***P<0.001, ****P<0.0001)

1.4.11. In-vivo analysis of SIRT1 Inh III

The schematic of establishing the *in-vivo* model for OvCa in C57BL/6 mice and the treatment regime is illustrated in Figure 11A. The survival status increased and the death rate decreased under the treated group (Figure 11B). Additionally, the number of peritoneal implants and volume of ascitic fluid were significantly reduced in the treated ones (Figure 11C-D). The individual organs are represented in Figure 11E. The tumor-infiltrating lymphocytes (TILs) in ovarian tumor were higher under treatment conditions than the non-treated ones, revealing the recruitment of immune cells in treating the disease by H&E staining (Figure 11F).

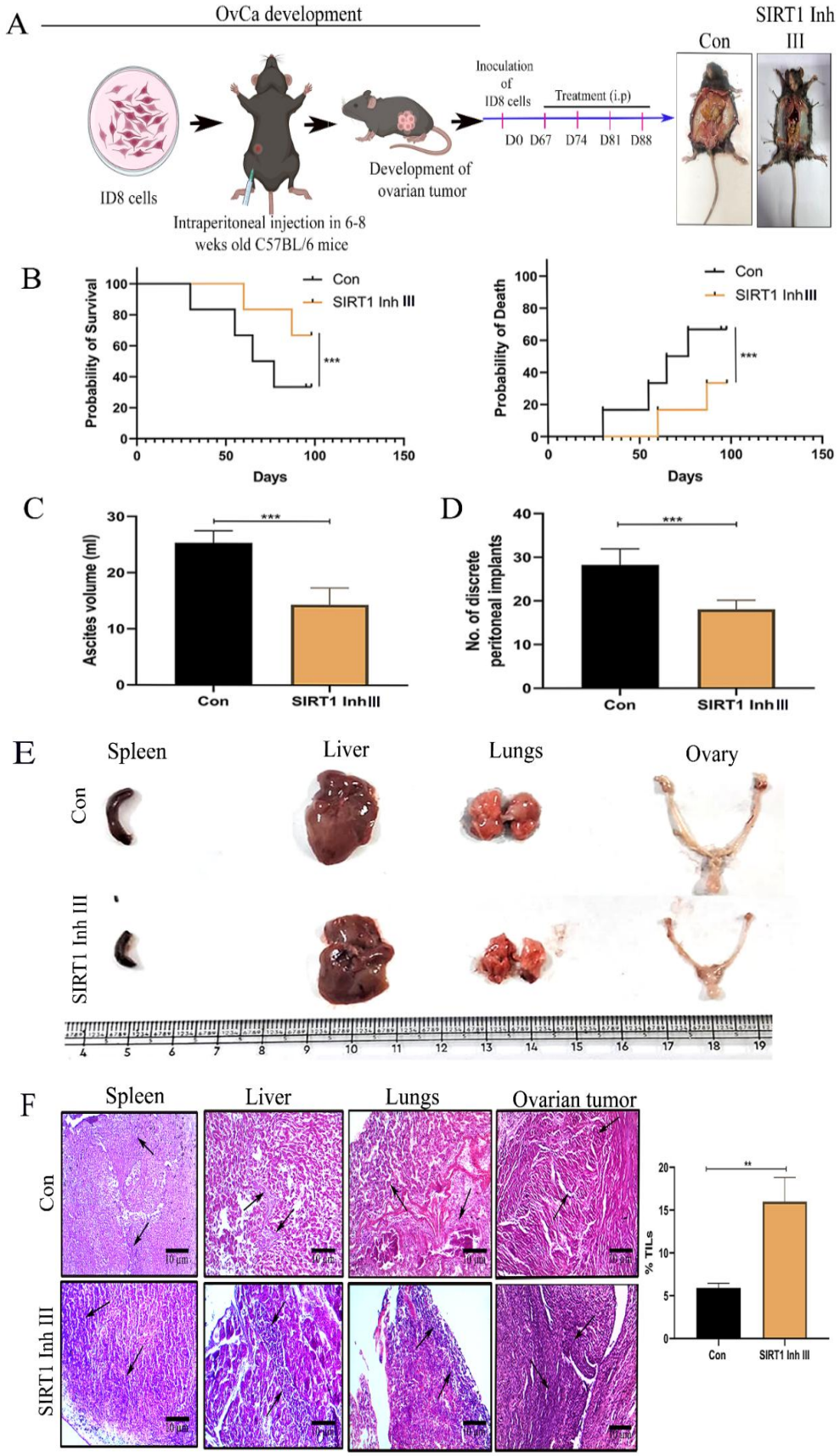

Figure 11. A. Schematic representation of the development of OvCa in C57BL/6 mice and treatment doses; B. Analysis of survival and death under control (Con) and treatment

condition; C. Estimation of ascites volume in con and treatment condition; D. Estimation of the number of discrete peritoneal implants under con and treatment condition; E. Representation of individual organs under con and treated groups; F. Representation of TILs count in con and treated categories in ovarian tumor; (*P<0.05, **P<0.01, ***P<0.001, ****P<0.0001)

1.4.12. Apoptotic cells and ROS generation analysis with expression of proliferation and epithelial markers

Annexin V+ cells increased under the treatment condition (Figure 12A), revealing the cells to be apoptotic. Surprisingly, ROS producing cells were higher under the treated conditions as compared to the control (Figure 12B). Furthermore, the Ki-67 (Figure 12C), α-SMA (Figure 12D), Fibronectin (Figure 12E) and Collagen (Figure 12F) expression status decreased considerably under the treated group as compared to the non-treated ones.

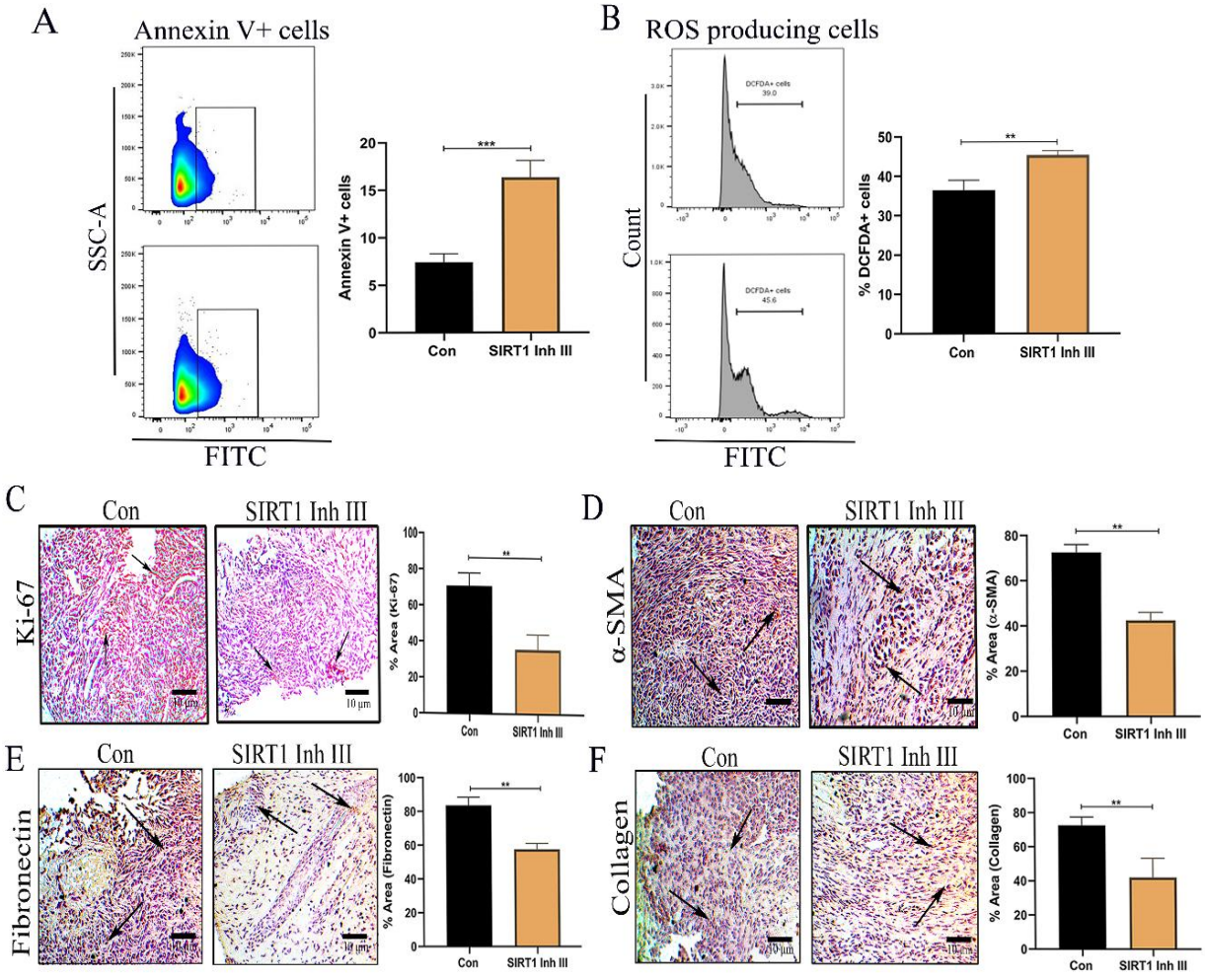

Figure 12. A. Flow cytometric analysis of percentage of Annexin V+ cells in con and treated groups; B. Flow cytometric analysis of percentage of DCFDA+ ROS producing cells in con

and treated groups; C. Expression status of Ki-67 by IHC in con and treated groups; D. Expression status of α-SMA by IHC in con and treated groups; E. Expression status of Fibronectin by IHC in con and treated groups; F. Expression status of Collagen by IHC in con and treated groups. (*P<0.05, **P<0.01, ***P<0.001, ****P<0.0001)

1.5. Discussion

SIRT1 along with p53 family, Nuclear factor-κB family and FOXO transcription factors play pivotal roles in cell survival and cell death [42]. The role of SIRT1 as a tumor promoter is validated in OvCa [22] and HCC [43]. Upon pan-cancer analysis of the expressional and mutational status of SIRT1 and p53, it was observed that both were highly expressed and mutated in OvCa. We also observed that their protein expression was higher in the tumor samples as compared to the normal. Additionally, their expression level increased with increase in grade of the disease. Interestingly, SIRT1 was highly expressed in the p53 mutant samples as compared to the non-mutant ones. To validate these observations, we have deduced similar results in their colocalized expression in clinical samples where the expression levels of SIRT1 and p53 increased in the tumor ones as normal ones. Interestingly Under this doctrine, to validate our observations, the underlying mechanism revealed that p53 being deacetylated by SIRT1 would have been expressed less but since it is mutated it acquires gain of function, resulting its overexpression which in turn triggers its oncogenic functionalities. The overexpressed p53 gets highly accumulated in the cytosol as its translocation into the nucleus is blocked which might augment the tumor promoting functions of SIRT1 by increasing its expression level [44]. Additionally, intracellular ROS is increased due to stimulated mitochondrial O_2^- causing damage to mitochondrial DNA due to their abnormal accumulation upon blockage of the SESN/AMPK complex by p53-R175H, p53-R248H, and p53-R273H (mutant variants of p53). This baseline mechanism aids the survival and proliferation of the cancer cells [45]. The OS and DFS in SIRT1 overexpressed patients were lower as compared to the p53 mutant patients thus, we proceeded for further studies with SIRT1 and its inhibition with SMIs and natural products still needs attention to improve the survival rates of the patients.

Furthermore, it was evaluated that positive regulation of cell migration, regulation of cytokines, regulation of TP53 degradation, receptor tyrosine kinase signaling, PI3K/AKT pathway are regulated by *SIRT1* and its associated genes like *AKT1, PTEN, PIK3CA, MMP2, MMP9, IL-6, PTGS2, EGFR*. Previous findings demonstrate that activation of

PI3K/AKT/mTOR pathway regulates the invasiveness and proliferation of OvCa cells [46], which further validates our observations. GSCA analysis showed EMT to be highly regulated by the *SIRT1* and related genes. Furthermore, their significant correlation with the immune infiltration score is also linked with the *SIRT1* and associated genes.

Since SIRT1 has been established as a potent target in OvCa, we were inclined to investigate a potent inhibitor of the molecule, either a natural product or a SMI, so that the disease can be combatted. We investigated and found that chromones (flavone and isoflavone) and coumarins, bichalchones are natural inhibitors of SIRT1 [10]. In this context, we deduced Hyperforin, a natural SIRT1 Inh in the IMPPAT database, to be suitable for our further study comparing it with SIRT1 Inh III (EX527) for further validation. Since we deduced from our database mining study that EMT might be regulated by PI3K/AKT pathway under the effect of SIRT1 and its associated molecule, we analyzed the effect of these two inhibitors in regulating SIRT1, PI3K and AKT molecules. The molecular docking study depicted that SIRT1 Inh III has a better binding energy with all the molecules as compared to Hyperforin. We evaluated complex stability using metrics like RMSD, which provides the average deviation of the complexed protein's backbone atom throughout the simulation period compared to the initial complex [47]. SIRT1 Inh III significantly showed better RMSD for AKT protein. Similar to RMSD, RMSF provides the average fluctuation of each amino acid's backbone atom during simulation concerning the initial individual amino acid residues of the complex [47]. SIRT1 Inh III displayed better RMSF for SIRT1 and AKT. Rg is a key measurement in biophysical research that provides vital information about the spatial arrangement and conformational compactness of proteins and SASA is the surface area (nm^2) of a molecule that can directly interact with the solvent [48][49]. In this case, SIRT1 Inh III also showed better Rg and SASA for SIRT1 and AKT. Additionally, we assessed the average number of hydrogen bonds formed between the target protein and the ligand to ensure the strength of molecular interactions throughout the simulation [50][51]. Our potent inhibitor SIRT1 Inh III showed more inter-molecular H-bonds in the case of PI3K and AKT. The hydrogen bond pair distance between the donor and the acceptor was also analyzed to assess the strength of the H-bond. Here we could see that SIRT1 Inh III had less pair distance for all the proteins, indicating a great potential for inhibiting their functions.

Furthermore, Hyperforin violated Lipinski’s rule of 5 by not following two fundamental properties (molecular weight >500g/mol and logP >5) whereas SIRT1 Inh III passed all the rules. Additionally, according to IMPPAT 2.0, Hyperforin violated different

important rules like Ghose rule, Veber rule, Egan rule, GSK 4/400 rule, Pfizer 3/75 rule, and QEDw score (Weighted quantitative estimate of drug-likeness).

These findings proved SIRT1 Inh III to be a more potent inhibitor SIRT1 as compared to Hyperforin and thus continued our further investigations in *in-vitro* and *in-vivo* models to validate the potential of the SMI in OvCa. The results of *in-vitro* analysis revealed that SIRT1 Inh III retarded the migration of the OvCa cells. Furthermore, *in-vivo* analysis also corroborated our findings, revealing that the survival rate increased and the death rate decreased in the treatment group, proving SIRT1 Inh III to be a potent inhibitor of OvCa. Additionally, the ascites volume and number of peritoneal implants also decreased in the treatment category as compared to the control group. The inhibitor also triggered apoptosis in the cancer cells by generating greater levels of ROS in the treatment group. The proliferation of the cancer cells was reduced, as evident from the lowered expression status of Ki-67 in the treatment group. The positive expression of EMT marker α-SMA in serous and clear cell OvCa cells demonstrated the mesenchymal attributes in the cancer cells [52]. Furthermore, collagen and other ECM components were found to be overexpressed in numerous OvCa drug-resistant cell lines, suggesting their crucial roles in mediating drug resistance in OvCa [53]. Fibronectin was found to be highly expressed in primary tumor, validating its role in metastasis [54]. Surprisingly, we deduced their lower expression in the treatment group as compared to the control.

Despite the presence of multiple regulatory and modulatory molecules in OvCa, SIRT1 has proved to be one of the most potent factors that can be targeted in combatting the disease. Keeping in mind the cytotoxicity caused by the synthetic drug over natural inhibitors, when we opted Hyperforin after a strenuous investigation of searching for a potent natural inhibitor and compared it with the SMI, our study revealed that the SMI was the more potent inhibitor as compared to the natural one. These derivations show that the SIRT1 Inh III performs a pivotal role in controlling the growth and migration of the OvCa cells and can be implemented as a potent SIRT1 Inh for further experiments.

1.6. References

[1] Z. Mei, X. Zhang, J. Yi, J. Huang, J. He, Y. Tao, Sirtuins in metabolism, DNA repair and cancer, J. Exp. Clin. Cancer Res. 35 (2016) 182. https://doi.org/10.1186/s13046-016-0461-5.

[2] Y. Tang, W. Ju, Y. Liu, Q. Deng, The role of SIRT1 in autophagy and drug resistance: unveiling new targets and potential biomarkers in cancer therapy, Front. Pharmacol. 15 (2024). https://doi.org/10.3389/fphar.2024.1469830.

[3] M. Hou, X. Zuo, C. Li, Y. Zhang, Y. Teng, Mir-29b Regulates Oxidative Stress by Targeting SIRT1 in Ovarian Cancer Cells., Cell. Physiol. Biochem. 43 (2017) 1767–1776. https://doi.org/10.1159/000484063.

[4] M.B. Kastan, O. Onyekwere, D. Sidransky, B. Vogelstein, R.W. Craig, Participation of p53 protein in the cellular response to DNA damage., Cancer Res. 51 (1991) 6304–11.

[5] A. Parrales, T. Iwakuma, Targeting Oncogenic Mutant p53 for Cancer Therapy, Front. Oncol. 5 (2015). https://doi.org/10.3389/fonc.2015.00288.

[6] J. Ford, M. Jiang, J. Milner, Cancer-specific functions of SIRT1 enable human epithelial cancer cell growth and survival, Cancer Res. 65 (2005) 10457–10463. https://doi.org/10.1158/0008-5472.CAN-05-1923.

[7] A. Vaquero, M. Scher, D. Lee, H. Erdjument-Bromage, P. Tempst, D. Reinberg, Human SirT1 interacts with histone H1 and promotes formation of facultative heterochromatin, Mol. Cell. 16 (2004) 93–105. https://doi.org/10.1016/J.MOLCEL.2004.08.031.

[8] M.F. Fraga, E. Ballestar, A. Villar-Garea, M. Boix-Chornet, J. Espada, G. Schotta, T. Bonaldi, C. Haydon, S. Ropero, K. Petrie, N.G. Iyer, A. Pérez-Rosado, E. Calvo, J.A. Lopez, A. Cano, M.J. Calasanz, D. Colomer, M.Á. Piris, N. Ahn, A. Imhof, C. Caldas, T. Jenuwein, M. Esteller, Loss of acetylation at Lys16 and trimethylation at Lys20 of histone H4 is a common hallmark of human cancer, Nat. Genet. 37 (2005) 391–400. https://doi.org/10.1038/NG1531.

[9] H. Vaziri, S.K. Dessain, E.N. Eaton, S.-I. Imai, R.A. Frye, T.K. Pandita, L. Guarente, R.A. Weinberg, hSIR2SIRT1 Functions as an NAD-Dependent p53 Deacetylase, Cell. 107 (2001) 149–159. https://doi.org/10.1016/S0092-8674(01)00527-X.

[10] B. Karaman Mayack, W. Sippl, F. Ntie-Kang, Natural Products as Modulators of Sirtuins, Molecules. 25 (2020) 3287. https://doi.org/10.3390/molecules25143287.

[11] Q. Zhang, S.X. Zeng, Y. Zhang, Y. Zhang, D. Ding, Q. Ye, S.O. Meroueh, H. Lu, A small molecule Inauhzin inhibits SIRT1 activity and suppresses tumour growth through activation of p53., EMBO Mol. Med. 4 (2012) 298–312. https://doi.org/10.1002/emmm.201100211.

[12] R. Asaka, T. Miyamoto, Y. Yamada, H. Ando, D.H. Mvunta, H. Kobara, T. Shiozawa, Sirtuin 1 promotes the growth and cisplatin resistance of endometrial carcinoma cells: a novel therapeutic target, Lab. Investig. 95 (2015) 1363–1373. https://doi.org/10.1038/labinvest.2015.119.

[13] M.P. Ceballos, G. Decándido, A.D. Quiroga, C.G. Comanzo, V.I. Livore, F. Lorenzetti, F. Lambertucci, L. Chazarreta-Cifre, C. Banchio, M. de L. Alvarez, A.D. Mottino, M.C. Carrillo, Inhibition of sirtuins 1 and 2 impairs cell survival and migration and modulates the expression of P-glycoprotein and MRP3 in hepatocellular carcinoma cell lines., Toxicol. Lett. 289 (2018) 63–74. https://doi.org/10.1016/j.toxlet.2018.03.011.

[14] C.E. Oon, C. Strell, K.Y. Yeong, A. Östman, J. Prakash, SIRT1 inhibition in pancreatic cancer models: contrasting effects in vitro and in vivo., Eur. J. Pharmacol. 757 (2015) 59–67. https://doi.org/10.1016/j.ejphar.2015.03.064.

[15] C. Gey, S. Kyrylenko, L. Hennig, L.D. Nguyen, A. Büttner, H.D. Pham, A. Giannis, Phloroglucinol Derivatives Guttiferone G, Aristoforin, and Hyperforin: Inhibitors of Human Sirtuins SIRT1 and SIRT2, Angew. Chemie Int. Ed. 46 (2007) 5219–5222. https://doi.org/10.1002/anie.200605207.

[16] G. Pinton, S. Zonca, A.G. Manente, M. Cavaletto, E. Borroni, A. Daga, P. V Jithesh, D. Fennell, S. Nilsson, L. Moro, SIRT1 at the crossroads of AKT1 and ERβ in malignant pleural mesothelioma cells., Oncotarget. 7 (2016) 14366–79. https://doi.org/10.18632/oncotarget.7321.

[17] X. Jin, Y. Wei, F. Xu, M. Zhao, K. Dai, R. Shen, S. Yang, N. Zhang, SIRT1 promotes formation of breast cancer through modulating Akt activity, J. Cancer. 9 (2018) 2012–2023. https://doi.org/10.7150/jca.24275.

[18] M. Riggio, M.L. Polo, M. Blaustein, A. Colman-Lerner, I. Lüthy, C. Lanari, V. Novaro, PI3K/AKT pathway regulates phosphorylation of steroid receptors, hormone independence and tumor differentiation in breast cancer., Carcinogenesis. 33 (2012) 509–18. https://doi.org/10.1093/carcin/bgr303.

[19] V. Byles, L.K. Chmilewski, J. Wang, L. Zhu, L.W. Forman, D. V. Faller, Y. Dai, Aberrant Cytoplasm Localization and Protein Stability of SIRT1 is Regulated by PI3K/IGF-1R Signaling in Human Cancer Cells, Int. J. Biol. Sci. (2010) 599–612. https://doi.org/10.7150/ijbs.6.599.

[20] M. Charan, S. Das, S. Mishra, N. Chatterjee, S. Varikuti, K. Kaul, S. Misri, D.K. Ahirwar, A.R. Satoskar, R.K. Ganju, Macrophage migration inhibitory factor inhibition as a novel therapeutic approach against triple-negative breast cancer, Cell Death Dis. 11 (2020) 774. https://doi.org/10.1038/s41419-020-02992-y.

[21] S.K. Das, S. Roy, A. Das, A. Chowdhury, N. Chatterjee, A. Bhaumik, A conjugated 2D covalent organic framework as a drug delivery vehicle towards triple negative breast cancer malignancy, Nanoscale Adv. (2022) 2313–2320. https://doi.org/10.1039/d2na00103a.

[22] S. Roy, A. Das, M. Vernekar, S. Mandal, N. Chatterjee, Understanding the Correlation between Metabolic Regulator SIRT1 and Exosomes with CA-125 in Ovarian Cancer: A Clinicopathological Study, Biomed Res. Int. 2022 (2022) 5346091. https://doi.org/10.1155/2022/5346091.

[23] D.A. Cohen, D.J. Dabbs, K.L. Cooper, M. Amin, T.E. Jones, M.W. Jones, M. Chivukula, G.A. Trucco, R. Bhargava, Interobserver agreement among pathologists for semiquantitative hormone receptor scoring in breast carcinoma, Am. J. Clin. Pathol. 138 (2012) 796–802. https://doi.org/10.1309/AJCP6DKRND5CKVDD.

[24] C.J. Liu, F.F. Hu, M.X. Xia, L. Han, Q. Zhang, A.Y. Guo, GSCALite: A web server for gene set cancer analysis, Bioinformatics. 34 (2018) 3771–3772. https://doi.org/10.1093/bioinformatics/bty411.

[25] K. Mohanraj, B.S. Karthikeyan, R.P. Vivek-Ananth, R.P.B. Chand, S.R. Aparna, P. Mangalapandi, A. Samal, IMPPAT: A curated database of Indian Medicinal Plants, Phytochemistry And Therapeutics, Sci. Rep. 8 (2018) 4329. https://doi.org/10.1038/s41598-018-22631-z.

[26] N.M. O'Boyle, M. Banck, C.A. James, C. Morley, T. Vandermeersch, G.R. Hutchison, Open Babel: An open chemical toolbox - 1758-2946-3-33.pdf, J. Cheminform. 3 (2011) 1–14. http://www.jcheminf.com/content/3/1/33%0Ahttp://www.biomedcentral.com/content/pdf/1758-2946-3-33.pdf.

[27] S. Dallakyan, A.J. Olson, Small-Molecule Library Screening by Docking with PyRx, in: 2015: pp. 243–250. https://doi.org/10.1007/978-1-4939-2269-7_19.

[28] M.F. Adasme, K.L. Linnemann, S.N. Bolz, F. Kaiser, S. Salentin, V.J. Haupt, M. Schroeder, PLIP 2021: expanding the scope of the protein–ligand interaction profiler to DNA and RNA, Nucleic Acids Res. 49 (2021) W530–W534. https://doi.org/10.1093/nar/gkab294.

[29] C.A. Lipinski, F. Lombardo, B.W. Dominy, P.J. Feeney, Experimental and computational approaches to estimate solubility and permeability in drug discovery and development settings 1PII of original article: S0169-409X(96)00423-1. The article was originally published in Advanced Drug Delivery Reviews 23 (1997) 3–25. 1, Adv. Drug Deliv. Rev. 46 (2001) 3–26. https://doi.org/10.1016/S0169-409X(00)00129-0.

[30] D.E. V. Pires, T.L. Blundell, D.B. Ascher, pkCSM: Predicting Small-Molecule Pharmacokinetic and Toxicity Properties Using Graph-Based Signatures, J. Med. Chem. 58 (2015) 4066–4072. https://doi.org/10.1021/acs.jmedchem.5b00104.

[31] P. Bjelkmar, P. Larsson, M.A. Cuendet, B. Hess, E. Lindahl, Implementation of the CHARMM Force Field in GROMACS: Analysis of Protein Stability Effects from Correction Maps, Virtual Interaction Sites, and Water Models, J. Chem. Theory Comput. 6 (2010) 459–466. https://doi.org/10.1021/ct900549r.

[32] M.Z. Sabri, A.A. Abdul Hamid, S.M. Sayed Hitam, M.Z. Abdul Rahim, In Silico Screening of Aptamers Configuration against Hepatitis B Surface Antigen, Adv. Bioinformatics. 2019 (2019) 6912914. https://doi.org/10.1155/2019/6912914.

[33] T.-S. Lee, D.S. Cerutti, D. Mermelstein, C. Lin, S. LeGrand, T.J. Giese, A. Roitberg, D.A. Case, R.C. Walker, D.M. York, GPU-Accelerated Molecular Dynamics and Free Energy Methods in Amber18: Performance Enhancements and New Features, J. Chem. Inf. Model. 58 (2018) 2043–2050. https://doi.org/10.1021/acs.jcim.8b00462.

[34] J. Wang, R.M. Wolf, J.W. Caldwell, P.A. Kollman, D.A. Case, Development and testing of a general amber force field, J. Comput. Chem. 25 (2004) 1157–1174. https://doi.org/10.1002/jcc.20035.

[35] A.H. Fischer, K.A. Jacobson, J. Rose, R. Zeller, Hematoxylin and eosin staining of tissueand cell sections, Cold Spring Harb. Protoc. 3 (2008) 3–5. https://doi.org/10.1101/pdb.prot4986.

[36] P. Das, S. Roy, C. Das, R. Biswas, N. Chaterjee, J. Dinda, Structure-based design to explore the anticancer efficacy of organometallic Pt(ii)- and Au(iii)-N-heterocyclic carbene (NHC) complexes, New J. Chem. 48 (2024) 16189–16201. https://doi.org/10.1039/d4nj02853h.

[37] L. Zhang, N. Yang, J.-R. Conejo Garcia, A. Mohamed, F. Benencia, S.C. Rubin, D. Allman, G. Coukos, Generation of a Syngeneic Mouse Model to Study the Effects of Vascular Endothelial Growth Factor in Ovarian Carcinoma, Am. J. Pathol. 161 (2002) 2295–2309. https://doi.org/10.1016/S0002-9440(10)64505-1.

[38] N. Chatterjee, S. Das, D. Bose, S. Banerjee, T. Jha, K. Das Saha, Lipid from Infective L. donovani Regulates Acute Myeloid Cell Growth via Mitochondria Dependent MAPK Pathway, PLoS One. 10 (2015) e0120509. https://doi.org/10.1371/journal.pone.0120509.

[39] D.F. Veber, S.R. Johnson, H.-Y. Cheng, B.R. Smith, K.W. Ward, K.D. Kopple, Molecular Properties That Influence the Oral Bioavailability of Drug Candidates, J. Med. Chem. 45 (2002) 2615–2623. https://doi.org/10.1021/jm020017n.

[40] T. Lynch, A. Price, The effect of cytochrome P450 metabolism on drug response, interactions, and adverse effects., Am. Fam. Physician. 76 (2007) 391–6.

[41] M.C. Sanguinetti, HERG1 channel agonists and cardiac arrhythmia, Curr. Opin. Pharmacol. 15 (2014) 22–27. https://doi.org/10.1016/j.coph.2013.11.006.

[42] G. Blander, L. Guarente, The Sir2 Family of Protein Deacetylases, Annu. Rev. Biochem. 73 (2004) 417–435. https://doi.org/10.1146/annurev.biochem.73.011303.073651.

[43] C. Hao, P.X. Zhu, X. Yang, Z.P. Han, J.H. Jiang, C. Zong, X.G. Zhang, W.T. Liu, Q.D. Zhao, T.T. Fan, L. Zhang, L.X. Wei, Overexpression of SIRT1 promotes

metastasis through epithelial-mesenchymal transition in hepatocellular carcinoma, BMC Cancer. 14 (2014) 1–10. https://doi.org/10.1186/1471-2407-14-978.

[44] M.-K. Han, E.-K. Song, Y. Guo, X. Ou, C. Mantel, H.E. Broxmeyer, SIRT1 Regulates Apoptosis and Nanog Expression in Mouse Embryonic Stem Cells by Controlling p53 Subcellular Localization, Cell Stem Cell. 2 (2008) 241–251. https://doi.org/10.1016/j.stem.2008.01.002.

[45] M. Cordani, G. Butera, I. Dando, M. Torrens-Mas, E. Butturini, R. Pacchiana, E. Oppici, C. Cavallini, S. Gasperini, N. Tamassia, M. Nadal-Serrano, M. Coan, D. Rossi, G. Gaidano, M. Caraglia, S. Mariotto, R. Spizzo, P. Roca, J. Oliver, M.T. Scupoli, M. Donadelli, Mutant p53 blocks SESN1/AMPK/PGC-1α/UCP2 axis increasing mitochondrial $O_2^{-}\cdot$ production in cancer cells, Br. J. Cancer. 119 (2018) 994–1008. https://doi.org/10.1038/s41416-018-0288-2.

[46] H. Bai, H. Li, W. Li, T. Gui, J. Yang, D. Cao, K. Shen, The PI3K/AKT/mTOR pathway is a potential predictor of distinct invasive and migratory capacities in human ovarian cancer cell lines, Oncotarget. 6 (2015) 25520–25532. https://doi.org/10.18632/oncotarget.4550.

[47] V. Srivastava, B. Naik, P. Godara, D. Das, V.S.K. Mattaparthi, D. Prusty, Identification of FDA-approved drugs with triple targeting mode of action for the treatment of monkeypox: a high throughput virtual screening study, Mol. Divers. 28 (2024) 1093–1107. https://doi.org/10.1007/s11030-023-10636-4.

[48] M.I. Lobanov, N.S. Bogatyreva, O. V Galzitskaia, [Radius of gyration is indicator of compactness of protein structure]., Mol. Biol. (Mosk). 42 (2008) 701–6.

[49] Z. Yuan, F. Zhang, M.J. Davis, M. Bodén, R.D. Teasdale, Predicting the Solvent Accessibility of Transmembrane Residues from Protein Sequence, J. Proteome Res. 5 (2006) 1063–1070. https://doi.org/10.1021/pr050397b.

[50] S. Singh, H.N. Banavath, P. Godara, B. Naik, V. Srivastava, D. Prusty, Identification of antiviral peptide inhibitors for receptor binding domain of SARS-CoV-2 omicron and its sub-variants: an in-silico approach, 3 Biotech. 12 (2022) 198. https://doi.org/10.1007/s13205-022-03258-4.

[51] S. Singh, V. Srivastava, P. Godara, H.N. Banavath, H. Tak, A. Nayak, D. Kumari, B. Naik, D. Prusty, An in-silico-based study identified peptide inhibitors that can block the egression of the monkeypox virus by inhibiting the p37 protein target, Pept. Sci. 115 (2023) e24325. https://doi.org/10.1002/pep2.24325.

[52] N. Anggorowati, C. Ratna Kurniasari, K. Damayanti, T. Cahyanti, I. Widodo, A. Ghozali, M.M. Romi, D.C.R. Sari, N. Arfian, Histochemical and Immunohistochemical Study of α-SMA, Collagen, and PCNA in Epithelial Ovarian Neoplasm., Asian Pac. J. Cancer Prev. 18 (2017) 667–671. https://doi.org/10.22034/APJCP.2017.18.3.667.

[53] R. Januchowski, P. Zawierucha, M. Ruciński, M. Zabel, Microarray-based detection and expression analysis of extracellular matrix proteins in drug-resistant ovarian cancer cell lines., Oncol. Rep. 32 (2014) 1981–90. https://doi.org/10.3892/or.2014.3468.

[54] K.A. Kujawa, E. Zembala-Nożyńska, A.J. Cortez, T. Kujawa, J. Kupryjańczyk, K.M. Lisowska, Fibronectin and Periostin as Prognostic Markers in Ovarian Cancer., Cells. 9 (2020) 149. https://doi.org/10.3390/cells9010149.

Chapter 2

"Evaluation of clinicopathological parameters and studying the association of SIRT1 and exosomes with CA-125"

2.1. Introduction

Early diagnosis in OvCa is challenging to monitor due to the local invasion of the cancer cells into the deep pelvis and their seeding in peritoneal organs which leads to metastasis. Therefore, despite the presence of multiple biomarkers, a reliable diagnostic and prognostic factor is necessary to detect the disease at an early stage. The OvCa tumor exhibits highly heterogeneous histopathological and clinical attributes that make the assessment of the disease strenuous at the early stage. However, serum cancer/carbohydrate antigen-125 (CA-125), an endogenous glycoprotein generated by neoplastic OvCa cells has proven to be an effective tumor marker that correlates effectively with tumor load and can be easily measured [1]. Additionally, effective tumor molecular markers like proliferation markers Ki-67, p53, estrogen receptors, progesterone receptors, E-cad in OvCa tissues are analyzed by immunohistochemical analysis for better diagnosis [2][3]. The expression levels of all these markers depict the metastatic properties of the cancer cells. Thus, keeping in mind that altered metabolism is a hallmark of cancer and metabolic deregulation onsets the process of metastasis [4], we were inclined to investigate their associated modulatory effect on OvCa aggressiveness, which needed further exploration. Additionally, important nutrients are supplied to the cancer cells by upregulated interconnected metabolic cascades. This metabolic plasticity allows them to effectively adapt to the rapid metabolic alterations in the TME for their survival, proliferation and invasiveness [5]. Moreover, the involvement of metabolic reprogramming in elevating the longevity of the cancer cells is evident [6].

Metabolic plasticity and metabolic flexibility are two intertwined concepts that instigate the cancer cells to survive either by utilizing one metabolite to fuel the multiple metabolic necessities required for distinct stages of the metastatic cascade or by using different metabolites to meet the same metabolic requirements by a particular step of the metastatic pathway [7]. Additionally, as we know, that the cancer cells undergo Warburg effect with upregulated glucose metabolism [8] and NAD serve as the thus, to understand the altered metabolic bioenergetics, Along with the tumor markers being assessed for diagnosis, in this research work we have analyzed the expression status of SIRT1, as it is a NAD-dependent enzyme and performs as a metabolic sensor by its deacetylating property that regulates the cellular metabolic homeostasis [9]. Literature reveals the multifarious roles of exosomes in reprogramming the cellular metabolism which in turn promotes the alterations in the tumor milieu by increasing the proliferation, invasion, angiogenesis, immunosuppression

that eventually augments the metastasis [10]. Exosomes are responsible for intercellular communication by unloading their cargoes into the recipient cells thereby promoting peritoneal dissemination [11].

Metabolic alterations have a huge contribution in promoting cancer cell progression and metastasis thus the migrating cancer cells from the primary to the secondary site, there is a demand for them to adapt to metabolic state in the newly developed TME. Amino acids like asparagine, proline, serine, metabolic byproducts like pyruvate, acetate, lactate along with by-products released by fatty acid oxidation (FAO) help the migrating cancer cells to adapt and proliferate at the new site by providing adequate energy for their survival [12]. Secondly, metastasis is aided by the production of CO_2, lactate, and other organic acids leading to the formation of an acidic extracellular space which degrades the ECM [13]. Furthermore, abruptions in the enzymatic reactions involved in glycogen metabolism lead to higher glycogen synthesis and storage which aid the cancer cells in growing and promoting metastasis [14]. Evidence reveals that FAO aids the OvCa cells metabolically at a higher rate than aerobic glycolysis by providing increased ATP that nurtures the cancer cells thereby promoting their growth and proliferation [15]. Increased glycogen storage augments the glycolytic pathway in the cancer cells in nutrient scarcity and metabolically stressed TME [16]. A hypoxic condition prevails in the TME due to lower oxygen levels which in turn metabolically regulate the cancer cells to secrete a higher number of exosomes [17][18]. Hypoxia-inducible factor 1α (HIF-1α) regulates the hypoxic TME and thus affects the cancer cell metabolism and exosomes secretion. So, in this cohort study, we explored diagnostic serum levels of CA-125 and correlated these with additional clinical parameters and based on the significant correlated clinicopathological parameters discussed the expression of metabolic and metastatic biomolecules in this cohort which may subsequently be proved as therapeutic targets and biomarkers for early diagnosis.

2.2. Specific objectives

- Analysis of the prevalence of clinicopathological parameters and their association with CA-125.
- Analysis of metabolic and metastatic markers in the OvCa tissues.
- Identifying risk factors for developing OvCa with survival analysis.

2.3. Materials and Methods

2.3.1. Materials

The antibodies and reagents used in the study have been enlisted in Table 1.

Table 1. List of reagents

Serial No.	Reagent Name	Company	Catalogue No.
1.	Hematoxylin Solution (Mayer's, Modified)	ABCAM	ab220365
2.	DAB Substrate	Sigma Aldrich	11718096001
3.	Collagenase Type IV	Sigma Aldrich	C4-22
4.	DPX new	Sigma Aldrich	1005790500
5.	Schiff's reagent	Sigma Aldrich	1090332500
6.	Periodic acid	Sigma Aldrich	P0430
7.	Phosphate buffered saline	Sigma Aldrich	P4474
8.	Xylene pure, 99% (500 ml)	Sisco Research Laboratories Pvt. Ltd.	54717
9.	Acetic Acid Glacial extrapure AR, 99.9%	Sisco Research Laboratories Pvt. Ltd.	85801 (0129168)
10.	Methanol extrapure AR, 99.8%	Sisco Research Laboratories Pvt. Ltd.	65524
11.	eBioscience™ 1X RBC Lysis Buffer	Invitrogen	00-4333-57
12.	Dulbecco′s Modified Eagle′s Medium - high glucose	Sigma Aldrich	D6429
13.	Rabbit polyclonal anti-human SIRT1 antibody	Cell Signalling Technology	D739
14.	Rabbit anti-human polyclonal HIF-1α antibody	Santa Cruz Biotechnology	sc10790
15.	Mouse anti-rabbit IgG-HRP secondary antibody	Santa Cruz	sc-2357
16.	Purified mouse anti-human CD81 antibody	Biolegend	349501
17.	Anti-human CD63 antibody	Biolegend	353027
18.	Ki-67 rabbit pAB	Abclonal	A2094
19.	Hydrogen peroxide solution	MERCK	88597
Buffer Composition			
20.	Citrate Buffer	12.044g Sodium Citrate Dihydrate; 11.341g Citric acid; H_2O to 1000mL; pH-6	
21.	PBS (1X)	8g NaCl; 0.2g KCl; 1.44g Na_2HPO_4.7H2O; 0.24g KH_2PO_4; H_2O to 1L; pH-7.4	

2.3.2. Methods

2.3.2A. Study population and data collection

Institute Ethics Committee (CNCI-IEC-40104) approved the study and includes women who visited Chittaranjan National Cancer Institute, Regional Centre, Kolkata India for their treatment from 2019-2021. The clinicopathological characteristics included are age, BMI, potent tumor markers like carcinoembryonic antigen levels (CEA), CA-125 and cancer antigen 19.9 (CA-19.9), ascites level, malignancy present in ascites, degree of spread of the disease, differentiation of tumor cells, tumor type, FIGO stage of tumor, TNM grading, laterality of tumor and size of tumor. The relevant information was collected from the clinical records by the attending clinicians and was kept confidential.

2.3.2B. Study design and patient sample collection

Our study included all the patients (N=248) diagnosed with OvCa irrespective of the age criteria and histopathological characteristics. Patients irrespective of their treatment regimen have been considered in the study. Patients with comorbidities like cardiac issues or abdominal problems, pregnant or lactating mothers and those diagnosed with other cancer forms were excluded from the study. Apart from a retrospective analysis of the clinicopathological attributes, the status of factors associated with metabolic and metastatic regulations in OvCa tissues collected from patients with CA-125 levels >35 U/ml irrespective of the histological subtypes was analyzed to understand their expression level compared to the adjacent normal collected from had CA-125 levels below ≤35 U/ml (N=21) with proper informed consent and details were anonymized.

2.3.2C. Immunohistochemistry

Immunohistochemistry (IHC) staining was performed on paraffin-embedded tissue section slides. Deparaffination using xylene was performed, followed by submersion in alcohol gradient (100%, 90%, 70% and 50%) for rehydration. For antigen expression, the rehydrated slides were subjected to submersion in 10Mm citrate buffer solution (pH 6.0), followed by treatment with 3% hydrogen peroxide diluted in 100% methanol and incubated for 15min in the dark. To terminate the endogenous peroxidase activity the slides were washed in 1X PBS for 5min followed by the addition of primary antibodies of SIRT1, HIF-1α, Ki-67 and CD81 (1:500) and kept at 4ºC overnight. On the following day, after washing away the unbound

primary antibody with 1X PBS, anti-rabbit secondary antibody (1:1000) was added and incubated for 2hrs at RT. The expression was detected by incubating the slides with DAB for 10min in the dark. In the end, as a counterstain, haematoxylin was added to the slides and dehydration was performed using a reverse gradient alcohol wash and mounted with DPX [19]. The images were captured in a brightfield compound microscope (Leica Microsystems: #Model DM1000) and were further analyzed for their expression by Fiji-ImageJ software and graphical representation by GraphPad prism.

2.3.2D. Flow cytometry

Single primary cells from the tissues were obtained after overnight collagenase IV treatment, followed by straining and centrifugation for 10min at 2000rpm. RBC lysis buffer (1X) was added to the single cells for 5min at RT and then centrifuged to obtain a fresh single cell suspension [20]. The single cells were then incubated with APC/Fire tagged CD63 antibody (1:500) for 1hr [21] and the stained cells were analyzed using a BD LSRFortessa flow cytometer (San Jose, CA, USA) and analyzed using FCS Express 7.

2.3.2E. Periodic acid/Schiff (PAS) staining for detecting glycogen accumulation

The slides were deparaffinized using xylene for 5min followed by treatment with Carnoy's fixative for 10min. After rinsing the slides with distilled water, Periodic acid solution was added for 10min for staining followed by the addition of Schiff reagent for 5min. The slides were washed with distilled water to remove excessive stains and then dehydrated in ascending alcohol gradient solutions (50%, 70%, 90%, 100%). DPX was used for mounting and images were captured under a Leica brightfield microscope in 20x and 40x magnification and analyzed using Fiji-ImageJ software [22].

2.3.2F. Statistical Analysis

IBM SPSS25 Statistics software was used for statistical analysis of the clinical records and to prepare the frequency table and cross-tabulation for the Chi-square test. Receiver-operating characteristic curve (ROC) and Cox regression analysis were also performed using this software. Image analysis was performed using Fiji-ImageJ Software https://imagej.net/Fiji. The graphs of expression status in the clinical images were prepared using GraphPad Prism software (Version 5). Flow cytometry analysis was performed using FCS Express7 software. P value <0.001 and <0.05 was considered statistically significant.

2.4. Results

2.4.1. Analysis of the prevalence of clinicopathological attributes of OvCa patients' cohort

A total of N=248 case records have been found eligible to be included in the study. Table 2 comprises the frequency distribution of the clinicopathological data of the OvCa patients. The age group 41-60 years experienced the maximum incidence of OvCa. OvCa was prevalent in patients with a BMI ≥25 kg/sq.m (overweight and obese patients). 56.9% of the patients had higher CEA levels (≥5 ng/ml). To understand the prevalence of CA-125 levels in the patients and were categorized under four groups. The lowest number of patients had lower CA-125 (≤35 U/ml). 39.9% were under the sub-category 35.1-499.9 U/ml range. 68.5% of patients had CA 19.9 level greater than ≥28 U/ml and the remaining were below this level. Most of the patients had high ascites levels, with 50% of the patients showing ascites malignancy leading to poor survival. 41.5% of the patients experienced pelvic dissemination (PD), the majority (50%) being poorly differentiated cancer tissues. 93.5% of the cases were epithelial form and the remaining were non-epithelial. Most of the patients were observed to be diagnosed at stage III, which is considered to be an advanced stage. As per TNM grading, the T3 stage with involvement of both the ovaries and peritoneal metastasis was highest along 36.3% with regional lymph node metastasis (N1) and in 42.7% of patients, distant metastasis (DM) was not observed (Mx). Unilateral tumor was more prevalent (62.9%) and tumor size less than <5*5*5 ccm (63.7%) was higher in number.

Table 2. Frequency profiles of clinicopathological parameters assessed in the study subjects.

Clinicopathological parameters	**Frequency (N)**	**Percentages (%)**
Age		
≤18	6	2.4
19-40	53	21.4
41-60	136	54.8
>60	53	21.4
BMI		
Underweight	25	10.1
Normal	96	38.7
Overweight/Obese	127	51.2

Clinicopathological parameters	**Frequency (N)**	**Percentages (%)**
CEA (ng/ml)		
<5	107	43.1
≥5	141	56.9
CA-125 (U/ml)		
≤35	30	12.1
35.1-499.9	99	39.9
500-999.9	49	19.9
≥1000	70	28.2
CA 19.9 (U/ml)		
<28	78	31.5
≥28	170	68.5
Ascites level		
High	97	39.1
Moderate	83	33.5
Low	68	27.4
Ascites malignancy		
Negative	112	45.2
Positive	136	54.8
Degree of dissemination		
Pelvic Dissemination (PD)	103	41.5
Distant Metastasis (DM)	55	22.2
Localized	90	36.3
Tumor differentiation		
Well differentiated	59	23.8
Moderately differentiated	65	26.2
Poorly differentiated	124	50
Tumor type		
Epithelial	232	93.5
Non-epithelial	16	6.5

Clinicopathological parameters	Frequency (N)	Percentages (%)
FIGO stage		
I	58	23.4
II	65	26.2
III	72	29
IV	53	21.4
T stage		
T1	58	23.4
T2	82	33.1
T3	108	43.5
N stage		
N0	83	33.5
Nx	75	30.2
N1	90	36.3
M stage		
M0	81	32.7
Mx	106	42.7
M1	61	24.6
Laterality		
Unilateral	156	62.9
Bilateral	92	37.1
Tumor Size (ccm)		
<5*5*5	158	63.7
≥5*5*5	90	36.3

2.4.2. CA-125 level is associated with clinicopathological parameters

The distribution of the clinicopathological attributes in the patients' cohort with respect to the CA-125 levels recorded at the time of diagnosis has been represented in Table 3 where CA-125 levels were categorized into low (≤35 U/ml) and high (>35 U/ml). The high level was further subcategorized into 35.1-499.9, 500-999.9, ≥1000 U/ml sections. A significant correlation was observed with all the factors except with age (P = 0.1968), CEA (P = 0.0610) and CA-19.9 (P = 0.0836).

Table 3. Association of CA-125 levels with clinicopathological parameters.

Clinicopathological parameters	**CA-125 (U/ml)**				**χ^2**	**P value**
	Low	High				
	≤35	35.1-499.9	500-999.9	≥1000		
Age						
<18	1	3	2	0	12.3	0.1968
19-40	8	28	9	8		
41-60	13	50	29	44		
>60	8	18	9	18		
BMI						
Underweight	2	11	3	9	15.73	0.0153
Normal	14	49	17	16		
Overweight/Obese	14	39	29	45		
CEA (ng/mL)						
<5	14	52	17	24	7.369	0.061
≥5	16	47	32	46		
CA 19.9 (U/mL)						
<28	6	40	13	19	6.658	0.0836
≥28	24	59	36	51		
Ascites level						
High	0	15	25	57	135.7	<0.0001
Moderate	5	46	19	13		
Low	25	38	5	0		
Ascites malignancy						
Positive	1	39	33	63	79.71	<0.0001
Negative	29	60	16	7		
Degree of dissemination						
Pelvic Dissemination	3	40	29	31	108.3	<0.0001
Distant Metastasis	0	7	13	35		
Localized	27	52	7	4		
Tumor differentiation						

Clinicopathological parameters	**CA-125 (U/ml)**				**χ^2**	**P value**
Well differentiated	21	32	4	2		
Moderately differentiated	9	34	13	9	94.56	<0.0001
Poorly differentiated	0	33	32	59		
Tumor type						
Epithelial	24	92	46	70	14.02	0.0029
Non-epithelial	6	7	3	0		
FIGO stage						
I	21	32	3	2	114.2	<0.0001
II	9	34	13	9		
III	0	26	22	24		
IV	0	7	11	35		
T stage						
T1	22	31	3	2	87.55	<0.0001
T2	8	39	14	21		
T3	0	29	32	47		
N stage						
N0	15	38	16	14	34.97	<0.0001
Nx	14	35	10	16		
N1	1	26	23	40		
M stage						
M0	13	31	19	18	53.25	<0.0001
Mx	17	58	14	17		
M1	0	10	16	35		
Laterality						
Unilateral	28	69	24	35	22.93	<0.0001
Bilateral	2	30	25	35		
Tumor size (ccm)						
<5*5*5	3	52	39	64	71.4	<0.0001
≥5*5*5	27	47	10	6		

2.4.3. Elevated SIRT1 expression strongly correlates with higher HIF-1α expression in OvCa tissues

In order to understand the association of SIRT1 with HIF-1α as hypoxic condition prevails in the TME and SIRT1 is the downstream target of HIF-1α, we have analyzed the expression of the markers in the tumor tissues and compared it with the expression in the adjacent normal tissues. We have surprisingly observed that the expression of both SIRT1 and HIF-1α were significantly higher in the tumor tissues and compared to the normal ones (Figure 1A-J), which validates an association of the metabolic biomarker, SIRT1 and hypoxia marker HIF-1α. Thus, it can be deduced that hypoxic TME regulates SIRT1 expression, which in turn plays a pivotal role in cell proliferation and disease progression.

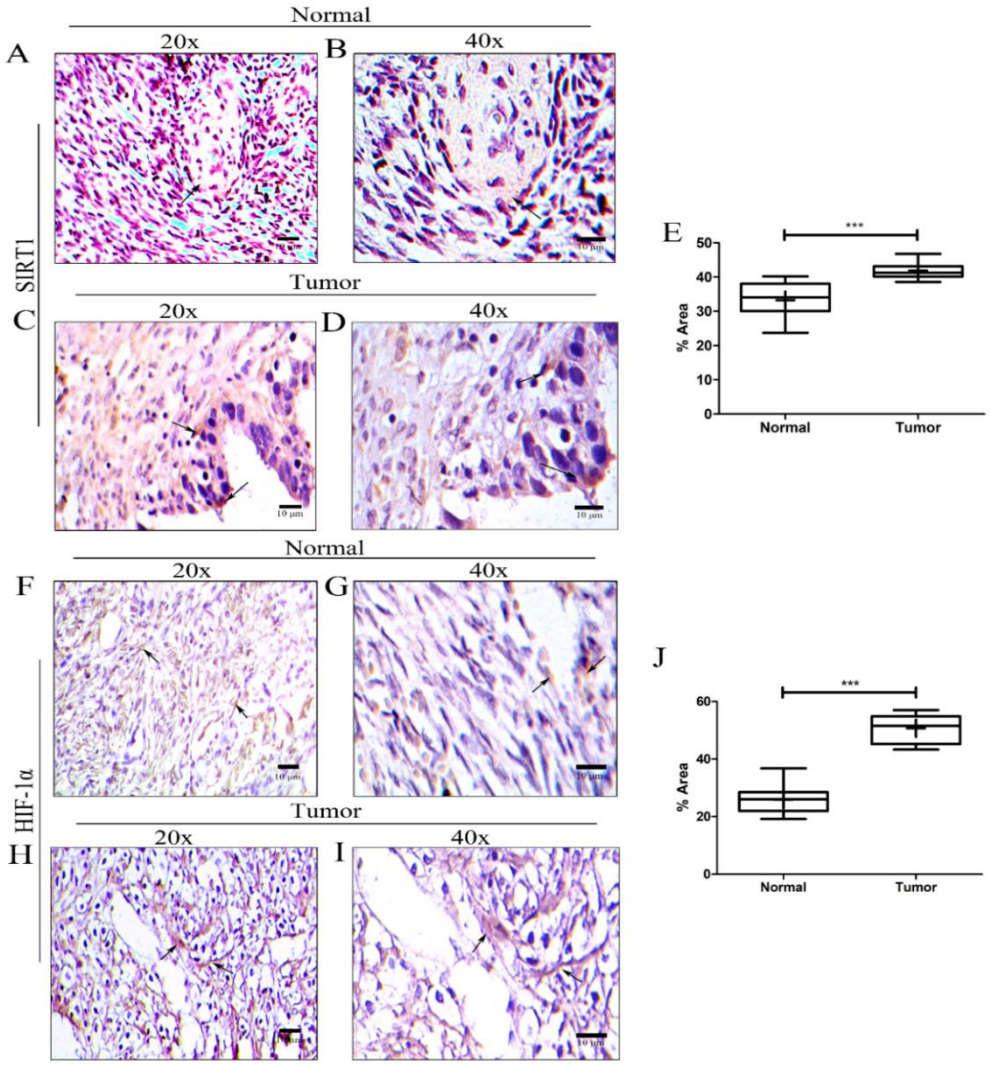

Figure 1. A-D. SIRT1 expression in normal and tumor ovarian tissues; E. Graphical representation of SIRT1 expression; F-I. HIF-1α expression in normal and tumor ovarian tissues; J. Graphical representation of HIF-1α expression. (*P<0.05, **P<0.01, ***P<0.001, ****P<0.0001)

2.4.4. Greater secretion of exosomes is induced by SIRT1 overexpression in hypoxic TME

IHC analysis of exosomal marker CD81 in the tumor tissues and the adjacent normal, revealed its higher expression in the tumor tissues as compared to the normal tissues (Figures 2A-E). Additionally, the expression of CD63 in the cancer cells was significantly more as normal cells (Figure 2F). This depicted that SIRT1 overexpression in hypoxic tumor milieu modulates the exosomal secretion which in turn promotes the migration of the cancer cells by creating a suitable niche for the cancer cells for their survival.

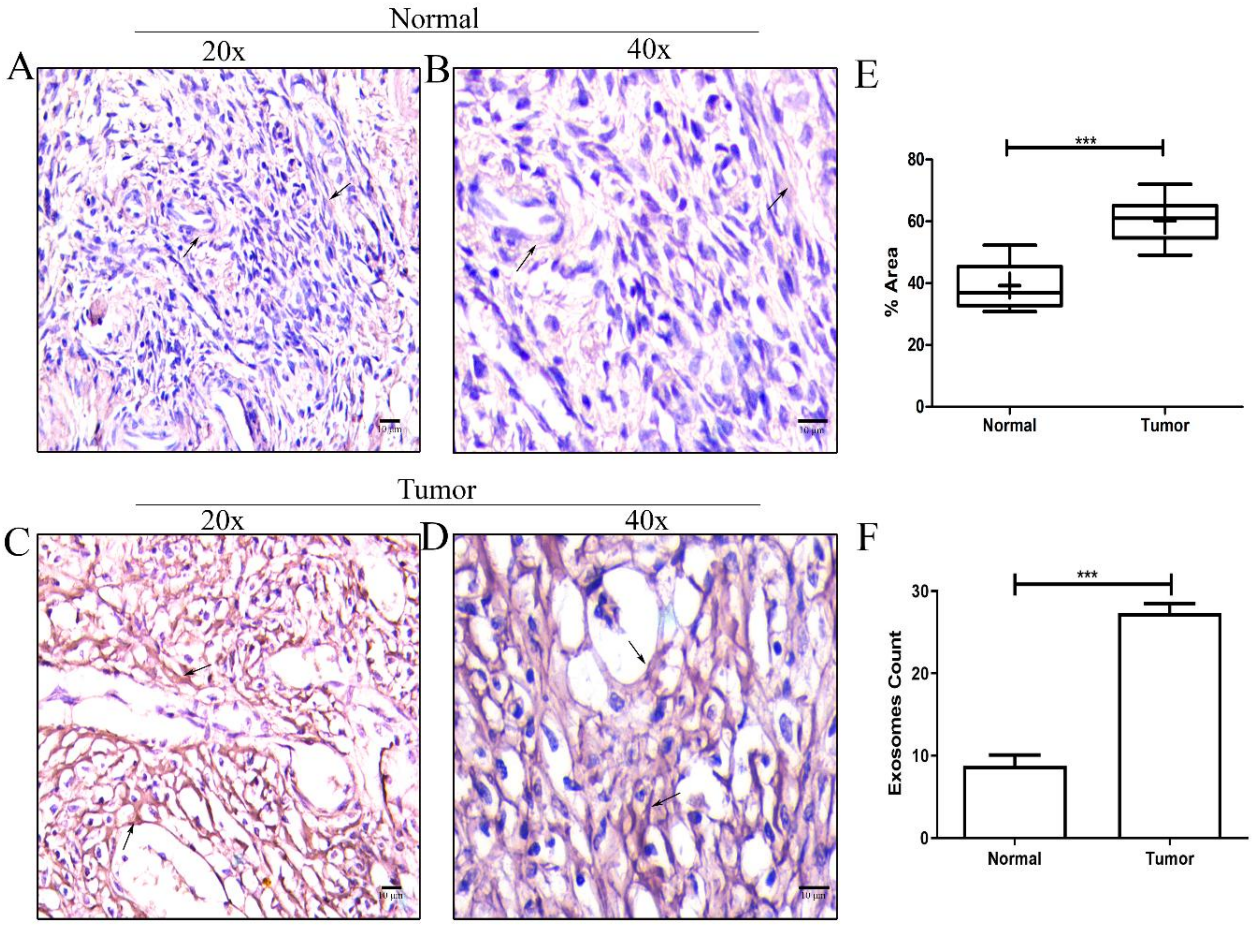

Figure 2. A-D. CD81 expression in normal and tumor ovarian tissues (20x); E. Graphical representation of CD81 expression; F. Graphical representation of CD63 in normal and tumor tissues analyzed by flow cytometry. (*P<0.05, **P<0.01, ***P<0.001, ****P<0.0001)

2.4.5. Proliferation of cancer cells is influenced by overexpressed SIRT1 under higher exosomal load

Upon analyzing the expression of proliferation marker Ki-67 by IHC, we observed its higher expression in the cancer tissues as compared to the adjacent normal tissues (Figure 3A-E).

This indicated that abnormal levels of SIRT1 regulate the proliferation rate of the cancer cells by increasing Ki-67 expression, which is additionally fuelled by elevated concentrations of exosomes in the tumor milieu and eventually promotes metastasis.

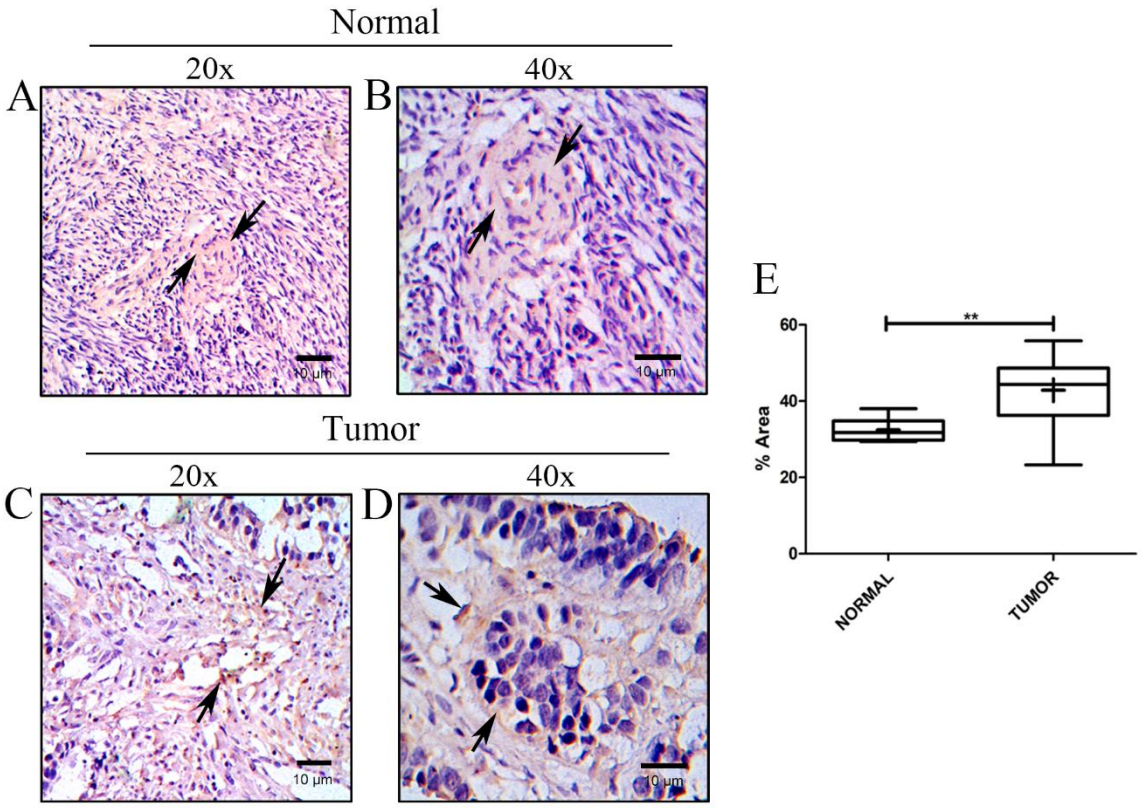

Figure 3. A-D. Ki-67 expression in normal and tumor ovarian tissues; E. Graphical representation of Ki-67 expression. (*P<0.05, **P<0.01, ***P<0.001, ****P<0.0001)

2.4.6. Glycogen deposition in OvCa tissues is regulated by overexpressed SIRT1

PAS staining of the tumor tissues and normal tissues depicted significantly higher deposition of glycogen in the tumor tissues compared to the normal ones (Figures 4A-E). This depicted that greater deposition of glycogen in the tissues supply nutrient for the proliferating cancer cells in nutrient deficient TME and being a storage of glucose molecules enhances the glycolysis in the cancer cells to supply with energy for the growth of the cancer cells. Thus, in the hypoxic TME overexpressed SIRT1 also modulates the glycogen deposition aiding the cancer cells to survive in the TME.

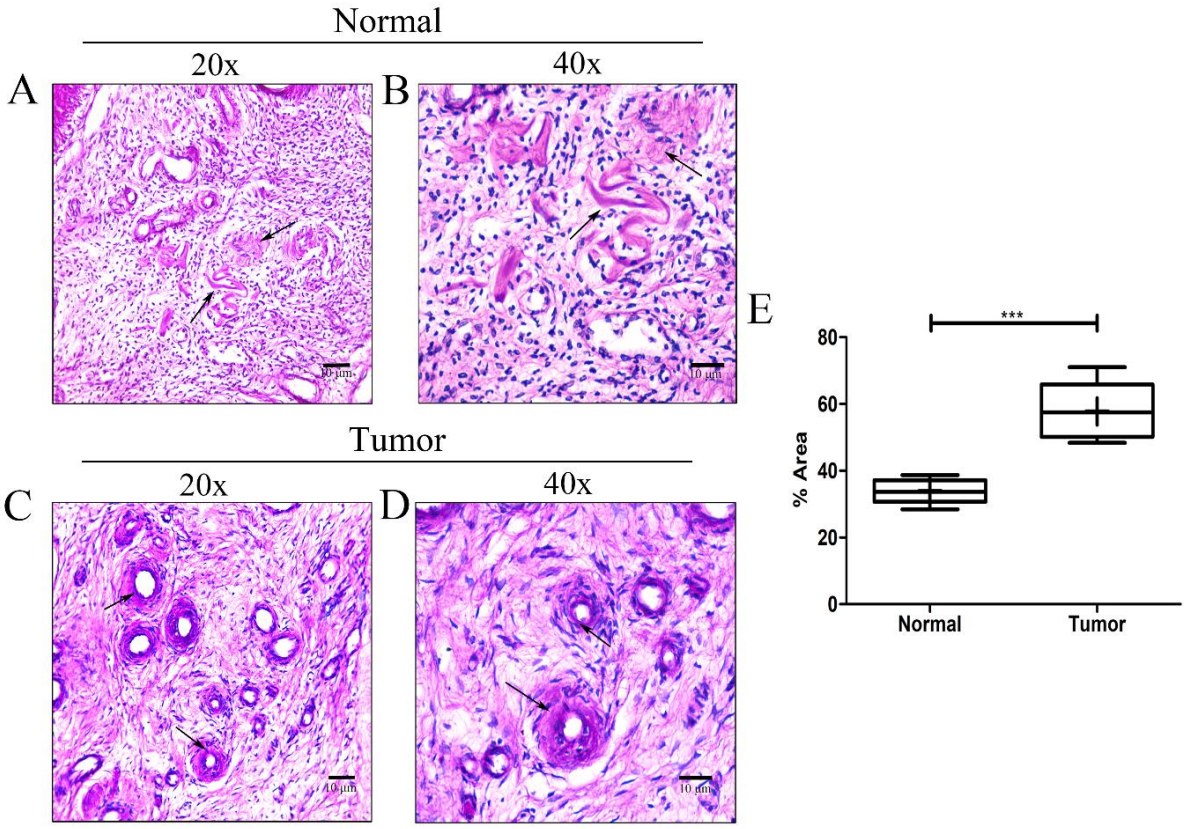

Figure 4. A. Glycogen deposition in normal and tumor ovarian tissues; E. Graphical representation of glycogen deposition. (*P<0.05, **P<0.01, ***P<0.001, ****P<0.0001)

2.4.7. Overall survival is linked with the clinicopathological parameters

The ROC curve of CA-125 (Figure 5A) revealed area under curve (AUC) to be 0.719 which was statistically significant with 327.7 U/ml of CA-125 as the best cut off point (Sensitivity = 82.4%; Specificity = 52.3%). Kaplan-Meier plots upon log rank test revealed OS of CA-125 ($\chi 2 = 26.841$) was significant along with and BMI ($\chi 2 = 13.473$), degree of dissemination ($\chi 2 = 85.033$) and ascites malignancy ($\chi 2 = 45.042$) as represented in Figure 5C-E. 18.780 months with 95% CI 17.754 - 19.805 was depicted to be the overall mean survival time for all the factors.

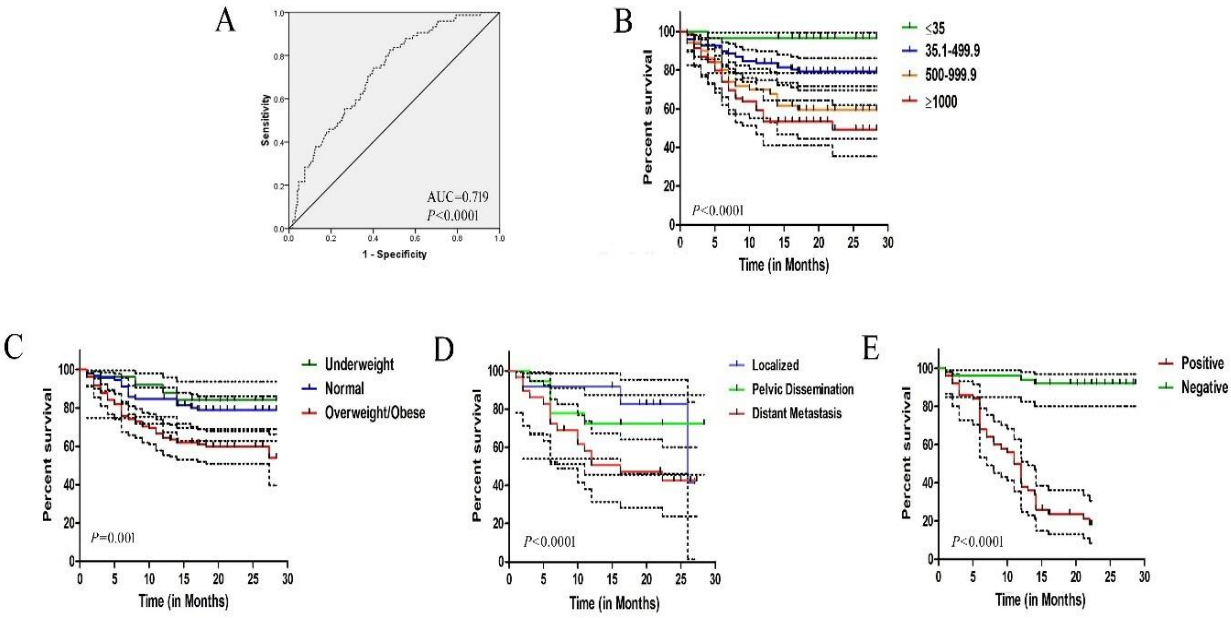

Figure 5. A. ROC curve of CA-125; B. OS graph of CA-125; C. OS graph of BMI; D. OS graph of degree of dissemination; E. OS graph of ascites malignancy. (*P<0.05, **P<0.01, ***P<0.001, ****P<0.0001)

2.4.8. Association of clinicopathological parameters as risk factors in the survival of OvCa patients

Multivariate Cox regression analysis of BMI, ascites malignancy, degree of dissemination, tumor differentiation, FIGO stage, tumor size and the tumor marker CA-125 revealed that BMI [Hazard ratio (HR) 1.759; 95% confidence interval (CI) 1.156 - 2.677; P=0.008], ascites malignancy [HR 0.336; 95% CI 0.124 - 0.911; P=0.032] and degree of dissemination [HR 1.994; 95% CI 1.251 - 3.178; P=0.004] are independent predictors of the OS of the OvCa patients (Table 4).

Table 4. Multivariate Cox regression analysis of clinicopathological parameters on OS.

Clinicopathological parameters	Overall survival			
	P value	HR	95% CI	
			Lower	Upper
BMI	0.008	1.759	1.156	2.677
Ascites level	0.158	0.616	0.315	1.206
Ascites malignancy	0.032	0.336	0.124	0.911
Degree of dissemination	0.004	1.994	1.251	3.178
Tumor differentiation	0.278	2.052	0.559	7.523
Tumor type	0.960	0.000	0.000	4.006E+185
FIGO stage	0.842	1.074	0.531	2.172
T stage	0.223	0.664	0.343	1.284
N stage	0.068	1.378	0.977	1.945
M stage	0.837	0.959	0.642	1.433
Laterality	0.650	1.123	0.681	1.850
Tumor size (ccm)	0.392	0.594	0.180	1.959

2.5. Discussion

Despite multiple advances in treatment strategies, improvement in the survival of patients remains a challenge to the clinicians thus early diagnosis of OvCa is an absolute necessity. The survival of the patients remains compromised despite CA-125 serving as an effective diagnostic marker. In this context, an early detection technique for the patients is required for better survival. In this research work, a correlation between CA-125 and clinicopathological characteristics was established which revealed a significant relation. This provided us the lead in targeting important targets specifically related to metabolism like BMI, degree of dissemination, etc. as they affect the survival of the patients. Thus, upon observing this, we have investigated the expression of SIRT1, HIF-1α, Ki-67, glycogen deposition level, exosomal burden, which provided a preliminary idea for planning the treatment regimen by targeting them at the diagnostic level. To establish these molecules as effective biomarkers for OvCa further research is needed.

To facilitate rapid proliferation rate and invasion, metabolic reprogramming plays a crucial role in the process. Approximately 39 metabolically altered genes have been

identified that were significantly correlated with the prognosis of OvCa, thus indicating the upliftment in the research on energy metabolism [23]. SIRT1, a class III histones deacetylases (HDACs), is considered the key metabolic regulator. SIRT1 is reported to deacetylate histidine triad nucleotide-binding protein (HINT) 1 and thereby increase tumor suppressive function by binding to microphthalmia transcription factor (MITF) and HINT by enhancing its boing efficacy to β-catenin in colon cancer and melanoma [24]. In lung adenocarcinoma, SIRT1 promotes oncogenicity by inducing the rapid growth and survival of the cancer cells [25]. NAD+ serves as a crucial substrate for the modulatory activity of SIRT1 as its functionality is regulated by cellular levels of NAD+/NADH [26]. Previous studies suggested that cancer stem cells like characteristics are conferred to the OvCa cells in the hypoxic milieu of OvCa by upregulated expression of SIRT1 under the effect of HIF-1α [27]. Additionally, in poorly differentiated serous OvCa, HIF-1α is an established expression prognostic marker [28]. Interestingly, our results also revealed an elevated expression of HIF-1α in the OvCa tissues which might regulate the expressional status of SIRT1 which in turn regulate the level of glycogen deposition in the cancer cells [29]. Meanwhile it is also reported that the exosomal secretion is more under the hypoxic conditions which in turn enhance the aggressiveness of the prostate cancer cells [30]. The validation of the association of SIRT1 overexpression with CA-125 in OvCa was established by two interlinking studies where it was shown that exponential cell growth is related with higher levels of CA-125 production. Furthermore, the inhibition of cell cycle of cell cycle by cycloheximide decreased the exponential cell growth as well as CA-125 release from the cancer cells [31]. Moreover, the secretory levels of CA-125 are dependent upon the epidermal growth factor receptor (EGFR) signaling cascade of the cancer cells and are phosphorylated and cleaved by extracellular protease before its release from the cells [32][33]. Furthermore, an interconnected association between SIRT1, EGFR and BRCA1 axis with their higher expressions is deduced in promoting cisplatin resistance OvCa cells [34]. Under this doctrine, our hypothesis that elevated SIRT1 expression regulates the CA-125 secretion levels from OvCa is validated. Thus, analyzing the SIRT1 levels at the diagnostic levels can also serve as a metabolic biomarker in OvCa.

Furthermore, an association between SIRT1 and exosomes secretion is established by *Latfikar et al.* in BC where elevated SIRT1 expression minimizes the release rate of exosomes thus playing a tumor suppressive role in BC [35]. In OvCa, SIRT1 regulates the exosomes secretion in relation to elevated levels of CA-125 [36]. However, as per our findings in OvCa, we can deduce that SIRT1 modulates the exosomal secretion to be higher,

thus performing a tumor promotive function in OvCa as observed by higher expression of exosomal marker in the tumor tissues as compared to the adjacent normal [37]. The relation of greater exosomal load with higher levels of CA-125 is further validated by finding where OvCa diagnostic efficacy is enhanced by evaluating the levels of exosomal CA-125 [38]. This finding further confirms that a greater concentration of exosomes is associated with higher CA-125 levels. Indeed, the CA-125 synthesized by the epithelial cells [39] and during cargo loading gets incorporated in the exosomes and is eventually released by the cancer cells via exosomes. Therefore, it could be concluded that under hypoxic conditions, the expression of SIRT1 is enhanced, which in turn influences the secretory levels of exosomes that release CA-125 at an increased level as exosomal cargo. Moreover, CA-125 bearing exosomal context can be established as a biomarker for OvCa even after the patients have undergone treatment since it is reported that a 5 U/ml increase of CA-125 within the normal limits, after the treatment, is associated with both relapse and survival of OvCa patients [40]. Moreover, analysis of exosomal load in patients' blood can be highly important as a potent biomarker for OvCa [41].

Apart from being a detection biomarker, SIRT1-mediated energy metabolism and metastasis in OvCa patients are also driven by exosomes. In TME, the exosomes impart metastatic potential to the recipient cells upon internalization of the exosomes [42]. Exosome cargoes are also involved in energy metabolism as evident from exosomal miR-122 released by BC cells initiates metastasis by altering glucose metabolism in PMN thereby supplying resources for the survival of the BC cells [43]. In CRC, exosomal content from hypoxic tumor cells transfers aggressiveness phenotype to the recipient normoxic cells [44]. *Abdough et al.* reported exosomes isolated from the sera of cancer patients delivered malignant characteristics to onco-suppressor mutated cells by revealing 85-90% Ki-67 positive OvCa cells along with other malignant markers like PAX8, WT1 etc., [45]. This demonstrates metastasis in OvCa is augmented by the transfer of exosomal Ki-67 content into the recipient cells which further confirms our hypothesis that with increasing exosomal content, the Ki-67 expression also gets elevated.

Among the risk factors in OvCa progression, obesity is also a crucial one thus investigating the metabolic alterations that augment obesity is essential to establish targeted potential therapy. An investigation inferred that obesity and OvCa are interlinked as obese people have an altered metabolic status that demonstrates an increased risk of the disease accompanied by a higher yield of CA-125 secretion [46]. A higher demand for glucose is

required by cancer cells to survive in TME. In our study, a higher glycogen deposition in the cancer tissues was observed, thereby serving as the reservoir of glucose for higher glycolysis in the cancer cells. Glucose metabolic flux in human adipocytes leading to glycogen deposition is well established in obese conditions [47]. Additionally, HIF-1α induced hypoxia has been reported to promote glycogen deposition in human ovarian clear cell carcinoma cells [29]. While these findings are significant, additional work must be done to further evaluate these biomarkers associated with metabolic changes in OvCa. Finally, all the clinicopathological parameters considered in the study are related to the OvCa patients' study which can ease the path of analyzing the disease. For instance, moderately to poorly differentiated OvCa cells were mostly observed in the later stages and associated with a significant risk of poor prognosis [48]. The schematic of the underlying mechanism of action is represented in Figure 6.

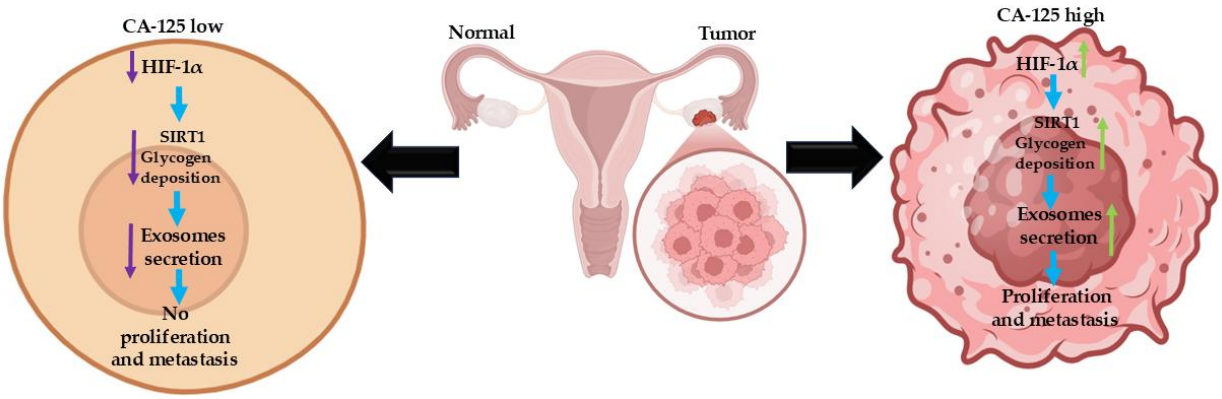

Figure 6. Schematic of the synergistic roles performed by metabolic and metastatic factors and mechanism of action

CA-125 can be a prognostic factor for OvCa patients as most of the clinicopathological parameters were significantly linked with distinct levels of CA-125. Based on the data obtained from IHC reports, we propose that due to the hypoxic milieu induced by upregulated HIF-1α, expression of SIRT1 is elevated, leading to the enhanced levels of exosomes in TME correlated with promoting a larger accumulation of glycogen in the tumor tissues as compared with those in normal tissues. Based on the analysis in this study, the correlation of serum biomolecule CA-125 with clinicopathological factors has given an initial lead in our research to study the biomolecules responsible for establishing new targets for OvCa treatment.

2.6. References

[1] H. Pant, A. Prakash, R. Khandelwal, S. Pandey, Correlation of serum CA-125 with histopathological findings in ovarian tumors, IP J. Diagnostic Pathol. Oncol. 4 (2019) 81–85. https://doi.org/10.18231/j.jdpo.2019.016.

[2] D.R. Bhagora, D.R. Malik, D.V.K. Trichal, Expression of estrogen receptor, progesterone receptor and KI 67 in epithelial ovarian tumors and their histopathological correlation, Int. J. Med. Res. Rev. 5 (2017) 554–561. https://doi.org/10.17511/ijmrr.2017.i06.03.

[3] K.K. Wong, K.H. Lu, A. Malpica, D.C. Bodurka, H.S. Shvartsman, R.E. Schmandt, A.D. Thornton, M.T. Deavers, E.G. Silva, D.M. Gershenson, Significantly greater expression of ER, PR, and ECAD in advanced-stage low-grade ovarian serous carcinoma as revealed by immunohistochemical analysis, Int. J. Gynecol. Pathol. 26 (2007) 404–409. https://doi.org/10.1097/pgp.0b013e31803025cd.

[4] D. Hanahan, R.A. Weinberg, Hallmarks of cancer: the next generation, Cell. 144 (2011) 646–674. https://doi.org/10.1016/J.CELL.2011.02.013.

[5] L.M. Phan, S.C.J. Yeung, M.H. Lee, Cancer metabolic reprogramming: importance, main features, and potentials for precise targeted anti-cancer therapies, Cancer Biol. Med. 11 (2014) 1–19. https://doi.org/10.7497/j.issn.2095-3941.2014.01.001.

[6] C.Y. Han, D.A. Patten, R.B. Richardson, M.E. Harper, B.K. Tsang, Tumor metabolism regulating chemosensitivity in ovarian cancer, Genes and Cancer. 9 (2018) 155–175. https://doi.org/10.18632/genesandcancer.176.

[7] G. Bergers, S.M. Fendt, The metabolism of cancer cells during metastasis, Nat. Rev. Cancer. 21 (2021) 162. https://doi.org/10.1038/S41568-020-00320-2.

[8] O. Warburg, On the origin of cancer cells, Science. 123 (1956) 309–314. https://doi.org/10.1126/SCIENCE.123.3191.309.

[9] J.R.P. Knight, J. Milner, SIRT1, metabolism and cancer., Curr. Opin. Oncol. 24 (2012) 68–75. https://doi.org/10.1097/cco.0b013e32834d813b.

[10] E. Yang, X. Wang, Z. Gong, M. Yu, H. Wu, D. Zhang, Exosome-mediated metabolic reprogramming: the emerging role in tumor microenvironment remodeling and its

influence on cancer progression, Signal Transduct. Target. Ther. 5 (2020) 242. https://doi.org/10.1038/s41392-020-00359-5.

[11] K. Nakamura, K. Sawada, M. Kobayashi, M. Miyamoto, A. Shimizu, M. Yamamoto, Y. Kinose, T. Kimura, Role of the exosome in ovarian cancer progression and its potential as a therapeutic target, Cancers (Basel). 11 (2019) 1147. https://doi.org/10.3390/cancers11081147.

[12] K. Ohshima, E. Morii, Metabolic reprogramming of cancer cells during tumor progression and metastasis, Metabolites. 11 (2021) 28. https://doi.org/10.3390/metabo11010028.

[13] B. Faubert, A. Solmonson, R.J. DeBerardinis, Metabolic reprogramming and cancer progression, Science (80-.). 368 (2020) eaaw5473. https://doi.org/10.1126/science.aaw5473.

[14] T. Khan, M.A. Sullivan, J.H. Gunter, T. Kryza, N. Lyons, Y. He, J.D. Hooper, Revisiting Glycogen in Cancer: A Conspicuous and Targetable Enabler of Malignant Transformation, Front. Oncol. 10 (2020) 592455. https://doi.org/10.3389/fonc.2020.592455.

[15] R.R. Chen, M.M.H. Yung, Y. Xuan, S. Zhan, L.L. Leung, R.R. Liang, T.H.Y. Leung, H. Yang, D. Xu, R. Sharma, K.K.L. Chan, S.F. Ngu, H.Y.S. Ngan, D.W. Chan, Targeting of lipid metabolism with a metabolic inhibitor cocktail eradicates peritoneal metastases in ovarian cancer cells, Commun. Biol. 2 (2019) 281. https://doi.org/10.1038/s42003-019-0508-1.

[16] A. Fadaka, B. Ajiboye, O. Ojo, O. Adewale, I. Olayide, R. Emuowhochere, Biology of glucose metabolization in cancer cells, J. Oncol. Sci. 3 (2017) 45–51. https://doi.org/10.1016/j.jons.2017.06.002.

[17] B. Muz, P. de la Puente, F. Azab, A.K. Azab, The role of hypoxia in cancer progression, angiogenesis, metastasis, and resistance to therapy, Hypoxia. 3 (2015) 83–92. https://doi.org/10.2147/hp.s93413.

[18] C. Shao, F. Yang, S. Miao, W. Liu, C. Wang, Y. Shu, H. Shen, Role of hypoxia-induced exosomes in tumor biology, Mol. Cancer. 17 (2018) 120. https://doi.org/10.1186/s12943-018-0869-y.

[19] M. Khushman, A. Bhardwaj, G.K. Patel, J. Ariel, K. Roveda, M.C. Tan, M.C. Patton, S. Singh, W. Taylor, A.P. Singh, Exosomal Markers (CD63 and CD9) Expression Pattern Using Immunohistochemistry in Resected Malignant and Non- malignant Pancreatic Specimens, Pancreas. 46 (2017) 782–788. https://doi.org/10.1097/MPA.0000000000000847.Exosomal.

[20] S.K. Yeo, X. Zhu, T. Okamoto, M. Hao, C. Wang, P. Lu, L.J. Lu, J.L. Guan, Single-cell RNA-sequencing reveals distinct patterns of cell state heterogeneity in mouse models of breast cancer, Elife. 9 (2020) e58810. https://doi.org/10.7554/ELIFE.58810.

[21] C.I.M. Baeten, J. Wagstaff, I.C.L. Verhoeven, H.F.P. Hillen, A.W. Griffioen, Flow cytometric quantification of tumour endothelial cells; an objective alternative for microvessel density assessment, Br. J. Cancer. 87 (2002) 344–347. https://doi.org/10.1038/sj.bjc.6600457.

[22] N. Chatterjee, S. Das, D. Bose, S. Banerjee, T. Jha, K. Das Saha, Leishmanial lipid affords protection against oxidative stress induced hepatic injury by regulating inflammatory mediators and confining apoptosis progress, Toxicol. Lett. 232 (2015) 499–512. https://doi.org/10.1016/j.toxlet.2014.11.023.

[23] L. Wang, X. Li, Identification of an energy metabolism-related gene signature in ovarian cancer prognosis, Oncol. Rep. 43 (2020) 1755–1770. https://doi.org/10.3892/or.2020.7548.

[24] T.Y. Jung, G.R. Jin, Y. Bin Koo, M.M. Jang, C.W. Kim, S.Y. Lee, H. Kim, C.Y. Lee, S.Y. Lee, B.G. Ju, H.S. Kim, Deacetylation by SIRT1 promotes the tumor-suppressive activity of HINT1 by enhancing its binding capacity for β-catenin or MITF in colon cancer and melanoma cells, Exp. Mol. Med. 52 (2020) 1075–1089. https://doi.org/10.1038/s12276-020-0465-2.

[25] X. Chen, D. Hokka, Y. Maniwa, C. Ohbayashi, T. Itoh, Y. Hayashi, Sirt1 is a tumor promoter in lung adenocarcinoma, Oncol. Lett. 8 (2014) 387–393. https://doi.org/10.3892/ol.2014.2057.

[26] X. Li, SIRT1 and energy metabolism, Acta Biochim Biophys Sin. 45 (2013) 51–60. https://doi.org/10.1093/abbs/gms108.Review.

[27] J. Qin, Y. Liu, Y. Lu, M. Liu, M. Li, J. Li, L. Wu, Hypoxia-inducible factor 1 alpha promotes cancer stem cells-like properties in human ovarian cancer cells by upregulating SIRT1 expression, Sci. Rep. 7 (2017) 10592. https://doi.org/10.1038/s41598-017-09244-8.

[28] A. Daponte, M. Ioannou, I. Mylonis, G. Simos, M. Minas, I.E. Messinis, G. Koukoulis, Prognostic significance of hypoxia-inducible factor 1 alpha(HIF-1alpha) expression in serous ovarian cancer: An immunohistochemical study, BMC Cancer. 8 (2008) 335. https://doi.org/10.1186/1471-2407-8-335.

[29] Y. Iida, K. Aoki, T. Asakura, K. Ueda, N. Yanaihara, S. Takakura, K. Yamada, A. Okamoto, T. Tanaka, K. Ohkawa, Hypoxia promotes glycogen synthesis and accumulation in human ovarian clear cell carcinoma, Int. J. Oncol. 40 (2012) 2122–2130. https://doi.org/10.3892/ijo.2012.1406.

[30] G.K. Panigrahi, P.P. Praharaj, T.C. Peak, J. Long, R. Singh, J.S. Rhim, Z.Y.A. Elmageed, G. Deep, Hypoxia-induced exosome secretion promotes survival of African-American and Caucasian prostate cancer cells, Sci. Rep. 8 (2018) 3853. https://doi.org/10.1038/s41598-018-22068-4.

[31] N.L. E P Beck , A Moldenhauer, E Merkle, F Kiesewetter, W Jäger, L Wildt, CA 125 production and release by ovarian cancer cells in vitro, Int. J. Biol. Markers. 13 (1998) 200–6. https://pubmed.ncbi.nlm.nih.gov/10228901/ (accessed February 25, 2022).

[32] I. Konishi, J.L. Fendrick, T.H. Parmley, J.G. Quirk, T.J. O'brien, Epidermal Growth Factor Enhances Secretion of the Ovarian Tumor-Associated Cancer Antigen CA125 From the Human Amnion WISH Cell Line, J. Soc. Gynecol. Investig. 1 (1994) 89–96. https://doi.org/10.1177/107155769400100118.

[33] T.J. O'Brien, J.B. Beard, L.J. Underwood, R.A. Dennis, A.D. Santin, L. York, The CA 125 gene: An extracellular superstructure dominated by repeat sequences, Tumor Biol. 22 (2001) 348–366. https://doi.org/10.1159/000050638.

[34] D. Li, Q.J. Wu, F.F. Bi, S.L. Chen, Y.M. Zhou, Y. Zhao, Q. Yang, Effect of the BRCA1-SIRT1-EGFR axis on cisplatin sensitivity in ovarian cancer, Am. J. Transl. Res. 8 (2016) 1601–1608.

[35] A. Latfikar, L. Ling, A. Hingorani, E. Johansen, A. Clement, Loss of Sirtuin 1 Alters the Secretome of Breast Cancer Cells by Impairing Lysosomal Integrity, Dev. Cell. 49 (2019) 393–408. https://doi.org/10.1016/j.devcel.2019.03.011.Loss.

[36] S. Roy, A. Das, M. Vernekar, S. Mandal, N. Chatterjee, Understanding the Correlation between Metabolic Regulator SIRT1 and Exosomes with CA-125 in Ovarian Cancer: A Clinicopathological Study, Biomed Res. Int. 2022 (2022) 5346091. https://doi.org/10.1155/2022/5346091.

[37] D.H. Mvunta, T. Miyamoto, R. Asaka, Y. Yamada, H. Ando, S. Higuchi, K. Ida, H. Kashima, T. Shiozawa, Overexpression of SIRT1 is Associated with Poor Outcomes in Patients with Ovarian Carcinoma, Appl. Immunohistochem. Mol. Morphol. 25 (2017) 415–421. https://doi.org/10.1097/PAI.0000000000000316.

[38] Z. Chen, Q. Liang, H. Zeng, Q. Zhao, Z. Guo, R. Zhong, M. Xie, X. Cai, J. Su, Z. He, L. Zheng, K. Zhao, Exosomal CA125 as A promising biomarker for ovarian cancer diagnosis, J. Cancer. 11 (2020) 6445–6453. https://doi.org/10.7150/jca.48531.

[39] P. Bischof, What do we know about the origin of CA 125?, Eur. J. Obstet. Gynecol. Reprod. Biol. 49 (1993) 93–98. https://doi.org/10.1016/0028-2243(93)90131-U.

[40] S. Piatek, G. Panek, Z. Lewandowski, M. Bidzinski, D. Piatek, P. Kosinski, M. Wielgos, Rising serum CA-125 levels within the normal range is strongly associated recurrence risk and survival of ovarian cancer, J. Ovarian Res. 13 (2020) 102. https://doi.org/10.1186/s13048-020-00681-0.

[41] M.K.S. Tang, A.S.T. Wong, Exosomes: Emerging biomarkers and targets for ovarian cancer, Cancer Lett. 367 (2015) 26–33. https://doi.org/10.1016/j.canlet.2015.07.014.

[42] W. Tian, S. Liu, B. Li, Potential Role of Exosomes in Cancer Metastasis, Biomed Res. Int. 2019 (2019) 4649705. https://doi.org/10.1155/2019/4649705.

[43] F.M. Y., Z. Weiying, L. L, A. AY, C. M, A. J, C. A, O. ST, L. S, C. AR, S. G., Breast cancer-secreted miR-122 reprograms glucose metabolism in pre-metastatic niche to promote metastasis, Nat. Cell Biol. 17 (2015) 183–194. https://doi.org/10.1038/ncb3094.Breast.

[44] Z. Huang, M. Yang, Y. Li, F. Yang, Y. Feng, Exosomes derived from hypoxic colorectal cancer cells transfer wnt4 to normoxic cells to elicit a prometastatic phenotype, Int. J. Biol. Sci. 14 (2018) 2094–2102. https://doi.org/10.7150/ijbs.28288.

[45] M. Abdouh, D. Hamam, Z.H. Gao, V. Arena, M. Arena, G.O. Arena, Exosomes isolated from cancer patients' sera transfer malignant traits and confer the same phenotype of primary tumors to oncosuppressor-mutated cells, J. Exp. Clin. Cancer Res. 36 (2017) 113. https://doi.org/10.1186/s13046-017-0587-0.

[46] A.M. Soile BO, Plasma Levels of CA125, CEA, AFP and Cortisol in Obesity, J. Steroids Horm. Sci. 06 (2015) 23–25. https://doi.org/10.4172/2157-7536.1000154.

[47] V. Ceperuelo-Mallafré, M. Ejarque, C. Serena, X. Duran, M. Montori-Grau, M.A. Rodríguez, O. Yanes, C. Núñez-Roa, K. Roche, P. Puthanveetil, L. Garrido-Sánchez, E. Saez, F.J. Tinahones, P.M. Garcia-Roves, A.M. Gómez-Foix, A.R. Saltiel, J. Vendrell, S. Fernández-Veledo, Adipose tissue glycogen accumulation is associated with obesity-linked inflammation in humans, Mol. Metab. 5 (2016) 5–18. https://doi.org/10.1016/j.molmet.2015.10.001.

[48] N. Wentzensen, E.M. Poole, B. Trabert, E. White, A.A. Arslan, A. V. Patel, V.W. Setiawan, K. Visvanathan, E. Weiderpass, H.O. Adami, A. Black, L. Bernstein, L.A. Brinton, J. Buring, L.M. Butler, S. Chamosa, T. V. Clendenen, L. Dossus, R. Fortner, S.M. Gapstur, M.M. Gaudet, I.T. Gram, P. Hartge, J. Hoffman-Bolton, A. Idahl, M. Jones, R. Kaaks, V. Kirsh, W.P. Koh, J. V. Lacey, I.M. Lee, E. Lundin, M.A. Merritt, N.C. Onland-Moret, U. Peters, J.N. Poynter, S. Rinaldi, K. Robien, T. Rohan, D.P. Sandler, C. Schairer, L.J. Schouten, L.K. Sjöholm, S. Sieri, A. Swerdlow, A. Tjonneland, R. Travis, A. Trichopoulou, P.A. Van Den Brandt, L. Wilkens, A. Wolk, H.P. Yang, A. Zeleniuch-Jacquotte, S.S. Tworoger, Ovarian cancer risk factors by histologic subtype: An analysis from the Ovarian Cancer Cohort Consortium, J. Clin. Oncol. 34 (2016) 2888–2898. https://doi.org/10.1200/JCO.2016.66.8178.

Chapter 3

"Deciphering the interference of exosomes in inflammation mediated metastasis in ovarian cancer by targeting metabolic factor, SIRT1"

3.1. Introduction

Apart from the clinical parameters associated with the occurrence of the disease, multiple evidences are reporting the sociodemographic factors being responsible for the occurrence of the disease [1][2]. Several risk factors for OvCa studied so far are gynaecological parameters like parity, intake of oral contraceptive pills, menstruation-related factors, hormonal factors, mode of delivery, tubectomy, age at pregnancy and demographic features like age, obesity, lifestyle, dietary habits, lower socioeconomic status, etc. [3][4]. In high-incidence countries like North America and Europe, multiple epidemiologic and sociodemographic studies are conducted but Asian countries, including India, need further attention [5]. A pooled investigation on socioeconomic status, a known predictor of survival in multiple cancers, of populations stated that low-educated group is at elevated risk of advanced tumor stage diagnosis [6]. Additionally, females with increased deprivation of socioeconomic status are more prone to be diagnosed with OvCa at an advanced stage [7]. Adapting Western culture is contributing to alterations in reproductive, anthropometric and nutritional parameters that in turn are responsible for a higher incidence rate of OvCa [8]. However, in low incidences in high country populations like India with a reported rise in cases each year, this arena of research is still unmet and demands sociodemographic analysis. However, hormone-based ovulatory events can be a causative factor for OvCa revealed by an epidemiologic case-control study in Indian females and also reported that tubal ligation might serve as a protective factor [9]. Late diagnosis of the disease remains a threat. *Goff et al.* first described a symptom trio associated with OvCa which are often neglected including bloating, difficulty eating/feeling full and pelvic/abdominal discomfort [10]. Thus, analysis of the most prevalent symptoms among the symptoms' triad is necessary for the early diagnosis or awareness programs of OvCa. The impact of external factors such as stratified lifestyle, social life of masses, common symptoms and how they are responsible for the occurrence and progression of the disease needs to be studied extensively.

The traditional subclassification of OvCa is based on the kind and level of differentiation. However, observing the increasing cases of the disease, it is becoming clear that each main histopathological kind contains distinctive genetic flaws that disrupt particular signaling pathways in tumor cells, thus challenging the treatment regimen. Furthermore, depending on the degree of tumor differentiation, the molecular pathogenicity appears to be diverse in well differentiated (grade 1 or low-grade), moderately differentiated (grade 2) and

poorly differentiated (grade 3 or high grade) tumors [11]. Since differentiation of the tumor is correlated with the progression of the cancer to distant sites, the interactions between the cells and exosomes, in the TME that account for the alterations in the signaling cascades, need to be explored. These crosstalks are driven by several factors present in the TME and one such factor is the exosomes which are extracellular vesicles being secreted from the cells, migrate to distant sites and upon internalization by the recipient cells, change and modulate the regulations of the host cells' machinery [12]. Additionally, the process of metastasis holds a strong interconnection with metabolism and inflammation. Cancer cells adopt aerobic glycolysis (Warburg effect) as a source of energy instead of mitochondrial OXPHOS [13]. An inflammatory milieu is established due to higher secretion of metabolic products like prostaglandins, arachidonic acid, lactate and nitric oxide (NO), generation of ROS, several growth factors, MMPs from metabolically altered tumor cells which in turn influences the secretory levels of different cytokines and chemokines in the TME. Thus, the elevated inflammatory status promotes the development of a tumor-progressive environment [13]. Thus, all these interrelated phenomena driving the process of metastasis and generation of pain need to be explored. Additionally, since our study encompasses the SIRT1 activity in OvCa due to its multifarious roles in metabolism, inflammation, apoptosis and other tumor-associated processes [14], we were inclined to understand the baseline mechanism of how the pain occurring due to metastasis is associated with SIRT1 levels. Furthermore, evidence reveals that OvCa metastasis is influenced by the SIRT1/NRF2 signaling cascade regulated by FOXQ1 (Forkhead Box Q1) [15]. The contribution of exosomes in promoting metastasis in OvCa has been reviewed by *Feng et al.*[16]. However, the roles of SIRT1 in regulating inflammation-mediated metastasis under the effect of the exosomes in OvCa remain elusive.

3.2. Specific objectives

- Evaluation of sociodemographic and gynaecological parameters as risk factors of OvCa
- Identifying symptoms as a sign of metastasis in OvCa
- Understanding the baseline mechanism driving the metastatic process revealed as a symptom in OvCa.

3.3. Materials and methods:

3.3.1. Materials

Primary antibodies e.g. SIRT1, Cyclooxygenase (COX)-2, IL-6, E-cad, Vim, Bax, Bcl-2, MMP2, MMP9, VEGF, Angiopoeitin (ANGPT) 2, PTEN and related secondary antibodies, both tagged and untagged were used for the conduction of the study. All the antibodies and reagents have been listed in Table 1.

Table 1. List of reagents

Serial No.	Product	Company	Catalogue No.
1.	DKXRB FITC AFFINITY	Invitrogen	A16024
2.	Goat anti-rabbit IgG APC	Invitrogen	31984
3.	Donkey anti-Goat IgG (H+L) Secondary Antibody, TRITC	Invitrogen	A16004
4.	Goat anti-Mouse IgG (H+L) Secondary Antibody, TRITC	Invitrogen	A16071
5.	Goat anti-Mouse IgG (H+L) Cross-Adsorbed Secondary Antibody, PE	Invitrogen	P-852
6.	SIRT1 Monoclonal Antibody (OTI5B2)	Invitrogen	MA5-27217
7.	CD326 (EpCAM) Monoclonal Antibody (1B7), Alexa Fluor™ 700, eBioscience™	Invitrogen	56-9326-42
8.	CD45 Monoclonal Antibody (HI30), PerCP	Invitrogen	MHCD4531
9.	Annexin V Conjugates for Apoptosis Detection	Invitrogen	A13199
10.	MMP9 Monoclonal Antibody (5G3)	Invitrogen	MA5-15886
11.	TRYPSIN 0.25% EDTA	Invitrogen	25200056
12.	4-6-DIAMIDINO-2-PHENYLIN (DAPI)	Invitrogen	D1306
13.	PENICILLIN STREPTOMYCIN SOL, 100ML	Invitrogen	15140122
14.	SUPERSIGNAL WEST PICO PLUS	Invitrogen	34580
15.	5-(and-6)-Carboxyfluorescein Diacetate Succinimidyl Ester (CFDA-SE, CFSE)	Invitrogen	65-0850-84
16.	Rabbit polyclonal anti-human SIRT1 antibody	Cell Signalling Technology	D739
17.	HRP-linked anti-rabbit antibody	Cell Signalling Technology	7074P2
18.	miRCURY Exosome Serum/Plasma Kit	Qiagen	76603
19.	miRCURY Exosome Cell/Urine/CSF Kit	Qiagen	76743
20.	TSG101 Rabbit pAb	Abclonal	A2216
21.	E-cadherin Rabbit pAb	Abclonal	A3044

Serial No.	Product	Company	Catalogue No.
22.	Vimentin Rabbit pAb	Abclonal	A2584
23.	CXCR4- pAb	Abclonal	A12534
24.	CXCL12- pAb	Abclonal	A1325
25.	IL6 Rabbit pAb	Abclonal	A0286
26.	IL10 Rabbit mAb	Abclonal	A12255
27.	TNF-α Rabbit pAb	Abclonal	A11534
28.	TGF beta 1	Abclonal	A2124
29.	VEGF pAb	Abclonal	A12303
30.	MMP2 pAb	Abclonal	A6247
31.	CXCR2 Rabbit pAb	Abclonal	A3301
32.	COX2/PTGS2 Rabbit pAb	Abclonal	A1253
33.	ALIX / PDCD6IP Rabbit pAb	Abclonal	A2215
34.	Bcl-2 Rabbit pAb	Abclonal	A0208
35.	Bax Rabbit pAb	Abclonal	A12009
36.	β-Actin Rabbit mAb	Abclonal	AC038
37.	5(6)-Carboxy-2′,7′-dichlorofluorescein diacetate (DCFDA)	MERCK	21884
38.	Eosin Y-solution 0.5% aqueous	MERCK	109844
39.	Hydrogen peroxide solution	MERCK	88597
40.	Anti-PTEN antibody	MERCK	SAB2501614
41.	Human/Mouse COX-2 Antibody	R&D Systems	AF4198
42.	Human Angiopoietin-2 Antibody	R&D Systems	AF623
43.	CXCL1 Polyclonal antibody	Proteintech	12335-1-AP
44.	Recombinant Human TGF-β1 (CHO derived)	Peprotech	100-21C
45.	SIRT1 INHIBITOR III 1PC X 5MG	Sigma	566322-5MG-M
46.	DAB Substrate	Sigma Aldrich	11718096001
47.	Bradford reagent	Sigma	B6916-500ML
48.	Dibutylphthalate polystyrene xylene (DPX) Mountant for histology	Sisco Research Laboratories Pvt. Ltd.	88147
49.	Dimethyl Sulphoxide (DMSO) extrapure, 99%	Sisco Research Laboratories Pvt. Ltd.	43404
50.	Albumin Bovine (pH 7) fraction V (Bovine Serum Albumin, BSA), 98%	Sisco Research Laboratories Pvt. Ltd.	83803
51.	Xylene pure, 99% (500 ml)	Sisco Research Laboratories Pvt. Ltd.	54717
52.	Methanol extrapure AR, 99.8%	Sisco Research Laboratories Pvt. Ltd.	65524

Serial No.	Product	Company	Catalogue No.
53.	Fetal Bovine Serum, exosome-depleted	Gibco ™	A2720803
54.	3-(4,5-dimethylthiazol-2-yl)-2,5 diphenyltetrazolium bromide (MTT) tetrazolium	HIMEDIA	MB186
55.	RIPA buffer Sterile chloride	HIMEDIA	TCL131
56.	TMB Substrate solution (for ELISA)	HIMEDIA	ML168
57.	Paraformaldehyde Solution, 4%	HIMEDIA	TCL119
58.	Collagenase Type IV	Sigma Aldrich	C4-22
59.	DPX new	Sigma Aldrich	1005790500
60.	Dulbecco′s Modified Eagle′s Medium - high glucose	Sigma Aldrich	D6429
61.	Collagenase Type IV	Sigma Aldrich	C4-22
62.	Hematoxylin Solution (Mayer's, Modified)	ABCAM	ab220365
Buffer composition			
63.	PBS (1X)	8g NaCl; 0.2g KCl; 1.44g $Na_2HPO_4.7H_2O$; 0.24g KH_2PO_4; H_2O to 1L; pH-7.4	
64.	Resolving Buffer	Resolving Buffer 1.5M Tris, 30%Acrylamide, 10%SDS, 10%APS, 5 µl TEMED 8; pH-8.8	
65.	Sample Buffer	Laemmli Buffer (0.75gm,2gm SDS); 5% β-Mercapto ethanol; 1/10th Glycerol; 1-2 drops Bromophenol blue; pH-6.8	
66.	SDS-PAGE Buffer	1.5g Tris, 7g Glycine, 0.5g SDS, H2O to 0.5L; pH-8.3	
67.	Transfer Buffer	1.52g Tris, 7.2g Glycine, Methanol 100ml, H_2O to 0.5L; pH-8.3	
68.	Stacking Buffer	0.5M Tris, 30%Acrylamide, 10%SDS, 10%APS,10 µl TEMED; pH-6.8	
69.	TBS-T (1X)	580mg NaCl; 1mL Tris(1M); 20µl Tween-20; H_2O to 100mL; pH-7.5	
70.	Citrate Buffer	12.044g Sodium Citrate Dihydrate; 11.341g Citric acid; H_2O to 1000mL; pH-6	

3.3.2. Methods

3.3.2A. Study population and data collection

The study was approved by the Institute Ethics Committee (CNCI-IEC-40104) and the cohort comprises OvCa patients attending Chittaranjan National Institute for their treatment. All the patients (N=350) under different age groups were included in the study. The demographic parameters include age, BMI, religion, education, occupation, marital age, marital status, food habits, domicile, family income, family history, comorbidity, food timings, sleep hours, stress level, working hours, addiction. The gynaecological parameters comprised menarche, age at menopause, mode of menopause, menstruation type, parity, delivery, ligation and abortion. All the information was collected retrospectively and was kept anonymized. Upon interaction with the patients, they were asked to rate their pain in a range of 1-10 as per Numerical Rating Scale (NRS).

3.3.2B. Study design

The OvCa patients were categorized under well, moderate and poorly differentiated tumor tissues and analyzed with the sociodemographic and gynaecological parameters. Exclusion criteria included patients with a history of other cancer and with comorbidities. Samples were collected with informed consent from the patients for the collection of tissues and blood (N=73: well differentiated:15; moderately differentiated:19; poorly differentiated:39) for further analysis of metastatic factors like cytokines and proteins. For comparing the cytokines status with the healthy individuals, 21 normal volunteers were also included in the study with proper consent.

3.3.2C. Haematoxylin and Eosin staining

Tissue sectioning was performed from paraffin-embedded well, moderate and poorly differentiated tissues for haematoxylin and eosin (H&E) staining. After the deparaffinization and alcohol hydration of the slides, Mayer's hematoxylin was added and kept for 30s, followed by washing in distilled water to remove the unbound stain. Eosin Y solution was added to the slide for 30s and after dehydration in alcohol gradient and xylene each for 5min, DPX mounting was performed followed by imaging under brightfield microscope (Leica Microsystems: #Model DM1000) [17].

3.3.2D. Cell culture

Single cell suspension was prepared from poorly differentiated patients by treating the tissues with collagenase IV/DMEM cocktail (50:50 dilution), followed by filtering and centrifugation at 8000rpm for 10min at RT to obtain the cell pellet. Finally, the single cells pellet was resuspended in exosomes-depleted 10% FBS supplemented DMEM media with antibiotics (1% penicillin-streptomycin) and was used for further experiments [18].

3.3.2E. MTT assay

5×10^3 primary cells in a 96-well flat-bottom transparent plate were seeded, followed by a 24hrs treatment with SIRT1 Inh (0.01µM, 0.1 µM, 1µM and 10µM) at 37°C in 5% CO_2. On the following day, MTT solution (5mg/ml) was added into each well and after 3hrs of incubation, DMSO was added to the wells for recording the OD value under an ELISA plate reader (Infinite 200PRO-TECAN, 30050303) at 595nm [19].

3.3.2F. Immunohistochemistry

The slide preparation was done by tissue sectioning from paraffin-embedded tissues (both OvCa and adjacent normal). The process of deparaffinization and dehydration was performed by dipping the slides in xylene and alcohol gradient solutions, respectively, followed by 10Mm citrate buffer solution (pH 6.0) treatment to increase the expression of antigen. After treatment with 3% hydrogen peroxide diluted in 100% methanol, a PBS wash was followed to terminate the endogenous peroxidase activity. The slides were then blocked with 3% BSA for 1hr and then treated with COX-2 primary antibody (1:500 dilution) and incubated overnight at 4°C. On the following day, a secondary antibody in a dilution 1:1000 was added to the slides and incubated at RT for 2hrs. To visualize the reaction, DAB was added for 10min and finally, haematoxylin was added for 30s. After an alcohol gradient wash, DPX mounting was performed to prepare the slides for capturing images under a brightfield compound microscope (Leica Microsystems: #Model DM1000) [20] and analyzed using Fiji-ImageJ software. The H-score was calculated using the following formula,

H-score = [(0 X % negative cells) + (1 X % weak positive cells) + (2 X % moderate positive cells) + (3 x % strong positive cells)] where 0 means no staining visible, 1 means weak, 2 means moderate and 3 means strong and the H-score ranges from 0 (negative) to 300 (100% strong staining) [21].

3.3.2G. Enzyme-linked immunosorbent assay

96 well plate were coated with serum from well, moderate and poorly differentiated patients and primary cell culture supernatant and allowed to settle overnight at 4°C for Enzyme-linked immunosorbent assay (ELISA). The wells were subjected to blocking with 5% BSA for 2hrs, followed by washing with PBS and the addition of primary antibodies which include IL-6, tumor necrosis factor-α (TNF-α), TGF-β, IL-10, chemokine (C-X-C motif) ligand (CXCL)12, C-X-C chemokine receptor (CXCR)-4, CXCL1 and CXCR2 (1:500) and incubated overnight for 4°C. On the next day, HRP-conjugated secondary antibody (1:1000) was added after washing away the primary antibody with PBST and then incubated for 2hrs at RT. After discarding the secondary antibody, TMB substrate was added into the wells, followed by incubation for 15min and OD values were taken under ELISA plate reader (Infinite 200PRO-TECAN, 30050303) at 595nm.

3.3.2H. Immunofluorescence

The slide (both tumor and adjacent normal) preparation was done by deparaffinization of the slides of OvCa tumor and adjacent normal tissues using xylene for 10min followed by rehydration using graded ethanol (5min). After antigen retrieval using citrate buffer and the addition of 0.9% H_2O_2/Methanol solution. To avoid the non-specific binding, 5% BSA was used for blocking for 1hr and primary antibodies for SIRT1, PTEN, COX-2, VEGF, ANGPT2, MMP2, MMP9 (1:500) were added and kept overnight for 4°C [22]. FITC and TRITC tagged secondary antibodies were added the next day and incubated for 2hrs (1:1000) at RT. To remove the excess antibody the slides were subjected to washing with 1X PBS and DPX mounting was performed for imaging under OLYMPUS BX53 fluorescence microscope [23]. The images were analyzed using Fiji-ImageJ software.

3.3.2I. Isolation of exosomes

Qiagen miRCURY ® Exosome serum/plasma kit and miRCURY ® Exosome Cell/Urine/CSF Kit were used to isolate exosomes from serum and cell culture supernatant as per manufacturer protocol. After the addition of reagents in 600µl of patients' serum and cell culture supernatant and their incubation 1hr at 4°C, the samples were centrifuged at 1500×g for 30min at RT. The pellet fraction was frozen at -80°C after being resuspended in a resuspension buffer [24].

3.3.2J. Dynamic light scattering

For Dynamic light scattering (DLS), the isolated exosomes were diluted with 0.1µg/µl of DPBS that was eventually filled to the brim in a cuvette with 100µl of DPBS. Exosome-containing cuvette (NanoStar MicroCuvette Kit) was inserted into Dynapro Nanostar (WYATT Technology) DLS device. The Laser Wavelength was fixed at 663.87nm with Peak Radius Low Cutoff to be 0.5nm and Peak Radius Low Cutoff at 5000nm (Temperature Control: yes with 25°C as Set temperature) and Auto-attenuation time was set to 60. The size or homogeneity of exosomes was determined by the radius or the percentage of intensity, respectively [25].

3.3.2K. Nanoparticle tracking analysis

To ensure the accuracy of Nanoparticle tracking analysis (NTA), exosomes suspension at a range of 2×10^8 to 2×10^9/ml was prepared. Particle Metrix Zetaview-PMX 130-Mono laser with laser wavelength at 520nm and Filter Wavelength: Scatter; Sensitivity: 60; Shutter: 100 was preset for accurate analysis of the samples and Software ZetaView (version 8.05.16 SP3) was used to analyze the data [26].

3.3.2L. Scanning electron microscopy

The isolated exosomes were sonicated for 5min individually in acetone, ethanol, and distilled water. After flushing with distilled water, drying and immobilization, 1–5µl vesicle mixtures were added to cleaned silicon chips. Carbon paste was used to mount silicon chip samples on a Scanning electron microscopy (SEM) stage (Jeol Ltd. JSM-7500F). To make the surface conductive, a coating of 2–5nm gold–palladium alloy was deposited by sputtering before capturing the images (SPI–Module Sputtering, Argon as gas for plasma) [27].

3.3.2M. Exosomes labelling and internalization detection by Confocal microscopy

15µl of an EV-containing PBS solution was stained with 40µM 5-(and-6)-Carboxyfluorescein Diacetate Succinimidyl Ester (CFSE) solution by mixing and incubating for 2hrs at 37°C [28]. To analyze the exosomes internalization by the cancer cells, the cells were allowed to adhere and fixed using 4% paraformaldehyde followed by nuclear staining with DAPI for 10min at RT in the dark at 1µg/1000 ml concentration [29]. The cells were then incubated with CFSE-labeled exosomes for 2hrs in the dark at RT followed by washing with PBS and DPX mounting [30]. Imaging under a Confocal microscope (Carl Zeiss) was performed using Zen software (Carl Zeiss, Inc., Thornwood, NY).

3.3.2N. Western blotting

Isolation of protein was performed after lysing the exosomes using RIPA buffer and Bradford assay was performed to assess the exosomal protein content. On 12% acrylamide gel, 25µg of total protein was loaded to quantify the exosomal protein content for β-actin as control, TSG101, ALIX (1:5000). On the following day, the reaction was visualized by adding HRP-tagged secondary antibody (1:10000) and incubated for 2hrs, followed by band acquisition after development with ECL Ultra Western HRP Substrate [31].

3.3.2O. Flow Cytometry

2×10^5 primary cells were seeded in 60mm petri dish under four different conditions including Con, No treatment+Exosomes (NTExos), SIRT1 Inh + exosomes (SIRT1 Inh+Exos) and SIRT1 Inh treated at a drug concentration estimated from cell viability assay for 24hrs. The cells were then incubated for 2hrs at 4°C with SIRT1, COX-2, IL-6, E-cad, Vim, Bax and Bcl-2, EpCam and CD45 (1:100) followed by incubation with APC, Alexa Fluor, PerCP, PE tagged secondary antibodies as mentioned in Table 1 and data acquisition in BD LSFortessa flow cytometer. The apoptotic cancer cells and ROS generation in the cancer cells under the same conditions mentioned above, the cells were incubated with AnnexinV for 2hrs and DCFDA for 30min at RT in the dark. Data was acquired by BD LSRFortessa flow cytometer and analyzed using FlowJo software [32].

3.3.2P. Protein-protein interaction network construction using STRING

To understand the interaction pattern of DEGs associated with SIRT1, a PPI network was deduced using the STRING v11.0 database (https://string-db.org) with a combined score of >0.7. PPI is scored as a low confidence score of <0.4, medium confidence from 0.4< to <0.7, and high confidence score of >0.7. In the present study, we selected a high confidence score to eliminate PPIs with low significance [33].

3.3.2Q. Statistical analysis

IBM SPSS25 software was used to understand the frequency distribution of various sociodemographical and gynaecological parameters. Additionally, crosstabulation of the parameters with tumor differentiation was also performed by IBM SPSS25 to obtain corrected Pearson Chi-square (χ^2) to understand the correlation between the data variables along with analysis of the survival plot. Image analysis was conducted using Fiji-ImageJ Software https://imagej.net/Fiji. FlowJo software was used to analyze the flow cytometry

data. GraphPad Prism (Version 8.0) was used for Two-way ANOVA, One-way ANOVA and Student's t test wherever applicable $P<0.0001$ and $P\leq0.05$ were considered to be statistically significant.

3.4. Result

3.4.1. Frequency distribution of sociodemographic and gynaecological parameters

The total number of patients was stratified in different subcategories of the multiple parameters taken under consideration. The clinical diagnosis reports suspected 180 (51.4%) patients had poorly differentiated OvCa followed by 90 (25.7%) patients with moderately differentiated form and 80 (22.9%) patients were diagnosed with well differentiated forms of OvCa. Most of the patients belonged to the age group 41-60 years (N=172, 49.1%) whereas 89 (25.4%) and 72 (20.6%) patients were under >60 years and 19-40 years age group and the least was under 18 years of age with only 4.9%. Interestingly, more than 50% (N=187) of the patients were overweight or obese, 35.4% had normal BMI and only 11.1% were underweight. The prevalence of OvCa was mostly observed in the Hindus (67.1%) and 25.7% were Muslims, followed by a very nominal percentage of 7.1% were Christian. Among all, 31.1% were illiterate, 26% had received higher education and most of them (42.9%) were educated up to primary/secondary school educated. It was interestingly observed that housewives/unemployed patients had high occurrence rates (64.3%), followed by the working category (service/farmers) with 24.9% and equal distribution was observed among retired patients and students with 5.4%. Looking into the marital age, 38.3% were married between 18-25 years of age, 35.4% had an early age marriage, 13.1% were married at >25 years of age. Among the patients, 68.3% were married, 18.6% were widows or divorced and the remaining (13.1%) were unmarried. Non-vegetarians accounted to be 73.1% and the remaining 26.9% were vegetarians. 56% were dwelling in a rural habitat and the remaining 44% were from urban areas. The income status revealed that there was minimal difference in the income level with 48.6% under high-income group and 51.4% under the low-income group. 46.6% had a record of prior history of cancer cases in the family. 61.7% of the patients had comorbidities like diabetes, thyroid, blood pressure, etc. whereas near about 60% had discrepancies in the timings of food consumption. Moreover, we recorded three new parameters related to the lifestyle of OvCa patients: sleep hours, stress level and working hours stratified under different segments, data is shown in Table 2. 50% of the patients were addicted to tobacco in different forms like gutka, dokta, smoking etc. and 10% had an

addiction towards alcohol whereas remaining 40% were non-addicted. Among the gynaecological parameters, 45.1% of the study cohort had menarche age within 10-13 years of age followed by 28.6% above 13 years and 26.3% below 10 years of age. Early age menopause includes 44.6% (<45 years) whereas late age menopause includes 34.6%. Irregularity in menstruation was prevalent in 58.6% and the remaining 41.4% had regular menstruation. 48.9% had 1-2 times history of conception followed by 19.7% who had more than 3 children and 18.6% were nulliparous. 50.6% had pre-term delivery and only 18% had full-term pregnancy. As far as ligation and abortion are concerned 36.7% and 16.6%, respectively, had undergone these surgeries. The most prevalent symptom is pain (N=167; 47.75) and pain with abdominal distension (N=116; 33.15). The frequency distribution of tumor differentiation has been shown in Table 2 where poorly differentiated forms account to be the maximum.

Table 2. Frequency distribution of sociodemographic and gynaecological parameters of patients' cohort

Characteristics of participants (N=350)	**Frequency**	**Percentages (%)**
Age		
≤18 years	17	4.9
19-40 years	72	20.6
41-60 years	172	49.1
>60 years	89	25.4
BMI		
Underweight	39	11.1
Normal	124	35.4
Overweight/Obese	187	53.4
Religion		
Hindu	235	67.1
Muslim	90	25.7
Christian	25	7.1
Education		
Illiterate	109	31.1
School education	150	42.9

Characteristics of participants (N=350)	Frequency	Percentages (%)
Graduates and above	91	26.0
Occupation		
Housewife/unemployed	225	64.3
Service/Farmers	87	24.9
Retired	19	5.4
Students	19	5.4
Marital age (years)		
<18	124	35.4
18-25	134	38.3
>25	46	13.1
Non applicable (NA)	46	13.1
Marital status		
Unmarried	46	13.1
Married	239	68.3
Widow/Divorced	65	18.6
Food habits		
Vegetarian	94	26.9
Non-vegetarian	256	73.1
Domicile		
Urban	154	44.0
Rural	196	56.0
Family income (Rupees)		
≤5000	180	51.4
>5000	170	48.6
Family history		
Yes	163	46.6
No	187	53.4
Comorbidity		
Yes	216	61.7
No	134	38.3
Food timings		

Characteristics of participants (N=350)	**Frequency**	**Percentages (%)**
Proper	140	40.0
Improper	210	60.0
Sleep hours (hrs)		
≤5 hrs	91	26.0
6-8 hrs	214	61.1
≥9 hrs	45	12.9
Stress level		
High	148	42.3
Moderate	127	36.3
Little	75	21.4
Working hours (hrs)		
<8 hrs	137	39.1
≥8 hrs	213	60.9
Addiction		
No addiction	140	40.0
Tobacco	175	50.0
Alcohol	35	10.0
Menarche age (years)		
<10	92	26.3
10-13	158	45.1
>13	100	28.6
Age at menopause (years)		
<45	156	44.6
≥45	121	34.6
NA	73	20.9
Menstruation type		
Regular	145	41.4
Irregular	205	58.6
Parity		
Nil	65	18.6
1-2	171	48.9

Characteristics of participants (N=350)	Frequency	Percentages (%)
≥3	69	19.7
NA	45	12.9
Delivery		
Pre-term	177	50.6
Full-term	63	18.0
NA	110	31.4
Ligation		
Yes	106	30.3
No	244	69.7
Abortion		
Yes	58	16.6
No	292	83.4
Tumor Differentiation		
Well	80	22.9
Moderate	90	25.7
Poor	180	51.4
Symptoms		
Distension of abdomen	33	9.4
Pain with abdominal distension	116	33.1
Pain	167	47.7
Others	34	9.7

3.4.2. Correlation of sociodemographic attributes with tumor differentiation

A significant correlation of tumor differentiation was observed with age, BMI, education, occupation, marital age, marital status, monthly income, family history, comorbidity and addiction with tumor differentiation. Tumor differentiation significantly correlated with sleep hours, stress level and working hours. However, parameters like religion, food habits, domicile, food timings did not draw any significant links with tumor differentiation. The respective P values are enlisted in Table 3.

Table 3. Correlation of tumor differentiation with the sociodemographic parameters.

Sociodemographic parameters	**Tumor differentiation**			χ^2	**P value**
	Well	**Moderate**	**Poor**		
Age					
≤18 years	12	5	0	66.5	<0.001
19-40 years	31	23	18		
41-60 years	27	44	101		
>60 years	10	18	61		
BMI					
Underweight	15	11	13	40.283	<0.001
Normal	39	43	42		
Overweight/Obese	26	36	125		
Religion					
Hindu	58	59	118	2.607	0.626
Muslim	16	23	51		
Christian	6	8	11		
Education					
Illiterate	12	28	69	14.369	0.006
School education	42	37	71		
Graduates and above	26	25	40		
Occupation					
Housewife/unemployed	43	58	124	38.69	<0.001
Service/Farmers	19	23	45		
Retired	3	5	11		
Students	15	4	0		
Marital age (years)					
<18 years	16	32	76	23.035	0.001
18-25 years	36	31	67		
>25 years	8	15	23		
NA	20	12	14		

Sociodemographic parameters	**Tumor differentiation**			**χ^2**	**P value**
	Well	**Moderate**	**Poor**		
Marital status					
Unmarried	20	12	14	17.957	0.001
Married	49	66	124		
Widow/Divorced	11	12	42		
Food habit					
Vegetarian	27	30	37	7.495	0.24
Non-vegetarian	53	60	143		
Domicile					
Urban	35	41	78	0.123	0.94
Rural	45	49	102		
Monthly income (Rupees)					
≤5000	30	41	109	13.459	0.001
>5000	50	49	71		
Family history					
Yes	27	41	95	8.109	0.017
No	53	49	85		
Comorbidity					
Yes	34	60	122	16.235	<0.001
No	46	30	58		
Food timings					
Proper	39	37	64	4.08	0.13
Improper	41	53	116		
Sleep hours (hrs)					
≤5 hrs	4	19	68	41.951	<0.001
6-8 hrs	55	60	99		
≥9 hrs	21	11	13		

Sociodemographic parameters	**Tumor differentiation**			**χ^2**	**P value**
	Well	**Moderate**	**Poor**		
Stress level					
High	0	22	126	205.771	<0.001
Moderate	25	55	47		
Little	55	13	7		
Working hours (hrs)					
<8 hrs	49	38	50	26.531	<0.001
≥8 hrs	31	52	130		
Addiction					
No addiction	50	35	55	26.55	<0.001
Tobacco	25	42	108		
Alcohol	5	13	17		

3.4.3. Association of gynaecologic characteristics with the tumor differentiation

Poorly differentiated OvCa mostly occurred in the category of menopausal age less than 45 years, parity with 1-2 children, pre-term delivery holding significant correlation. However, our study could not show a significant association with parameters like menarche, menstruation type, ligation and abortion. All the data with respective P values have been shown in Table 4.

Table 4. Correlation of tumor differentiation with the gynaecologic parameters.

Gynaecological parameters	**Tumor differentiation**			**χ^2**	**P value**
	Well	**Moderate**	**Poor**		
Menarche					
<10	21	31	40	6.139	0.189
Oct-13	40	36	82		
>13	19	23	58		
Age at menopause					
<45 years	28	36	92	35.375	<0.001

Gynaecological parameters		**Tumor differentiation**		**χ^2**	**P value**
	Well	**Moderate**	**Poor**		
≥45 years	18	34	69		
NA	34	20	19		
Menstruation type					
Regular	38	36	71	3.991	0.407
Irregular	43	53	109		
Parity					
Null	10	8	47	29.126	<0.001
01-Feb	39	46	86		
≥3	11	24	34		
NA	20	12	13		
Delivery					
Pre-term	29	52	96	13.416	0.009
Full-term	21	18	24		
NA	30	20	60		
Ligation					
Yes	27	30	49	1.651	0.438
No	53	60	131		
Abortion					
Yes	11	17	30	0.811	0.667
No	69	73	150		

3.4.4. Morphological analysis of differentiated OvCa tissues

Well differentiated tissues tissue revealed that the nuclear size is small with no distortion in cellular morphology. The nuclear size increased comparatively with distorted cellular structure in moderately differentiated OvCa tissues. The greatest variation in nuclear size is observed in poorly differentiated OvCa tissues (Figure 1A). Interestingly, the survival of the patients gradually deteriorated in the poorly differentiated patients at a significant rate (Figure 1B).

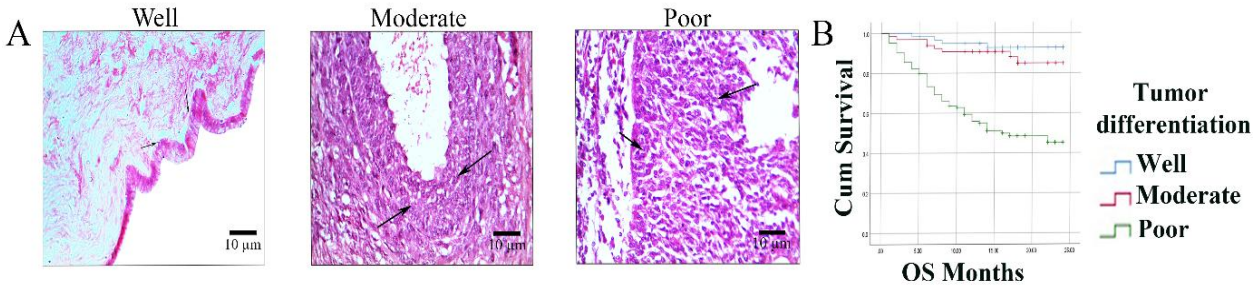

Figure 1. A. Morphological analysis of well, moderate and poorly differentiated OvCa tissues; B. Kaplan Meir Plot of survival with respect to tumor differentiation

3.4.5. Pain is a prevalent symptom in the poorly differentiated OvCa patients

Pain is one of the most common symptoms in OvCa followed by pain with distension of the abdomen and distention of abdomen and other symptoms, respectively (Table 5). Since pain was observed to be most predictable symptoms among all other, we have cross tabulated pain parameters with the tumor differentiation and observed that pain with abdominal distension (N=84;72.4%) and other pain forms (N=76; 45.5%) were most prevalent in the patients with poorly differentiated OvCa patients (Table 5). The tabulated data has been graphically represented in Figure 2A-B.

Table 5. Frequency distribution with percentages of symptoms with respect to tumor differentiation

Parameters			**Tumor differentiation**			**Total**
			Well	**Moderate**	**Poor**	
Symptoms	Distension of abdomen	Count	12	11	10	33
		% within Symptoms	36.4%	33.3%	30.3%	100.0%
	Pain with abdominal distension	Count	12	20	84	116
		% within Symptoms	10.3%	17.2%	72.4%	100.0%
	Pain	Count	39	52	76	167
		% within Symptoms	23.4%	31.1%	45.5%	100.0%
	Others	Count	17	7	10	34
		% within Symptoms	50.0%	20.6%	29.4%	100.0%
Total		Count	80	90	180	350
		% within Symptoms	22.9%	25.7%	51.4%	100.0%

Additionally, estimating the pain score with tumor differentiation and statistically analyzing the intensity of pain showed an increase in the poorly differentiated form of cancer followed by moderate and well differentiated form of OvCa ($F(2.347)=83.645$; $P<0.05$) as represented in Figure 2C-D and tabulated in Table 6.

Table 6. Frequency distribution with percentages of pain score with respect to tumor differentiation

Parameters			**Tumor differentiation**			**Total**
			Well	**Moderate**	**Poor**	
Pain Score	No pain	Count	29	18	20	67
		% within Pain Score	43.3%	26.9%	29.9%	100.0%
	1-4	Count	51	0	0	51
		% within Pain Score	100.0%	0.0%	0.0%	100.0%
	5-7	Count	0	69	2	71
		% within Pain Score	0.0%	97.2%	2.8%	100.0%
	8-10	Count	0	3	158	161
		% within Pain Score	0.0%	1.9%	98.1%	100.0%
Total		Count	80	90	180	350
		% within Pain Score	22.9%	25.7%	51.4%	100.0%

While estimating the frequency of other characteristics related to pain like pattern of pain, frequency of pain, site of pain and quality of pain, it was observed that the patients with poorly differentiated form of OvCa experienced constant continuous sharp pain, mostly in the abdominal or pelvic region (Figure 2E-H). This data focused on pain as one of the most important and predictable symptoms to detect OvCa.

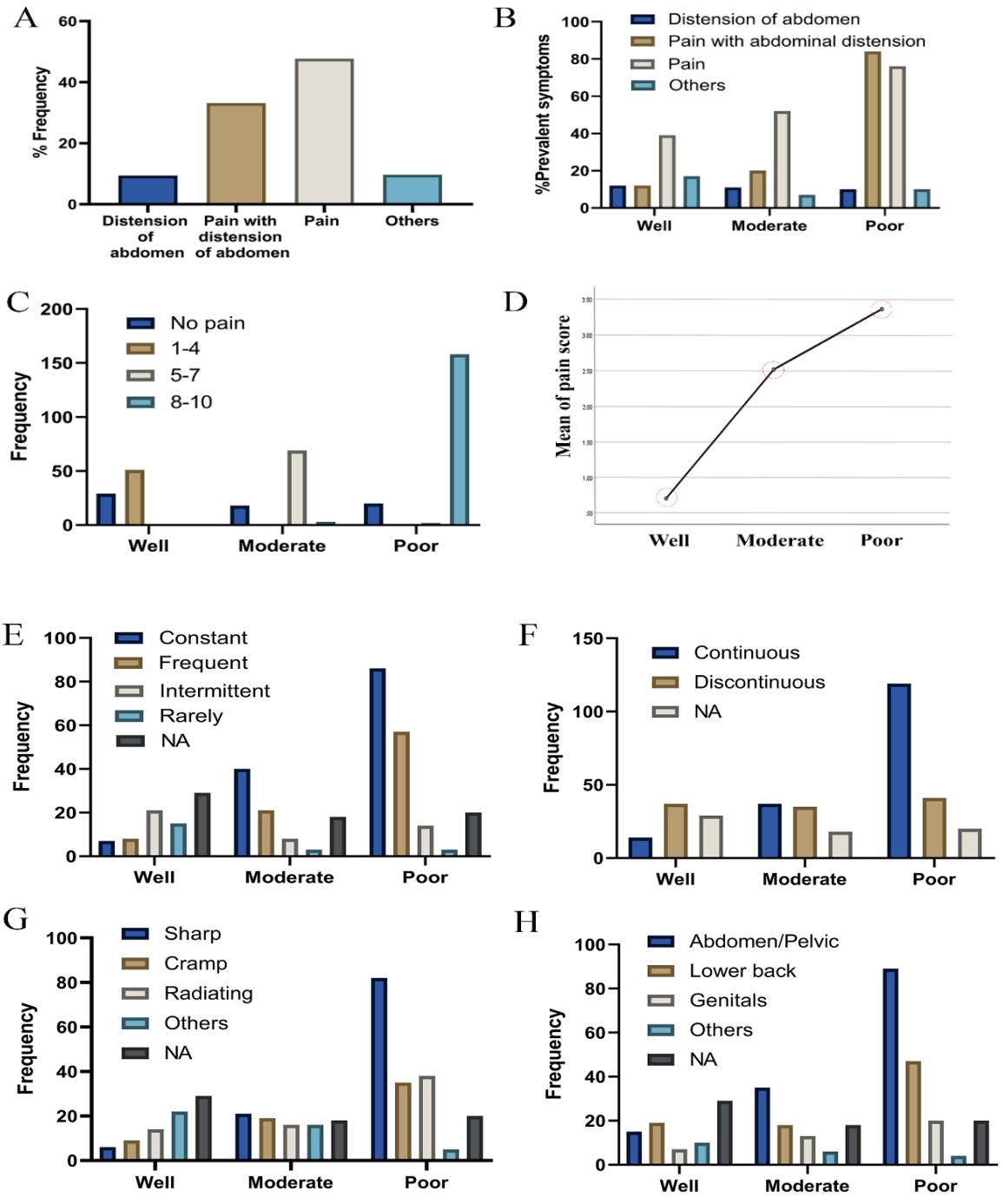

Figure 2. A. Frequency distribution of prevalence of symptoms; B. Frequency distribution of the symptoms with respect to tumor differentiation; C. Frequency of rating of pain in accordance with tumor differentiation; D. Trend analysis of pain score with respect to tumor differentiation; E-H. Frequency distribution of patterns of pain observed in accordance with tumor differentiation.

3.4.6. COX-2 is significantly higher in poorly differentiated patients demarking itself as a potent inducer of pain

COX-2 as a regulatory factor of pain, when analyzed in the tissue culture supernatant and blood serum that includes well differentiated (N=15), moderately differentiated (N=19) and poorly differentiated (N=39) OvCa patients, revealed elevated levels in both blood and primary cell culture supernatant of poorly differentiated patients as compared to the moderately and poorly differentiated patients (Figure 3A). Upon observing higher expression levels in poorly differentiated patients, IHC analysis of COX-2 was conducted in the tissues collected from poorly differentiated patients and adjacent normal which also corroborated with the previous findings where COX-2 expression was higher in the tumor tissues as compared to the adjacent normal (Figure 3B). Furthermore, with the increase in the pain intensity as determined by the NRS, the H-score of COX-2 expression also increased considerably in the poorly differentiated OvCa patients (Figure 3C).

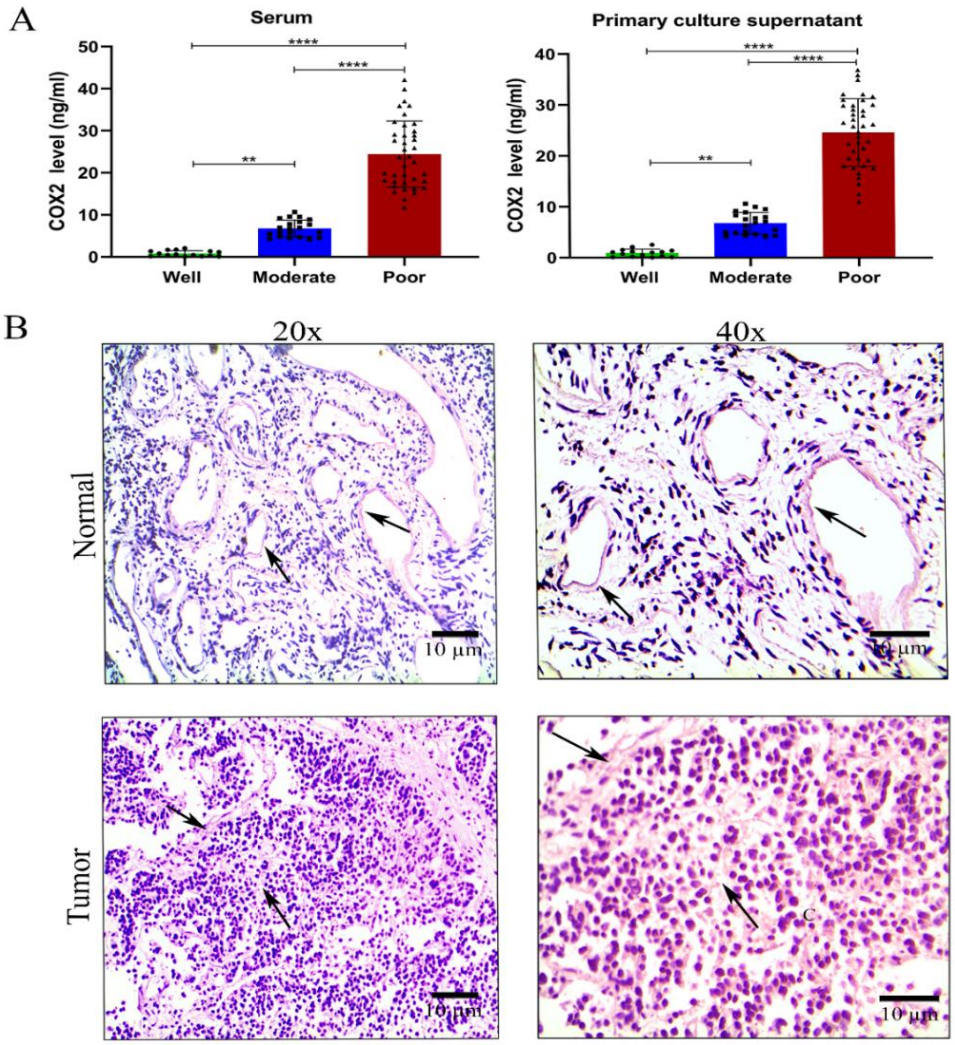

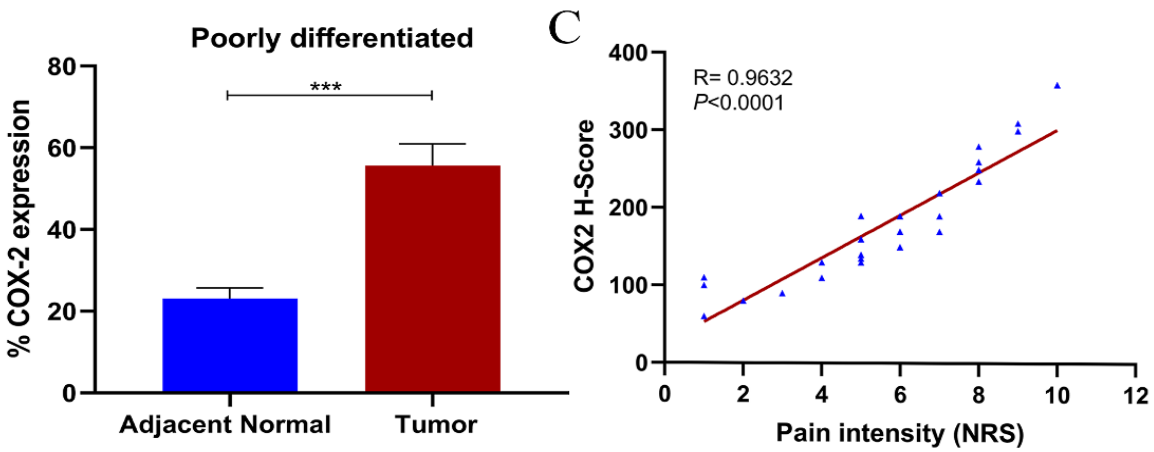

Figure 3. A. COX-2 secretion level analysis in serum and primary culture supernatant by ELISA; B. IHC analysis of COX-2 in normal and tumor tissues; C. COX-2 H-score in relation to pain intensity. (*P<0.05, **P<0.01, ***P<0.001, ****P<0.0001)

3.4.7. Angiogenic and metastatic factors are higher in poorly differentiated tumor tissues as compared to the adjacent normal

As we have observed pain and tumor differentiation are strongly correlated thus, to draw the link between these parameters, we analyzed angiogenic and metastatic markers: ANGPT2 and VEGF as well as MMP2 and MMP9. The results revealed that the expression of VEGF and ANGPT2 showed higher expression in the tumor tissues as compared to the adjacent normal ones and the colocalized expression of VEGF/ANGPT2 was also significantly higher in the tumor tissues (Figure 4A-C). MMP2/MMP9 expression has also revealed similar results where their individual expressions were significantly higher in the tumor as compared to adjacent normal tissue, along with their increased colocalized expression in the tumor tissues (Figure 4D-F). These results suggest that the SIRT1 and COX-2 axis certainly play a role in dictating the metastasizing tendency in the poorly differentiated OvCa patients.

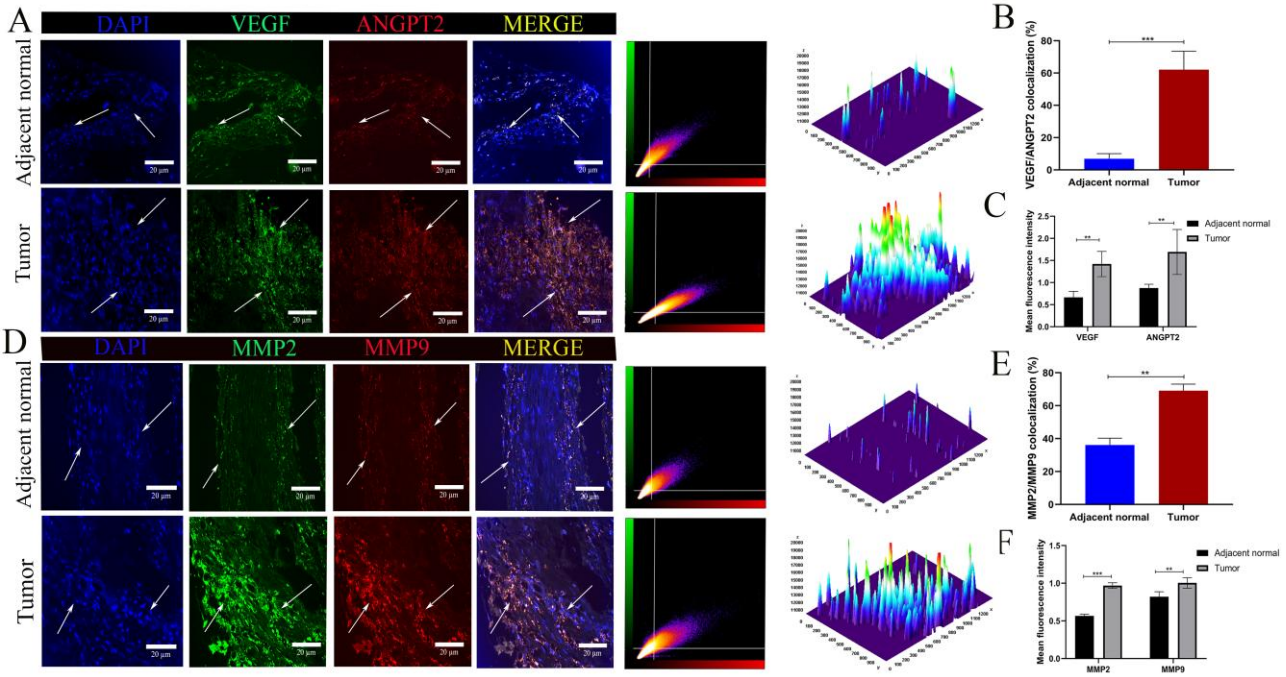

Figure 4. A-C, Colocalized expression and MFI of VEGF/ANGPT2 in tumor and adjacent normal tissues by IF; D-F, Colocalized expression and MFI of MMP2/MMP9 in tumor and adjacent normal tissues by IF. (*P<0.05, **P<0.01, ***P<0.001, ****P<0.0001)

3.4.8. Increased expression of COX-2 dictates the cytokines and chemokines profile in poorly differentiated OvCa patients

Since COX-2 is highly associated with inflammation, the cytokines and chemokines profiling in the serum of normal volunteers (N=21) and poorly differentiated OvCa patients' tissues (N=39) along with primary tumor cell supernatant from poorly differentiated patients (N=37). Interestingly, it was observed that IL-6 level was considerably higher in the poorly differentiated patients among the cytokines and chemokines. However, anti-inflammatory cytokines, IL-10 and TGF-β levels were less in comparison to the pro-inflammatory IL-6 and TNF-α. On the contrary, the levels of chemokines CXCL-12/CXCR-4 and CXCL1/CXCR2 were higher than all the cytokines, but it was observed that the levels in the normal and cancer patients were less significant in comparison to the cytokines (Figure 5A-B).

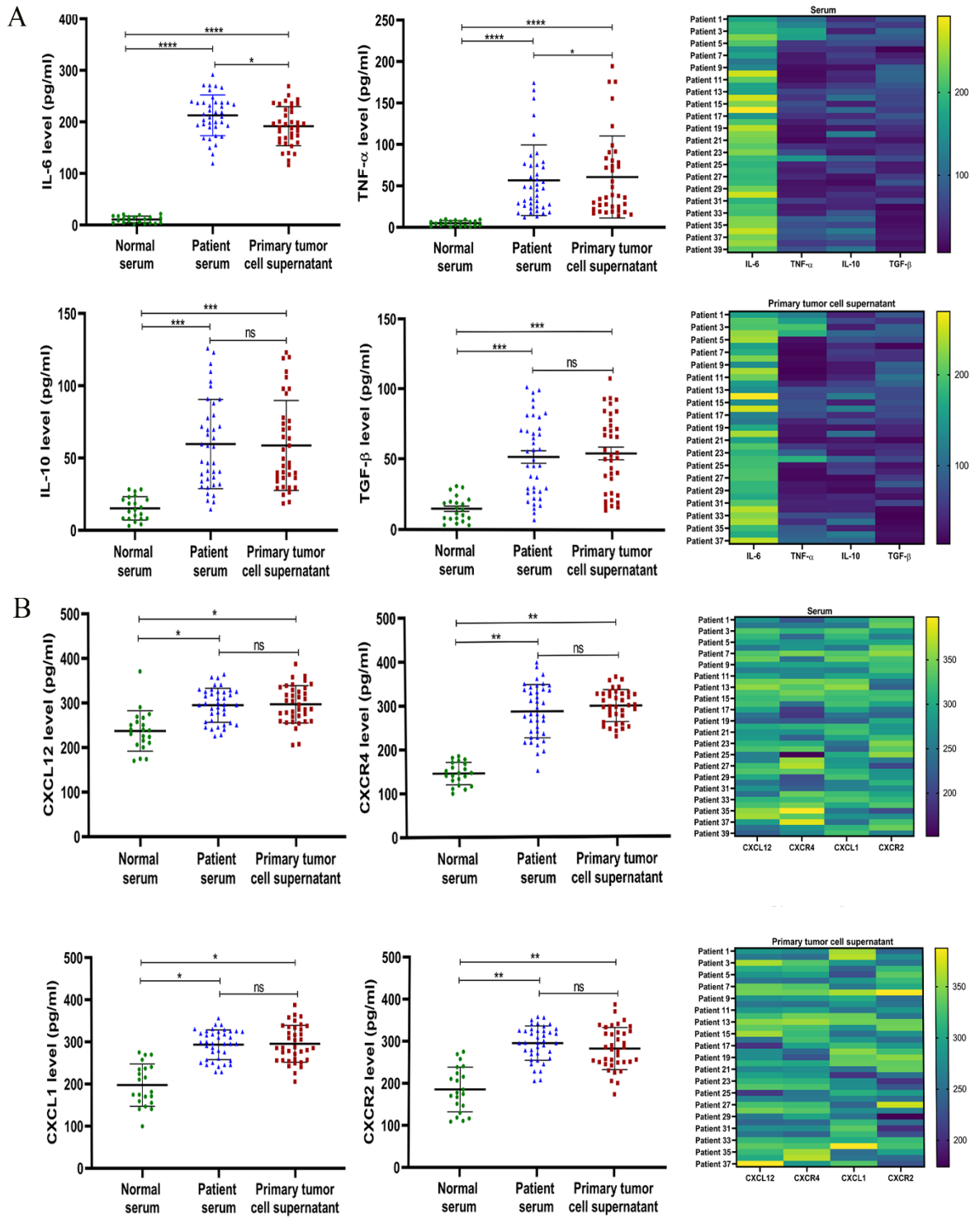

Figure 5. A. Analysis of cytokines in primary cancer cell supernatant and serum from poorly differentiated patients as compared to the normal volunteers by ELISA, as represented graphically and in heatmap; B. Analysis of chemokines in serum and primary cancer cell supernatant from poorly differentiated patients in comparison to the normal volunteers by ELISA, as represented graphically and in heatmap. (*P<0.05, **P<0.01, ***P<0.001, ****P<0.0001)

3.4.9. STRING database confirms higher interactive score of SIRT1 with metastatic and inflammatory factors

Upon deriving the higher colocalized expression of VEGF/ANGPT2 and MMP/MMP9 along with elevated secretion of IL-6 we were inclined to investigate the interaction confidence score between the molecules. Interestingly, COX-2 (0.96), SIRT1(0.726), MMP2 (0.847), MMP9 (0.959) held strong score with IL-6. Additionally, SIRT1 and PTEN are also indirectly related to IL-6 (Figure 6). We also observed significant confidence scores of MMP9 with exosomal marker CD63 which in turn is related to other exosomal markers CD81, TSG101, CD9. All these molecules are interconnected with each other, thus, we illustrated that SIRT1 is interconnected strongly with COX-2 and IL-6 and also with exosomes.

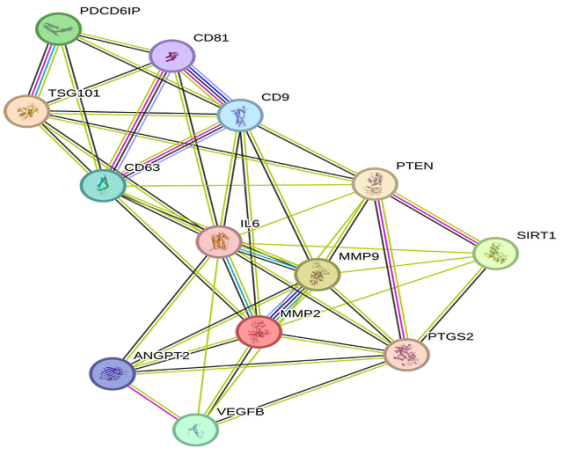

Node 1	Node 2	Score
ANGPT2	MMP2	0.606
ANGPT2	VEGFB	0.7
ANGPT2	PTGS2	0.462
ANGPT2	MMP9	0.629
ANGPT2	IL6	0.75
CD63	MMP2	0.431
CD63	TSG101	0.998
CD63	CD81	0.994
CD63	PTEN	0.447

Node 1	Node 2	Score
CD63	MMP9	0.7
CD63	CD9	0.994
CD63	IL6	0.562
CD63	PDCD6IP	0.836
CD81	TSG101	0.995
CD81	IL6	0.575
CD81	PDCD6IP	0.803
CD81	CD9	0.997
CD9	MMP2	0.412

Node 1	Node 2	Score
CD9	TSG101	0.995
CD9	PTEN	0.436
CD9	MMP9	0.48
CD9	IL6	0.54
CD9	PDCD6IP	0.808
IL6	SIRT1	0.726
IL6	MMP2	0.847
IL6	TSG101	0.451
IL6	VEGFB	0.608

Node 1	Node 2	Score
IL6	PTGS2	0.96
IL6	PTEN	0.681
IL6	MMP9	0.959
MMP2	SIRT1	0.449
MMP2	VEGFB	0.411
MMP2	PTEN	0.745
MMP2	PTGS2	0.764
MMP2	MMP9	0.918
MMP9	SIRT1	0.597

Node 1	Node 2	Score
MMP9	VEGFB	0.438
MMP9	PTGS2	0.815
MMP9	PTEN	0.766
PDCD6IP	TSG101	0.999
PTEN	SIRT1	0.757
PTEN	TSG101	0.428
PTEN	PTGS2	0.682
PTGS2	SIRT1	0.592
PTGS2	VEGFB	0.486

Figure 6. Establishment of PPI of metastatic and inflammatory factors with SIRT1

3.4.10. SIRT1 colocalized with COX-2 and PTEN at a highly significant rate in poorly differentiated OvCa tissues

To understand the association of SIRT1 with COX-2, IF data revealed their strong colocalized expression in the poorly differentiated tumor tissues as compared to the adjacent normal ones. Moreover, the individual expression of SIRT1 and COX-2 was also significantly higher in the tumor tissues (Figure 7A-C). Additionally, the colocalized expression of SIRT1 and PTEN also corroborated with SIRT1/COX-2 expression with higher expression in the poorly differentiated tumor, which was also revealed by their individual MFI (Figure 7D-F). This depicted that SIRT1 regulates COX-2 level, thereby inducing pain in the poorly differentiated OvCa patients and might also regulate the metastatic process.

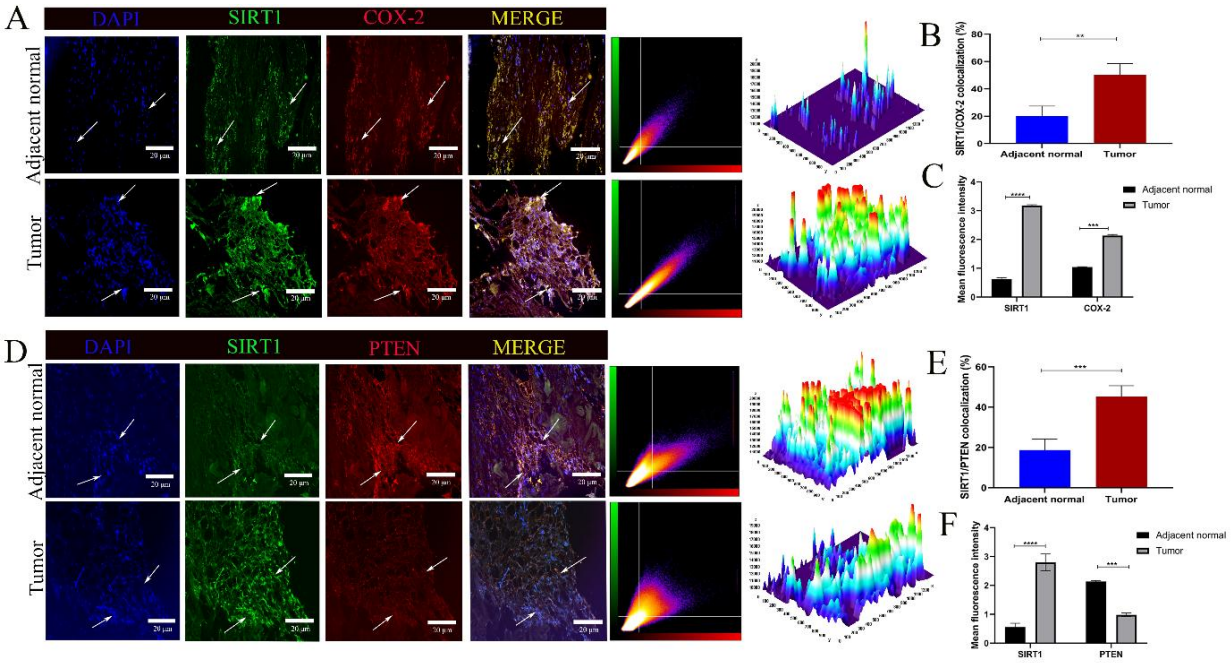

Figure 7. A-C. Colocalized expression and MFI of SIRT1/COX-2 in tumor and adjacent normal tissues by IF; D-F. Colocalized expression of SIRT1/PTEN in tumor and adjacent normal tissues by IF. (*P<0.05, **P<0.01, ***P<0.001, ****P<0.0001)

3.4.11. Isolation and characterization of exosomes from serum of poorly differentiated patients

Figure 8A schematically represents the process of isolation of exosomes. Upon characterization by western blot, we deduced that the expression of exosomes markers (ALIX and TSG-101) showed similar protein content in exosomes isolated from both serum and cell culture supernatant (Figure 8B). SEM revealed that the isolated exosomes were round in morphology, having a size range of 70nm-150nm (Figure 8C). Interestingly, DLS and NTA data validated the results of SEM where 81.5% particles/ml were of 108.8nm (FWHM/nm,118.3). The X50 value is 114.7 with a volume 243.1 and Zeta potential was recorded -5.22 ± 0.10 mV (Figure 8D-F). Additionally, the isolated exosomes also had the potential to internalise into host cells as revealed by increased MFI upon internalization of CFSE-tagged exosomes in cells after incubation with the tagged exosomes as compared to non incubated cells (Figure 8G).

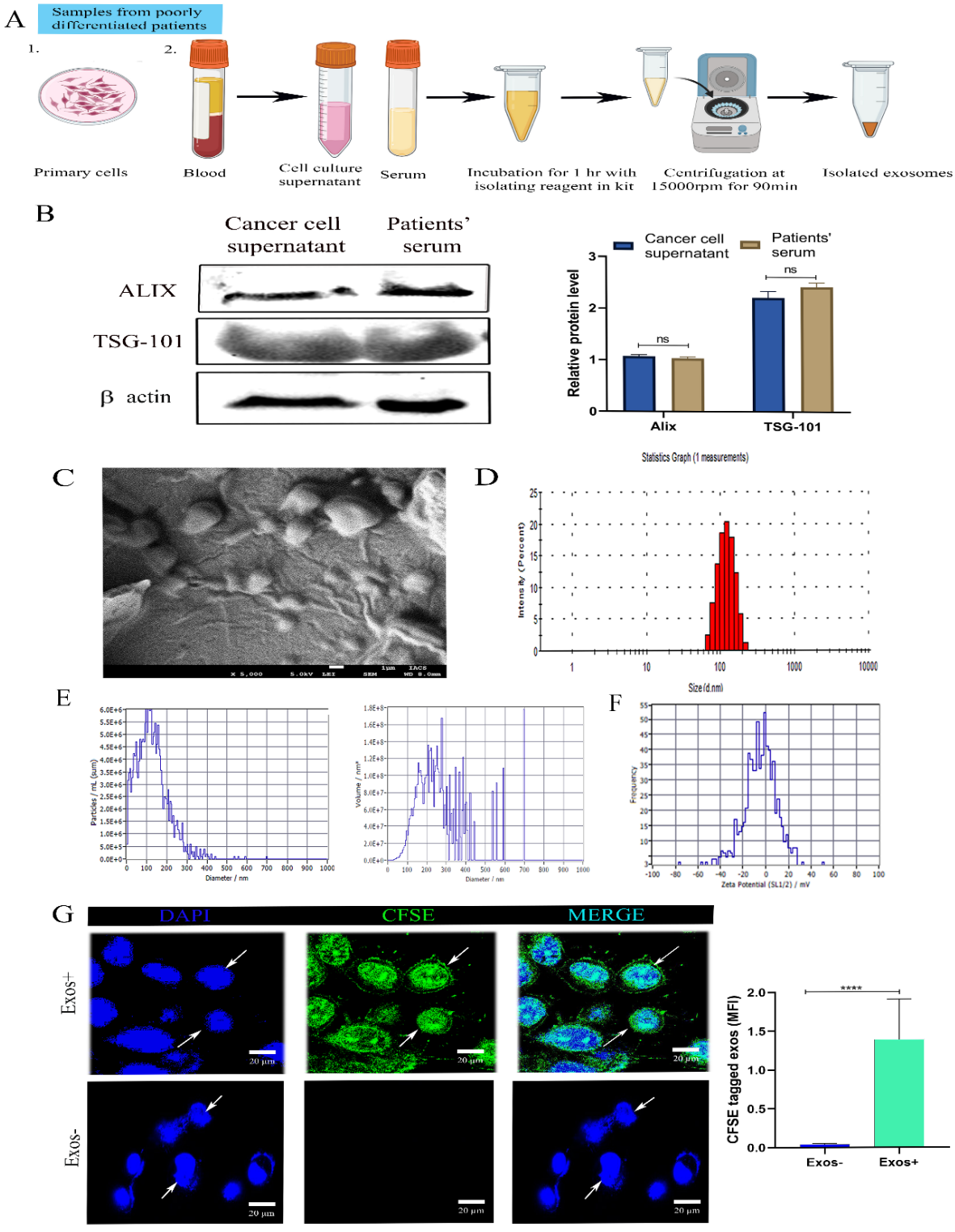

Figure 8. A. Schematic representation of isolation of exosomes; B. Western blot analysis of exosomal markers from cancer cell supernatant and patients' serum; C. SEM images for morphological evaluation; D. DLS for determination of size of isolated exosomes. E. NTA for concentration of exosomes; F. Zeta potential of exosomes; G. Internalization of CFSE-tagged exosomes by confocal microscopy. (*P<0.05, **P<0.01, ***P<0.001, ****P<0.0001)

3.4.12. Metabolic inhibitor decreases the elevated cytokines level induced by exosomal interference

Primary cells isolated from poorly differentiated OvCa tissues were treated under four categories as schematically represented in Figure 9A. SIRT1 Inh revealed an IC_{50} dose of 0.205µM in primary cancer cells (Figure 9B) and the primary cells were treated in this concentration in the presence and absence of exogenous exosomes. The secretion levels of pro-inflammatory cytokines (IL-6 and TNF-α) increased considerably upon the addition of exosomes, depicting that exosomes are responsible for establishing an inflammatory milieu, however, the levels decreased upon treatment with SIRT1 Inh (Figure 9C). Interestingly, the levels of anti-inflammatory markers (IL-10 and TGF-β) decreased under the effect of exosomes and increased significantly under the treatment with SIRT1 Inh, depicting that the inhibitor is potent in mitigating the inflammation in the TME (Figure 9D).

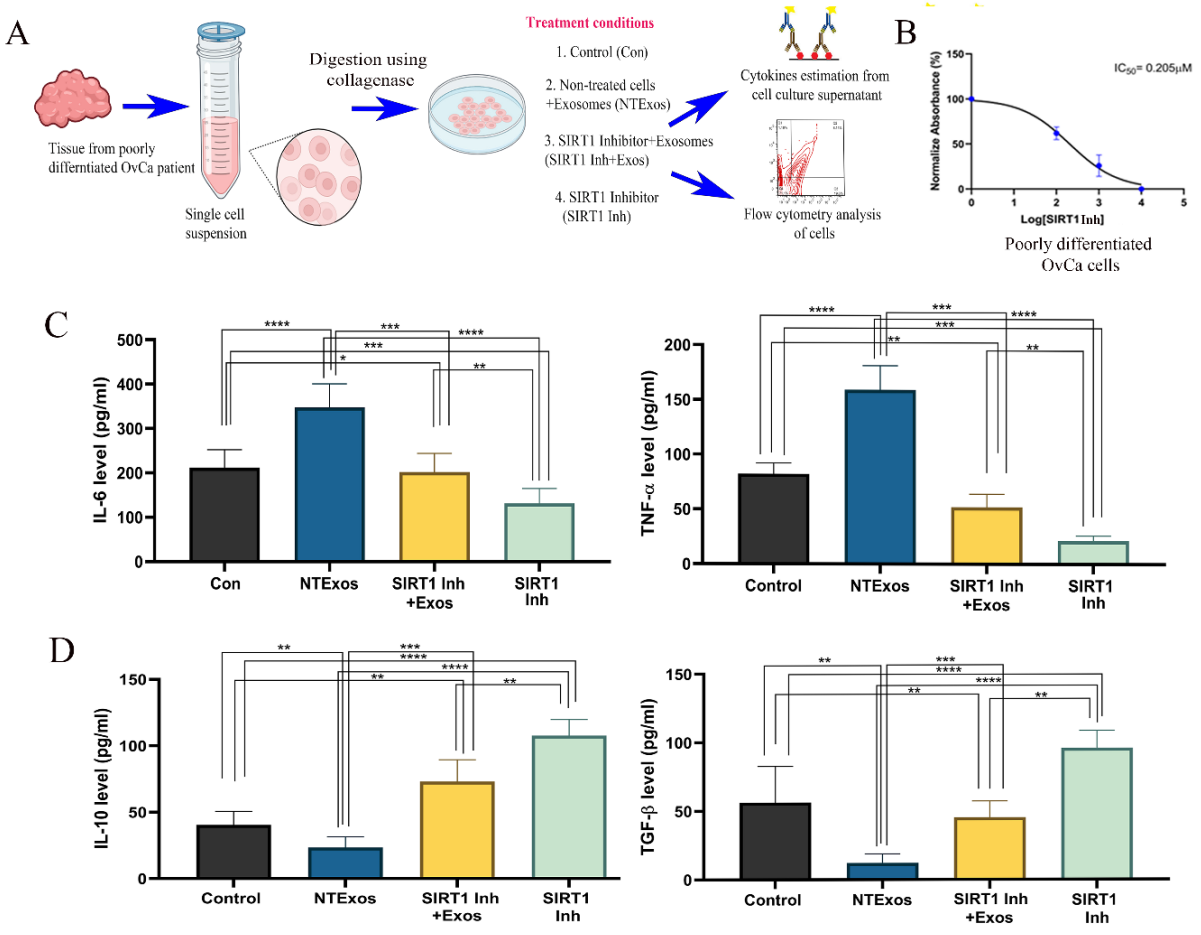

Figure 9. A. Schematic representation of isolation of single cells from poorly differentiated OvCa tissues; B. MTT assay of SIRT1 Inh on primary OvCa cells; C. Analysis of pro-inflammatory cytokines by ELISA; D. Analysis of anti-inflammatory cytokines by ELISA. (*P<0.05, **P<0.01, ***P<0.001, ****P<0.0001)

3.4.13. Levels of SIRT1/COX-2/IL-6 decrease under the effect of SIRT1 Inh modulating the expression levels of EMT markers

The gating strategy of the flow cytometric analysis of primary OvCa epithelial cells under the above mentioned treatment parameters is represented in Figure 10A. The expression levels of SIRT1, COX-2 and IL-6 were high under the effect of exogenous exosomes (Figure 10B-D). Surprisingly, SIRT1, COX-2 and IL-6 levels increased considerably under the effect of exogenous exosomes, however, under the SIRT1 Inh treatment group, their expression decreased significantly (Figure 10E-G). Upon deducing this, we were inclined to estimate the levels of EMT markers, where it was observed that epithelial marker E-cad decreased considerably under the effect of exogenous exosomes but increased under the treatment group. Interestingly, mesenchymal marker Vim increased at a significant rate when exogenous exosomes were added and decreased under SIRT1 Inh treatment (Figure 10H-I).

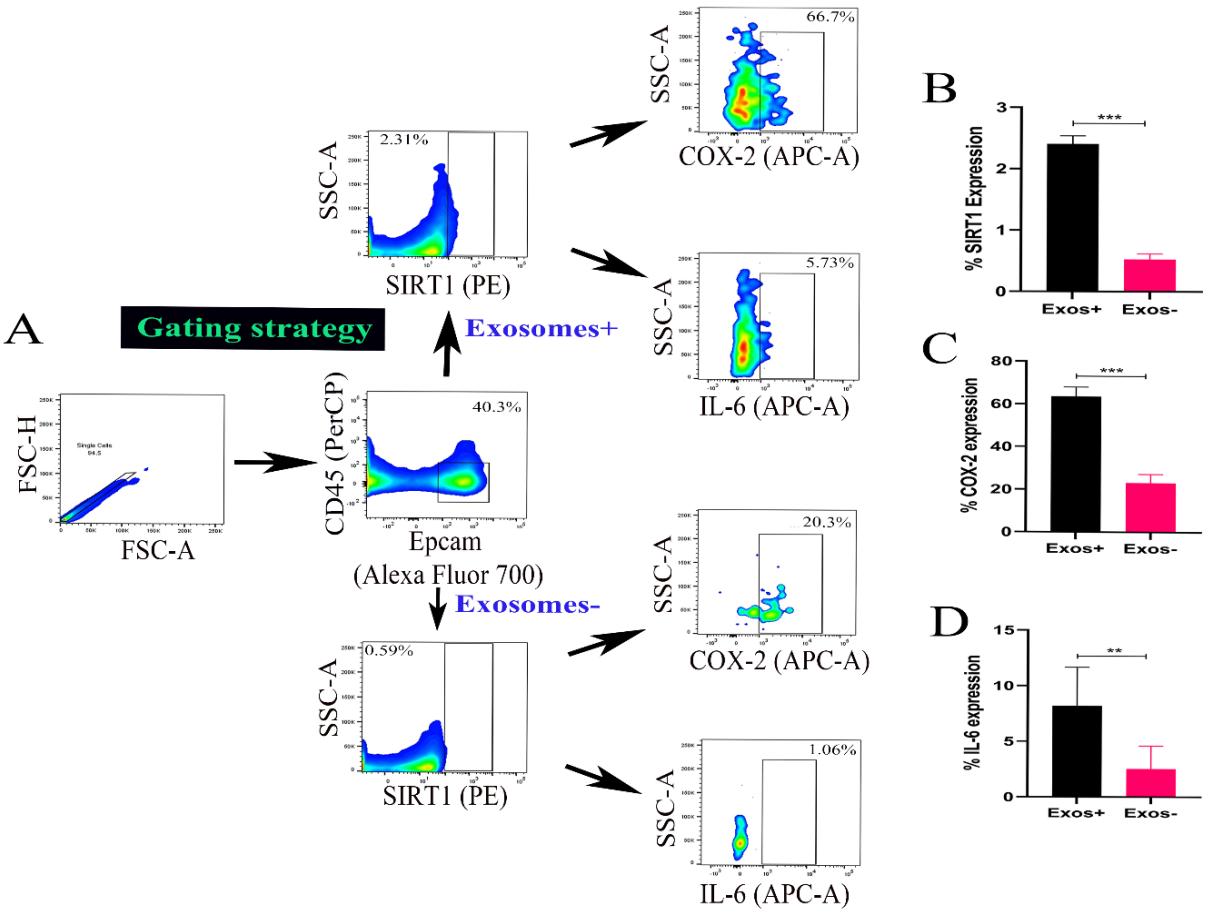

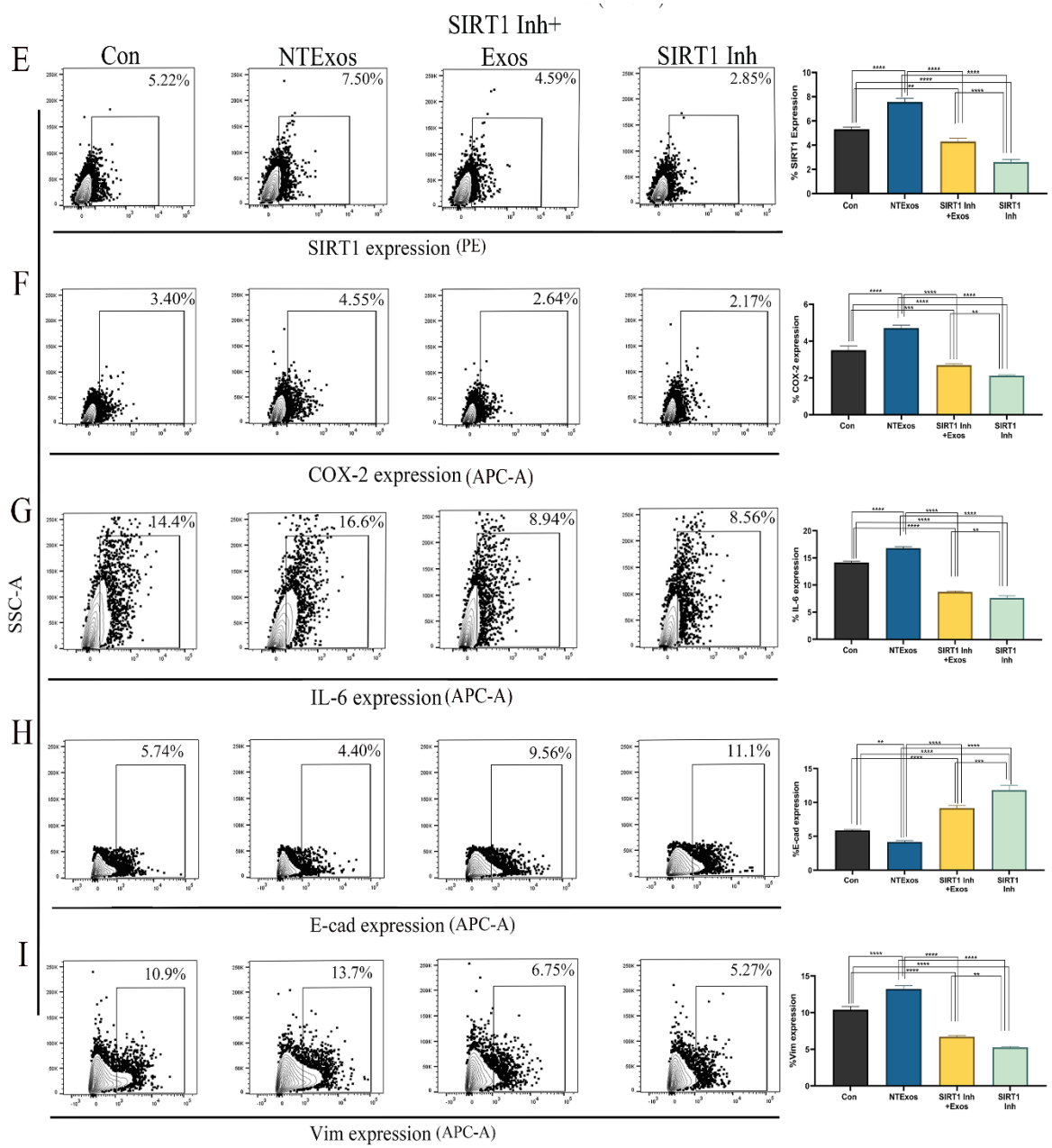

Figure 10. A. Gating strategy for estimating the epithelial cells in the heterogenous primary OvCa cells. B. Expression of SIRT1 in primary epithelial cells in the presence (Exos+) and absence of exosomes (Exos-); C. Expression of COX-2 in primary epithelial cells in the presence (Exos+) and absence of exosomes (Exos-) by flow cytometry; D. Expression of IL-6 in primary epithelial cells in primary epithelial cells in the presence (Exos+) and absence of exosomes (Exos-) by flow cytometry; E. Flow cytometric analysis of SIRT1 level in primary epithelial cells under Con, NTExos, SIRT1 Inh+Exos and SIRT1 Inh; F. Flow cytometric analysis of COX-2 level in primary epithelial cells under Con, NTExos, SIRT1 Inh+Exos and SIRT1 Inh; G. Flow cytometric analysis of IL-6 level in primary epithelial cells under Con, NTExos, SIRT1 Inh+Exos and SIRT1 Inh; H. Flow cytometric analysis of E-cad level in

primary epithelial cells under Con, NTExos, SIRT1 Inh+Exos and SIRT1 Inh; I. Flow cytometric analysis of Vim level in primary epithelial cells under Con, NTExos, SIRT1 Inh+Exos and SIRT1 Inh. (*P<0.05, **P<0.01, ***P<0.001, ****P<0.0001)

3.4.14. Generation of ROS and apoptotic cells count increase under the effect of SIRT1 Inh

Upon deducing the above results, which revealed SIRT1 regulates the metastatic process by creating an inflammatory TME, we were inclined to study the effect on ROS and apoptosis related factors under the above mentioned treatment conditions. Interestingly, we observed both ROS and Annexin V+ cells decreased under the effect of exogenous exosomes, whereas the generation of ROS and Annexin V+ cells increased under the SIRT1 Inh treatment category in primary cancer cells (Figure 11A-B). Further analysis of pro-apoptotic, Bax and anti-apoptotic Bcl-2, we observed that the Bax level decreased under the effect of exogenous exosomes but increased under the treatment of SIRT1 Inh (Figure 11C). The expression level of Bcl-2, however, increased under exosomal interference and decreased under the effect of SIRT1 Inh (Figure 11D).

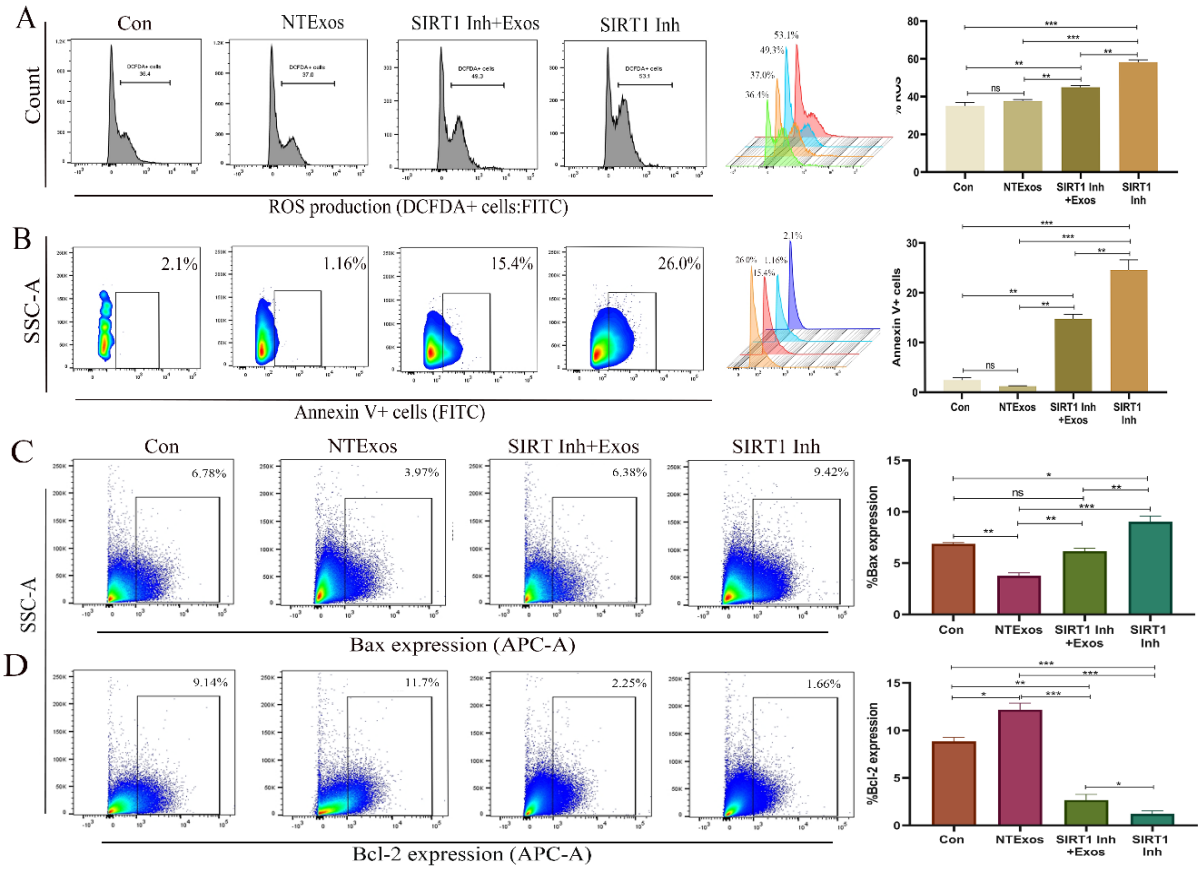

Figure 11. A. Flow cytometric determination of generation of ROS level in OvCa primary cells by DCFDA assay under Con, NTExos, SIRT1 Inh+Exos and SIRT1 Inh; B. Flow

cytometric determination of the percentage of AnnexinV+ OvCa primary cells under Con, NTExos, SIRT1 Inh+Exos and SIRT1 Inh; C. Flow cytometric determination of Bax level in OvCa primary cells under Con, NTExos, SIRT1 Inh+Exos and SIRT1 Inh; D. Flow cytometric determination of Bcl-2 level in OvCa primary cells under Con, NTExos, SIRT1 Inh+Exos and SIRT1 Inh. (*P<0.05, **P<0.01, ***P<0.001, ****P<0.0001)

3.5. Discussion

The signs and symptoms of OvCa mostly resemble normal symptoms that a woman can experience on any given day like abdominal bloating and pain, changes in faecal excretion habits, frequency in urine discharge, etc. Proper education on the signs and symptoms of OvCa is essential to create awareness for not neglecting the symptoms as it results in late diagnosis of the disease [34]. Established risk factors for the occurrence of OvCa, mainly EOC, can be reproductive, gynaecologic, hormonal, genetic, age, and lifestyle.

OvCa is more prevalent in older age (median age 50-79 years, mostly above 64 years) with an advanced stage compared to younger women. OvCa is a postmenopausal menace as with increasing age the administration of the treatment gets compromised leading to poor survival of the patients [4]. However, obese women in the premenopausal period experience a higher risk of OvCa compared to the postmenopausal period [35]. Additionally, obesity in the pre-pregnancy period is also a risk factor for OvCa [36]. Interestingly, our data also revealed similar results with a significant association with tumor differentiation determining the association of obesity and menopausal status with the aggressiveness of the disease in the patients of Eastern India. The occurrence of OvCa is reported to be inversely correlated with physical activity or occupation [37]. However, a significant association between occupation and tumor association was deduced from our retrospective data analysis. This result is further validated by the significant association of working hours and stress level with tumor differentiation, as discussed later. Our data has derived a significant correlation with the marital status and marital age of the patients, which is consistent with a prior cohort study where the widow or divorced patients were at a higher risk of OvCa [38]. It has also been established recently that the unmarried patients with ovarian serous carcinoma, generally poorly differentiated, had experienced a higher HR of OS [39]. Previous data revealed that dietary habits like intake of meat and high fat held a significant relation with OvCa occurrence [40] but in our data scenario, there was a non-significant correlation between food

habits (vegetarians/non-vegetarians) and the degree of tumor differentiation which might be due to the lower number of patients.

Women with records for incidence of cancer in one third degree biological relatives (great grandparents, great aunt, first cousin etc.) or two or more blood relatives with BC and/or OvCa are more prone to develop OvCa [41]. However, no significant association with the family history was deduced in our study. A recent study conducted by *Liang et al.* revealed no significant correlation with the risk of developing OvCa with variances in sleeping patterns and sleep habits [39]. Our data also corroborated with this finding thus nullifying altered sleeping patterns as a risk factor for developing OvCa. An epidemiologic meta-analysis of various cancers relating to the risk of cancer development with work stress demonstrated that no significant correlation was associated with OvCa [42] but on the contrary, our study has suggested a strong correlation with stress level and working hours. A pooled analysis in Asian women depicted that the women consuming alcohol results in inactivation of acetaldehyde dehydrogenase2 (ALDH2) due to ALDH2 polymorphism rs671 (Glu504Lys) increased the acetaldehyde exposure. This had an inverse genetic relation with mucinous ovarian cancer [43]. In a study, it was observed that red wine drinkers are less likely to develop OvCa as compared to non-drinkers. However, beer and spirit consumers are more prone to develop Ovca [44]. In our study, no significant association was revealed between addiction and the risk of OvCa. Furthermore, in this cohort study, we have included a few more distinct stratified parameters like religion, education, cooking fuels and food timings but there was no association of them with the tumor differentiation that might impose the risk of OvCa.

Uninterrupted ovulation causes damage to the epithelial cells of the ovaries which emerges as a high risk factor for OvCa. Thus, reducing the ovulation cycle upon the usage of oral contraceptive pills, pregnancy tenure, etc. can minimize the risk of OvCa [45,46]. On the contrary, irregularity in menstrual cycles leading to a decrease in ovulation cycles can be a high risk factor for OvCa [47]. Late age pregnancy reduces the risk of OvCa whereas early age menarche and late age menopause increases the risk for OvCa development [48]. However, no significant association was observed between tumor differentiation and menstruation related factors like menstruation type and age of menarche and menopause. Tubec cauterization (tubectomy) reduces the risk of OvCa [49] and thus held no association with tumor differentiation in our study. However, mode of delivery and parity held a significant correlation with the tumor differentiation.

Simultaneously, upon studying the symptoms, we observed that pain is the most prominent symptom accompanied by distension of the abdomen, which in turn serve as indicators of aggressiveness and progression of the disease creating physical ailment and mental distress to the patients. When we underwent a trend analysis we observed that pain was more intense in the advanced stage i.e. poorly differentiated tumor OvCa patients which directed us to continue our further study with the poorly differentiated OvCa patients.

The association of inflammation mediated cancer symptoms linked to advanced stage cancer is evident from multiple studies [50][51] but this parameter still needs to be explored in OvCa. Under this doctrine, one important factor that has been previously related to pain is COX-2. The involvement of COX-2 as a regulatory factor for pain induction is reported in patients with mandibular surgeries [52] and other medical conditions [53] but not in cancer yet. In our study, we have analyzed the level of COX-2 in the serum and primary culture supernatant of the poorly differentiated OvCa and additionally, we have also checked the expression status of COX-2 in poorly differentiated cancer tissues and compared it with adjacent normal tissues. Interestingly, it was observed that the COX-2 level was significantly higher in the cancer patients which in turn fitted our hypothesis of the involvement of COX-2 in inducing elevated pain in the late-stage patients. Interestingly multiple evidence suggests the interconnected roles of COX-2 and inflammatory cytokines in cancer [54]. Pain in cancer patients can be the outcome of tumor growth, metastasis, systemic inflammation and psychological reasons leading to worse patients' conditions [55]. Pro-inflammatory cytokines inducing pain are reported to exhibit possible mechanisms including spontaneous nerve fiber discharge [56], altering neurotransmission [57], and variability of the phenotype of the nerve end receptor [58]. *Laired et al.* deduced TNF- α and IL-1β modulate systemic inflammation in the animal hyperalgesia model. In the same study, clinically a strong association of IL-6 inducing pain was observed [59]. Another similar study by *Cohen et al.* reported that initiation of EMT in BC occurred under the influence of TNF- α, IL-6, TGF- β in BC [60]. This further led us to study the cytokines and chemokines pattern in the serum and primary culture supernatant of OvCa patients compared to the serum of healthy volunteers. Surprisingly, we deduced that although the pro- and anti-inflammatory cytokines were all significantly higher in the cancer patients among them, IL-6 was surprisingly higher. The findings by *Zhang et al.* strengthened our findings by demonstrating that in osteosarcoma, inhibiting IL-6 in both *in-vitro* and *in-vivo* systems reduced the proliferation and invasiveness of cancer cells and also combatted the seeding of the circulating tumor cells [61].

Additionally, the outcomes in a clinical study conducted by *Kampan et al.* corroborated our findings stating that higher levels of IL-6 in high grade serous cancer OvCa patients might be a potent biomarker at diagnostic level [62]. In deducing this, we have confronted to lead the study with pro-inflammatory cytokine IL-6.

The relationship between cancer and chronic inflammation became apparent after the groundbreaking research of Rudolf Virchow more than 150 years ago. However, it was not possible to determine the cause of the relationship between inflammation and cancer until about a decade ago by following the directions of research through experimental models known to date for many types of cancer. As many as 20% of human cancer cases are evolutionary consequences of chronic inflammation that continues in the context of anesthetic infection. Proinflammatory cytokines along with immune cells and tumor-invasive myeloid cells perform their roles in the initiation and progression of metastasis in inflammation-mediated cancer [63][64]. Since inflammation and metastasis go hand in hand, we were also inclined to evaluate the tumor markers responsible for angiogenesis and metastasis. We have checked the coexpression status of VEGF, ANGPT2, MMP2, and MMP9 and observed their increased colocalization in the poorly differentiated tumor tissues compared to the adjacent normal. Our results were strengthened by the finding that EP2, the subtype of prostaglandin 2 (PGE2) receptor, instigates VEGF induced angiogenesis which in turn regulates the survival and migration of endothelial cells in cancer [65]. There exists numerous evidence documenting the tumor promoting roles of MMP2 and MMP9. They are extensively studied in OvCa revealing that they are highly secreted and activated and eventually participate in promoting metastasis of OvCa which resulted in poor survival of the patients [66]. *Brun et al.* documented that MMP2 and MMP9 are higher in serous compared to the mucinous form. MMP2 is reported to be higher in benign form whereas MMP9 is elevated in malignant serous OvCa patients. However, MMP2 and MMP9 were higher in the mucinous form [67]. *Liu et al.,* by their meta-analysis reported increasing levels of MMP9 with increasing stages of tumor, thereby demonstrating its diagnostic and prognostic value [68]. Autocrine secretion of IL-6 augments the expression status of MMP2 and MMP9 in OvCa which in turn confers the aggressiveness to the cancer cells, thereby revealing the association of IL-6 and MMP2/9 in OvCa progression [69].

Additionally, with these findings, we have surprisingly deduced a correlation between all these markers involved in driving the progression of cancer cells with the master regulator of metabolism SIRT1. Moreover, when the BMI with tumor differentiation, it held a

significantly higher strong correlation which illustrates metabolism plays a role in the metastasis of OvCa. It was previously validated by *Roy et al.* suggesting that elevated expression of SIRT1 in the OvCa patients is in correlation with CA-125 and exosomes as compared to the adjacent normal [20]. The scores related to inflammation, metastasis and metabolism have been vividly illustrated in the result section. Upon this finding, we were inclined to investigate the coexpression of SIRT1 and COX-2 which surprisingly revealed that both were highly coexpressed in the tumor tissues of the poorly differentiated OvCa patients as compared to the adjacent normal. However, evidence reveals that SIRT1 activation downregulates the COX-2 expression in lung cancer [70] but in OvCa there exists a strong positive interconnection between these parameters. We also checked the coexpression of SIRT1 and PTEN where we observed that with increasing SIRT1 expression the PTEN expression decreased in the tumor tissues as compared to the normal. This result has also corroborated the finding that SIRT1 inhibits PTEN expression by deacetylating it in thyroid cancer [71]. Moreover, SIRT1 deacetylates and inhibits PTEN which in turn activate the PI3K/AKT pathway [72]. The hypothesis in our study that SIRT1/COX-2/IL-6 axis interplay roles to drive the metastasis in OvCa is supported by all the previous findings (Figure 12).

Upon deriving and validating the relation of COX-2, IL-6 and SIRT1, we were inclined to investigate the effect of exosomes upon these factors that in turn contribute to the process of metabolism and inflammation mediated metastasis by inhibiting SIRT1. To evaluate this we isolated exosomes from the serum of poorly differentiated patients and characterized those. Additionally, we exogenously applied these exosomes into the primary cells derived from poorly differentiated OvCa tumor tissues under the effect of SIRT1 Inh. We have observed that under the effect of exosomes, the levels of COX-2 and IL-6 increased drastically but eventually, the SIRT1 Inh reduced their levels. Similar results were observed with the mesenchymal marker Vim. Still, surprisingly it was observed that the E-cad level increased under the effect of the SIRT1 Inh even though exogenous exosmes reduced the E-cad level. Evidence reveals that upregulated SIRT1 drives the process of EMT in EC and inhibiting it reverses the process of initiation of metastasis [73]. Furthermore, in NSCLC, EMT associated with metastasis is upregulated by SIRT1 regulated by B7-H3 [74]. Thus, the earlier findings supported our results in OvCa. These results suggest that exosomes when enter the cancer cells, regulate the metabolic factor SIRT1 thereby inducing higher expression of COX-2 which in turn promotes elevated secretion of pro-inflammatory

cytokine, IL-6. This regulatory pathway instigates the process of metastasis by initiating EMT and increasing the progressiveness of the OvCa cells thus inhibiting SIRT1 can shed light on the complex molecular mechanisms dictating cancer progression and provide valuable insights for the development of novel therapeutic strategies. Thus, inhibiting SIRT1 comprehens the development of novel treatment strategies in OvCa. Furthermore, we have deduced that SIRT1 Inh exhibits the capability to induce ROS production in the cancer cells that promotes apoptosis of the OvCa cells. This result was validated by findings illustrating isoalantolactone downregulates SIRT1 which resulted in increased ROS production thereby inducing apoptosis in BC cells [75]. Another study where pemetrexed induces apoptosis by inhibiting SIRT1 and increasing ROS production in mesothelioma and A549 cells [76]. Thus, it can be deduced from our findings that SIRT1 inhibition can also induce apoptosis in OvCa.

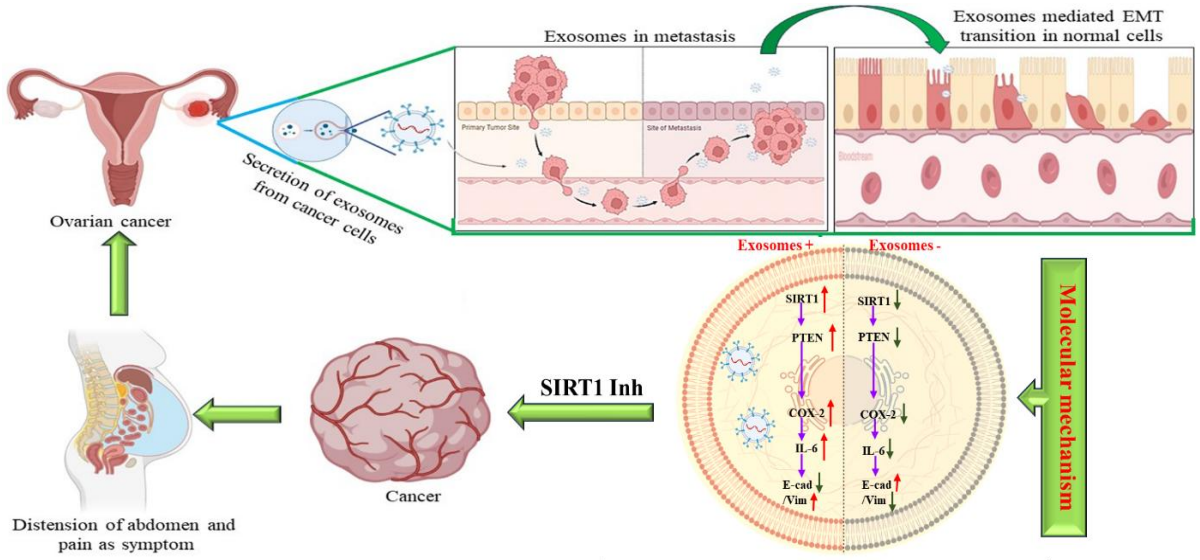

Figure 12. Schematic representation of molecular circuitry

The present study encompasses a new insight into OvCa cancer research depicting sociodemographic and gynaecological parameters. The parameters included in the study were new aspects to be analyzed. Our brief analysis revealed a valid correlation with risk factors detecting the degree of tumor differentiation in the participants of Eastern India. Thus, spreading awareness through OvCa control programs and proper health policies can provide a new dimension by analyzing the risks of OvCa and also planning the treatment strategy accordingly. Additionally, evaluation of the role of exosomes in inducing higher metastatic characteristics and their mitigation with the SIRT1 Inh can be a novel therapeutic approach to combat the proliferation and invasiveness of poorly differentiated OvCa cells.

3.6. References

[1] M.S. Zayyan, Risk Factors for Ovarian Cancer, in: Intech, 2016: p. 13.

[2] S. Shabir, P.K. Gill, Global scenario on ovarian cancer – Its dynamics, relative survival, treatment, and epidemiology, Adesh Univ. J. Med. Sci. Res. 2 (2020) 17–25. https://doi.org/10.25259/aujmsr_16_2019.

[3] C. La Vecchia, Ovarian cancer: Epidemiology and risk factors, Eur. J. Cancer Prev. 26 (2017) 55–62. https://doi.org/10.1097/CEJ.0000000000000217.

[4] Z. Momenimovahed, A. Tiznobaik, S. Taheri, H. Salehiniya, Ovarian cancer in the world: Epidemiology and risk factors, Int. J. Womens. Health. 11 (2019) 287–299. https://doi.org/10.2147/IJWH.S197604.

[5] M. Zhang, A.H. Lee, C.W. Binns, Reproductive and dietary risk factors for epithelial ovarian cancer in China, Gynecol. Oncol. 92 (2004) 320–326. https://doi.org/10.1016/j.ygyno.2003.10.025.

[6] C.M.N. C. Præstegaard, S.K. Kjaer, T.S. Nielsen, S.M. Jensen, P.M. Webb, The association between socioeconomic status and tumour stage at diagnosis of ovarian cancer: a pooled analysis of 18 case-control studies, Cancer Epidemiol. 41 (2017) 71–79. https://doi.org/10.1016/j.canep.2016.01.012.The.

[7] C. Karpinskyj, M. Burnell, A. Gonzalez-Izquierdo, A. Ryan, J. Kalsi, I. Jacobs, M. Parmar, U. Menon, A. Gentry-Maharaj, Socioeconomic status and ovarian cancer stage at diagnosis: A study nested within UKCToCs, Diagnostics. 10 (2020) 89. https://doi.org/10.3390/diagnostics10020089.

[8] B. Park, S. Park, T.J. Kim, S.H. Ma, B.G. Kim, Y.M. Kim, J.W. Kim, S. Kang, J. Kim, T.J. Kim, K.Y. Yoo, S.K. Park, Epidemiological characteristics of ovarian cancer in Korea, J. Gynecol. Oncol. 21 (2010) 241–247. https://doi.org/10.3802/jgo.2010.21.4.241.

[9] H.S.N. A. Devi, A Krishnan, Epidemiological Risk Factors for Primary Ovarian Malignancy in Indian Population- A Case Control Study from a Tertiary Care Centre in Kerala, J. Med. Sci. Clin. Res. 05 (2017) 15664–15669. https://doi.org/10.18535/jmscr/v5i1.77.

[10] B.A. Goff, L.S. Mandel, C.H. Melancon, H.G. Muntz, Frequency of symptoms of ovarian cancer in women presenting to primary care clinics, JAMA. 291 (2004) 2705–2712. https://doi.org/10.1001/JAMA.291.22.2705.

[11] K.R. Cho, I.M. Shih, Ovarian cancer, Annu. Rev. Pathol. Mech. Dis. 4 (2009) 287–313. https://doi.org/10.1146/annurev.pathol.4.110807.092246.

[12] D. Sinha, S. Roy, P. Saha, N. Chatterjee, A. Bishayee, Trends in Research on Exosomes in Cancer Progression and Anticancer Therapy, Cancers 2021, Vol. 13, Page 326. 13 (2021) 326. https://doi.org/10.3390/CANCERS13020326.

[13] M. Neagu, C. Constantin, I.D. Popescu, D. Zipeto, G. Tzanakakis, D. Nikitovic, C. Fenga, C.A. Stratakis, D.A. Spandidos, A.M. Tsatsakis, Inflammation and metabolism in cancer cell—mitochondria key player, Front. Oncol. 9 (2019) 1–15. https://doi.org/10.3389/fonc.2019.00348.

[14] D.K. Alves-Fernandes, M.G. Jasiulionis, The role of SIRT1 on DNA damage response and epigenetic alterations in cancer, Int. J. Mol. Sci. 20 (2019) 3153. https://doi.org/10.3390/ijms20133153.

[15] Y. Lv, R. He, J. Lu, A. Wei, R. Chen, FOXQ1 promotes proliferation and metastasis of epithelial ovarian cancer via activation of SIRT1/NRF2 signaling pathway, Trop. J. Pharm. Res. 18 (2019) 1397–1404. https://doi.org/10.4314/tjpr.v18i7.5.

[16] W. Feng, D.C. Dean, F.J. Hornicek, H. Shi, Z. Duan, Exosomes promote pre-metastatic niche formation in ovarian cancer, Mol. Cancer. 18 (2019) 124. https://doi.org/10.1186/s12943-019-1049-4.

[17] A.H. Fischer, K.A. Jacobson, J. Rose, R. Zeller, Hematoxylin and eosin staining of tissueand cell sections, Cold Spring Harb. Protoc. 3 (2008) 3–5. https://doi.org/10.1101/pdb.prot4986.

[18] B.L. Thériault, L. Portelance, A.M. Mes-Masson, M.W. Nachtigal, Establishment of primary cultures from ovarian tumor tissue and ascites fluid, Methods Mol. Biol. 1049 (2013) 323–336. https://doi.org/10.1007/978-1-62703-547-7_24.

[19] S.K. Das, S. Roy, A. Das, A. Chowdhury, N. Chatterjee, A. Bhaumik, A conjugated 2D covalent organic framework as a drug delivery vehicle towards triple negative breast cancer malignancy, Nanoscale Adv. (2022) 2313–2320. https://doi.org/10.1039/d2na00103a.

[20] S. Roy, A. Das, M. Vernekar, S. Mandal, N. Chatterjee, Understanding the Correlation between Metabolic Regulator SIRT1 and Exosomes with CA-125 in Ovarian Cancer: A Clinicopathological Study, Biomed Res. Int. 2022 (2022) 5346091. https://doi.org/10.1155/2022/5346091.

[21] D.A. Cohen, D.J. Dabbs, K.L. Cooper, M. Amin, T.E. Jones, M.W. Jones, M. Chivukula, G.A. Trucco, R. Bhargava, Interobserver agreement among pathologists for semiquantitative hormone receptor scoring in breast carcinoma, Am. J. Clin. Pathol. 138 (2012) 796–802. https://doi.org/10.1309/AJCP6DKRND5CKVDD.

[22] M.I. Lutz, C. Schwaiger, B. Hochreiter, G.G. Kovacs, J.A. Schmid, Novel approach for accurate tissue-based protein colocalization and proximity microscopy, Sci. Rep. 7 (2017) 2668. https://doi.org/10.1038/s41598-017-02735-8.

[23] M. Charan, S. Das, S. Mishra, N. Chatterjee, S. Varikuti, K. Kaul, S. Misri, D.K. Ahirwar, A.R. Satoskar, R.K. Ganju, Macrophage migration inhibitory factor inhibition as a novel therapeutic approach against triple-negative breast cancer, Cell Death Dis. 11 (2020) 774. https://doi.org/10.1038/s41419-020-02992-y.

[24] M. Mercadal, C. Herrero, O. López-Rodrigo, M. Castells, A. de la Fuente, F. Vigués, L. Bassas, S. Larriba, Impact of extracellular vesicle isolation methods on downstream mirna analysis in semen: A comparative study, Int. J. Mol. Sci. 21 (2020) 5949. https://doi.org/10.3390/ijms21175949.

[25] T.S. Lyu, Y. Ahn, Y.J. Im, S.S. Kim, K.H. Lee, J. Kim, Y. Choi, D. Lee, E.S. Kang, G. Jin, J. Hwang, S.I. Lee, J.A. Cho, The characterization of exosomes from fibrosarcoma cell and the useful usage of Dynamic Light Scattering (DLS) for their evaluation, PLoS One. 16 (2021) e0231994. https://doi.org/10.1371/journal.pone.0231994.

[26] W. Zhang, P. Peng, Y. Kuang, J. Yang, D. Cao, Y. You, K. Shen, Characterization of exosomes derived from ovarian cancer cells and normal ovarian epithelial cells by nanoparticle tracking analysis, Tumor Biol. 37 (2016) 4213–4221. https://doi.org/10.1007/s13277-015-4105-8.

[27] K.D.J. Wu Y, Deng W, Exosomes: Improved methods to characterize their morphology, RNA content, and surface protein biomarkers, Analyst. 140 (2015) 6631–6642. https://doi.org/10.1039/c5an00688k.Exosomes.

[28] A. Morales-Kastresana, B. Telford, T.A. Musich, K. McKinnon, C. Clayborne, Z. Braig, A. Rosner, T. Demberg, D.C. Watson, T.S. Karpova, G.J. Freeman, R.H. Dekruyff, G.N. Pavlakis, M. Terabe, M. Robert-Guroff, J.A. Berzofsky, J.C. Jones, Labeling extracellular vesicles for nanoscale flow cytometry, Sci. Rep. 7 (2017) 1878. https://doi.org/10.1038/s41598-017-01731-2.

[29] S. Lin, Z. Ke, K. Liu, S. Zhu, Z. Li, H. Yin, Z. Chen, Identification of DAPI-stained normal, inflammatory, and carcinoma hepatic cells based on hyperspectral microscopy, Biomed. Opt. Express. 13 (2022) 2082. https://doi.org/10.1364/boe.451006.

[30] C. Escrevente, S. Keller, P. Altevogt, J. Costa, Interaction and uptake of exosomes by ovarian cancer cells, BMC Cancer. 11 (2011) 108. https://doi.org/10.1186/1471-2407-11-108.

[31] E. Hosseini-Beheshti, S. Pham, H. Adomat, N. Li, E.S. Tomlinson Guns, Exosomes as biomarker enriched microvesicles: Characterization of exosomal proteins derived from a panel of prostate cell lines with distinct AR phenotypes, Mol. Cell. Proteomics. 11 (2012) 863–885. https://doi.org/10.1074/mcp.M111.014845.

[32] N. Chatterjee, S. Das, D. Bose, S. Banerjee, T. Jha, K. Das Saha, Lipid from infective L. Donovani regulates acute myeloid cell growth via mitochondria dependent MAPK pathway, PLoS One. 10 (2015). https://doi.org/10.1371/journal.pone.0120509.

[33] H. Hozhabri, R.S.G. Dehkohneh, S.M. Razavi, S.M. Razavi, F. Salarian, A. Rasouli, J. Azami, M.G. Shiran, Z. Kardan, N. Farrokhzad, A.M. Namini, A. Salari, Comparative analysis of protein-protein interaction networks in metastatic breast cancer, PLoS One. 17 (2022) e0260584. https://doi.org/10.1371/journal.pone.0260584.

[34] C. Stewart, C. Ralyea, S. Lockwood, Ovarian Cancer: An Integrated Review, Semin. Oncol. Nurs. 35 (2019) 151–156. https://doi.org/10.1016/j.soncn.2019.02.001.

[35] Z. Liu, T.T. Zhang, J.J. Zhao, S.F. Qi, P. Du, D.W. Liu, Q.B. Tian, The association between overweight, obesity and ovarian cancer: A meta-analysis, Jpn. J. Clin. Oncol. 45 (2015) 1107–1115. https://doi.org/10.1093/jjco/hyv150.

[36] R. Kessous, E. Davidson, M. Meirovitz, R. Sergienko, E. Sheiner, Prepregnancy obesity: A risk factor for future development of ovarian and breast cancer, Eur. J. Cancer Prev. 26 (2017) 151–155. https://doi.org/10.1097/CEJ.0000000000000228.

[37] J. Lee, Physical activity, sitting time, and the risk of ovarian cancer: A brief research report employing a meta-analysis of existing, Health Care Women Int. 40 (2019) 433–458. https://doi.org/10.1080/07399332.2018.1505892.

[38] S.S.T. C. Trudel-Fitzgerald, E.M. Poole, A.K. Sood, O.I. Okereke, I. Kawachi, L.D. Kubzansky, Social integration, marital status, and ovarian cancer risk: A 20- year prospective cohort study, Psychosom. Med. 81 (2019) 833–840. https://doi.org/10.1097/PSY.0000000000000747.Social.

[39] J.L. X. Liang, H.R. Harris, M. Hendry, A.H. Shadyab, L. Hale, Y. Li, T.E. Crane , E.M.C. Feliciano, M.L. Stefanick, Sleep characteristics and risk of ovarian cancer among postmenopausal women, Cancer Prev. Res. (Philadelphia Pa.). 14 (2021) 55–64. https://doi.org/10.1158/1940-6207.CAPR-20-0174.Sleep.

[40] F. Kolahdooz, T.I. Ibiebele, J.C. Van Der Pols, P.M. Webb, Dietary patterns and ovarian cancer risk, Am. J. Clin. Nutr. 89 (2009) 297–304. https://doi.org/10.3945/ajcn.2008.26575.

[41] C.A. Doubeni, A.R.B. Doubeni, A.E. Myers, Diagnosis and management of ovarian cancer, Am. Fam. Physician. 93 (2016) 937–944. https://doi.org/10.1080/21548331.1987.11707701.

[42] T. Yang, Y. Qiao, S. Xiang, W. Li, Y. Gan, Y. Chen, Work stress and the risk of cancer: A meta-analysis of observational studies, Int. J. Cancer. 144 (2019) 2390–2400. https://doi.org/10.1002/ijc.31955.

[43] T. Ugai, L.E. Kelemen, M. Mizuno, J.S. Ong, P.M. Webb, G. Chenevix-Trench, K.G. Wicklund, J.A. Doherty, M.A. Rossing, P.J. Thompson, L.R. Wilkens, M.E. Carney, M.T. Goodman, J.M. Schildkraut, A. Berchuck, D.W. Cramer, K.L. Terry, H. Cai, X.O. Shu, Y.T. Gao, Y.B. Xiang, D. Van Den Berg, M.C. Pike, A.H. Wu, C.L. Pearce, K. Matsuo, Ovarian cancer risk, ALDH2 polymorphism and alcohol drinking: Asian data from the Ovarian Cancer Association Consortium, Cancer Sci. 109 (2018) 435–445. https://doi.org/10.1111/cas.13470.

[44] L.S. Cook, A.C.Y. Leung, K. Swenerton, R.P. Gallagher, A. Magliocco, H. Steed, M. Koebel, J. Nation, S. Eshragh, A. Brooks-Wilson, N.D. Le, Adult lifetime alcohol consumption and invasive epithelial ovarian cancer risk in a population-based case-

control study, Gynecol. Oncol. 140 (2016) 277–284. https://doi.org/10.1016/j.ygyno.2015.12.005.

[45] K.A. Michels, R.M. Pfeiffer, L.A. Brinton, B. Trabert, Modification of the associations between duration of oral contraceptive use and ovarian, endometrial, breast, and colorectal cancers, JAMA Oncol. 4 (2018) 516–521. https://doi.org/10.1001/jamaoncol.2017.4942.

[46] M.F. Fathalla, Incessant ovulation and ovarian cancer - a hypothesis re-visited., Facts, Views Vis. ObGyn. 5 (2013) 292–7. http://www.ncbi.nlm.nih.gov/pubmed/24753957%0Ahttp://www.pubmedcentral.nih.gov/articlerender.fcgi?artid=PMC3987381.

[47] K.L.T. Harris, H.R., L.J. Titus, D.W. Cramer, Long and irregular menstrual cycles, polycystic ovary syndrome, and ovarian cancer risk in a population-based case- control study, Int J Cancer. 140 (2017) 139–148. https://doi.org/doi:10.1002/ijc.30441.

[48] B.M. Reid, J.B. Permuth, T.A. Sellers, Epidemiology of ovarian cancer: a review, Cancer Biol. Med. 14 (2017) 9–32. https://doi.org/10.20892/j.issn.2095-3941.2016.0084.

[49] K. Gaitskell, J. Green, K. Pirie, G. Reeves, Tubal ligation and ovarian cancer risk in a large cohort: Substantial variation by histological type, Int. J. Cancer. 138 (2016) 1076–1084. https://doi.org/10.1002/ijc.29856.

[50] B.J. Laird, D.C. McMillan, P. Fayers, K. Fearon, S. Kaasa, M.T. Fallon, P. Klepstad, The systemic inflammatory response and its relationship to pain and other symptoms in advanced cancer, Oncologist. 18 (2013) 1050–1055. https://doi.org/10.1634/THEONCOLOGIST.2013-0120.

[51] B.J.A. Laird, M. Fallon, M.J. Hjermstad, S. Tuck, S. Kaasa, P. Klepstad, D.C. McMillan, Quality of Life in Patients With Advanced Cancer: Differential Association With Performance Status and Systemic Inflammatory Response, J. Clin. Oncol. 34 (2016) 2769–2775. https://doi.org/10.1200/JCO.2015.65.7742.

[52] A.A. Khan, M. Iadarola, H.Y.T. Yang, R.A. Dionne, Expression of COX-1 and COX-2 in a clinical model of acute inflammation, J. Pain. 8 (2007) 349–354. https://doi.org/10.1016/J.JPAIN.2006.10.004.

[53] P. Waelkens, E. Alsabbagh, A. Sauter, G.P. Joshi, H. Beloeil, Pain management after complex spine surgery: A systematic review and procedure-specific postoperative pain management recommendations, Eur. J. Anaesthesiol. 38 (2021) 985–994. https://doi.org/10.1097/EJA.0000000000001448.

[54] R.E. Harris, B.C. Casto, Z.M. Harris, Cyclooxygenase-2 and the inflammogenesis of breast cancer, World J. Clin. Oncol. 5 (2014) 677–692. https://doi.org/10.5306/wjco.v5.i4.677.

[55] A. Caraceni, R.K. Portenoy, T. Force, <Caraceni-1999-An international sur.pdf>, Pain. 82 (1999) 263–274.

[56] S.B. Oh, P.B. Tran, S.E. Gillard, R.W. Hurley, D.L. Hammond, R.J. Miller, Chemokines and glycoprotein 120 produce pain hypersensitivity by directly exciting primary nociceptive neurons, J. Neurosci. 21 (2001) 5027–5035. https://doi.org/10.1523/jneurosci.21-14-05027.2001.

[57] E. Eliav, U. Herzberg, M.A. Ruda, G.J. Bennett, Neuropathic pain from an experimental neuritis of the rat sciatic nerve, Pain. 83 (1999) 169–182. https://doi.org/10.1016/S0304-3959(99)00102-5.

[58] R.D. Martin, © 19 9 6 Nature Publishing Group, Nature. 363 (1993) 223–234. https://doi.org/10.1038/363223a0.

[59] B.J.A. Laird, A.C. Scott, L.A. Colvin, A.L. McKeon, G.D. Murray, K.C.H. Fearon, M.T. Fallon, Cancer pain and its relationship to systemic inflammation: An exploratory study, Pain. 152 (2011) 460–463. https://doi.org/10.1016/j.pain.2010.10.035.

[60] E.N. Cohen, H. Gao, S. Anfossi, M. Mego, N.G. Reddy, B. Debeb, A. Giordano, S. Tin, Q. Wu, R.J. Garza, M. Cristofanilli, S.A. Mani, D.A. Croix, N.T. Ueno, W.A. Woodward, R. Luthra, S. Krishnamurthy, J.M. Reuben, Inflammation Mediated Metastasis: Immune Induced Epithelial-To-Mesenchymal Transition in Inflammatory Breast Cancer Cells, PLoS One. 10 (2015) e0132710. https://doi.org/10.1371/JOURNAL.PONE.0132710.

[61] Y. Zhang, Q. Ma, T. Liu, G. Guan, K. Zhang, J. Chen, N. Jia, S. Yan, G. Chen, S. Liu, K. Jiang, Y. Lu, Y. Wen, H. Zhao, Y. Zhou, Q. Fan, X. Qiu, Interleukin-6 suppression reduces tumour self-seeding by circulating tumour cells in a human osteosarcoma nude

mouse model, Oncotarget. 7 (2016) 446–458. https://doi.org/10.18632/ONCOTARGET.6371.

[62] N.C. Kampan, M.T. Madondo, J. Reynolds, J. Hallo, O.M. McNally, T.W. Jobling, A.N. Stephens, M.A. Quinn, M. Plebanski, Pre-operative sera interleukin-6 in the diagnosis of high-grade serous ovarian cancer, Sci. Rep. 10 (2020) 2213. https://doi.org/10.1038/s41598-020-59009-z.

[63] K. Wang, M. Karin, Tumor-Elicited Inflammation and Colorectal Cancer, 1st ed., Elsevier Inc., 2015. https://doi.org/10.1016/bs.acr.2015.04.014.

[64] S. Hibino, T. Kawazoe, H. Kasahara, S. Itoh, T. Ishimoto, M. Sakata-Yanagimoto, K. Taniguchi, Inflammation-induced tumorigenesis and metastasis, Int. J. Mol. Sci. 22 (2021) 1–37. https://doi.org/10.3390/ijms22115421.

[65] S.H. Chang, C.H. Liu, M.T. Wu, T. Hla, Regulation of vascular endothelial cell growth factor expression in mouse mammary tumor cells by the EP2 subtype of the prostaglandin E2 receptor, Prostaglandins Other Lipid Mediat. 76 (2005) 48–58. https://doi.org/10.1016/j.prostaglandins.2004.12.001.

[66] B. Davidson, I. Goldberg, W.H. Gotlieb, J. Kopolovic, G. Ben-Baruch, J.M. Nesland, A. Berner, M. Bryne, R. Reich, High levels of MMP-2, MMP-9, MT1-MMP and TIMP-2 mRNA correlate with poor survival in ovarian carcinoma, Clin. Exp. Metastasis. 17 (1999) 799–808. https://doi.org/10.1023/A:1006723011835.

[67] M. Furuya, H. Ishikura, Y. Kawarada, Y. Ogawa, N. Sakuragi, S. Fujimoto, T. Yoshiki, Expression of matrix metalloproteinases and related tissue inhibitors in the cyst fluids of ovarian mucinous neoplasms, Gynecol. Oncol. 78 (2000) 106–112. https://doi.org/10.1006/gyno.2000.5856.

[68] C. Liu, Y. Shen, Q. Tan, Diagnostic and prognostic values of MMP-9 expression in ovarian cancer: A study based on bioinformatics analysis and meta-analysis, Int. J. Biol. Markers. 38 (2023) 15–24. https://doi.org/10.1177/03936155221140421.

[69] A. Rabinovich, L. Medina, B. Piura, S. Segal, M. Huleihel, Regulation of ovarian carcinoma SKOV-3 cell proliferation and secretion of MMPs by autocrine IL-6, Anticancer Res. 27 (2007) 267–272.

[70] W. Lim, C. Kang, Avenanthramide C suppresses hypoxia-induced cyclooxygenase-2 expression through sirtuin1 activation in non-small-cell lung cancer cells, Animal Cells Syst. (Seoul). 24 (2020) 79–83. https://doi.org/10.1080/19768354.2020.1748108.

[71] D. Herranz, A. Maraver, M. Cañamero, G. Gómez-López, L. Inglada-Pérez, M. Robledo, E. Castelblanco, X. Matias-Guiu, M. Serrano, SIRT1 promotes thyroid carcinogenesis driven by PTEN deficiency, Oncogene. 32 (2013) 4052–4056. https://doi.org/10.1038/onc.2012.407.

[72] T. Ikenoue, K. Inoki, B. Zhao, K.L. Guan, PTEN acetylation modulates its interaction with PDZ domain, Cancer Res. 68 (2008) 6908–6912. https://doi.org/10.1158/0008-5472.CAN-08-1107.

[73] M. Wang, Y. Wu, Y. He, J. Liu, Y. Chen, J. Huang, G. Qi, P. Li, SIRT1 upregulation promotes epithelial-mesenchymal transition by inducing senescence escape in endometriosis, Sci. Rep. 12 (2022) 12302. https://doi.org/10.1038/s41598-022-16629-x.

[74] H. Liao, M. Ding, N. Zhou, Y. Yang, L. Chen, B7-H3 promotes the epithelial-mesenchymal transition of NSCLC by targeting SIRT1 through the PI3K/AKT pathway, Mol. Med. Rep. 25 (2022) 79. https://doi.org/10.3892/mmr.2022.12595.

[75] Z. Li, B. Qin, X. Qi, J. Mao, D. Wu, Isoalantolactone induces apoptosis in human breast cancer cells via ROS-mediated mitochondrial pathway and downregulation of SIRT1, Arch. Pharm. Res. 39 (2016) 1441–1453. https://doi.org/10.1007/s12272-016-0815-8.

[76] K.E. Hwang, Y.S. Kim, Y.R. Hwang, S.J. Kwon, D.S. Park, B.K. Cha, B.R. Kim, K.H. Yoon, E.T. Jeong, H.R. Kim, Pemetrexed induces apoptosis in malignant mesothelioma and lung cancer cells through activation of reactive oxygen species and inhibition of sirtuin 1, Oncol. Rep. 33 (2015) 2411–2419. https://doi.org/10.3892/or.2015.3830.

Chapter 4

"Exosomes induce an oncogenic shift to the normal cells and inhibiting it can mitigate the process of metastasis"

4.1. Introduction

Metastasis of OvCa is life threating to the patients and throws a challenge to the clinicians regardless of technical and clinical improvements in treatment processes like radiation, chemotherapy and debulking surgery. Metastasis is a result of crosstalks between the cancer cells with other cells in the TME which aid the cancer cells in migrating from a primary site to a secondary site [1]. The interactions of the primary cancer cells with the ECM is the initiation of metastatic process which involves the decorin loss, upregulated versican, stiffness due to remodelled collagen into thick fibrils [2][3][4]. *Marchini et al.* stated that EMT is an outcome of development of resistance to chemotherapeutic drugs [5]. Thus, the deregulated signaling pathway in the cancer cells with SMI are in limelight in research for improving the conventional therapeutic approaches [6].

Intensive research in the field of cancer biology has revealed methods of communication between cells through extracellular vesicles called exosomes. Exosomes are released from various cells and serve as serviceable mediators resulting into dysregulations in the recipient cells. Evidences reveal OvCa derived exosomes migrate and interact with the resident cells and form a permissive TME by promoting angiogenesis, escape from immunosurveillance, the transformation of normal fibroblasts to CAFs, mesothelial remodeling for the cancer cells [7]. OvCa cells, SKOV-3 derived exosomes are reported to enhance the proliferation and migration of normal fibroblasts by increasing CAFs associated markers like α-SMA and tissue inhibitor of metalloproteinase 2 (TIMP2) [8]. Hence, inhibiting the release of exosomes can be a useful in blocking the progression of the cancer cell by stopping the intercellular communications in the TME. Understanding the biology of the cancer cells under the effect of exosomal Inh and has become an arena of research. In this regard, a potent exosomal Inh, GW4869, is investigated in OvCa metastasis. It is a neutral sphingomyelinase 2 (nSMase2) blocker which prevent the production of ceramide that in turn is a key regulator of exosomes biogenesis. Evidently, GW4869 diminishes CD44 expression and mitigates EMT in OvCa which might be an outcome of exosomes resulting in less malignant cancer cells [9]. Therefore, development of exosomes inhibitors as research tools and as drug delivery agents is in focus to be included in clinical trials. Thus, studies on exosomes may lead to a breakthrough in cancer research, for which new clinical targets for different types of cancers are urgently needed.

Exosomes are also involved in modulating metabolism which is one of the hallmarks of cancer, and deregulated metabolism accounts for secondary metastasis in cancer. For instance, CAFs derived exosomes augment glycolytic pathway of cancer cells by inhibiting mitochondrial OXPHOS and glutamine-dependent reductive carboxylation which allows rapid proliferation of the cancer cells to proliferate rapidly [10]. Moreover, exosomal Aldolase A (ALDOA) and Aldehyde Dehydrogenase 3 Family Member A1 (ALDH3A1) from irradiated LC cells promote migration and invasion of recipient cells through promoting glycolysis. This implies that the metabolic enzymes might be delivered to recipient cells via exosomes that can induce activation of metabolic pathways promoting cancer progression [11]. In addition to this, exosomes also reprogram stromal cells in the TME. Evidently, cisplatin treated primary cells derived from exosomes induce glycolysis in bone marrow stromal cells (BMSCs) that leads to upregulated lactic acid formation which provides a suitable niche for the cancer cells to proliferate and reproduce within the bone marrow [12]. *Rai et al.* stated overexpression of GLUT 1 thereby increasing the glycolytic rate under the effect of exosomes and fueling the cancer cells as an energy source for their survival and growth in CRC [13]. Our previous findings established SIRT1 as a potent target in OvCa and evidence suggests inhibition of SIRT1 arrests the growth of the OvCa cells. For instance, MHY2245, a SIRT1 Inh, induces autophagy and inhibits PKM2/mTOR pathway. SIRT1 inhibition by MHY2245 arrests G2/M phase of cell cycle and induces apoptotic death of SKOV3 cell enhanced expression of cytochrome c, cleaved-PARP, cleaved caspase-3 and Bax [14]. Under this doctrine, in this study, we have focused on identifying the roles of exosomes in imparting oncogenic attributes to the cancer cells and the effect of combination treatment of a metabolic and exosomal Inh on the EMT of OvCa cells, resulting in secondary metastasis.

Additionally, from our previous findings, we have deduced that PI3K/AKT is the most deregulated pathway in OvCa, we were inclined to investigate the interference of exosomes in modulating this signaling. Previous, research also demonstrated the roles of exosomes in other cancer forms. For instance, in bladder cancer, exosomal miR-21 promotes M2 polarization upon activation of the STAT3 pathway and inhibition of PI3K/AKT pathway thereby mitigating the metastasis of bladder cancer [15].

4.2. Specific objectives

- Evaluation of the oncogenic potential of exosomes in transforming normal cells
- In-vitro validation of the combination treatment in combatting metastasis.
- 4.2.3. Evaluation of the effect of combination treatment of SIRT1 Inh and exosomes Inh in mitigating EMT in *in-vivo* mice model by regulating metabolism.

4.3. Materials and Methods

4.3.1. Materials

The list of reagents used in this study is enlisted in Table 1.

Table 1. List of reagents

Serial No.	Product	Company	Catalogue No.
1.	DKXRB FITC AFFINITY	Invitrogen	A16024
2.	Goat anti-rabbit IgG APC	Invitrogen	31984
3.	Goat anti-Human IgG (H+L) Secondary Antibody, TRITC	Invitrogen	A18810
4.	Donkey anti-Goat IgG (H+L) Secondary Antibody, TRITC	Invitrogen	A16004
5.	Goat anti-Mouse IgG (H+L) Secondary Antibody, TRITC	Invitrogen	A16071
6.	MMP9 Monoclonal Antibody (5G3)	Invitrogen	MA5-15886
7.	TWIST1 Monoclonal Antibody (10E4E6)	Invitrogen	MA5-38652
8.	Goat anti-Mouse IgG (H+L) Cross-Adsorbed Secondary Antibody, PE	Invitrogen	P-852
9.	TRYPSIN 0.25% EDTA	Invitrogen	25200056
10.	4-6-DIAMIDINO-2-PHENYLIN (DAPI)	Invitrogen	D1306
11.	PENICILLIN STREPTOMYCIN SOL, 100ML	Invitrogen	15140122
12.	SUPERSIGNAL WEST PICO PLUS	Invitrogen	34580
13.	5-(and-6)-Carboxyfluorescein Diacetate Succinimidyl Ester (CFDA-SE, CFSE)	Invitrogen	65-0850-84
14.	5(6)-Carboxy-2′,7′-dichlorofluorescein diacetate (DCFDA)	MERCK	21884
15.	Hydrogen peroxide solution	MERCK	88597
16.	Eosin Y-solution 0.5% aqueous	MERCK	109844
17.	Rabbit polyclonal anti-human SIRT1 antibody	Cell Signalling Technology	D739

18.	HRP-linked anti-rabbit antibody	Cell Signalling Technology	7074P2
19.	SIRT1 Activity Assay Kit	Abcam	ab156065
20.	Pyruvate Assay Kit	Abcam	ab65342
21.	L-Lactate Assay Kit (Colorimetric)	Abcam	ab65331
22.	Glucose Uptake Assay Kit (Colorimetric)	Abcam	ab136955
23.	NAD/NADH Assay Kit II (colorimetric)	Abcam	ab221821
24.	ATP Assay Kit	Abcam	ab83355
25.	E-cadherin Rabbit pAb	Abclonal	A3044
26.	Vimentin Rabbit pAb-20ul	Abclonal	A2584
27.	IL-6 Rabbit pAb-20ul	Abclonal	A0286
28.	VEGF- pAb-20ul	Abclonal	A12303
29.	MMP2 pAb-20ul	Abclonal	A6247
30.	COX2/PTGS2 Rabbit pAb	Abclonal	A1253
31.	Ki-67 rabbit pAb	Abclonal	A2094
32.	Hexokinase II Rabbit pAb	Abclonal	A0994
33.	GLUT1/SLC2A1 Rabbit pAb	Abclonal	A6982
34.	PKM2-specific Rabbit pAb	Abclonal	A18799
35.	Snail rabbit pAb	Abclonal	A5243
36.	pAKT-s473 rabbit pAb	Abclonal	AP1068
37.	AKT1 rabbit mAb	Abclonal	A17909
38.	PIK3CA rabbit pAb	Abclonal	A0265
39.	β-Actin Rabbit mAb	Abclonal	AC038
40.	Human/Mouse COX-2 Antibody	R&D Systems	AF4198
41.	Human Angiopoietin-2 Antibody	R&D Systems	AF623
42.	Recombinant Human TGF-β1 (CHO derived)	Peprotech	100-21C
43.	GW 4869 (hydrochloride hydrate)	Cayman Chemical Company, USA	13127
44.	SIRT1 INHIBITOR III 1PC X 5MG	Sigma	566322
45.	DAB Substrate	Sigma Aldrich	11718096001
46.	Bradford reagent	Sigma	B6916
47.	Rabbit anti-human polyclonal HIF-1α antibody	Santa Cruz Biotechnology	sc10790
48.	Dibutylphthalate polystyrene xylene (DPX) Mountant for histology	Sisco Research Laboratories Pvt. Ltd.	88147

49.	Dimethyl Sulphoxide (DMSO) extrapure, 99%	Sisco Research Laboratories Pvt. Ltd.	43404
50.	Albumin Bovine (pH 7) fraction V (Bovine Serum Albumin, BSA), 98%	Sisco Research Laboratories Pvt. Ltd.	83803
51.	Xylene pure, 99% (500 ml)	Sisco Research Laboratories Pvt. Ltd.	54717
52.	Methanol extrapure AR, 99.8%	Sisco Research Laboratories Pvt. Ltd.	65524
53.	Crystal Violet (Gentian Violet) ACS, ExiPlus	Sisco Research Laboratories Pvt. Ltd.	17610
54.	Fetal Bovine Serum (FBS)	Gibco ™	10270-106
55.	Fetal Bovine Serum (FBS), exosome-depleted	Gibco ™	A2720803
56.	3-(4,5-dimethylthiazol-2-yl)-2,5 diphenyltetrazolium bromide (MTT) tetrazolium	HIMEDIA	MB186
57.	RIPA buffer Sterile chloride	HIMEDIA	TCL131
58.	TMB Substrate solution (for ELISA)	HIMEDIA	ML168
59.	Paraformaldehyde Solution, 4%	HIMEDIA	TCL119
60.	Collagenase Type IV	Sigma Aldrich	C4-22
61.	DPX new	Sigma Aldrich	1005790500
62.	Dulbecco′s Modified Eagle′s Medium (DMEM)- high glucose	Sigma Aldrich	D6429
63.	Hematoxylin Solution (Mayer's, Modified)	ABCAM	ab220365
64.	Schiff's reagent	Sigma Aldrich	1090332500
65.	Periodic acid	Sigma Aldrich	P0430
Buffer composition			
66.	PBS (1X)	8g NaCl; 0.2g KCl; 1.44g Na_2HPO_4.7H2O; 0.24g KH_2PO_4; H_2O to 1L; pH-7.4	
67.	Resolving Buffer	Resolving Buffer 1.5M Tris, 30%Acrylamide, 10%SDS, 10%APS, 5 µl TEMED 8; pH-8.8	

68.	Sample Buffer	Laemmli Buffer (0.75g,2g SDS); 5% β-Mercapto ethanol; 1/10th Glycerol; 1-2 drops Bromophenol blue; pH-6.8
69.	SDS-PAGE Buffer	1.5g Tris, 7g Glycine, 0.5g SDS, H_2O to 0.5L; pH-8.3
70.	Transfer Buffer	1.52g Tris, 7.2g Glycine, Methanol 100ml, H_2O to 0.5L; pH-8.3
71.	Stacking Buffer	0.5M Tris, 30%Acrylamide, 10%SDS, 10%APS,10 µl TEMED; pH-6.8
72.	TBS-T (1X)	580mg NaCl; 1mL Tris(1M); 20µl Tween-20; H_2O to 100mL; pH-7.5
73.	Citrate Buffer	12.044g Sodium Citrate Dihydrate; 11.341g Citric acid; H_2O to 1000mL; pH-6

4.3.2. Methods

4.3.2A. Cell culture

HaCaT cells were cultured in exosomes depleted FBS (10%) supplemented DMEM media and ID8 cells were cultured in DMEM with exosomes non-depleted 10% FBS, both supplemented with 1% penicillin-streptomycin at 37°C in 5% CO_2. After the cells reached 75-80% confluency, trypsinization (0.25%) was done and cells were seeded at desired densities for respective experiments. HaCaT cells were further treated with TGFβ (2ng/ml for 72hrs) for induction of EMT [16][17] in FBS (exosomes depleted) supplemented DMEM media for further experiments.

4.3.2B. MTT assay

To check the viability of the cells, both HaCaT and ID8 cells were inoculated in a 96 well flat bottom transparent plate at a concentration of 5×10^3 cells and allowed to seed overnight in a CO_2 incubator. SIRT1 Inh was added at concentrations of 0.01µM, 0.1 µM, 1µM and 10 µM for both HaCaT cells and ID8 cells for 24hrs. 5µM, 10µM, 20µM and 40µM concentrations of GW4869 was added only in ID8 cells and treated for a period of 24hrs. On the following day, MTT (5mg/ml) dissolved in 1X PBS was added into each well and incubated in the dark

for 3hrs at RT and finally, 150µl DMSO was added to each well before taking the final reading in an ELISA plate reader (Infinite 200PRO-TECAN, 30050303) at 595nm [18].

4.3.2C. Western blotting

To determine the oncogenic characteristics of the isolated exosomes, the HaCaT cells were incubated with exogenous exosomes for 24hrs. HaCaT cells were also treated under four different conditions (Con, NTExos, SIRT1 Inh+Exos, SIRT1 Inh) and the total protein from the cells of different experimental setups was isolated after the addition of RIPA buffer and sonication of the cells. Bradford assay was performed to estimate the protein concentration.

Additionally, the protein estimation from the primary cells obtained from mice tumors under four different treatment conditions (Con, SIRT1 Inh, GW4869, SIRT1 Inh+GW4869) was performed as described above. On 10% acrylamide gel was used for protein expression estimation. Primary antibodies of SIRT1, COX-2, IL-6, E-cad, Vim, PI3K, AKT and pAKT (Table 1) were used to quantify relative protein levels (1:5000). HRP-tagged secondary antibody (1:10000) was added and incubated for 2hrs, to visualize the reaction and band acquisition after development with ECL Ultra Western HRP Substrate was taken under Invitrogen iBright^{TM} FL1500 [19].

4.3.2D. Colony formation assay

HaCaT cells at different treatment conditions (Con, TGF-β+, TGF-β + Exos) for analyzing the oncogenic potential of exosomes and to analyze the changes in the cancer cells after the addition of the inhibitor, HaCaT cells were subjected to different sets of treatment (Con, NTExos, SIRT1 Inh+Exos, SIRT1 Inh). Under both the experimental set up the cells were treated with TGF-β at a concentration of 2ng/ml for 72hrs and ID8 cells under the treatment conditions (Con, SIRT1 Inh, GW4869 and SIRT1 Inh+GW4869) were seeded at a very low concentration (500 cells/plate) in 6 well plates and colony growth was allowed for 10 days with addition of exosomes depleted FBS supplemented fresh media for colony assessment in HaCaT cells and full media in every three days. On the 10th day, 4% paraformaldehyde was used to fix the cells and then washed with 1X PBS followed by staining with 0.1% crystal violet. The excess stain was removed after washing with 1X PBS. The colonies were counted using Fiji software. The assay was repeated with three biological replicates [20].

4.3.2E. Immunocytochemistry

HaCaT cells were inoculated on coverslips and allowed to seed overnight. On the next day, desired treatment conditions were provided for each cell type, as mentioned above and incubated for 24hrs. Upon fixation with ethanol, the cells were subjected to blocking by 3% BSA for 30min. Primary antibody (Snail) was added to the HaCaT cells and kept overnight, followed by TRITC-conjugated secondary antibody (Con, TGF-β+, TGF-β + Exos) and FITC tagged secondary antibodies (Con, NTExos, SIRT1 Inh+Exos, SIRT1 Inh) for 2hrs at RT in the dark.

For ID8 cells, the cells were allowed to adhere on coverslips overnight and on the following day after fixation by methanol and blocking with 3% BSA for 30min primary antibodies (E-cad, Vim and Ki-67) were added to the cells, which were visualised on the following day by adding and incubating with FITC tagged secondary antibodies (Con, SIRT1 Inh, GW4869 and SIRT1 Inh+GW4869) for 2hrs in the dark at RT. Nuclear staining of both HaCaT cells and ID8 cells, DAPI was added. To remove the excessive dye, the coverslips were washed with 1XPBS, and DPX was used for mounting the slides and evaluated under a fluorescence microscope (Olympus) [21].

4.3.2F. Flow Cytometry

2×10^5 HaCaT and ID8 cells were separately seeded in 60mm petri dishes under four different conditions for each cell type as mentioned above. After the desired treatment for 24hrs, the HaCaT cells were incubated with E-cad, Vim for 2hrs at 4°C, followed by incubation with APC tagged secondary antibody and data acquisition in BD LSRFortessa flow cytometer. For ID8 cells, after the desired treatment, the ROS level was measured by flow cytometer after adding DCFDA for an incubation period of 30min [22].The analysis was done using FlowJo software.

4.3.2G. Transwell migration assay

5×10^3 ID8 cells were inoculated on the upper chamber of the Transwell and loaded into the upper chamber of the Transwell, and 500µl DMEM containing 10% exosomes supplemented FBS was added to the bottom of Transwell for incubation overnight. The next day, the Transwell was removed, and cells remaining on the upper chamber were removed with a cotton swab. Following washing with PBS, the cells attached to the membrane were fixed in

4% paraformaldehyde for 30min at RT. Cells were stained with 0.1% crystal violet for 20min at RT. Following washing with PBS, imaging under an inverted microscope (Nikon ECLIPSE Ts2), and images were captured for enumeration of the cells [23]

4.3.2H. Protein-Protein Interaction network construction

To predict the interaction pattern of DEGs the PPI of DEGs was visualized using the STRING database (https://string-db.org) with a combined score of >0.7. In the present study, we selected a high confidence score >0.7 to eliminate PPIs with low probability/significance and obtain more reliable results [24].

4.3.2I. DOT blot assay

Protein extraction from treated HaCaT cells was done using RIPA buffer and protein estimation was done using Bradford assay. Quantified protein, at a concentration of 10µg, was added onto methanol-activated nitrocellulose membrane in a wet chamber. The membrane was then blocked using 5% BSA and incubated overnight after the addition of primary antibodies PI3K, AKT and pAKT, β-actin at 4°C (1:5000). HRP-tagged secondary antibody (1:10000) was added to the membrane and incubated for 1hr. The fluorescence signal was developed using ECL Ultra Western HRP Substrate after washing with 1X PBS and the results were observed in Invitrogen iBright^{TM} FL1500.

4.3.2J. Experimental animals

Female C57BL/6 mice (6-8 weeks old) were purchased from West Bengal Livestock Development Corporation Ltd, Buddhapark Kalyani, Nadia-741235, West Bengal, India. All experiments were conducted with the approval of the Institutional Animal Ethics Committee at Chittaranjan National Cancer Institute (IAEC-1774/NC-4/2022/16).

4.3.2K. Establishment of OvCa model and experimental outline

The mice were quarantined for 2 weeks at a temperature of 22 ± 2°C and 12hrs light/dark cycle. Inoculation of tumor cells was performed via intra-peritoneal (i.p.) injection with a total volume of 7×10^6 cells in 0.7ml of 1x PBS. For the next 8 weeks, the animals were followed up for survival and tumor growth. The treatment under four different treatment conditions started after 8 weeks following inoculation. The mice (N=24) were segregated into four groups with N=6 mice in each group (Group 1: Vehicle control, Group 2: SIRT1 Inh treated, Group 3: GW4869 treated, Group 4: Combination treatment of SIRT1 Inh and GW4869). The SIRT1 Inh was dissolved in DMSO diluted with normal saline at a

concentration of 0.5%. The mice were treated intraperitoneally once a week with EX-527 (10mg/kg) [25]. GW4869 was dissolved in DMSO at 8mg/ml concentration and injected intraperitoneally with 200µl of 0.3mg/mL GW4869 in 0.9% normal saline (60µg/mouse; 2-2.5µg/g body weight) once a week for 4 weeks [26].

4.3.2L. Sample preparation from in-vivo model

The mice were sacrificed after the completion of the treatment as mentioned above. Before the sacrifice, the blood was collected by retro-orbital bleeding and allowed to be clotted for 1hr at RT to analyze the cytokine level [27]. The control and tumor tissues were collected from the mice of distinct treatment groups. The tissues were processed under two different conditions. Firstly, the tissues were either paraformaldehyde fixed for cryosectioning. Secondly, the primary cell suspension was prepared by overnight digestion using collagenase IV and DMEM cocktail (50:50 dilution) at 37°C, 5% CO_2 after mincing of the tissues. The cell pellet was obtained after centrifugation at 8000rpm for 10min at RT followed by dissolving the pellet with 1X RBC lysis buffer to get rid of any remaining red blood cells. Finally, the pellet was washed in 1X PBS and resuspended in FBS-supplemented (Exosomes depleted and with exosomes) DMEM media with 1% penicillin and streptomycin. The cells were then allowed to grow and were subsequently used for downstream experiments [28]. The isolated organs from each mice group (Lungs, Liver, Spleen and Ovary) were fixed with 4% paraformaldehyde for H&E staining.

4.3.2M. Immunohistochemistry

The mice tissue section slides were deparaffinized using xylene (10min) followed by rehydration in a series of graded concentrations (100%, 90%, 70%, 50%) of alcohol (5min each). To augment the expression of antigen 10Mm citrate buffer solution was added to the slides. The slides were further treated with 3% hydrogen peroxide diluted in 100% methanol and kept at RT for 15min, followed by a PBS wash to stop the endogenous peroxidase activity. After blocking the slides with 3% BSA for 1hr, the slides were kept at 4ºC overnight after the addition of primary antibodies (SIRT1, HIF-1α, COX-2, PTEN, GLUT1, hexokinase (HK) II, PKM2, Ki-67, E-cad and Vim) in humified chambers in a dilution of (1:500). On the following day, after washing off the excess primary antibody with 1X PBS, anti-rabbit secondary antibody was added (1:1000). After the incubation at RT in the dark for 2hrs, DAB was added for 10min and counterstained with. Finally, hematoxylin was added to counterstain

the specimen and dehydrated using a gradient alcohol wash, followed by sealing the slides with coverslips using DPX [29]. The images for each sample were taken in a brightfield compound microscope (OLYMPUS CX40) and analyzed using Fiji software.

4.3.2N. Immunofluorescence

The tumor tissue slides from mice were deparaffinized and dehydrated using xylene and alcohol gradient solutions (100%, 90%, 70%, 50%). The slides were then subjected to Methanol/H_2O_2 solution for fixation, followed by citrate buffer treatment for antigen retrieval. After the blocking with 5% BSA, primary antibodies for VEGF, ANGPT2, MMP2, MMP9 and Snail (1:500) were added and kept overnight at 4°C [30]. FITC and TRITC tagged secondary antibodies were added the next day and incubated for 2hrs (1:1000) at RT. After staining the nucleus with DAPI, the slides were washed with 1X PBS to remove the excess stains, followed by DPX mounting required for imaging under OLYMPUS fluorescent microscope [31]. The images were further analyzed using Fiji software.

4.3.2O. Haematoxylin and eosin staining

The tissue sections from the organs (Lungs, Liver, Spleen and Ovary) and tumor obtained from the four distinct groups of mice were deparaffinized using xylene and hydrated using distilled water to remove any fixative that could interfere with staining. The slides were then dipped into a solution of Mayer's hematoxylin for 30s followed by rinsing with water for 1min to remove the excess. 1% Eosin Y solution stain was added to the slides for 10-30s. The tissue sections were dehydrated using two changes of 95% alcohol and two changes of 100% alcohol, each for 30s followed by xylene wash for 5min, and finally, DPX mounting was performed for imaging under a brightfield microscope (OLYMPUS CX40) [32].

4.3.2P. Periodic Acid Schiff staining

The slides were deparaffinized using xylene for 5min followed by treatment with Carnoy's fixative for 10min. After rinsing the slides with distilled water, Periodic acid solution was added (10min) for staining followed by the addition of Schiff reagent for 5min. The slides were washed with distilled water to remove excessive stains and then dehydrated in ascending alcohol gradient solutions. DPX was used for mounting and imaging was performed under a Leica brightfield microscope and analyzed using Fiji-ImageJ software [33].

4.3.2Q. Enzyme-linked immunosorbent assay

The cell culture supernatant of HaCaT cells under the presence and absence of exosomes were coated in the 96 well ELISA plates and allowed to settle overnight at 4°C. Additionally, serum collected from mice blood from four different groups was also coated in 96 well ELISA plates. On the following day, 5% BSA was used for blocking for 2hrs and washed with PBS. Primary antibodies IL-6 and TNF-α (1:500) for HaCaT cell culture supernatant and IL-6 (1:500) for mice serum were added and kept overnight at 4°C. HRP-conjugated secondary antibody (1:1000) was added the next day after the primary antibody was discarded, washed with PBST, and kept in incubation for 2hrs at RT in a shaker. After the incubation was over, the wells were washed with PBST and TMB substrate was added into the wells in the dark and incubated for 15min before taking OD values under an ELISA plate reader (Infinite 200PRO-TECAN, 30050303) at 595nm.

4.3.2R. Metabolism related assays

4.3.2R1. Glucose uptake assay

5×10^6 primary tumor cells from mice were inoculated in 6 well plates and seeded at 37°C for 24hrs. The cells were then subjected to serum-free DMEM media for serum deprivation for 4hrs to augment glucose uptake. The cells were lysed and centrifuged to obtain the lysate required for the assay. 200µl of the lysate was incubated with the detection solution for 30min and the glucose uptake was performed as per the manufacturer's protocol. Finally, the OD value was taken in a microplate reader (Infinite 200PRO-TECAN, 30050303) at 540nm [34].

4.3.2R2. Pyruvate and lactate assay

For pyruvate and lactate assay, 3×10^5 primary cells from mice tumor were plated per well in a 6 well plate and incubated at 37°C for 24hrs. RIPA buffer was used to homogenize the cells to obtain the cell supernatant after centrifugation and finally, 50µl detection solution was added to each well and incubated dark at RT for 30min. The pyruvate and lactate assessment was conducted as per the manufacturer's protocol and measurement was taken in a microplate reader (Infinite 200PRO-TECAN, 30050303) at 540nm [34].

4.3.2R3. SIRT1 activity assay

SIRT1 activity was quantified using the fluorometric SIRT1 assay kit as per the manufacturer's guidelines. The fluorescence intensity was measured using an excitation

wavelength of 355nm and an emission wavelength of 450nm every 2min for a duration of 30min [35].

4.3.2R4. NAD+ and NADH Measurement

The NAD+/NADH ratios were determined using the NAD+/NADH assay kit as per manufacturer's instructions [36]. NAD+ and NADH concentrations in µM were determined from a standard curve and normalized to the total protein concentrations.

4.3.2R5. ATP measurement assay

1×10^6 primary cells obtained from different treatment conditions of mice were homogenized in ATP assay buffer and finally, the ATP levels were assessed according to the manufacturer's instruction. All outcomes were adjusted based on the number of cells [34].

4.3.2S. Statistical analysis

GraphPad Prism (version 8.0) was used to perform Two-way ANOVA, One-way ANOVA and Student's t-test wherever applicable. FlowJo software was used for flow cytometric data analysis. Fiji-ImageJ software (https://imagej.net/Fiji) was used to analyze the IHC image analysis, colocalization and MFI of the fluorescence images. $P<0.0001$ and $P\leq0.05$ were considered to be statistically significant.

4.4. Results

4.4.1. Exosomes transfer oncogenic attributes to normal cells

To investigate whether the exosomes derived from poorly differentiated OvCa patients confer oncogenic properties to normal cells or not, we incubated the HaCaT cells with TGF-β to confirm the initiation of EMT and exogenously added the isolated exosomes. Under this condition, colony forming assay revealed that the number of colonies increased under the exosomal added state (Figure 1A). Western blot analysis revealed that E-cad expression decreased in exosomes added condition whereas in the non-exosomal state, E-cad expression was higher, whereas the expression of Vim increased under the exogenous exosomes as compared to the non-exosomes condition (Figure 1B). Additionally, upon investigating the expression of Snail under the above-mentioned conditions, we observed that the expression of Snail increased under the effect of exogenous exosomes (Figure 1C). The secretion of pro-inflammatory cytokines, IL-6 and TNF-α increased significantly under exosomes added state as compared to the non-exosomes state (Figure 1D). These results suggest that the isolated exosomes carry oncogenic characteristics which can confer oncogenic properties into the

normal cells by transferring their cargoes inducing their oncogenic transformation schematically represented in Figure 1E.

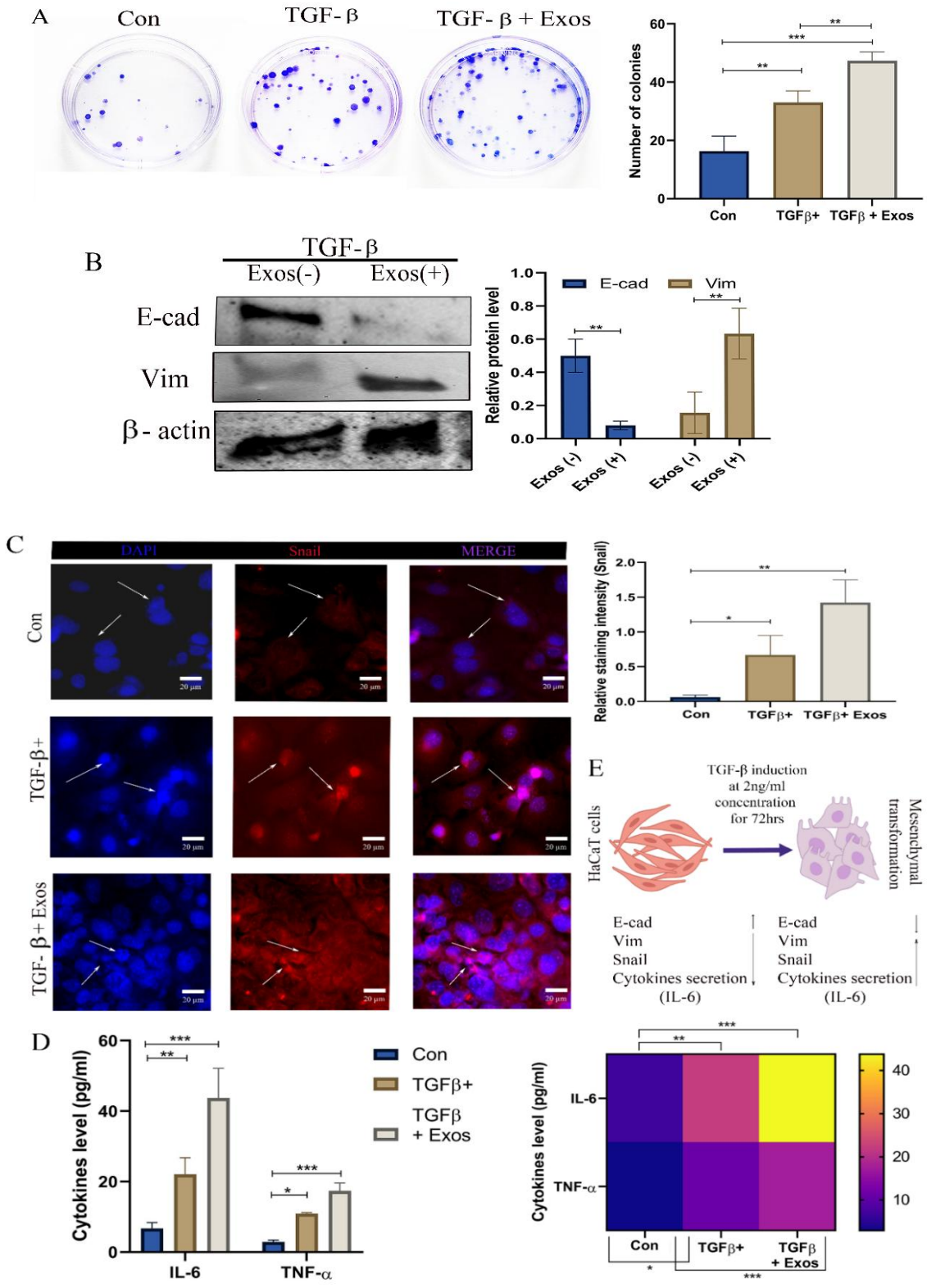

Figure 1. A. Determination of proliferation of HaCaT cells by colony formation assay; B. Protein expression of EMT markers in HaCaT cells; C. Evaluation of Snail expression in

HaCaT cells; D. Cytokines level analysis by ELISA; E. Schematic of TGF-β induced HaCaT cells transformation. (*P<0.05, **P<0.01, ***P<0.001, ****P<0.0001)

4.4.2. The influence of exosomes on the normal cells regulates inflammation via SIRT1/COX-2/IL-6 axis

TGF-β induced HaCaT cells under four distinct treatment parameters were used for further experiments, schematically illustrated in Figure 2A and to analyze the regulatory effect of SIRT1/COX-2/IL-6 axis on the normal cells we have performed MTT assay of SIRT1 Inh on HaCaT cells to estimate the drug dose which revealed an IC_{50} of 0.07505µM (Figure 2B). Analysis of pro-inflammatory cytokines (IL-6 and TNF-α) in cell culture supernatant revealed elevated secretion under exosomal incubation, however, the secretion of both IL-6 and TNF-α decreased when treated with the SIRT1 Inh in the presence and absence of exosomes as compared to the control as represented in Figure 2C. The protein expression level of SIRT1, COX-2, IL-6 also revealed similar results where the expression of SIRT1, COX-2, IL-6 increased under the exosomal effect but significantly decreased under the inhibitory effect of SIRT1 Inh in the absence of exosomes as compared to the presence of exosomes (Figure 2D). To understand the connectivity of the molecules, we performed a STRING analysis and revealed PI3K/AKT to be strongly interconnected with the molecules of interest (Figure 2E).

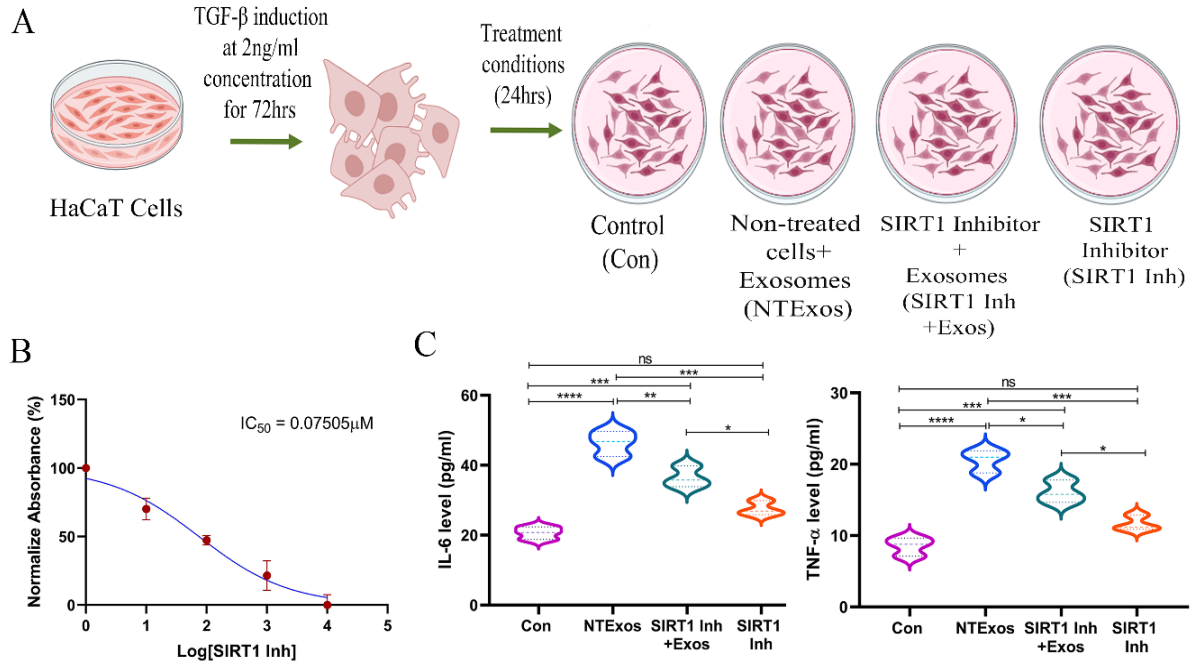

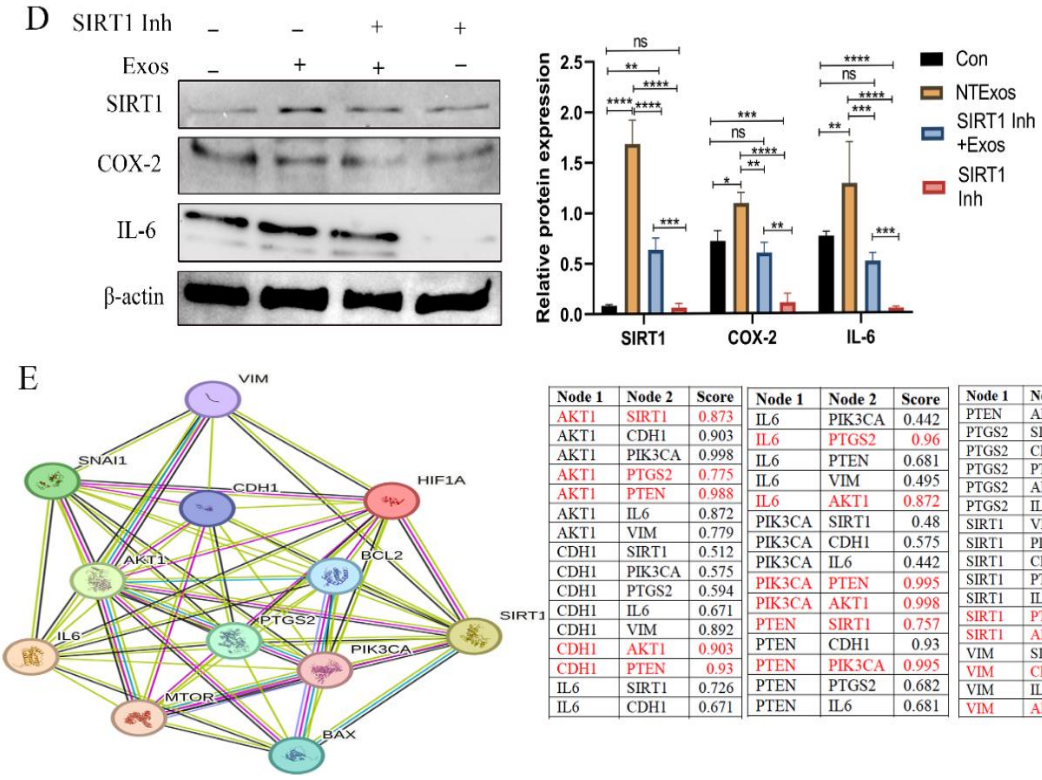

Node 1	Node 2	Score
AKT1	SIRT1	0.873
AKT1	CDH1	0.903
AKT1	PIK3CA	0.998
AKT1	PTGS2	0.775
AKT1	PTEN	0.988
AKT1	IL6	0.872
AKT1	VIM	0.779
CDH1	SIRT1	0.512
CDH1	PIK3CA	0.575
CDH1	PTGS2	0.594
CDH1	IL6	0.671
CDH1	VIM	0.892
CDH1	AKT1	0.903
CDH1	PTEN	0.93
IL6	SIRT1	0.726
IL6	CDH1	0.671

Node 1	Node 2	Score
IL6	PIK3CA	0.442
IL6	PTGS2	0.96
IL6	PTEN	0.681
IL6	VIM	0.495
IL6	AKT1	0.872
PIK3CA	SIRT1	0.48
PIK3CA	CDH1	0.575
PIK3CA	IL6	0.442
PIK3CA	PTEN	0.995
PIK3CA	AKT1	0.998
PTEN	SIRT1	0.757
PTEN	CDH1	0.93
PTEN	PIK3CA	0.995
PTEN	PTGS2	0.682
PTEN	IL6	0.681

Node 1	Node 2	Score
PTEN	AKT1	0.988
PTGS2	SIRT1	0.592
PTGS2	CDH1	0.594
PTGS2	PTEN	0.682
PTGS2	AKT1	0.775
PTGS2	IL6	0.96
SIRT1	VIM	0.43
SIRT1	PIK3CA	0.48
SIRT1	CDH1	0.512
SIRT1	PTGS2	0.592
SIRT1	IL6	0.726
SIRT1	PTEN	0.757
SIRT1	AKT1	0.873
VIM	SIRT1	0.43
VIM	CDH1	0.892
VIM	IL6	0.495
VIM	AKT1	0.779

Figure 2. A. Schematic representation of TGF-β induction of HaCaT cells followed by different treatment conditions: Control (Con), Non-treated+Exosomes (NTExos), SIRT1 Inhibitor+Exosomes, (SIRT1 Inh+Exos) and SIRT1 Inhibitor (SIRT1 Inh); B. MTT assay of SIRT1 Inh in HaCaT cells; B-C. Cytokines analysis by ELISA from HaCaT cell culture supernatant; D. Western blot analysis of SIRT1/COX-2/IL-6 under the above-mentioned treatment conditions; E. STRING analysis of interconnected DEGs involved in reprogramming of normal cells. (*P<0.05, **P<0.01, ***P<0.001, ****P<0.0001)

4.4.3. The oncogenic properties conferred by exogenous exosomes are mitigated under the effect of SIRT1 Inh by regulating PI3K/AKT pathway

Upon deriving that the exosomes impart oncogenic transformation into the normal cells, we were inclined to study the effect of SIRT1 Inh on the exosomes incubated normal cells. Colony forming assay revealed that the number of colonies was maximum under the effect of exogenous exosomes followed by SIRT1 Inh + Exos and least number of colonies under the inhibitory effect of SIRT1 Inh without any exosomes (Figure 3A) revealing that the proliferative capacity of the cells which was imparted by oncogenic exosomes was inhibited by SIRT1 Inh. The protein expression of E-cad and Vim also corroborated our hypothesis. We observed that E-cad expression increased under the SIRT1 Inh effect and least under the

effect of exogeneous exosomes whereas Vim expression was maximum under exosomal effect and least in case of SIRT1 Inh (Figure 3B). Upon observing that EMT could be targeted with SIRT1 Inh, we further strengthened our findings with flow cytometric analysis of the EMT markers. The results obtained also revealed a similar expression pattern as deduced in the protein expression level analysed by western blot (Figure 3C). The expression of Snail also corroborated significantly with the previous findings (Figure 3D). Thus, to define the underlying mechanism, dot blot assay revealed expression of PI3K/AKT/pAKT to corroborate with our previous findings (Figure 3E), which stated an orchestra between SIRT1/COX-2/IL-6 axis mediated inflammation thereby modulating metastasis in OvCa regulated by PI3K/AKT signaling cascade.

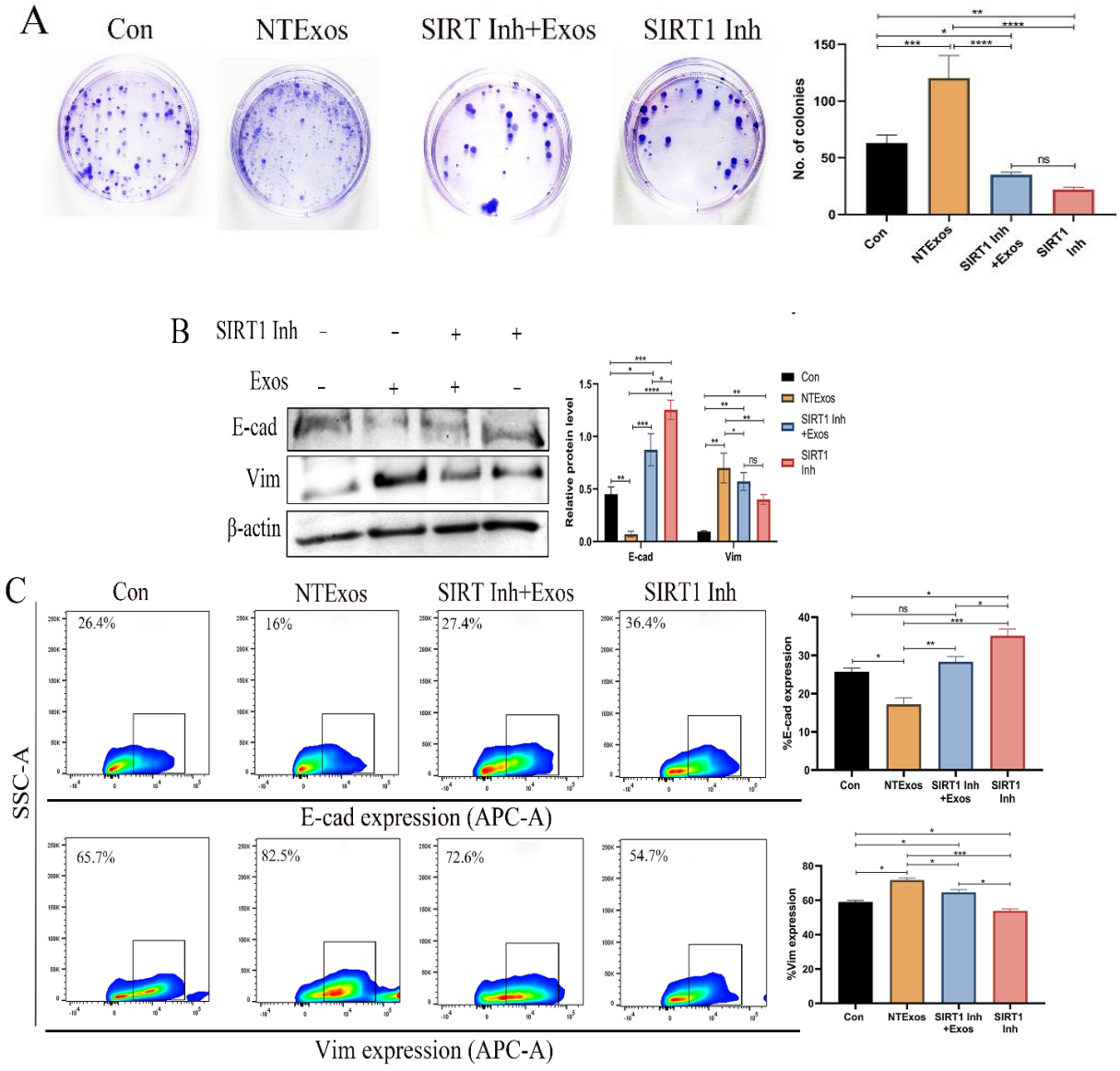

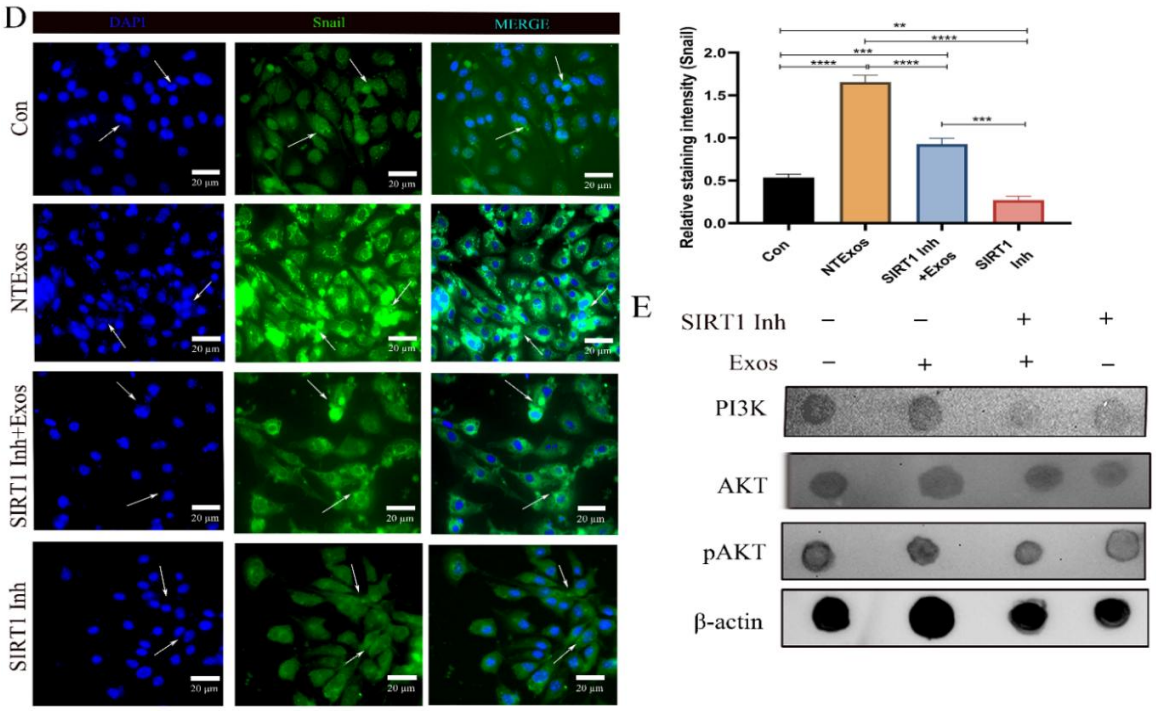

Figure 3. A. Colony-forming capacity of HaCaT cells; B. Western blot analysis of E-cad and Vim under the Control (Con), Non-treated+Exosomes (NTExos), SIRT1 Inhibitor+Exosomes, (SIRT1 Inh+Exos) and SIRT1 Inhibitor (SIRT1 Inh) in HaCaT cells; C. Flow cytometric analysis of E-cad and Vim under Con, NTExos, SIRT1 Inh+Exos and SIRT1 Inh in HaCaT cells; D. Expression status of Snail by IF under Con, NTExos, SIRT1 Inh+Exos and SIRT1 Inh in HaCaT cells; E. DOT blot analysis of PI3K/AKT/pAKT pathway under Con, NTExos, SIRT1 Inh+Exos and SIRT1 Inh in HaCaT cells. (*P<0.05, **P<0.01, ***P<0.001, ****P<0.0001)

4.4.4. The increased growth and migration of the cancer cells are mitigated by the combination treatment by increasing ROS generation

Upon deriving that SIRT1 Inh was arresting the EMT by regulating PI3K/AKT pathway, we performed an *in-vitro* analysis on ID8 cells to understand its effect in combination with exosomes Inh, GW4869. Firstly, the doses determined from the MTT assay revealed the drugs SIRT1 Inh and GW4869 to be 0.8964µM and 7.887µM, respectively (Figure 4A-B). We observed that proliferation of the colonies got more compromised under the combination treatment of SIRT1 Inh and GW4869 as compared to their individual treatment (Figure 4C-D). Interestingly, we observed that ROS generation is also increased at a significant level under the combination treatment (Figure 4E) revealing that the proliferative and migration of cancer cells were affected by the combination treatment.

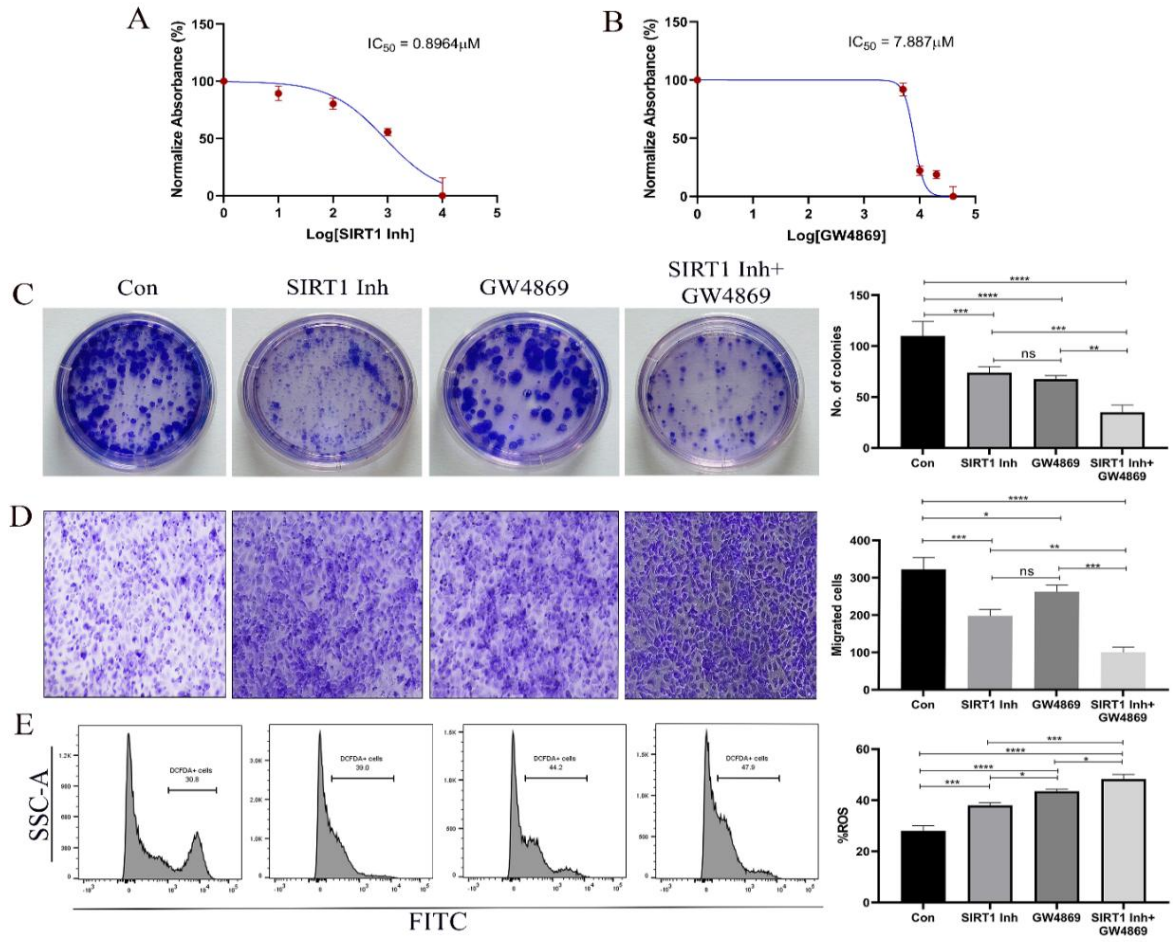

Figure 4. A-B. MTT analysis of SIRT1 Inh and GW4869 in ID8 cells; C. Colony formation assay in ID8 cells under Con, SIRT1 Inh, GW4869 and SIRT1 Inh+GW4869; D. Transwell migration of ID8 cells under Con, SIRT1 Inh, GW4869 and SIRT1 Inh+GW4869; E. ROS generation in ID8 cells by DCFDA assay under Con, SIRT1 Inh, GW4869 and SIRT1 Inh+GW4869. (*P<0.05, **P<0.01, ***P<0.001, ****P<0.0001)

4.4.5. Exosomal interference in EMT and proliferation of cancer cells are combatted by the combination treatment of SIRT1 Inh and GW4869

Since, we observed that growth of colonies and migration of the cancer cells are combatted by the combination treatment, we were inclined to investigate the baseline mechanism responsible for the results deduced previously. Interestingly, we observed that the expression of EMT markers E-cad increased whereas Vim expression decreased under the combination treatment (Figure 5A-B). The same results were observed in case of proliferation marker, Ki-67, with its decreased expression level under the combination treatment whereas no significant decrease between the individual treatment of SIRT1 and GW4869, however, the expression decreased as compared to the control (Figure 5C).

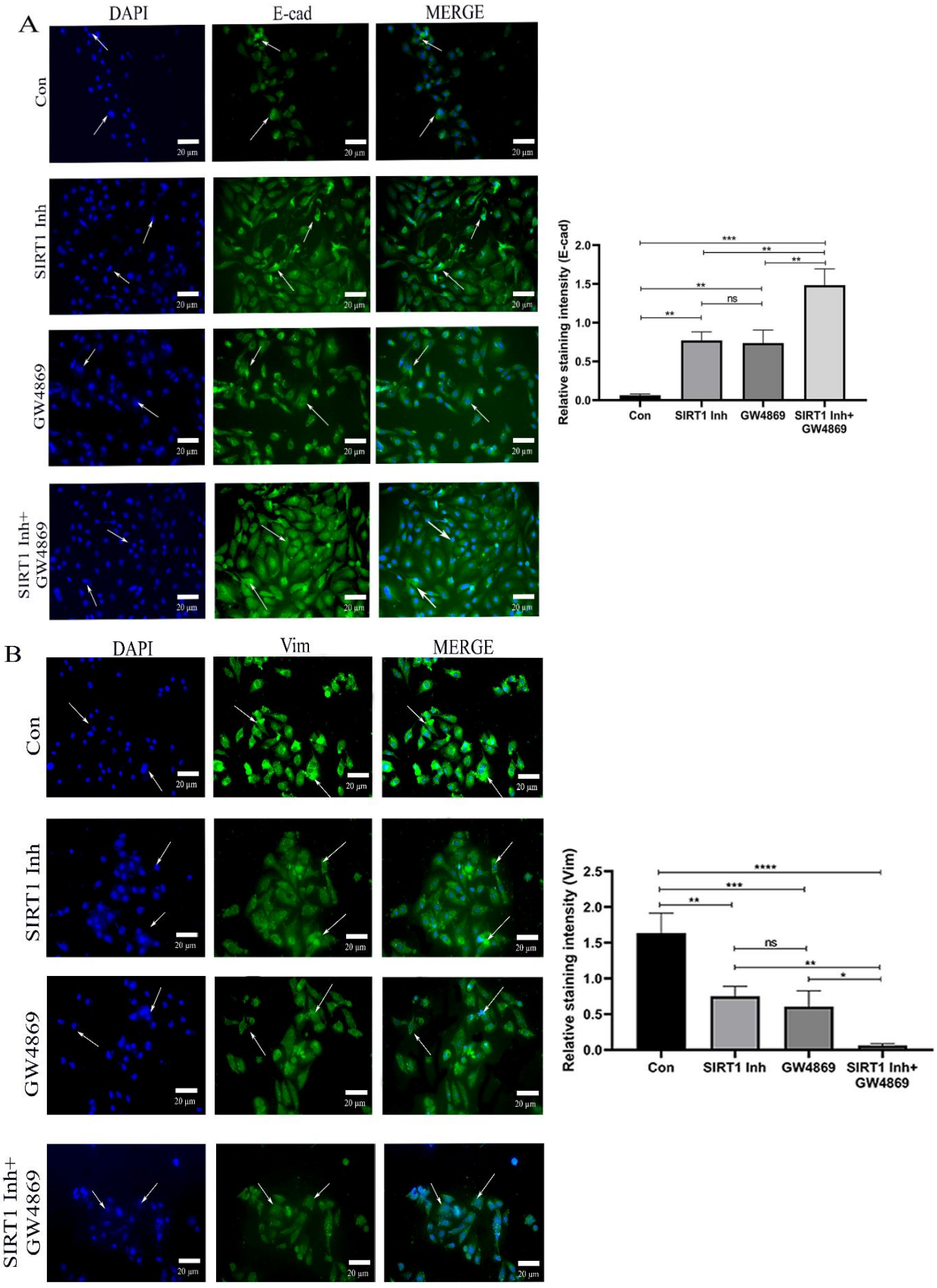
A
DAPI
E-cad
MERGE
Con
SIRT1 Inh
GW4869
SIRT1 Inh+ GW4869
20 µm
Relative staining intensity (E-cad)
2.0
1.5
1.0
0.5
0.0
***
**
**
**
ns
**
Con
SIRT1 Inh
GW4869
SIRT1 Inh+ GW4869
B
DAPI
Vim
MERGE
Con
SIRT1 Inh
GW4869
SIRT1 Inh+ GW4869
20 µm
Relative staining intensity (Vim)
2.5
2.0
1.5
1.0
0.5
0.0
****
***
**
ns
**
*
Con
SIRT1 Inh
GW4869
SIRT1 Inh+ GW4869

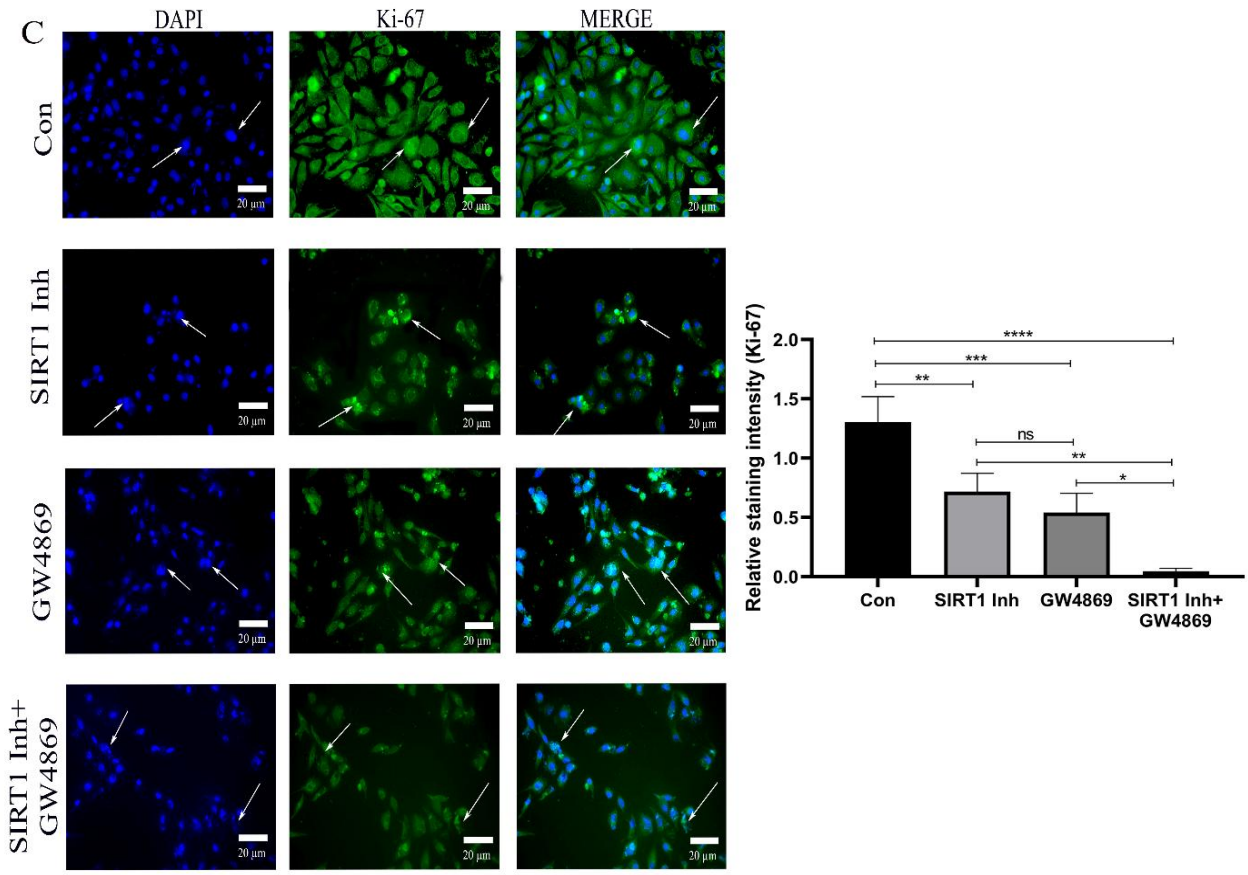

Figure 5. A. IF analysis of E-cad expression in ID8 cells under Con, SIRT1 Inh, GW4869 and SIRT1 Inh+GW4869; B. IF analysis of Vim in ID8 cells expression under Con, SIRT1 Inh, GW4869 and SIRT1 Inh+GW4869; C. IF analysis of Ki-67 in ID8 cells under Con, SIRT1 Inh, GW4869 and SIRT1 Inh+GW4869. (*P<0.05, **P<0.01, ***P<0.001, ****P<0.0001)

4.4.6. Combination treatment of SIRT1 Inh and GW4869 increases the survival of the mice

The representation of OvCa development by injecting ID8 cells into C57BL/6 mice and the treatment strategy is schematically revealed in Figure 6A. The sacrificed mice revealed decreased metastatic implants in the omentum of the combination treatment group as compared to the SIRT1 Inh and GW4869 followed by the vehicle control as represented in Figure 6A. The TILs count increased within the treatment groups, maximum in the combination treatment category, however, the glycogen deposition decreased under the combination treatment group as compared to their individual treatment as compared to normal (Figure 6B-C). There was a significant increase in %OS and a decrease in death rate in the combination treatment group as compared to the SIRT1 Inh, GW4869 and vehicle control (Figure 5D-E). The number of peritoneal implants and the volume of ascitic fluid

decreased considerably in the combination treatment group (Figure 5F-G). H&E staining of organs from the mice bearing ovarian tumors treated with the drugs revealed no sign of necrosis or thrombosis in the histological analysis of vital organs, including liver, spleen, lung and ovary (Figure H-K), demonstrating the drugs to be highly selective.

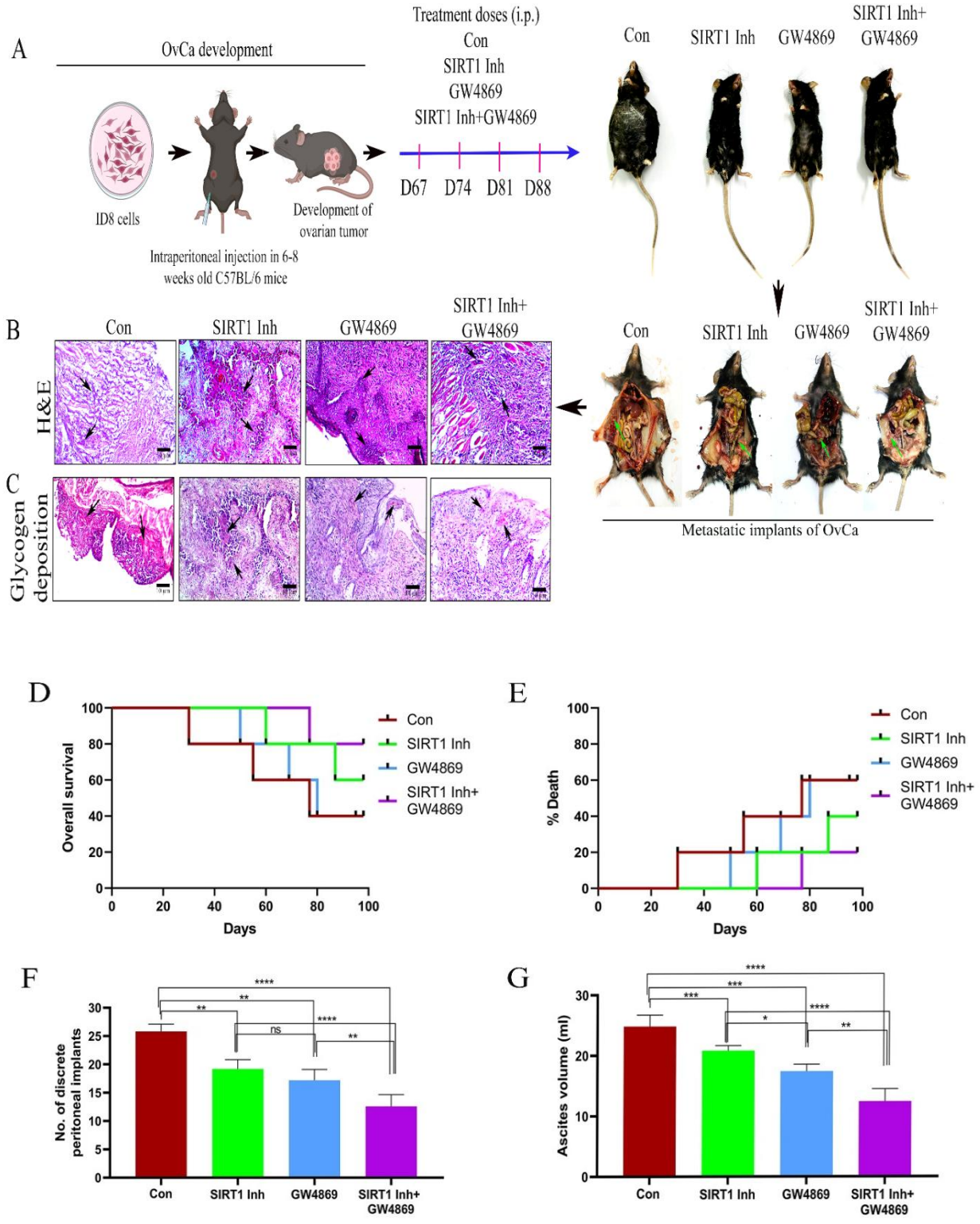

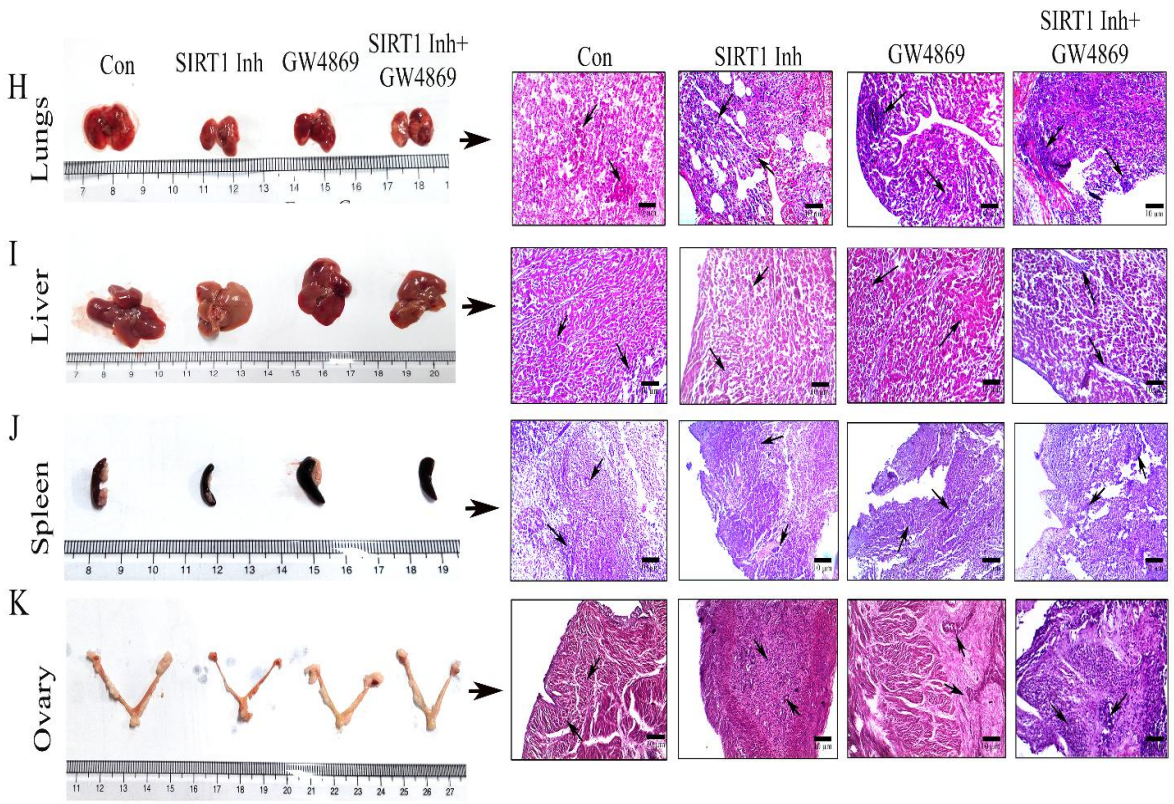

Figure 6. A. Experimental outline of *in-vivo* mice model; B. H&E staining of ovarian tumor under Group 1: Vehicle control, Group 2: SIRT1 Inh treated, Group 3: GW4869 treated, Group 4: Combination treatment of SIRT1 Inh and GW4869; C. Level of glycogen deposition under Group 1: Vehicle control, Group 2: SIRT1 Inh treated, Group 3: GW4869 treated, Group 4: Combination treatment of SIRT1 Inh and GW4869; D. Percentage of OS status; E. Percentage of death; F. Determination of peritoneal implants; G. Measurement of ascitic fluid; H-K, Representation of liver, spleen, lungs and ovary and their respective H&E staining from different treatment groups. (*P<0.05, **P<0.01, ***P<0.001, ****P<0.0001)

4.4.7. SIRT1/COX-2 is modulated by hypoxic TME under the combination treatment by increasing PTEN

The expression of SIRT1, COX-2 corroborated with our previous findings where their expression decreased with the treatment of SIRT1 Inh but surprisingly when we administered the exosomal inhibitor, GW4869 in combination with the SIRT1 Inh, we observed there was a considerable decrease in the expression of SIRT1 (Figure 7A) and COX-2 (Figure 7C). To check whether the HIF-1α performs a role in modulating with SIRT1 and COX-2 expression, we observed its lower expression under the combination treatment (Figure 7B). However, the

PTEN expression increased significantly under the combination treatment as compared to the individual treatment of SIRT1 Inh and GW4869 (Figure 7D).

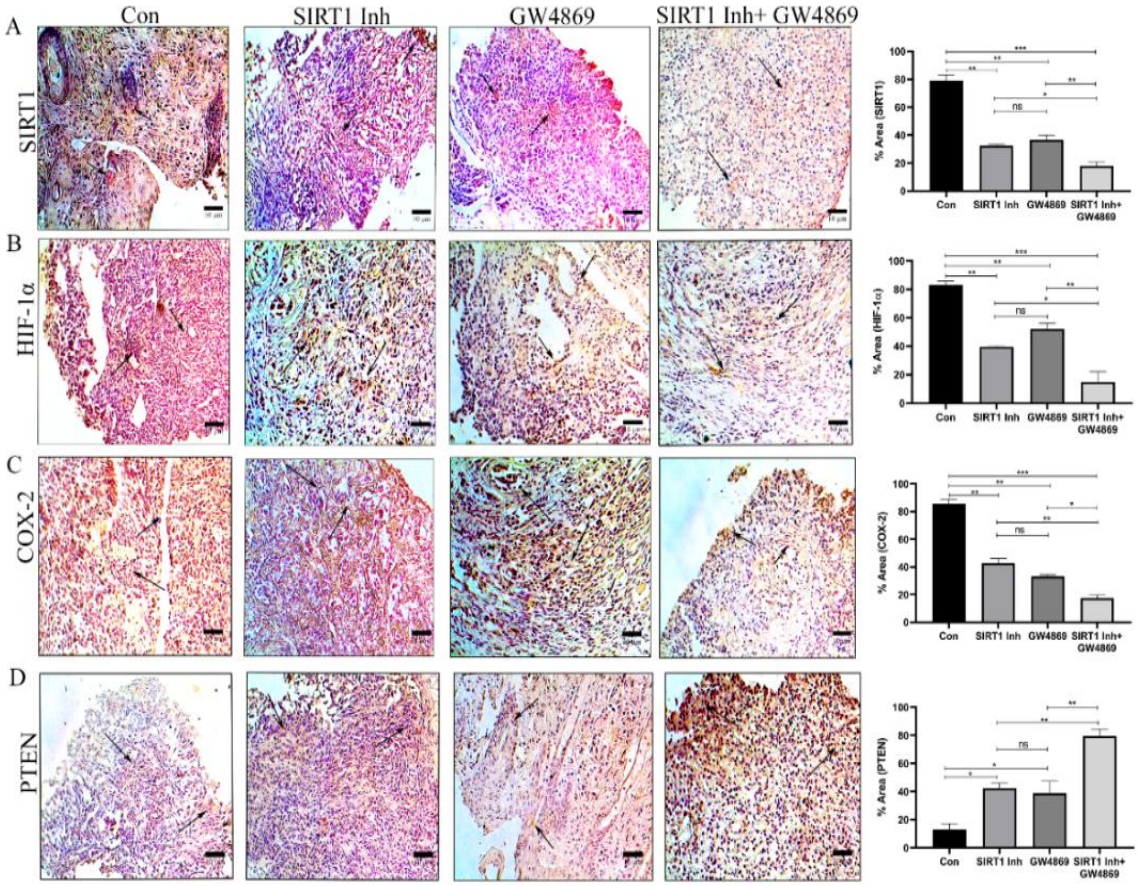

Figure 7. IHC analysis of A. SIRT1, B. HIF-1α, C. COX-2, D. PTEN under Group 1: Vehicle control, Group 2: SIRT1 Inh treated, Group 3: GW4869 treated, Group 4: Combination treatment of SIRT1 Inh and GW4869. (*P<0.05, **P<0.01, ***P<0.001, ****P<0.0001)

4.4.8. Combination treatment reduces the proliferation, metastatic and angiogenesis markers in OvCa tissues

Upon having a lead in observing that SIRT1 expression decreased under the combination treatment (SIRT1 Inh+GW4869), we were inclined to understand the expression of the proliferation marker and metastatic markers. Interestingly, we have observed Ki-67 status decreased under the combination treatment group (Figure 8A), which strengthens our findings of the colony formation in the *in-vitro* model. Furthermore, their colocalized expression and the MFI of MMP2/MMP9 decreased under the combination treatment as compared to SIRT1 Inh and GW4869 treatment alone as represented in Figure 8B-D.

Surprisingly, angiogenesis markers VEGF and ANGPT2 also corroborated with the expressional status of MMP2/MMP9 (Figure 8E-G).

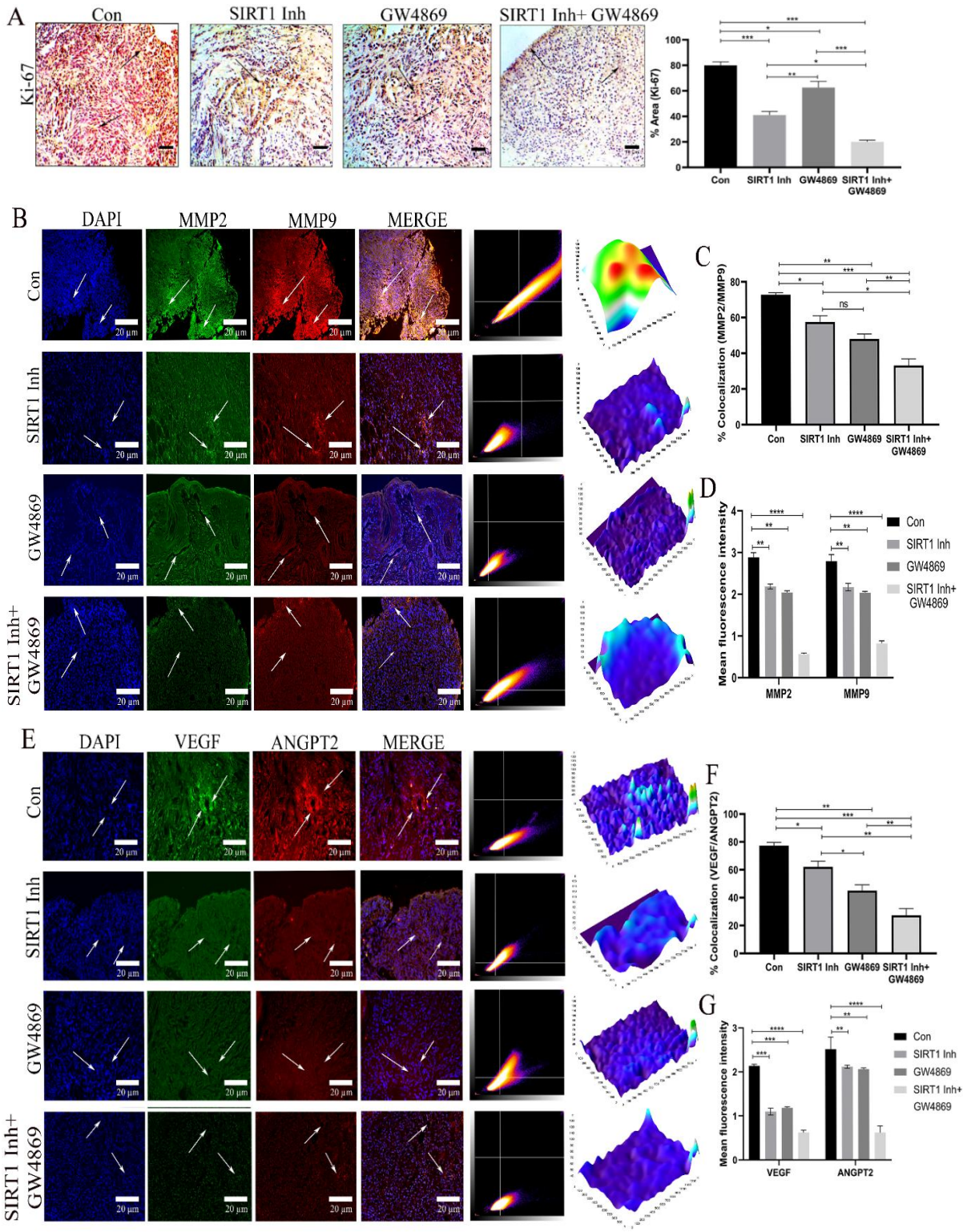

Figure 8. A. IHC analysis of proliferation marker Ki-67; B. IF analysis of metastatic markers MMP2/MMP9; C. Colocalized expression of MMP2/MMP9; D. MFI of MMP2/MMP9; E. IF analysis of metastatic markers VEGF/ANGPT2; F. Colocalized expression of

VEGF/ANGPT2; G. MFI of VEGF/ANGPT2 under Group 1: Vehicle control, Group 2: SIRT1 Inh treated, Group 3: GW4869 treated, Group 4: Combination treatment of SIRT1 Inh and GW4869. (*P<0.05, **P<0.01, ***P<0.001, ****P<0.0001)

4.4.9. Evaluation of EMT markers revealed their decreased expression under the combination treatment

When we observed that the metastasis related factors decreased under the combination treatment, we analyzed the expression of EMT markers (E-cad/Vim/Snail/Twist). Surprisingly, we have observed that the epithelial marker E-cad was significantly increased under the combination treatment whereas the mesenchymal markers like Vim decreased (Figure 9A-B) and Snail/Twist expression decreased under the combination treatment as revealed by their colocalized expression and their MFI under four distinct treatment groups (Figure 9C-E).

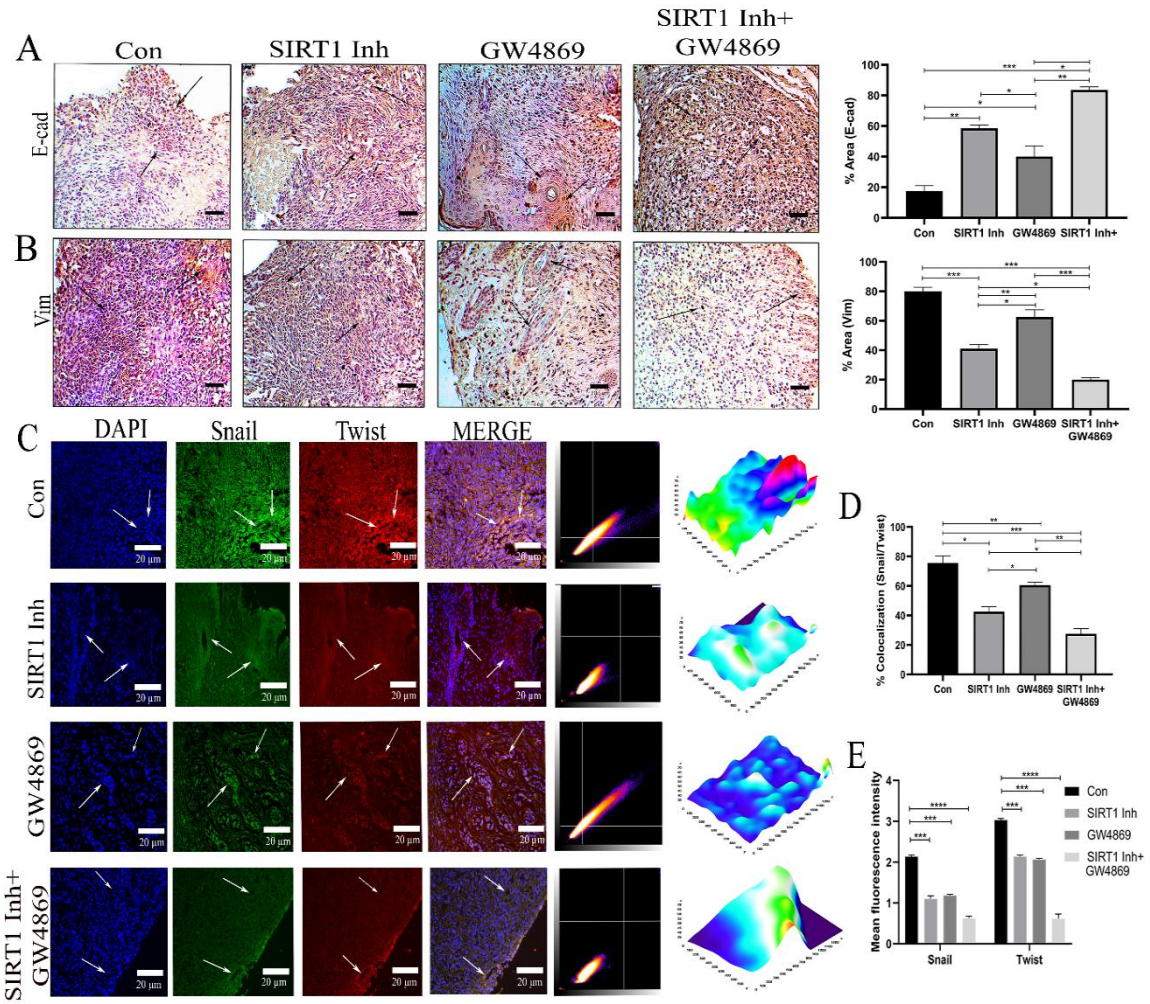

Figure 9. IHC analysis of A. Epithelial marker E-cad; B. IHC analysis of mesenchymal marker Vim; C. IF analysis of Snail/Twist; D. Colocalized expression of Snail/Twist; E. MFI

of Snail/Twist under Group 1: Vehicle control, Group 2: SIRT1 Inh treated, Group 3: GW4869 treated, Group 4: Combination treatment of SIRT1 Inh and GW4869. (*P<0.05, **P<0.01, ***P<0.001, ****P<0.0001)

4.4.10. Dysregulated glycolytic factors contribute to the metastasis of the cancer cells

After deducing the metastasis related factors, we were inclined to investigate the expression of glycolytic markers and surprisingly, we observed that the expression of GLUT1, HKII and PKM2 were increased in the control group. However, their expressions were comparatively reduced under the treatment of SIRT1 Inh and GW4869. The combination treatment of SIRT1 Inh and GW4869 significantly reduced the expression of GLUT1, HKII and PKM2 as compared to their individual treatment, as represented in Figure 10A-C.

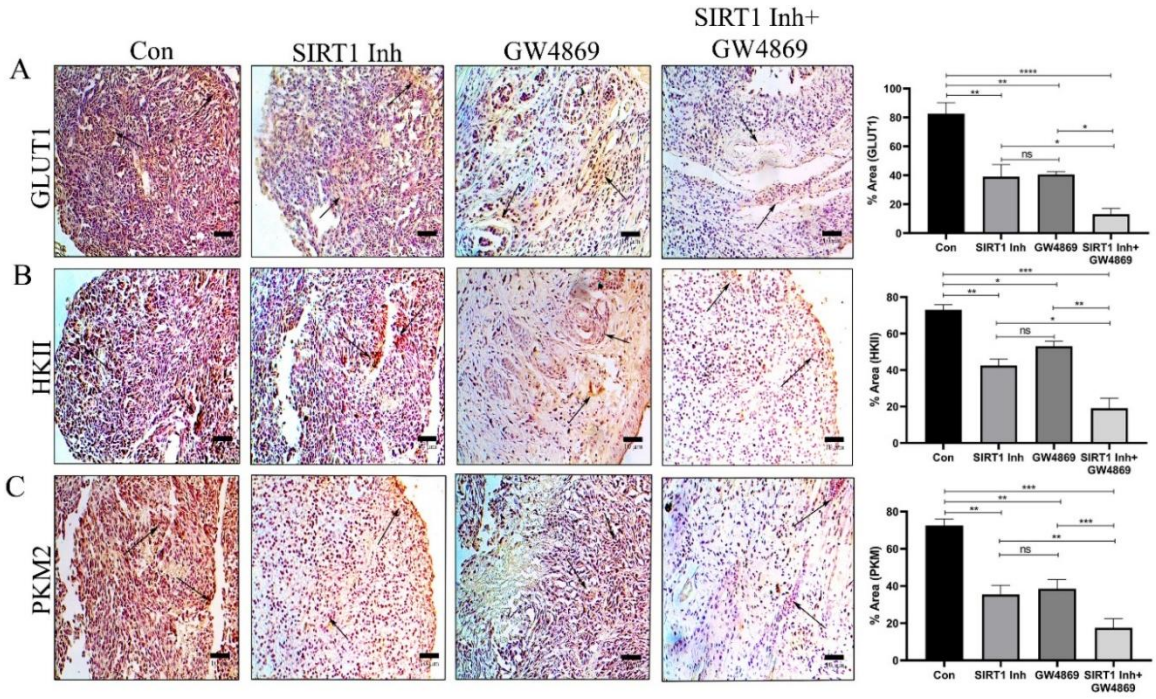

Figure 10. IHC analysis of A. GLUT1; B. IHC analysis HKII; C. IHC analysis of PKM2 under Group 1: Vehicle control, Group 2: SIRT1 Inh treated, Group 3: GW4869 treated, Group 4: Combination treatment of SIRT1 Inh and GW4869. (*P<0.05, **P<0.01, ***P<0.001, ****P<0.0001

4.4.11. Altered metabolism was restored under the effect of SIRT1 Inh and GW4869 in combination

After analyzing the interrelated factors associated with metabolism and metastasis, we were inclined to understand the altered metabolic reprogramming in OvCa. The protein was isolated from the tumor tissues from all four different treatment categories (Figure 11A). We

have observed that the glucose consumption level decreased under the combination treatment (Figure 11B) and expectedly the pyruvate production increased (Figure 11C) whereas lactate production decreased (Figure 11D) under the similar combination effect. To assess the involvement of SIRT1 in it, we have performed SIRT1 activity assay which revealed that SIRT1 activity decreased under the combination treatment (Figure 11E). Along with that, the NAD/NADH ratio level (Figure 11F) as well as relative ATP levels also decreased under the same treatment conditions (Figure 11G). Upon observing that PTEN expression decreases with the treatment, to understand how the signaling cascade works, we analyzed the PI3K/AKT/pAKT and observed that the results corroborated with our previous finding in the normal cells. However, the combination treatment reduced their protein levels considerably (Figure 11H). A similar result was observed in the case of IL-6 analyzed from the blood serum as represented in Figure 11I.

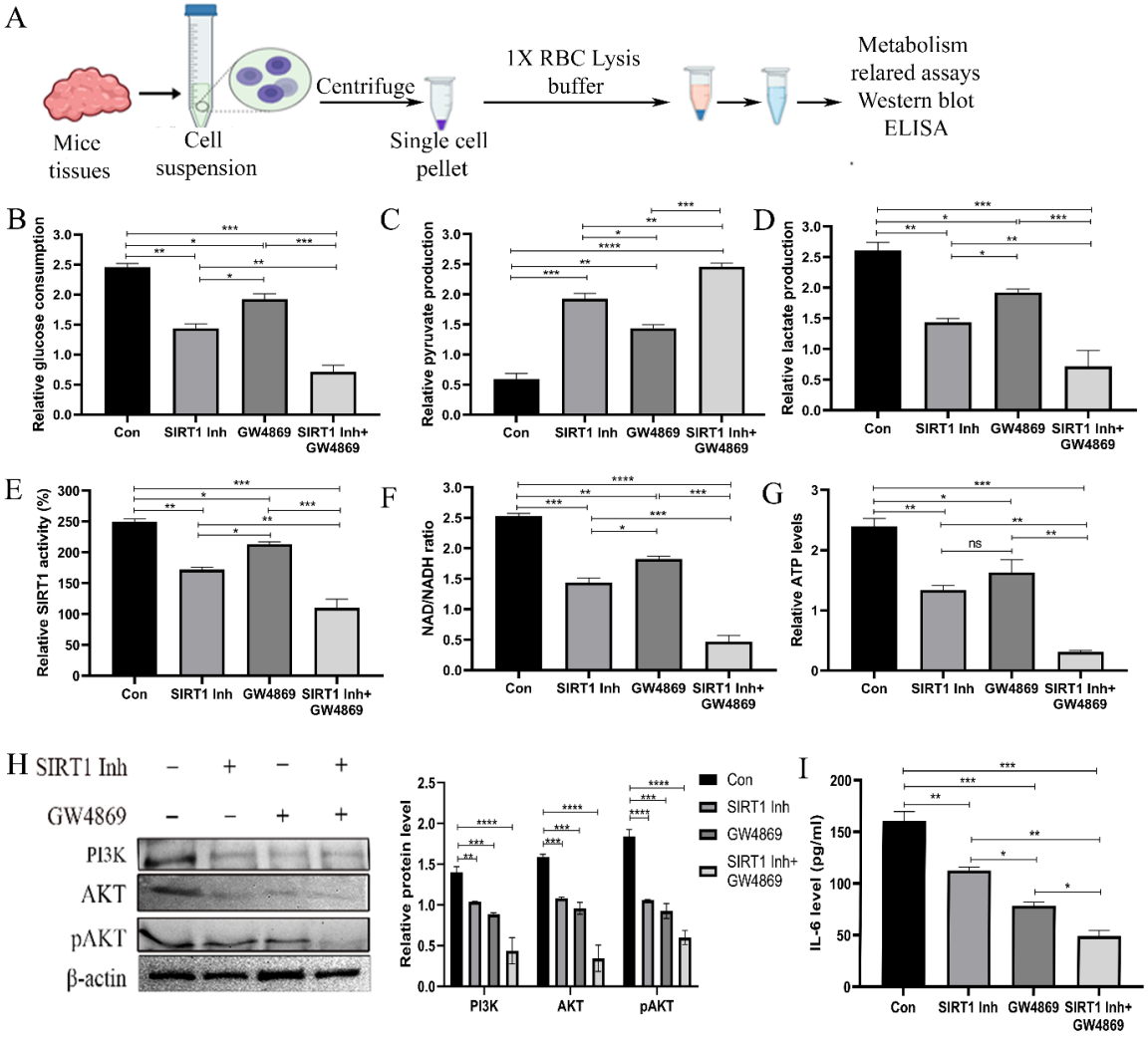

Figure 11. A. Schematic representation of sample preparation for metabolic assays from mice tissues; B. Glucose uptake assay; C. Pyruvate production assay; D. Lactate production assay;

E. SIRT1 activity assay; F. NAD/NADH ratio estimation; G. ATP measurement assay; H. Western Blot of PI3K/AKT/pAKT; I. Determination of IL-6 secretion under Group 1: Vehicle control, Group 2: SIRT1 Inh treated, Group 3: GW4869 treated, Group 4: Combination treatment of SIRT1 Inh and GW4869. (*P<0.05, **P<0.01, ***P<0.001, ****P<0.0001)

4.5. Discussion

Metabolism driven metastasis under an inflammatory milieu is a critical condition to control the aggressiveness of OvCa. A correlation was established between SIRT1/COX-2/IL-6 axis under the effect of exosomes in primary OvCa cells which triggered the metastatic switch. The outcome of this signaling cascade was mitigated under the effect of SIRT1 Inh which performs its role by promoting apoptosis in the cancer cells induced by increased ROS production. In this report, we investigated the potential of the OvCa derived exosomes in imparting oncogenic attributes to normal cells. In this context, after induction of EMT in the normal cells by TGF-β, upon addition of exosomes, the results reflected decreased epithelial marker E-cad, increased mesenchymal marker, Vim, elevated expression of Snail, increased number of colonies and higher secretion of IL-6. These results confirmed that the isolated exosomes from the poorly differentiated patient blood possessed oncogenic properties that are conferred into the normal cells thereby influencing their oncogenic transformation.

To explore the effect of SIRT1 Inh in modulating the transformed normal cells, we evaluated the secretion of pro-inflammatory cytokines. Interestingly, our results corroborated with our previous findings revealing their increased secretion levels under the effect of exosomes, however, the secretory levels decreased under the effect of SIRT1 Inh. Surprisingly, we also deduced that protein expression levels of SIRT1, COX-2 and IL-6 which increased significantly under the effect of exogenous exosomes but upon inhibiting SIRT1 their expression status decreased. Upon evaluating the EMT markers, E-cad and Vim, also corroborated with our previous findings, where under the effect of SIRT1 Inh E-cad expression increased and Vim decreased. Upon observing the expression of Snail, it was deduced that the nuclear translocation of Snail decreased under the effect of SIRT1 Inh which was increased under exosomal effect. This result validated the hypothesis that SIRT1 interferes with the initiation of EMT under the influence of exosomes by regulating the translocation of Snail which in turn affects the proliferation capacity of the transformed normal cells. Previous findings also strengthened our findings that exosomes impart oncogenic transformations in healthy cells. For instance, *Elmageed et al.* revealed that normal adipocyte-derived stem cells undergo neoplastic transformation when incubated with PC

adipocyte-derived by transferring exosomes into the normal cells [37]. Furthermore, *Melo et al.* demonstrated that BC derived exosomes contain carry RNA-induced silencing complex (RISC) loading complex proteins, Dicer, TRBP, and AGO2 pre-miRNAs which imparts oncogenic attributes to the non-transformed epithelial cells by altering the transcriptome of the host cells [38]. Additionally, healthy fibroblasts transform into CAFs under the effect of bladder cancer-derived exosomes by enhancing IL-6 secretion which in turn regulates the process of EMT [39]. Mesenchymal-epithelial transition (MET) is also modulated by exosomes. Evidently, PC derived exosomes regulate patients' adipose derived stem cells (ADSCs) by inducing MET and developing a prostate tumor in an *in-vivo* model [40]. In nasopharyngeal carcinoma, the oncogenic exosomes transcriptionally regulate the host cells by increasing the expression of HIF-1α as cargo on the exosomes influenced by latent membrane protein 1 (LMP1), the principal oncoprotein of Epstein-Barr Virus (EBV) [41].

Under this doctrine, when we confirmed that the exogenous exosomes actively participate in the metastatic process whose effect is affected by the treatment of SIRT1 Inh, we were interested in exploring the underlying mechanism responsible for this phenomenon, thus we evaluated the PI3K/AKT pathway, as our previous findings illustrated that PI3K/AKT is altered in OvCa. We interestingly deduced that the PI3K expression decreased under the effect of SIRT1 Inh, which was previously increased under the effect of exosomes. PI3K/AKT pathway is altered under the effect of SIRT1 Inh cancer cell derived exosomes, which in turn promote oncogenic attributes in cancer cells. Evidently, *Dai et al.* stated that CRC-derived oncogenic exosomes contain high levels of miR-10 which regulate the fibroblasts in the TME and enhance the migration of the cancer cells by the PI3K/AKT pathway [42]. Metastasis in GC is also modulated by oncogenic exosomes by the exosomal transfer of LINC01559 from mesenchymal stem cells to GC cells and regulates the PI3K/AKT pathway [43]. Interestingly, we deduced similar results in the expression of AKT and pAKT. Literature survey revealed that SIRT1 deacetylates and inhibits PTEN, which in turn triggers the PI3K/AKT signaling cascade. Our findings of increased SIRT1 expression in the tumor tissues with decreased PTEN expression was interestingly validated by a study by *Ikenoue et al.* where the deacetylation of PTEN by SIRT1 was proven, resulting in lower expression of PTEN [44]. Lower expression and inactivation of PTEN by deacetylation in OvCa activates the PI3K/AKT pathway which promotes the tumorigenesis, cell proliferation, differentiation, angiogenesis and anti-apoptosis of the OvCa cells. The observations by *Gao et al.* stated that PI3K regulates the growth of OvCa cells by activation of an AKT/mTOR/p70S6K1 signaling pathway [45]. Moreover, activated PI3K phosphorylate

AKT in HCC [46] and this might be the underlying mechanism in case of the OvCa cancer cells. Interestingly, in a research work by *Wang et al.,* in lung adenocarcinoma, PI3K/AKT expression controls the expression of COX-2 and inhibiting the signaling cascade decreases the prostaglandin E2 (PGE) induced COX-2 expression [47]. Interestingly, COX-2 regulated the secretory levels of IL-6 levels in microglia cells via activating STAT3 pathway [48] and this establishes a strong interconnection between COX-2 and its downstream molecule IL-6. The connection between COX-2 and IL-6 is also established in CRC patients [49]. COX-2 is also highly expressed in PTEN mutated endometrial cancer cells which is regulated by AKT [50]. As this regulatory signaling cascade driving the metastasis encompassing SIRT1, COX-2, IL-6, PTEN, PI3K, AKT has not yet been evaluated in OvCa, thus our data indicates that activation of PI3K/AKT induces the COX-2 expression. These findings encompassing all these parameters have been evaluated for the first time in OvCa and as hypothesized, it can be a beneficial finding in OvCa treatment strategies.

Keeping in mind, the pivotal roles played by exosomes in transferring oncogenic attributes to non-tumor cells, we hypothesized that inhibiting the exosomal secretion can be a potential therapeutic strategy for controlling tumor development. A well-known inhibitor of exosomes biogenesis is GW4869 which by inhibiting nSMase2, GW4869 reduces the biosynthesis and release of exosomes, thereby combatting the pro-tumorigenic signaling mediated by exosomes [51]. For instance, in non-small cell lung cancer, EMT and extracellular heat shock protein 90 alpha (HSP90α) are inhibited by GW4869 which enhances the sensitivity of conventional drug gefitinib [52]. The expression of CD44 is compromised and EMT is reversed in peritoneal mesothelial cells (PMCs) in OvCa by inhibiting the exosomes release by GW4869 [53]. GW4869 also combats the uptake of miR-205 by human umbilical vein endothelial cells (HUVECs) and this underscores the pivotal role of exosomes and microRNAs in cancer progression. This finding demonstrates that targeting exosome-mediated communication can affect the aggressive behaviour of the OvCa cells [54]. Additionally, in SKOV3 cells, the oncogenic transfer of miR-205 by exosomes induces cell proliferation, migration and invasion with attenuation of OvCa cells apoptosis with down regulation of E-cad and increased Vim expression and upon treatment with GW4869 the oncogenic attributes are reversed in SKOV-3 cells [55]. Exosomal transfer of Annexin A2 (ANXA2) from OvCa cells to HMrSV5 cells induces morphological changes and fibrosis of HMrSV5 cells by degrading ECM and inducing MMT by activating PI3K/AKT/mTOR pathway. This provides a new theoretical basis for the mechanism of intraperitoneal implantation and metastasis of OvCa [56]. These findings strengthened our results that the

expression of metastatic markers, MMP2/MMP9, angiogenesis markers (VEGF/ANGPT2), proliferation marker, Ki-67 and Vim decreased considerably under the effect of combination treatment of SIRT1 Inh and GW4869, illustrating that metabolic inhibitor along with inhibition of exosomes secretion can arrest the metastasis of OvCa. Additionally, PTEN and E-cad increased under combination treatment.

Since metabolism is deregulated in OvCa, we were inclined to investigate the metabolical changes under the inhibition of SIRT1 Inh, GW4869 and both in combination in comparison to the control. KRAS mutant CRC cells have elevated expression of GLUT1, which increases the uptake of glucose in the cancer cells that in turn contributes to metabolic alterations in the cancer cells [57]. HIF-1 plays a role in exosome secretion from hepatic stellate cells (HSCs) and the expression of glycolysis-related proteins GLUT1, PKM2 in HSC exosomes underlines a new mechanism of HIF-1 in the metabolic reprogramming and activation of HSCs, which is regulating glycolysis via exosomes. This novel mode of activation and metabolic switch of HSCs and other liver non-parenchymal cells provides a better understanding of the role of exosomes in the pathogenesis of liver fibrosis [58]. These findings validated our results where the expression of GLUT1, HKII, PKM2 decreased under combination treatment as compared to the individual treatment of SIRT1 Inh and GW4869. Additionally, triple negative BC (TNBC) cells derived exosomes regulate metabolic reprogramming in CAFs, which induces mitophagy and lactate production [59]. Glucose uptake, lactate production, pyruvate production SIRT1 activity, NAD/NADH ratio and ATP decreased significantly under the combination treatment.

In a nutshell, we deduced that the exosomes derived from serum of poorly differentiated OvCa patients carry oncogenic characteristics that have the capability to transform the non-tumor cells into tumorous ones. However, the transformation can be mitigated by SIRT1 Inh treatment since SIRT1 regulates the expression of EMT markers E-cad and Vim by modulating the PI3K/AKT pathway. Additionally, when we treated the cancer cells by a combination treatment of SIRT1 Inh and GW4869 we deduced that the EMT and metastatic markers were decreased in an *in-vivo* setup. Interestingly, our results revealed metabolic factors to be involved in driving the process thus the metabolical reprogramming can be targeted to control the progression and aggressiveness of the disease.

4.6. References

[1] T.L. Yeung, C.S. Leung, K.P. Yip, C.L.A. Yeung, S.T.C. Wong, S.C. Mok, Cellular and molecular processes in ovarian cancer metastasis. A review in the theme: Cell and molecular processes in cancer metastasis, Am. J. Physiol. - Cell Physiol. 309 (2015) C444–C456. https://doi.org/10.1152/ajpcell.00188.2015.

[2] A. Cho, V.M. Howell, E.K. Colvin, The extracellular matrix in epithelial ovarian cancer - A piece of a puzzle, Front. Oncol. 5 (2015) 245. https://doi.org/10.3389/fonc.2015.00245.

[3] R.O. Hynes, A. Naba, Overview of the matrisome-An inventory of extracellular matrix constituents and functions, Cold Spring Harb. Perspect. Biol. 4 (2012) a004903. https://doi.org/10.1101/cshperspect.a004903.

[4] C. Bonnans, J. Chou, Z. Werb, 1. Bonnans, C.; Chou, J.; Werb, Z. No Title. Nat. Rev. Mol. Cell Biol. 2014, 15., Nat. Rev. Mol. Cell Biol. 15 (2014) 786–801. https://doi.org/10.1038/nrm3904.Remodelling.

[5] S. Marchini, R. Fruscio, L. Clivio, L. Beltrame, L. Porcu, I.F. Nerini, D. Cavalieri, G. Chiorino, G. Cattoretti, C. Mangioni, R. Milani, V. Torri, C. Romualdi, A. Zambelli, M. Romano, M. Signorelli, S. Di Giandomenico, M. D'Incalci, Resistance to platinum-based chemotherapy is associated with epithelial to mesenchymal transition in epithelial ovarian cancer, Eur. J. Cancer. 49 (2013) 520–530. https://doi.org/10.1016/j.ejca.2012.06.026.

[6] M. Teeuwssen, R. Fodde, Wnt signaling in ovarian cancer stemness, EMT, and therapy resistance, J. Clin. Med. 8 (2019) 1658. https://doi.org/10.3390/jcm8101658.

[7] Y. Liu, X. Cao, Characteristics and Significance of the Pre-metastatic Niche, Cancer Cell. 30 (2016) 668–681. https://doi.org/10.1016/j.ccell.2016.09.011.

[8] I. Giusti, M. Di Francesco, S.D. Ascenzo, M.G. Palmerini, G. Macchiarelli, G. Carta, V. Dolo, Ovarian cancer-derived extracellular vesicles affect normal human fibroblast behavior, Cancer Biol. Ther. 19 (2018) 722–734. https://doi.org/10.1080/15384047.2018.1451286.

[9] K. Nakamura, K. Sawada, Y. Kinose, A. Yoshimura, A. Toda, E. Nakatsuka, K. Hashimoto, S. Mabuchi, K.I. Morishige, H. Kurachi, E. Lengyel, T. Kimura,

Exosomes Promote Ovarian Cancer Cell Invasion through Transfer of CD44 to Peritoneal Mesothelial Cells, Mol. Cancer Res. 15 (2017) 78–92. https://doi.org/10.1158/1541-7786.MCR-16-0191.

[10] H. Zhao, L. Yang, J. Baddour, A. Achreja, V. Bernard, T. Moss, J.C. Marini, T. Tudawe, E.G. Seviour, F.A. San Lucas, H. Alvarez, S. Gupta, S.N. Maiti, L. Cooper, D. Peehl, P.T. Ram, A. Maitra, D. Nagrath, Tumor microenvironment derived exosomes pleiotropically modulate cancer cell metabolism, Elife. 5 (2016) e10250. https://doi.org/10.7554/ELIFE.10250.

[11] C. Wang, J. Xu, D. Yuan, Y. Bai, Y. Pan, J. Zhang, C. Shao, Exosomes carrying ALDOA and ALDH3A1 from irradiated lung cancer cells enhance migration and invasion of recipients by accelerating glycolysis, Mol. Cell. Biochem. 469 (2020) 77–87. https://doi.org/10.1007/S11010-020-03729-3.

[12] J. Xu, X. Feng, N. Yin, L. Wang, Y. Xie, Y. Gao, J. Xiang, Exosomes from cisplatin-induced dormant cancer cells facilitate the formation of premetastatic niche in bone marrow through activating glycolysis of BMSCs, Front. Oncol. 12 (2022) 922465. https://doi.org/10.3389/FONC.2022.922465/BIBTEX.

[13] A. Rai, D.W. Greening, M. Chen, R. Xu, H. Ji, R.J. Simpson, Exosomes Derived from Human Primary and Metastatic Colorectal Cancer Cells Contribute to Functional Heterogeneity of Activated Fibroblasts by Reprogramming Their Proteome, Proteomics. 19 (2019) e1800148. https://doi.org/10.1002/pmic.201800148.

[14] I.H. Tae, J.Y. Son, S.H. Lee, M.Y. Ahn, K. Yoon, S. Yoon, H.R. Moon, H.S. Kim, A new SIRT1 inhibitor, MHY2245, induces autophagy and inhibits energy metabolism via PKM2/mTOR pathway in human ovarian cancer cells, Int. J. Biol. Sci. 16 (2020) 1901–1916. https://doi.org/10.7150/IJBS.44343.

[15] F. Lin, H. Bin Yin, X.Y. Li, G.M. Zhu, W.Y. He, X. Gou, Bladder cancer cell-secreted exosomal miR-21 activates the PI3K/AKT pathway in macrophages to promote cancer progression, Int. J. Oncol. 56 (2020) 151–164. https://doi.org/10.3892/ijo.2019.4933.

[16] K. Räsänen, A. Vaheri, TGF-beta1 causes epithelial-mesenchymal transition in HaCaT derivatives, but induces expression of COX-2 and migration only in benign, not in malignant keratinocytes, J. Dermatol. Sci. 58 (2010) 97–104. https://doi.org/10.1016/j.jdermsci.2010.03.002.

[17] A.C. Midgley, M. Rogers, M.B. Hallett, A. Clayton, T. Bowen, A.O. Phillips, R. Steadman, Transforming growth factor-β1 (TGF-β1)-stimulated fibroblast to myofibroblast differentiation is mediated by hyaluronan (HA)-facilitated epidermal growth factor receptor (EGFR) and CD44 co-localization in lipid rafts, J. Biol. Chem. 288 (2013) 14824–14838. https://doi.org/10.1074/jbc.M113.451336.

[18] S.K. Das, S. Roy, A. Das, A. Chowdhury, N. Chatterjee, A. Bhaumik, A conjugated 2D covalent organic framework as a drug delivery vehicle towards triple negative breast cancer malignancy, Nanoscale Adv. (2022) 2313–2320. https://doi.org/10.1039/d2na00103a.

[19] E. Hosseini-Beheshti, S. Pham, H. Adomat, N. Li, E.S. Tomlinson Guns, Exosomes as biomarker enriched microvesicles: Characterization of exosomal proteins derived from a panel of prostate cell lines with distinct AR phenotypes, Mol. Cell. Proteomics. 11 (2012) 863–885. https://doi.org/10.1074/mcp.M111.014845.

[20] L. Gong, G. Li, X. Yi, Q. Han, Q. Wu, F. Ying, L. Shen, Y. Cao, X. Liu, L. Gao, W. Li, Z. Wang, J. Cai, Tumor-derived small extracellular vesicles facilitate omental metastasis of ovarian cancer by triggering activation of mesenchymal stem cells, Cell Commun. Signal. 22 (2024) 47. https://doi.org/10.1186/s12964-023-01413-9.

[21] N. Chatterjee, S. Das, D. Bose, S. Banerjee, S. Das, D. Chattopadhyay, K. Das Saha, Exploring the anti-inflammatory activity of a novel 2-phenylquinazoline analog with protection against inflammatory injury, Toxicol. Appl. Pharmacol. 264 (2012) 182–191. https://doi.org/10.1016/j.taap.2012.07.032.

[22] N. Chatterjee, S. Das, D. Bose, S. Banerjee, T. Jha, K. Das Saha, Lipid from Infective L. donovani Regulates Acute Myeloid Cell Growth via Mitochondria Dependent MAPK Pathway, PLoS One. 10 (2015) e0120509. https://doi.org/10.1371/journal.pone.0120509.

[23] Q. Wang, W. Shi, UNBS5162 inhibits SKOV3 ovarian cancer cell proliferation by regulating the PI3K/AKT signalling pathway, Oncol. Lett. 17 (2019) 2976–2982. https://doi.org/10.3892/ol.2019.9890.

[24] H. Hozhabri, R.S.G. Dehkohneh, S.M. Razavi, S.M. Razavi, F. Salarian, A. Rasouli, J. Azami, M.G. Shiran, Z. Kardan, N. Farrokhzad, A.M. Namini, A. Salari, Comparative

analysis of protein-protein interaction networks in metastatic breast cancer, PLoS One. 17 (2022) e0260584. https://doi.org/10.1371/journal.pone.0260584.

[25] G. Luo, Z. Jian, Y. Zhu, Y. Zhu, B. Chen, R. Ma, F. Tang, Y. Xiao, Sirt1 promotes autophagy and inhibits apoptosis to protect cardiomyocytes from hypoxic stress, Int. J. Mol. Med. 43 (2019) 2033–2043. https://doi.org/10.3892/ijmm.2019.4125.

[26] M.B. Dinkins, S. Dasgupta, G. Wang, G. Zhu, E. Bieberich, Exosome Reduction In Vivo Is Associated with Lower Amyloid Plaque Load in the 5XFAD Mouse Model of Alzheimer's Disease, Neurobiol. Aging. 35 (2014) 1792–1800. https://doi.org/10.1016/j.neurobiolaging.2014.02.012.Exosome.

[27] L. Zhang, N. Yang, J.R. Conejo Garcia, A. Mohamed, F. Benencia, S.C. Rubin, D. Allman, G. Coukos, Generation of a syngeneic mouse model to study the effects of vascular endothelial growth factor in ovarian carcinoma, Am. J. Pathol. 161 (2002) 2295–2309. https://doi.org/10.1016/S0002-9440(10)64505-1.

[28] B.L. Thériault, L. Portelance, A.M. Mes-Masson, M.W. Nachtigal, Establishment of primary cultures from ovarian tumor tissue and ascites fluid, Methods Mol. Biol. 1049 (2013) 323–336. https://doi.org/10.1007/978-1-62703-547-7_24.

[29] S. Roy, A. Das, M. Vernekar, S. Mandal, N. Chatterjee, Understanding the Correlation between Metabolic Regulator SIRT1 and Exosomes with CA-125 in Ovarian Cancer: A Clinicopathological Study, Biomed Res. Int. 2022 (2022) 5346091. https://doi.org/10.1155/2022/5346091.

[30] M.I. Lutz, C. Schwaiger, B. Hochreiter, G.G. Kovacs, J.A. Schmid, Novel approach for accurate tissue-based protein colocalization and proximity microscopy, Sci. Rep. 7 (2017) 2668. https://doi.org/10.1038/s41598-017-02735-8.

[31] M. Charan, S. Das, S. Mishra, N. Chatterjee, S. Varikuti, K. Kaul, S. Misri, D.K. Ahirwar, A.R. Satoskar, R.K. Ganju, Macrophage migration inhibitory factor inhibition as a novel therapeutic approach against triple-negative breast cancer, Cell Death Dis. 11 (2020) 774. https://doi.org/10.1038/s41419-020-02992-y.

[32] A.H. Fischer, K.A. Jacobson, J. Rose, R. Zeller, Hematoxylin and eosin staining of tissueand cell sections, Cold Spring Harb. Protoc. 3 (2008) 3–5. https://doi.org/10.1101/pdb.prot4986.

[33] N. Chatterjee, S. Das, D. Bose, S. Banerjee, T. Jha, K. Das Saha, Leishmanial lipid affords protection against oxidative stress induced hepatic injury by regulating inflammatory mediators and confining apoptosis progress, Toxicol. Lett. 232 (2015) 499–512. https://doi.org/10.1016/j.toxlet.2014.11.023.

[34] Z.M. Peng, X.J. Han, T. Wang, J.J. Li, C.X. Yang, F.F. Tou, Z. Zhang, PFKP deubiquitination and stabilization by USP5 activate aerobic glycolysis to promote triple-negative breast cancer progression, Breast Cancer Res. 26 (2024) 10. https://doi.org/10.1186/s13058-024-01767-z.

[35] J. wen Yang, Y. Zou, J. Chen, C. Cui, J. Song, M. meng Yang, J. Gao, H. qing Hu, L. qing Xia, L. ming Wang, X. yu Lv, L. Chen, X. guo Hou, Didymin alleviates metabolic dysfunction-associated fatty liver disease (MAFLD) via the stimulation of Sirt1-mediated lipophagy and mitochondrial biogenesis, J. Transl. Med. 21 (2023) 921. https://doi.org/10.1186/S12967-023-04790-4.

[36] M. Ahn, E. Oh, E.M. McCown, X. Wang, R. Veluthakal, D.C. Thurmond, A requirement for PAK1 to support mitochondrial function and maintain cellular redox balance via electron transport chain proteins to prevent β-cell apoptosis, Metabolism. 115 (2021) 154431. https://doi.org/10.1016/j.metabol.2020.154431.

[37] C. Zhang, C. Qin, S. Dewanjee, H. Bhattacharya, P. Chakraborty, N.K. Jha, M. Gangopadhyay, S.K. Jha, Q. Liu, Tumor-derived small extracellular vesicles in cancer invasion and metastasis: molecular mechanisms, and clinical significance, Mol. Cancer. 23 (2024) 983–97. https://doi.org/10.1186/s12943-024-01932-0.

[38] S.A. Melo, H. Sugimoto, J.T. O'Connell, N. Kato, A. Villanueva, A. Vidal, L. Qiu, E. Vitkin, L.T. Perelman, C.A. Melo, A. Lucci, C. Ivan, G.A. Calin, R. Kalluri, Cancer Exosomes Perform Cell-Independent MicroRNA Biogenesis and Promote Tumorigenesis, Cancer Cell. 26 (2014) 707–721. https://doi.org/10.1016/j.ccell.2014.09.005.

[39] C.R. Goulet, A. Champagne, G. Bernard, D. Vandal, S. Chabaud, F. Pouliot, S. Bolduc, Cancer-associated fibroblasts induce epithelial-mesenchymal transition of bladder cancer cells through paracrine IL-6 signalling, BMC Cancer. 19 (2019) 137. https://doi.org/10.1186/s12885-019-5353-6.

[40] Z.Y.A. Elmageed, Y. Yang, R. Thomas, M. Ranjan, D. Mondal, K. Moroz, Z. Fang, B.M. Rezk, K. Moparty, S.C. Sikka, O. Sartor, A.B. Abdel-Mageed, Neoplastic reprogramming of patient-derived adipose stem cells by prostate cancer cell-associated exosomes, Stem Cells. 32 (2014) 983–997. https://doi.org/10.1002/stem.1619.

[41] M. Aga, G.L. Bentz, S. Raffa, M.R. Torrisi, S. Kondo, N. Wakisaka, T. Yoshizaki, J.S. Pagano, J. Shackelford, Exosomal HIF1α supports invasive potential of nasopharyngeal carcinoma-associated LMP1-positive exosomes, Oncogene. 33 (2014) 4613–4622. https://doi.org/10.1038/onc.2014.66.

[42] G. Dai, X. Yao, Y. Zhang, J. Gu, Y. Geng, F. Xue, J. Zhang, Colorectal cancer cell–derived exosomes containing miR-10b regulate fibroblast cells via the PI3K/Akt pathway, Bull. Cancer. 105 (2018) 336–349. https://doi.org/10.1016/j.bulcan.2017.12.009.

[43] L. Wang, X. Bo, X. Yi, X. Xiao, Q. Zheng, L. Ma, B. Li, Exosome-transferred LINC01559 promotes the progression of gastric cancer via PI3K/AKT signaling pathway, Cell Death Dis. 11 (2020) 723. https://doi.org/10.1038/s41419-020-02810-5.

[44] T. Ikenoue, K. Inoki, B. Zhao, K.L. Guan, PTEN acetylation modulates its interaction with PDZ domain, Cancer Res. 68 (2008) 6908–6912. https://doi.org/10.1158/0008-5472.CAN-08-1107.

[45] N. Gao, D.C. Flynn, Z. Zhang, X.S. Zhong, V. Walker, K.J. Liu, X. Shi, B.H. Jiang, G1, cell cycle progression and the expression of G1 cyclins are regulated by PI3K/AKT/mTOR/p70S6K1 signaling in human ovarian cancer cells, Am. J. Physiol. - Cell Physiol. 287 (2004) 281–291. https://doi.org/10.1152/ajpcell.00422.2003.

[46] H. Wang, H. Liu, K. Chen, J. Xiao, K. He, J. Zhang, G. Xiang, SIRT1 promotes tumorigenesis of hepatocellular carcinoma through PI3K/PTEN/AKT signaling, Oncol. Rep. 28 (2012) 311–318. https://doi.org/10.3892/or.2012.1788.

[47] J. Yang, X. Wang, Y. Gao, C. Fang, F. Ye, B. Huang, L. Li, Inhibition of PI3K-AKT signaling blocks PGE2-induced COX-2 expression in lung adenocarcinoma, Onco. Targets. Ther. 13 (2020) 8197–8208. https://doi.org/10.2147/OTT.S263977.

[48] J. Zhu, S. Li, Y. Zhang, G. Ding, C. Zhu, S. Huang, A. Zhang, Z. Jia, M. Li, Cox-2 contributes to LPS-induced Stat3 activation and IL-6 production in microglial cells, Am. J. Transl. Res. 10 (2018) 966–974.

[49] C. Maihöfner, M.P. Charalambous, U. Bhambra, T. Lightfoot, G. Geisslinger, N.J. Gooderham, J. Barrett, D.T. Bishop, A.R. Boobis, D. Forman, R.C. Garner, C. Sachse, G. Smith, R. Waxman, C.R. Wolf, Expression of cyclooxygenase-2 parallels expression of interleukin-1beta, interleukin-6 and NF-kappaB in human colorectal cancer, Carcinogenesis. 24 (2003) 665–671. https://doi.org/10.1093/carcin/bgg006.

[50] M.E. St-Germain, V. Gagnon, I. Mathieu, S. Parent, E. Asselin, Akt regulates COX-2 mRNA and protein expression in mutated-PTEN human endometrial cancer cells., Int. J. Oncol. 24 (2004) 1311–1324. https://doi.org/10.3892/ijo.24.5.1311.

[51] C. Tallon, K.R. Hollinger, A. Pal, B.J. Bell, R. Rais, T. Tsukamoto, K.W. Witwer, N.J. Haughey, B.S. Slusher, Nipping disease in the bud: nSMase2 inhibitors as therapeutics in extracellular vesicle-mediated diseases, Drug Discov. Today. 26 (2021) 1656–1668. https://doi.org/10.1016/J.DRUDIS.2021.03.025.

[52] X. Wan, Y. Fang, J. Du, S. Cai, H. Dong, GW4869 Can Inhibit Epithelial-Mesenchymal Transition and Extracellular HSP90α in Gefitinib-Sensitive NSCLC Cells, Onco. Targets. Ther. 16 (2023) 913–922. https://doi.org/10.2147/OTT.S428707.

[53] K. Nakamura, K. Sawada, Y. Kinose, A. Yoshimura, A. Toda, E. Nakatsuka, K. Hashimoto, S. Mabuchi, K.I. Morishige, H. Kurachi, E. Lengyel, T. Kimura, Exosomes promote ovarian cancer cell invasion through transfer of CD44 to peritoneal mesothelial cells, Mol. Cancer Res. 15 (2017) 78–92. https://doi.org/10.1158/1541-7786.MCR-16-0191.

[54] L. He, W. Zhu, Q. Chen, Y. Yuan, Y. Wang, J. Wang, X. Wu, Ovarian cancer cell-secreted exosomal miR-205 promotes metastasis by inducing angiogenesis, Theranostics. 9 (2019) 8206–8220. https://doi.org/10.7150/thno.37455.

[55] L. Wang, F. Zhao, Z. Xiao, L. Yao, Exosomal microRNA-205 is involved in proliferation, migration, invasion, and apoptosis of ovarian cancer cells via regulating VEGFA, Cancer Cell Int. 19 (2019) 281. https://doi.org/10.1186/s12935-019-0990-z.

[56] L. Gao, X. Nie, R. Gou, Y. Hu, H. Dong, X. Li, B. Lin, Exosomal ANXA2 derived from ovarian cancer cells regulates epithelial-mesenchymal plasticity of human peritoneal mesothelial cells, J. Cell. Mol. Med. 25 (2021) 10916–10929. https://doi.org/10.1111/jcmm.16983.

[57] R. Preet, D.A. Dixon, Mutant KRAS Exosomes Influence the Metabolic State of the Colon Microenvironment, Cell. Mol. Gastroenterol. Hepatol. 5 (2018) 647. https://doi.org/10.1016/J.JCMGH.2018.01.021.

[58] L. Wan, T. Xia, Y. Du, J. Liu, Y. Xie, Y. Zhang, F. Guan, J. Wu, X. Wang, C. Shi, Exosomes from activated hepatic stellate cells contain GLUT1 and PKM2: a role for exosomes in metabolic switch of liver nonparenchymal cells, FASEB J. 33 (2019) 8530–8542. https://doi.org/10.1096/fj.201802675R.

[59] J.S. Sung, C.W. Kang, S. Kang, Y. Jang, Y.C. Chae, B.G. Kim, N.H. Cho, ITGB4-mediated metabolic reprogramming of cancer-associated fibroblasts, Oncogene. 39 (2020) 664–676. https://doi.org/10.1038/S41388-019-1014-0.

Conclusion

Conclusion

Investigations on the advancements in the field of translational research for the managing risk factors of cancer are ongoing for improving survival of the patients. However, possible explanation for the increasing cases of OvCa is that it had been a challenging issue for gynaecology oncologists to uncover an absolutely potent cure for the disease. The heterogeneity of OvCa disease limits evidences for the dynamic etiological factors to understand the onset of the disease. The lack of effective screening process and improper symptoms also restrains the diagnosis at an early stage which in turn makes the treatment complicated due to its advanced stage.

Our study highlights the functions of SIRT1 as an important therapeutic target in OvCa due to its modulatory functions in cancer-associated signaling pathways by facilitating EMT process and initiating metastasis of the disease. Moreover, our study provides quality evidence to demonstrate the efficacy of SIRT1 inhibitors both natural compounds and SMIs. This unfolds the theme for future identification of better SIRT1 inhibitors. This resulted in SIRT1 Inh III as a new specific and potent hit, much more potent than Hyperforin. These data indicate that SIRT1 Inh III blocks the metastatic process and regulates the disease progression. Thus, this study not only identified SIRT1 as a promising target but also recognised SIRT1 Inh III as a potent therapeutic agent that may merit further investigation.

The association of CA-125 with the clinicopathological parameters revealed its strong correlation with BMI, degree of dissemination, tumor differentiation, ascitic fluid. In this context, since SIRT1 is a metabolic factor, upon analyzing its expression revealed its higher expression in the hypoxic TME of OvCa under the excess burden of exosomes. Thus, segregated levels of CA-125 in relation with expression of SIRT1 and its associated factors can detect the aggressiveness of the disease by detecting metabolic dysregulations in cancer cells and exosome concentrations. This provides a guideline to target the mechanism involving them, offering an improved therapeutic outcome for the OvCa patients.

The lead provided in the previous study inclined us to study the sociodemographical parameters revealing pain as a detectable factor that correlated with the tumor differentiation. Since most of the symptoms are undetectable at an early stage however, analysis of pain can be a symptomatic indication on the status of the disease. Additionally, pain is an outcome of

inflammation and metastasis mediated by inflammation is an important criteria of cancer aggressiveness. Thus, hypothesizing a circuitry in OvCa where SIRT1 is proven to be a regulator of an inflammatory TME, influencing the metastasis under the oncogenic exosomes needed exploration. Surprisingly, SIRT1 was found to regulate the metastasis and was surprisingly observed the involvement of exosomes fueled the process but was eventually mitigated by the SIRT1 Inh. Thus, targeting SIRT1 can be a novel treatment approach, which can mitigate the metastatic cascade and also minimizes exosomal interference thereby it was expected to minimize the pain in late-stage patients and improve the quality of life of patients by decreasing the metastatic capability of the OvCa cells.

Under the context that exosomes confer oncogenic properties to non-transformed cells it was deduced that the isolated exosomes from poorly differentiated patients were oncogenic proven by imparting metastatic and proliferative properties to the normal cells. Thus, targeting exosome biogenetic, secretion, may interrupt the metastatic cascade by controlling the metabolic interactions, thus suppressing cancer development. Metabolic reprogramming by alterations in the glycolytic cascade in OvCa also accounts for supplementing the SIRT1 expression by replenishing NAD levels which in turn modulates the metastatic cascade is a complete circuitry to be considered as a target for OvCa treatment. This reprogramming drive tumorigenesis and could define therapeutic targets.

Future prospects

For improvising the patient survival, controlling devastating malignant precedes are essential that could be addressed via regulating metastasis, altering metabolism, developing body response and importantly minimizing the '*off target on side*' toxicities by not disturbing other cellular mechanisms. Target cell specificity remains a challenge as exosomes are ubiquitously released from almost all cells, either in malignant or normal conditions. Thus, tumor specific delivery of inhibitors for exosomes release or any associated protein molecules remains a challenge. Although the establishment of exosomal inhibitors is a dependable avenue for cancer therapy, the above-mentioned limitations restrain the process. Additionally, despite the identification of multiple metabolic factors, the presence of adverse side effects, plasticity and flexibility as well as metabolic heterogeneity, creates challenges in therapeutic strategies. There is also an urgency to establish potent therapeutic approaches that can mitigate the

development of resistance against metabolic or exosomal inhibitors. Importantly, implementing this with other therapeutic regimens can prove to be a novel therapeutic avenue in cancer therapy. This will potentially lead clinicians and researchers to break through the drawbacks in understanding the molecular mechanisms to combat this disease. Continued research and clinical trials are required to completely investigate the targeting capability of the exosomes inhibitors and metabolic inhibitors which in turn will aid in understanding the exosome-mediated communication in cancer. Thus, targeting exosome biogenesis and secretion, especially in combination with other therapeutic agents like SIRT1 inhibitors, may offer promising strategies for inhibiting OvCa metastasis.

Appendix

Publications

Conference proceedings

Oral/Poster presentation

Workshops/ Seminars/ Symposiums/

Conferences

Publications

1. **Roy S**, Das A, Vernekar M, Mandal S, Chatterjee N. Understanding the Correlation between Metabolic Regulator SIRT1 and Exosomes with CA-125 in Ovarian Cancer: A Clinicopathological Study. Biomed Res Int. 2022;2022:5346091. doi: 10.1155/2022/5346091.

2. **Roy S**, Das A, Bairagi A, Das D, Jha A, Srivastava AK, Chatterjee N. Mitochondria act as a key regulatory factor in cancer progression: current concepts on mutations, mitochondrial dynamics, and therapeutic approach. Mutat Res Rev Mutat Res. 2024 Mar 7:108490. doi: 10.1016/j.mrrev.2024.108490.

3. Sinha D, **Roy S**, Saha P, Chatterjee N, Bishayee A. Trends in Research on Exosomes in Cancer Progression and Anticancer Therapy. Cancers (Basel). 2021;13(2):326. Published 2021 Jan 17. doi:10.3390/cancers13020326

4. Das A, **Roy S**, Bairagi A, Alam N, Chatterjee N. IL-6 mediated $CD206^{+}ARG\text{-}1^{+}$ tumor associated macrophage polarization induces Treg infiltration in non-responder luminal A breast cancer. FEBS Lett. 2025 Feb 4. doi: 10.1002/1873-3468.70000.

5. Das P, **Roy S**, Das C, Biswas R, Chaterjee N, Dinda J. Structure-based design to explore the anticancer efficacy of organometallic Pt(ii)- and Au(iii)-N-heterocyclic carbene (NHC) complexes. New Journal of Chemistry, 2024; 48(37). 1144-0546. doi. 10.1039/D4NJ02853H.

6. Hassan A, **Roy S**, Das A, Wahed SA, Bairagi A, Mondal S, Chatterjee N, Das N. Covalent Organic Frameworks as Potential Drug Carriers and Chemotherapeutic Agents for Ovarian Cancers. ACS Biomater Sci Eng. 2024 Jul 8;10(7):4227-4236. doi: 10.1021/acsbiomaterials.4c00351.

7. Behera PK, Maity L, **Roy S**, Das A, Sahu P, Kisan HK, Changotra A, Isab AA, Fetthouhi MB, Bairagi A, Chatterjee N, Dinda J. Therapeutic Potential of Ag(I)-, Au(I)-, Au(III)-NHC complexes of 3-pyridyl wingtip N-heterocyclic carbene (NHC) against lung cancer. New Journal of Chemistry. 2023;47(40). Published 2023 Jan. doi: 10.1039/D3NJ02882H.

8. Das SK, **Roy S**, Das A, Chowdhury A, Chatterjee N, Bhaumik A. A conjugated 2D covalent organic framework as a drug delivery vehicle towards triple negative breast cancer malignancy. Nanoscale Adv. 2022;2313–20. doi.org/10.1039/D2NA00103A.

9. Das A, **Roy S**, Swarnakar S, Chatterjee N. Understanding the immunological aspects of SARS-CoV-2 causing COVID-19 pandemic: A therapeutic approach. Clin Immunol. 2021;231:108804. doi:10.1016/j.clim.2021.108804.

10. Chatterjee N, Das D, Jha A, **Roy S**. Role of Mitochondrial-mediated Pathways in Breast Cancer: An Overview. E-book: Current Advances in Breast Cancer Research: A Molecular Approach, Bentham Science publishers, 2020, 304-325. doi: 10.2174/9789811451447120010015.

Conference proceedings:

- **Roy S**, Das A, Vernekar M, Das S, Chatterjee N. SIRT1 regulates ovarian cancer metastasis via altering the exosome release and glycogen deposition. *Cancer Res* (2021) 81 (13_Supplement): 2461. 10.1158/1538-7445.AM2021-2461

- Das A, **Roy S**, Nanda D, Das S, Chatterjee N. Study the synergistic role of trastuzumab along with docetaxel in immune profiling of HER2+ breast cancer patients. 2021, FASEB 35(S1). June.10.1096/FASEBJ.2021.35.02844.

- Chatterjee N, **Roy S**, Das A. 151 Poster - Role of miR-21 in chemotherapeutic drug resistance of oral squamous cell carcinoma. 2020, EJC 138 (S2). October. 10.1016/S0959-8049(20)31183-7

Oral/Poster presentation:

1. **Roy S.,** Das A., Vernekar M., Chatterjee N. "Exosomes participate in metabolically regulating metastatic ovarian cancer in obese patients" - Oral presentation at 8th International Conference on Molecular Signaling and 4th CeSin Symposium: Signaling in Disease Management and Diagnostics on 16th-18th Mar, 2023.
2. **Roy S.,** Das A., Bairagi A., Vernekar M., Tiwari Nk., Chatterjee N. "Increased body mass index influences the metastasizing capability of ovarian cancer cells regulated by extracellular vesicles"- Poster presentation at NIOS'24 Global Conference for Oncology on 6th-7th Jan, 2024.
3. **Roy** S., Das A., Bairagi A., Roy A., Maiti K., P Chandra Sekar, Vernekar M., Chatterjee N., "Targeting upregulated SIRT1 expression downgrades oncogenic attributes of ovarian cancer"- Poster presentation at IACR'25, International Conference on 'Convergence of Fundamental and Translational Approaches in Cancer Theranostics' on 16 – 18 January, 2025.

Workshops/Seminars/Symposiums/Conferences

1. Certificate of participation in One Day Symposium on Digital Health and Cancer Registry at Chittaranjan National Cancer Institute on 30th Dec 2019.
2. Certificate of participation in Cancer Research: Bench to Bedside at Chittaranjan National Cancer Institute on 11th Jan 2020.
3. Certificate of participation in a One-day National-Level Seminar and Poster Presentation organized by the Department of Zoology at Ramkrishna Mission Vidyamandira on 6th Mar 2020.
4. Certificate for Online Workshop on Single-cell RNA sequencing from 22nd Jun-26th Jun 2020.
5. Certificate of participation in One day Seminar on National Science Day 28th Feb 2022.
6. Certificate of participation in Two-day symposium on "When Science Meets Life" by Society of Biological Chemists(I), Kolkata Chapter on 9th -10th Apr, 2022.
7. Certificate of participation in One day International Seminar on "Targeted Oncology in Therapeutics and Diagnostics" on 23rd Apr 2022.
8. Certificate of Training for Workshop on Basic of Flow Cytometry (Becton Dickinson India Pvt Ltd) on 22nd - 24th, Nov, 2022.
9. Certificate of achievement in cancer biology at Asia International Research Awards Congress at Tamil Nadu, India; on 1st Oct, 2023.

Hindawi
BioMed Research International
Volume 2022, Article ID 5346091, 16 pages
https://doi.org/10.1155/2022/5346091

Research Article

Understanding the Correlation between Metabolic Regulator SIRT1 and Exosomes with CA-125 in Ovarian Cancer: A Clinicopathological Study

Sraddhya Roy,[1] Ananya Das,[1] Manisha Vernekar,[2] Syamsundar Mandal,[3] and Nabanita Chatterjee[1]

[1]*Department of Receptor Biology and Tumor Metastasis, Chittaranjan National Cancer Institute, Kolkata, India*
[2]*Department of Gynaecological Oncology, Chittaranjan Cancer Hospital, Kolkata, India*
[3]*Department of Epidemiology and Biostatistics, Chittaranjan National Cancer Institute, Kolkata, India*

Correspondence should be addressed to Nabanita Chatterjee; nabanita.chatterje@yahoo.com

Received 6 January 2022; Accepted 10 March 2022; Published 20 April 2022

Academic Editor: Sheba Mohankumar

Background. Ovarian cancer (OvCa), the deadliest gynaecological malignancy, is associated with poor prognosis and high mortality rate. Ovarian cancer has been related with CA-125 and metabolic reprogramming by SIRT1 leading to metastasis with the involvement of exosomes. *Methods*. Clinicopathological data of OvCa patients were collected to perform the analysis. Patients' samples were collected during surgery for immunohistochemistry and flow cytometric analysis of SIRT1, HIF-1α, exosomal markers (CD81 and CD63), ki-67, and PAS staining for glycogen deposition. Adjacent normal and tumor tissues were collected as per the CA-125 levels. *Results*. CA-125, a vital diagnostic marker, has shown significant correlation with body mass index (BMI) ($P = 0.0153$), tumor type ($P = 0.0029$), ascites level, ascites malignancy, degree of dissemination, tumor differentiation, FIGO stage, TNM stage, laterality, and tumor size at $P < 0.0001$. Since significant correlation was associated with BMI and degree of dissemination, as disclosed by IHC analysis, metabolic marker SIRT1 ($P = 0.0003$), HIF-1α ($P < 0.0001$), exosomal marker CD81 ($P < 0.0001$), ki-67 status ($P = 0.0034$), and glycogen deposition ($P < 0.0001$) were expressed more in tumor tissues as compared to the normal ones. ROC analysis of CA-125 had shown 327.7 U/ml has the best cutoff point with 82.4% sensitivity and specificity of 52.3%. In addition, Kaplan-Meier plots of CA-125 ($P < 0.0001$), BMI ($P = 0.001$), degree of dissemination ($P < 0.0001$), and ascites level ($P < 0.0001$) reflected significant correlation with overall survival (OS). Upon multivariate Cox-regression analysis for overall survival (OS), BMI ($P = 0.008$, HR 1.759, 95% CI 1.156-2.677), ascites malignancy ($P = 0.032$, HR 0.336, 95% CI 0.124-0.911), and degree of dissemination ($P = 0.004$, HR 1.994, 95% CI 1.251-3.178) were significant proving to be independent indicators of the disease. *Conclusion*. Clinicopathological parameters like BMI, degree of dissemination, and ascites level along with CA-125 can be prognostic factors for the disease. Levels of CA-125 can depict the metabolic and metastatic factors. Thus, by targeting SIRT1 and assessing exosomal concentrations to overcome metastasis and glycogen deposition, individualized treatment strategy could be designed. In-depth studies are still required.

1. Introduction

Ovarian cancer (OvCa) is the third most common gynaecological malignancy after cervical and uterine cancer with the highest mortality and morbidity rate among all gynaecological malignancies [1, 2]. Limitation of early diagnosis is the major reason for poor survival and increased mortality rates among the patients [3]. Late diagnosis is the result of nonspecific and inappropriate symptoms which are mostly misinterpreted as normal gastrointestinal and urinary symptoms. In addition to this, several other factors possess the risk of developing OvCa like age, menopausal status, body mass index (BMI), parity, and family history [4]. As per World Health Organization (WHO) classification, 60% of all primary OvCa is of

epithelial origin, followed by germ cell (30%) and sex cord stromal tumor (8%). Carcinomas of epithelial origin is the most frequent form of OvCa having 80-85% occurrence rate and is subcategorized depending on the proliferation rate of epithelial cells and on histopathological types [5]. Epithelial OvCa (EOC) is a heterogeneous group of neoplasms which has been categorized under various histological subtypes, namely, serous, mucinous, endometrioid, clear cell, transitional cell tumors (Brenner tumors), carcinosarcoma, mixed epithelial tumor, and undifferentiated carcinoma [6]. India ranks the highest in mortality rate among the Asian countries whereas incidences among young females have reduced in Europe and North America [7]. The age-adjusted OvCa occurrence rates in India lie between 0.9 to 8.4 per 100,000 population distributed in different parts of the country [8]. It has been estimated that by the end of 2020, there would be 59,276 new OvCa cases in India, and it has been assessed that the rate of incidences would increase by 55% by the end of 2035 while mortality rate would be uplifted by 67% [9]. In Indian scenario, where the patients are diagnosed at a later stage and with bleak chances of good prognosis, there is an absolute necessity to assess the disease at an early stage to improve the survival.

Accurate monitoring of the disease is hindered by local invasion of the tissues deep within the pelvis and peritoneal seeding leads to metastasis, thereby making early diagnosis difficult to assess. Thus, there is a need to detect the disease with preferably good diagnostic and prognostic factor. A wide range of clinical and histopathological characteristics have been exhibited by the primary OvCa lesions. Out of the various clinicopathological parameters, serum cancer/carbohydrate antigen-125 (CA-125), a glycoprotein synthesized by neoplastic OvCa cells, has been proven to be a potent tumor marker, which is closely associated with tumor burden and easy to assay [10].

Persistent efforts are being conducted to assess the tumor molecular markers like ki-67 (a proliferation marker), p53, estrogen receptors, progesterone receptors, and E-cadherin (E-cad) of EOC by immunohistochemical (IHC) analysis [11, 12]. Substantial evidences have reflected that metabolic reprogramming contributes to survival of the cancer cells [13], but the relation with metastasis and recurrence in OvCa needs attention. Keeping in pace with the detection of tumor markers, we have assessed by performing IHC the expression of metabolic marker, silent information regulator 1 (sirtuin 1/SIRT1), since dysfunction in metabolic reprogramming is one of the hallmarks of cancer. SIRT1 being NAD+ dependent acts as metabolic sensor, and its deacetylating property hampers cellular metabolism [14]. Recent evidences have suggested the role of extracellular vesicles, the exosomes in metabolic reprogramming of the cancer cells, which promotes their proliferation, angiogenesis, and immunosuppression in the tumor microenvironment (TME) and eventually leads to metastasis [15]. In these efforts, we have tried to evaluate the status of exosomes which are responsible for intercellular communication via transfer of distinct cargoes carried by them and promote peritoneal dissemination [16]. Metabolic alterations have a huge contribution in promoting cancer cell progression and metastasis. When the cancer cells migrate from their primary tumor sites to a secondary location, they need to adapt with the metabolic state in the new metastatic niche. Metabolic factors including several amino acids like asparagine, proline, and serine and several by-products from metabolic pathways like pyruvate, acetate, and lactate as well as the by-products of fatty acid oxidation (FAO) aid the cancer cells to adapt to the metabolic environment of the new TME by supplying energy [17]. Secondly, the acidification of extracellular space due to the release of CO_2, lactate, and other organic acids from metabolically active cancer cells also contributes in degrading extracellular matrix, thereby promoting metastasis [18]. Furthermore, the accumulation of glycogen in the cancer cells has introduced a new arena of research. The dysregulations of the enzymes involved in glycogen metabolism have been related to tumor cell proliferation, migration, and invasion, which eventually lead to malignancy of the cancer [19]. Recent study has revealed that OvCa cell metabolism requires more FAO in comparison to aerobic glycolysis for increasing the availability of ATP to nourish the cancer cells for proliferation and migration [20]. Glycogen fuels glycolysis to nurture the cancer cells during nutrient deficiency and metabolically compromised conditions in the TME [21]. An oxygen tension level always prevails in the tumor condition leading to a hypoxic atmosphere that can alter cancer cell metabolism as well as induce elevated secretion of the exosomes [22, 23]. As a mode of survival in hypoxic TME, the cancer cells accommodate themselves in small vasculatures of size 100-200 μm which in turn regulates the oxygen limit in the tissues [24]. Cells can directly sense oxygen level that influences cellular physiology by the aid of several regulatory elements [25]. One such controlling element is hypoxia inducible factor 1α (HIF-1α) which induces the hypoxic TME and is associated with tumor cell metabolism and exosome release. Thus, HIF-1α is also taken under consideration in order to develop a compact coordination among the factors considered in this study.

Therefore, in this cohort study, we have analyzed the serum levels of CA-125 at the diagnostic stage and related it to other clinical parameters, and depending on the significant correlated clinicopathological parameters, we have also analyzed the expression of metabolic and metastatic biomolecules which can be further established as therapeutic targets and biomarkers for early diagnosis.

2. Materials and Methods

2.1. Antibodies and Reagents. Primary antibodies were applied to analyze the expression of SIRT1, HIF-1α, CD81, and CD63. Rabbit polyclonal anti-human SIRT1 antibody (Cell Signaling Technology: D739) was used to detect the expression in both normal and tumor samples. For evaluating the expression of HIF-1α, we have used rabbit anti-human polyclonal antibody (Santa Cruz Biotechnology: sc10790) and CD81 expression was evaluated using purified mouse anti-human CD81 antibody (BioLegend: #349501). Flow cytometric analysis was observed by anti-human CD63 antibody (BioLegend: #353027). Mouse anti-rabbit

IgG-HRP secondary antibody (Santa Cruz: sc-2357) was utilized against the primary antibody. Other reagents used are included in Supplementary file 1.

2.2. Study Population and Data Collection. The study population includes women who attended the Cancer Detection Centre at Chittaranjan National Cancer Institute, Regional Centre, Kolkata, India. The study has been approved by the Institute Ethics Committee (CNCI-IEC-40104). The data set comprises clinical characteristics including age, BMI, potent tumor markers like carcinoembryonic antigen levels (CEA), CA-125 and cancer antigen 19.9 (CA 19.9), ascites level, malignancy present in ascites, degree of spread of the disease, differentiation of tumor cells, tumor type, FIGO stage of tumor, TNM grading, laterality of tumor, and size of tumor. The relevant clinicopathological characteristics have been collected from their clinical records. All the information was recorded by the attending physicians.

2.3. Study Design. This retrospective study comprises data collected from the records of the patients in the year 2019-2021. Our study includes all the patients ($N = 248$) who have been diagnosed with OvCa irrespective of the age criteria. Patients who have undergone or not undergone surgery and/or chemotherapy with variable clinical characteristics have been considered in the study. The exclusion criteria include those patients who had comorbidities like cardiac problem or gastrointestinal problems, those who were pregnant or lactating, and those who had prior diagnosis of different forms of cancer. Along with the analysis of clinicopathological parameters retrospectively, we were also inclined to evaluate the expression of biomolecules related to metabolic and metastatic regulations in OvCa irrespective of the histological subtypes in order to get the molecular status in patients ($N = 21$).

2.4. Patient Sample Collection. OvCa samples were collected from patients who have undergone surgery at Chittaranjan National Cancer Hospital. Tumor tissues and adjacent normal tissues were collected from patients during surgery according to the segregation of CA-125 level at the diagnostic stage with written consent form from the respective patients. The clinical records were collected retrospectively, thus, the written consent information was not required from the patients and prior to analysis, patient details were anonymised.

2.5. Immunohistochemical Analysis. Paraffin embedding and tissue sectioning from both tumor tissues and adjacent normal tissues were conducted and IHC staining was followed. The tissue section slides were deparaffinized using xylene followed by rehydration in a series of graded concentrations of alcohol. In order to augment the expression of antigen, 10 Mm citrate buffer solution (pH 6.0) was added to the slides. The slides were further treated with 3% hydrogen peroxide dilute in 100% methanol and kept at room temperature for 15 min, followed by a PBS wash to stop the endogenous peroxidase activity. The slides were kept at 4°C overnight after addition of primary antibody in humidified chambers. A 1 : 500 dilution of SIRT1, HIF-1α, ki-67, and CD81 was used as the primary antibodies. After overnight incubation, the slides were washed in PBS and anti-rabbit

Table 1: Frequency profiles of clinicopathological parameters assessed in the study subjects.

Clinicopathological parameters	Frequency (N)	Percentages (%)
Age		
≤18	6	2.4
19-40	53	21.4
41-60	136	54.8
>60	53	21.4
Body mass index (BMI)		
Underweight	25	10.1
Normal	96	38.7
Overweight/obese	127	51.2
CEA (ng/ml)		
<5	107	43.1
≥5	141	56.9
CA-125 (U/ml)		
≤35	30	12.1
35.1-499.9	99	39.9
500-999.9	49	19.9
≥1000	70	28.2
CA 19.9 (U/ml)		
<28	78	31.5
≥28	170	68.5
Ascites level		
High	97	39.1
Moderate	83	33.5
Low	68	27.4
Ascites malignancy		
Negative	112	45.2
Positive	136	54.8
Degree of dissemination		
Pelvic dissemination	103	41.5
Distant metastasis	55	22.2
Localized	90	36.3
Tumor differentiation		
Well differentiated	59	23.8
Moderately differentiated	65	26.2
Poorly differentiated	124	50.0
Tumor type		
Epithelial	232	93.5
Nonepithelial	16	6.5
FIGO stage		
I	58	23.4
II	65	26.2
III	72	29.0
IV	53	21.4
T stage		
T1	58	23.4
T2	82	33.1
T3	108	43.5
N stage		

Table 1: Continued.

Clinicopathological parameters	Frequency (N)	Percentages (%)
N0	83	33.5
Nx	75	30.2
N1	90	36.3
M stage		
M0	81	32.7
Mx	106	42.7
M1	61	24.6
Laterality		
Unilateral	156	62.9
Bilateral	92	37.1
Tumor size (ccm)		
$<5*5*5$	158	63.7
$\geq 5*5*5$	90	36.3

secondary antibody in a dilution 1 : 1000 was added, followed by incubation at room temperature for 2 hours. The reaction was visualised by adding 3,3′-diaminobenzidine tetrahydrochloride, which reacted for 10 minutes. Finally, haematoxylin was added to counterstain the specimen and dehydrated using a gradient alcohol wash, followed by sealing the slides with coverslips using DPX [26]. The images for each sample were taken in a brightfield compound microscope (Leica Microsystems: #Model DM1000) and analyzed.

2.6. Flow Cytometric Analysis. Firstly, single cell suspension was prepared by collagenase IV treatment to the tissues followed by straining the tissue through a 0.4 μm strainer and then centrifuging at 2000 rpm for 10 min. The supernatants for each sample were discarded and incubated in RBC lysis buffer for 5 min at RT, followed by centrifugation at 400g for 5 min and the cells were stored at -80°C in 10% DMEM freezing media for subsequent flow cytometry [27]. The single cell suspension was thawed and centrifuged at 2000 rpm for 5 min. After discarding the supernatant, APC/Fire-tagged CD63 antibody in a dilution of 1 : 500 was added and incubated for 1 h [28]. The stained cells were acquired using a BD LSRFortessa Flow Cytometry (San Jose, CA, USA) and analyzed using FCS Express 7.

2.7. PAS Staining for Detecting Glycogen Accumulation. PAS staining was conducted following Chatterjee et al. [29]. Briefly, paraffinized slides were deparaffinized using xylene, and then, the slides were taken in Columbia staining dish for treatment with Carnoy's fixative for 10 min. The slides were rinsed 3 times with distilled water, followed by addition of periodic acid solution for staining (10 min). The slides were again washed 3 times with distilled water. After removal of excessive periodic acid stain, Schiff reagent was added to the slides and kept for 5 min. In order to remove the excess Schiff reagent, the slides were again washed with distilled water followed by their dehydration in ascending alcohol solutions (50%, 70%, 90% and 100%). After the dehydration process, the slides were mounted with DPX and covered with coverslips. Images were taken after 1 h of mounting in Leica brightfield microscope in 20x and 40x magnifications and analyzed using Fiji-ImageJ software.

2.8. Statistical Analysis. The statistical analysis of the clinical records was performed using IBM SPSS25 Statistics software. The frequency table and cross tabulation were prepared using this software whereas the graphs for the frequency distribution were prepared using GraphPad Prism software by one-way analysis of variance (ANOVA) and unpaired t-test wherever applicable. The chi-square test was performed using GraphPad Prism software (version 5). Image analysis was carried out using Fiji-ImageJ software (https://imagej.net/Fiji). Statistical analysis of the clinical images was conducted using GraphPad Prism software. Flow cytometry analysis was performed using FCS Express 7 software. Cox-regression analysis and ROC analysis were done using IBM SPSS25 Statistics software. P value < 0.001 and <0.05 was considered statistically significant.

3. Results

3.1. Analysis of Clinicopathological Data of OvCa Patients' Cohort. A total of $N = 248$ case records have been found eligible to be included in the study. Table 1 comprises frequency distribution of the clinicopathological data of the ovarian cancer patients. The parameters associated with OvCa including age, levels of tumor markers like CA-125, CEA, and CA 19.9, ascites level, ascites malignancy, degree of dissemination, tumor differentiation, tumor type, FIGO stage, TNM staging, laterality of tumor, and tumor size were considered for the study. Ovarian cancer seems to be more prevalent in patients belonging to the age group 41-60 years (54.8%), and the least occurrence was observed in the age group below 18 years (2.4%), whereas age group 19-40 and greater than 60 years shared the same proportion of patients (21.4%). BMI was observed to be associated with occurrence of the disease where overweight and obese patients (BMI $\geq$ 25 kg/sq.m) were more likely to develop ovarian cancer (51.2%) as compared to the normal (38.7%) lying within 18.5 kg/sq.m-24.9 kg/sq.m and underweighted patients (10.1%) whose BMI was <18.5 kg/sq.m. The levels of antigen markers like CA-125, CEA, and CA 19.9 have been associated with diagnosis of the disease [30]. Most of the patients had CEA levels $\geq$ 5 ng/ml (56.9%) whereas 43.1% of victims had CEA levels < 5 ng/ml. CA-125 has been subdivided into four groups in order to derive the distribution of patients at different levels of CA-125. ≤35 U/ml is considered to be a normal range, but still this level consisted of 12.1% of patients with OvCa. The maximum patients who were diagnosed with cancer were in the range 35.1-499.9 (39.9%), followed by ≥1000 U/ml and 500-999.9 U/ml with 28.2% and 19.9%, respectively. CA 19.9 level greater than ≥28 U/ml was associated with maximum number of patients (68.5%) and 31.5% of patients had CEA levels < 28 U/ml, which is considered to be normal. All the patients considered for the study were associated with different ascites levels determined upon radiological findings. 39.1% of the patients had high levels of ascites, followed by 33.5% having

Table 2: Association of CA-125 levels with clinicopathological parameters.

Clinicopathological parameters	CA-125 (U/ml)				χ^2	*P* value
	Low		High			
	≤35	35.1-499.9	500-999.9	≥1000		
Age						
<18	1	3	2	0	12.30	0.1968
19-40	8	28	9	8		
41-60	13	50	29	44		
>60	8	18	9	18		
Body mass index (BMI)						
Underweight	2	11	3	9	15.73	0.0153
Normal	14	49	17	16		
Overweight/obese	14	39	29	45		
CEA (ng/ml)						
<5	14	52	17	24	7.369	0.0610
≥5	16	47	32	46		
CA 19.9 (U/ml)						
<28	6	40	13	19	6.658	0.0836
≥28	24	59	36	51		
Ascites level						
High	0	15	25	57	135.7	<0.0001
Moderate	5	46	19	13		
Low	25	38	5	0		
Ascites malignancy						
Positive	1	39	33	63	79.71	<0.0001
Negative	29	60	16	7		
Degree of dissemination						
Pelvic dissemination	3	40	29	31	108.3	<0.0001
Distant metastasis	0	7	13	35		
Localized	27	52	7	4		
Tumor differentiation						
Well differentiated	21	32	4	2	94.56	<0.0001
Moderately differentiated	9	34	13	9		
Poorly differentiated	0	33	32	59		
Tumor type						
Epithelial	24	92	46	70	14.02	0.0029
Nonepithelial	6	7	3	0		
FIGO stage						
I	21	32	3	2	114.2	<0.0001
II	9	34	13	9		
III	0	26	22	24		
IV	0	7	11	35		
T stage						
T1	22	31	3	2	87.55	<0.0001
T2	8	39	14	21		
T3	0	29	32	47		
N stage						
N0	15	38	16	14	34.97	<0.0001
Nx	14	35	10	16		
N1	1	26	23	40		

Table 2: Continued.

Clinicopathological parameters	CA-125 (U/ml)				χ^2	P value
M stage						
M0	13	31	19	18		
Mx	17	58	14	17	53.25	<0.0001
M1	0	10	16	35		
Laterality						
Unilateral	28	69	24	35	22.93	<0.0001
Bilateral	2	30	25	35		
Tumor size (ccm)						
$<5*5*5$	3	52	39	64	71.40	<0.0001
$\geq 5*5*5$	27	47	10	6		

moderate levels and mild ascites were found in 27.4% of the patients. Malignant ascites has been associated with prognosis of the disease leading to poor quality of life and leads to mortality. In our study, we had deduced that more than 50% of the patients had ascites malignancy and 45.2% of the patients had no malignant ascites. Since OvCa has been associated with tumor metastasis or degree of dissemination, it was observed that pelvic dissemination (PD) was recorded to the highest (41.5%), followed by localized tumor (36.3%) and 22.2% was associated with distant metastasis (DM). Differentiation of tumor cells also plays a pivotal role in spread of the disease. Moderately to poorly differentiated OvCa cells were mostly observed in the later stages and associated with significant risk of poor prognosis [31]. Here, it was observed that 50% of the patients had poorly differentiated tumor cells and the remaining half either had well differentiated (23.8%) or moderately differentiated (26.2%) depending on the stage of the cancer. Since EOC is the most common form of OvCa and that was also reflected in our results (93.5%), the remaining 6.5% was of non-EOC. Early diagnosis of OvCa remains the main challenge for survival; thus, it was observed that most of the patients diagnosed were at stage III (29%), followed by stage II (26.2%), stage I (23.4%), and stage IV (21.4%), respectively. The patients were further categorized based on TNM grading where T3 stage (43.5%) with involvement of both the ovaries with peritoneal metastasis, N1 stage (36.3%) with regional lymph node metastasis, and Mx stage (42.7%) where distant metastasis was not observed was maximum shown in Table 1. In respect to laterality of tumor, unilateral tumor was higher (62.9%) than bilateral tumor (37.1%) and tumor size less than $<5*5*5$ ccm (63.7%) was more in comparison to tumor more than $\geq 5*5*5$ ccm (36.3%). Graphical representation of frequency distribution with $P < 0.05$ being statistically significant has been presented in Supplementary file 2.

3.2. Association of CA-125 Level with Clinicopathological Features. The levels of CA-125 at the time of diagnosis were recorded and categorized into low and high. Low level included CA-125 level ≤ 35 U/ml, and high level (>35 U/ml) was subdivided into three sections as 35.1-499.9, 500-999.9, and ≥1000 U/ml. Table 2 summarizes the data of patient cohort distributed among the various levels of CA-125. A nonsignificant relation was deduced in case of CA-125 with age ($P = 0.1968$) and other tumor marker levels CEA ($P = 0.0610$) and CA 19.9 ($P = 0.0836$) whereas a strong association of CA-125 was observed with the other clinicopathological parameters like BMI ($P = 0.0153$), ascites level and ascites malignancy, and tumor differentiation ($P < 0.0001$).

3.3. SIRT1 Expression Increases in Ovarian Tumor in Association with Overexpression of HIF-1α in the Tumor Tissues. We have evaluated the metabolic biomarker SIRT1 expression in the ovarian tissue both in cancerous state and normal state. It was observed that SIRT1 expression was remarkedly higher in the cancer tissue in comparison to the adjacent normal ovarian tissue ($P = 0.0003$). SIRT1 is the downstream target of HIF-1α which is one of the major factors to create a hypoxic TME, contributing to tumor development and progression. In order to determine the nonphysiological oxygen tension level (hypoxia) in the TME, we have evaluated the level of expression of HIF-1α in both cancer and normal tissues. HIF-1α expression was significantly high in cancer tissues in comparison to normal tissues ($P < 0.0001$). Moreover, a decreased expression of HIF-1α with reduced SIRT1 expression in the normal tissues further validated the fact that hypoxic TME created by HIF-1α regulates the expression of SIRT1 in the cancer tissues with a significant correlation (Figures 1(a)–1(j)).

3.4. Overexpressed SIRT1 in TME Induces Greater Secretion of Exosomes from OvCa Cells. We have performed IHC analysis for exosomal surface marker CD81 in OvCa tissues as exosomes participate in preparing a premetastatic niche (PMN) for the migrating cancer cells at the secondary site and promote metastasis [32]. We observed an elevated expression of CD81 in the cancer tissues as compared to normal tissues (Figures 2(a)–2(d)), and the significant graphical representation is found in Figure 2(e) ($P < 0.0001$). Further, to validate the IHC result, flow cytometric analysis for exosomes detection with CD63 antibody depicted increased levels of CD63 in the cancer cells in comparison to the normal cells (Figure 2(f)).

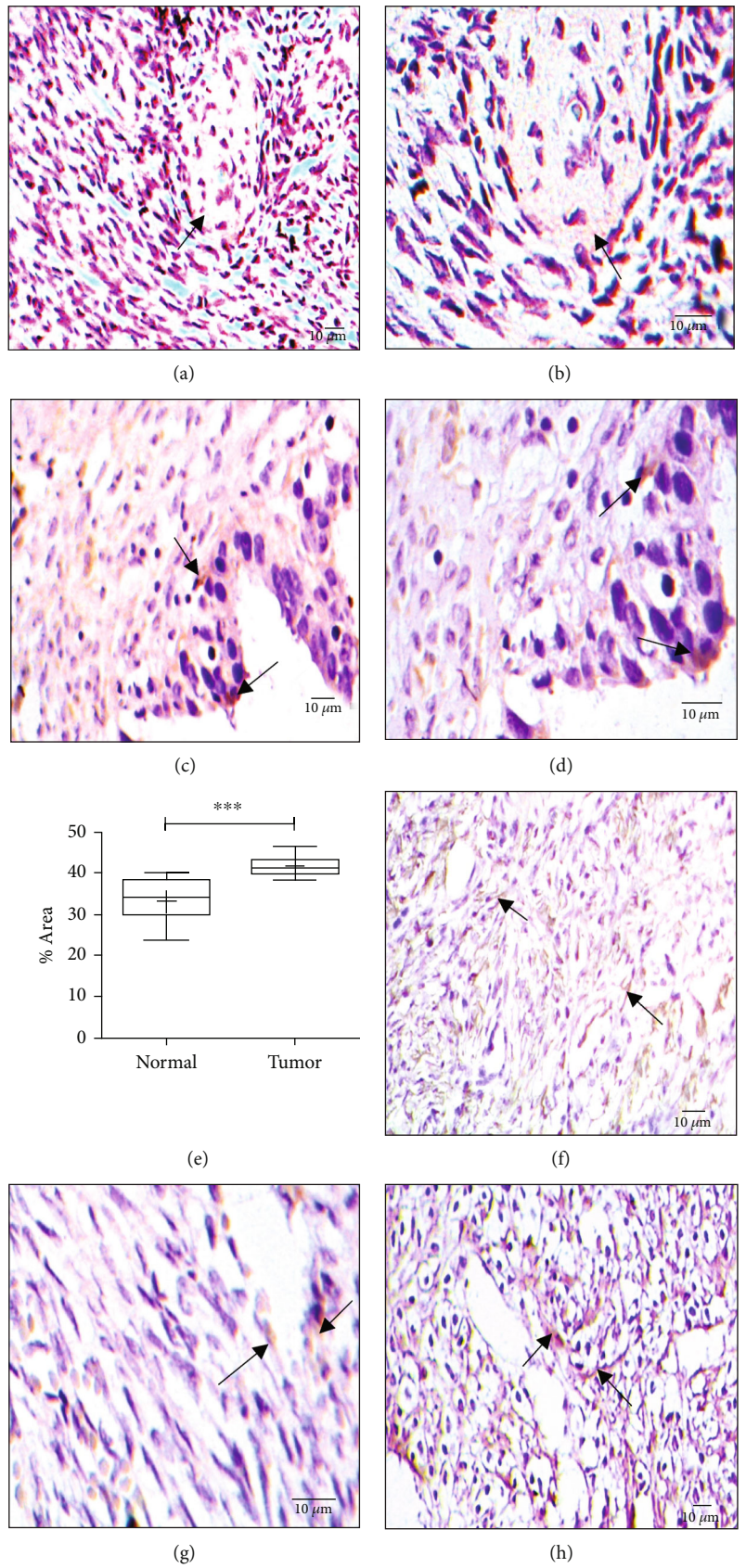

Figure 1: Continued.

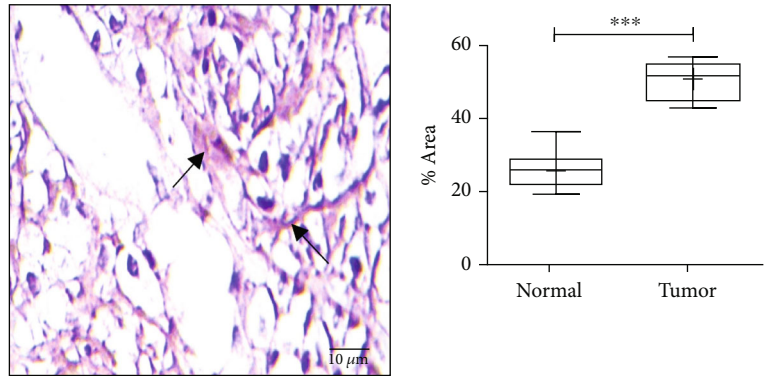

Figure 1: Expression of SIRT1 and HIF-1α. (a) SIRT1 expression in normal ovarian tissue (20x). (b) SIRT1 expression in normal ovarian tissue (40x). (c) SIRT1 expression in ovarian tumor tissue (20x). (d) SIRT1 expression in ovarian tumor tissue (40x). (e) Graphical representation of SIRT1 expression, $P = 0.0003$. Expression of HIF-1α. (f) HIF-1α expression in normal ovarian tissue (20x). (g) HIF-1α expression in normal ovarian tissue (40x). (h) HIF-1α expression in ovarian tumor tissue (20x). (i) HIF-1α expression in ovarian tumor tissue (40x). (j) Graphical representation of HIF-1α expression, $P < 0.0001$.

3.5. Overexpression of SIRT1 and Exosomes Influences the Metastasizing Capacity of the OvCa Cells. Imbalance in the SIRT1 expression and exosome concentration shows a positive correlation with the proliferation marker, ki-67. IHC was conducted to evaluate the metastasizing ability of the OvCa cancer cells (Figures 3(a)–3(e)); it was observed that expression of ki-67 was significantly higher in the tumor cells as compared to the normal cells ($P = 0.0034$). This indicated that the chances of metastasis were enhanced when SIRT1 is overexpressed which in turn influences the exosomes concentration in the tumor cells.

3.6. Dysregulated SIRT1 Influences the Deposition of Glycogen in OvCa. Deposition of glycogen serves as nutritional source for the survival of cancer cells; thus, periodic acid/Schiff (PAS) staining was conducted to determine the accumulation of glycogen in both the tissues which revealed that the glycogen deposition was remarkably more in the cancer cells than in the normal cells ($P < 0.0001$), illustrating that the cancer cells have huge storage of glycogen for their usage during nutrient deprivation stage for their growth and survival (Figures 4(a)–4(e)).

3.7. Correlation between Clinical Factors and Overall Survival. Survival analysis was conducted with clinically defined endpoint, i.e., OS. Kaplan-Meier plots upon log rank test revealed OS of CA-125 ($\chi^2 = 26.841$) was significant ($P < 0.0001$) represented in Figure 5(b). Similarly, OS of both degree of dissemination ($\chi^2 = 85.033$) and ascites malignancy ($\chi^2 = 45.042$) and BMI ($\chi^2 = 13.473$) had shown significance at $P < 0.0001$ and $P = 0.001$, respectively (Figures 5(c)–5(e)). The overall mean survival time for all the factors was observed to be 18.780 months with 95% CI 17.754–19.805. The ROC curve of CA-125 (Figure 5(a)) has been evaluated which revealed an area under curve (AUC) of 0.719 which was statistically significant ($P < 0.0001$). The best cutoff point for CA-125 in this study is 327.7 U/ml with sensitivity = 82.4% and specificity = 52.3%.

3.8. Risk Attributes of Clinicopathological Parameters in Survival of OvCa Patients. Depending on the correlation of CA-125 with the clinicopathological characteristics, we have performed overall survival analysis of the patients in relation to BMI, ascites malignancy, degree of dissemination, tumor differentiation, FIGO stage and tumor size. Univariate analysis revealed BMI, CA-125, ascites level, ascites malignancy, tumor differentiation, degree of dissemination, FIGO stage, tumor type, T stage, N stage, M stage, laterality, and tumor size (Supplementary file 3). Based on these findings, multivariate Cox-regression analysis was conducted. Table 3 unveils the multivariate Cox regression analysis of the parameters taken under consideration in which BMI (HR 1.759; 95% CI 1.156–2.677; $P = 0.008$), ascites malignancy (HR 0.336; 95% CI 0.124–0.911; $P = 0.032$), and degree of dissemination (HR 1.994; 95% CI 1.251–3.178; $P = 0.004$) are independent predictors of the OS of the patients.

4. Discussion

Early diagnosis of OvCa, which helps to improve the survival rate of the patients, remains a challenge for the clinicians. However, CA-125 level serves as a promising diagnostic marker, but still the survival of the patients remains compromised in most of the cases. Thus, there is a need to develop personalised treatment strategy for the patients for better response. This research work has analyzed the CA-125 levels and correlated with the clinicopathological parameters. Since most of the parameters held a significant correlation, we have targeted only those parameters that were related to metabolism like BMI and the spreading of cancer like degree of dissemination (metastasis) that hold the risk for the survival of the patients. Thus, we were more inclined to analyze the expression level of SIRT1, ki-67, status of glycogen deposition, HIF-1α, and intercellular communicators, i.e., exosomes, so that a preliminary idea can be provided for designing the individualized treatment regimen by targeting them at the diagnostic level. Upon further investigation and validation, they can be established as biomarkers for OvCa.

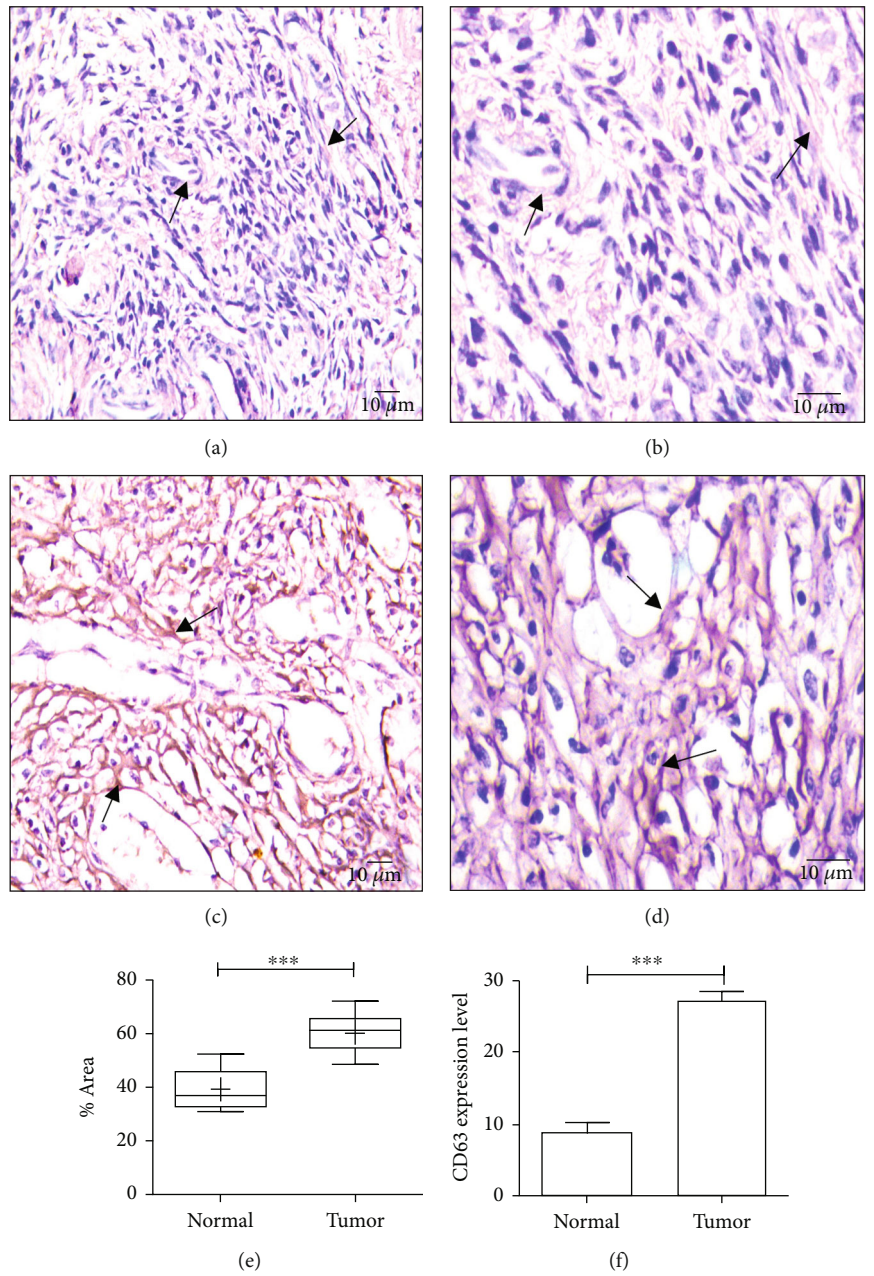

Figure 2: Expression of CD81 and CD63. (a) CD81 expression in normal ovarian tissue (20x). (b) CD81 expression in normal ovarian tissue (40x). (c) CD81 expression in ovarian tumor tissue (20x). (d) CD81 expression in ovarian tumor tissue (40x). (e) Graphical representation of CD81 expression, $P < 0.0001$. (f) Flow cytometric graphical representation of CD63 in normal and tumor tissues ($P < 0.0001$).

Metabolic reprogramming is essential for the cancer cells to facilitate cellular growth, proliferation, and their persistence. Current researches on energy metabolism in OvCa have also been steered, where 39 energy metabolism-related genes significantly correlated with disease prognosis [33]. SIRT1, a class III histone deacetylases (HDACs), is considered as the key metabolic regulator. In response to various external stimuli, it impacts the metabolic status of the cancer cells in regulating the chromatin structure and gene expression [34]. Among the seven members of the sirtuin family, SIRT1 is the most extensively studied in the cancer types as there are conflicting evidences regarding the association of SIRT1 and tumorigenesis [35]. For instance, in colon cancer and melanoma, it acts as a tumor suppressor by deacetylating histidine triad nucleotide-binding protein (HINT) 1 and enhances its binding efficacy with oncogenic transcription factor β-catenin and microphthalmia transcription factor (MITF) [36]. Simultaneously, in lung adenocarcinoma, it induces the tumorigenicity of the cancer cells, thus fuelling the cancer progression and survival of the cancer cells [37]. Activity of SIRT1 is tightly regulated by NAD +/NADH levels in a cell, where for deacetylation of targeted proteins, NAD+ serves as a major substrate for SIRT1 [34]. Evidences suggest that hypoxia is one of the hallmarks of malignant tumors and SIRT1 being a downstream target of HIF-1α is observed to be upregulated in OvCa, thereby

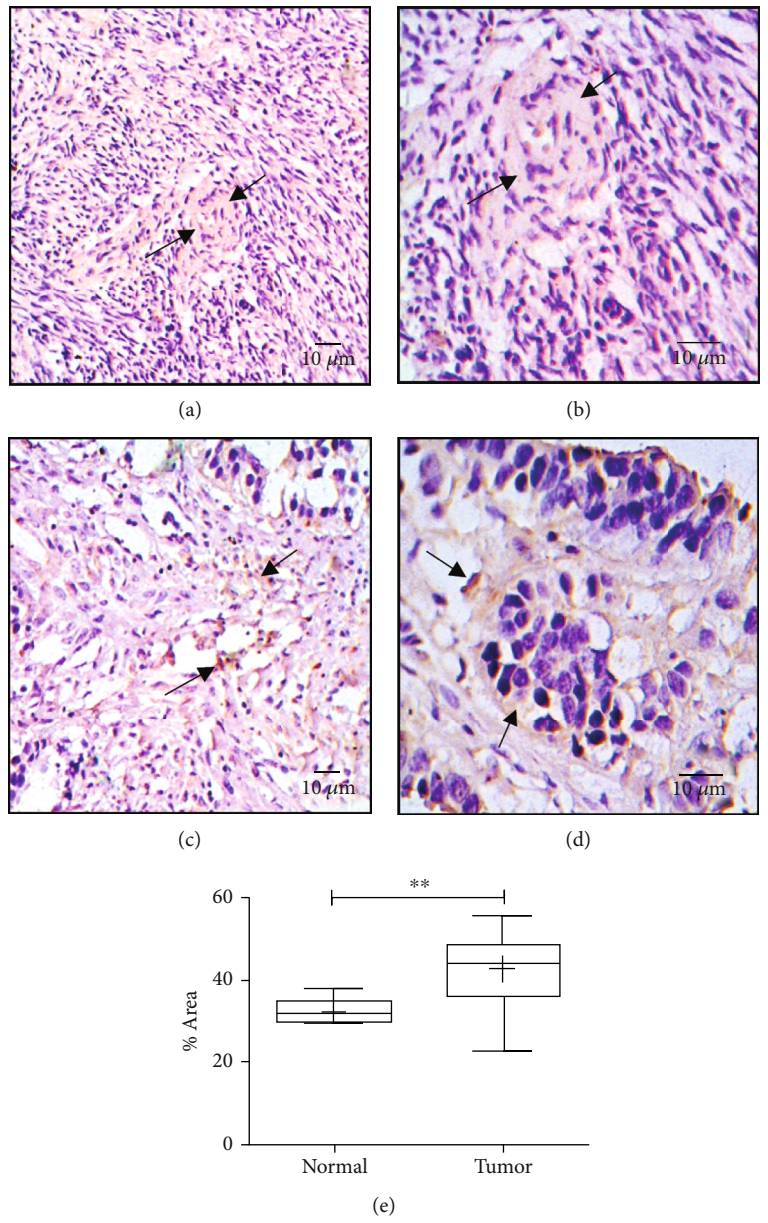

Figure 3: Expression of ki-67. (a) ki-67 expression in normal ovarian tissue (20x). (b) ki-67 expression in normal ovarian tissue (40x). (c) ki-67 expression in ovarian tumor tissue (20x). (d) ki-67 expression in ovarian tumor tissue (40x). (e) Graphical representation of ki-67 expression, $P = 0.0034$.

conferring cancer stem cell-like properties [38]. HIF-1α expression can be a prognostic biological marker in poorly differentiated serous ovarian carcinoma [39]. Our data revealed that HIF-1α was expressed more in the OvCa tissues as compared to the adjacent normal ones, which might have regulated the expression of SIRT1 which could influence glycogen deposition in the cells [40]. Interestingly, hypoxic TME also facilitates greater secretion of minute extracellular biomolecules especially exosomes which aids in the promotion of the aggressiveness of cancer cells [41]. In an earlier study, it has been established that CA-125 production and release are related to exponential cell growth. Inhibition of the cell cycle at the G2/M phase by cyclohexamide not only resulted in the death of the cells but also significantly minimized the rate of secretion of CA-125 from the cancer cells [42]. The secretion of CA-125, a heavily glycosylated membrane-bound protein, relies upon the epidermal growth factor receptor (EGFR) signal transduction pathway signaling of the cancer cells [43], and prior to its release, it undergoes phosphorylation at the serine/threonine followed by its cleavage by extracellular protease [44]. In addition to this, Li et al. have also established a link between SIRT1, EGFR, and BRCA1 axis in enhancing the resistance of the OvCa cells towards cisplatin. They have observed that the expression levels of SIRT1, EGFR, and BRCA1 were significantly high in the cisplatin-resistant OvCa cells as

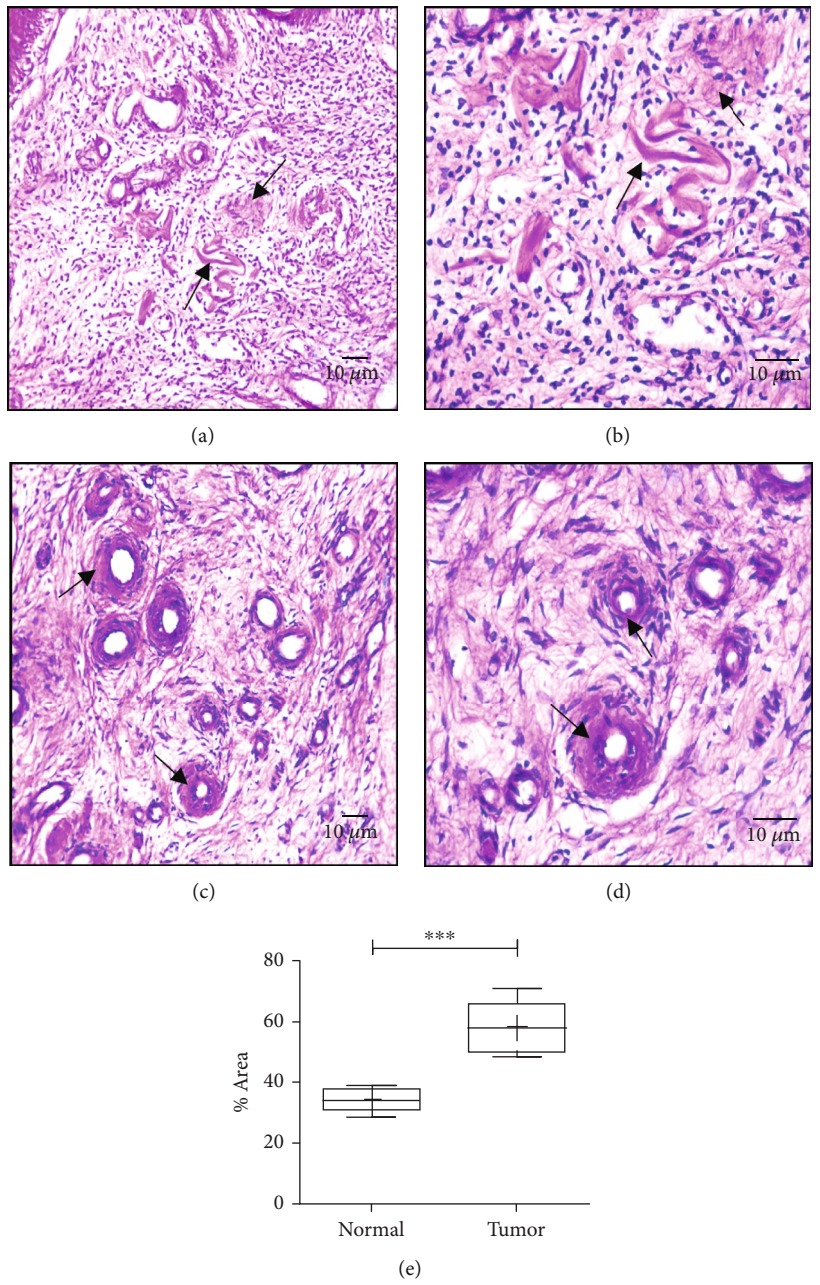

Figure 4: Levels of glycogen deposition. (a) Glycogen deposition in normal ovarian tissue (20x). (b) Glycogen deposition in normal ovarian tissue (40x). (c) Glycogen deposition in ovarian tumor tissue (20x). (d) Glycogen deposition in ovarian tumor tissue (40x). (e) Graphical representation of glycogen deposition, $P < 0.0001$.

compared to the cisplatin-sensitive cancer cells [45]. Since an underlying signaling cascade involving BRCA1-mediated SIRT1 transcriptional regulation of EGFR expression has been evaluated, it validates our hypothesis that increased SIRT1 expression directly modulates the CA-125 levels. Thus, estimating the SIRT1 levels at the diagnostic level can also be established as a metabolic biomarker of OvCa. In addition, the association of SIRT1 and exosomes has been also deduced by Latfikar et al. illustrating that SIRT1 exhibits a tumor suppressive role in breast cancer and reduction in SIRT1 expression promotes elevated secretion of exosomes [46]. It is definite that SIRT1 influences the release of exosomes, but according to our data, it may be said that SIRT1 has tumor promotive function by inducing greater secretion of exosomes in OvCa [47], which can be estimated by observing its relatively higher expression in the tumor tissues as compared to the normal ones. Recently, it has been evaluated that exosomal CA-125 increases OvCa diagnostic efficacy [48]. This finding further confirms that greater concentration of exosomes can be related to higher CA-125 levels. CA-125 being synthesized by the epithelial cells [49] may get incorporated into the exosomes to be secreted during their cargo loading. Since the hypoxic state of TME enhances the production of exosomes, it can be

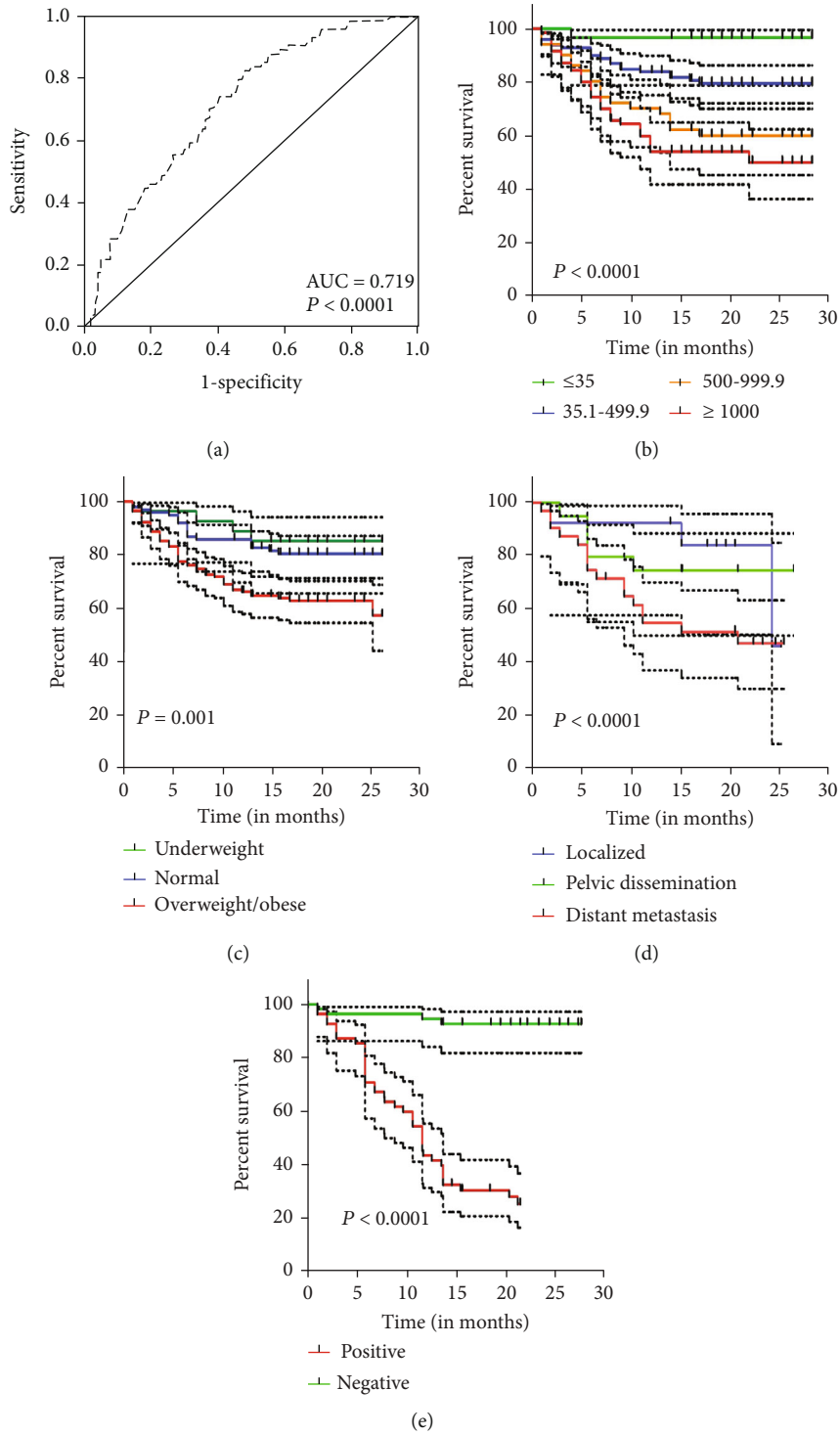

Figure 5: ROC curve and Kaplan-Meier overall survival (OS) graphs of clinicopathological parameters. (a) ROC curve of CA-125. (b) OS graph of CA-125. (c) OS graph of BMI. (d) OS graph of degree of dissemination. (e) OS graph of ascites malignancy.

established that hypoxic condition mediated by HIF-1α regulates the expression of SIRT1 which in turn enhances the secretion of CA-125 and exosomes. Exosomes, being 30 nm-150 nm in size, have the capability to cross all the biological barriers and migrate to different parts of the body [50]. So, these exosomes carrying CA-125 may be assessed easily in the serum of the patients. Exosomes perform both protumorigenic and antitumorigenic roles in cancer [51]. Furthermore, the increase in levels of CA-125 by 5 U/ml, within the normal range, after the treatment has been observed to be associated with the recurrence and survival in OvCa patients [52]. This finding paves a new way in analyzing the risk of recurrence by estimating the concentration of exosomes carrying CA-125 present in the patients' blood,

Table 3: Multivariate Cox regression analysis of clinicopathological parameters on OS.

Clinicopathological parameters	Overall survival			
	P value	HR	95% CI	
			Lower	Upper
Body mass index (BMI)	0.008	1.759	1.156	2.677
Ascites level	0.158	0.616	0.315	1.206
Ascites malignancy	0.032	0.336	0.124	0.911
Degree of dissemination	0.004	1.994	1.251	3.178
Tumor differentiation	0.278	2.052	0.559	7.523
Tumor type	0.960	0.000	0.000	$4.006E+185$
FIGO stage	0.842	1.074	0.531	2.172
T stage	0.223	0.664	0.343	1.284
N stage	0.068	1.378	0.977	1.945
M stage	0.837	0.959	0.642	1.433
Laterality	0.650	1.123	0.681	1.850
Tumor size (ccm)	0.392	0.594	0.180	1.959

at a gap of 3-6 months, following the prescribed treatment, thus establishing it as post-treatment biomarker for OvCa. Moreover, elevated level of exosomes can itself be considered as a potent biomarker and therapeutic target in OvCa patients [53]. Exosomal cargoes have also been reported to influence energy metabolism such as in breast cancer exosomal miR-122 induces metastasis by reprogramming glucose metabolism in PMN thereby providing nutrient for the cancer cells [54]. Apart from being a diagnostic tool, exosomes may also participate in SIRT1-driven energy metabolism in OvCa patients and promote metastasis. The distinguished cross-talks between the exosomes and other cells in the TME potentiate the host cells to acquire metastasizing capability which in turn show a direct negative impact in the survival of such patients [55]. In colorectal cancer, it has been observed that under hypoxia the exosomes derived from hypoxic tumor cells when internalized by the normoxic cells impart a metastatic phenotype to the recipient cells. These exosomes transfers Wnt4 depending on HIF-1α which in turn activates the β-catenin signaling pathway and facilitates metastasis, contributing to cancer progression [56]. Similarly, an investigation conducted by Abdouh et al. has stated that exosomes derived from the sera of cancer patients transmitted potent cargoes which influence the recipient cells to acquire malignant traits. Upon IHC of serum-derived exosome-treated cells, a positivity of 85-90% ki-67 has been observed in the ovarian cells along with remarkable increase in other malignancy markers like PAX8 and WT1 [57]. This confirmed the fact that exosomes carry ki-67 and transfer it to the recipient cells to enhance metastasis. According to our investigation, increased concentration of exosomes indicates that the metastasizing potential of the cancer cells is enhanced, validated by greater expression of ki-67 in tumor tissues.

It was observed that 5.5% of all cancer types in UK were related to overweight and obesity [58]. In 2007 and 2008, a meta-analysis in 28 populations and 12 cohort studies, respectively, demonstrated that the obese patients were at a greater risk of developing OvCa [59]. In India, there is a higher prevalence of obesity which affects more than 135 million people [60] because of rapid urbanization. From this study, it has been deduced that a greater proportion of patients are obese and overweight which has interestingly corroborated with the fact that obesity and OvCa are associated with each other. The modulations in metabolism of obese individuals increase the risks of developing the disease. Moreover, evidences have revealed that obesity induces metabolic changes which can also contribute to the increased levels of CA-125 [61]. Since obesity is one of the risk factors in OvCa development, understanding the baseline metabolic alterations leading to obesity is essential to develop targeted potential therapy. Evidences have suggested that the demand for glucose in TME is higher for the survival of the cancer cells. So, we were inclined to analyze the level of glycogen deposition in the cancer cells which serves as a storage for glucose to be utilized for increased glycolysis. However, it has been well established that obesity redirects glucose metabolic flux which in turn induces glycogen deposition in human adipocytes [62]. Glycogen deposition is not only limited to adipocytes, rather hypoxia induced by HIF-1α has been reported to promote glycogen deposition in human ovarian clear cell carcinoma cells [63]. Our data has revealed the distinct level of glycogen deposition between the adjacent normal and cancerous ovarian tissue, inferring that the serum CA-125 levels can also provide a lead to metabolic regulations of OvCa glycogen deposition. Although in depth, further investigations are necessary for the biomarkers related to metabolic alterations in OvCa.

Statistical analysis from data of the patients' cohort revealed that different levels of CA-125 in OvCa patients are significantly correlated with all the clinicopathological parameters except the age, CEA, and CA 19.9 levels. Thus, CA-125 can be a prognostic factor for patients with OvCa. From the IHC data, we can hypothesize that, under hypoxic TME created by upregulation of HIF-1α, the expression level of SIRT1 is elevated which may be correlated with the increased levels of exosomes in the TME and also promotes greater accumulation of glycogen in the tumor tissues as compared to the normal tissues. The key findings from this preliminary data of our research are based on the clinicopathological correlation of serum marker CA-125 with the clinicopathological factors which has provided a lead in the study to analyze the biomolecules in order to establish new targets for OvCa treatment.

5. Conclusion

This comprehensive study has correlated serum CA-125 levels with the clinicopathological parameters indicating that CA-125 apart from a diagnostic element can also be a prognostic factor that can provide a perception on the metastatic and probability of recurrence in the OvCa patients. This reflected a number of significant outcomes both in analyzing the clinicopathological parameters and in the clinical analysis. In addition to it, CA-125 level

variations can also be implemented to detect the dysregulations in the cancer cell metabolism and concentrations of exosomes. The disruption in the normal balance of metabolic pathways as well as elevated metastatic regulations can be responsible for significant level of CA-125. Since a better diagnostic and prognostic factor is essential in the treatment strategy of OvCa, the evaluation of the expression level of biomolecules like SIRT1, HIF-1α, glycogen deposition, and exosome level provides a preliminary idea to target the mechanisms involving them for a better therapeutic outcome for the OvCa patients. According to our study, since CA-125 levels can aid in depicting the metabolic rate and risk of metastasis, individualized treatment strategies can be planned for better survival of the patients by targeting the biomolecules related to metabolism and metastasis. Further intensive explorations are essential in this new arena of research for detecting the underlying invloved biomolecules and signaling cascades, driving the increased metabolism rate and risk of metastasis, which can be further established as potent biomarkers for OvCa.

Abbreviations

AUC: Area under curve
BMI: Body mass index
CA 19.9: Cancer antigen 19.9
CA-125: Cancer/carbohydrate antigen-125
CEA: Carcinoembryonic antigen
DM: Distant metastasis
EGFR: Epidermal growth factor receptor
EOC: Epithelial ovarian cancer
FAO: Fatty acid oxidation
HDACs: Histone deacetylases
HIF-1α: Hypoxia inducible factor-1α
HINT1: Histidine triad nucleotide-binding protein 1
HR: Hazard ratio
IHC: Immunohistochemistry
MITF: Microphthalmia transcription factor
NAD: Nicotinamide adenine diphosphate
OS: Overall survival
OvCa: Ovarian cancer
PAS: Periodic acid/Schiff
PD: Pelvic dissemination
PMN: Premetastatic niche
SIRT1: Silent information regulator 1
TME: Tumor microenvironment.

Data Availability

The data used to support the findings of this study are available from the corresponding author upon request.

Conflicts of Interest

The authors declare that there are no conflicts of interest regarding the publication of this paper.

Authors' Contributions

NC participated in conceptualization, designing the work, supervising the work, analyzing the data, and editing the study. SR participated in designing the work, conducting the experiments, writing the manuscript, and analyzing the data. AD participated in conducting the experiments. SM participated in the statistical analysis. MV participated in providing the patients' samples. All authors have read and approved the manuscript.

Acknowledgments

The authors are thankful to Dr. Jayanta Chakraborti, Director, Chittaranjan National Cancer Institute, Kolkata, for providing infrastructural facilities. The authors are thankful to UGC and CSIR for student fellowships. This study was supported by grants from the Ministry of Health and Family Welfare, Govt. of India, and University Grants Commission, Govt. of India, has granted fellowship to Sraddhya Roy.

Supplementary Materials

Supplementary 1. List of reagents.

Supplementary 2. Graphical representation of frequency profile of clinicopathological parameters in the patient cohort ($N = 248$).

Supplementary 3. Univariate Cox regression analysis of clinicopathological parameters.

References

[1] F. Bray, J. Ferlay, I. Soerjomataram, R. L. Siegel, L. A. Torre, and A. Jemal, "Global cancer statistics 2018: GLOBOCAN estimates of incidence and mortality worldwide for 36 cancers in 185 countries," *CA: a Cancer Journal for Clinicians*, vol. 68, no. 6, pp. 394–424, 2018.

[2] B. F. Ferlay J, M. Ervik, F. Lam et al., "Ovarian Cancer Incidence and Mortality," 2020.

[3] S. Narod, "Can advanced-stage ovarian cancer be cured?," *Nature Reviews. Clinical Oncology*, vol. 13, no. 4, pp. 255–261, 2016.

[4] C. Stewart, C. Ralyea, and S. Lockwood, "Ovarian cancer: an integrated review," *Seminars in Oncology Nursing*, vol. 35, no. 2, pp. 151–156, 2019.

[5] M. Devouassoux-Shisheboran and C. Genestie, "Pathobiology of ovarian carcinomas," *Chinese Journal of Cancer*, vol. 34, no. 1, pp. 50–55, 2015.

[6] T. Kaku, S. Ogawa, Y. Kawano et al., "Histological classification of ovarian cancer," *Medical Electron Microscopy*, vol. 36, no. 1, pp. 9–17, 2003.

[7] M. Malvezzi, G. Carioli, T. Rodriguez, E. Negri, and C. La Vecchia, "Global trends and predictions in ovarian cancer mortality," *Annals of Oncology*, vol. 27, no. 11, pp. 2017–2025, 2016.

[8] Indian Council of Medical Research, "Consensus document for management of epithelial ovarian cancer," 2019.

[9] N. S. Murthy, S. Shalini, G. Suman, S. Pruthvish, and A. Mathew, "Changing trends in incidence of ovarian cancer - the Indian scenario," *Asian Pacific Journal of Cancer Prevention*, vol. 10, no. 6, pp. 1025–1030, 2009.

[10] H. Pant, A. Prakash, R. Khandelwal, and S. Pandey, "Correlation of serum CA-125 with histopathological findings in ovarian tumors," *IP Journal of Diagnostic Pathology and Oncology*, vol. 4, no. 2, pp. 81–85, 2019.

[11] D. R. Bhagora, D. R. Malik, and D. V. K. Trichal, "Expression of estrogen receptor, progesterone receptor and KI 67 in epithelial ovarian tumors and their histopathological correlation," *International Journal of Medical Research*, vol. 5, no. 6, pp. 554–561, 2017.

[12] K. K. Wong, K. H. Lu, A. Malpica et al., "Significantly greater expression of ER, PR, and ECAD in advanced-stage low-grade ovarian serous carcinoma as revealed by immunohistochemical analysis," *International Journal of Gynecological Pathology*, vol. 26, no. 4, pp. 404–409, 2007.

[13] C. Y. Han, D. A. Patten, R. B. Richardson, M. E. Harper, and B. K. Tsang, "Tumor metabolism regulating chemosensitivity in ovarian cancer," *Genes & Cancer*, vol. 9, no. 5–6, pp. 155–175, 2018.

[14] J. R. P. Knight and J. Milner, "SIRT1, metabolism and cancer," *Current Opinion in Oncology*, vol. 24, no. 1, pp. 68–75, 2012.

[15] E. Yang, X. Wang, Z. Gong, M. Yu, H. Wu, and D. Zhang, "Exosome-mediated metabolic reprogramming: the emerging role in tumor microenvironment remodeling and its influence on cancer progression," *Signal Transduction and Targeted Therapy*, vol. 5, no. 1, p. 242, 2020.

[16] K. Nakamura, K. Sawada, M. Kobayashi et al., "Role of the exosome in ovarian cancer progression and its potential as a therapeutic target," *Cancers*, vol. 11, no. 8, p. 1147, 2019.

[17] K. Ohshima and E. Morii, "Metabolic reprogramming of cancer cells during tumor progression and metastasis," *Metabolites*, vol. 11, no. 1, p. 28, 2021.

[18] B. Faubert, A. Solmonson, and R. J. DeBerardinis, "Metabolic reprogramming and cancer progression," *Science*, vol. 368, no. 6487, article eaaw5473, 2020.

[19] T. Khan, M. A. Sullivan, J. H. Gunter et al., "Revisiting glycogen in cancer: a conspicuous and targetable enabler of malignant transformation," *Frontiers in Oncology*, vol. 10, p. 592455, 2020.

[20] R. R. Chen, M. M. H. Yung, Y. Xuan et al., "Targeting of lipid metabolism with a metabolic inhibitor cocktail eradicates peritoneal metastases in ovarian cancer cells," *Communications Biology*, vol. 2, no. 1, p. 281, 2019.

[21] A. Fadaka, B. Ajiboye, O. Ojo, O. Adewale, I. Olayide, and R. Emuowhochere, "Biology of glucose metabolization in cancer cells," *Journal of Oncological Sciences*, vol. 3, no. 2, pp. 45–51, 2017.

[22] B. Muz, P. de la Puente, F. Azab, and A. K. Azab, "The role of hypoxia in cancer progression, angiogenesis, metastasis, and resistance to therapy," *Hypoxia.*, vol. 3, pp. 83–92, 2015.

[23] C. Shao, F. Yang, S. Miao et al., "Role of hypoxia-induced exosomes in tumor biology," *Molecular Cancer*, vol. 17, no. 1, p. 120, 2018.

[24] R. K. J. G. Helmlinger, F. Yuan, M. Dellian, and R. K. Jain, "Interstitial pH and pO2 gradients in solid tumors in vivo: high-resolution measurements reveal a lack of correlation," *Nature Medicine*, vol. 3, no. 2, pp. 177–182, 1997.

[25] P. Lee, N. S. Chandel, and M. C. Simon, "Cellular adaptation to hypoxia through hypoxia inducible factors and beyond," *Nature Reviews. Molecular Cell Biology*, vol. 21, no. 5, pp. 268–283, 2020.

[26] M. Khushman, A. Bhardwaj, G. K. Patel et al., "Exosomal markers (CD63 and CD9) expression pattern using immunohistochemistry in resected malignant and nonmalignant pancreatic specimens," *Pancreas*, vol. 46, no. 6, pp. 782–788, 2017.

[27] S. K. Yeo, X. Zhu, T. Okamoto et al., "Single-cell RNA-sequencing reveals distinct patterns of cell state heterogeneity in mouse models of breast cancer," *Elife*, vol. 9, article e58810, 2020.

[28] C. I. M. Baeten, J. Wagstaff, I. C. L. Verhoeven, H. F. P. Hillen, and A. W. Griffioen, "Flow cytometric quantification of tumour endothelial cells; an objective alternative for microvessel density assessment," *British Journal of Cancer*, vol. 87, no. 3, pp. 344–347, 2002.

[29] N. Chatterjee, S. Das, D. Bose, S. Banerjee, T. Jha, and K. Das Saha, "Leishmanial lipid affords protection against oxidative stress induced hepatic injury by regulating inflammatory mediators and confining apoptosis progress," *Toxicology Letters*, vol. 232, no. 2, pp. 499–512, 2015.

[30] F. Chen, J. Shen, J. Wang, P. Cai, and Y. Huang, "Clinical analysis of four serum tumor markers in 458 patients with ovarian tumors: diagnostic value of the combined use of HE4, CA125, CA19-9, and CEA in ovarian tumors," *Cancer Management and Research*, vol. 10, pp. 1313–1318, 2018.

[31] N. Wentzensen, E. M. Poole, B. Trabert et al., "Ovarian cancer risk factors by histologic subtype: an analysis from the Ovarian Cancer Cohort Consortium," *Journal of Clinical Oncology*, vol. 34, no. 24, pp. 2888–2898, 2016.

[32] W. Feng, D. C. Dean, F. J. Hornicek, H. Shi, and Z. Duan, "Exosomes promote pre-metastatic niche formation in ovarian cancer," *Molecular Cancer*, vol. 18, no. 1, p. 124, 2019.

[33] L. Wang and X. Li, "Identification of an energy metabolism-related gene signature in ovarian cancer prognosis," *Oncology Reports*, vol. 43, no. 6, pp. 1755–1770, 2020.

[34] X. Li, "SIRT1 and energy metabolism," *Acta Biochimica et Biophysica Sinica*, vol. 45, no. 1, pp. 51–60, 2013.

[35] N. Y. Song and Y. J. Surh, "Janus-faced role of SIRT1 in tumorigenesis," *Annals of the New York Academy of Sciences*, vol. 1271, no. 1, pp. 10–19, 2012.

[36] T. Y. Jung, G. R. Jin, Y. Bin Koo et al., "Deacetylation by SIRT1 promotes the tumor-suppressive activity of HINT1 by enhancing its binding capacity for β-catenin or MITF in colon cancer and melanoma cells," *Experimental & Molecular Medicine*, vol. 52, no. 7, pp. 1075–1089, 2020.

[37] X. Chen, D. Hokka, Y. Maniwa, C. Ohbayashi, T. Itoh, and Y. Hayashi, "Sirt1 is a tumor promoter in lung adenocarcinoma," *Oncology Letters*, vol. 8, no. 1, pp. 387–393, 2014.

[38] J. Qin, Y. Liu, Y. Lu et al., "Hypoxia-inducible factor 1 alpha promotes cancer stem cells-like properties in human ovarian cancer cells by upregulating SIRT1 expression," *Scientific Reports*, vol. 7, no. 1, p. 10592, 2017.

[39] A. Daponte, M. Ioannou, I. Mylonis et al., "Prognostic significance of hypoxia-inducible factor 1 alpha(HIF-1alpha) expression in serous ovarian cancer: an immunohistochemical study," *BMC Cancer*, vol. 8, no. 1, p. 335, 2008.

[40] S. Roy, A. Das, M. Vernekar, S. Das, and N. Chatterjee, "SIRT1 regulates ovarian cancer metastasis via altering the exosome release and glycogen deposition [abstract]," in *Proceedings of the American Association for Cancer Research Annual Meeting 2021*, Philadelphia (PA): AACR; Cancer Res 2021;81(13_Suppl):Abstract nr 2461, 2021 Apr 10-15 and May 17-21.

[41] G. K. Panigrahi, P. P. Praharaj, T. C. Peak et al., "Hypoxia-induced exosome secretion promotes survival of African-American and Caucasian prostate cancer cells," *Scientific Reports*, vol. 8, no. 1, p. 3853, 2018.

[42] E. P. Beck, A. Moldenhauer, E. Merkle et al., "CA 125 production and release by ovarian cancer cells in vitro," *The International Journal of Biological Markers*, vol. 13, no. 4, pp. 200–206, 1998.

[43] I. Konishi, J. L. Fendrick, T. H. Parmley, J. G. Quirk, and T. J. O'brien, "Epidermal growth factor enhances secretion of the ovarian tumor-associated cancer antigen CA 125 from the human amnion WISH cell line," *Journal of the Society for Gynecologic Investigation*, vol. 1, no. 1, pp. 89–96, 1994.

[44] T. J. O'Brien, J. B. Beard, L. J. Underwood, R. A. Dennis, A. D. Santin, and L. York, "The CA 125 gene: an extracellular superstructure dominated by repeat sequences," *Tumor Biology*, vol. 22, no. 6, pp. 348–366, 2001.

[45] D. Li, Q. J. Wu, F. F. Bi et al., "Effect of the BRCA1-SIRT1-EGFR axis on cisplatin sensitivity in ovarian cancer," *American Journal of Translational Research*, vol. 8, no. 3, pp. 1601–1608, 2016.

[46] A. Latfikar, L. Ling, A. Hingorani et al., "Loss of sirtuin 1 alters the secretome of breast cancer cells by impairing lysosomal integrity," *Developmental Cell*, vol. 49, no. 3, pp. 393–408.e7, 2019.

[47] D. H. Mvunta, T. Miyamoto, R. Asaka et al., "Overexpression of SIRT1 is associated with poor outcomes in patients with ovarian carcinoma," *Applied Immunohistochemistry & Molecular Morphology*, vol. 25, no. 6, pp. 415–421, 2017.

[48] Z. Chen, Q. Liang, H. Zeng et al., "Exosomal CA125 as a promising biomarker for ovarian cancer diagnosis," *Journal of Cancer*, vol. 11, no. 21, pp. 6445–6453, 2020.

[49] P. Bischof, "What do we know about the origin of CA 125?," *European Journal of Obstetrics, Gynecology, and Reproductive Biology*, vol. 49, no. 1–2, pp. 93–98, 1993.

[50] R. O. Elliott and M. He, "Unlocking the power of exosomes for crossing biological barriers in drug delivery," *Pharmaceutics*, vol. 13, no. 1, p. 122, 2021.

[51] D. Sinha, S. Roy, P. Saha, N. Chatterjee, and A. Bishayee, "Trends in research on exosomes in cancer progression and anticancer therapy," *Cancers*, vol. 13, no. 2, pp. 326–331, 2021.

[52] S. Piatek, G. Panek, Z. Lewandowski et al., "Rising serum CA-125 levels within the normal range is strongly associated recurrence risk and survival of ovarian cancer," *Journal of Ovarian Research*, vol. 13, no. 1, p. 102, 2020.

[53] M. K. S. Tang and A. S. T. Wong, "Exosomes: emerging biomarkers and targets for ovarian cancer," *Cancer Letters*, vol. 367, no. 1, pp. 26–33, 2015.

[54] M. Y. Fong, W. Zhou, L. Liu et al., "Breast-cancer-secreted miR-122 reprograms glucose metabolism in premetastatic niche to promote metastasis," *Nature Cell Biology*, vol. 17, no. 2, pp. 183–194, 2015.

[55] W. Tian, S. Liu, and B. Li, "Potential role of exosomes in cancer metastasis," *BioMed Research International*, vol. 2019, Article ID 4649705, 12 pages, 2019.

[56] Z. Huang, M. Yang, Y. Li, F. Yang, and Y. Feng, "Exosomes derived from hypoxic colorectal cancer cells transfer wnt4 to normoxic cells to elicit a prometastatic phenotype," *International Journal of Biological Sciences*, vol. 14, no. 14, pp. 2094–2102, 2018.

[57] M. Abdouh, D. Hamam, Z. H. Gao, V. Arena, M. Arena, and G. O. Arena, "Exosomes isolated from cancer patients' sera transfer malignant traits and confer the same phenotype of primary tumors to oncosuppressor-mutated cells," *Journal of Experimental & Clinical Cancer Research*, vol. 36, no. 1, p. 113, 2017.

[58] D. M. Parkin and L. Boyd, "8. Cancers attributable to overweight and obesity in the UK in 2010," *British Journal of Cancer*, vol. 105, no. S2, pp. S34–S37, 2011.

[59] M. F. Leitzmann, C. Koebnick, K. N. Danforth et al., "Body mass index and risk of ovarian cancer," *Cancer*, vol. 115, no. 4, pp. 812–822, 2009.

[60] P. Ravi Varma, "The obesity epidemic and cancer in India – the Cochin Cancer Research Centre initiative," *Research and Reviews on Healthcare: Open Access Journal*, vol. 4, no. 2, pp. 356–362, 2019.

[61] M. O. Akiibinu, B. O. Soile, M. Ajibola, U. Amzat, and T. K. Olatunji, "Plasma levels of CA125, CEA, AFP and cortisol in obesity," *Journal of Steroids and Hormonal Science*, vol. 6, no. 2, pp. 23–25, 2015.

[62] V. Ceperuelo-Mallafré, M. Ejarque, C. Serena et al., "Adipose tissue glycogen accumulation is associated with obesity-linked inflammation in humans," *Molecular Metabolism*, vol. 5, no. 1, pp. 5–18, 2016.

[63] Y. Iida, K. Aoki, T. Asakura et al., "Hypoxia promotes glycogen synthesis and accumulation in human ovarian clear cell carcinoma," *International Journal of Oncology*, vol. 40, no. 6, pp. 2122–2130, 2012.

Mutation Research-Reviews in Mutation Research 793 (2024) 108490

Contents lists available at ScienceDirect

Mutation Research-Reviews in Mutation Research

journal homepage: www.elsevier.com/locate/mutrev

Mitochondria act as a key regulatory factor in cancer progression: Current concepts on mutations, mitochondrial dynamics, and therapeutic approach

Sraddhya Roy [a], Ananya Das [a], Aparajita Bairagi [a], Debangshi Das [a], Ashna Jha [a], Amit Kumar Srivastava [b], Nabanita Chatterjee [a,*]

[a] Chittaranjan National Cancer Institute, 37 S. P. Mukherjee Road, Kolkata 700026, India
[b] CSIR-IICB Translational Research Unit Of Excellence, CN-6, Salt Lake, Sector – V, Kolkata 700091, India

ARTICLE INFO

Keywords:
Mitochondria
Mitochondrial alterations
mitochondrial dynamics
cancer progression, immune cells

ABSTRACT

The diversified impacts of mitochondrial function vs. dysfunction have been observed in almost all disease conditions including cancers. Mitochondria play crucial roles in cellular homeostasis and integrity, however, mitochondrial dysfunctions influenced by alterations in the mtDNA can disrupt cellular balance. Many external stimuli or cellular defects that cause cellular integrity abnormalities, also impact mitochondrial functions. Imbalances in mitochondrial activity can initiate and lead to accumulations of genetic mutations and can promote the processes of tumorigenesis, progression, and survival. This comprehensive review summarizes epigenetic and genetic alterations that affect the functionality of the mitochondria, with considerations of cellular metabolism, and as influenced by ethnicity. We have also reviewed recent insights regarding mitochondrial dynamics, miRNAs, exosomes that play pivotal roles in cancer promotion, and the impact of mitochondrial dynamics on immune cell mechanisms. The review also summarizes recent therapeutic approaches targeting mitochondria in anti-cancer treatment strategies.

1. Introduction

Mitochondria, the energy feeders of the cells, were presumably minuscule bacterial descendants that acquired identity as important cell organelles after undergoing endosymbiotic relationships with prokaryotic cells over millions of years. They have evolved as bi-layered subcellular organelles that serve as a prime source of energy required for eukaryotic cell survival, except for erythrocytes because in erythrocytes

Abbreviations: AK4, adenylate kinase 4; Akt, protein kinase B; ALL, acute lymphoblastic leukemia; BTICs, brain tumor initiating cells; AML, acute myeloid leukemia; BHD, Birt–Hogg–Dubé; CAFs, cancer associated fibroblasts; CJs, crista junctions; COX, cyclooxygenase; CRC, colorectal cancer; D loop, displacement loop; DDK3, Dickkopf-related protein 3; DHODH, dihydroorotate dehydrogenase; DNM2, dynamin 2; DNMT, DNA methyltransferases; Drp1, dynamin related protein 1; EMT, epithelial mesenchymal transition; ER, endoplasmic reticulum; FAO, fatty acid oxidation; FH, fumarate hydratase; Glut1, glucose transporter 1; GTP, guanosine triphosphate; HCC, hepatocellular carcinoma; HIF-1, hypoxia inducible factor 1; HOXA, Homeobox A Cluster; IBM, inner boundary membrane; IDH, isocitrate dehydrogenase; IMM, inner mitochondrial membrane; LSC-NPs, lipid membrane- coated inorganic silica–carbon nanoparticles; LZTS1, Leucine Zipper Tumor Suppressor 1; MAF, minor allele frequency; Mdivi1, mitochondrial division inhibitor 1; MDR, multidrug resistance; MFN1, mitofusin 1; Mgrap, mitochondria-localized glutamic acid-rich protein; MICOS, mitochondrial contact site and cristae organizing system complex; MLL, mixed lineage leukemia; Mrps12, mitochondrial ribosomal protein S12; MtDNA, mitochondrial DNA; MTOR, mammalian target for rapamycin; NAD, nicotinamide; ND, NADH dehydrogenase; NDNA, nuclear DNA; NF-κb, nuclear transcription factor-κB; NLRP3, NLR family pyrin domain containing 3; NOS, nitric oxide synthase; NRF-1, nuclear respiratory factor 1; OGG1, 8-oxoguanine DNA glycosylase; OMM, outer mitochondrial membrane; OPA1, optic atrophy 1; OSCC, oral squamous cell carcinoma; OXPHOS, oxidative phosphorylation; PARP, poly ADP Ribose Polymerase 2; PDAC, pancreatic ductal adenocarcinoma; PDK1, pyruvate dehydrogenase lipoamide kinase isozyme 1; PDT, photodynamic therapy; PGC-1-α, peroxisome-proliferator activated receptor gamma coactivator 1-α; PKM2, pyruvate kinase isozyme2; POLG, DNA polymerase; POLMRT, mitochondrial RNA polymerase; PTC, papillary thyroid carcinoma; ROS, reactive oxygen species; SDH, succinate dehydrogenase; SFRP2, secreted frizzled-related protein 2; SNHG3, small nucleolar RNA host gene 3; SNPs, single nucleotide polymorphism; SOD2, superoxide dismutase 2; TCA, tricarboxylic acid cycle; TET, ten-eleven translocations; TFAM, mitochondrial transcription A; TME, tumor microenvironment; Tmem70, transmembrane protein 70; TPP, tetraphenylphosphonium; Trp, tryptophan; TSGs, tumor suppressing genes; UBE2E2, ubiquitin-conjugating enzyme E2E 2; UCP, uncoupling protein; UPRmt, mitochondrial unfolded protein response; VHL, Von Hippel-Lindau.

* Corresponding author.
E-mail address: nabanita.chatterje@yahoo.com (N. Chatterjee).

https://doi.org/10.1016/j.mrrev.2024.108490
Received 26 April 2022; Received in revised form 12 February 2024; Accepted 22 February 2024
Available online 8 March 2024

both the nucleus and mitochondria are eliminated due to oxidative stress [1]. Furthermore, various cellular metabolic pathways in the cells are nourished by mitochondrial metabolites. Mitochondrial functions and dysfunctions participate in a wide range of diseases and physiological conditions, mainly cancer and aging. Though aging and cancer are distinct processes, they share some common mechanisms including alterations in the mitochondrial genome/DNA (mtDNA), activation of mitochondria- to-nucleus signaling pathways (retrograde signaling), and telomere shortening. Aging is associated with the accumulation of mtDNA mutations because disruption of the mitochondrial respiratory chain aids in the increased generation of reactive oxygen species (ROS). Further, the ongoing accumulation of mtDNA mutations play a decisive role in the aging process [2]. However, in cancer, mitochondria promote cancer cells' survival, proliferation, and progression by generating ROS, which in turn induces DNA defects and activates oncogenic signaling. This results in the accumulation of oncogenic metabolites as well as abnormal functioning of the mitochondrial permeability transition. Whole genome sequencing of various cancer types has provided satisfying evidence relating genomic mutations and cancer [3,4], but the multiple factors underlying the role of mtDNA mutations and their impacts on cancer susceptibility are still being explored [5]. Therefore, widespread global research is ongoing to illuminate the diverse roles of mitochondria in tumorigenesis and cancer progression. According to emerging studies, the fusion, and fission events in mitochondria (mitochondrial dynamics) influence various cellular functions such as cell division, metabolism, and cell migration, such that alterations in mitochondrial dynamics can induce the emergence and progression of cancer. Investigations examining genetic and epigenetic alterations in the mitochondrial genome, accompanied by studies of mitochondrial dynamics contributing to cancer, are active arenas of cancer research. The novelty of this review is that it showcases alterations of mitochondrial dynamics at genetic and epigenetic levels, as well as reviews the emerging roles of miRNAs in influencing mitochondrial functionality. This review also discusses the mitochondrial impact on immunological aspects, metabolism and mitochondrial targeting strategies. Taken together, the review offers an extensive overview of how mitochondrial dysfunctions participate in the process of tumorigenesis and promote cancer.

2. Mitochondrial alterations in cancer

Mitochondria have been associated with various cellular functions including energy generation, cellular metabolism and signaling, cell cycle control, and cell death. Despite their multiple constitutive roles, mitochondria dysfunction has also been depicted in the initiation and spread of cancer due to their deviations in malfunctioning cells. Mitochondrial DNA (mtDNA) alterations leading to cancer can include reduction or alterations in mtDNA content or mitochondrial proteins encoded by the nuclear genome (nDNA), resulting in several cancer promoting factors such as resistance to apoptosis and epithelial-mesenchymal transition (EMT), etc [6]. Genetic alterations in both nDNA and mtDNA, as well as in miRNAs, transcription factors, tumor suppressor genes and oncogenes can elevate the risk of developing cancer in various ethnicities. Altered communications between mitochondria and the nucleus at genetic and epigenetic levels can increase cancer susceptibility [6]. The involvement of mtDNA in tumorigenesis is sometimes difficult to interpret because of abnormalities present in the mitochondrial genome. Germline mitochondrial mutations are inherited from mothers to offspring, and somatic mitochondrial mutations can occur in the proliferating cells during the lifetime of an individual. Further, quantitative mtDNA alterations leading to changes in mtDNA copy number have been associated with a wide range of cancer types [7]. Table 1 illustrates the large variety of mitochondrial dysfunctions that have been cataloged in different cancer types.

2.1. Mitochondrial mutations in cancer

Considering germline mitochondrial genome variations, many haplogroups (the existence of certain unique mutations in a population) have been denoted. According to restriction fragment length polymorphisms, respective human populations possess distinctive haplogroups of mtDNA [37]. Polymorphisms in the coding regions of mitochondrial genome give rise to distinct haplotypes in respective haplogroups. Some individual haplotypes have been observed to be linked to the development of cancer. For instance, nine distinct haplotypes, namely H, I, J, K, T, U, V, W, and X were observed to be associated with renal and prostate cancer in North American white men of European origin. Among them, the risk of prostate cancer increased by 2 times and by 2.5 times for renal cancer because of the presence of haplogroup U [38]. mtDNA single nucleotide polymorphisms (SNPs) have also been associated with an increased risk of breast cancer; e.g in an Indian population, the substitution of G10398A in N haplogroup has increased the susceptibility to breast and esophageal cancer [39]. An increased probability of invasive serous ovarian cancer has been found in haplotypes of the European population who inherited SNP rs2857285 in the NADH dehydrogenase 4 (*ND4*) gene with a minor allele frequency (MAF) level less than 5% [40]. A multi-ethnic cohort study encompassing colorectal cancer (CRC) has demonstrated that a missense 4917 SNP in *ND2* increased the susceptibility to CRC in European Americans but not in Asian Americans, African Americans, Latinos, or Native Hawaiians. In the same study, the T haplogroup has been found to be more susceptible to cancer development [41]. In Saudi Arabia, haplotype G (34%) and haplotype C (13%) were newly discovered in acute lymphoblastic leukemia (ALL) patients, along with 31 mutations at 14 locations in ATP synthase subunit 6 of mtDNA [42]. A total of 17 mutations in mitochondrial DNA polymerase γ (POL) at T251I (exonuclease domain), P587L (linker region), and E1143G (polymerase domain), including one silent (A703A) and one missense (R628Q) at the linker region, have been identified in 63% of breast tumors [43]. *Jensen et al.* have evaluated that polymorphism in the CAG region of the *POLG* allele has been associated with the development of testicular cancer [44]. Frameshift mutations in mitochondrial transcription A (TFAM) have led to mitochondrial copy number reduction and mitochondrial instability in CRC [45]. Among Indian populations, increased risk of oral leukoplakia and cancer has been associated with two SNPs, rs41553913 at POLMRT and rs9905016 at POLG2, at both genetic and allelic levels, thus contributing to increased mtDNA synthesis [46]. In a cohort study of German populations, breast cancer risk has been associated with one SNP in Poly ADP Ribose Polymerase 2 (PARP2) and three SNPs in POLG [47]. Somatic mtDNA mutations also contribute to the development of various cancers. These mutations are more likely to occur in the displacement (D) loop located in between nucleotides and contain mitochondrial transcription and replication components, which makes this region a mutational hot spot [48]. D-loop regions have been observed to be the most sensitive region of mtDNA to oxidative phosphorylation (OXPHOS). Since mtDNA replication depends on transcription, mtDNA damage can affect mitochondrial gene expression in three different ways: by generating transcriptional mutagenesis or premature transcript termination, by interfering with the mitochondrial RNA polymerase's priming during mtDNA replication, or by causing errors in DNA polymerase γ nucleotide incorporation that result in mutations [49]. *Yuan et al.* have depicted nine mtDNA mutations in the D-loop region of oral squamous cell carcinoma (OSCC), which have a mutation rate of 27%, that have favored cancer development [50]. On the contrary, another study by *Lin et al.* has stated that somatic mutations in the D loop, with a mutation rate of 62.5%, were not associated with poor survival of OSCC patients but rather increased the 5 years survival rate [51]. In a similar study carried out by *Zhao et al.* in gastric cancer, 18 mutated genes have been observed, out of which 4 mutation sites are present in the mtDNA D-loop region [52]. Furthermore, polymorphisms in nucleotides like 263 A>G in Tunisian females have made

Table 1
Mitochondrial dysfunctions in cancer types.

Cancer Types	Mitochondrial Dysfunction	Mechanism	Effect	Ref.
Bladder cancer	Alterations in mitochondrial proteins: Lon protease ↑	Switch from respiratory metabolic pathway to glycolytic pathway ROS ↑ c-Jun N-terminal kinase (JNK) phosphorylation ↑	Apoptosis ↓ Cell survival and proliferation ↑ Chemoresistance↑	[8,9]
	Mitofusin (MFN) 2 ↓	Ras-ERK MAPK signaling pathway ↑ caspase-3 ↓ cleavage of poly (ADP-ribose) polymerase PARP ↓	Cell survival and proliferation ↑ Cell cycle arrest at G1 phase ↑ Apoptosis ↓	
	Mitochondrial transcription factor A (TFAM) ↑	microRNA 590–3p ↓ which directly target TFAM	Cell proliferation ↑ Migration ↑ Colony-forming ability↑	
Acute myeloid Leukemia	Somatic point mutations in the D loop of mtDNA mtDNA copy number↑ TFAM ↑	ROS ↑ Disturb the flow of electrons in electron transport chain (ETC)	Transformation of chronic granulocytic leukemia to acute myeloid leukemia	[10, 11]
Melanoma	mtDNA copy number↑ TFAM ↑	Glucose consumption ↑ ATP ↑	Tumorigenesis ↑	[12]
Non-Small Cell Lung carcinoma (NSCLC)	TFAM ↓	ROS)-induced c-Jun amino-terminal kinase (JNK)/ p38 MAPK signaling ↑ Cellular bioenergentics ↓	Cell cycle arrest at G1 phase ↑ Apoptosis ↑ Sensitivity to cisplatin ↑ Tumorigenesis ↓	[13]
	Mfn2 upregulation	Downregulation of AIM2 Inactivation of MAPK/ERK pathway	Decreased ROS production	[14]
	Inhibition of Drp1 phosphorylation by sirt4	Inactivation of ERK	Cell cycle arrest and rapid invasion	[15]
	PIM1-inhibition induced Drp1 upregulation	↑ROS	chemosensitivity	[16]
Clear cell renal cell carcinoma (ccRCC)	SIRT3 (involved in mitochondrial proteostasis) ↑ Expression of TFAM ↑ Acetylation of TFAM ↓	Mitochondrial biogenesis ↑ Warburg effect ROS/oxidative stress ↑	Cell proliferation ↓ EMT ↓	[17]
Colorectal cancer	Demethylation of D-loop of mtDNA in the CpG islands at the position of 4th and 6th/ 7th	mtDNA copy number↑	Cell proliferation ↑ Apoptosis ↓ Cell cycle arrest at G0/G1 phase ↓	[18]
	Drp1 phosphorylation	↑ERK pathway	chemo resistance	[19]
	Suppression of Drp1 phosphorylation	inhibition of IKKβ and p65 translocation, suppression of NF-κB	Inhibition of carcinogenesis	[20]
Oral squamous cell carcinoma (OSCC)	Hypermethylation at CpG sites in the *COX1* and *CYTB* genes of mtDNA	ROS ↑ Glycolysis ↑	Cisplatin sensitivity ↓ Cell proliferation ↑	[21]
Human laryngeal squamous cell carcinoma (LSCC)	Somatic mutations in D-loop of mtDNA at Hypervariable region I and II (HVI/II) and D310 region	mtDNA copy number↑ Polymorphism	Carcinogenesis ↑	[22]
Colon cancer	mtDNA copy number↑ TFAM ↑	ROS ↑ Lactate fermentation ↑ COX-II ↑ Snail ↑ Vimentin↑ N-cadherin ↑	EMT ↑ Invasion ↑	[23]
	SIRT3 (involved in mitochondrial proteostasis) ↓	Mitochondrial biogenesis ↓ Peroxisome proliferator-activated receptor γ (PPAR γ) coactivator-1 alpha (PGC-1α) ↓	Cell proliferation ↑	[24]
Hepatocellular carcinoma	↑Dynamin-1-like protein ↓Mfn1	Activating Ca2+/CaMK II/ERK/FAK pathway	Cell migration ↑	[25]
	↓ Mfn1	↓ Glycolysis	Modulate cancer metastasis via metabolic shift	[26]
	↑ Drp1	Modulate NFKB and TP53 pathway	↑ Infiltration of tumor associated macrophages	[27]
Breast cancer	↓ Mfn1	Modulate NOTCH1 pathway	Cancer cell survival	[28]
	DRP1 phosphorylation on Ser637	↑SIRT3 phosphorylation of AMPK at Ser 485/491.	Tamoxifen resistance	[29]
	Liensinine treatment induced fission via DNM1L activation	↓ autophagic degradation	Cellular apoptosis	[30]
Pancreatic cancer	↑Drp1 phosphorylation	Activation of MAPK pathway	Tumor growth	[31]
Pancreatic ductal adenocarcinoma	↑Mitochondrial fission	↑ ROS generation	Cell proliferation and invasion	[32]
Prostate cancer	Mff repression resulting from BRD4 knockdown		CSCs exhaustion	[33]
	Increased fission	ER-localized isoform of the formin protein inverted formin 2 (INF2) mediates polymerization of actin at ER-mitochondria intersections	Tumorigenesis	[34]
T-ALL	Drp1 phosphorylation on Ser616	Modulate ROS production	Drug resistance	[35]
AML	Fission upregulation In LSC	Modulate AMPK pathway	LSCs self-renewal	[36]

↑, increase; ↓, decrease

them more susceptible to developing breast cancer [53]. The 16189 T>C polymorphism that affects mtDNA replication and cellular copy number in peripheral blood cells [54] has also been observed to be associated with endometrial cancer [55], polycystic astrocytoma [56], and breast cancer [57]. The accumulation of ROS due to the imbalance in OXPHOS as a result of mtDNA mutations facilitates the ability of cancer cells to survive the stress associated with mitochondrial unfolded protein response (UPRmt). This has been elucidated by *Kenny et al.*, reporting that the SIRT3/FOXO/SOD2 axis remains activated in highly metastatic breast cancer cells with elevated levels of superoxide dismutase 2 (SOD2) as compared to the less metastatic ones [58]. The mtDNA mutation T8993G, affecting the functionality of the *cytochrome oxidase subunit I (COI)* gene by increasing the generation of ROS, has been observed to promote prostate tumor growth to about 7 times larger than in non-mtDNA associated prostate cancers [59]. In colorectal cancer (CRC) cells, somatic mutations in *ND1, ND4L, ND5, cytochrome b, MTCOI, MTCOII,* and *MTCOIII* genes, as well as in the 12 S and 16 S rRNA genes, are mostly homoplasmic in nature i.e. they were present in every mitochondrial genome. The mutations were mainly transitions at the purines (T-to-C or G-to-A) are due to the effect of increased ROS in the cancer cells [60]. Although most of the mutations have been observed to be homoplasmic i.e. they are present in almost every mitochondrial genome but sometimes the mutations are present along with the wild type genome or more than one different variant of mtDNA coexisting within a cell (heteroplasmy) has been observed in oral cancer. Furthermore, insertions or deletions have been observed to occur in the poly C region of the D-loop, missense mutations have been noted to occur in NADH dehydrogenase 2, and frameshift mutations have been found to occur in complex III [61]. In pancreatic ductal adenocarcinoma (PDAC), the non- coding control regions that contain sites of mtDNA transcription and replication harbour a maximum number of mtDNA somatic mutations. Among the mutations, *ND4* and *ND6* mutated genes are associated with poor survival of the patients, along with *ND5, RNR2,* and *CO1* being frequently mutated [62].

2.2. Impact of mtDNA mutations on cancer progression

The mitochondrial OXPHOS machinery is encoded by several mtDNA genes and is susceptible to damage due to the production of ROS [2]. Cancer cells possess mtDNA both in wild-type and in mutated forms in a heteroplasmic state, however most of the mtDNA mutations in non-coding and coding regions acquire homoplasmy due to a drift in the proportion of the mutant mtDNAs in the cells. In this scenario, the increased levels of somatic mtDNA mutations have been associated with different forms of cancer. These mutations are responsible to confer pro-tumorigenic properties to the cancer cells. For instance, *Smith et al.,* observed in their *in-vivo* study that deletion of the tumor suppressor Apc in age-associated OXPHOS deficient mice upregulates the *de novo* serine synthesis pathway, which in turn promotes the growth of intestinal tumors [63]. In non-small cell lung cancer (NSCLC) and colon cancer cells, the *ND6* 13885insC mutation induces overexpression of metastatic and angiogenesis related genes accompanied by resistance towards stress-induced apoptosis, thereby promoting metastasis [64]. *Arnold et al.* have demonstrated a recurrent missense mtDNA mutation in the *ND3* gene at nucleotide position 10398 to be responsible for bone metastasis in prostate cancer patients [65]. The metastatic potential of CRC has also been observed to be elevated due to the microsatellite instability in the D310, D514, and D16184 positions of the D-loop [66]. *Tan et al.* have reported various types of mutations such as deletions or insertions, single base substitutions within the D-loop, or in coding and non-coding regions of the mitochondrial genome in breast cancer [67]. However, in ovarian cancer, the mutational hotspots have been depicted to be in the D-loop, 12 S rRNA, 16 S rRNA, and cytochrome b, as most of the transition changes from T-C or G-A are prevalent in these regions [68]. In papillary thyroid carcinoma (PTC), most of the somatic mtDNA mutations have been observed in complex I of the respiratory chain, which might be involved in early-stage tumor development [69]. Heteroplasmic levels of shared mutations are highly correlated with the intratumoral recurrence of mtDNA mutations in hepatocellular carcinoma (HCC) and CRC [70]. In a cohort study of prostate cancer patients, mtDNA mutations were apparently more common in the older age patients in comparison to the younger ones. Co-occurrence of mutations has also been observed in the nuclear and mitochondrial mutational indexes, e.g. mitochondrial single nucleotide variants (mtSNVs) co-occur with the increase in function of the *MYC* oncogene has been associated with patient survival [71]. Sequence analysis of mtDNA has revealed the presence of a m.10875 T>C missense mutation of a conserved residue (p.39Leu>Pro) in the *MTND4* gene encoding the CI subunit in ovarian cancer cells [72]. However, in contrast, evidence of the anti- tumorigenic role of mutation has also been reported for instance. in osteosarcoma, *m.3571insC/MT-ND1* and *m.3243 A>G/MT-TL1* mutations in the mitochondrial complex I have resulted in structural and functional alterations, which in turn minimize the tumorigenic potential of the cancer cells [73]. mtDNA repair by targeting 8-oxoguanine DNA glycosylase (OGG1) has been reported to confer an anti-metastatic effect on breast cancer cells [74]. CI disassembly caused by high loads of *MTND1* m.3571insC also offers anti-tumorigenic and antimetastatic effects. The genes that exhibit the ability to regulate either oncogenic or suppressive functions in mitochondrial settings during tumorigenesis depending on a threshold load beyond which tumor growth and invasiveness get markedly inhibited is termed oncojanus genes [75].

In this context, the study of oncocytomas is a major arena of recent research. Oncocytomas are neoplasms that have amassed excessive amounts of mitochondria in epithelial cells, resulting in a swollen appearance. Mitochondrial respiratory complex I is the major site for mtDNA mutations in oncocytic tumors [76]. The 3571insC ND1 mutation has been observed to ablate ND1 content and diminish the levels of nuclear-coded NDUFA9 and the mitochondria-coded ND6 in thyroid oncocytic tumors [77]. In nasopharyngeal oncocytic tumors, truncated frameshift mutations in the ND5 region of complex I promote the disassembly of complex I due to the loss of other ND subunits like ND6 and have been associated with the oncocytic transformations [78]. Frameshift mutations in ND1, ND4, and ND5 of the mitochondrial respiratory complex I have been associated with its loss of enzymatic activity, marking it as a major cause of renal oncocytomas [79]. Furthermore, a loss in chromosome 1, or overexpression of cyclin D1 in a subset of renal oncocytomas dictating functional changes in complex I, might be underlying reasons for the early genetic events leading to tumor development by altering glutathione metabolism [80]. Interstingly, oncocytomas are capable of destabilizing hypoxia-inducible factor (HIF)-1α by hyperhydroxylating it due to the effect of several mutations in the mitochondrial respiratory chain. This leads to the accumulation of hyperhydroxylated HIF-1α in Von Hippel-Lindau (VHL) deficient renal oncocytomas, which confers a benign nature to the tumor by minimizing the glycolysis rate [81]. The study conducted by *Lang et al.* has stated that mtDNA mutations aid in distinguishing between renal tumors of Birt–Hogg–Dubé (BHD) patients and other renal oncocytomas, indicating that mitochondrial alterations could be a potential diagnostic marker for renal oncocytomas [82].

2.3. Mito-epigenetics in cancer

Apart from the genetic changes in mtDNA discussed above, there has also been a recent focus on the epigenetic regulation of mtDNA and the potential impacts on cancer. This field of study has been termed mitoepigenetics. Epigenetic regulation of mtDNA occurs mainly due to DNA methylation and hydroxymethylation which are driven by four DNA methyltransferases (DNMT1, 3 A, 3B, and 3 L) and three demethylases, i.e. ten-eleven translocations (TET1–3) [83]. Epigenetic alterations in mitochondria structure and function under the influences of multiple external and intra-mitochondrial factors can result in cellular

malfunctions leading to cancer. These mutations, instead of attenuating energy metabolism, hamper the bioenergetic and biosynthetic states of mitochondria.

In HCC, transmembrane protein 70 (*Tmem70*) and ubiquitin-conjugating enzyme E2E 2 (*UBE2E2*) genes have been reported to undergo epigenetic modulation by hypermethylation, resulting in a shift of cellular respiration from OXPHOS to glycolysis and aberrant cell cycle regulation facilitating cell proliferation [84]. The D-loop region of mtDNA in breast cancer has been reported to possess eight methylation sites, which are maternally inherited [85]. mtDNA methylation has been negatively correlated with mtDNA copy number and tumor spread. For instance, in osteosarcoma and glioblastoma, 5hmC in the D-loop region of mtDNA has been observed to be low during tumor progression, with increased mtDNA copy numbers in the transformed cells. Moreover, tumorigenesis is catalyzed by methylation in the D-loop which is negatively correlated with ND5 and ND6 transcription [86]. Ample evidence suggest that mitochondrial epigenetic dysfunctions can also lead to nDNA methylation, histone methylation, and acetylation [87]. In the mitochondrial respiratory chain and Krebs cycle, dysfunction of two enzymes, namely succinate dehydrogenase (SDH) and isocitrate dehydrogenase (IDH) has been observed to promote nDNA hypermethylation in pheochromocytomas, gastrointestinal stromal tumors, paragangliomas, and gliomas [88]. Epigenetic alterations in the subunits of mitochondrial respiratory changes encoded by mtDNA might impose positive regulation of proto-oncogenes and negatively regulate tumor-suppressor genes (TSGs) that lead to tumorigenesis [83].

5-hydroxymethyl cytosine (5hmC) is the second most common epigenetic mutation after DNA methylation in both nuclear genome and mtDNA [89]. Levels of 5hmC have been observed to be lower in the tumor tissues as compared to the normal tissues [90,91]. Evidence revealed that in cancers, mutations in genes like *IDH1/2, SDH, and fumarate hydratase (FH)* controlled the levels of 5hmC at genomic levels by regulating the activity of TET proteins [91,92]. The diversified roles of 5hmC either as tumor suppressing or promoting, can be evaluated by identifying the locus-specific modifications in different forms of cancer. In the genomic context, reduced levels of 5hmC influencing gene body hypermethylation have been observed in kidney cancer and also promote hypermethylation of TSGs in different cancer forms [93]. In breast cancer, loss of 5hmC in the *Homeobox A Cluster* (*HOXA)* gene promotes cancer cell invasion [94]. Similarly, the loss of 5hmC in the miR-200 promoter region and the *Leucine Zipper Tumor Suppressor 1* (*LZTS1)* gene enables EMT. This also enhances the metastasizing capability of the cancer cells by promoting hypermethylation in the promoter regions of *mir-200* and *LZTS1* [95,96]. In squamous cells and adenocarcinomas, the loss of 5hmC at the promoter region of the metabolic enzyme SOD3 due to demethylation facilitated by the TET proteins, downregulates its expression [97]. In colon cancer, an *in-vivo* study has revealed that *Dickkopf-related protein 3* (DDK3) at its promoter region undergoes a loss in 5hmC that in turn activates Wnt signaling which regulates tumor growth [98]. Furthermore, the mutation in the *TET1* gene leads to an increase in the levels of 5hmC which signifies its oncogenic role in mixed lineage leukemia (MLL) [99]. However, a recent study by *Yu et al.* has stated that TET1 expression is lower in PTC with reduced levels of 5hmC and thus exhibits a tumor suppressive role in PTC [100]. Similarly, a previous study concerning pancreatic tumor has stated that TET1 and 5hmc are reduced in the tumor cells and inhibit EMT by altering the Wnt signaling cascade upon binding to the secreted frizzled-related protein 2 (SFRP2) promoter [101]. Thus, mitoepigenetics can affect both pro-tumorigenic and anti-tumorigenic properties of cells.

2.4. Mutations in the complexes of the electron transport chain (ETC)

Complex I (NADH dehydrogenase) is enriched with seven mtDNA subunit genes, namely *ND1, ND2, ND3, ND4, ND4L, ND5*, *ND6,* and their associated mutations are mostly related to tumorigenesis [102]. A research study demonstrated that Complex I malfunction can lead to tumorigenesis upon inducing oxidative stress and activation of the AKT pathway. Moreover, the investigation by the same group has revealed that mutations in mtDNA encoded by the Complex I *ND5* gene have increased the apoptotic rate and resistance capacity of cancer cells [103]. MT-ND1 mutations have been associated with the recurrence of renal cell carcinoma after surgery [104]. MT-ND5 mutations have increased ROS production that epigenetically modulates apoptotic pathways to transform cells into pro-cancerous phenotypes [105]. The *CYTB* subunit gene is the only gene encoded by mtDNA in Complex III and has been associated with fewer somatic mutations. However, urothelial cell carcinoma patients are an exception to this as Complex III has been observed to be more affected than in other cancers [106]. Complex IV (cytochrome C oxidase) is composed of three genes encoded by mtDNA *COX1, COX2, and COX3*. Specific mutations in mtDNA causing structural changes to Complex IV have been observed in colon cancer patients where substitutions of Ser458Pro and Gly125Asp in subunit I of Complex IV occur and affect proteins, ions, and metabolite transport. Lastly, in Complex V, two mtDNA encoded genes, namely *ATP6* and *ATP8* in which *ATP6* have been observed to be more prone to undergo mutations than *ATP8* in breast cancer [107].

The mitochondrial enzymes in the ETC accumulate to form supramolecular assemblies known as supercomplexes. The most common and widely accepted form of supercomplexes is the respirasome. Although the three components, i.e. complex I, II, and IV, can function individually, they can also aggregate to form the supercomplexes to promote catalysis by channeling the metabolic intermediates from complex to complex in a more efficient manner. These supercomplexes are also associated with cancer. For instance, it has been recently evaluated that PDAC respiratory supercomplexes potentiate mitochondrial activity, which in turn promotes cancer growth in a highly hypoxic environment [108]. Mitochondrial supercomplexes have also been associated with tumorigenicity of endometrial and breast cancers where COX7RP/-COX7A2L/SCAF1, a stabilizing factor for mitochondrial supercomplex, remain overexpressed in the tumors. Metabolomic analysis revealed that specifically COX7RP modulates the metabolic status in the cancer cells and stimulates their growth [109]. Similarly, overexpression of COX7RP has induced tumor cell growth and promoted EMT by facilitating ROS production and activation of the nuclear transcription factor-κB (NF-κB) pathway in HCC cells [110]. In $HER2^{high}$ metastatic breast cancer, targeting mitochondrial supercomplexes could be a potent anti-cancer therapeutic strategy upon targeting complex I via Mitotam, which in turn elevates the ROS level and promotes cell death [111].

3. Effect of miRNAs on mitochondria

A family of small non-coding RNAs (miRNAs) called mitomiRs serves as crosstalk mediators between the mitochondria and the nucleus, which can highly regulate the functions of mitochondria including mitophagy, and also impact mitochondrial fusion and fission processes. Mitochondria have their own genetic system and serve as a potent site for mitomiRs mediating post-transcriptional regulation. A total of 57 miRNAs have been evaluated by *Bandiera et al.* in the cytosolic fractions and mitochondria of HeLa cells, out of which 13 miRNAs are nuclear coded. The characterization of their genomic context, cross-species conservation, and intrinsic features such as their size and thermodynamic parameters signify their localization in the mitochondria [112]. It has been observed that mitomiRs can target several mitochondrial mRNAs, rRNAs, and tRNAs along with mitochondria-associated mRNAs encoded by the nucleus, thereby indicating their involvement in mitochondrial regulation [113].

In both ER-negative and ER-positive breast cancer cells, miR-195 acts as a modulator of mitochondrial dynamics and associated functions. It influences the mitochondria to undergo a fission event by targeting and decreasing mitofusin 2 (MFN2) and optic atrophy 1 (OPA1), while increasing dynamin-related protein 1 (DRP1) expression [114]. Furthermore, the Fis1 protein located on the outer mitochondrial

membrane (OMM) is regulated by oncomiR-484 and influences mitochondrial fusion by increasing its level when the cells undergo apoptosis [115,116]. miR-200–3p, a member of the miR-200 family, has been observed to be differentially expressed in different cancers and regulates the process of tumorigenesis. However, it exhibits some intrinsic role in mitochondrial dynamics by promoting mitochondrial fission via targeting mitochondrial fission factor (MFF) and thus elevating basal respiratory rate and mitochondrial membrane potential [117]. Furthermore, *Li et al.* have shown that in gastric cancer, miR-148a-3p induces mitochondrial fission and suppresses cytoprotective autophagy, thereby increasing the cytotoxicity levels of cisplatin [118]. MiR-494 has been shown to reduce the growth of renal cancer cells by increasing multilamellar bodies, lipid droplets, and mitochondrial changes. The changes in mitochondria, including

Drp1 localization and reduced PINK1 protein, have been involved in altering mitochondrial structural patterns [119]. It has also been observed that miR-484 inhibits mitochondrial fission and apoptosis by targeting the Fis1 protein in adrenocortical cancer cells and cardiomyocytes [116].

MitomiRs also perform a crucial role in driving the process of mitophagy. They play a role in tumor suppression as well as in tumor promotion (Table 2). For instance, it has been observed that in breast cancer stem cells, miR-137 suppresses mitophagy by negatively targeting the FUN14 domain containing 1 (FUNDC1), NIP-3-like protein X (NIX), and LC3-II. This elevates mitochondrial biogenesis and bioenergetics, whereas it decreases ROS level and cell apoptosis to induce tumor growth in breast cancer [120]. On the other hand, *Zhang et al.* have shown that overexpressed miR-1 performs a tumor suppressive role in breast cancer by inducing mitophagy after targeting mitophagy-associated genes including MINOS1 (mitochondrial inner membrane organizing system 1), GPD2 (glycerol-3-phosphate dehydrogenase 2), and LRPPRC (leucine-rich pentatricopeptide-repeat containing) [121]. The lack of unambiguous molecular targets in cancer clinical treatment remains a challenge despite tremendous research. Mitochondrial health and altered metabolism are hallmarks of a new arena of research. Thus, evaluating miRs and mito-miRs and their impacts on mitochondria can offer potential new approaches to clinical treatment.

4. Effect of exosomes on mitochondrial metabolism

Extracellular vesicles, namely exosomes are the key intermediates between various cells present in the tumor microenvironment (TME), which help in developing a pre-metastatic niche for the migrating tumor cells [134]. Cancer-associated fibroblasts (CAFs), one of the major components of TME, release exosomes, which when internalized by the cancer cells, drive regulatory changes in their metabolism. For instance, in prostate and pancreatic cancers, the CAFs derived exosomes inhibit mitochondrial oxidative metabolism and increase the glycolytic rate by supplying essential metabolites [135]. There is evidence suggesting that exosomal contents also participate in regulating mitochondrial metabolism. Exosomes, derived from human melanoma cells, are enriched in miR-155 as well as miR-210. Upon internalization by the stromal cells, they induce the cells to undergo metabolic reprogramming by suppressing OXPHOS and enhancing aerobic glycolysis, thereby promoting a pre-metastatic niche formation [136]. According to *Bland et al.* the exosomes derived from melanoma cells altered the transcriptomics of T cells, which influences their mitochondrial respiration [137]. Furthermore, melanoma-derived exosomes could induce apoptosis of $CD4^+$ T cells by activating caspase-3, caspase-7, and caspase-9 but not caspase-8, indicating that these exosomes activate mitochondrial apoptotic pathway probably through their cargoes like miR- 690 [138]. Small nucleolar RNA host gene 3 (SNHG3), a new lncRNA, has been observed to be overexpressed in breast cancer cells. It positively regulates PKM expression by acting as a sponge for miR-330–5p. Additionally, it minimizes mitochondrial OXPHOS, elevates glycolysis and thereby promotes the proliferation of breast cancer cells [139]. Hypoxia-induced tumor derived exosomes enhance OXPHOS in bone marrow-derived macrophages by transferring let-7a miRNA, resulting in inhibition of the insulin-Akt-mTOR signaling pathway. This suggests that exosomes are capable of modifying the immunometabolic profile of monocytes-macrophages, which in turn facilitates tumor progression upon escaping host immunity [140]. In breast cancer, the extracellular

Table 2
Role of mitomiRs in cancer.

MitomiRs	Cancer	Mechanism of action	Ref
miR-17–3p	Prostate Cancer	Inhibits manganese superoxide dismutase (MnSOD), glutathione peroxidase 2 (Gpx2), and thioredoxin reductase 2 (TrxR2), increase ROS accumulation in cancer cells and enhances radiosensitivity	[122]
miR-195	Breast cancer	Targets polypeptide 1 (CYP27B1), that occurs in the internal mitochondrial membrane which remains upregulated in breast cancer and reduced proliferation, invasion and migration.	[123]
miR-761	Hepatocellular carcinoma	Targets MFN2 and downregulates it which hampers the apoptosis inducing capacity of MFN2.	[124]
miR-483–5p	Tongue squamous cell carcinoma (TSCC)	Targets FIS1 protein and dysregulates its apoptosis inducing capacity and decreases cisplatin sensitiveness.	[125–127]
miR-2392		Regulates cisplatin resistance and induces apoptosis. Inhibited polycistronic mtDNA transcription in a cell-specific manner.	
miR-5787		Its downregulation induces cisplatin resistance and affect oxidative phosphorylation and aerobic glycolysis by inhibiting translation of mitochondrial *cytochrome c oxidase subunit 3* (*MT-COX3*).	
miR-210	Colorectal cancer	Induces apoptosis by a ROS dependent mechanism	[128]
miR-98	Bladder cancer	Targets LASS2 and regulates bladder cancer chemoresistance through modulation of mitochondrial function	[129]
miR-210	Lung cancer	Targets SDH complex of ETC and regulates cell metabolism and survival by modulating of HIF-1 activity	[130]
miR-31	Oral carcinoma	Targets SIRT3 and induced cell proliferation and invasion by disturbing mitochondrial membrane potential and generating ROS	[131]
miR-26b	Laryngeal cancer	Targets activating transcription factor (ATF) 2 by inhibiting its phosphorylation under the cisplatin treatment and induces mitochondrial apoptosis	[132]
miR-181a-5p	Liver cancer	Targets the *cytochrome B* (*mt-CYB*) and *cytochrome C oxidase II* (*mt-COX2*) genes thereby modulating ETC which results in decreased mitochondrial membrane potential and reprogramming of glucose metabolism occur	[133]

vesicles released by the cancer cells mediate the crosstalk with normal epithelial cells. These interactions activate mitochondrial dynamics, increase organelle accumulation, and promote mitochondrial movements in the host epithelial cells which in turn influence the EMT markers in hypoxic TME [141]. In-depth studies are required in this field to further understand the fast emerging importance of cancer-derived exosomes on mitochondrial metabolism.

5. Mitochondrial dynamics

According to recent studies, genetic screening and live cell imaging have revealed that mitochondria are not stable organelles. In the cytoplasm, mitochondria not only change their position but also change their shape by two opposing mechanisms called mitochondrial fission and fusion (Fig. 1). A perfect balance between these two opposing mechanisms is referred to as "mitochondrial dynamics", and it maintains the shape and size of mitochondria. Mitochondrial fusion is the generation of an interconnected mitochondrion from two parental mitochondria, and fission is the division of one mitochondrion into two daughter mitochondria. Mainly two GTPase proteins namely, MFN1 and MFN2 and OPA1, a large GTPase located at the inner mitochondrial membrane (IMM), are responsible for the fusion of the OMM and the IMM respectively [142]. On the other hand, another set of proteins namely Drp1 and dynamin 2 (DNM2), regulate the fission of mitochondria. Apart from this mechanism, electron microscopy of mitochondria has revealed numerous infoldings called cristae, which were previously thought to be stable structures, but later they were found to be extensively dynamic as they can restructure themselves by elongation, shortening, fusion, division, and detachment of mitochondrial inner boundary membrane (IBM) very rapidly depending on the cellular conditions. The key molecules involved in the cristae dynamics and crista junctions (CJs) are the mitochondrial contact site and cristae organizing system (MICOS) complex, OPA1, F1Fo ATP synthase, and the lipid microenvironment [143].

Mitochondrial fusion occurs by the docking of the outer membranes of the two mitochondria to increase the surface of contact and decrease the distance between them, followed by the tethering of the adjacent layers. Mitochondrial fission and fusion have become great aspects of research to understand all the biological processes such as apoptosis, and mitochondrial transposition. Guanosine triphosphate (GTP) hydrolysis induces the conformational change for the final fusion of OMM [144,145]. MFN1 is involved in GTP- dependent mitochondrial membrane tethering but MFN2 not only participates in membrane tethering, but also regulates mitochondrial-endoplasmic reticulum membrane contact site tethering. According to MFN topology, OMM tethering occurs between the trans-HR2 or GTPase domain of MFN situated on the outer surface of opposing mitochondria, followed by a conformational change induced by GTP hydrolysis that ultimately results in fusion [146]. The IMM fusion happens with the help of OPA1-dependent GTP hydrolysis. In mitochondrial fission, the recruited Drp1 forms a ring-like structure in OMM around the mitochondria and narrows the membrane, followed by GTP hydrolysis to increase membrane constriction. Drp1 oligomerizes at the middle domain to form Drp-oligomeric helices that start from two different points of the mitochondrial membrane and always maintain a balance between the dimeric and oligomeric forms in the cytosol and mitochondrial membrane, respectively [147–149].

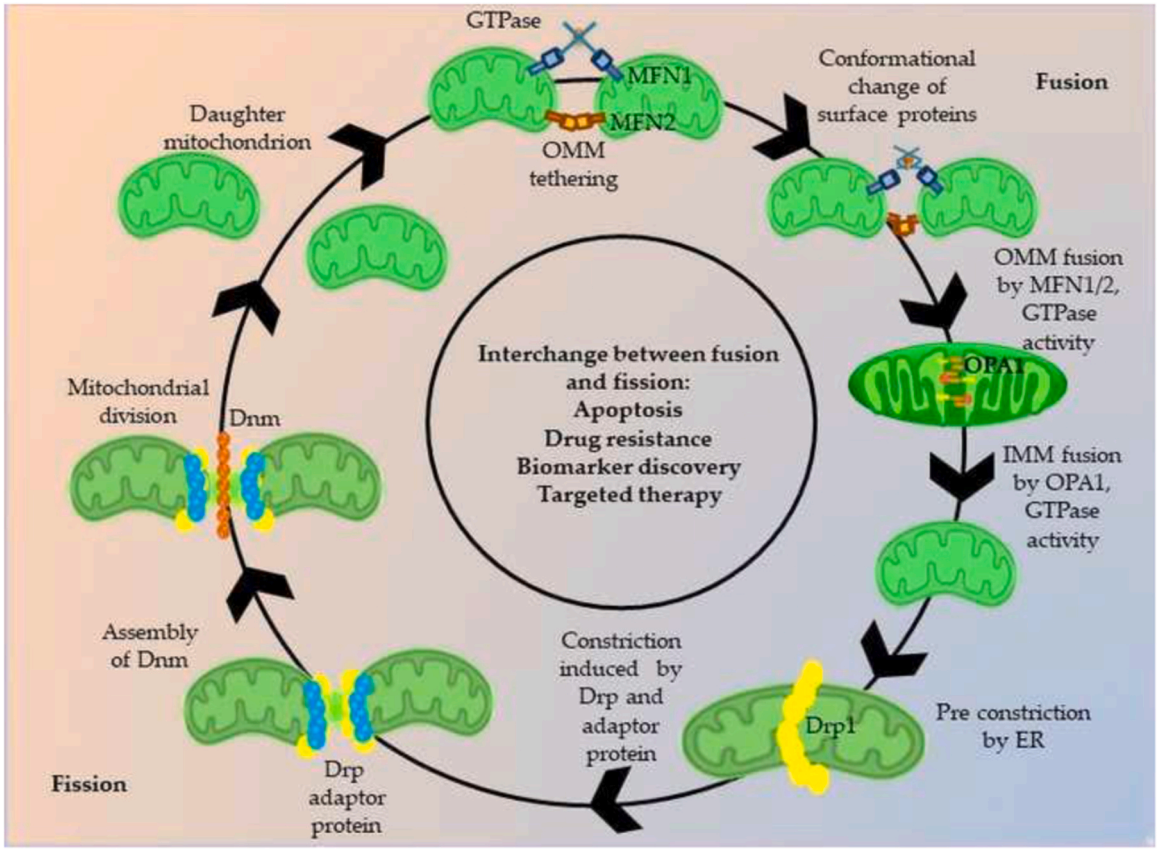

Fig. 1. Mitochondrial fusion and fission. The fusion of mitochondria occurs in both outer and inner membrane. The tethering of OMM is led by either homotypic (MFN1- MFN1/MFN2-MFN2) or heterotypic interactions (MFN1-MFN2) and GTPase leads to the fusion of two opposing mitochondrial membranes. Then the IMM fusion is regulated by OPA1 (left) and GTPase that leads to the fusion of two mitochondria. Mitochondrial fission initiates at site which is marked by the ER and actin. The DRP1, recruited by mitochondrial adaptor protein, forms a spiral around the mitochondrion. Then the assembly of DNM results in the pinching of the mitochondrion membrane and forms two separate mitochondria (right). These two processes are interchangeable process that are responsible for apoptosis, drug resistance, biomarker discovery and targeted therapy in cancer.

Finally, DNM2 assembles and terminates the scission of the membrane in the constriction of the neck region and leads to the generation of two daughter mitochondria [150]. These fusion and fission events of mitochondria, called "mitochondrial dynamics", are not only involved in many cellular processes but also regulate cells' fate. A detailed description of mitochondrial dynamics has been extensively reviewed by *Yu et al.* [151]. An exploration of the baseline mechanisms involving different molecules that control the mitochondrial dynamics is essential to understand how defects in mitochondria are responsible for the occurrence and development of diseases related to them.

5.1. Impact of mitochondrial dynamics on cancer progression

Mitochondrial dynamics lead to the genesis and progression of various cancer types. Understanding the role of mitochondrial dynamics in cancer will enlighten new insights into mitochondria-related therapeutic approaches. Upregulation and downregulation of fusion and fission related proteins, respectively, have been observed in a variety of cancers. Moreover, the development of cancer has been related to changes in the cellular environment that in turn drive alterations in the mitochondrial dynamics of the cells, as reviewed by *Wang et al.* [152]. OSKM-induced cell reprogramming constitutes an organized series of events that starts with the downregulation of somatic cell markers. Mitochondrial dynamics play a huge role in cellular reprogramming. Studies have shown that both Drp1 total protein and Drp1-S579 phosphorylation are increased during the stochastic phase of cellular reprogramming. During this phase, activated Erk1/2 phosphorylates Drp1-S579, which induces mitochondrial fission [153]. Evidence suggests that the activity of Drp1/MFN2 varies among cancer types. An elevated expression of Drp1/MFN2 in the lung cancer cells modulated mitochondrial dynamics by promoting mitochondrial fusion, thereby arresting the cell cycle and minimizing their proliferation [154]. On the contrary, an increase in mitochondrial fission upon phosphorylation of Drp1 has been observed in brain tumor initiating cells (BTICs). Therefore, targeting activated Drp1 has been established as a targeted therapeutic approach in glioblastoma [155]. Scientists have investigated the role of mitochondrial dynamics in Ras and MAPK-driven cancers. For instance, activation and phosphorylation of Drp1 at Ser616 by ERK has promoted mitochondrial fragmentation under the effect of expressed Ras and Raf oncogenes [156,157]. In parallel research, it has been shown that ERK mediated phosphorylation and inactivation of MFN1 modulate both apoptosis and mitochondrial shape [158]. These findings demonstrated that cellular transformation demands a fragmented mitochondrial phenotype, thereby marking the importance of mitochondrial shape in cancer development. *Kong et al.* have reviewed the suppression of apoptosis and enhancement of mitochondrial fusion in chemoresistant cancer cells. They have informed that cisplatin is efficient enough to dephosphorylate Drp1 and phosphorylate p53, thereby increasing Bax translocation to mitochondria and apoptosis. However, cisplatin has reduced efficacy to enhance apoptosis by phosphorylating and dephosphorylating p53 and Drp1, respectively, in chemoresistant cells. Additionally, a shift in OPA1 has been observed in the chemoresistant cancer cells, which promotes mitofusion but reduces apoptosis [159]. Mitochondrial fission plays an important role in different stages of the cell cycle, which is one of the prime dysregulated mechanisms in cancer cells. Drp1 has been positively associated with tumor cell progression, and thus its downregulation induces ROS production in the S phase of the cell cycle, which in turn contributes to higher DNA damage. Furthermore, the downregulation of Drp1 has increased the piling up of a nearly compact mitochondrial network and thus increased the mitosis period, thereby hampering cell division [160]. Overexpressed Drp1 increases mitochondrial fission in HCC by regulating the p53/p21 and NF-κB/cyclins pathways. It also promotes cancer cell proliferation by facilitating the G1/S phase transition of the cell cycle [161]. *Huang et al.* have stated that mitochondrial fission is significantly increased due to overexpressed DNM1L compared to MFN1. It has been stated that the increased expression of DNML1 inhibits mitochondrial-dependent apoptosis and facilitates autophagy in cancer cells, which in turn contributes to the poor prognosis of the disease [27]. It has already been established that the apoptotic protein, Bax regulates mitochondrial morphology and colocalizes with MFN1 and Drp1 at the initial stages of apoptosis, which eventually become mitochondrial fragmentation sites [162].

According to the literature, mitochondrial fission has been reported to promote cell migration, autophagy, and infiltration of tumor associated macrophages (TAMs) in HCC with a higher ratio of Drp1/MFN1 expression, which has led to a poor prognosis of the disease. *In- vitro* and *in-vivo* studies have shown that elevated ROS-mediated mitochondrial fission promotes the survival of cancer cells [25]. On the contrary, the depletion of MFN1 induces the EMT transition in HCC cells [26]. Furthermore, *Li et al.* have stated that under energy-stressed conditions, mitochondria exhibit morphological changes through cristae formation, and assembly of respiratory complexes. This phenomenon enhances OXPHOS and promotes the survival of tumor cells under such conditions in HCC via regulating glucose metabolism [163].

Another study has shown that mitochondrial fusion also mediates tumor cell growth in the liver [164]. Metabolic reprogramming via mitochondrial elongation promotes the survival of HCC cells and also mediates adaptation to energy stress [163]. Previous studies have found that Drp1 is highly expressed in ovarian cancer and co-expressed with cell cycle genes that promote the proliferation of ovarian cancer cells [165]. In ovarian cancer, overexpression of OPA1 and prohibitin (PHB)2 has been associated with reduced crista width and diameter. This, along with other factors like SIRT3, coordinated to define a "mitochondrial signature" via the cAMP pathway [166]. Mitochondrial dynamics also show some effects on the chemosensitivity of cancer cells. A study has reported that in hypoxic conditions, mitochondrial fission leads to cisplatin resistance in ovarian cancer cells [167].

Piperlongumin, a phytochemical, can downregulate protein Drp1 (Ser637) phosphorylation, which regulates platinum-based resistance in ovarian cancer cells, thereby inducing apoptosis [168]. *Sambus nigra* agglutinin, a lectin, activates protein kinase B (Akt), and ERK1/2 pathway in ovarian cancer cells, which in turn stimulates Drp1 translocation. Upon translocation of Drp1, the mitochondria start gaining a fragmented phenotype, and thus mitochondrial fission induces apoptosis in the cancer cells [169]. In addition, salt-inducible kinase 2 has been shown to enhance the Warburg effect via Drp1-mediated fission in ovarian cancer cells [170]. The oncoprotein MYC indirectly inhibits YAP/TAZ coactivators and suppresses cancer development in breast cancer cells. PLD6, an OMM-localized phospholipase, mediates the activity of MYC by increasing mitochondrial fusion [170]. On the other hand, mitochondrial fission facilitates the apoptosis and drug resistance of breast cancer cells [163,171]. Liensinine, a major isoquinoline alkaloid, is an efficient inhibitor of autophagy and mitophagy when used in combination with chemotherapeutic agents like doxorubicin in breast cancer. It is capable of decreasing the viability of cancer cells and inducing apoptosis by triggering mitochondrial fission by DNM1L [30]. In invasive breast cancer cells, an upregulation of the Drp1 protein has been observed. Upon silencing Drp1, the formation of lamellipodia in the cancer cells has been restricted, thus illustrating that increased Drp1 influences the migration of the cancer cells [172]. In another study, it was determined that Drp1 not only facilitates the migration of breast cancer cells but also sensitizes the cancer cells towards cisplatin [173]. According to the literature, Drp1 inhibitors, Drpitor1 and Drpitor1a, have antineoplastic potency in breast cancer cells [174]. *Qiu et al.* have demonstrated the involvement of MICOS in OSCC, where the transcriptional factor, SOX2 upregulates the expression of dihydroorotate dehydrogenase (DHODH). DHODH stabilizes the MICOS complex to support rapid tumor growth by facilitating mitochondrial respiration [175]. Fig. 2 outlines the mechanisms related to mitochondrial dynamics and cancer progression. In addition, FAM49B is a tumor suppressor in pancreatic ductal adenocarcinomas. Knockdown

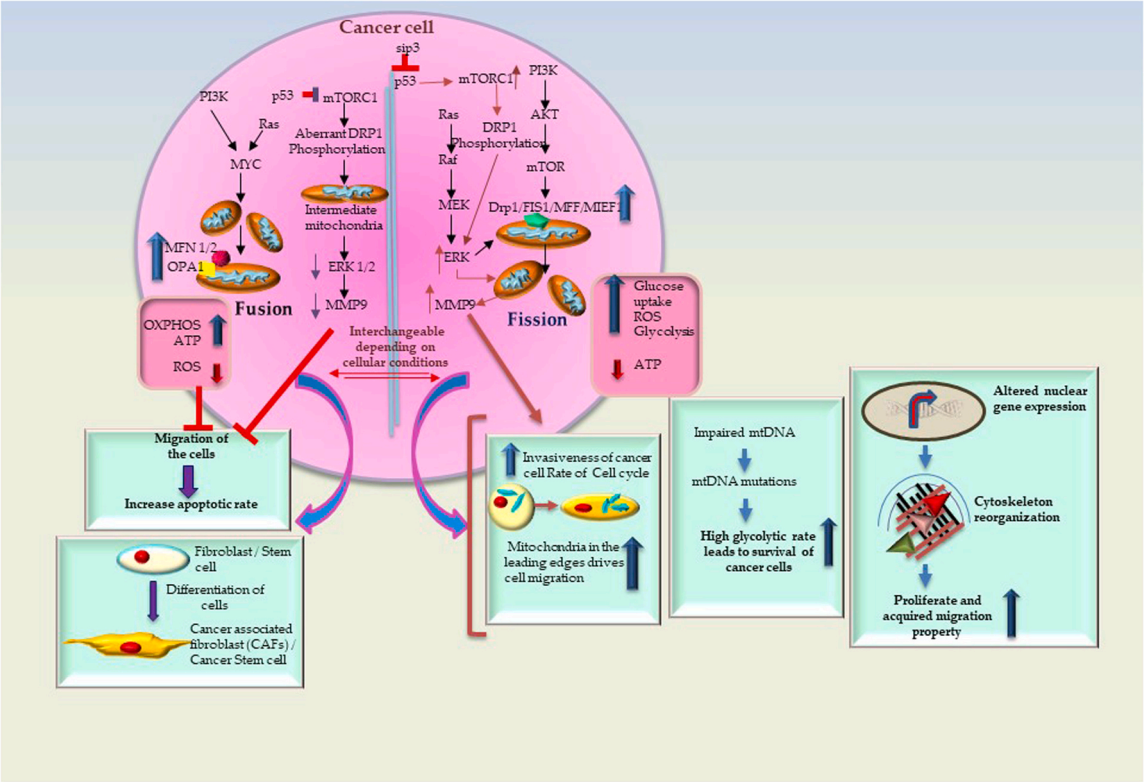

Fig. 2. Role of mitochondrial dynamics in promoting cancer. Oncogenic signaling pathways like Ras-Raf, p53 mediated mTORC1 and PI3K/AKT influences the mitochondrial dynamics in cancer cells. Ras-Raf and PI3K/AKT individually promotes mitochondrial fission which in turn increases glucose uptake, ROS generation, and decreases OXPHOS that leads to a metabolic switch to glycolysis. This results in the promotion of cell cycle, increased migrating potential as the fragmented mitochondria accumulate at the edges of the cells. It fuels the mtDNA mutations rate thereby increasing the glycolytic rate and thus promotes survival of the cancer cells. Furthermore, mitochondrial fission promotes cytoskeleton reorganization that enhances the proliferation rate and migration properties of the cancer cells. SIP3 inhibiting p53 stimulates mTORC1 pathway, phosphorylating Drp1 and enhancing ERK/MMP9 activity, thereby increasing invasiveness of cancer cells. However, fused mitochondria perform dual function, i.e. when influenced by MYC oncogenic signaling, it exhibits increased oxidative metabolism, ATP production, and decreased ROS generation and participates in cellular differentiation of fibroblasts and stem cells into cancer associated (CAFs or stem) cells that in turn aids in the tumorigenic process and mostly it promotes the apoptosis of the cells. p53 inhibiting mTORC1 causes aberrant DRP1 phosphorylation causing intermediate fusion of mitochondria which decreases ERK1/2 and MMP9 expression, thereby arresting the migration of cells.

of FAM49B induces phosphorylation of Drp1 and favors mitochondrial fission in cancer cells [32]. However, the knockdown of myoferlin induces mitochondrial fission to inhibit cancer cell proliferation in pancreatic ductal adenocarcinoma [176]. *L Fu et. al.* have shown that SIRT4 inhibits cancer progression by decreasing mitochondrial fission in NSCLC [15]. Inhibition of PIM sensitizes NSCLC cells to chemotherapy by inducing mitochondrial fragmentation [16]. Depletion of MDM2 enhances the phosphorylation of DRP1 on Ser637, which leads to increased mitochondrial fission. However, increased mitochondrial MDM2 levels increase the migration and invasiveness of cancer cells [16]. Factors related to mitochondrial dynamics have been proven to be therapeutic targets for cancer. A potent inhibitor of Drp1, namely mitochondrial division inhibitor 1 (Mdivi-1), reduces glioblastoma cell migration induced by hypoxia [177]. In gliomas, NF-κB-inducing kinase promotes mitochondrial fission and cell invasion [16].

6. Mitochondrial metabolism and cancer development

Mitochondria are not only responsible for energy production but also facilitate both anabolic and catabolic reactions to accomplish the necessities of cellular bioenergetics as well as their biogenesis. The anaplerotic pathway is considered to be a major pathway that can regulate the metabolic intermediates needed for the rapid proliferation of myeloma cells. The intermediates produced during the TCA cycle are used as a carbon source for anaplerotic activity such as the formation of α-ketoglutarate by glutaminolysis from glutamine, the production of oxaloacetate by pyruvate carboxylation from pyruvate, etc. [178–180]. Several important cellular signaling pathways like PI3K-Akt- mTORC1, K-Ras, and Myc play major roles in regulating the mitochondrial metabolism in cancer cells. Thus, enhanced glycolytic activity has been observed upon decoupling of glucose and glutamine metabolism by the oncoprotein K-Ras, which in turn utilizes a greater amount of glutamine, the carbon source for the TCA cycle [181]. PI3K-Akt signaling is often modified in tumorigenic conditions. In a cancer metabolic environment, active Akt-targeted mTORC1 modifies the energy state, and growth factors mediate cell signaling, oxygen, and nutrient availability in the cells [182]. The activation of Myc, regulated the genes involved in glutamine and glucose metabolism as well as the biogenesis of the mitochondria [183,184].

IDH1 and IDH2, two isoforms of IDH, have shown recurrent mutations in several tumors specifically glioblastoma and myeloid leukemia [185–187]. IDH has shown gain- of-function mutation effects through which α-ketoglutarate is again metabolized to an oncometabolite, i.e. 2-hydroxyglutarate and thereby deregulates the pathways that require α- ketoglutarate as a substrate [185,186,188]. These altered cascades imparted pleiotropic effects like epigenetic regulation, histone methylation, collagen synthesis, and HIF signaling which contribute to oncogenesis. As the mutated IDH1 and IDH2 are cancer cell specific, they can be potential therapeutic targets. Interestingly, highly expressed wild-type IDH2 has also been reported to protect CRC cells from oxidative stress. This has been validated when both abrogated and suppressed IDH2 induced ROS and oxidative DNA damage, resulting in

cell cycle arrest and eventually cancer cell death [189]. The tumor promoting function of overexpressed wild-type IDH2 has been evaluated in AML, where lipid synthesis is enhanced due to glutamine overconsumption upon conversion of α-ketoglutarate (α-KG) to isocitrate/citrate in the IDH2-mediated reductive TCA cycle [190].

FH and SDH are the two most important enzymes in the TCA cycle. Derivatives of fumaric and succinic acids are accumulated upon inactivation of FH and SDH, respectively, due to mutation. These metabolites, released in the cytosol, inhibit prolyl hydroxylase and either induce resistance towards apoptosis or activate the pseudohypoxic response to trigger HIF-1 mediated glycolysis [92,191]. In the case of renal carcinoma, FH has shown a loss-of- function mutation as a result of which fumarate increases and malate and citrate decrease [192]. Fumarate can exert oncogenic effects because it directly inhibits prolyl 4-hydroxylase, the negative regulator of HIF, and thus activates hypoxia signaling [193]. The inhibition of dioxygenase activity that is dependent on α-KG like 5-methylcytosine hydroxylases and histone demethylases (TET family members), fumarate, and succinate can alter DNA methylation and histone modifications [194,195]. The FH-deficient cancer cells are killed due to inhibition of the haem oxygenase activity, thus suggesting a therapeutic approach too. Mutations in the four subunits of SDH incorporated in complex II can cause cancer of the neuroendocrine system which is known as paragangliomas. Similar to fumarate, the accumulated succinate can activate HIF signaling by inhibiting prolyl 4-hydroxylase. A study has suggested that SDH-deficient cancer cells can exert extracellular pyruvate by sustaining a Warburg-like metabolic state for their survival [196].

7. Impact of mitochondrial dynamics on the metabolism and function of immune cells

The immune system is a crucial part of the cancer microenvironment and recent research has established a bridge between the role of the mitochondrial dynamics and the cancer immune system. Interestingly, mitochondrial dynamics have been observed to be associated with both innate and adaptive immune responses, which direct both cancer aggression and defense. Immune cells like NK cells and T cells are regulated by mitochondrial dynamics and perform in either tumor promotion or suppression. Moreover, mitochondrial dynamics are involved in the escape of tumor cells from immune surveillance in the TME. Differentiation and functioning of immune cells mostly rely upon mitochondria- driven metabolism which circumvents ATP production and catalyses macromolecules. Several mitochondrial mechanisms are closely associated with the polarization and functioning of several immune cells. Mitochondrial dynamics interchanges the cross-talk within immune cells that regulates cellular functions and triggers an immune response. Recent pieces of literature have shown that not only metabolism but mitochondria also regulate the immune cells transcriptionally by mtDNA and mtROS production.

Mitochondria and immunity are interlinked in various ways. Firstly, changes in aerobic and anaerobic mitochondrial metabolic pathways affect immune cell functionalities. For instance, proinflammatory macrophages possess a discontinued TCA cycle whereas anti- inflammatory macrophages are dependent upon β-oxidation [197,198]. Secondly, activation of the inflammatory anti-viral response can be activated by mitochondria through the NLR family pyrin domain containing 3 (NLRP3) pathway [199,200] in which MFN1 attenuates the NLRP3 inflammasome activation. Downregulation of Drp1 has also been observed during inflammasome activation, which shows mitochondrial fission augmented inflammatory response through the NLRP3 pathway [200,201]. Thirdly, mitochondrial fission and fusion influence the functions of immune cells. Finally, mitochondria and endoplasmic reticulum (ER) being in close proximity to each other, interact with each other for different signaling pathways, which in turn influence immune cell metabolism. However, *Bao et al.* have demonstrated that mtDNA stress caused by the release of mtDNA into the cell cytoplasm under the effect of Drp1-mediated fission induces infiltration and polarization of TAMs by enhancing the CCL2 secretion from HCC cells by TLR9-mediated NF-κB signaling pathway [202]. Mitochondrial dynamics are involved in cancer by regulating the immune system in various ways, such as the formation of the inflammasome, M2 polarization, and modulating the T cell profile. Fig. 3 illustrates how mitochondrial dynamics contribute to modulating the altered immune responses, with special respect to cancer.

7.1. Mitochondrial dynamics and polarization of T cells

Cellular behavior is also regulated by mitochondrial dynamics, especially in T cells' repertoire. The activation and polarization of T cells crucially depend on mitochondrial metabolism as T cells use glucose as the primary fuel to generate ATP. T cell proliferation and differentiation mainly depend on glycolysis, OXPHOS, fatty acid oxidation (FAO), and amino acid metabolism. Upon stimulation by several signal activators like interleukins, cluster molecules that activates T cell receptors, enhance glucose uptake and increase glycolytic rate via the induction of Akt-PI3K-signaling [203]. The Akt pathway upregulates the expression of glucose transporters (Glut1) on the surface of the T cell membrane and enhances the uptake of glucose [204]. Downregulation of glucose metabolism in T cells results in a reduced level of cytokines, followed by an altered immune response and cell death. Glycolysis and FAO, occurring in mitochondria, highly control the polarization and activation of T cell subtypes. T cell subtypes (Th1, Th2, and Th17) not only show increased glycolysis but also express a higher level of Glut1. On the other hand, memory T cells and regulatory T cells depend on FAO with lower Glut1 expression [205]. Besides this, metabolomic data analysis has shown that intercellular L-arginine increases OXPHOS in activated T cells together with anti-tumor activity and also promotes the generation of memory T cells [206]. Another essential metabolite, L-tryptophan (trp), an important source of nicotinamide (NAD) synthesis, helps in CD4+ T cell differentiation. Depletion of Trp promotes T cell apoptosis due to increased L-kynurenine, facilitating immune tolerance [206]. Moreover, the activation and differentiation of T cell phenotypes are facilitated by mitochondrial dynamics along with changes in their mass, number, and mtDNA content. Drp1 also helps in the activation of a proper T cell repertoire, thereby controlling mitochondrialmetabolismto activate T_E cells by reducing the OXPHOS rate [207]. Conversely, OPA1 induces OXPHOS and FAO to generate memory-like T cells as an anti-tumor response triggered by mitochondrial fusion [208]. In cancer cells, the blockage of PGC1α-mediated mitochondrial biogenesis influences the cancer-specific T_E cells to lose their mitochondrial functions, which in turn leads to a considerable reduction in their number. The inhibition of PGC1α is due to the activation of AKT signaling and reduces the anti-tumor activity of the T cells [141]. *Menk et al.* have suggested that the co-stimulation of 4–1BB which is highly expressed in exhausted T cells, increased mitochondrial fusion and activated the p38-MAPK cascade, which in turn influenced the PGC1α-mediated pathways in cancer [209]. Dephosphorylation of serine637 in Drp1 by mitochondrial phosphatase phosphoglycerate mutase5 has facilitated the production of cytokines in NKT cells [210]. The chemotaxis of the lymphocytes has been facilitated by mitochondrial fission which relocates the organelles to promote the migration of lymphocytes [211]. This has validated that the T cell activation and differentiation in TME directly or indirectly relies on the mitochondrial dynamics. It has been observed that in nasopharyngeal carcinoma, T cells acquire an exhaustion phenotype with lower expression of MFN1. This has resulted in lower ATP production and decreased mitochondrial OXPHOS activity under hypoxic conditions [212]. Thus, mitochondrial dynamics may be involved in modulating the immune response in TME.

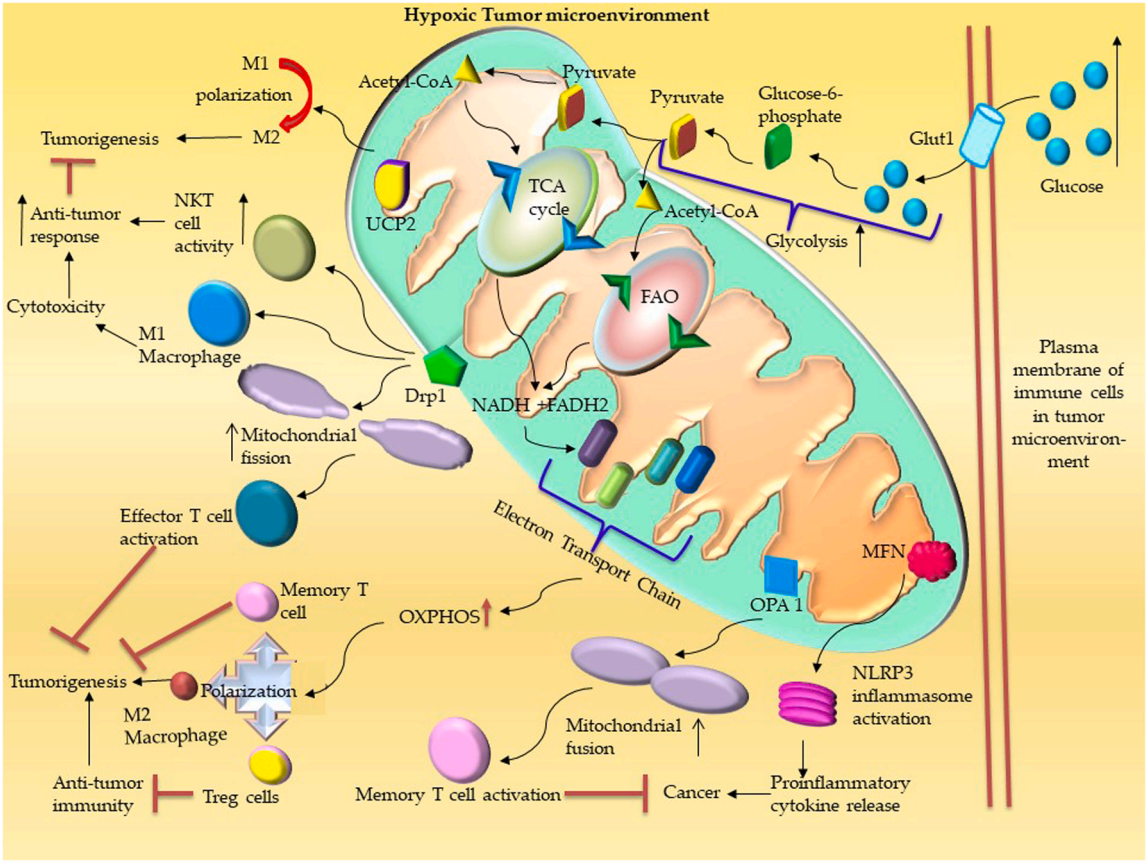

Fig. 3. Impact of mitochondrial dynamics on immune cells. Increase in glycolysis in cancer cells is initiated by increased uptake of glucose molecules via GLUT1 and produce the by- products like pyruvate and acetyl-CoA in high amount that in turn enters metabolic mechanisms like the TCA cycle and FAO. NADH and FADH2 produced from TCA cycle and FAO enters the ETC which results in increased OXPHOS. OXPHOS further facilitates the polarization of immune cells like M2 macrophages (promotes tumorigenesis), memory T cells (inhibit tumorigenesis), Tregs (suppress antitumor immunity). Mitochondrial proteins like DRP1, OPA1, UCP2, MFN also helps in activation and increase the respective functionality of various immune cells like NKT cells (increase anti-tumor response, polarization of M1 to M2 phenotype (promote tumorigenesis), memory T cells and NLRP3 inflammasome activation that increase proinflammatory cytokine release thereby promoting cancer. DRP1 also aids in mitochondrial fission event which in turn helps in activation of effector T cells that inhibits tumorigenesis.

7.2. Impact of mitochondrial dynamics on the innate immune system and polarization of macrophages in cancer

Mitochondrial dynamics has an interesting role in TME, which regulates the cells of the innate immune system. Innate immune cells such as dendritic cells, natural killer (NK) cells, and macrophages recognize damage-associated molecular patterns (DAMPs), secreted by tumor cells, via pattern-recognition receptors (PRRs). These show proinflammatory activity through the formation of inflammasomes and secrete proinflammatory cytokines such as IL- 1β, and IL-10. Interestingly, mitochondria play an important role in the formation of an inflammasome. MFN-2 acted as a docking site for the interaction with NLRP3 to promote inflammasome assembly [200,201]. Mitochondrial dynamics may have some impact on NK cells as well. As there is an established study on the role of Drp1-mediated mitochondrial fission in T cell synapse formation [213], thus it can be assumed that mitochondrial fission has the same function in tumor-NK-cell contact site (NK cell immune synapse). Mitochondrial dynamics play an important role in macrophage polarization. Metabolic variability is found in the subtypes of macrophages. The classically activated macrophages of the M1 phenotype, stimulated by IFN-γ, mainly rely on glycolysis [214]. On the other hand, alternatively activated macrophages, or M2 phenotype, stimulated by IL-4 or IL-13, have high β oxidation and OXPHOS metabolism level [214]. Glutaminolysis is another important metabolism that causes the synthesis of ketoglutarate which directs macrophages into the M2 phenotype [215].

Mitochondrial dynamics differentiate monocytes into macrophages and further subtypes upon polarization. A high NOS level inhibits mitochondrial fusion to facilitate M1 polarization [216]. Mitochondrial uncoupling protein (UCP) 2, present in the IMM along with matrix shuttle proteins, polarizes macrophages into the M2 phenotype by controlling ROS levels [217]. The classically activated macrophages are associated with mitochondrial fission whereas the alternatively activated macrophages are related to mitochondrial fusion. Drp1 in M2 macrophages increases the level of L-lactate, a major product in glycolysis, stimulates M1 polarization, and also helps in the CCL2/CCR2 mediated chemotaxis of macrophages [218]. The knockout of FAM73b (also known as mitoguradin 2), a mitochondrial outer membrane fusion protein, induces TLR (toll-like receptor)- mediated IL-12 production and inhibits the secretion of IL-10 and IL-13 by macrophages and dendritic cells to facilitate an antitumor immune response [219]. mtDNA acts as DAMPs that induce the oligomerization of the inflammasome and, in turn, facilitate the activation of macrophages. M2 macrophages play a crucial role in metastatic niche formation by facilitating tumor cell growth and proliferation and also immunosuppression by inhibiting NK cell and T cell activity in TME [220]. Taken together, mitochondrial fusion proteins which are involved in M2 polarization can be therapeutic targets in cancer. In nutshell, mitochondrial dynamics play a crucial role in cancer by regulating innate immune cells, but a more detailed study is needed to understand the proper regulatory mechanisms.

8. Targeting mitochondria for anti-cancer therapy: an insight into Mitocans

Mitochondria play a key role in tumor development and promotion as they are the main regulator of the intrinsic apoptosis pathway, which remains dormant at the time of tumor generation and gains resistance properties. In addition to this, mutations in mtDNA and preeminent ROS levels are the major factors that increase tumor occurrence [221]. Under such circumstances, targeting mitochondria as an anti-tumor treatment strategy has come into focus in recent era. For specific and targeted delivery of drugs to the mitochondria, some small molecules with unique features like lipophilicity, positive potential, etc. and those with increased potential to interact with the mitochondrial membrane or with increased affinity for substances released by mitochondria are being used. An outstanding representation of Mitocans has been elucidated by *Neuzil et al.,* where a vivid classification of Mitocans has been provided based on their mode of action [222]. Table 3 encompasses some important drugs used for targeting mitochondria.

Positively charged lipophilic small molecules, e.g. tetraphenylphosphonium (TPP) carrying doxorubicin, have been used to treat breast cancer cells, resulting in increased cellular uptake and the reversal of multidrug resistance (MDR). Furthermore, increased levels of caspase 3 and PARP, induced apoptosis in the cells [234]. Small molecule ligands like glycyrrhetinic acid, an active ingredient extracted from the root of the traditional herb licorice, are potent in delivering a drug to the mitochondrial matrix of HCC cells through 4-fold higher cellular internalization and 8.8-fold higher accumulation in mitochondria [235]. Other than this, peptide-based drug delivery molecules like TAT (RKKRRQRRR) and R8 (RRR RRR RR), mitochondrial target sequences in combination with cell-penetrating peptides like TAT, mitochondrial penetrating peptides like Szeto–Schiller (SS) peptides, vehicle-based mitochondrial targeting modes like MITO-porter, and mesoporous silicon nanoparticles have been used for greater cellular internalization and targeted delivery of drugs [236]. Apart from this, microbial metabolites or cellular components have also been observed to attenuate cancer cells. As evaluated by *Chatterjee et al.,* leishmanial lipid performs an anti-neoplastic role in AML via the mitochondrial-regulated MAPK pathway [237]. Parallelly, attenuated *L. donovani* has been observed to exhibit a cytotoxic effect on HCC cells via the ROS-mediated p53-dependent mitochondrial pathway [238].

An increase in the accumulation of doxorubicin in mitochondria enhances mtROS production, thereby inducing cellular apoptosis by increasing caspase levels and also hampering the ETC components of the cancer cells [239,240]. Mitochondrial targeting has also been associated with the reversal of MDR. For instance, membrane penetrating peptide modified doxorubicin coupled with HPMA polymers proved to be efficient in drug transfer into resistant breast cancer cells. It has also increased mtROS production and minimized drug efflux, and thus decreasing resistant cell growth [241]. MDR has also been reversed by combining mitochondrial targeting and photodynamic therapy (PDT), where the monocarboxylate transporters present on the OMM facilitate the selective distribution of lipid membrane-coated inorganic silica-carbon nanoparticles (LSC-NPs) loaded with doxorubicin in the mitochondria. This increases mtROS production, which oxidizes the NADH into NAD+ to deploy the ATP required for drug efflux and thus reverses MDR to inhibit the growth of the resistant tumor cells and cancer stem cells [242]. Evidence also suggests mitochondrial targeting for anti-metastatic activities, e.g. *Wang et al.* have found that the cuprous oxide nanoparticles without chemical modification could selectively distribute in tumor cell mitochondria, which in turn activates the apoptotic proteins caspase 3 and caspase 9 and releases cytochrome C thus minimizing lung metastasis of melanoma cells [243] [244]. Furthermore, targeting mitochondrial cancer metabolism has emerged as a new anticancer treatment strategy. *Yang et al.* have shown that reversal from glycolysis to glucose oxidation occurs when dichloroacetate conjugated with mitochondria-targeted rhenium (I) complex

Table 3
Drugs targeting mitochondria for anti-cancer treatment.

Drug	Mechanism of action	Cancer types	Drug status	Ref
Enasidenib	Inhibits mutated IDH2 and blocks DNA and histone hypermethylation in AML	AML	Clinical	[223]
Mito Tam	Inhibits Complex I, increase ROS and causes death of cancer cells in breast cancer	Breast cancer	Clinical	[107]
ME-344	It induced apoptosis by inhibiting heme-oxygenase 1.	Lung cancer	Investigational	[224]
ME-143 and ME-344	Targets complex I subunit NDUFA9, as well as the complex IV subunit COXIV and induces cancer cell death by disrupting metabolism	Osteosarcoma and cervical cancer	Investigational	[225]
Cyclopamine tartrate (CycT)	Induced apoptosis by suppressing oxygen consumption in lung cancer cells. Increased ROS generation, mitochondrial membrane hyperpolarization, and mitochondrial fragmentation	Lung cancer	Investigational	[226]
Tigecycline	Inhibits mitochondrial protein translation and inhibit anchorage dependent growth of K-Ras mutant cancer cells	AML	Clinical	[227, 228]
VLX600	Reduces mitochondrial respiration or OXPHOS and reduces the growth of cancer cells	Colon cancer	Investigational	[229]
Gamitrinib	Disassembles mitochondrial integrity and ATPase activity of Tumor Necrosis Factor Receptor-Associated Protein-1 (TRAP-1) Induces apoptosis prostate cancer cells by accumulating in the cells	Prostate cancer	Investigational	[230, 231]
Gboxin	Inhibits the activity of F0F1 ATP synthase (Complex V) affecting OXPHOS in glioblastoma cells	Glioblastoma multiforme	Investigational	[232]
Deguilin	Reduces oxygen consumption by inhibiting Complex I in vemurafenib-resistant melanoma cells and thus inhibits their growth	Melanoma	Investigational	[233]

efficiently accumulates in the mitochondria and selectively destroys the cancer cells co- cultured with the normal cells by targeting pyruvate dehydrogenase kinase, which attenuates tumor invasion [245]. Mitochondrial targeting for immunotherapy is a new therapeutic approach. *Chen et al.* have shown that inducing mitochondrial stress with a designed organic photosensitizer (named TPE-DPA-TCyP) results in large scale immunogenic cell death [246]. Parallelly, exogenous exosomes can also target the mitochondria to constrain the growth of cancer cells. For instance, macrophage-derived exosomal miR-503–3p reduces the glycolytic rate, and increases mitochondrial OXPHOS for which DACT2 is overexpressed and inhibits the Wnt/β-catenin pathway to limit the growth of breast cancer cells [247]. CAFs derived exosomes when cultured with prostate cancer cells, significantly reduce OXPHOS. Moreover, exosomal miRNAs target OXPHOS genes, thereby determining that exogenous exosomes modulate mitochondrial activity to promote tumor growth and can be targeted as an anti-cancer strategy [135]. *Bland et al.* have evaluated that CTLL2 cells when treated with exogenous exosomes derived from B16Fo cells increase the gene expression associated with mitochondrial activity and increase mitochondrial respiration despite the lack of substrate and oxygen [248]. Interaction of breast cancer cell derived exosomes with normal human primary mammary epithelial cells has revealed that internalization of the exosomes induces ROS in the recipient cells and initiates autophagy. This results in the secretion of breast cancer promoting factors from the transformed recipient cells, which can be targeted for anti-cancer therapy [249]. To sum up, mitochondrial targeting as an anti-cancer treatment strategy has gained a lot of focus in recent years, and further investigations are required to explore this field with more attempts and efforts to combat cancer.

9. Discussion

A plethora of mitochondrial dysfunctions occurring due to mutations in mtDNA, altered expression of mitochondrial proteins and enzymes, along with the impact of mitoepigenetics in cancer have been elucidated in this review along with some mitochondrial targeted treatment strategies. Furthermore, this review also summarizes information on the effect of mitochondrial dynamics in transformed cells and their effect on the various immune cells that drive the progression of cancer. Signaling pathways from mitochondria to the nucleus occurring in the cytosol are generally activated under the effect of these mitochondrial alterations, which results in altered gene expression in the nucleus that fuels tumorigenesis [250]. The baseline alterations in mitochondrial dynamics mark possibilities not only for hampering immune cells, but also causing malfunctions in normal mitochondrial functionalities. A detailed understanding of the oncogenic signaling occurring in mitochondria can depict the undetected somatic and germline mutations that are essential to attenuate the tumorigenicity by targeting them. The emerging research on exosomes and their effects on mitochondrial metabolism will be an innovative field of study for anti-cancer treatment strategies. Moreover, in the era of personalized medicine, an extensive study is adopted worldwide to study and target mitochondrial dynamics to develop fruitful anti-cancer therapy. The detection of mitochondrial mutations at different levels, and the varied expression of mitochondria-related factors and proteins, will serve as signature indicators for cancer development. Thus, studies on mitochondria driven cancers provide opportunities for researchers to investigate new factors responsible for cancer development and progression.

Since cancer is convoluted and heterogeneous in nature, therapeutic approaches may vary based on several factors, including genetic/epigenetic, metabolic, environmental, lifestyle, and others. Mitochondria serve as a source of metabolites for various biosynthetic pathways, like fatty acid metabolism. However, alterations in the mitochondrial proteins can drive tumorigenesis by generating oncometabolites and helping the cancer cells survive in hypoxic and nutrient depleted TME. The study of these alterations in mitochondrial dynamics exhibited by tumor cells is essential for novel drug discovery for antitumor therapy. Research into the mechanisms of apoptosis and mitophagy has focused on the regulations of mitochondrial fission and fusion machinery for a detailed study of the physiological processes. Elucidation of the underlying molecular mechanisms involved in these processes will be critical for a better understanding of mammalian mitochondrial dynamics. However, a great challenge lies in elucidating the expression of mitochondrial proteins and genes in various types of cancer. In other words, identification of the specific induced or inhibited proteins related to mitochondrial dynamics in cancer cells in response to multiple stimuli that might help in fighting tumor cells remains a challenge. Questions remain about the link between metabolic heterogeneity and cancer cell migration due to alterations in mitochondrial dynamics. The evaluation of mitochondrial dynamics in the metabolic regulations of the stem cells and how they contribute to tumorigenesis still needs to be addressed. Identification of the mechanisms involving the actin cytoskeleton, ER, and mitochondrial proteins that contribute to the mitochondrial division also remain as challenges to developing targetable treatment strategies. The establishment of potent mitochondrial proteins as diagnostic or prognostic markers, depending on their expression and activity, is an essential area of ongoing research. Future discoveries in these areas have implications for cancer and will also impact our knowledge of fundamental cell biology.

Funding

Not applicable

Declaration of Competing Interest

Authors declare that no conflict of interest exist for this publication.

Data availability

No data was used for the research described in the article.

Acknowledgements

We are thankful to our Director, Chittaranjan National Cancer, Kolkata for his support and encouragement to complete this scientific input. We are thankful to UGC and CSIR for providing student fellowships.

CRediT authorship contributions statement

All authors have contributed equally to the writing as well as drafting of the manuscript. All authors have approved the final version of the manuscript.

Institutional review board statement

Not applicable.

Informed consent statement

Not applicable.

References

[1] Z.W. Zhang, J. Cheng, F. Xu, Y.E. Chen, J.B. Du, M. Yuan, F. Zhu, X.C. Xu, S. Yuan, Red blood cell extrudes nucleus and mitochondria against oxidative stress, IUBMB Life. 63 (2011) 560–565, https://doi.org/10.1002/iub.490.
[2] H.A. Prag, M.P. Murphy, mtDNA mutations help support cancer cells, Nat. Cancer 1 (2020) 941–942, https://doi.org/10.1038/s43018-020-00128-x.
[3] S. Nik-Zainal, H. Davies, J. Staaf, M. Ramakrishna, D. Glodzik, X. Zou, I. Martincorena, L.B. Alexandrov, S. Martin, D.C. Wedge, P. Van Loo, Y.S. Ju, M. Smid, A.B. Brinkman, S. Morganella, M.R. Aure, O.C. Lingjærde, A. Langerød, M. Ringnér, S.M. Ahn, S. Boyault, J.E. Brock, A. Broeks, A. Butler, C. Desmedt, L. Dirix, S. Dronov, A. Fatima, J.A. Foekens, M. Gerstung, G.K.J. Hooijer, S.

J. Jang, D.R. Jones, H.Y. Kim, T.A. King, S. Krishnamurthy, H.J. Lee, J.Y. Lee, Y. Li, S. McLaren, A. Menzies, V. Mustonen, S. O'Meara, I. Pauporté, X. Pivot, C. A. Purdie, K. Raine, K. Ramakrishnan, F.G. Rodríguez-González, G. Romieu, A. M. Sieuwerts, P.T. Simpson, R. Shepherd, L. Stebbings, O.A. Stefansson, J. Teague, S. Tommasi, I. Treilleux, G.G. Van Den Eynden, P. Vermeulen, A. Vincent-Salomon, L. Yates, C. Caldas, L.V. t Veer, A. Tutt, S. Knappskog, B.K. T. Tan, J. Jonkers, Å. Borg, N.T. Ueno, C. Sotiriou, A. Viari, P.A. Futreal, P. J. Campbell, P.N. Span, S. Van Laere, S.R. Lakhani, J.E. Eyfjord, A.M. Thompson, E. Birney, H.G. Stunnenberg, M.J. Van De Vijver, J.W.M. Martens, A.L. Børresen-Dale, A.L. Richardson, G. Kong, G. Thomas, M.R. Stratton, Landscape of somatic mutations in 560 breast cancer whole-genome sequences, Nature 534 (2016) 47–54, https://doi.org/10.1038/nature17676.

[4] J. Vinagre, A. Almeida, H. Pópulo, R. Batista, J. Lyra, V. Pinto, R. Coelho, R. Celestino, H. Prazeres, L. Lima, M. Melo, A.G. Da Rocha, A. Preto, P. Castro, L. Castro, F. Pardal, J.M. Lopes, L.L. Santos, R.M. Reis, J. Cameselle-Teijeiro, M. Sobrinho-Simões, J. Lima, V. Máximo, P. Soares, Frequency of TERT promoter mutations in human cancers, Nat. Commun. 4 (2013), https://doi.org/10.1038/ncomms3185.

[5] Y.S. eo Ju, L.B. Alexandrov, M. Gerstung, I. Martincorena, S. Nik-Zainal, M. Ramakrishna, H.R. Davies, E. Papaemmanuil, G. Gundem, A. Shlien, N. Bolli, S. Behjati, P.S. Tarpey, J. Nangalia, C.E. Massie, A.P. Butler, J.W. Teague, G. S. Vassiliou, A.R. Green, M.Q. Du, A. Unnikrishnan, J.E. Pimanda, B.T. ea Teh, N. Munshi, M. Greaves, P. Vyas, A.K. El-Naggar, T. Santarius, V.P. Collins, R. Grundy, J.A. Taylor, D.N. Hayes, D. Malkin, C.S. Foster, A.Y. Warren, H. C. Whitaker, D. Brewer, R. Eeles, C. Cooper, D. Neal, T. Visakorpi, W.B. Isaacs, G. S. Bova, A.M. Flanagan, P.A. Futreal, A.G. Lynch, P.F. Chinnery, U. McDermott, M.R. Stratton, P.J. Campbell, Origins and functional consequences of somatic mitochondrial DNA mutations in human cancer, Elife 3 (2014) e02935, https://doi.org/10.7554/eLife.02935.

[6] A.R. Choudhury, K.K. Singh, Mitochondrial determinants of cancer health disparities, Semin. Cancer Biol. 47 (2017) 125–146, https://doi.org/10.1016/j.semcancer.2017.05.001.

[7] M. Yu. Somatic Mitochondrial DNA Mutations in Human Cancers, 1st ed., Elsevier Inc, 2012 https://doi.org/10.1016/B978-0-12-394384-2.00004-8.

[8] A. Cormio, F. Sanguedolce, C. Musicco, V. Pesce, G. Calò, P. Bufo, G. Carrieri, L. Cormio, Mitochondrial dysfunctions in bladder cancer: exploring their role as disease markers and potential therapeutic targets, Crit. Rev. Oncol. Hematol. 117 (2017) 67–72, https://doi.org/10.1016/j.critrevonc.2017.07.001.

[9] M. Mo, F. Peng, L. Wang, L. Peng, G. Lan, S. Yu, Roles of mitochondrial transcription factor A and microRNA-590-3p in the development of bladder cancer, Oncol. Lett. 6 (2013) 617–623, https://doi.org/10.3892/ol.2013.1419.

[10] J. Boultwood, C. Fidler, K.I. Mills, P.M. Frodsham, R. Kusec, A. Gaiger, R.E. Gale, D.C. Linch, T.J. Littlewood, P.A.H. Moss, J.S. Wainscoat, Amplification of mitochondrial DNA in acute myeloid leukaemia, Br. J. Haematol. 95 (1996) 426–431, https://doi.org/10.1046/j.1365-2141.1996.d01-1922.x.

[11] M. Saadaoui, L. Aissaoui, V. Salaun, M. Manai, S. Allouche, Mitochondrial DNA alterations and oxidative stress in acute leukemia, Open Leuk. J. 5 (2013) 1–6, https://doi.org/10.2174/1876816420130418001.

[12] L.F. Araujo, A.D.D. Siena, J.R. Plaça, D.B. Brotto, I.I. Barros, B.R. Muys, C.A. O. Biagi, K.C. Peronni, J.F. Sousa, G.A. Molfetta, L.C. West, A.P. West, A. M. Leopoldino, E.M. Espreafico, W.A. Silva, Mitochondrial transcription factor A (TFAM) shapes metabolic and invasion gene signatures in melanoma, Sci. Rep. 8 (2018) 14190, https://doi.org/10.1038/s41598-018-31170-6.

[13] D. Xie, X. Wu, L. Lan, F. Shangguan, X. Lin, F. Chen, S. Xu, Y. Zhang, Z. Chen, K. Huang, R. Wang, L. Wang, X. Song, Y. Liu, B. Lu, Downregulation of TFAM inhibits the tumorigenesis of non-small cell lung cancer by activating ROS-mediated JNK/p38MAPK signaling and reducing cellular bioenergetics, Oncotarget 7 (2016) 11609–11624, https://doi.org/10.18632/oncotarget.7018.

[14] M. Qi, D. Dai, J. Liu, Z. Li, P. Liang, Y. Wang, L. Cheng, Y. Zhan, Z. An, Y. Song, Y. Yang, X. Yan, H. Xiao, H. Shao, AIM2 promotes the development of non-small cell lung cancer by modulating mitochondrial dynamics, Oncogene 39 (2020) 2707–2723, https://doi.org/10.1038/s41388-020-1176-9.

[15] L. Fu, Q. Dong, J. He, X. Wang, J. Xing, E. Wang, X. Qiu, Q. Li, SIRT4 inhibits malignancy progression of NSCLCs, through mitochondrial dynamics mediated by the ERK-Drp1 pathway, Oncogene 36 (2017) 2724–2736, https://doi.org/10.1038/onc.2016.425.

[16] 2 Shailender S. Chauhan1, Rachel K. Toth2, Corbin C. Jensen3, Andrea L. Casillas3, David F. Kashatus4, Noel A. Warfel1, PIM kinases alter mitochondrial dynamics and chemosensitivity in lung cancer, Methods Mol. Biol. 39 (2020) 2597–2611, https://doi.org/10.1038/s41388-020-1168-9.PIM.

[17] H. Liu, S. Li, X. Liu, Y. Chen, H. Deng, S.I.R.T.3 Overexpression, Inhibits growth of kidney tumor cells and enhances mitochondrial biogenesis, J. Proteome Res. 17 (2018) 3143–3152, https://doi.org/10.1021/acs.jproteome.8b00260.

[18] H. Tong, L. Zhang, J. Gao, S. Wen, H. Zhou, S. Feng, Methylation of mitochondrial DNA displacement loop region regulates mitochondrial copy number in colorectal cancer, Mol. Med. Rep. 16 (2017) 5347–5353, https://doi.org/10.3892/mmr.2017.7264.

[19] C.Y. Huang, S.F. Chiang, W.T.L. Chen, T.W. Ke, T.W. Chen, Y.S. You, C.Y. Lin, K.S. C. Chao, C.Y. Huang, HMGB1 promotes ERK-mediated mitochondrial Drp1 phosphorylation for chemoresistance through RAGE in colorectal cancer, Cell Death Dis. 9 (2018), https://doi.org/10.1038/s41419-018-1019-6.

[20] M. Chen, K. Ye, B. Zhang, Q. Xin, P. Li, A.N. Kong, X. Wen, J. Yang, Paris Saponin II inhibits colorectal carcinogenesis by regulating mitochondrial fission and NF-κB pathway, Pharmacol. Res. 139 (2019) 273–285, https://doi.org/10.1016/j.phrs.2018.11.029.

[21] A. Aminuddin, P.Y. Ng, C.O. Leong, E.W. Chua, Mitochondrial DNA alterations may influence the cisplatin responsiveness of oral squamous cell carcinoma, Sci. Rep. 10 (2020) 7885, https://doi.org/10.1038/s41598-020-64664-3.

[22] W. Guo, D. Yang, H. Xu, Y. Zhang, J. Huang, Z. Yang, X. Chen, Z. Huang, Mutations in the D-loop region and increased copy number of mitochondrial DNA in human laryngeal squamous cell carcinoma, Mol. Biol. Rep. 40 (2013) 13–20, https://doi.org/10.1007/s11033-012-1939-7.

[23] C.S. Lin, L.T. Liu, L.H. Ou, S.C. Pan, C.I. Lin, Y.H. Wei, Role of mitochondrial function in the invasiveness of human colon cancer cells, Oncol. Rep. 39 (2018) 316–330, https://doi.org/10.3892/or.2017.6087.

[24] M. Torrens-Mas, R. Hernández-López, D.G. Pons, P. Roca, J. Oliver, J. Sastre-Serra, Sirtuin 3 silencing impairs mitochondrial biogenesis and metabolism in colon cancer cells, Am. J. Physiol. - Cell Physiol. 317 (2019) C398–C404, https://doi.org/10.1152/ajpcell.00112.2019.

[25] Xiacheng Sun, Haiyan Cao, Lei Zhan, Mitochondrial fission promotes cell migration by Ca2+/CaMKII/ERK/FAK pathway in hepatocellular carcinoma, Liver Int. (2017), https://doi.org/10.1111/liv.13660.

[26] Z. Zhang, T.E. Li, M. Chen, D. Xu, Y. Zhu, B.Y. Hu, Z.F. Lin, J.J. Pan, X. Wang, C. Wu, Y. Zheng, L. Lu, H.L. Jia, S. Gao, Q.Z. Dong, L.X. Qin, MFN1-dependent alteration of mitochondrial dynamics drives hepatocellular carcinoma metastasis by glucose metabolic reprogramming, Br. J. Cancer 122 (2020) 209–220, https://doi.org/10.1038/s41416-019-0658-4.

[27] Q. Huang, L. Zhan, H. Cao, J. Li, Y. Lyu, X. Guo, J. Zhang, L. Ji, T. Ren, J. An, B. Liu, Y. Nie, J. Xing, Increased mitochondrial fission promotes autophagy and hepatocellular carcinoma cell survival through the ROS-modulated coordinated regulation of the NFKB and TP53 pathways, Autophagy 12 (2016) 999–1014, https://doi.org/10.1080/15548627.2016.1166318.

[28] L. Chen, J. Zhang, Z. Lyu, Y. Chen, X. Ji, H. Cao, M. Jin, J. Zhu, J. Yang, R. Ling, J. Xing, T. Ren, Y. Lyu, Positive feedback loop between mitochondrial fission and Notch signaling promotes survivin-mediated survival of TNBC cells, Cell Death Dis. 9 (2018), https://doi.org/10.1038/s41419-018-1083-y.

[29] V. Tomková, C. Sandoval-Acuña, N. Torrealba, J. Truksa, Mitochondrial fragmentation, elevated mitochondrial superoxide and respiratory supercomplexes disassembly is connected with the tamoxifen-resistant phenotype of breast cancer cells, Free Radic. Biol. Med. 143 (2019) 510–521, https://doi.org/10.1016/j.freeradbiomed.2019.09.004.

[30] J. Zhou, G. Li, Y. Zheng, H.M. Shen, X. Hu, Q.L. Ming, C. Huang, P. Li, N. Gao, A novel autophagy/mitophagy inhibitor liensinine sensitizes breast cancer cells to chemotherapy through DNM1L-mediated mitochondrial fission, Autophagy 11 (2015) 1259–1279, https://doi.org/10.1080/15548627.2015.1056970.

[31] (and) D.F.K. Jennifer A. Kashatus1, 4, Aldo Nascimento1, 4, Lindsey J. Myers1, Annie Sher2, Frances L. Byrne3, Kyle L. Hoehn3, Christopher M. Counter2, Erk2 phosphorylation of Drp1 promotes mitochondrial fission and MAPK-driven tumor growth, Physiol. Behav. 176 (2017) 139–148, https://doi.org/10.1016/j.molcel.2015.01.002.Erk2.

[32] M.S. Chattaragada, C. Riganti, M. Sassoe, M. Principe, M.M. Santamorena, C. Roux, C. Curcio, A. Evangelista, P. Allavena, R. Salvia, B. Rusev, A. Scarpa, P. Cappello, F. Novelli, FAM49B, a novel regulator of mitochondrial function and integrity that suppresses tumor metastasis, Oncogene 37 (2018) 697–709, https://doi.org/10.1038/onc.2017.358.

[33] G. Civenni, R. Bosotti, A. Timpanaro, R. Vàzquez, J. Merulla, S. Pandit, S. Rossi, D. Albino, S. Allegrini, A. Mitra, S.N. Mapelli, L. Vierling, M. Giurdanella, M. Marchetti, A. Paganoni, A. Rinaldi, M. Losa, E. Mira-Catò, R. D'Antuono, D. Morone, K. Rezai, G. D'Ambrosio, L.H. Ouafik, S. Mackenzie, M.E. Riveiro, E. Cvitkovic, G.M. Carbone, C.V. Catapano, Epigenetic control of mitochondrial fission enables self-renewal of stem-like tumor cells in human prostate cancer, e6, Cell Metab. 30 (2019) 303–318, https://doi.org/10.1016/j.cmet.2019.05.004.

[34] X. Jin, J. Wang, K. Gao, P. Zhang, L. Yao, Y. Tang, L. Tang, J. Ma, J. Xiao, E. Zhang, J. Zhu, B. Zhang, S.M. Zhao, Y. Li, S. Ren, H. Huang, L. Yu, C. Wang, Dysregulation of INF2-mediated mitochondrial fission in SPOP-mutated prostate cancer, PLoS Genet 13 (2017) 1–24, https://doi.org/10.1371/journal.pgen.1006748.

[35] J. Cai, J. Wang, Y. Huang, H. Wu, T. Xia, J. Xiao, X. Chen, H. Li, Y. Qiu, Y. Wang, T. Wang, H. Xia, Q. Zhang, A.P. Xiang, ERK/Drp1-dependent mitochondrial fission is involved in the MSC-induced drug resistance of T-cell acute lymphoblastic leukemia cells, e2459-11, Cell Death Dis. 7 (2016), https://doi.org/10.1038/cddis.2016.370.

[36] S. Pei, M. Minhajuddin, B. Adane, N. Khan, M. Brett, S.C. Mack, S. Lai, J.N. Rich, A. Inguva, M. Kevin, H. Kim, A. Tan, J.R. Myers, J.M. Ashton, D.A. Pollyea, C. A. Smith, C.T. Jordan, AMPK/FIS1-mediated mitophagy is required for self-renewal of human AML stem cells 23 (2018) 86–100, https://doi.org/10.1016/j.stem.2018.05.021.AMPK/FIS1-mediated.

[37] R.S. Malhi, H.M. Mortensen, J.A. Eshleman, B.M. Kemp, J.G. Lorenz, F.A. Kaestle, J.R. Johnson, C. Gorodezky, D.G. Smith, Native American mtDNA prehistory in the American Southwest, Am. J. Phys. Anthropol. 120 (2003) 108–124, https://doi.org/10.1002/ajpa.10138.

[38] L.M. Booker, G.M. Habermacher, B.C. Jessie, Q.C. Sun, A.K. Baumann, M. Amin, S.D. Lim, C. Fernandez-Golarz, R.H. Lyles, M.D. Brown, F.F. Marshall, J.A. Petros, North American white mitochondrial haplogroups in prostate and renal cancer, J. Urol. 175 (2006) 468–473, https://doi.org/10.1016/S0022-5347(05)00163-1.

[39] K. Darvishi, S. Sharma, A.K. Bhat, E. Rai, R.N.K. Bamezai, Mitochondrial DNA G10398A polymorphism imparts maternal Haplogroup N a risk for breast and esophageal cancer, Cancer Lett. 249 (2007) 249–255, https://doi.org/10.1016/j.canlet.2006.09.005.

[40] M.A. Earp, A. Brooks-Wilson, L. Cook, N. Le, Inherited common variants in mitochondrial DNA and invasive serous epithelial ovarian cancer risk, BMC Res. Notes 6 (2013) 425, https://doi.org/10.1186/1756-0500-6-425.
[41] Y. Li, K.B. Beckman, C. Caberto, R. Kazma, A. Lum-Jones, C.A. Haiman, L. Le Marchand, D.O. Stram, R. Saxena, I. Cheng, Association of genes, pathways, and haplogroups of the mitochondrial genome with the risk of colorectal cancer: the multiethnic cohort, PLoS One 10 (2015) e0136796, https://doi.org/10.1371/journal.pone.0136796.
[42] H.A. Yacoub, W.M. Mahmoud, H.A.E. El-Baz, O.M. Eid, R.I. El-Fayoumi, M. M. Mahmoud, S. Harakeh, O.H.A. Abuzinadah, New haplotypes of the ATP synthase subunit 6 gene of mitochondrial DNA are associated with acute lymphoblastic leukemia in Saudi Arabia, Asian Pac. J. Cancer Prev. 15 (2014) 10433–10438, https://doi.org/10.7314/APJCP.2014.15.23.10433.
[43] K.K. Singh, V. Ayyasamy, K.M. Owens, M.S. Koul, M. Vujcic, B. Life, S. Building, C. Streets, Mutat. mitochondrial DNA Polym. γ Promot. Breast Tumor 54 (2009) 516–524, https://doi.org/10.1038/jhg.2009.71.Mutations.
[44] M. Blomberg Jensen, H. Leffers, J.H. Petersen, G. Daugaard, N.E. Skakkebaek, E. Rajpert-De Meyts, Association of the polymorphism of the CAG repeat in the mitochondrial DNA polymerase gamma gene (POLG) with testicular germ-cell cancer, Ann. Oncol. 19 (2008) 1910–1914, https://doi.org/10.1093/annonc/mdn407.
[45] S.N.L. Guo, J, L. Zheng, L. Wang, Z. Wang, Z. Wang, A.J. French, D. Kang, L. Chen, Thibodeau, Frequent Truncating Mutation of TFAM Induces Mitochondrial DNA Depletion and Apoptotic Resistance in Microsatellite- Unstable Colorectal Cancer, Bone 23 (2008) 1–7, https://doi.org/10.1158/0008-5472.CAN-10-3482.Frequent.
[46] S. Datta, A. Ray, R. Roy, B. Roy, Association of DNA sequence variation in mitochondrial DNA polymerase with mitochondrial DNA synthesis and risk of oral cancer, Gene 575 (2016) 650–654, https://doi.org/10.1016/j.gene.2015.09.039.
[47] O. Popanda, P. Seibold, I. Nikolov, C.C. Oakes, B. Burwinkel, S. Hausmann, D. Flesch- Janys, C. Plass, J. Chang-Claude, P. Schmezer, Germline variants of base excision repair genes and breast cancer: a polymorphism in DNA polymerase gamma modifies gene expression and breast cancer risk, Int. J. Cancer 132 (2013) 55–62, https://doi.org/10.1002/ijc.27665.
[48] J. Xu, Xue Li, Mengzhi Hu, Jun Chen, Zheng Yu, Jinyu Dong, Yan Sun, Chengtao Han, Somatic mitochondrial DNA D - loop mutations in meningioma discovered: A preliminary data A comprehensive overview of mitochondrial, DNA 4977-bp, J. Cancer Res. Ther. 14 (2018) 1525–1534, https://doi.org/10.4103/jcrt.JCRT.
[49] S.D. Cline, Mitochondrial DNA damage and its consequences for mitochondrial gene expression, Biochim. Biophys. Acta - Gene Regul. Mech. 1819 (2012) 979–991, https://doi.org/10.1016/j.bbagrm.2012.06.002.
[50] R.T. Yuan, Y. Sun, L.X. Bu, M.Y. Jia, Gene mutations in the D-loop region of mitochondrial DNA in oral squamous cell carcinoma, Mol. Med. Rep. 11 (2015) 4496–4500, https://doi.org/10.3892/mmr.2015.3240.
[51] J.C. Lin, C.C. Wang, R.S. Jiang, W.Y. Wang, S.A. Liu, Impact of somatic mutations in the D-Loop of mitochondrial DNA on the survival of oral squamous cell carcinoma patients, PLoS One 10 (2015) e0124322, https://doi.org/10.1371/journal.pone.0124322.
[52] Y.B. Zhao, H.Y. Yang, X.W. Zhang, G.Y. Chen, Mutation in D-loop region of mitochondrial DNA in gastric cancer and its significance, World J. Gastroenterol. 11 (2005) 3304–3306, https://doi.org/10.3748/wjg.v11.i21.3304.
[53] B. Yacoubi Loueslati, W. Troudi, L. Cherni, K.B. Rhomdhane, L. Mota-Vieira, Germline HVR-II mitochondrial polymorphisms associated with breast cancer in Tunisian women. Genet. Mol. Res. 9 (2010) 1690–1700, https://doi.org/10.4238/vol9-3gmr778.
[54] C.W. Liou, T.K. Lin, J.B. Chen, M.M. Tiao, S.W. Weng, S.D. Chen, Y.C. Chuang, J. H. Chuang, P.W. Wang, Association between a common mitochondrial DNA D-loop polycytosine variant and alteration of mitochondrial copy number in human peripheral blood cells, J. Med. Genet. 47 (2010) 723–728, https://doi.org/10.1136/jmg.2010.077552.
[55] V.W.S. Liu, Y. Wang, H.J. Yang, P.C.K. Tsang, T.Y. Ng, L.C. Wong, P. Nagley, H.Y. S. Ngan, Mitochondrial DNA variant 16189T>C is associated with susceptibility to endometrial cancer, Hum. Mutat. 22 (2003) 173–174, https://doi.org/10.1002/humu.10244.
[56] M. Lueth, L. Wronski, A. Giese, R. Kirschner-Schwabe, T. Pietsch, A. von Deimling, G. Henze, A. Kurtz, P.H. Driever, Somatic mitochondrial mutations in pilocytic astrocytoma, Cancer Genet. Cytogenet. 192 (2009) 30–35, https://doi.org/10.1016/j.cancergencyto.2009.03.002.
[57] N.R. Tipirisetti, S. Govatati, P. Pullari, S. Malempati, M.K. Thupurani, S. Perugu, P. Guruvaiah, L. Rao K, R.R. Digumarti, V. Nallanchakravarthula, M. Bhanoori, V. Satti, Mitochondrial control region alterations and breast cancer risk: A study in south Indian population, PLoS One 9 (2014) 1–8, https://doi.org/10.1371/journal.pone.0085363.
[58] T.T. Kenny, P. Hart, M. Ragazzi, M. Sersinghe, J. Chipuk, M.A.K. Sagar, K. K. Eliceiri, T. LaFramboise, S. Grandhi, J. Santos, A.A. Riar, L. Papa, M. D'Aurello, G. Manfredi, M.M. Bonini, D. Germain, Selected mitochondrial DNA landscapes activate the SIRT3 axis of the UPRmt to promote metastasis, Oncogene 36 (2017) 4393–4404, https://doi.org/10.1038/onc.2017.52.
[59] J.A. Petros, A.K. Baumann, E. Ruiz-Pesini, M.B. Amin, C.Q. Sun, J. Hall, S.D. Lim, M.M. Issa, W.D. Flanders, S.H. Hosseini, F.F. Marshall, D.C. Wallace, MtDNA mutations increase tumorigenicity in prostate cancer, Proc. Natl. Acad. Sci. U. S. A. 102 (2005) 719–724, https://doi.org/10.1073/pnas.0408894102.
[60] K. Polyak, Y. Li, H. Zhu, C. Lengauer, J.K.V. Willson, S.D. Markowitz, M.A. Trush, K.W. Kinzler, B. Vogelstein, Somatic mutations of the mitochondrial genome in human colorectal tumours, Nat. Genet. 20 (1998) 291–293, https://doi.org/10.1038/3108.
[61] D.J. Tan, J. Chang, W.L. Chen, L.J. Agress, K.T. Yeh, B. Wang, L.J.C. Wong, Novel heteroplasmic frameshift and missense somatic mitochondrial DNA mutations in oral cancer of betel quid chewers, Genes Chromosom. Cancer 37 (2003) 186–194, https://doi.org/10.1002/gcc.10217.
[62] J.F. Hopkins, R.E. Denroche, J.A. Aguiar, F. Notta, A.A. Connor, J.M. Wilson, L. D. Stein, S. Gallinger, P.C. Boutros, Mutations in mitochondrial DNA from pancreatic ductal adenocarcinomas associate with survival times of patients and accumulate as tumors progress, e5, Gastroenterology 154 (2018) 1620–1624, https://doi.org/10.1053/j.gastro.2018.01.029.
[63] A.L.M. Smith, J.C. Whitehall, C. Bradshaw, D. Gay, F. Robertson, A.P. Blain, G. Hudson, A. Pyle, D. Houghton, M. Hunt, J.N. Sampson, C. Stamp, G. Mallett, S. Amarnath, J. Leslie, F. Oakley, L. Wilson, A. Baker, O.M. Russell, R. Johnson, C. A. Richardson, B. Gupta, I. McCallum, S.A.C. McDonald, S. Kelly, J.C. Mathers, R. Heer, R.W. Taylor, N.D. Perkins, D.M. Turnbull, O.J. Sansom, L.C. Greaves, Age-associated mitochondrial DNA mutations cause metabolic remodeling that contributes to accelerated intestinal tumorigenesis, Nat. Cancer 1 (2020) 976–989, https://doi.org/10.1038/s43018-020-00112-5.
[64] N. Koshikawa, M. Akimoto, J.I. Hayashi, H. Nagase, K. Takenaga, Association of predicted pathogenic mutations in mitochondrial ND genes with distant metastasis in NSCLC and colon cancer, Sci. Rep. 7 (2017) 15535, https://doi.org/10.1038/s41598-017-15592-2.
[65] R.S. Arnold, S.A. Fedewa, M. Goodman, A.O. Osunkoya, H.T. Kissick, C. Morrissey, L.D. True, J.A. Petros, Bone metastasis in prostate cancer: Recurring mitochondrial DNA mutation reveals selective pressure exerted by the bone microenvironment, Bone 78 (2015) 81–86, https://doi.org/10.1016/j.bone.2015.04.046.
[66] B. Kleist, T. Meurer, M. Poetsch, Mitochondrial DNA alteration in primary and metastatic colorectal cancer: Different frequency and association with selected clinicopathological and molecular markers, 1010428317692246, Tumour Biol. 39 (2017), https://doi.org/10.1177/1010428317692246.
[67] D.J. Tan, R.K. Bai, L.J.C. Wong, Comprehensive scanning of somatic mitochondrial DNA mutations in breast cancer, Cancer Res 62 (2002) 972–976.
[68] V.W.S. Liu, H. Hui Shi, A.N.Y. Cheung, P. Man Chiu, T.W. Leung, P. Nagley, L. Wong Wong, H.Y.S. Ngan, High incidence of somatic mitochondrial DNA mutations in human ovarian carcinomas, Cancer Res 61 (2001) 5998–6001.
[69] K.K. Abu-Amero, A.S. Alzahrani, M. Zou, Y. Shi, High frequency of somatic mitochondrial DNA mutations in human thyroid carcinomas and complex I respiratory defect in thyroid cancer cell lines, Oncogene 24 (2005) 1455–1460, https://doi.org/10.1038/sj.onc.1208292.
[70] X. Li, X. Guo, D. Li, X. Du, C. Yin, C. Chen, W. Fang, Z. Bian, J. Zhang, B. Li, H. Yang, J. Xing, Multi-regional sequencing reveals intratumor heterogeneity and positive selection of somatic mtDNA mutations in hepatocellular carcinoma and colorectal cancer, Int. J. Cancer 143 (2018) 1143–1152, https://doi.org/10.1002/ijc.31395.
[71] J.F. Hopkins, V.Y. Sabelnykova, J. Weischenfeldt, R. Simon, J.A. Aguiar, R. Alkallas, L.E. Heisler, J. Zhang, J.D. Watson, M.L.K. Chua, M. Fraser, F. Favero, C. Lawerenz, C. Plass, G. Sauter, J.D. McPherson, T. Van Der Kwast, J. Korbel, T. Schlomm, R.G. Bristow, P.C. Boutros, Mitochondrial mutations drive prostate cancer aggression, Nat. Commun. 8 (2017), https://doi.org/10.1038/s41467-017-00377-y.
[72] F. Guerra, A.M. Perrone, I. Kurelac, D. Santini, C. Ceccarelli, M. Cricca, C. Zamagni, P. De Iaco, G. Gasparre, Mitochondrial DNA mutation in serous ovarian cancer: Implications for mitochondria-coded genes in chemoresistance, J. Clin. Oncol. 30 (2012) e373–e378, https://doi.org/10.1200/JCO.2012.43.5933.
[73] L. Iommarini, I. Kurelac, M. Capristo, M.A. Calvaruso, V. Giorgio, C. Bergamini, A. Ghelli, P. Nanni, C. De giovanni, V. Carelli, R. Fato, P.L. Lollini, M. Rugolo, G. Gasparre, A.M. Porcelli, Different mtDNA mutations modify tumor progression in dependence of the degree of respiratory complex I impairment, Hum. Mol. Genet. 23 (2014) 1453–1466, https://doi.org/10.1093/hmg/ddt533.
[74] L.V. Yuzefovych, A.G. Kahn, M.A. Schuler, L. Eide, R. Arora, G.L. Wilson, M. Tan, L.I. Rachek, Mitochondrial DNA repair through OGG1 activity attenuates breast cancer progression and metastasis, Cancer Res. 76 (2016) 30–34, https://doi.org/10.1158/0008-5472.CAN-15-0692.
[75] G. Gasparre, I. Kurelac, M. Capristo, L. Iommarini, A. Ghelli, C. Ceccarelli, G. Nicoletti, P. Nanni, C. De Giovanni, K. Scotlandi, C.M. Betts, V. Carelli, P. L. Lollini, G. Romeo, M. Rugolo, A.M. Porcelli, A mutation threshold distinguishes the antitumorigenic effects of the mitochondrial gene MTND1, an Oncojanus function, Cancer Res. 71 (2011) 6220–6229, https://doi.org/10.1158/0008-5472.CAN-11-1042.
[76] G. Gasparre, G. Romeo, M. Rugolo, A.M. Porcelli, Learning from oncocytic tumors: why choose inefficient mitochondria? Biochim. Biophys. Acta - Bioenerg. 1807 (2011) 633–642, https://doi.org/10.1016/j.bbabio.2010.08.006.
[77] E. Bonora, A.M. Porcelli, G. Gasparre, A. Biondi, A. Ghelli, V. Carelli, A. Baracca, G. Tallini, A. Martinuzzi, G. Lenaz, M. Rugolo, G. Romeo, Defective oxidative phosphorylation in thyroid oncocytic carcinoma is associated with pathogenic mitochondrial DNA mutations affecting complexes I and III, Cancer Res 66 (2006) 6087–6096, https://doi.org/10.1158/0008-5472.CAN-06-0171.
[78] G. Gasparre, L. Iommarini, A.M. Porcelli, M. Lang, G.G. Ferri, I. Kurelac, R. Zuntini, E. Mariani, L.F. Pennisi, E. Pasquini, G. Pasquinelli, A. Ghelli, E. Bonora, C. Ceccarelli, M. Rugolo, N. Salfi, G. Romeo, V. Carelli, An inherited mitochondrial DNA disruptive mutation shifts to homoplasmy in oncocytic tumor cells, Hum. Mutat. 30 (2009) 391–396, https://doi.org/10.1002/humu.20870.

[79] J.A. Mayr, D. Meierhofer, F. Zimmermann, R. Feichtinger, C. Kögler, M. Ratschek, N. Schmeller, W. Sperl, B. Kofler, Loss of complex I due to mitochondrial DNA mutations in renal oncocytoma, Clin. Cancer Res 14 (2008) 2270–2275, https://doi.org/10.1158/1078-0432.CCR-07-4131.
[80] R.K. Gopal, S.E. Calvo, A.R. Shih, F.L. Chaves, D. McGuone, E. Mick, K.A. Pierce, Y. Li, A. Garofalo, E.M. Van Allen, C.B. Clish, E. Oliva, V.K. Mootha, Early loss of mitochondrial complex I and rewiring of glutathione metabolism in renal oncocytoma, Proc. Natl. Acad. Sci. U. S. A. 115 (2018) E6283–E6290, https://doi.org/10.1073/pnas.1711888115.
[81] M. De Luise, V. Guarnieri, C. Ceccarelli, L. D'Agruma, A.M. Porcelli, G. Gasparre, A nonsense mitochondrial DNA mutation associates with dysfunction of HIF1α in a von Hippel-Lindau renal oncocytoma, Oxid. Med. Cell. Longev. 2019 (2019) 1–6, https://doi.org/10.1155/2019/8069583.
[82] M. Lang, C.D. Vocke, M.J. Merino, L.S. Schmidt, W.M. Linehan, Mitochondrial DNA mutations distinguish bilateral multifocal renal oncocytomas from familial Birt-Hogg- Dubé tumors, Mod. Pathol. 28 (2015) 1458–1469, https://doi.org/10.1038/modpathol.2015.101.
[83] A. Ferreira, T.L. Serafim, V.A. Sardão, T. Cunha-Oliveira, Role of mtDNA-related mitoepigenetic phenomena in cancer, Eur. J. Clin. Invest. 45 (2015) 44–49, https://doi.org/10.1111/eci.12359.
[84] S. Mizukami, A. Yafune, Y. Watanabe, K. Nakajima, M. Jin, T. Yoshida, M. Shibutani, Identification of epigenetically downregulated Tmem70 and Ube2e2 in rat liver after 28- day treatment with hepatocarcinogenic thioacetamide showing gene product downregulation in hepatocellular preneoplastic and neoplastic lesions produced by tumor promoti, Toxicol. Lett. 266 (2017) 13–22, https://doi.org/10.1016/j.toxlet.2016.11.022.
[85] X. Han, Z. Zhao, M. Zhang, G. Li, C. Yang, F. Du, J. Wang, Y. Zhang, Y. Wang, Y. Jia, B. Li, Y. Sun, Maternal trans-general analysis of the human mitochondrial DNA pattern, Biochem. Biophys. Res. Commun. 493 (2017) 643–649, https://doi.org/10.1016/j.bbrc.2017.08.138.
[86] X. Sun, V. Vaghjiani, W.S.N. Jayasekara, J.E. Cain, J.C. St John, The degree of mitochondrial DNA methylation in tumor models of glioblastoma and osteosarcoma, Clin. Epigenetics. 10 (2018) 157, https://doi.org/10.1186/s13148-018-0590-0.
[87] A.R. Cyr, M.J. Hitchler, F.E. Domann, Regulation of SOD2 in cancer by histone modifications and CpG Methylation: Closing the loop between redox biology and epigenetics, Antioxid. Redox Signal 18 (2013) 1946–1955, https://doi.org/10.1089/ars.2012.4850.
[88] J.K. Killian, S.Y. Kim, M. Miettinen, C. Smith, M. Merino, M. Quezado, W.I.S. Jr, M.S. Jahromi, P. Xekouki, E. Szarek, R.L. Walker, J. Lasota, M. Raffeld, B. Klotzle, L. Jones, Y. Zhu, Y. Wang, J.J. Waterfall, J. Maureen, O. Sullivan, M. Bibikova, K. Pacak, C. Stratakis, A. Katherine, J.D. Schiffman, J. Fan, L. Helman, P. S. Meltzer, Succinate Dehydrogenase Mutation Underlies Global Epigenomic Divergence in Gastrointestinal Stromal Tumor, Cancer Discov. 3 (2014) 648–657, https://doi.org/10.1158/2159-8290.CD-13-0092.Succinate.
[89] M. Münzel, D. Globisch, T. Carell, 5-Hydroxymethylcytosine, the Sixth Base of the Genome, Angew. Chem. - Int. Ed. 50 (2011) 6460–6468, https://doi.org/10.1002/anie.201101547.
[90] K.D. Rasmussen, K. Helin, Role of TET enzymes in DNA methylation, development, and cancer, Genes Dev. 30 (2016) 733–750, https://doi.org/10.1101/gad.276568.115.
[91] G.P. J.S. Pfeifer, W. Xiong, M.A. Hahn, The role of 5-hydroxymethylcytosine in human cancer, Cell Tissue Res 356 (2014) 631–641, https://doi.org/10.1007/s00441-014-1896-7.
[92] A. King, M.A. Selak, E. Gottlieb, Succinate dehydrogenase and fumarate hydratase: Linking mitochondrial dysfunction and cancer, Oncogene 25 (2006) 4675–4682, https://doi.org/10.1038/sj.onc.1209594.
[93] K. Chen, J. Zhang, Z. Guo, Q. Ma, Z. Xu, Y. Zhou, Z. Xu, Z. Li, Y. Liu, X. Ye, X. Li, B. Yuan, Y. Ke, C. He, L. Zhou, J. Liu, W. Ci, Loss of 5-hydroxymethylcytosine is linked to gene body hypermethylation in kidney cancer, Cell Res 26 (2016) 103–118, https://doi.org/10.1038/cr.2015.150.
[94] M. Sun, C.X. Song, H. Huang, C.A. Frankenberger, D. Sankarasharma, S. Gomes, P. Chen, J. Chen, K.K. Chada, C. He, M.R. Rosner, HMGA2/TET1/HOXA9 signaling pathway regulates breast cancer growth and metastasis, Proc. Natl. Acad. Sci. U. S. A. 110 (2013) 9920–9925, https://doi.org/10.1073/pnas.1305172110.
[95] S.J. Song, L. Poliseno, M.S. Song, U. Ala, K. Webster, C. Ng, G. Beringer, N. J. Brikbak, X. Yuan, L.C. Cantley, A.L. Richardson, P.P. Pandolfi, MicroRNA-Antagonism Regulates Breast Cancer Stemness and Metastasis via, Cell 154 (2013) 311–324, https://doi.org/10.1016/j.cell.2013.06.026.microRNA-antagonism.
[96] M. Wielscher, W. Liou, W. Pulverer, C.F. Singer, C. Rappaport-Fuerhauser, D. Kandioler, G. Egger, A. Weinhäusel, Cytosine 5-hydroxymethylation of the LZTS1 gene is reduced in breast cancer, Transl. Oncol. 6 (2013) 715–721, https://doi.org/10.1593/tlo.13523.
[97] T. Kamiya, R. Nakahara, N. Mori, H. Hara, T. Adachi, Ten-eleven translocation 1 functions as a mediator of SOD3 expression in human lung cancer A549 cells, Free Radic. Res. 51 (2017) 329–336, https://doi.org/10.1080/10715762.2017.1313415.
[98] F. Neri, D. Dettori, D. Incarnato, A. Krepelova, S. Rapelli, M. Maldotti, C. Parlato, P. Paliogiannis, S. Oliviero, TET1 is a tumour suppressor that inhibits colon cancer growth by derepressing inhibitors of the WNT pathway, Oncogene 34 (2015) 4168–4176, https://doi.org/10.1038/onc.2014.356.
[99] H. Huang, X. Jiang, Z. Li, Y. Li, C.X. Song, C. He, M. Sun, P. Chen, S. Gurbuxani, J. Wang, G.M. Hong, A.G. Elkahloun, S. Arnovitz, J. Wang, K. Szulwach, L. Lin, C. Street, M. Wunderlich, M. Dawlaty, M.B. Neilly, R. Jaenisch, F.C. Yang, J. C. Mulloy, P. Jin, P.P. Liu, J.D. Rowley, M. Xu, C. He, J. Chen, TET1 plays an essential oncogenic role in MLL-rearranged leukemia, Proc. Natl. Acad. Sci. U. S. A. 110 (2013) 11994–11999, https://doi.org/10.1073/pnas.1310656110.
[100] S. Yu, Y. Yin, S. Hong, S. Cao, Y. Huang, S. Chen, Y. Liu, H. Guan, Q. Zhang, Y. Li, H. Xiao, TET1 is a Tumor Suppressor That Inhibits Papillary Thyroid Carcinoma Cell Migration and Invasion, Int. J. Endocrinol. 2020 (2020), https://doi.org/10.1155/2020/3909610.
[101] J. Wu, H. Li, M. Shi, Y. Zhu, Y. Ma, Y. Zhong, C. Xiong, H. Chen, C. Peng, TET1-mediated DNA hydroxymethylation activates inhibitors of the Wnt/β-catenin signaling pathway to suppress EMT in pancreatic tumor cells, J. Exp. Clin. Cancer Res. 38 (2019) 348, https://doi.org/10.1186/s13046-019-1334-5.
[102] I. Kurelac, A. MacKay, M.B.K. Lambros, E. Di Cesare, G. Cenacchi, C. Ceccarelli, I. Morra, A. Melcarne, L. Morandi, F.M. Calabrese, M. Attimonelli, G. Tallini, J. S. Reis- Filho, G. Gasparre, Somatic complex I disruptive mitochondrial DNA mutations are modifiers of tumorigenesis that correlate with low genomic instability in pituitary adenomas, Hum. Mol. Genet. 22 (2013) 226–238, https://doi.org/10.1093/hmg/dds422.
[103] L.K. Sharma, H. Fang, J. Liu, R. Vartak, J. Deng, Y. Bai, Mitochondrial respiratory complex I dysfunction promotes tumorigenesis through ROS alteration and AKT activation, Hum. Mol. Genet 20 (2011) 4605–4616, https://doi.org/10.1093/hmg/ddr395.
[104] H. Kim, T. Komiyama, C. Inomoto, H. Kamiguchi, H. Kajiwara, H. Kobayashi, N. Nakamura, T. Terachi, Mutations in the mitochondrial ND1 gene are associated with postoperative prognosis of localized renal cell carcinoma, Int. J. Mol. Sci. 17 (2016) 2049, https://doi.org/10.3390/ijms17122049.
[105] R.K. Singh, S. Saini, D. Verma, P. Kalaiarasan, R.N.K. Bamezai, Mitochondrial ND5 mutation mediated elevated ROS regulates apoptotic pathway epigenetically in a P53 dependent manner for generating pro-cancerous phenotypes, Mitochondrion 35 (2017) 35–43, https://doi.org/10.1016/j.mito.2017.05.001.
[106] S. Dasgupta, C. Shao, T.E. Keane, D.P. Duberow, R.A. Mathies, P.B. Fisher, L. A. Kiemeney, D. Sidransky, Detection of mitochondrial deoxyribonucleic acid alterations in urine from urothelial cell carcinoma patients, Int. J. Cancer 131 (2012) 158–164, https://doi.org/10.1002/ijc.26357.
[107] M. Ghaffarpour, R. Mahdian, F. Fereidooni, B. Kamalidehghan, N. Moazami, M. Houshmand, The mitochondrial ATPase6 gene is more susceptible to mutation than the ATPase8 gene in breast cancer patients, Cancer Cell Int 14 (2014) 21, https://doi.org/10.1186/1475-2867-14-21.
[108] K.E.R. Hollinshead, S.J. Parker, V.V. Eapen, J. Encarnacion-Rosado, A. Sohn, T. Oncu, M. Cammer, J.D. Mancias, A.C. Kimmelman, Respiratory supercomplexes promote mitochondrial efficiency and growth in severely hypoxic pancreatic cancer, Cell Rep. 33 (2020) 108231, https://doi.org/10.1016/j.celrep.2020.108231.
[109] K. Ikeda, K. Horie-Inoue, T. Suzuki, R. Hobo, N. Nakasato, S. Takeda, S. Inoue, Mitochondrial supercomplex assembly promotes breast and endometrial tumorigenesis by metabolic alterations and enhanced hypoxia tolerance, Nat. Commun. 10 (2019) 4108, https://doi.org/10.1038/s41467-019-12124-6.
[110] G. Wang, B. Popovic, J. Tao, A. Jiang, Overexpression of COX7RP promotes tumor growth and metastasis by inducing ROS production in hepatocellular carcinoma cells, Am. J. Cancer Res. 10 (2020) 1366–1383. ⟨http://www.ncbi.nlm.nih.gov/pubmed/32509385%0Ahttp://www.pubmedcentral.nih.gov/articlerender.fcgi?artid=PMC7269779⟩.
[111] K. Rohlenova, K. Sachaphibulkij, J. Stursa, A. Bezawork-Geleta, J. Blecha, B. Endaya, L. Werner, J. Cerny, R. Zobalova, J. Goodwin, T. Spacek, E. Alizadeh Pesdar, B. Yan, M.N. Nguyen, M. Vondrusova, M. Sobol, P. Jezek, P. Hozak, J. Truksa, J. Rohlena, L.F. Dong, J. Neuzil, Selective Disruption of Respiratory Supercomplexes as a New Strategy to Suppress Her2high Breast Cancer, Antioxid. Redox Signal 26 (2017) 84–103, https://doi.org/10.1089/ars.2016.6677.
[112] S. Bandiera, S. Rüberg, M. Girard, N. Cagnard, S. Hanein, D. Chrétien, A. Munnich, S. Lyonnet, A. Henrion-Caude, Nuclear outsourcing of RNA interference components to human mitochondria, PLoS One 6 (2011) e20746, https://doi.org/10.1371/journal.pone.0020746.
[113] N. Dasgupta, Y. Peng, Z. Tan, G. Ciraolo, D. Wang, R. Li, miRNAs in mtDNA-less cell mitochondria, Cell Death Discov. 1 (2015) 15004, https://doi.org/10.1038/cddiscovery.2015.4.
[114] P.K. Purohit, R. Edwards, K. Tokatlidis, N. Saini, MiR-195 regulates mitochondrial function by targeting mitofusin-2 in breast cancer cells, RNA Biol. 16 (2019) 918–929, https://doi.org/10.1080/15476286.2019.1600999.
[115] A.Yang-ja Lee, Seon-Yong Jeong, Mariusz Karbowski, Carolyn L. Smith, R. J. Youle, Roles of the Mammalian Mitochondrial Fission and Fusion Mediators Fis1, Drp1, and Opa1 in Apoptosis, Mol. Biol. Cell 15 (2004) 5001–5011, https://doi.org/10.1091/mbc.e04-04-0294.
[116] K. Wang, B. Long, J.Q. Jiao, J.X. Wang, J.P. Liu, Q. Li, P.F. Li, MiR-484 regulates mitochondrial network through targeting Fis1, Nat. Commun. 3 (2012) 781–789, https://doi.org/10.1038/ncomms1770.
[117] H. Lee, H. Tak, S.J. Park, Y.K. Jo, D.H. Cho, E.K. Lee, microRNA-200a-3p enhances mitochondrial elongation by targeting mitochondrial fission factor, BMB Rep. 50 (2017) 214–219, https://doi.org/10.5483/BMBRep.2017.50.4.006.
[118] B. Li, W. Wang, Z. Li, Z. Chen, X. Zhi, J. Xu, Q. Li, L. Wang, X. Huang, L. Wang, S. Wei, G. Sun, X. Zhang, Z. He, L. Zhang, D. Zhang, H. Xu, W. El-Rifai, Z. Xu, MicroRNA-148a-3p enhances cisplatin cytotoxicity in gastric cancer through mitochondrial fission induction and cyto-protective autophagy suppression, Cancer Lett. 410 (2017) 212–227, https://doi.org/10.1016/j.canlet.2017.09.035.
[119] P. Dutta, E. Haller, A. Sharp, M. Nanjundan, MIR494 reduces renal cancer cell survival coinciding with increased lipid droplets and mitochondrial changes, BMC Cancer 16 (2016) 33, https://doi.org/10.1186/s12885-016-2053-3.

[120] Q. Hu, Y. Yuan, Y. Wu, Y. Huang, Z. Zhao, C. Xiao, MicroRNA-137 exerts protective effects on hypoxia-induced cell injury by inhibiting autophagy/mitophagy and maintaining mitochondrial function in breast cancer stem-like cells, Oncol. Rep. 44 (2020) 1627–1637, https://doi.org/10.3892/or.2020.7714.
[121] S. Zhang, C. Liu, X. Zhang, Mitochondrial damage mediated by miR-1 overexpression in cancer stem cells, Mol. Ther. - Nucleic Acids 18 (2019) 938–953, https://doi.org/10.1016/j.omtn.2019.10.016.
[122] Z. Xu, Y. Zhang, J. Ding, W. Hu, C. Tan, M. Wang, J. Tang, Y. Xu, miR-17-3p Downregulates Mitochondrial Antioxidant Enzymes and Enhances the Radiosensitivity of Prostate Cancer Cells, Mol. Ther. - Nucleic Acids 13 (2018) 64–77, https://doi.org/10.1016/j.omtn.2018.08.009.
[123] R. Singh, V. Yadav, S. Kumar, N. Saini, MicroRNA-195 inhibits proliferation, invasion and metastasis in breast cancer cells by targeting FASN, HMGCR, ACACA and CYP27B1, Sci. Rep. 5 (2015) 17454, https://doi.org/10.1038/srep17454.
[124] X. Zhou, L. Zhang, B. Zheng, Y. Yan, Y. Zhang, H. Xie, L. Zhou, S. Zheng, W. Wang, MicroRNA-761 is upregulated in hepatocellular carcinoma and regulates tumorigenesis by targeting Mitofusin-2, Cancer Sci. 107 (2016) 424–432, https://doi.org/10.1111/cas.12904.
[125] S. Fan, W.X. Chen, X. Bin Lv, Q.L. Tang, L.J. Sun, B. Du Liu, J.L. Zhong, Z.Y. Lin, Y.Y. Wang, Q.X. Li, X. Yu, H.Q. Zhang, Y.L. Li, B. Wen, Z. Zhang, W.L. Chen, J. S. Li, MiR-483-5p determines mitochondrial fission and cisplatin sensitivity in tongue squamous cell carcinoma by targeting FIS1, Cancer Lett. 362 (2015) 183–191, https://doi.org/10.1016/j.canlet.2015.03.045.
[126] S. Fan, T. Tian, W. Chen, X. Lv, X. Lei, H. Zhang, S. Sun, L. Cai, G. Pan, L. He, Z. Ou, X. Lin, X. Wang, M.F. Perez, Z. Tu, S. Ferrone, B.A. Tannous, J. Li, Mitochondrial miRNA determines chemoresistance by reprogramming metabolism and regulating mitochondrial transcription, Cancer Res 79 (2019) 1069–1084, https://doi.org/10.1158/0008-5472.CAN-18-2505.
[127] W. Chen, P. Wang, Y. Lu, T. Jin, X. Lei, M. Liu, P. Zhuang, J. Liao, Z. Lin, B. Li, Y. Peng, G. Pan, X. Lv, H. Zhang, Z. Ou, S. Xie, X. Lin, S. Sun, S. Ferrone, B. A. Tannous, J. Li, S. Fan, Y. Ruan, Decreased expression of mitochondrial mir-5787 contributes to chemoresistance by reprogramming glucose metabolism and inhibiting MT-CO3 translation, Theranostics 9 (2019) 5739–5754, https://doi.org/10.7150/thno.37556.
[128] K.E. Tagscherer, A. Fassl, T. Sinkovic, J. Richter, S. Schecher, S. Macher-Goeppinger, W. Roth, MicroRNA-210 induces apoptosis in colorectal cancer via induction of reactive oxygen, Cancer Cell Int 16 (2016) 42, https://doi.org/10.1186/s12935-016-0321-6.
[129] T. Luan, S. Fu, L. Huang, Y. Zuo, M. Ding, N. Li, J. Chen, H. Wang, J. Wang, MicroRNA-98 promotes drug resistance and regulates mitochondrial dynamics by targeting LASS2 in bladder cancer cells, Exp. Cell Res. 373 (2018) 188–197, https://doi.org/10.1016/j.yexcr.2018.10.013.
[130] M.P. Puisségur, N.M. Mazure, T. Bertero, L. Pradelli, S. Grosso, K. Robbe-Sermesant, T. Maurin, K. Lebrigand, B. Cardinaud, V. Hofman, S. Fourre, V. Magnone, J.E. Ricci, J. Pouysségur, P. Gounon, P. Hofman, P. Barbry, B. Mari, MiR-210 is overexpressed in late stages of lung cancer and mediates mitochondrial alterations associated with modulation of HIF-1 activity, Cell Death Differ. 18 (2011) 465–478, https://doi.org/10.1038/cdd.2010.119.
[131] Y.Y. Kao, C.H. Chou, L.Y. Yeh, Y.F. Chen, K.W. Chang, C.J. Liu, C.Y. Fan Chiang, S.C. Lin, MicroRNA miR-31 targets SIRT3 to disrupt mitochondrial activity and increase oxidative stress in oral carcinoma, Cancer Lett. 456 (2019) 40–48, https://doi.org/10.1016/j.canlet.2019.04.028.
[132] L. Tian, J. Zhang, X. Ren, X. Liu, W. Gao, C. Zhang, Y. Sun, M. Liu, Overexpression of miR-26b decreases the cisplatin-resistance in laryngeal cancer by targeting ATF2, Oncotarget 8 (2017) 79023–79033, https://doi.org/10.18632/oncotarget.20784.
[133] B.H. Zhuang X, Y. Chen, Z. Wu, Q. Xu, M. Chen, M. Shao, X. Cao, Y. Zhou, M. Xie, Y. Shi, Y. Zeng, Mitochondrial miR-181a-5p promotes glucose metabolism reprogramming in liver cancer by regulating the electron transport chain Xiang, Carcinogenesis 41 (2014) 972–983.
[134] Y. Guo, X. Ji, J. Liu, D. Fan, Q. Zhou, C. Chen, W. Wang, G. Wang, H. Wang, W. Yuan, Z. Ji, Z. Sun, Effects of exosomes on pre-metastatic niche formation in tumors, Mol. Cancer 18 (2019) 1–11, https://doi.org/10.1186/s12943-019-0995-1.
[135] H. Zhao, L. Yang, J. Baddour, A. Achreja, V. Bernard, T. Moss, J.C. Marini, T. Tudawe, E.G. Seviour, F.A. San Lucas, H. Alvarez, S. Gupta, S.N. Maiti, L. Cooper, D. Peehl, P.T. Ram, A. Maitra, D. Nagrath, Tumor microenvironment derived exosomes pleiotropically modulate cancer cell metabolism, Elife 5 (2016) e10250, https://doi.org/10.7554/eLife.10250.
[136] S. La Shu, Y. Yang, C.L. Allen, O. Maguire, H. Minderman, A. Sen, M.J. Ciesielski, K.A. Collins, P.J. Bush, P. Singh, X. Wang, M. Morgan, J. Qu, R.B. Bankert, T. L. Whiteside, Y. Wu, M.S. Ernstoff, Metabolic reprogramming of stromal fibroblasts by melanoma exosome microRNA favours a pre-metastatic microenvironment, Sci. Rep. 8 (2018) 12905, https://doi.org/10.1038/s41598-018-31323-7.
[137] C.L. Bland, C.N. Byrne-Hoffman, A. Fernandez, S.L. Rellick, W. Deng, D.J. Klinke, Exosomes derived from B16F0 melanoma cells alter the transcriptome of cytotoxic T cells that impacts mitochondrial respiration, FEBS J. 285 (2018) 1033–1050, https://doi.org/10.1111/febs.14396.
[138] J. Zhou, Y. Yang, W.W. Wang, Y. Zhang, Z.R. Chen, C.L. Hao, J.P. Zhang, Melanoma- released exosomes directly activate the mitochondrial apoptotic pathway of CD4+ T cells through their microRNA cargo, Exp. Cell Res. 371 (2018) 364–371, https://doi.org/10.1016/j.yexcr.2018.08.030.
[139] Y. Li, Z. Zhao, W. Liu, X. Li, SNHG3 functions as miRNA sponge to promote breast cancer cells growth through the metabolic reprogramming, Appl. Biochem. Biotechnol. 191 (2020) 1084–1099, https://doi.org/10.1007/s12010-020-03244-7.
[140] J.E. Park, B. Dutta, S.W. Tse, N. Gupta, C.F. Tan, J.K. Low, K.W. Yeoh, O.L. Kon, J. P. Tam, S.K. Sze, Hypoxia-induced tumor exosomes promote M2-like macrophage polarization of infiltrating myeloid cells and microRNA-mediated metabolic shift, Oncogene 38 (2019) 5158–5173, https://doi.org/10.1038/s41388-019-0782-x.
[141] N.E. Scharping, A.V. Menk, R.S. Moreci, R.D. Whetstone, R.E. Dadey, S. C. Watkins, R.L. Ferris, G.M. Delgoffe, Tumor Microenviron. Represses T Cell Mitochondrial Biog. Drive Intrat T Cell Metab. Insufficiency Dysfunct. 45 (2017) 374–388, https://doi.org/10.1016/j.immuni.2016.07.009.The.
[142] L. Pernas, L. Scorrano, Mito-Morphosis: Mitochondrial Fusion, Fission, and Cristae Remodeling as Key Mediators of Cellular Function, Annu. Rev. Physiol. 78 (2016) 505–531, https://doi.org/10.1146/annurev-physiol-021115-105011.
[143] A.K. Kondadi, R. Anand, A.S. Reichert, Cristae membrane dynamics – a paradigm change, Trends Cell Biol. 30 (2020) 923–936, https://doi.org/10.1016/j.tcb.2020.08.008.
[144] T. Brandt, L. Cavellini, W. Kühlbrandt, M.M. Cohen, A mitofusin-dependent docking ring complex triggers mitochondrial fusion in vitro, Elife 5 (2016) e14618, https://doi.org/10.7554/eLife.14618.
[145] A. Scherl, Y. Coute, C. De, A. Calle, J. Sanchez, A. Greco, D. Hochstrasser, J. Diaz, R.T.H. Laennec, Functional Proteomic Analysis of Human Nucleolus□, Mol. Biol. Cell. 13 (2002) 4100–4109, https://doi.org/10.1091/mbc.E02.
[146] T. Koshiba, Structural basis of mitochondrial tethering by mitofusin complexes, Science 858 (2014) 858–862, https://doi.org/10.1126/science.1099793.
[147] C. Fröhlich, S. Grabiger, D. Schwefel, K. Faelber, E. Rosenbaum, J. Mears, O. Rocks, O. Daumke, Structural insights into oligomerization and mitochondrial remodelling of dynamin 1-like protein, EMBO J. 32 (2013) 1280–1292, https://doi.org/10.1038/emboj.2013.74.
[148] S. Koirala, Q. Guo, R. Kalia, H.T. Bui, D.M. Eckert, A. Frost, J.M. Shaw, Interchangeable adaptors regulate mitochondrial dynamin assembly for membrane scission, Proc. Natl. Acad. Sci. U. S. A. 110 (2013) E1342–E1351, https://doi.org/10.1073/pnas.1300855110.
[149] W.K. Ji, A.L. Hatch, R.A. Merrill, S. Strack, H.N. Higgs, Actin filaments target the oligomeric maturation of the dynamin GTPase Drp1 to mitochondrial fission sites, Elife 4 (2015) e11553, https://doi.org/10.7554/eLife.11553.
[150] L. Tilokani, S. Nagashima, V. Paupe, J. Prudent, Mitochondrial dynamics: Overview of molecular mechanisms, Essays Biochem 62 (2018) 341–360, https://doi.org/10.1042/EBC20170104.
[151] R. Yu, U. Lendahl, M. Nistér, J. Zhao, Regulation of mammalian mitochondrial dynamics: opportunities and challenges, Front. Endocrinol. 11 (2020) 374, https://doi.org/10.3389/fendo.2020.00374.
[152] Y. Wang, H.H. Liu, Y.T. Cao, L.L. Zhang, F. Huang, C. Yi, The role of mitochondrial dynamics and mitophagy in carcinogenesis, metastasis and therapy, Front. Cell Dev. Biol. 8 (2020) 413, https://doi.org/10.3389/fcell.2020.00413.
[153] J. Prieto, M. León, X. Ponsoda, R. Sendra, R. Bort, R. Ferrer-Lorente, A. Raya, C. López-Garciá, J. Torres, Early ERK1/2 activation promotes DRP1-dependent mitochondrial fission necessary for cell reprogramming, Nat. Commun. 7 (2016) 1–13, https://doi.org/10.1038/ncomms11124.
[154] J. Rehman, H.J. Zhang, P.T. Toth, Y. Zhang, G. Marsboom, Z. Hong, R. Salgia, A. N. Husain, C. Wietholt, S.L. Archer, Inhibition of mitochondrial fission prevents cell cycle progression in lung cancer, FASEB J. 26 (2012) 2175–2186, https://doi.org/10.1096/fj.11-196543.
[155] Q. Xie, Q. Wu, C.M. Horbinski, W.A. Flavahan, K. Yang, W. Zhou, S. M. Dombrowski, Z. Huang, X. Fang, Y. Shi, A.N. Ferguson, D.F. Kashatus, S. Bao, J.N. Rich, Mitochondrial control by DRP1 in brain tumor initiating cells, Nat. Neurosci. 18 (2015) 501–510, https://doi.org/10.1038/nn.3960.
[156] M.N. Serasinghe, S.Y. Wieder, T.T. Renault, R. Elkholi, J.J. Asciolla, J.L. Yao, O. Jabado, K. Hoehn, Y. Kageyama, H. Sesaki, J.E. Chipuk, Mitochondrial division is requisite to RAS-induced transformation and targeted by oncogenic MAPK pathway inhibitors, Mol. Cell. 57 (2015) 521–536, https://doi.org/10.1016/j.molcel.2015.01.003.
[157] J.A. Kashatus, A. Nascimento, L.J. Myers, A. Sher, F.L. Byrne, K.L. Hoehn, C. M. Counter, D.F. Kashatus, Erk2 phosphorylation of Drp1 promotes mitochondrial fission and MAPK-driven tumor growth, Mol. Cell. 57 (2015) 537–551, https://doi.org/10.1016/j.molcel.2015.01.002.
[158] A. Pyakurel, C. Savoia, D. Hess, L. Scorrano, Extracellular regulated kinase phosphorylates mitofusin 1 to control mitochondrial morphology and apoptosis, Mol. Cell. 58 (2015) 244–254, https://doi.org/10.1016/j.molcel.2015.02.021.
[159] B. Kong, H. Tsuyoshi, M. Orisaka, D. Bin Shieh, Y. Yoshida, B.K. Tsang, Mitochondrial dynamics regulating chemoresistance in gynecological cancers, Ann. N. Y. Acad. Sci. 1350 (2015) 1–16, https://doi.org/10.1111/nyas.12883.
[160] W. Qian, J. Wang, V. Roginskaya, L.A. McDermott, R.P. Edwards, D.B. Stolz, F. Llambi, D.R. Green, B. Van Houten, Novel combination of mitochondrial division inhibitor 1 (mdivi-1) and platinum agents produces synergistic pro-apoptotic effect in drug resistant tumor cells, Oncotarget 5 (2014) 4180–4194, https://doi.org/10.18632/oncotarget.1944.
[161] L. Zhan, H. Cao, G. Wang, Y. Lyu, X. Sun, J. An, Z. Wu, Q. Huang, B. Liu, J. Xing, Drp1-mediated mitochondrial fission promotes cell proliferation through crosstalk of p53 and NF-κB pathways in hepatocellular carcinoma, Oncotarget 7 (2016) 65001–65011, https://doi.org/10.18632/oncotarget.11339.
[162] M. Karbowski, Y.J. Lee, B. Gaume, S.Y. Jeong, S. Frank, A. Nechushtan, A. Santel, M. Fuller, C.L. Smith, R.J. Youle, Spatial and temporal association of Bax with mitochondrial fission sites, Drp1, and Mfn2 during apoptosis, J. Cell Biol. 159 (2002) 931–938, https://doi.org/10.1083/jcb.200209124.

[163] J. Li, Q. Huang, X. Long, X. Guo, X. Sun, X. Jin, Z. Li, T. Ren, P. Yuan, X. Huang, H. Zhang, J. Xing, Mitochondrial elongation-mediated glucose metabolism reprogramming is essential for tumour cell survival during energy stress, Oncogene 36 (2017) 4901–4912, https://doi.org/10.1038/onc.2017.98.
[164] M. Li, L. Wang, Y. Wang, S. Zhang, G. Zhou, R. Lieshout, B. Ma, J. Liu, C. Qu, M. M.A. Verstegen, D. Sprengers, J. Kwekkeboom, L.J.W. van der Laan, W. Cao, M. P. Peppelenbosch, Q. Pan, Mitochondrial fusion via OPA1 and MFN1 Supports Liver Tumor Cell Metabolism and Growth, Cells 9 (2020) 1–16, https://doi.org/10.3390/cells9010121.
[165] D.K. Tanwar, D.J. Parker, P. Gupta, B. Spurlock, R.D. Alvarez, M.K. Basu, K. Mitra, Crosstalk between the mitochondrial fission protein, Drp1, and the cell cycle is identified across various cancer types and can impact survival of epithelial ovarian cancer patients, Oncotarget 7 (2016) 60021–60037, https://doi.org/10.18632/oncotarget.11047.
[166] A. Signorile, D. De Rasmo, A. Cormio, C. Musicco, R. Rossi, F. Fortarezza, L. L. Palese, V. Loizzi, L. Resta, G. Scillitani, E. Cicinelli, F. Simonetti, A. Ferretta, S. Russo, A. Tufaro, G. Cormio, Human ovarian cancer tissue exhibits increase of mitochondrial biogenesis and cristae remodeling, Cancers 11 (2019) 1350, https://doi.org/10.3390/cancers11091350.
[167] Y. Han, B. Kim, U. Cho, I.S. Park, S.I. Kim, D.N. Dhanasekaran, B.K. Tsang, Y. S. Song, Mitochondrial fission causes cisplatin resistance under hypoxic conditions via ROS in ovarian cancer cells, Oncogene 38 (2019) 7089–7105, https://doi.org/10.1038/s41388-019-0949-5.
[168] L. Farrand, J.Y. Kim, A. Im-Aram, J.Y. Suh, H.J. Lee, B.K. Tsang, An improved quantitative approach for the assessment of mitochondrial fragmentation in chemoresistant ovarian cancer cells, PLoS One 8 (2013) e74008, https://doi.org/10.1371/journal.pone.0074008.
[169] S.R. Chowdhury, U. Ray, B.P. Chatterjee, S.S. Roy, Targeted apoptosis in ovarian cancer cells through mitochondrial dysfunction in response to Sambucus nigra agglutinin, Cell Death Dis. 8 (2017) e2762, https://doi.org/10.1038/cddis.2017.77.
[170] S.L.P. Tian Gao, Xiaohong Zhang, Jing Zhao, Feng Zhou, Yaya Wang, Zh.Tian Gao, Xiaohong Zhang, Jing Zhao, Feng Zhou, Yaya Wang, Zheng Zhao, Jinliang Xing, Biliang Chen, Jibin Li, Shujuan Liu PII:eng Zhao, Jinliang Xing, Biliang Chen, Jibin Li, SIK2 promotes reprogramming of glucose metabolism through PI3K,AKT,HIF-1α.pdf, (2019).
[171] Cheng1, 2 2 Chun-Ting, Kuo1 Ching-Ying, Ouyang3 Ching, Li4, 5 Chien-Feng, Chung1 Yiying, Chan6 David C, Kung7, 8 Hsing-Jien, Ann1 David K, Metabolic stress- induced phosphorylation of KAP1 Ser473 blocks mitochondrial fusion in breast cancer cells, Cancer Res. 76 (2016) 5006–5018, https://doi.org/10.1158/0008- 5472.CAN-15-2921.Metabolic.
[172] J. Zhao, J. Zhang, M. Yu, Y. Xie, Y. Huang, D.W. Wolff, P.W. Abel, Y. Tu, Mitochondrial dynamics regulates migration and invasion of breast cancer cells, Oncogene 32 (2013) 4814–4824, https://doi.org/10.1038/onc.2012.494. Mitochondrial.
[173] X.J. Han, Z.J. Yang, L.P. Jiang, Y.F. Wei, M.F. Liao, Y. Qian, Y. Li, X. Huang, J. Bin Wang, H.B. Xin, Y.Y. Wan, Mitochondrial dynamics regulates hypoxia-induced migration and antineoplastic activity of cisplatin in breast cancer cells, Int. J. Oncol. 46 (2015) 691–700, https://doi.org/10.3892/ijo.2014.2781.
[174] D. Wu, A. Dasgupta, K.H. Chen, M. Neuber-Hess, J. Patel, T.E. Hurst, J. D. Mewburn, P.D.A. Lima, E. Alizadeh, A. Martin, M. Wells, V. Snieckus, S. L. Archer, Identification of novel dynamin-related protein 1 (Drp1) GTPase inhibitors: therapeutic potential of Drpitor1 and Drpitor1a in cancer and cardiac ischemia-reperfusion injury, FASEB J. 34 (2020) 1447–1464, https://doi.org/10.1096/fj.201901467R.
[175] X. Qiu, S. Jiang, Y. Xiao, Y. He, T. Ren, L. Jiang, R. Liu, Q. Chen, SOX2-dependent expression of dihydroorotate dehydrogenase regulates oral squamous cell carcinoma cell proliferation, Int. J. Oral. Sci. 13 (2021) 3, https://doi.org/10.1038/s41368-020-00109-x.
[176] G. Rademaker, V. Hennequière, L. Brohée, M.J. Nokin, P. Lovinfosse, F. Durieux, S. Gofflot, J. Bellier, B. Costanza, M. Herfs, R. Peiffer, L. Bettendorff, C. Deroanne, M. Thiry, P. Delvenne, R. Hustinx, A. Bellahcène, V. Castronovo, O. Peulen, Myoferlin controls mitochondrial structure and activity in pancreatic ductal adenocarcinoma, and affects tumor aggressiveness, Oncogene 37 (2018) 4398–4412, https://doi.org/10.1038/s41388-018-0287-z.
[177] Y.Y. Wan, J.F. Zhang, Z.J. Yang, L.P. Jiang, Y.F. Wei, Q.N. Lai, J. Bin Wang, H. B. Xin, X.J. Han, Involvement of Drp1 in hypoxia-induced migration of human glioblastoma U251 cells, Oncol. Rep. 32 (2014) 619–626, https://doi.org/10.3892/or.2014.3235.
[178] R.J. DeBerardinis, J.J. Lum, G. Hatzivassiliou, C.B. Thompson, The biology of cancer: metabolic reprogramming fuels cell growth and proliferation, Cell Metab. 7 (2008) 11–20, https://doi.org/10.1016/j.cmet.2007.10.002.
[179] R. Possemato, K.M. Marks, Y.D. Shaul, M.E. Pacold, D. Kim, K. Birsoy, S. Sethumadhavan, H.K. Woo, H.G. Jang, A.K. Jha, W.W. Chen, F.G. Barrett, N. Stransky, Z.Y. Tsun, G.S. Cowley, J. Barretina, N.Y. Kalaany, P.P. Hsu, K. Ottina, A.M. Chan, B. Yuan, L.A. Garraway, D.E. Root, M. Mino-Kenudson, E. F. Brachtel, E.M. Driggers, D.M. Sabatini, Functional genomics reveal that the serine synthesis pathway is essential in breast cancer, Nature 476 (2011) 346–350, https://doi.org/10.1038/nature10350.
[180] K. Sellers, M.P. Fox, M.B. Ii, S.P. Slone, R.M. Higashi, D.M. Miller, Y. Wang, J. Yan, M.O. Yuneva, R. Deshpande, A.N. Lane, T.W.M. Fan, Pyruvate carboxylase is critical for non-small-cell lung cancer proliferation, J. Clin. Invest 125 (2015) 687–698, https://doi.org/10.1172/JCI72873.
[181] D. Gaglio, C.M. Metallo, P.A. Gameiro, K. Hiller, L.S. Danna, C. Balestrieri, L. Alberghina, G. Stephanopoulos, F. Chiaradonna, Oncogenic K-Ras decouples glucose and glutamine metabolism to support cancer cell growth, Mol. Syst. Biol. 7 (2011) 523, https://doi.org/10.1038/msb.2011.56.
[182] M. Osaki, M. Oshimura, H. Ito, PI3K-Akt pathway: Its functions and alterations in human cancer, Apoptosis 9 (2004) 667–676, https://doi.org/10.1023/B:APPT.0000045801.15585.dd.
[183] R.C. Osthus, H. Shim, S. Kim, Q. Li, R. Reddy, M. Mukherjee, Y. Xu, D. Wonsey, L. A. Lee, C.V. Dang, Deregulation of glucose transporter 1 and glycolytic gene expression by c-Myc, J. Biol. Chem. 275 (2000) 21797–21800, https://doi.org/10.1074/jbc.C000023200.
[184] F. Li, Y. Wang, K.I. Zeller, J.J. Potter, D.R. Wonsey, K.A. O'Donnell, J. Kim, J. T. Yustein, L.A. Lee, C.V. Dang, Myc stimulates nuclearly encoded mitochondrial genes and mitochondrial biogenesis, Mol. Cell. Biol. 25 (2005) 6225–6234, https://doi.org/10.1128/mcb.25.14.6225-6234.2005.
[185] C. Lu, S. Venneti, A. Akalin, F. Fang, P.S. Ward, R.G. DeMatteo, A.M. Intlekofer, C. Chen, J. Ye, M. Hameed, K. Nafa, N.P. Agaram, J.R. Cross, R. Khanin, C. E. Mason, J.H. Healey, S.W. Lowe, G.K. Schwartz, A. Melnick, C.B. Thompson, Induction of sarcomas by mutant IDH2, Genes Dev. 27 (2013) 1986–1998, https://doi.org/10.1101/gad.226753.113.
[186] C. Chen, Y. Liu, C. Lu, J.R. Cross, J.P. Morris IV, A.S. Shroff, P.S. Ward, J. E. Bradner, C. Thompson, S.W. Lowe, Cancer-associated IDH2 mutants drive an acute myeloid leukemia that is susceptible to Brd4 inhibition, Genes Dev. 27 (2013) 1974–1985, https://doi.org/10.1101/gad.226613.113.
[187] D. Rohle, J. Popovici-muller, N. Palaskas, S. Turcan, C. Campos, J. Tsoi, O. Clark, B. Oldrini, K. Kunii, A. Pedraza, S. Schalm, L. Silverman, A. Miller, F. Wang, H. Yang, Y. Chen, A. Kernytsky, K. Marc, W. Liu, S.A. Biller, S.M. Su, C. W. Brennan, A. Chan, T.G. Graeber, K.E. Yen, I.K. Mellinghoff, An inhibitor of mutant IDH1 delays growth and promotes differentiation of glioma cells, Science 340 (2013) 626–630, https://doi.org/10.1126/science.1236062.
[188] L. Dang, D.W. White, S. Gross, B.D. Bennett, M.A. Bittinger, E.M. Driggers, V. R. Fantin, H.G. Jang, S. Jin, M.C. Keenan, K.M. Marks, R.M. Prins, P.S. Ward, K. E. Yen, L.M. Liau, J.D. Rabinowitz, L.C. Cantley, C.B. Thompson, M.G. Vander Heiden, S.M. Su, Cancer-associated IDH1 mutations produce 2-hydroxyglutarate, Nature 462 (2009) 739–744, https://doi.org/10.1038/nature08617.
[189] S. Qiao, W. Lu, C. Glorieux, J. Li, P. Zeng, N. Meng, H. Zhang, S. Wen, P. Huang, Wild-type IDH2 protects nuclear DNA from oxidative damage and is a potential therapeutic target in colorectal cancer, Oncogene 40 (2021) 5880–5892, https://doi.org/10.1038/s41388-021-01968-2.
[190] P. Zeng, W. Lu, J. Tian, S. Qiao, J. Li, C. Glorieux, S. Wen, H. Zhang, Y. Li, P. Huang, Reductive TCA cycle catalyzed by wild-type IDH2 promotes acute myeloid leukemia and is a metabolic vulnerability for potential targeted therapy, J. Hematol. Oncol. 15 (2022) 1–22, https://doi.org/10.1186/s13045-022-01245-z.
[191] J.S. Isaacs, J.J. Yun, D.R. Mole, S. Lee, C. Torres-Cabala, Y.L. Chung, M. Merino, J. Trepel, B. Zbar, J. Toro, P.J. Ratcliffe, W.M. Linehan, L. Neckers, HIF overexpression correlates with biallelic loss of fumarate hydratase in renal cancer: novel role of fumarate in regulation of HIF stability, Cancer Cell 8 (2005) 143–153, https://doi.org/10.1016/j.ccr.2005.06.017.
[192] S. Picaud, K.L. Kavanagh, W.W. Yue, W.H. Lee, S. Muller-Knapp, O. Gileadi, J. Sacchettini, U. Oppermann, Structural basis of fumarate hydratase deficiency, J. Inherit. Metab. Dis. 34 (2011) 671–676, https://doi.org/10.1007/s10545-011-9294-8.
[193] L. O'Flaherty, J. Adam, L.C. Heather, A.V. Zhdanov, Y.L. Chung, M.X. Miranda, J. Croft, S. Olpin, K. Clarke, C.W. Pugh, J. Griffiths, D. Papkovsky, H. Ashrafian, P. J. Ratcliffe, P.J. Pollard, Dysregulation of hypoxia pathways in fumarate hydratase-deficient cells is independent of defective mitochondrial metabolism, Hum. Mol. Genet 19 (2010) 3844–3851, https://doi.org/10.1093/hmg/ddq305.
[194] A.S. Hoekstra, M.A. de Graaff, I.H. Briaire-de Bruijn, C. Ras, R.M. Seifar, I. van Minderhout, C.J. Cornelisse, P.C.W. Hogendoorn, M.H. Breuning, J. Suijker, E. Korpershoek, H.P.M. Kunst, N. Frizzell, P. Devilee, J.P. Bayley, J.V.M.G. Bovée, Inactivation of SDH and FH cause loss of 5hmC and increased H3K9me3 in paraganglioma/pheochromocytoma and smooth muscle tumors, Oncotarget 6 (2015) 38777–38788, https://doi.org/10.18632/oncotarget.6091.
[195] M. Xiao, H. Yang, W. Xu, S. Ma, H. Lin, H. Zhu, L. Liu, Y. Liu, C. Yang, Y. Xu, S. Zhao, D. Ye, Y. Xiong, K.L. Guan, Inhibition of α-KG-dependent histone and DNA demethylases by fumarate and succinate that are accumulated in mutations of FH and SDH tumor suppressors, Genes Dev. 26 (2012) 1326–1338, https://doi.org/10.1101/gad.191056.112.
[196] S. Cardaci, L. Zheng, G. Mackay, N.J.F. Van Den Broek, E.D. Mackenzie, C. Nixon, D. Stevenson, S. Tumanov, V. Bulusu, J.J. Kamphorst, A. Vazquez, S. Fleming, F. Schiavi, G. Kalna, K. Blyth, D. Strathdee, E. Gottlieb, Pyruvate carboxylation enables growth of SDH-deficient cells by supporting aspartate biosynthesis, Nat. Cell Biol. 17 (2015) 1317–1326, https://doi.org/10.1038/ncb3233.
[197] J. Van den Bossche, L.A. O'Neill, D. Menon, Macrophage Immunometabolism: where are we (Going)? Trends Immunol. 38 (2017) 395–406, https://doi.org/10.1016/j.it.2017.03.001.
[198] A. Viola, F. Munari, R. Sánchez-Rodríguez, T. Scolaro, A. Castegna, The metabolic signature of macrophage responses, Front. Immunol. 10 (2019) 1–16, https://doi.org/10.3389/fimmu.2019.01462.
[199] R.C. Coll, C.L. Holley, K. Schroder, Mitochondrial DNA synthesis fuels NLRP3 inflammasome, Cell Res 28 (2018) 1046–1047, https://doi.org/10.1038/s41422-018-0093-8.
[200] T. Ichinohe, T. Yamazaki, T. Koshiba, Y. Yanagi, Mitochondrial protein mitofusin 2 is required for NLRP3 inflammasome activation after RNA virus infection, Proc. Natl. Acad. Sci. U. S. A. 110 (2013) 17963–17968, https://doi.org/10.1073/pnas.1312571110.

[201] S. Park, J.H. Won, I. Hwang, S. Hong, H.K. Lee, J.W. Yu, Defective mitochondrial fission augments NLRP3 inflammasome activation, Sci. Rep. 5 (2015) 15489, https://doi.org/10.1038/srep15489.
[202] D. Bao, J. Zhao, X. Zhou, Q. Yang, Y. Chen, J. Zhu, P. Yuan, J. Yang, T. Qin, S. Wan, J. Xing, Mitochondrial fission-induced mtDNA stress promotes tumor-associated macrophage infiltration and HCC progression, Oncogene 38 (2019) 5007–5020, https://doi.org/10.1038/s41388-019-0772-z.
[203] K.A. Frauwirth, J.L. Riley, M.H. Harris, R.V. Parry, J.C. Rathmell, D.R. Plas, R. L. Elstrom, C.H. June, C.B. Thompson, The CD28 Signaling Pathway Regulates Glucose Metabolism ability of resting cells to take up and utilize nutrients at levels sufficient to maintain viability (Rathmell et al in fat and muscle cells insulin induces glucose uptake in excess of that required, Immunity 16 (2002) 769–777, https://doi.org/10.1016/S1074-7613(02)00323-0.
[204] H.L. Wieman, J.A. Wofford, J.C. Rathmell, Cytokine stimulation promotes glucose uptake via phosphatidylinositol-3 kinase/Akt regulation of Glut1 activity and trafficking, Mol. Biol. Cell. 18 (2007) 1437–1446, https://doi.org/10.1091/mbc.E06-07-0593.
[205] A. Perl, M. Tan, Diverse roles of mitochondria in immune responses: novel insights into immuno-metabolism, Front. Immunol. 9 (2018) 1605, https://doi.org/10.3389/fimmu.2018.01605.
[206] R. Geiger, J.C. Rieckmann, T. Wolf, C. Basso, Y. Feng, T. Fuhrer, M. Kogadeeva, P. Picotti, F. Meissner, M. Mann, N. Zamboni, F. Sallusto, A. Lanzavecchia, L-Arginine modulates T Cell Metabolism and Enhances Survival and Anti-tumor Activity, e13, Cell 167 (2016) 829–842, https://doi.org/10.1016/j.cell.2016.09.031.
[207] L. Simula, I. Pacella, A. Colamatteo, C. Procaccini, V. Cancila, M. Bordi, C. Tregnago, M. Corrado, M. Pigazzi, V. Barnaba, C. Tripodo, G. Matarese, S. Piconese, S. Campello, Drp1 Controls Effective T Cell Immune-Surveillance by Regulating T Cell Migration, Proliferation, and cMyc-Dependent Metabolic Reprogramming, e10, Cell Rep. 25 (2018) 3059–3073, https://doi.org/10.1016/j.celrep.2018.11.018.
[208] M.D.D. Buck, D. O'Sullivan, R.I.I. Klein Geltink, J.D.D. Curtis, C.H. Chang, D.E. E. Sanin, J. Qiu, O. Kretz, D. Braas, G.J.J.W. van der Windt, Q. Chen, S.C. C. Huang, C.M.M. O'Neill, B.T.T. Edelson, E.J.J. Pearce, H. Sesaki, T.B.B. Huber, A.S.S. Rambold, E.L.L. Pearce, Mitochondrial dynamics controls T cell fate through metabolic programming, Cell 166 (2016) 63–76, https://doi.org/10.1016/j.cell.2016.05.035.
[209] A.V. Menk, N.E. Scharping, D.B. Rivadeneira, M.J. Calderon, M.J. Watson, D. Dunstane, S.C. Watkins, G.M. Delgoffe, 4-1BB costimulation induces T cell mitochondrial function and biogenesis enabling cancer immunotherapeutic responses, J. Exp. Med. 215 (2018) 1091–1100, https://doi.org/10.1084/jem.20171068.
[210] Y.J. Kang, B.R. Bang, K.H. Han, L. Hong, E.J. Shim, J. Ma, R.A. Lerner, M. Otsuka, Regulation of NKT cell-mediated immune responses to tumours and liver inflammation by mitochondrial PGAM5-Drp1 signalling, Nat. Commun. 6 (2015) 8371, https://doi.org/10.1038/ncomms9371.
[211] S. Campello, R.A. Lacalle, M. Bettella, S. Mañes, L. Scorrano, A. Viola, Orchestration of lymphocyte chemotaxis by mitochondrial dynamics, J. Exp. Med. 203 (2006) 2879–2886, https://doi.org/10.1084/jem.20061877.
[212] Y.N. Liu, J.F. Yang, D.J. Huang, H.H. Ni, C.X. Zhang, L. Zhang, J. He, J.M. Gu, H. X. Chen, H.Q. Mai, Q.Y. Chen, X.S. Zhang, S. Gao, J. Li, Hypoxia induces mitochondrial defect that promotes T cell exhaustion in tumor microenvironment through MYC- regulated pathways, Front. Immunol. 11 (2020) 1–16, https://doi.org/10.3389/fimmu.2020.01906.
[213] F. Baixauli, N.B. Martín-Cófreces, G. Morlino, Y.R. Carrasco, C. Calabia-Linares, E. Veiga, J.M. Serrador, F. Sánchez-Madrid, The mitochondrial fission factor dynamin- related protein 1 modulates T-cell receptor signalling at the immune synapse, EMBO J. 30 (2011) 1238–1250, https://doi.org/10.1038/emboj.2011.25.
[214] L.A.J. O'Neill, E.J. Pearce, Immunometabolism governs dendritic cell and macrophage function, J. Exp. Med. 213 (2016) 15–23, https://doi.org/10.1084/jem.20151570.
[215] P.-S. Liu, H. Wang, X. Li, T. Chao, T. Teav, S. Christen, G. Di Conza, W.-C. Cheng, C.-H. Chou, M. Vavakova, C. Muret, K. Debackere, M. Mazzone, H.-D. Huang, S.-M. Fendt, J. Ivanisevic, P.-C. Ho, a-ketoglutarate orchestrates macrophage activation through metabolic and epigenetic reprogramming, Nat. Immunol. 18 (2017) 985–994, https://doi.org/10.1038/ni.3796.
[216] Y. Li, Y. He, K. Miao, Y. Zheng, C. Deng, T.M. Liu, Imaging of macrophage mitochondria dynamics in vivo reveals cellular activation phenotype for diagnosis, Theranostics 10 (2020) 2897–2917, https://doi.org/10.7150/thno.40495.
[217] R. De Simone, M.A. Ajmone-Cat, M. Pandolfi, A. Bernardo, C. De Nuccio, L. Minghetti, S. Visentin, The mitochondrial uncoupling protein-2 is a master regulator of both M1 and M2 microglial responses, J. Neurochem. 135 (2015) 147–156, https://doi.org/10.1111/jnc.13244.
[218] R. Umezu, J.I. Koga, T. Matoba, S. Katsuki, L. Wang, L. Wang, N. Hasuzawa, N. Hasuzawa, M. Nomura, M. Nomura, H. Tsutsui, K. Egashira, K. Egashira, Macrophage (Drp1) dynamin-related protein 1 accelerates intimal thickening after vascular injury, Arterioscler. Thromb. Vasc. Biol. (2020) E214–E226, https://doi.org/10.1161/ATVBAHA.120.314383.
[219] Z. Gao, Y. Li, F. Wang, T. Huang, K. Fan, Y. Zhang, J. Zhong, Q. Cao, T. Chao, J. Jia, S. Yang, L. Zhang, Y. Xiao, J.Y. Zhou, X.H. Feng, J. Jin, Mitochondrial dynamics controls anti-Tumour innate immunity by regulating CHIP-IRF1 axis stability, Nat. Commun. (2017), https://doi.org/10.1038/s41467-017-01919-0.
[220] J.W. R. Pollard, Tumor-associated macrophages: from mechanisms to therapy, Immunity 41 (2015) 49–61, https://doi.org/10.1016/j.immuni.2014.06.010.Tumor-associated.
[221] D.C. Wallace, Mitochondria and cancer, Nat. Rev. Cancer 12 (2012) 685–698, https://doi.org/10.1038/nrc3365.
[222] J. Neuzil, L.F. Dong, J. Rohlena, J. Truksa, S.J. Ralph, Classification of mitocans, anti- cancer drugs acting on mitochondria, Mitochondrion 13 (2013) 199–208, https://doi.org/10.1016/j.mito.2012.07.112.
[223] E.M. Stein, C.D. DiNardo, D.A. Pollyea, A.T. Fathi, G.J. Roboz, J.K. Altman, R. M. Stone, D.J. Deangelo, R.L. Levine, I.W. Flinn, H.M. Kantarjian, R. Collins, M. R. Patel, A.E. Frankel, A. Stein, M.A. Sekeres, R.T. Swords, B.C. Medeiros, C. Willekens, P. Vyas, A. Tosolini, Q. Xu, R.D. Knight, K.E. Yen, S. Agresta, S. De Botton, M.S. Tallman, Enasidenib in mutant IDH2 relapsed or refractory acute myeloid leukemia, Blood 130 (2017) 722–731, https://doi.org/10.1182/blood-2017-04-779405.
[224] L. Zhang, J. Zhang, Z. Ye, Y. Manevich, L.E. Ball, R. Jennifer, Y. Jiang, A. Broome, A.C. Dalton, G.Y. Wang, D.M. Townsend, K.D. Tew, Isoflavone ME-344 disrupts redox homeostasis and mitochondrial function by targeting Heme Oxygenase 1. Leilei, Cancer Res 79 (2020) 4072–4085, https://doi.org/10.1158/0008-5472.CAN-18-3503.Isoflavone.
[225] S.C. Lim, K.T. Carey, M. McKenzie, Anti-cancer analogues ME-143 and ME-344 exert toxicity by directly inhibiting mitochondrial NADH: Ubiquinone oxidoreductase (Complex I), Am. J. Cancer Res. 5 (2015) 689–701.
[226] M.M. Alam, S. Sohoni, S.P. Kalainayakan, M. Garrossian, L. Zhang, Cyclopamine tartrate, an inhibitor of Hedgehog signaling, strongly interferes with mitochondrial function and suppresses aerobic respiration in lung cancer cells, BMC Cancer 16 (2016) 1–10, https://doi.org/10.1186/s12885-016-2200-x.
[227] T.D. Martin, D.R. Cook, M.Y. Choi, M.Z. Li, K.M. Haigis, S.J. Elledge, A Role for Mitochondrial Translation in Promotion of Viability in K-Ras Mutant Cells, Cell Rep. 20 (2017) 427–438, https://doi.org/10.1016/j.celrep.2017.06.061.
[228] M. Škrtić, S. Sriskanthadevan, B. Jhas, M. Gebbia, X. Wang, Z. Wang, R. Hurren, Y. Jitkova, M. Gronda, N. Maclean, C.K. Lai, Y. Eberhard, J. Bartoszko, P. Spagnuolo, A.C. Rutledge, A. Datti, T. Ketela, J. Moffat, B.H. Robinson, J. H. Cameron, J. Wrana, C.J. Eaves, M.D. Minden, J.C.Y. Wang, J.E. Dick, K. Humphries, C. Nislow, G. Giaever, A.D. Schimmer, INHIBITION OF MITOCHONDRIAL TRANSLATION AS A THERAPEUTIC STRATEGY FOR HUMAN ACUTE MYELOID LEUKEMIA, Cancer Cell 20 (2011) 674–688, https://doi.org/10.1016/j.ccr.2011.10.015.
[229] X. Zhang, M. Fryknäs, E. Hernlund, W. Fayad, A. De Milito, M.H. Olofsson, V. Gogvadze, L. Dang, S. Påhlman, L.A.K. Schughart, L. Rickardson, P. D'Arcy, J. Gullbo, P. Nygren, R. Larsson, S. Linder, Induction of mitochondrial dysfunction as a strategy for targeting tumour cells in metabolically compromised microenvironments, Nat. Commun. 5 (2014) 3295, https://doi.org/10.1038/ncomms4295.
[230] H.K. Byoung, J. Plescia, Y.S. Ho, M. Meli, G. Colombo, K. Beebe, B. Scroggins, L. Neckers, D.C. Altieri, Combinatorial drug design targeting multiple cancer signaling networks controlled by mitochondrial Hsp90, J. Clin. Invest. 119 (2009) 454–464, https://doi.org/10.1172/JCI37613.
[231] I. Leav, J. Plescia, H.L. Goel, J. Li, Z. Jiang, R.J. Cohen, L.R. Languino, D. C. Altieri, Cytoprotective mitochondrial chaperone TRAP-1 as a novel molecular target in localized and metastatic prostate cancer, Am. J. Pathol. 176 (2010) 393–401, https://doi.org/10.2353/ajpath.2010.090521.
[232] Y. Shi, S.K. Lim, Q. Liang, S.V. Iyer, H. Wang, Z. Wang, X. Xie, D. Sun, Y. Chen, V. Tabar, P. Gutin, J.K. De Brabander, L.F. Parada, Gboxin is an oxidative phosphorylation inhibitor that targets glioblastoma, Nature 567 (2019) 341–346, https://doi.org/10.1038/s41586-019-0993-x.Gboxin.
[233] E.L. Carpenter, S. Chagani, D. Nelson, P.B. Cassidy, G. Ganguli-indra, A.K. Indra, U. States, O. Health, U. States, U. States, O. Health, U. States, Mitochondrial Complex I Inhibitor Deguelin induces metabolic reprogramming and sensitizes vemurafenib resistant BRAFV600E mutation bearing metastatic melanoma cells, Mol. Carcinog. 58 (2020) 1680–1690, https://doi.org/10.1002/mc.23068.Mitochondrial.
[234] M. Han, M.R. Vakili, H. Soleymani Abyaneh, O. Molavi, R. Lai, A. Lavasanifar, Mitochondrial delivery of doxorubicin via triphenylphosphine modification for overcoming drug resistance in MDA-MB-435/DOX cells, Mol. Pharm. 11 (2014) 2640–2649, https://doi.org/10.1021/mp500038g.
[235] Y. Liu, Z. Zhou, X. Lin, X. Xiong, R. Zhou, M. Zhou, Y. Huang, Enhanced reactive oxygen species generation by mitochondria targeting of anticancer drug to overcome tumor multidrug resistance, Biomacromolecules 20 (2019) 3755–3766, https://doi.org/10.1021/acs.biomac.9b00800.
[236] Q. Li, Y. Huang, Mitochondrial targeted strategies and their application for cancer and other diseases treatment, J. Pharm. Investig. 50 (2020) 271–293, https://doi.org/10.1007/s40005-020-00481-0.
[237] N. Chatterjee, S. Das, D. Bose, S. Banerjee, T. Jha, K. Das Saha, Lipid from Infective L. donovani Regulates Acute Myeloid Cell Growth via Mitochondria Dependent MAPK Pathway, PLoS One 10 (2015) e0120509, https://doi.org/10.1371/journal.pone.0120509.
[238] D. Bose, S. Banerjee, S. Das, N. Chatterjee, K. Das Saha, Heat killed attenuated leishmania induces apoptosis of HepG2 cells through ROS mediated p53 dependent mitochondrial pathway, Cell. Physiol. Biochem. 38 (2016) 1303–1318, https://doi.org/10.1159/000443125.
[239] A. Rogalska, A. Koceva-Chyła, Z. Jóźwiak, Aclarubicin-induced ROS generation and collapse of mitochondrial membrane potential in human cancer cell lines, Chem. Biol. Interact. 176 (2008) 58–70, https://doi.org/10.1016/j.cbi.2008.07.002.

[240] S.S. Malhi, A. Budhiraja, S. Arora, K.R. Chaudhari, K. Nepali, R. Kumar, H. Sohi, R.S.R. Murthy, Intracellular delivery of redox cycler-doxorubicin to the mitochondria of cancer cell by folate receptor targeted mitocancerotropic liposomes, Int. J. Pharm. 432 (2012) 63–74, https://doi.org/10.1016/j.ijpharm.2012.04.030.

[241] M. Zhou, L. Li, L. Li, X. Lin, F. Wang, Q. Li, Y. Huang, Overcoming chemotherapy resistance via simultaneous drug-efflux circumvention and mitochondrial targeting, Acta Pharm. Sin. B. 9 (2019) 615–625, https://doi.org/10.1016/j.apsb.2018.11.005.

[242] H. Wang, Z. Gao, X. Liu, P. Agarwal, S. Zhao, D.W. Conroy, G. Ji, J. Yu, C. P. Jaroniec, Z. Liu, X. Lu, X. Li, X. He, Targeted production of reactive oxygen species in mitochondria to overcome cancer drug resistance, Nat. Commun. 9 (2018) 562, https://doi.org/10.1038/s41467-018-02915-8.

[243] Y. Wang, X.Y. Zi, J. Su, H.X. Zhang, X.R. Zhang, H.Y. Zhu, J.X. Li, M. Yin, F. Yang, Y.P. Hu, Cuprous oxide nanoparticles selectively induce apoptosis of tumor cells, Int. J. Nanomed. 7 (2012) 2641–2652, https://doi.org/10.2147/IJN.S31133.

[244] Y. Wang, F. Yang, H.X. Zhang, X.Y. Zi, X.H. Pan, F. Chen, W.D. Luo, J.X. Li, H. Y. Zhu, Y.P. Hu, Cuprous oxide nanoparticles inhibit the growth and metastasis of melanoma by targeting mitochondria, Cell Death Dis. 4 (2013) e783, https://doi.org/10.1038/cddis.2013.314.

[245] J. Yang, Q. Cao, H. Zhang, L. Hao, D. Zhou, Z. Gan, Z. Li, Y.X. Tong, L.N. Ji, Z. W. Mao, Targeted reversal and phosphorescence lifetime imaging of cancer cell metabolism via a theranostic rhenium(I)-DCA conjugate, Biomaterials 176 (2018) 94–105, https://doi.org/10.1016/j.biomaterials.2018.05.040.

[246] C. Chen, X. Ni, S. Jia, Y. Liang, X. Wu, D. Kong, D. Ding, Massively Evoking Immunogenic Cell Death by Focused Mitochondrial Oxidative Stress using an AIE Luminogen with a Twisted Molecular Structure, Adv. Mater. 31 (2019) e1904914, https://doi.org/10.1002/adma.201904914.

[247] S. Huang, P. Fan, C. Zhang, J. Xie, X. Gu, S. Lei, Z. Chen, Z. Huang, Exosomal microRNA-503-3p derived from macrophages represses glycolysis and promotes mitochondrial oxidative phosphorylation in breast cancer cells by elevating DACT2, Cell Death Discov. 7 (2021), https://doi.org/10.1038/s41420-021-00492-2.

[248] C.L. Bland, A. Byrne-Hoffman, C.N. Fernandez, S.L. Rellick, D.J. Deng, W. Klinke, Exosomes derived from B16F0 melanoma cells alter the transcriptome of cytotoxic T cells that impacts mitochondrial respiration, FEBS J. 285 (2018) 1033–1050, https://doi.org/doi:10.1111/febs.14396.

[249] S. Dutta, C. Warshall, C. Bandyopadhyay, D. Dutta, B. Chandran, Interactions between exosomes from breast cancer cells and primary mammary epithelial cells leads to generation of reactive oxygen species which induce DNA damage response, stabilization of p53 and autophagy in epithelial cells, PLoS One 9 (2014) e97580, https://doi.org/10.1371/journal.pone.0097580.

[250] N. Chatterjee, D. Das, A. Jha, S. Roy, Role of mitochondrial-mediated pathways in breast cancer: An overview. Current advances in breast cancer research: A molecular approach, Bentham Science Publications, 2020, pp. 305–327, https://doi.org/10.2174/9789811451447120010015.

cancers

MDPI

Review

Trends in Research on Exosomes in Cancer Progression and Anticancer Therapy

Dona Sinha [1,*], Sraddhya Roy [1], Priyanka Saha [1], Nabanita Chatterjee [1] and Anupam Bishayee [2,*]

[1] Department of Receptor Biology and Tumour Metastasis, Chittaranjan National Cancer Institute, Kolkata 700 026, India; sraddhya1@gmail.com (S.R.); poojasaha.saha79@gmail.com (P.S.); nabanita.chatterje@yahoo.com (N.C.)

[2] Lake Erie College of Osteopathic Medicine, Bradenton, FL 34211, USA

* Correspondence: dona.sinha@cnci.org.in or donasinha2012@gmail.com (D.S.); abishayee@lecom.edu or abishayee@gmail.com (A.B.)

Simple Summary: Intensive research in the field of cancer biology has discovered a unique mode of interplay between cells via extracellular bioactive vesicles called exosomes. Exosomes serve as intermediators among cells via their cargoes that, in turn, contribute in the progression of cancer. They are ubiquitously present in all body fluids as they are secreted from both normal and tumor cells. These minuscules exhibit multiple unique properties that facilitate their migration to distant locations and modulate the microenvironment for progression of cancer. This review summarizes the multifarious role of exosomes in various aspects of cancer research with its pros and cons. It discusses biogenesis of exosomes, their functional role in cancer metastasis, both protumorigenic and antitumorigenic, and also their applications in anticancer therapy.

Abstract: Exosomes, the endosome-derived bilayered extracellular nanovesicles with their contribution in many aspects of cancer biology, have become one of the prime foci of research. Exosomes derived from various cells carry cargoes similar to their originator cells and their mode of generation is different compared to other extracellular vesicles. This review has tried to cover all aspects of exosome biogenesis, including cargo, Rab-dependent and Rab-independent secretion of endosomes and exosomal internalization. The bioactive molecules of the tumor-derived exosomes, by virtue of their ubiquitous presence and small size, can migrate to distal parts and propagate oncogenic signaling and epigenetic regulation, modulate tumor microenvironment and facilitate immune escape, tumor progression and drug resistance responsible for cancer progression. Strategies improvised against tumor-derived exosomes include suppression of exosome uptake, modulation of exosomal cargo and removal of exosomes. Apart from the protumorigenic role, exosomal cargoes have been selectively manipulated for diagnosis, immune therapy, vaccine development, RNA therapy, stem cell therapy, drug delivery and reversal of chemoresistance against cancer. However, several challenges, including in-depth knowledge of exosome biogenesis and protein sorting, perfect and pure isolation of exosomes, large-scale production, better loading efficiency, and targeted delivery of exosomes, have to be confronted before the successful implementation of exosomes becomes possible for the diagnosis and therapy of cancer.

Keywords: tumor-derived exosomes; exosomal cargoes; protumorigenic effect; drug resistance; anticancer therapy

Citation: Sinha, D.; Roy, S.; Saha, P.; Chatterjee, N.; Bishayee, A. Trends in Research on Exosomes in Cancer Progression and Anticancer Therapy. *Cancers* **2021**, *13*, 326. https://doi.org/10.3390/cancers13020326

Received: 23 November 2020
Accepted: 14 January 2021
Published: 17 January 2021

1. Introduction

Exosomes are bilayered endosomal nanovesicles, first discovered in 1983, as transferrin conjugated vesicles (50 nm) released by reticulocytes [1]. Due to the increasing interest of scientists in exosome biology, a consensus guideline was proposed by board members of International Society of Extracellular Vesicles under "minimal experimental requirements for definition of extracellular vesicles and their functions" (MISEV2014) which was

later updated in 2018 (MISEV2018). The guidelines advocated norms for nomenclature, isolation, separation, characterization, functional studies, and reporting requirements for proper identification of and experimentation with extracellular vesicles and exosomes [2,3]. Exosomes are generally formed by inward budding of late endosomes, also known as multivesicular bodies (MVBs). Intraluminal vesicles (ILVs) of MVBs engulf a variety of biomolecules which are released into extracellular space as exosomes. Exosomes are anucleated particles naturally released by cells, surrounded by lipid bilayer and are not capable of replication. Exosomes are identified by size (30–200 nm) and surface markers, such as membrane-associated proteins, e.g., lysosome-associated membrane glycoprotein 3 (LAMP3)/CD63; intercellular adhesion molecule (ICAM1)/CD81; and tetraspanin membrane protein/CD9. Exosomes are observed in various body fluids, such as blood, plasma, saliva, urine, synovial fluid, amniotic fluid, and breast milk [4,5].

All cellular types (normal and diseased) secrete exosomes, mediating intercellular communications [6]. Exosomes exhibit heterogeneity in size—Exo-Large (90–120 nm), Exo-Small (60–80 nm), and the membrane-less exomere (<50 nm). Exosome-mediated intercellular transfer of specific repertoire of proteins, lipids, RNA and DNA confer physiological and/or pathological functions to the recipient targets. Exosomes regulate physiological functions, such as neuronal communication, immune responses, reproductive activity, cell proliferation homeostasis, maturation and cellular waste disposition. They also contribute in clinical disorders, including inflammation, cancer, cardiovascular diseases, neuronal pathologies and pathogenic infections [5].

Our review deals with exosomal contents, exosome-associated protumorigenic, antitumorigenic effect and therapeutics, unlike other reviews, which discuss combinational roles of all microvesicles in cancer progression [7,8] or have primarily focused on tumor-derived exosomes (TEXs) with little information on therapeutics [9]. In contrast to reviews which have focused on specific exosomal cargoes and therapeutics [10,11], we have envisaged the exosomal contents, the mechanisms influencing cancer progression and their therapeutic implications in cancer management. The inexplicable nature of exosomes has raised concern about their role in the invasion and metastasis of cancer cells, encompassing epithelial-to-mesenchymal transition (EMT), angiogenesis, and immune regulation [12]. Thus, instead of reviewing the isolated impact of exosomes, e.g., evasion of immune surveillance [13] for cancer progression, we have tried to encompass exosome-mediated propagation of oncogenic signaling, epigenetic regulation, modulation of tumor microenvironment (TME) and immune escape, EMT, angiogenesis, metastasis and drug resistance. Considering the clinical applications, the exosomes serve as potent diagnostic and prognostic biomarkers because of their bioavailability, low toxicity and differentiated surface markers [5]. Recent reviews on exosomes have focused on therapeutic efficacy of exosomes by addressing extracellular vesicular interaction with the host immune system [14], constraints and opportunities available with bioengineering of exosomes [15–17], success against multiple cancers [18] and exosome-based drug delivery [19–21]. Anticancer treatments sometimes experience shortfall in their efficacy due to unwanted side effects of the therapeutic agents or shortened shelf-life, but exosomes serve as natural agents to overcome these issues and become a potent therapeutic agent [22]. However, instead of perceiving specific therapeutic potential of exosomes, the present review has tried to decipher the entire repertoire of exosomes, including both protumorigenic and antitumorigenic impact.

2. Cargo Composition of Exosomes

Exosomes are rich in enzymes, transcription factors, heat shock proteins (Hsps), major histocompatibility complex (MHC), cytoskeleton components, signal transducers, tetraspanins, lipids, RNAs and DNAs [6,23]. Detailed information about the exosomal components can be accessed via databases, such as ExoCarta [www.exocarta.org], EVpedia [http://evpedia.info] and Vesiclepedia [www.microvesicles.org]. Though exosomes diverge in size and biomolecular inclusions, some common components are observed in all types [5]. Lipid components are cholesterol, sphingomyelin, glycosphingolipids,

phosphatidylcholine, phosphatidylserines, phosphatidylethanolamines and saturated fatty acids [4]. RNAs include specific microRNAs (miRNAs), long non-coding RNAs (lncRNAs), vault RNA, Y-RNA, transfer RNAs (tRNAs), ribosomal RNA (rRNA) fragments (such as 28S and 18S rRNA subunits) and messenger RNAs (mRNAs) [24]. Exosomal cargo components also include mitochondrial DNA (mtDNA), single-stranded DNA, double-stranded DNA and retrotransposons [4,6]. Different protein forms include components of the immune system (MHC class I and II molecules, cytokines), endosomal sorting complexes required for the transport (ESCRT) complex, those involved in trafficking (tetraspanins, glycosylphosphatidylinositol-anchored proteins, Rabs, soluble N-ethylmaleimide-sensitive fusion protein attachment protein receptors (SNARES), flotillins, lipid-rafts residents [25] and those involved in carcinogenesis (oncoproteins, tumor suppressor proteins, and transcriptional factors) [4]. The plasma membrane (PM) proteins constitute the vesicle membrane for maintaining composition parity with the cell membrane which helps in sequestration of soluble ligands. Exosomal proteins are involved in (i) antigen presentation, (ii) cell adhesion, (iii) cell structure and motility, (iv) stress regulation, (v) transcription and protein synthesis, and (vi) trafficking and membrane fusion [26]. The structure of exosome with membrane proteins and cargoes have been depicted in Figure 1.

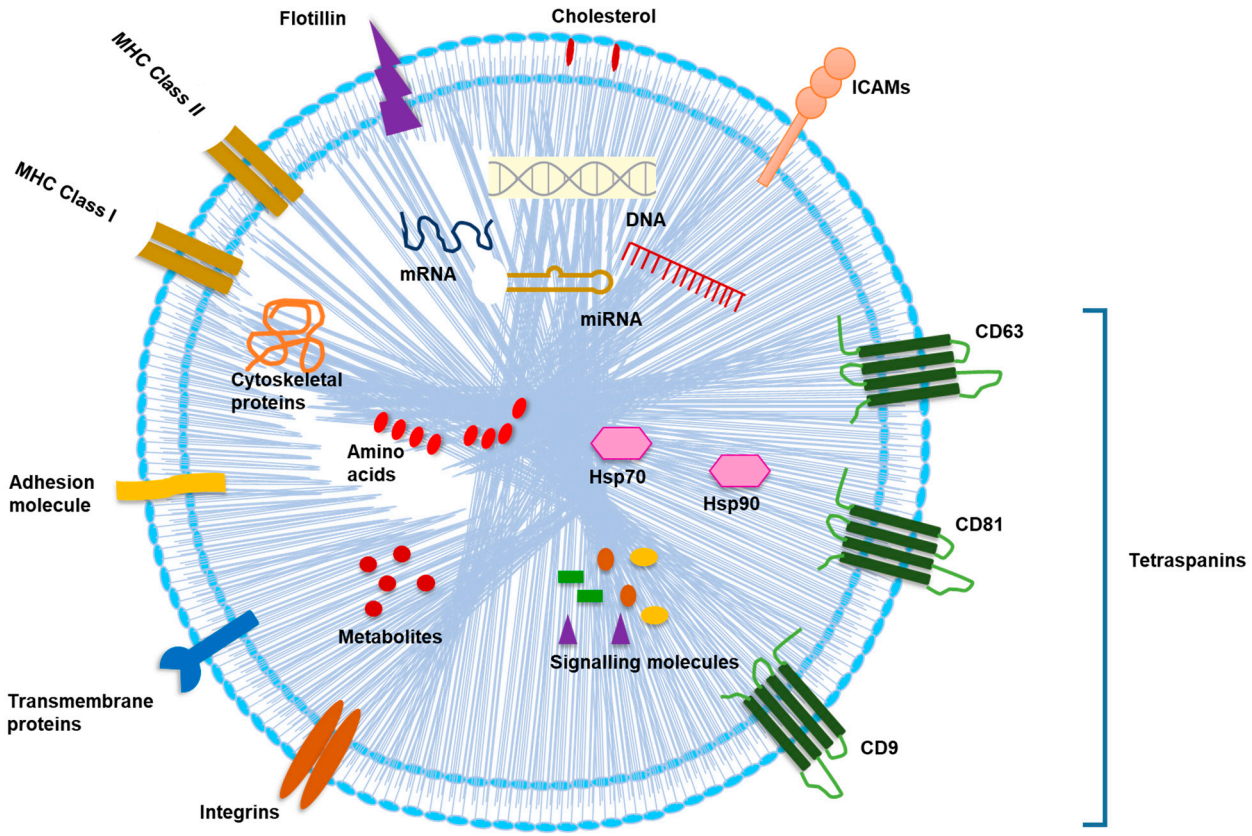

Figure 1. Structure of exosome with membrane proteins and cargoes. Exosomes consist of many constituents of a cell including DNA, RNAs, amino acids, proteins, metabolites, enzymes, lipids (cholesterol) and Hsps along with several cytosolic and cell-surface signaling proteins which are involved in intercellular communications. Exosomal membrane is rich in transmembrane proteins (tetraspanins such as CD81, CD63 and CD9), flotillin, ICAMs, integrins and adhesion molecules. They consist of immune components including MHC class I and class II molecules. Abbreviations: CD, cluster of differentiation; DNA, deoxyribonucleic acids; Hsps, heat shock proteins; ICAMs, intercellular adhesion molecules; MHC, major histocompatibility complex; mRNA, messenger RNA; miRNA, microRNA.

3. Exosome Biogenesis

Endocytosis generates early endosomes via invagination of PM rich in lipid rafts. This internalizes the PM receptors which are either recycled or degraded. The exosome biogenesis involves a complex network of enzymatic actions and signal transductions. Early endosomes mature to MVBs or late endosomes upon internal budding of endosomes, forming ILVs [23]. MVB budding is primed with actin polymerization at PM lipid domains [27,28]. ADP ribosylation factor 6 (ARF6), along with phospholipase D2 (PLD2), converts ILVs into mature MVBs [29]. Heparanase enzyme stimulates the syndecan-syntenin-ALG-2 interacting protein X (ALIX) axis, upregulating exosome formation [30]. ARF6-induced actomyosin contractility and ESCRTs promote ILVs shedding from MVBs as exosomes [31]. The MVBs undergo one of the three type consequences [23,32] mentioned below:

(i) Recycling through the trans-Golgi network (TGN) which may be subdivided into a fast and a slow pathway, considering the duration taken by the specific proteins/lipids from internalization to re-exposure at the cell surface or exocytosis.
(ii) Lysosomal degradation by hydrolytic enzymes which are able to digest complex macromolecules.
(iii) Fusion of MVBs with the cell surface release exosomes via exocytosis. Additional materials may be incorporated to the TGN at any juncture and processed through the canonical secretory pathways.

4. Sorting of Exosomal Cargoes

4.1. ESCRT-Dependent Sorting Pathway

The ESCRT pathway participates in sorting ubiquitinated proteins of exosome, after being internalized within ILVs. The complex includes ESCRT-0, which identifies and processes ubiquitin-dependent cargo inside the vesicles; ESCRT-I and ESCRT-II evoke budding and ESCRT-III causes vesicle scission from endosomal membrane. Other accessory proteins such as ALIX aid in vesicle budding and vacuolar protein sorting associated protein 4 (VPS4) promotes scission [30,33].

4.2. ESCRT-Independent Exosomal Sorting

Ceramide and cholesterol, PLD2, or tetraspanins mediates ESCRT independent sorting machinery. Tetraspanins may promote incorporation of specific cargoes into exosome, e.g., CD9 facilitates encapsulation of metalloproteinase CD10 and CD63. Even the lipid composition and membrane dynamics of the early endosome and MVBs may regulate exosomal cargoes. Ceramide and neutral sphingomyelinase 2 (nSMase2) play a pivotal role in an ESCRT independent process of exosome formation, loading, and release [23]. Podoplanin, a transmembrane glycoprotein, is another regulator of exosome biogenesis and cargo sorting [31].

5. Exocytosis and Secretion of Exosomes

Exocytosis is exosomal secretion into the extracellular matrix (ECM) which is regulated by Rab GTPases, molecular motors, cytoskeletal proteins, SNAREs, intracellular Ca^{2+} levels (increased Ca^{2+} results in increased exosome secretion) and extracellular/intracellular pH gradients [23]. Vesicular SNAREs (v-SNARE) on the MVB bind with the target SNARE (t-SNARE), Syx 5, on the inner surface of the PM for mediating fusion of MVB with the cell membrane [34]. The fusion of exosome with PM occurs at the actin-rich zones of the invadopodia, promoting ECM degradation and metastasis, followed by their exocytosis into extracellular space [34]. Peptidyl arginine deiminases aid exosomal secretion by deaminating actin [35]. A negative feedback mechanism limits excess exosome secretion from the same cells [34].

Rabs Control Endocytic Pathway

The Rab GTPases belong to a large family of highly conserved proteins with 60 members, which regulate vesicular trafficking in eukaryotes. Different Rab forms are involved

in endocytic trafficking—Rab4, 5, 9, 11a, 11b, 25 and 35 control recycling [36–39]; Rab5 and 7 cause endosomal maturation [40]; Rab 7 regulates sorting and degradation [41]; Rab 7, 27a and b control secretion of exosomes [42,43] and Rab5 overexpression causes release of exosomal markers [44]. Deregulation of the Rabs perturb the progression of cargo at specific endocytic locations. Rabs also play a crucial role in the regulation of tumor-derived exosomes. Rab11 influenced extrusion of exosome and interaction of MVB with autophagosomes [45] and promoted calcium dependent docking of MVBs to the PM [46] in K562 cells. Rab27A, in association with its GTPase activator, EP164, promoted exosome secretion by A549 lung cancer cells [47]. Rab27A/B are associated with exchange of exosomes between different cells of TME as well as with exosome secretion by macrophages [6]. Various types of Rabs involved in endocytic cargo trafficking have been depicted in Table 1.

Table 1. Different types of Rabs and their function in endocytic trafficking.

Rabs	Effects	Functions	References
Rab27	Secretion of exosomes	Release of markers MHC II, CD63, and CD81 in cancer cells	[32]
Rab7, Rab27a/b		Fusion with plasma membrane	[43]
Rab5, Rab4, Rab35	Recycling	Fast delivery of cargo to the plasma membrane	[36]
Rab5, Rab11a, Rab11b, Rab25		Slow delivery of cargo to the plasma membrane	[37,38]
Rab9		Transportation to TGN	[39]
Rab5, Rab7	Endosome maturation	Release of Rab5	[40]
Rab7	Sorting and degradation	Reduction in pH and acquisition of hydrolytic enzymes	[41]
Rab5 overexpression<break/>Note: may be rescued by Rab7	Suppression of release of exosomal markers syndecan, CD63, and ALIX	Inhibition of progression of endocytosed material from early endosomes	[44]

Abbreviations: ALIX, ALG-2 interacting protein X; MHC-II, major histocompatibility complex II; TGN, trans-Golgi network.

6. Exosomal Internalization by Recipient Cells

Exosomes float in the ECM after their release and exosomal surface proteins help in detecting the target cells for their internalization [48]. Exosomes attach to specific target cells by receptor-ligand binding, mediated through integrins, tetraspanins and intercellular adhesion molecules, which then internalizes exosomes (Figure 2) by (i) clathrin/caveolin-mediated endocytosis, (ii) uptake via lipid raft, (iii) macropinocytosis, (iv) direct fusion with the PM and (v) phagocytosis.

Clathrin protein forms a mesh like structure around the exosomes for its internalization. The PM of the recipient cells forms an inward invagination, followed by pinching off the clathrin coated vesicle from the membrane. The exosome empties all its contents in recipient cell's endosomes to perform specific functions [49]. Endocytosis, similar to the clathrin-dependent process, may be also mediated by caveolin-1 whose aggregations in PM form rafts. The invagination of the PM (caveolae) is rich in glycolipids, cholesterol and caveolin 1 [50]. Macropinocytosis involves distortion of PM forming protrusions from the membrane which encompass a region of extracellular fluid and exosomes, thereby internalizing exosomes. This process is Rac1-, actin- and cholesterol-dependent and it requires Na^+/H^+ exchange [51]. LAMP-1, integrins or tetraspanins are involved in the fusion of exosomes with the PM of recipient cells [52,53]. Phagocytosis is similar to macropinocytosis where exosomes are internalized along with some extracellular fluids. This process is followed by both phagocytic cells—like macrophages and dendritic cells (DCs)—and non-phagocytic cells like γδ T cells [54]. During exosome uptake by soluble signaling, exosomal ligands are cleaved by cytoplasmic proteases and are bound to their respective

receptors present on the PM of the recipient cells. In case of juxtacrine signaling, the ligands and receptors need to be in close proximity for efficient ligand–receptor binding [55]. Exosomal tetraspanins (CD9, CD63, CD81 and CD82) regulate cell fission and fusion, target cell selection [42], migration, adhesion, proliferation, and interaction between exosomes and recipient cells [56]. Size distribution in exosomes facilitates their internalization since cells have a propensity for loading smaller exosomes [5]. Oncogenic integrins play a dominant role during internalization of tumor-derived exosomes by recipient cells. Metastasis has been observed to be associated with exosome-integrins, such as αvβ6 integrin in prostate, αvβ5 integrins in liver and α6β4 and α6β1 integrins in lung [56].

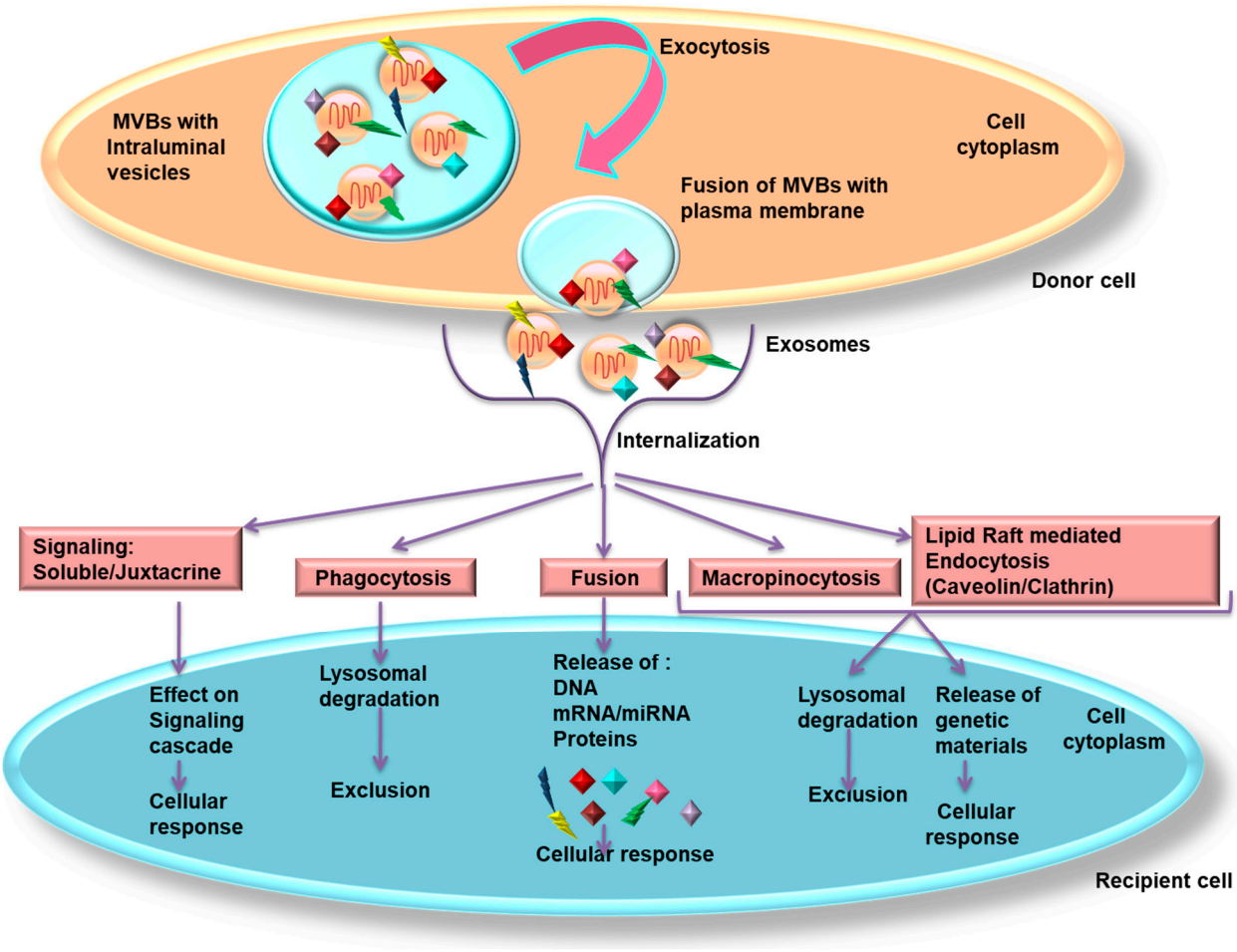

Figure 2. Mechanisms of internalization of exosomes. The exosomes inside the MVBs are extruded out from the donor cells by exocytosis on merging with plasma membrane. The released exosomes are then internalized via different modes: soluble/juxtacrine signaling; phagocytosis; fusion; micropinocytosis and lipid raft mediated endocytosis. The lipid raft mediated endocytosis can be either clathrin or caveolin protein dependent. Exosomes internalized by soluble/juxtacrine signaling affect the signaling cascade of the recipient cell. During phagocytosis, the exosomes undergo degradation, whereas, in the fusion event, genetic material is released that causes cellular response. In macropinocytosis and lipid raft-mediated endocytosis, the exosomes either undergo lysosomal degradation or mediate cellular response. Abbreviations: mRNA, messenger RNA; miRNA, microRNA; MVBs, multivesicular bodies.

7. TEX

The TEXs influence shaping of the TME, tumor progression, invasion and premetastatic niche formation, metastasis, angiogenic switch, and immune escape by paracrine subversion of local and distant microenvironments [57].

7.1. Oncogenic Signaling Involved in Exosomal Trafficking

According to the genometastatic theory, complex biomolecules in exosomes transfer oncogenic traits to target cells. Matrix cells in the TME interact with their oncogenic counterparts through exosomes and mediate tumor evolution and progression. Exosomal cargoes confer oncogenic transformation, EMT, immune surveillance evasion, invasion, and metastatic properties to the recipient cells [58]. Hypoxia and extracellular acidity culminate in greater release of TEXs [58]. Cells having even one oncosuppressor mutation are more prone towards uptake of exosomal oncogenic factors. Mutations leading to upregulated mitogen-activated protein kinase (MAPK) signaling in cancer cells elevated exosomes release [59]. Secretion of exosomes by activated platelets promoted MAPK and phosphoinositide 3-kinase (PI3K)/protein kinase B (Akt)/matrix metalloproteinase (MMP) signaling during cancer progression [31]. Expression of oncogenic RAS in non-tumorigenic epithelial cells promoted secretion of oncoprotein-rich exosomes [60]. Robust expression of oncogenic and truncated forms of epidermal growth factor receptor (EGFR) vIII in glioma cells augmented exosomal secretion and transfer of oncogenic activity to other normal cells [61]. Mutation of liver kinase B1 (STK11), a tumor suppressor, increased exosome secretion in lung cancer [62]. Secretion of exosomal mtDNA induced anaerobic metabolism and dormancy in cancer cells [31].

7.2. Exosomal miRNA-Mediated Cancer Promotion

Breast TEXs, enriched with Dicer, Protein Argonaut 2, and transactivation response element RNA-binding protein, processed precursor miRNAs into mature miRNAs for gene silencing in target cells and induced non-tumorigenic epithelial cells to form tumors [63]. Exosomal miRNAs suppressed cell proliferation by downregulating the C-X-C motif chemokine ligand 12 (CXCL12); exosomal-miR-23b augmented cell quiescence by inhibiting myristoylated alanine-rich C-kinase substrate expression in the metastatic niche [64]; miR-10b molded the TME to promote tumor metastasis [65] of breast cancer (BC) cells. Astrocyte-derived exosomes suppressed phosphatase and tensin homolog (PTEN) by intracellular trafficking of miR-19a in metastatic BC and melanoma brain metastasis models [66]. Release of exosomal miR-1245 from mutant p53 cancer cells reoriented macrophages to transforming growth factor-β (TGF-β)-rich tumor-associated macrophages (TAMs) which, in turn, propagated tumor progression [67]. Exosomal miR-105 and miR-939 in BC and miR-181c in brain cancer dissolved tight junctions, caused vascular leakiness and induced metastasis [31].

7.3. Exosomes and TME

TEXs are well documented for immune suppression by multiple interactions with immune cells of the TME (Figure 3). They hinder helper and cytotoxic T-cell activation and function, activate regulatory T-cell (Tregs), inhibit cytotoxicity of natural killer (NK) cells, augment differentiation of myeloid-derived suppressor cells (MDSCs) and reduce leukocyte adhesion [34]. Exosomes modulate the TME by extracellular signal-regulated kinase (ERK)-mediated cell growth or apoptosis. Interaction of stromal cells and tumor via exosomes inflict dissemination of tight junctions, generating a suitable niche for metastasis [68]. TEXs induced cancer-associated fibroblasts (CAFs) for exosomes' release [69]. The transfer of CAF-derived exosomal cargoes in the form of metabolic intermediates of the tricarboxylic acid cycle to cancer cells promotes neoplastic growth by alteration of glycolysis and glutamine-dependent reductive carboxylation [70]. Exosomes transformed fibroblasts into CAFs in melanoma [71]. CAFs or mesenchymal stem cells (MSCs) derived exosomes maneuvered Wnt signaling-induced migration [68]. Exosomes expressing Fas ligand activated CD8+ T-cell apoptosis [72]. Exosomal αvβ6 integrin inhibited the signal transducer and activator of transcription 1 (STAT1)/MX1/2 signaling in cancer cells and reprogramed monocytes into the M2 phenotype [73]. Exosomal miR-146a-5p from hepatocellular carcinoma (HCC) cells induced M2 polarization [74]. BC cell derived exosomes inhibited NK cells [75] and infiltrated neutrophils into tumors [76]. Melanoma-derived

exosomes perturbed maturation of DCs in lymph nodes [77]. However, TEXs can supply antigens to DCs for cross-presentation to cytotoxic T cells [78]. Administration of topotecan/radiation induced the release of exosomal immunostimulatory DNA, which inflicted DC maturation and cytotoxic T cell activation [31]. Programmed death ligand 1 (PD-L1)-positive exosomes positively correlated with head and neck squamous cancer cells (HNSCC) progression in patients and administration of anti-PD-L-1 antibodies inhibited the immunosuppressive function of PD-L1 [79].

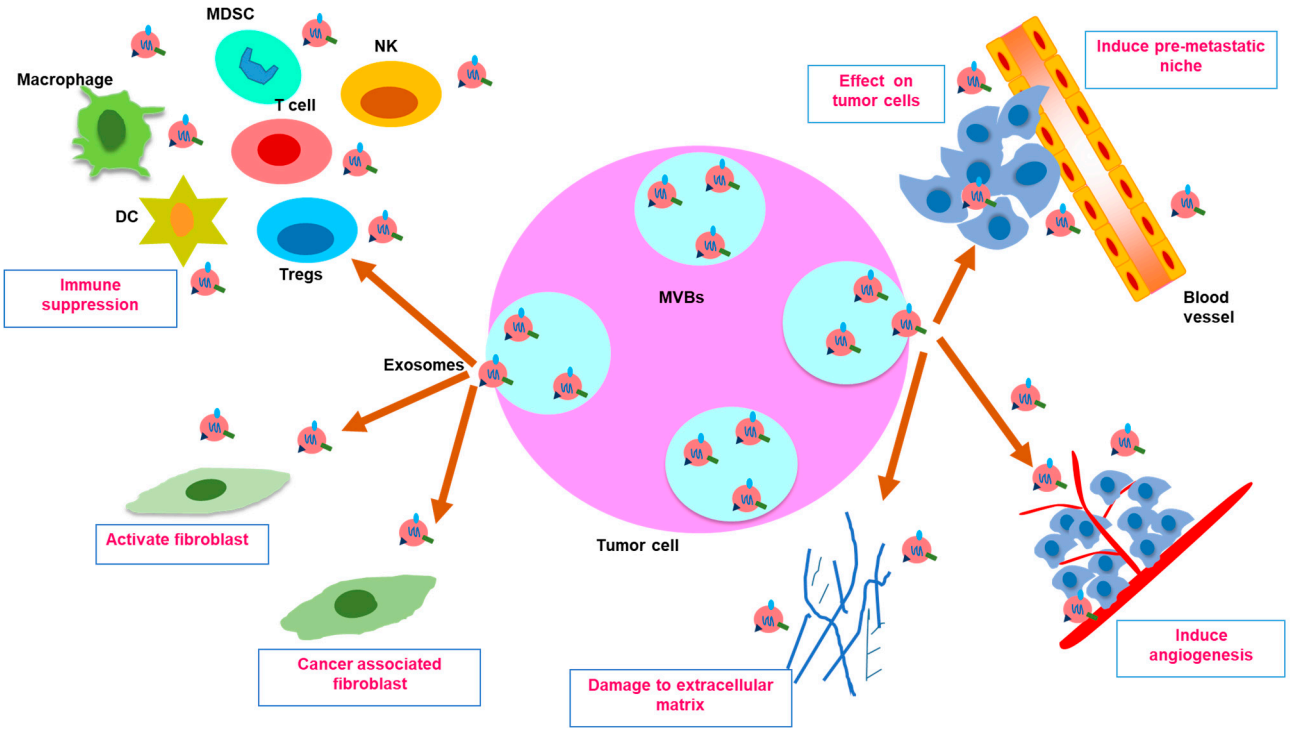

Figure 3. Exosomes in tumor microenvironment. Exosomes secreted from tumor cells containing MVBs exhibited a dynamic signaling between tumor cells and the TME. Exosomes may lead to immune suppression by downregulating macrophages, DC, T cells and NK cells and upregulating immunosuppressive cells like Tregs, MDSCs and TAMs. Exosomes induced differentiation of fibroblasts, activation of CAFs and degradation of ECM, which are associated with TME construction. They are involved in the alteration of ECM, hypoxia-mediated angiogenesis and the formation of pre-metastatic niches that trigger the metastatic escape of tumor cells. Abbreviations: CAFs, cancer-associated fibroblasts; ECM, extracellular matrix; DCs, dendritic cells; MDSCs, myeloid-derived suppressor cells; NK cells, natural killer cells; TAMs, tumor-associated macrophages; TME, tumor microenvironment; Tregs, tumor regulatory cells.

7.4. Impact of Exosomes on EMT, Invasion, Metastasis and Angiogenesis

Exosomal cargoes CD151 and Tspan8 are related with ECM degradation, stromal reprogramming, cell motility and tumor progression [80]. EMT was induced by exosomal miR-663b in bladder cancer [81]; lncRNA SOX2 overlapping transcript (Sox2ot) in pancreatic ductal adenocarcinoma (PDAC cells) [82]; and TGF-β-enriched TEXs in myofibroblasts [83]. Migration of tumor cells was facilitated by the exosome-mediated transfer of αvβ6 in prostate cancer [84]; miR-21 in bladder cancer [85]; TAM derived exosomes in gastric cancer (GC) cells [86]; and lncRNA ubiquitin-fold modifier conjugating enzyme 1 (UFC1) in non-small cell lung carcinoma (NSCLC) [87]. Exosomal lncRNA zinc finger antisense 1 (ZFAS1) induced EMT and migration in GC cells [88]. Metastasis was promoted by exosomal EGFR in GC [89]; MMP1 mRNA in ovarian cancer [90]; miR-25-3p, miR-130b-3p, miR-425-5p in colorectal cancer cells (CRC) [91]; miR-106b in lung cancer [92]; and miR-21 in oesophageal cancer [93]. Cell proliferation and invasion was induced by exosomal miR-1260b in lung adenocarcinoma [94] and miR-222 in PDAC [95]. Angiogenesis and

tumor progression were influenced by exosome mediated Wnt4/β-catenin signaling in CRC [96] and by vascular endothelial growth factor A (VEGF-A) enriched exosomes in brain endothelial cells [97]. Tumor progression was augmented by exosomal miRNAs from TP53-mutant cells in colon cancer cells [98] and by exosomal lncRNA ZFAS1 in GC [92]. Exosomal miR-21 reduced apoptosis in GC cells [99], exosomal IL-6 induced metastasis in BC cells [100], exosomal HSP70 induced tumor progression in MSC cells [101], and exosomal TGF-β promoted tumor growth in LAMA84 cells [102]. Various recent studies based on the tumor promoting effect of exosomes have been listed in Table 2.

Table 2. Tumor-promoting effects of exosomal cargoes on recipient cells.

Exosome Donor Cells	Exosomal Cargo	Target Cells	Effects	Mechanisms	References
Human prostate cancer (PC3) cells	Integrin $\alpha_V\beta_6$	Peripheral blood mononuclear cells and THP-1 monocyte cells	↑M2 polarization	↓STAT1/MX1/2 signaling	[73]
		Human prostate cancer DU145 cells	↑Cell adhesion and migration	↑Latency-associated peptide-TGF-β	[84]
HCC (mouse Hepa1-6, H22, and human HepG2, H7402) cells	miR-146a-5p	Mouse RAW264.7 cells, THP-1 cells, mice peritoneal macrophages	↑Pro-inflammatory factors, ↑M2 polarization, ↑T-cell exhaustion by M2 macrophages	↑NF-κB, ↑p-STAT3, ↓p-STAT1	[74]
Human Bladder cancer (T24 and 5637) cells	miR-663b	T24 and 5637 cells	↑Cell proliferation, ↑EMT	↓ERF, ↓E-cadherin, ↑Vimentin	[81]
Human PDAC (Hs 766 T) and metastatic (Hs 766T-L2) cells	lncRNA-Sox2ot	Human PDAC (BxPC-3) cells	↑EMT, ↑stemness, ↑invasion and metastasis	↑Sox-2	[82]
Human bladder cancer (T24) cells	miR-21	Human THP-1 cell-derived macrophages	↑M2 polarization, ↑tumor cell migration and invasion	↓PTEN, ↑PI3K/Akt-STAT3 signaling	[85]
M2 polarized macrophages (TAMs)	Apolipoprotein E	Mouse gastric carcinoma (MFC) cells	↑Cell migration	↑PI3K-Akt signaling	[86]
Human NSCLC (A549 and H1299) cells	lncRNA UFC1	A549 and H1299 cells	↑Cell proliferation, ↑migration, ↑invasion	↓PTEN via EZH2-mediated epigenetic silencing	[87]
Human GC (BGC-823) cells	lncRNA-ZFAS1	Human GC (MKN-28) cells	↑EMT, ↑cell proliferation, ↑migration	↑Cyclin D1, ↑Bcl-2, ↓Bax, ↓E-cad, ↑N-cad, ↑Slug	[88]
Human GC (SGC7901) cells	EGFR	Primary mouse liver cells	↑Cell proliferation, ↑metastasis	↓miR-26a/b, ↑HGF, ↑c-Met	[89]
Human CRC (HCT116) cells	miR-25-3p, miR-130b-3p and miR-425-5p	Macrophages RAW264.7	↑M2 polarization, ↑EMT, ↑liver metastasis	↑CXCL12/CXCR4 axis, ↓PTEN, ↑PI3K-Akt signaling	[91]
Human lung cancer (SPC-A-1 and H1299) cells	miR-106b	SPC-A-1 and H1229 cells	↑Migration and invasion	↓PTEN	[92]
Human esophageal cancer (EC9706) cells	miR-21	EC9706 cells	↑Metastasis	↓PDCD4, ↑MMP2, ↑MMP9	[93]
Human lung adenocarcinoma (H1299) cells	miR-1260b	Human A549 cells	↑Cell invasion, ↑cell proliferation, ↑drug resistance	↑Wnt/β-catenin signaling, ↓sFRP1, ↓Smad4	[94]
Human PDAC (Capan-1 and Hs 766T-L3) cells	miR-222	PDAC (Capan-1 and Hs 766T-L3 cells)	↑Cell invasion, ↑metastasis	↑Akt, ↓PPP2R2A, ↑p-P27	[95]

Table 2. *Cont.*

Exosome Donor Cells	Exosomal Cargo	Target Cells	Effects	Mechanisms	References
Hypoxic human CRC (HT29 and HCT116) cells	Wnt4	Endothelial (HUVECs) and CRC (HT29) cells	↑Proliferation, ↑angiogenesis, ↑migration	↑β-Catenin signaling	[96]
TP53-mutant (HT29) colon cancer cells	miR-1249-5p, miR-6737-5p, and miR-6819-5p	Human colon fibroblasts (CCD-18Co) cells	↑Tumor progression	↓TP53	[98]
Murine bone marrow–derived macrophages	miR-21	Human GC (MFC, MGC-803) cells	↓Apoptosis, ↑resistance to cisplatin	↑PI3K/AKT signalling, ↓PTEN	[99]
Co-culture of THP-1-derived macrophages exposed to apoptotic human BC (MCF-7 or MDA-MB-231) cells	IL-6	Naive (MCF-7 or MDA-MB-231) cells	↑Proliferation, ↑metastasis	↑p-STAT3, ↑cyclin D1, ↑MMP2, ↑MMP9	[100]
Human lung cancer (A549) cells	HSP70	MSCs extracted from human adipose tissue	Pro-inflammatory MSCs, ↑tumor growth	↑TLR-2/NF-κB signaling, ↑IL-6, ↑IL-8, ↑MCP-1	[101]
Human chronic myeloid leukemia (LAMA84) cells	TGF-β	LAMA84 cells	↑Proliferation, ↓apoptosis, ↑tumor growth	↑SMAD 2/3, ↑Bcl-w, ↑Bcl-xL, ↑survivin, ↓BAD, ↓BAX, ↓PUMA	[102]
Human BC (MCF-7) tamoxifen resistant cells	miR-221/222	Human BC (MCF-7) wild type cells	↑Resistance to tamoxifen	↓P27, ↓ERα,	[103]
Human cisplatin resistant A549 cells	miR-100-5p	Human A549 cells	↑Resistance to cisplatin	↑mTOR	[104]
Gemcitabine treated human PDAC CAFs	Snail and miR-146a	Human pancreatic cancer L3.6pl cells	↑proliferation, ↑resistance to gemcitabine	↑Snail, ↑miR-146a	[105]
Human HER-2-positive BC trastuzumab resistant (SKBR-3 and BT474) cells	lncRNA AFAP1-AS1	SKBR-3 and BT474 cells	↑Resistance to trastuzumab	↑ERBB2	[106]
Tamoxifen resistant BC (LCC2) cells	lncRNA UCA1	ER-positive BC MCF-7 cells	↑Cell viability, ↑resistance to tamoxifen	↓caspase-3	[107]
Human GC (MGC-803 and MKN-45) cisplatin resistant cells	lncRNA HOTTIP	MGC-803 and MKN-45 cells	↑Resistance to cisplatin	↑HMGA1	[108]

Symbols: ↑, upregulated; ↓, downregulated; Abbreviations: AFAP1-AS1, actin filament associated protein1 antisense RNA 1; Akt, protein kinase B; Bad, Bcl-2 associated agonist of cell death; Bax, Bcl-2-associated X protein; Bcl-2, B-cell lymphoma 2; c-Met, Mesenchymal-epithelial transition factor; CXCL12, C-X-C motif chemokine ligand 12; CXCR4, C-X-C chemokine receptor type 4; Erα, estrogen receptor-α; ERF, Ets2-repressor factor; ERBB2, erythroblastic oncogene B; HGF, hepatocyte growth factor; HMGA1, High-mobility group A1; HOTTIP, HOXA transcript at the distal tip; MCP-1, monocyte chemoattractant protein-1; MMP, matrix metalloproteinase; NF-κB, nuclear factor kappa-light-chain-enhancer of activated B cells; PDCD4, programmed cell death 4; PI3K, phosphoinositide 3-kinase; PPP2R2A, protein phosphatase 2 regulatory subunit B alpha; PTEN, phosphatase and tensin homolog; PUMA, p53 upregulated modulator of apoptosis; sFRP, secreted frizzled-related protein 1; STAT, signal transducer and activator of transcription; Sox-2, sex determining region Y-box 2; TGF-β, transforming growth factor-β; TLR-2, toll-like receptor 2; TP53, tumor protein p53.

7.5. Exosomes and Drug Resistance

Exosomes form a physical barrier against drug penetration and confer drug resistance by transfer of cargoes from resistant to sensitive cells [104]. Exosome-mediated drug resistance may be devised through trafficking of non-coding RNAs, drug transporters and neutralization of antibody-based drugs, which has been described in the following sections.

7.5.1. By Trafficking of Non-Coding RNAs

Non-coding RNAs, including miRNAs and lncRNAs, perpetuated drug resistance across an array of cancer cells. Exosomes from M2-macrophage exerted miR-21-mediated upregulation of PI3K/Akt signaling and reduced apoptosis and cisplatin resistance in GC [93]. Exosomal miR-221/222 modulated p27 and ERα for tamoxifen resistance [103] in BC cells. Exosomes derived from cisplatin resistant cells induced resistance in cisplatin sen-

sitive A549 cells in a miR-100-5p-dependent manner [104]. In ovarian cancer cells, exosomal miR-443 induced senescence and resistance against paclitaxel [109]. In prostate cancer, CAF derived exosomes conferred gemcitabine resistance via Snail and miR-146a [105]. Exosomal cargo-lncRNA UCA1 mediated tamoxifen resistance [107] and lncRNA actin filament associated protein1 antisense RNA 1 (AFAP1-AS1) conferred trastuzumab resistance by binding to AU binding factor 1 and translating erythroblastic oncogene B2 (ERBB2) [106] in BC cells. MSC-derived exosomes aided the transfer of lncRNA PSMA3-AS1 to myeloma cells and exerted resistance against proteasome inhibitor [110]. In GC, exosomal lncRNA HoxA transcript at a distal tip (HOTTIP) made sensitive GC cells cisplatin resistant [108].

7.5.2. By Trafficking of Drug Transporters and Neutralizing Antibody-Based Drugs

The exosome-mediated transfer of drug transporter molecules is intimately associated with the spread of drug resistance across diverse cancer forms. Exosomes transported P-glycoprotein (P-gp) from doxorubicin-resistant cells [68] and multidrug resistance protein-1 (MDR-1) from docetaxel-resistant cells [111] to confer drug resistance in sensitive BC cells. Recently, it has been evidenced that exosome-mediated transfer of chloride intracellular channel 1 upregulated P-gp and B cell lymphoma-2 (Bcl-2) and conferred vincristine resistance in GC cell line SGC-7901 [112].

B-cell lymphoma derived exosomes modulated ATP-binding cassette (ABC) transporter A3, carried CD20 antigen which shielded the cancer cells against therapeutic CD20 antibodies and evaded immune surveillance [113]. Exocytosis of TEXs from human epidermal growth factor receptor 2 (HER2) positive BC cells expressed specific decoy molecules and conferred resistance against monoclonal antibody trastuzumab, thus depicting that TEXs are also involved in neutralizing antibody based drugs [114].

8. Strategies against Tumor-Derived Exosomes

There have been, primarily, three approaches for the management of exosomes associated with pathogenesis, as described below.

8.1. Suppression of Exosome Biogenesis and Trafficking

Genetic knockdown of tumor suppressor TSG1 (protein involved with exosome biogenesis and trafficking) reduced Wnt5b-positive exosomes in colon cancer [115]. Suppression of annexin A1 (responsible for membrane contact sites, inward vesiculation and exosome biosynthesis) reduced the number of secreted exosomes in pancreatic cancer cells [116]. Manumycin A was reported to inhibit ESCRT-dependent exosome biogenesis by modulating Ras/Raf/ERK1/2/heterogeneous nuclear ribonucleoprotein H1 axis in prostate cancer cells [117].

Small molecule inhibitor GW4869 against nSMase2 reduced secretion of ceramide enriched exosomes [118] and sensitized breast tumors by inhibition of exosomal PD-L1 [119]. Knockout of nSMase2 reduced exosome secretion, angiogenesis and metastasis in breast tumors [120]. Another inhibitor of lipid metabolism, pantethine, a pantothenic acid (vitamin B_5) derivative, depleted the release of exosomes in MCF-7 variants and increased doxorubicin responsiveness [121]. Genetic silencing of Rab27A/B reduced exosomal secretion by HNSCC and macrophages, thereby minimizing metastasis in BC cells [76] and lung metastasis in melanoma [122]. PRAS40 downregulated Akt, downstream of TGF-β, and mediated antagonistic effects against exosome secretion and chemoresistance in breast and lung cancer cells [123]. WEB2086, a platelet-activating factor receptor (PAFR) antagonist, was shown to reduce gemcitabine-induced exosome release in PAFR-positive pancreatic cancer cells [124]. Other exosome extrusion inhibitors, such as chloramidine, bisindolylmaleimide-I, imipramine, d-pantethine, and calpeptin, and calcium chelators, such as ethylene glycol bis (2-aminoethyl ether) tetra-acetic acid, increased responsiveness toward 5-FU in prostate and BC cells [125]. The inhibition of protease-activated receptor 2 by an anticoagulant, apixaban, which binds to the tissue factor–factor VIIa complex, downregulated the secretion of TF-bearing exosomes from pancreatic cancer

cells [126]. Dasitinib inhibited exosome release and beclin-1/Vps34 mediated autophagy in imatinib resistant K562 cells [127]. Reduced exosome secretion by synthetic peptide (constructed with a derivative of the secretion modification region of HIV-1 Nef protein, a N-terminus anchored polyethylene glycol residue and a c-terminus cluster in peptide) [128] and by Docosahexaenoic acid (a polyunsaturated fatty acid) [34] inhibited metastasis and angiogenesis, respectively, in BC cells.

8.2. Depletion of Exosome Uptake

A synthetic nanoparticle, which is a prototype of high-density lipoprotein, was used as an agonist of the scavenger receptor type B-1 (SR-B1) which eliminated cholesterol from lipid rafts and prevented exosome uptake by SR-B1 expressing cancer cells [129]. Other agents, such as heparin sulfate proteoglycans, methyl-β cyclodextrin (molecule used for cholesterol removal from natural and artificial membranes) and dynasore (dynamin inhibitor), have been reported to abrogate exosome endocytosis in cancer cells [130]. Heparin and dynasore attenuated the uptake of multiple myeloma-derived exosome by bone marrow stromal cells and inhibited phosphorylation of STAT1, STAT3, and ERK1/2 signaling pathways [131]. Radiation-derived exosomes made the recipient cancer cells radiation-resistant and aggravated proliferation. Heparin and simvastatin attenuated radiation-derived exosome uptake by recipient cells in in vitro and in vivo models of glioblastoma [132].

8.3. Modulation of Harmful Exosomal Cargo and Inhibition of Exosome Dissemination

Alteration of exosomal cargoes was achieved by viral manipulation or by incorporation of viral proteins/RNA into secreted exosomes [133]. Curcumin culminated the immunosuppressive effect of exosomes in BC by deregulation of the ubiquitin-proteasome system and cargo sorting of ILVs [134]. Subscapular sinus CD169+ macrophages bound with exosomes restricted their interaction with B cells, promoting tumor progression [135]. Exosome release was inhibited by inhibitors like indometacin (COX2 inhibitor) in combination with rapamycin (interfere with MVB biogenesis) in B lymphoma cells, by suppressing ATP-binding cassette sub-family A member 3 expression of the lymphoma cells and induced the cells to undergo complement dependent cytolysis under the effect of drug rituximab [113].

8.4. Removal of Exosomes

A microfluidics-based technology-microscale acoustic standing wave technology facilitates clearance of exosomes from circulation [136]. Innate immune system in co-operation with opsonization effects of complement proteins may be used for elimination of exosomes [137]. Opsonization of exosomal markers CD9 and CD63 by targeting anti CD9 and anti CD63 antibodies elevated exosomes representation to the macrophages, leading to exosomes' elimination, which suppressed lung metastasis in vivo [138]. In colorectal cancer, dimethyl amiloride depleted exosomes, thereby elevating cyclophosphamide efficacy against the cancer cells [139].

9. Cancer Management with Exosomes

Exosomes have emerged as a new arena of clinical interest due to their prospective use in diagnostic applications as potential biomarkers, for carrying specific information of their progenitor cells, as well as for being ideal candidates for liquid biopsy [56].

9.1. Preclinical Studies on Anticancer Potential of Exosomal Cargoes

Uptake of exosomal contents does not always confer procarcinogenic signaling. There are instances where exosomal proteins promoted anticarcinogenic signaling pathways, e.g., exosomal uptake with payload of gastrokine1 suppressed H-Ras/Raf/MEK/ERK-mediated gastric carcinogenesis in gastric epithelial cells [140]. The miR-375 carried by exosomes inhibited cell proliferation and invasive capability in colon cancer cells through

Bcl-2 blocking [141]. Exosomal miR-520b derived from normal fibroblasts cells inhibited proliferation and migration of pancreatic cancer cells [142]. The migratory behavior of lung cancer cells was reduced by exosomal miR-497 through suppression of growth factors, cyclin E1 and VEGF [143]. Exosomal circulating RNA circ-0051443 inhibited tumor progression through apoptosis induction in HCC cells [144]. In BC cells, exosomal miR-100 derived from MSCs inhibited angiogenesis in vitro via modulating mTOR/HIF-1α/VEGF signaling [145].

9.2. Exosomes as Biomarkers

Cancer cells secrete exosomes ten times higher than normal cells, which makes TEXs major potential candidates for liquid biopsy needed for cancer diagnosis and prognosis [57]. The release of exosomes in the extracellular space also aids in cancer diagnosis by examining their increased levels in various body fluids, such as blood, ascites fluid, urine, and saliva [146]. Exosomal DNA represents the entire genome; therefore, liquid biopsies of plasma aid in early detection of cancer-specific mutations. Exosomal CD63 and caveolin-1 served as non-invasive markers of melanoma [121]. Exosomal lncRNA, either with miR-21 or alone, was correlated with tumor classification (III/IV), stage of tumor and lymph node/distant metastasis in many cancer types [5]. Differential expression of exosomal miR-150, miR-155, and miR-1246 in serum of normal individuals and acute myeloid leukemia patients detected minimal residual disease [147]. Phosphatidylserine present on the exosomal surface also serves as a biomarker for diagnosis of early-stage cancer [148]. However, exosomal biomarkers are often overshadowed by highly prevalent complex proteins of the body fluids. Exosome isolation from body fluids follows either of the three methods, namely differential centrifugation coupled with ultracentrifugation, immunoaffinity pull-down, and density gradient separation. Mining of exosomal biomarkers from body fluid of cancer patients has been explored with fluorescence-based analytical techniques, electrochemical aptamer-based detection methods, localized surface plasmon resonance and surface-enhanced Raman scattering [149]. Though exosome biomarker analysis has tremendous translational potential, a gold standard for exosome isolation under clinical settings is yet to be achieved [150]. Since there is no definite consensus for isolation of exosomes, the best suitable body fluid for exosome isolation is also under investigation.

9.3. Role of Exosomes in Immunotherapy and Vaccine Development

DCs and other antigen presenting cells (APCs) derived exosomes are loaded with specific drugs; miRNAs of interest or even exosomes alone are implemented to trigger immune response in the recipient individuals (Figure 4). DC-based exosomes, in therapy, are beneficial as they possess abundant surface lactadherin that helps in efficient exosome uptake [151]. The functional moieties, such as MHC-I, MHC-II, CD40, CD80, CD86 TNF, FasL, TRAIL and natural killer group 2D (NKG2D) ligands on the surface of DC-derived exosomes, facilitate in imparting innate and adaptive antitumor immune response [152]. DC-derived exosomes activated NK cells in NKG2D and interkeukin (IL)-15Rα ligand dependent mode, which restored 50% functionality of NK cells and was implemented as a cell free vaccination strategy [153]. The administration of adjuvants, such as IFN-γ, Toll-like receptor agonists, and polyinosinic: polycyctidylic acid, was explored for production of mature DC-derived exosomes which showed greater potential for activation of Th1 cells [154,155]. Immunogenic cell death was induced by melphalan, an anticancer drug, in multiple myeloma cells by increasing the damage-associated molecular pattern containing exosomes, thus triggering NK cell cytotoxicity [156]. A histone deacetylase inhibitor, MS-275, increased the release of Hsp70 and MHC-I polypeptide-related sequence B (MICB)-rich exosomes which induced NK cytotoxicity and lymphocyte proliferation [157]. Heat shock treatment increasing the immunostimulatory activities of TEXs has been demonstrated in A20 lymphoma/leukemia cells. Heat shock tumor derived exosomes were observed to possess more immune-stimulating activities due to elevated expression of MHC and increased levels of cytokines, such as IL-1β, IL-12p40, and TNF-α [158].

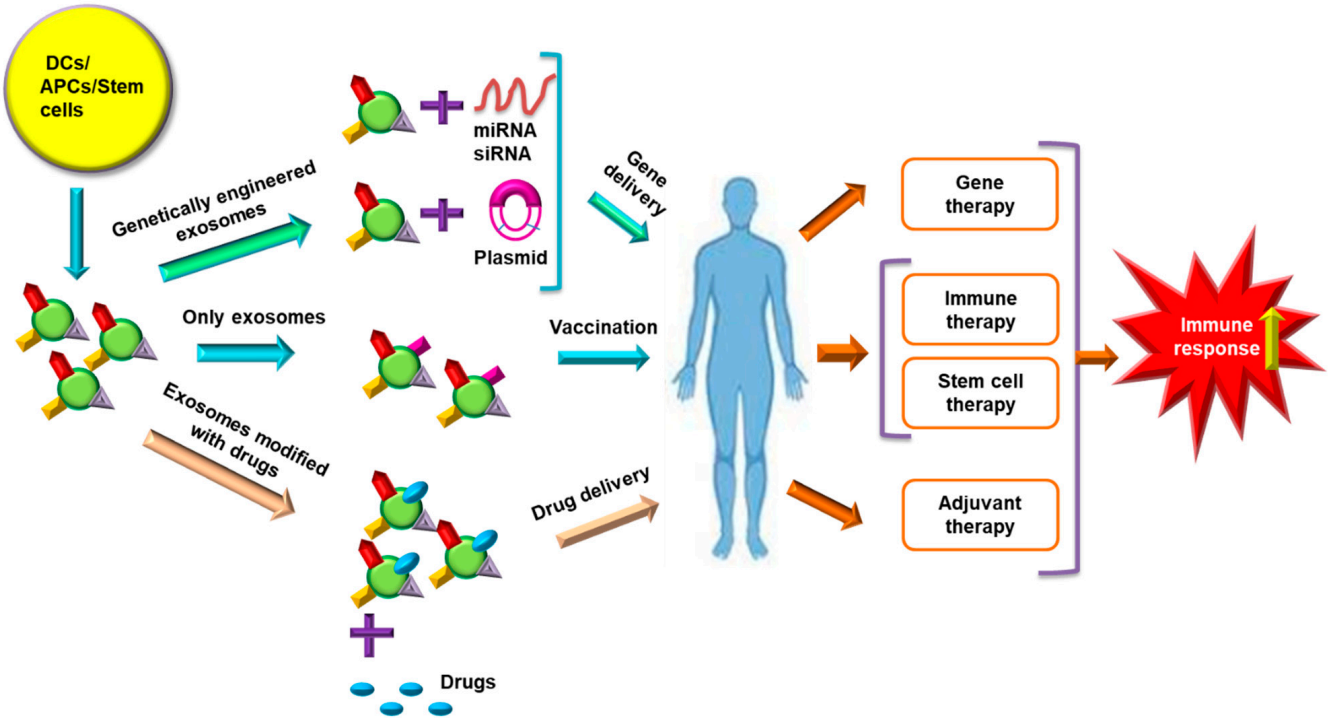

Figure 4. Exosomes in therapeutic approaches. Exosomes derived from DCs, APCs and stem cells can be utilized for immunotherapy, gene therapy, stem cell therapy and adjuvant therapy. Exosome based gene therapy is obtained by genetically engineered exosomes loaded with miRNA, siRNA and plasmids of interest. Stem cell or DC-derived exosomes can be implemented alone as vaccines and confer stem cell-based therapy or immunotherapy. The exosomes can also be utilized for drug delivery vectors by modifying them with drugs of interest. The DC-, APC- and stem cell-derived exosomes administered into the patient help in triggering immune response in combating cancer by targeting and regulating the mechanisms against which the exosomes are implemented. Abbreviations: APCs, antigen presenting cells; DCs, dendritic cells; miRNA, microRNA; siRNA, small interfering RNA.

Exosomes have potential use in vaccine development because the surface-bound proteins on exosomes of APCs, DCs and tumor cells originate from the progenitor cell membranes [5]. Nanoscale immunotherapy treatments with TEX, DC-derived exosomes and ascitic cell-derived exosomes have shown efficacy in stimulating the body's immune system against cancer cells [159]. Ascitic cell-derived exosomes obtained from peritoneal cavity fluid of cancer patients triggered cancer cell lysis via activation of dendritic cells and MHC-1-dependent T cell response. Membrane-bound Hsp70 of TEX exhibited robust priming of T helper cell 1 (Th1)- and NK-mediated antitumor immune response [160]. Chemotherapy accompanied with hyperthermia has evolved as a new treatment mode for cancer involving TEXs. For instance, heat stress has increased the antitumor effect of TEXs derived from doxorubicin-treated MCF-7 cells [161]. DC-derived exosomes control tumor growth by eliciting CD8+ and CD4+ T cell responses [162]. DC-derived exosomes incubated with cancer antigen triggered cancer specific T cell response [163]. Adjuvant-based exosomal vaccines are effective in eliciting immune response. For example, streptavidin-lactadherin protein fused with immunostimulatory biotinylated CpG DNA (adjuvant) after transfection into murine melanoma cells created genetically modified exosomes. These exosomes have the ability to trigger improved antigen presentation to the DCs and other immune cells, contributing to enhanced immune response [164]. DC-derived exosomes have been observed to be more efficient as cell-free vaccines in treating malignancies that respond poorly to immunotherapy. For instance, α-feto protein-rich DC derived exosomes triggered more effective antitumor immune responses and modulated the TME in a HCC mice model [165]. Recently, it was observed that vaccination with TEX-pulsed DC along with cytotoxic drugs specifically targeted immunosuppressive MDSCs in pancreatic cancer

cells [166]. DNA vaccines prepared by fusing ovalbumin antigen with lactadherin present on exosomal surface diminished fibrosarcoma, thymoma and melanoma metastasis by activating T lymphocytes [167].

9.4. Exosome-Based RNA Therapy

Exosome-based miRNA therapy exhibited immunosuppressive properties by controlling the gene expressions [19]. An early study reported that exosomes derived from human embryonic kidney cells were effective in regressing tumor growth by delivering miR-let7a in an EGFR-positive BC xenograft model [168]. The MSCs transfected with miR-124a enhanced exosomes carrying the RNA of interest production, which, when implemented against gliomas, reduced the cell viability and targeted FOXA2 that caused accumulation of lipids [169]. Transfer of lncRNA PTEN pseudogene 1 by exosomes derived from normal cells to bladder cancer cells reduced tumor progression in vitro and in vivo [170].

Exosomes also mediated targeted delivery of siRNA, e.g., siRNA transfected into exosomes targeted RAD51 and RAD52 in Hela and fibrosarcoma cells, which inhibited proliferation of the recipient cells [171]. Engineered exosomes containing IL-3 ligand or functional siRNA for BCR-ABL were successfully used against imatinib resistance in chronic myeloid leukemia patients [172]. Exosomes used for trafficking RNA interference (RNAi) mediators counteracted against oncogenic KRAS and improved overall survival in mouse models of pancreatic cancer [173]. Delivery of engineered exosome mediated siRNA inhibited post-operative metastasis of BC, indicating a promising strategy against tumor progression [174]. Successful delivery of antisense miRNA oligonucleotides against miR-21 by electroporating them in exosomal membrane improved the treatment efficacy for glioblastoma by inducing the expression of PTEN and PDCD4, resulting in decreased tumor size [175].

9.5. Exosomes in Stem Cell Therapy

Normal stem cell-derived exosomes are free of tumorigenic factors and are potential candidates for stem cell therapy [176]. MSC-derived exosomes can protect their cargoes from degradation, facilitate easier uptake by recipient cells, elicit low toxicity and immunogenicity, and these exosomes can be modified to enhance cell type-specific targeting and may be a prospective tool for cell-free based therapeutic approaches [177]. Exosomal miR-144 derived from bone marrow derived MSC retarded the spread of NSCLC by targeting cyclin E1 or E2 [178]. Exosomes released from miR-101-3p overexpressing MSCs negatively affected the proliferation and migration of oral cancer cells by targeting the collagen type X α1 chain [179]. MSC-derived exosomes were genetically engineered by loading them with polo-like kinase 1 (PLK-1)-siRNA and were utilized for PLK1 gene silencing in bladder cancer [180]. The primary hurdles of stem cell-based therapy, such as teratoma formation and embolization, are less frequent with exosome-based stem cell therapeutics. Exosomes secreted from induced pluripotent stem cells may exert better therapeutic effects [163].

9.6. Exosomes in Drug Delivery

Normal cell derived exosomes exhibit excellent biodistribution, biocompatibility, low immunogenicity, capacity to cross the blood–brain barrier and high target specificity, which make them potential candidates for drug delivery in cancer [5]. The exosomal surface proteins regulate efficient drug delivery because of their involvement in exosomes uptake by the tumorigenic recipient cells [181]. Exosomes derived from androgen-sensitive human prostate adenocarcinoma cells carrying paclitaxel negatively affect the cancer cells' viability [182]. DC-derived exosomes in BC and macrophage-derived exosomes in lung cancer were loaded with the drugs trastuzumab and paclitaxel, respectively, and successfully delivered to the recipients [183,184]. Moreover, exosomes loaded with doxorubicin conjugated with gold nanoparticles showed anticancer effect against lung cancer cells [185]. Exosomes with A disintegrin and metalloproteinase 15 (ADAM15) expression (A15-Exo) co-delivered with doxorubicin and cholesterol-modified miRNA 159 exhibited anticancer

effect in BC cells [186]. Paclitaxel loaded exosomes showed sensitivity towards MDR cancer cells via by-passing P-gp-mediated drug efflux and also inhibited metastasis in a lung cancer xenograft model [187]. Unmodified exosomes encapsulated with doxorubicin reduced tumor proliferation in a mouse mammary carcinoma xenograft model [137]. Exosomal delivery of doxorubicin induced its therapeutic activity in xenograft models of breast and ovarian cancer [188]. Exosomes isolated from engineered immature DCs (expressed Lamp2b fused with αv integrin-specific iRGD peptide (CRGDKGPDC)) loaded with doxorubicin successfully targeted αv integrin-positive breast tumor cells [189]. Exosome encapsulated gemcitabine exhibited anticancer properties in autologous pancreatic cancer cells and in a xenograft model [190].

Phytochemicals, administered via an exosome-mediated drug delivery system, can provide health benefits and anticancer properties [56]. Pancreatic adenocarcinoma cell-derived exosomes aided curcumin in inflicting its anticancer properties among tumor cells [191]. Milk-derived exosomes encapsulated with anthocyanidins exhibited antiproliferative effect in a xenograft lung carcinoma model [192]. Exosomal formulations of black bean extract exhibited pronounced antiproliferative effect in many cancer cells [193]. Exosomal formulations with berry anthocyanidins exhibited anticancer properties in ovarian cancer with enhanced sensitivity in chemoresistant tumors [194]. Exosomal encapsulation of celastrol (a triterpenoid) exhibited antiproliferative effect in lung cancer cells and in a xenograft model [195]. Recent studies on exosomal drug delivery of chemotherapeutic drugs and phytochemicals are listed in Table 3.

9.7. Induction of Chemosensitivity with Exosomes

TEXs impart drug resistance but may also be used for inducing drug sensitivity. Dimethyl amiloride augmented ABC transporter containing exosome secretion revived the cyclophosphamide sensitivity of cancer cells [31]. Downregulation of the GAIP-interacting protein C terminus mediated secretion of ABCG2 drug transporters containing exosomes and suppressed gemicitabine resistance in pancreatic cancer cells [196]. In oral squamous cell carcinoma, exosomal miR-155 increased chemoresistivity in cisplatin-sensitive cancer cells [197]. The exosomes loaded with CRISPR/Cas9 induced apoptosis and cisplatin chemosensitivity in ovarian cancer cells [198]. An increase in apoptosis and chemosensitivity was observed in cisplatin-resistant human gastric adenocarcinoma cells through treatment with si-c-Met containing exosomes derived from human kidney epithelial cell line [199]. Normal intestinal FHC cell-derived exosomes transferred miR-128-3p into oxiplatin resistant CRC cells which induced their chemosensitivity and decreased motility [200]. miR-122-transfected adipose tissue-derived MSCs (AMSCs) released exosomes carrying miR-122 and, when cocultured with hepatocyte carcinoma cells, induced sorafenib chemosensitivity [201]. miR-567 induced chemosensitivity in resistant BC cells towards trastuzumab and blocked autophagy [202]. Exosomal miR-200c induced chemosensitivity towards docetaxel and apoptosis in tongue squamous cell carcinoma [203]. Coculture of miR-199a carrying exosomes derived from AMSCs with HCC cells downregulated mammalian target of rapamycin (mTOR) pathway and induced chemosensitivity towards doxorubicin [204]. Various recent reports on exosome-mediated reversal of chemosensitivity have been listed in Table 4.

Table 3. Exosomes as delivery system for therapeutic implications against cancer.

Exosome Source	Modification of Exosomes with Drugs	Loading Method	Target Cells	Effect	Mechanism	References
Chemotherapeutic drugs						
Human mammary adenocarcinoma cells (M-CF-7), mouse mammary carcinoma cells (4T1), and human prostate adenocarcinoma cells (PC3)	Doxorubicin	Incubation	4T1 tumor-bearing BALB/c mice	↓Tumor growth, but no significant reduction in tumor growth with exosomes loaded with doxorubicin compared to free drug	-	[137]
Human prostate cancer (LNCaP and PC-3) cells	Paclitaxel	Incubation	LNCaP and PC-3 cells	↑Cytotoxic effect of paclitaxel	-	[182]
Human NSCLC (H1299) cells	Exo-gold nanoparticles-doxorubicin	Incubation	Human NSCLC (H1299 and A549) cells	↑DNA damage, ↑apoptosis	↑caspase-9, ↑ROS	[185]
Human monocyte (THP-1 cells)-derived macrophages	A15-Exo-doxorubicin-cho-miR159	Mixing in triethylamine solution overnight, Incubation	αvβ3+ and αvβ3- human BC (MDA-MB-231 and MCF-7) cells	↓Cell proliferation, ↑apoptosis	↓TCF7, ↓MYC	[186]
			MDA-MB-231 tumor-bearing BALB/c-nu mice	↓Tumor growth, ↑survival of mice	↓TCF7, ↓MYC, ↓Ki67, ↓CD31	
Mouse immature dendritic cells (imDCs)	Doxorubicin	Electroporation	MDA-MB-231 tumor-bearing BALB/c nude mice	↓Tumor growth	-	[189]
Human pancreatic cancer (Panc-1) cells	Gemcitabine	Sonication	Panc-1 and A549 cells	↓Cell viability	-	[190]
			Panc-1 tumor-bearing BALB/c nude mice	↓Tumor volume	↓Alanine aminotransferase, ↓aspartate aminotransferase, ↓TNF-α, ↓IL-6 in exo-gemcitabine group compared to gemcitabine	
Mouse (RAW 264.7) macrophages	Paclitaxel	Sonication	Murine Lewis lung carcinoma cell subline (3LL-M27 cells), Madin-Darby canine kidney (MDCK-WT) and (MDCK-MDR1) cells	↑Drug cytotoxicity, ↑chemosensitization of MDR cells	-	[187]
			8FlmC-FLuc-3LL-M27 tumor bearing C57BL/6 mice	↓Metastasis	-	
Human BC (MDA-MB-231) cells and mouse ovarian cancer (STOSE) cell	Doxorubicin	Electroporation	MDA-MB-231 and STOSE tumor bearing FVB/N mice	↑Doxorubicin efficacy, ↓tumor volume	-	[188]

Table 3. *Cont.*

Exosome Source	Modification of Exosomes with Drugs	Loading Method	Target Cells	Effect	Mechanism	References
Phytochemicals						
Human pancreatic adenocarcinoma (PANC-1, MIA PaCa-2) cells	Curcumin	Incubation	PANC-1 and MIA PaCa-2 cells	↓Cell viability,	-	[191]
Pooled raw milk from Jersey cows	Anthocyanidins	By mixing in a solution of acetonitrile: ethanol (1:1 *v*/*v*) and PBS	Human pancreatic cancer (PANC1 and Mia PaCa2), lung cancer (A549 and H1299), colon cancer (HCT116), BC (MDA-MB-231 and MCF7), prostate cancer (PC3 and DU145), and ovarian cancer (OVCA432) cells	↓Cell proliferation, ↓cell survival	↓NF-κB	[192]
			A549 tumor bearing female athymic nude (nu/nu) mice	↓Tumor growth	–	
MCF7, PC3, human liver (HepG2), colon cancer (Caco2) cells	Black bean extract	Electroporation	MCF7, PC3, HepG2 and Caco2 cells	↓Cell viability	–	[193]
Mature bovine milk	Anthocyanidins	By mixing	Human ovarian cancer (A2780, A2780/CP70, OVCA432, and OVCA433) cells	↓Cell survival	-	[194]
			A2780 tumor-bearing female athymic nude mice	↓Tumor volume	-	
Milk from pasture-fed Holstein and Jersey cows	Celastrol	By mixing	Human lung cancer (H1299 and A549) cells	↓Cell survival,	-	[195]
			H1299 and A549 tumor-bearing female athymic nude mice	↓Tumor volume	-	

Symbols: ↑, upregulated; ↓, downregulated; Abbreviations: MYC, master regulator of cell cycle entry and proliferative metabolism; NF-κB, nuclear factor kappa-light-chain-enhancer of activated B cells; ROS, reactive oxygen species; TCF7, transcription factor 7; TNF-α, tumor necrosis factor-α.

Table 4. Reversal of chemoresistance in resistant cancer cells with exosomal cargoes.

Exosome Source	Modification in Exosomal Cargo Content	Target Cells	Effects	Mechanisms	References
Human mesenchymal stem cells (MSCs)	Anti-miR-9	Glioblastoma (U87 and T98G) cells	↑Apoptosis ↑chemosensitivity towards temozolomide	↑Caspase-3 ↓P-gp ↓MDR1	[151]
Human kidney epithelial (HEK293T) cells	si-c-Met	Human gastric adenocarcinoma (SGC7901and SGC7901/DDP) cells	↑Apoptosis ↑chemosensitivity towards cisplatin	↓c-Met gene	[199]
Normal intestinal foetal human cells (FHC)	miR-128-3p	Human oxiplatin resistant colorectal cancer (HCT116OxR) cells	↑Oxiplatin accumulation ↑apoptosis ↓proliferation ↓self-renewal	↓Bmi1 ↓MRP5 ↓N-cadherin ↑E-cadherin	[200]
Human adipose tissue derived mesenchymal stem cells (AMSCs)	miR-122	Human HCC (HepG2, Huh7) cells	↑Apoptosis ↑cell cycle arrest ↑chemosensitivity towards sorafenib	↑G0/G1 arrest ↓CCNG1 ↓ADAM10 ↑Caspase-3 ↑Bax	[201]
Human normal breast epithelial (MCF 10A) cells	miR-567	Human trastuzumab resistant BC (SKBR-3/TR and BT474/TR) cells	↑Chemosensitivity towards trastuzumab ↑autophagy	↓ATG5 ↑p62 ↓LC3-11	[202]
Human normal tongue epithelial (NTECs) cells	miR-200c	Docetaxel resistant hepatic stellate cells (HSC-3DR) cells	↑Chemosensitivity towards docetaxel ↑apoptosis	↓TUBB3 ↓PPP2R1B	[203]
Human adipose tissue derived mesenchymal stem cells (AMSCs)	miR-199a	Human colorectal cancer (CRC) (Huh7, SMMC-7721, PLC/PRF/5) cells	↑Chemosensitivity towards doxorubicin	↓mTOR	[204]

Symbols: ↑, upregulated; ↓, downregulated; Abbreviations: ADAM10, A disintegrin and metalloproteinase 10; ATG5, autophagy related 5 protein; Bax, Bcl-2-associated X protein; BC, breast cancer; c-MET, mesenchymal epithelial transition factor; CCNG1, Cyclin G1; LC3, microtubule associated protein PIA/IB-light chain 3-I; MDR1, multidrug resistance protein-1; MRP5, multidrug resistant associated protein 5; mTOR, mammalian target of rapamycin; P-gp, P-glycoprotein; PPP2R1B, protein phosphatase 2 scaffold subunit 1β; TUBB3, class III β-tubulin gene.

9.8. Exosomes in Clinical Trials

According to the National Institutes of Health website, a large number of clinical trials are being conducted with exosomes (Table 5). In a study, plant exosomes were modified to deliver curcumin in colon cancer patients (ClinicalTrials.gov Identifier: NCT01294072). Phase I and II clinical trials with DC-derived exosomes indicated activation of T cell- and NK cell-based immune responses in NSCLC patients [154]. A phase II clinical trial (ClinicalTrials.gov Identifier: NCT01159288) on NSCLC observed that exosomes derived from TLR4L-or interferon-γ (IFN-γ)-maturated DCs enriched with MHC I- and MHC II-restricted cancer antigens as maintenance immunotherapy subsequent to first-line chemotherapy [205]. A study on HER2-positive BC patients measured HER2-HER3 dimer expression in exosomes (ClinicalTrials.gov Identifier: NCT04288141). Another trial led to a therapeutic analysis on cancer-derived exosomes via treatments with lovastatin and vildagliptin in thyroid cancer patients (ClinicalTrials.gov Identifier: NCT02862470). Characterization of exosomal non-coding RNAs was carried out in cholangiocarcinoma patients (ClinicalTrials.gov Identifier: NCT03102268). Another study reported exosome-mediated intercellular signaling in pancreatic cancer (ClinicalTrials.gov Identifier: NCT02393703). In metastatic pancreatic adenocarcinoma, exosomes with KrasG12D siRNA were used to treat pancreatic cancer with KrasG12D mutation (ClinicalTrials.gov Identifier: NCT03608631). In head and neck cancer, the effects of metformin hydrochloride on cytokines and exosomes were investigated (ClinicalTrials.gov Identifier: NCT03109873). A phase I clinical trial

(ClinicalTrials.gov Identifier: NCT01668849) investigated the ability of plant exosomes to prevent oral mucositis induced by combined chemotherapy and radiation in head and neck cancer patients. However, more clinical trials are needed with modified exosomes which may exhibit anticancer effect.

Table 5. Clinical trials on exosomes.

Trial No. (ClinicalTrials.gov Identifier:)	Study Type	Cancer Type	Study Perspective	Study Design	Status
NCT01294072	Phase I	Colon cancer	Interventional	Investigation of the ability of plant-derived exosomes to deliver curcumin	Active, not recruiting
NCT01159288	Phase II	Non-small cell lung cancer	Interventional	Trial of a vaccination with exosomes derived from dendritic cell loaded with tumor antigen	Completed
NCT04288141	Observational	Early HER2-positive BC, Metastatic HER2-positive BC	Prospective	Assessment of HER2-HER3 dimer expression in exosomes from HER2-positive patients receiving HER2 targeted therapies	Recruiting
NCT02862470	Observational	Anaplastic thyroid cancer, Follicular thyroid cancer	Prospective	Analysis of cancer-derived exosomes via lovastatin and vildagliptin treatments and prognostic study through urine exosomal markers	Active, not recruiting
NCT03102268	Observational	Cholangiocarcinoma	Prospective	Characterization of exosomal non-coding RNAs from cholangiocarcinoma patients before anticancer therapies	Unknown
NCT02393703	Observational	Pancreatic cancer	Prospective	Investigation of exosome mediated disease recurrence	Active, not recruiting
NCT03608631	Phase I	Metastatic pancreatic adenocarcinoma, Pancreatic ductal adenocarcinoma	Interventional	Study of the mesenchymal stromal cells-derived exosomes with KrasG12D siRNA (iExosomes) for pancreatic cancer patients having KrasG12D	Not yet recruiting
NCT03109873	Early phase I	Head and neck cancer	Randomized	Assessment of the effect of metformin hydrochloride on cytokines and exosomes in cancer patients	Completed
NCT01668849	Phase I	Head and neck cancer	Interventional	Investigation of the ability of plant-derived exosomes to prevent oral mucositis induced by combined chemotherapy and radiation	Active, not recruiting

10. Current Limitations and Challenges

Exosomes mediate intercellular communication and play significant roles in both physiological and pathological processes. A new hypothesis suggested that the target cells inhibit the incoming signals by forming exosome dimers based on the particle size, zeta potential and/or ligand–receptor pairs which facilitates cancer metastasis, cancer immunoregulation, intraocular pressure homoeostasis, tissue regeneration and many others [206].

Exosomes released by normal and malignant cells are endowed with heterogeneity and pleiotropic physiological and pathological effects. Inhibition of the release of TEXs may have both anti-carcinogenic and pro-carcinogenic effects. The majority of the exosome released inhibitors are not cancer-specific and also affect normal cells. Therefore,

inhibition of exosome release may act as a double-edged sword which should be carefully manipulated for minimal adverse effects [34].

Isolation of pure and specific exosomes is limited by technical constraints, the availability of suitable biomarkers for specific exosomes, and expensive technologies [5]. A major hurdle in the execution of liquid biopsy is isolation of exosomes by an economic user-friendly tool. Protein contaminated and heterogenous exosome pool is obtained using ultracentrifugation. Asymmetric flow field-flow fractionation, though a prospective tool, needs technical expertise and requires a huge amount of initial sample. Other exosome isolation methods like microfluidic devices, sucrose gradients, size exclusion chromatography, and affinity-based exosome isolation kits are accompanied with both advantages and disadvantages like lack of robustness and specificity [31]. A perfect exosome isolation method should be robust, reproducible, specific, economic and user friendly as a diagnostic tool.

Detailed research of exosome biogenesis, functional diversity of exosomes and the identification of cancer specific biomarkers may be effective for exosome-based therapeutic approaches with minimum adverse effects [34]. Determination of exosomal cargo sorting and releasing mechanisms holds great potential for the development of various applications in cancer research [31].

Normally, less than 1 μg of exosomal protein is yielded from 1 mL of culture medium, whereas the majority of studies have reported 10–100 μg of exosomal protein as an effective dose for in vivo models [163]. The introduction of exosome-mimetic vesicles (100–200 nm in diameter) has conquered exosomal limitations like low loading efficiency and low yields. These nanovesicles have been used for delivery of chemotherapeutic drugs [204,205] and RNAi [207] to target cancer cells. Hybrid nanocarriers formed by the fusion of exosomes with liposomes changed the exogenous lipid composition and was effective in the delivery of chemotherapeutic drugs [208].

11. Conclusions

It may be deciphered that the intercellular communication via exosomes is evident throughout cancer progression. Apart from cancer pathogenesis, exosome biology heralds the future arena of non-invasive diagnostic tools for cancer management, especially in the spheres of liquid biopsy, immunotherapy and vaccine development, RNA therapy, stem cell therapy, drug delivery, and reversal of chemoresistance. Preclinical studies have undoubtedly proven the immense potential of exosomes in cancer therapeutics, but a number of clinical trials have failed to achieve this success. These inconsistent results indicate major challenges including in-depth knowledge of exosome biogenesis and protein sorting, perfect and pure isolation of exosomes, large scale production, better loading efficiency targeted delivery of exosomes. These hurdles have to be confronted before successful implementation of exosomes for the diagnosis and therapy of cancer. This review has attempted to envisage the implication of exosomes in cancer pathogenesis and cancer therapeutics along with the current limitations so that researchers may be made aware of the existing lacunae with regard to exosomes in their use against cancer. This knowledge may help scientists to improvise innovative technologies for successful translation of the exosome-mediated diagnosis and treatment of malignant neoplasms.

Author Contributions: Conceptualization and writing, D.S.; writing and figure preparation, S.R., P.S. and N.C.; editing and suggestion of improvements, A.B. All authors have read and agreed to the published version of the manuscript.

Funding: This research received no external source of funding.

Institutional Review Board Statement: Not applicable.

Informed Consent Statement: Not applicable.

Data Availability Statement: Not applicable.

Acknowledgments: D.S., S.R., P.S., and N.C. are deeply grateful to Jayanta Chakrabarti, Director, Chittaranjan National Cancer Institute, Kolkata, for providing the infrastructural facilities. P.S. is thankful to Jayanta Chakrabarti for granting an institutional fellowship. S.R. is indebted to the University Grants Commission, New Delhi, India, for providing a fellowship.

Conflicts of Interest: The authors declare no conflict of interest.

Abbreviations

ABC	ATP-binding cassette;
ABCA3	ATP-binding cassette sub-family A member 3;
ADAM10	A disintegrin and metalloproteinase 10;
AFAP1-AS1	actin filament associated protein1 antisense RNA 1;
Akt	protein kinase B;
ALIX	ALG-2 interacting protein X;
AMSCs	adipose tissue-derived MSCs;
APC	antigen presenting cell;
ARF6	ADP ribosylation factor 6;
ATG5	autophagy related 5 protein;
CAFs	cancer-associated fibroblasts;
CCNG1	cyclin G1;
CRC	colorectal cancer cells;
CXCR4	C-X-C chemokine receptor type 4;
DCs	dendritic cells;
ECM	extracellular matrix;
EGFR	epidermal growth factor receptor;
EMT	epithelial mesenchymal transition;
ERBB2	erythroblastic oncogene B2;
ERF	Ets2-repressor factor;
ERK	extracellular signal-regulated kinase;
ERα	estrogen receptor-α;
ESCRT	endosomal sorting complexes required for the transport;
GC	gastric cancer;
HCC	hepatocellular carcinoma;
HER2	human epidermal growth factor receptor 2;
HGF	hepatocyte growth factor;
HNSCC	head and neck squamous cell carcinoma;
HOTTIP	HoxA transcript at a distal tip;
Hsps	heat shock proteins;
ICAM	intercellular adhesion molecule;
IL-6	interleukin-6;
ILV	intraluminal vesicles;
LAMP-1	lysosome-associated membrane glycoprotein-1 LncRNAs
LncRNAs	long non-coding RNAs;
MAPK	mitogen activated protein kinase;
MDR-1	multidrug resistance protein-1;
MDSCs	myeloid-derived suppressor cells;
MHC	major histocompatibility complex;
miRNAs	microRNA;
MMP	matrix metalloproteinase;
mRNA	messenger RNA;
MSCs	mesenchymal stem cells;
mtDNA	mitochondrial DNA;
MVB	multivesicular bodies;
NF-κB	nuclear factor κ-light-chain-enhancer of activated B cells;
NK	natural killer cells;
NKG2D	natural killer group 2D;

NSCLC	non-small cell lung carcinoma;
PAFR	a platelet-activating factor receptor;
PDAC	pancreatic ductal adenocarcinoma;
PDCD4	programmed cell death 4;
PD-L1	programmed death ligand 1;
P-gp	P-glycoprotein;
PI3K	phosphoinositide 3-kinase;
PLD2	phospholipase D2;
PLK-1	polo-like kinase 1;
PM	plasma membrane;
PPP2R1B	protein phosphatase 2 scaffold subunit 1β;
PTEN	phosphatase and tensin homolog;
rRNA	ribosomal RNA;
SNARES	soluble NSF attachment protein receptors;
Sox2ot	SOX2 overlapping transcript;
SR-B1	scavenger receptor type B-1;
STAT1	signal transducer and activator of transcription 1;
TAMs	tumor-associated macrophages;
TEX	tumor derived exosomes;
TGF-β	transforming growth factor-β;
TGN	trans-Golgi network;
TLR-2	toll like receptor-2;
TME	tumor microenvironment;
Tregs	T regulatory cells;
TUBB3	class III β-tubulin gene;
UFC1	Ubiquitin-fold modifier conjugating enzyme 1;
VEGF-A	vascular endothelial growth factor A;
Vps4	vacuolar protein sorting associated protein 4;
ZFAS1	zinc finger antisense 1.

References

1. Harding, C.; Stahl, P. Transferrin Recycling in Reticulocytes: pH and Iron Are Important Determinants of Ligand Binding and Processing. *Biochem. Biophys. Res. Commun.* **1983**, *113*, 650–658. [CrossRef]
2. Lötvall, J.; Hill, A.F.; Hochberg, F.; Buzás, E.I.; Vizio, D.D.; Gardiner, C.; Gho, Y.S.; Kurochkin, I.V.; Mathivanan, S.; Quesenberry, P.; et al. Minimal experimental requirements for definition of extracellular vesicles and their functions: A position statement from the International Society for Extracellular Vesicles. *J. Extracell. Vesicles* **2014**, *3*, 26913. [CrossRef]
3. Théry, C.; Witwer, K.W.; Aikawa, E.; Alcaraz, M.J.; Anderson, J.D.; Andriantsitohaina, R.; Antoniou, A.; Arab, T.; Archer, F.; Atkin-Smith, G.K.; et al. Minimal information for studies of extracellular vesicles 2018 (MISEV2018): A position statement of the International Society for Extracellular Vesicles and update of the MISEV2014 guidelines. *J. Extracell. Vesicles* **2018**, *7*, 1535750. [CrossRef]
4. Zhang, C.; Ji, Q.; Yang, Y.; Li, Q.; Wang, Z. Exosome: Function and role in cancer metastasis and drug resistance. *Technol. Cancer Res. Treat.* **2018**, *17*. [CrossRef]
5. He, C.; Zheng, S.; Luo, Y.; Wang, B. Exosome theranostics: Biology and translational medicine. *Theranostics* **2018**, *8*, 237–255. [CrossRef]
6. McAndrews, K.M.; Kalluri, R. Mechanisms associated with biogenesis of exosomes in cancer. *Mol. Cancer* **2019**, *18*, 52. [CrossRef]
7. Jurj, A.; Zanoaga, O.; Braicu, C.; Lazar, V.; Tomuleasa, C.; Irimie, A.; Berindan-neagoe, I. A comprehensive picture of extracellular vesicles and their contents. Molecular transfer to cancer cells. *Cancers* **2020**, *12*, 298. [CrossRef]
8. Lucchetti, D.; Tenore, C.R.; Colella, F.; Sgambato, A. Extracellular Vesicles and Cancer: A Focus on Metabolism, Cytokines, and Immunity. *Cancers* **2020**, *12*, 171. [CrossRef]
9. Tang, Z.; Li, D.; Hou, S.; Zhu, X. The cancer exosomes: Clinical implications, applications and challenges. *Int. J. Cancer* **2020**, *146*, 2946–2959. [CrossRef]
10. Mohammadi, S.; Yousefi, F.; Shabaninejad, Z.; Movahedpour, A.; Mahjoubin Tehran, M.; Shafiee, A.; Moradizarmehri, S.; Hajighadimi, S.; Savardashtaki, A.; Mirzaei, H. Exosomes and cancer: From oncogenic roles to therapeutic applications. *IUBMB Life* **2020**, *72*, 724–748. [CrossRef]
11. Parayath, N.N.; Padmakumar, S.; Amiji, M.M. Extracellular vesicle-mediated nucleic acid transfer and reprogramming in the tumor microenvironment. *Cancer Lett.* **2020**, *482*, 33–43. [CrossRef]
12. Wee, I.; Syn, N.; Sethi, G.; Goh, B.C.; Wang, L. Role of tumor-derived exosomes in cancer metastasis. *Biochim. Biophys. Acta Rev. Cancer* **2019**, *1871*, 12–19. [CrossRef]
13. Raimondo, S.; Pucci, M.; Alessandro, R.; Fontana, S. Extracellular vesicles and tumor-immune escape: Biological functions and clinical perspectives. *Int. J. Mol. Sci.* **2020**, *21*, 2286. [CrossRef]
14. Gilligan, K.E.; Dwyer, R.M. Extracellular Vesicles for Cancer Therapy: Impact of Host Immune Response. *Cells* **2020**, *9*, 224. [CrossRef]

15. Li, X.; Corbett, A.L.; Taatizadeh, E.; Tasnim, N.; Little, J.P.; Garnis, C.; Daugaard, M.; Guns, E.; Hoorfar, M.; Li, I.T.S. Challenges and opportunities in exosome research—Perspectives from biology, engineering, and cancer therapy. *APL Bioeng.* **2019**, *3*, 011503. [CrossRef]
16. Srivastava, A.; Amreddy, N.; Pareek, V.; Chinnappan, M.; Ahmed, R.; Mehta, M.; Razaq, M.; Munshi, A.; Ramesh, R. Progress in extracellular vesicle biology and their application in cancer medicine. *Wiley Interdiscip. Rev. Nanomed. Nanobiotechnol.* **2020**, *12*, e1621. [CrossRef]
17. Taghikhani, A.; Farzaneh, F.; Sharifzad, F.; Mardpour, S.; Ebrahimi, M.; Hassan, Z.M. Engineered Tumor-Derived Extracellular Vesicles: Potentials in Cancer Immunotherapy. *Front. Immunol.* **2020**, *11*, 221. [CrossRef]
18. Stevic, I.; Buescher, G.; Ricklefs, F.L. Monitoring Therapy Efficiency in Cancer through Extracellular Vesicles. *Cells* **2020**, *9*, 130. [CrossRef]
19. Pullan, J.E.; Confeld, M.I.; Osborn, J.K.; Kim, J.; Sarkar, K.; Mallik, S. Exosomes as Drug Carriers for Cancer Therapy. *Mol. Pharm.* **2019**, *16*, 1789–1798. [CrossRef]
20. Yong, T.; Wang, D.; Li, X.; Yan, Y.; Hu, J.; Gan, L.; Yang, X. Extracellular vesicles for tumor targeting delivery based on five features principle. *J. Control. Release* **2020**, *322*, 555–565. [CrossRef]
21. Zhao, X.; Wu, D.; Ma, X.; Wang, J.; Hou, W.; Zhang, W. Exosomes as drug carriers for cancer therapy and challenges regarding exosome uptake. *Biomed. Pharmacother.* **2020**, *128*, 110237. [CrossRef]
22. Pirisinu, M.; Pham, T.C.; Zhang, D.X.; Hong, T.N.; Nguyen, L.T.; Le, M.T. Extracellular vesicles as natural therapeutic agents and innate drug delivery systems for cancer treatment: Recent advances, current obstacles, and challenges for clinical translation. *Semin. Cancer Biol.* **2020**. [CrossRef]
23. Milane, L.; Singh, A.; Mattheolabakis, G.; Suresh, M.; Amiji, M.M. Exosome Mediated Communication within the Tumor Microenvironment. *J. Control. Release* **2015**, *10*, 278–294. [CrossRef]
24. Jenjaroenpun, P.; Kremenska, Y.; Nair, V.M.; Kremenskoy, M.; Joseph, B.; Kurochkin, I.V. Characterization of RNA in exosomes secreted by human breast cancer cell lines using next-generation sequencing. *PeerJ* **2013**, *1*, e201. [CrossRef]
25. Li, S.P.; Lin, Z.X.; Jiang, X.Y.; Yu, X.Y. Exosomal cargo-loading and synthetic exosome-mimics as potential therapeutic tools. *Acta Pharmacol. Sin.* **2018**, *39*, 542–551. [CrossRef]
26. Zhang, Y.; Liu, Y.; Liu, H.; Tang, W.H. Exosomes: Biogenesis, biologic function and clinical potential. *Cell Biosci.* **2019**, *9*, 19. [CrossRef]
27. Souza-Schorey, C.; Schorey, J.S. Regulation and mechanisms of extracellular vesicle biogenesis and secretion. *Essays Biochem.* **2018**, *62*, 125–133. [CrossRef]
28. Antonyak, M.A.; Cerione, R.A. Microvesicles as mediators of intercellular communication in cancer. *Methods Mol. Biol.* **2014**, *1165*, 147–173. [CrossRef]
29. Ghossoub, R.; Lembo, F.; Rubio, A.; Gaillard, C.B.; Bouchet, J.; Vitale, N.; Slavík, J.; Machala, M.; Zimmermann, P. Syntenin-ALIX exosome biogenesis and budding into multivesicular bodies are controlled by ARF6 and PLD2. *Nat. Commun.* **2014**, *5*, 3477. [CrossRef]
30. Kowal, J.; Tkach, M.; Théry, C. Biogenesis and secretion of exosomes. *Curr. Opin. Cell Biol.* **2014**, *29*, 116–125. [CrossRef]
31. Wortzel, I.; Dror, S.; Kenific, C.M.; Lyden, D. Exosome-Mediated Metastasis: Communication from a Distance. *Dev. Cell* **2019**, *49*, 347–360. [CrossRef]
32. Alenquer, M.; Amorim, M.J. Exosome biogenesis, regulation, and function in viral infection. *Viruses* **2015**, *7*, 5066–5083. [CrossRef]
33. Stoorvogel, W. Resolving sorting mechanisms into exosomes. *Cell Res.* **2015**, *25*, 531–532. [CrossRef]
34. Moloudizargari, M.; Asghari, M.H.; Abdollahi, M. Modifying exosome release in cancer therapy: How can it help? *Pharmacol. Res.* **2018**, *134*, 246–256. [CrossRef]
35. Lange, S.; Gallagher, M.; Kholia, S.; Kosgodage, U.S.; Hristova, M.; Hardy, J.; Inal, J.M. Peptidylarginine deiminases—Roles in cancer and neurodegeneration and possible avenues for therapeutic intervention via modulation of exosome and microvesicle (EMV) release? *Int. J. Mol. Sci.* **2017**, *18*, 1196. [CrossRef]
36. Mohrmann, K.; Leijendekker, R.; Gerez, L.; Van Sluijs, P. Der rab4 regulates transport to the apical plasma membrane in Madin-Darby canine kidney cells. *J. Biol. Chem.* **2002**, *277*, 10474–10481. [CrossRef]
37. Schlierf, B.; Fey, G.H.; Hauber, J.; Hocke, G.M.; Rosorius, O. Rab11b is essential for recycling of transferrin to the plasma membrane. *Exp. Cell Res.* **2000**, *259*, 257–265. [CrossRef]
38. Casanova, J.E.; Wang, X.; Kumar, R.; Bhartur, S.G.; Navarre, J.; Woodrum, J.E.; Altschuler, Y.; Ray, G.S.; Goldenring, J.R. Association of Rab25 and Rab11a with the apical recycling system of polarized Madin-Darby Canine Kidney cells. *Mol. Biol. Cell* **1999**, *10*, 47–61. [CrossRef]
39. Lombardi, D.; Soldati, T.; Riederer, M.A.; Goda, Y.; Zerial, M.; Pfeffer, S.R. Rab9 functions in transport between late endosomes and the trans Golgi network. *EMBO J.* **1993**, *12*, 677–682. [CrossRef]
40. Guerra, F.; Bucci, C. Multiple Roles of the Small GTPase Rab7. *Cells* **2016**, *5*, 34. [CrossRef]
41. Vitelli, R.; Santillo, M.; Lattero, D.; Chiariello, M.; Bifulco, M.; Bruni, C.B.; Bucci, C. Role of the small GTPase RAB7 in the late endocytic pathway. *J. Biol. Chem.* **1997**, *272*, 4391–4397. [CrossRef]
42. Chen, J.; Chopp, M. Exosome therapy for stroke. *Stroke* **2018**, *49*, 1083–1090. [CrossRef]
43. Ostrowski, M.; Carmo, N.B.; Krumeich, S.; Fanget, I.; Raposo, G.; Savina, A.; Moita, C.F.; Schauer, K.; Hume, A.N.; Freitas, R.P.; et al. Rab27a and Rab27b control different steps of the exosome secretion pathway. *Nat. Cell Biol.* **2010**, *12*, 19–30. [CrossRef]
44. Baietti, M.F.; Zhang, Z.; Mortier, E.; Melchior, A.; Degeest, G.; Geeraerts, A.; Ivarsson, Y.; Depoortere, F.; Coomans, C.; Vermeiren, E.; et al. Syndecan-syntenin-ALIX regulates the biogenesis of exosomes. *Nat. Cell Biol.* **2012**, *14*, 677–685. [CrossRef]
45. Savina, A.; Vidal, M.; Colombo, M.I. The exosome pathway in K562 cells is regulated by Rab11. *J. Cell Sci.* **2002**, *115*, 2505–2515.

46. Savina, A.; Fader, C.M.; Damiani, M.T.; Colombo, M.I. Rab11 promotes docking and fusion of multivesicular bodies in a calcium-dependent manner. *Traffic* **2006**, *6*, 131–143. [CrossRef]
47. Li, W.; Hu, Y.; Jiang, T.; Han, Y.; Han, G.; Chen, J.; Li, X. Rab27A regulates exosome secretion from lung adenocarcinoma cells A549: Involvement of EPI64. *APMIS* **2014**, *122*, 1080–1087. [CrossRef]
48. Heusermann, W.; Hean, J.; Trojer, D.; Steib, E.; von Bueren, S.; Graff-Meyer, A.; Genoud, C.; Martin, K.; Pizzato, N.; Voshol, J.; et al. Exosomes surf on filopodia to enter cells at endocytic hot spots, traffic within endosomes, and are targeted to the ER. *J. Cell Biol.* **2016**, *213*, 173–184. [CrossRef]
49. Tian, T.; Zhu, Y.L.; Zhou, Y.Y.; Liang, G.F.; Wang, Y.Y.; Hu, F.H.; Xiao, Z.D. Exosome uptake through clathrin-mediated endocytosis and macropinocytosis and mediating miR-21 delivery. *J. Biol. Chem.* **2014**, *289*, 22258–22267. [CrossRef]
50. Nabi, I.R.; Le, P.U. Caveolae/raft-dependent endocytosis. *J. Cell Biol.* **2003**, *161*, 673–677. [CrossRef]
51. Gonda, A.; Kabagwira, J.; Senthil, G.N.; Wall, N.R. Internalization of exosomes through receptor-mediated endocytosis. *Mol. Cancer Res.* **2019**, *17*, 337–347. [CrossRef]
52. Joshi, B.S.; de Beer, M.A.; Giepmans, B.N.G.; Zuhorn, I.S. Endocytosis of Extracellular Vesicles and Release of Their Cargo from Endosomes. *ACS Nano* **2020**, *14*, 4444–4455. [CrossRef]
53. Andreu, Z.; Yáñez-Mó, M. Tetraspanins in extracellular vesicle formation and function. *Front. Immunol.* **2014**, *5*, 442. [CrossRef]
54. Wu, Y.; Wu, W.; Wong, W.M.; Ward, E.; Thrasher, A.J.; Goldblatt, D.; Osman, M.; Digard, P.; Canaday, D.H.; Gustafsson, K. Human γδ T Cells: A Lymphoid Lineage Cell Capable of Professional Phagocytosis. *J. Immunol.* **2009**, *183*, 5622–5629. [CrossRef]
55. McKelvey, K.J.; Powell, K.L.; Ashton, A.W.; Morris, J.M.; McCracken, S.A. Exosomes: Mechanisms of Uptake. *J. Circ. Biomark.* **2015**, *4*, 7. [CrossRef]
56. Farooqi, A.A.; Desai, N.N.; Qureshi, M.Z.; Librelotto, D.R.N.; Gasparri, M.L.; Bishayee, A.; Nabavi, S.M.; Curti, V.; Daglia, M. Exosome biogenesis, bioactivities and functions as new delivery systems of natural compounds. *Biotechnol. Adv.* **2018**, *36*, 328–334. [CrossRef]
57. Datta, A.; Kim, H.; McGee, L.; Johnson, A.E.; Talwar, S.; Marugan, J.; Southall, N.; Hu, X.; Lal, M.; Mondal, D.; et al. High-Throughput screening identified selective inhibitors of exosome biogenesis and secretion: A drug repurposing strategy for advanced cancer. *Sci. Rep.* **2018**, *8*, 8161. [CrossRef]
58. Logozzi, M.; Spugnini, E.; Mizzoni, D.; Di Raimo, R.; Fais, S. Extracellular acidity and increased exosome release as key phenotypes of malignant tumors. *Cancer Metastasis Rev.* **2019**, *38*, 93–101. [CrossRef]
59. Agarwal, K.; Saji, M.; Lazaroff, S.M.; Palmer, A.F.; Ringel, M.D.; Paulaitis, M.E. Analysis of exosome release as a cellular response to MAPK pathway inhibition. *Langmuir* **2015**, *31*, 5440–5448. [CrossRef]
60. Lee, T.H.; Chennakrishnaiah, S.; Audemard, E.; Montermini, L.; Meehan, B.; Rak, J. Oncogenic ras-driven cancer cell vesiculation leads to emission of double-stranded DNA capable of interacting with target cells. *Biochem. Biophys. Res. Commun.* **2014**, *451*, 295–301. [CrossRef]
61. Al-Nedawi, K.; Meehan, B.; Micallef, J.; Lhotak, V.; May, L.; Guha, A.; Rak, J. Intercellular transfer of the oncogenic receptor EGFRvIII by microvesicles derived from tumour cells. *Nat. Cell Biol.* **2008**, *10*, 619–624. [CrossRef]
62. Zhang, C.; Xiao, X.; Chen, M.; Aldharee, H.; Chen, Y.; Long, W. Liver kinase B1 restoration promotes exosome secretion and motility of lung cancer cells. *Oncol. Rep.* **2018**, *39*, 376–382. [CrossRef]
63. Melo, S.A.; Sugimoto, H.; O'Connell, J.T.; Kato, N.; Villanueva, A.; Vidal, A.; Qiu, L.; Vitkin, E.; Perelman, L.T.; Melo, C.A.; et al. Cancer Exosomes Perform Cell-Independent MicroRNA Biogenesis and Promote Tumorigenesis. *Cancer Cell* **2014**, *26*, 707–721. [CrossRef]
64. Jia, Y.; Chen, Y.; Wang, Q.; Jayasinghe, U.; Luo, X.; Wei, Q.; Wang, J.; Xiong, H.; Chen, C.; Xu, B.; et al. Exosome: Emerging biomarker in breast cancer. *Oncotarget* **2017**, *8*, 41717–41733. [CrossRef]
65. Singh, R.; Pochampally, R.; Watabe, K.; Lu, Z.; Mo, Y.Y. Exosome-mediated transfer of miR-10b promotes cell invasion in breast cancer. *Mol. Cancer* **2014**, *13*, 256. [CrossRef]
66. Zhang, L.; Zhang, S.; Yao, J.; Lowery, F.J.; Zhang, Q.; Huang, W.C.; Li, P.; Li, M.; Wang, X.; Zhang, C.; et al. Microenvironment-induced PTEN loss by exosomal microRNA primes brain metastasis outgrowth. *Nature* **2015**, *527*, 100–104. [CrossRef]
67. Cooks, T.; Pateras, I.S.; Jenkins, L.M.; Patel, K.M.; Robles, A.I.; Morris, J.; Forshew, T.; Appella, E.; Gorgoulis, V.G.; Harris, C.C. Mutant p53 cancers reprogram macrophages to tumor supporting macrophages via exosomal miR-1246. *Nat. Commun.* **2018**, *9*, 771. [CrossRef]
68. Zhang, H.D.; Jiang, L.H.; Hou, J.C.; Zhong, S.L.; Zhu, L.P.; Wang, D.D.; Zhou, S.Y.; Yang, S.J.; Wang, J.Y.; Zhang, Q.; et al. Exosome: A novel mediator in drug resistance of cancer cells. *Epigenomics* **2018**, *10*, 1499–1509. [CrossRef]
69. Yang, X.; Li, Y.; Zou, L.; Zhu, Z. Role of Exosomes in Crosstalk Between Cancer-Associated Fibroblasts and Cancer Cells. *Front. Oncol.* **2019**, *9*, 356. [CrossRef]
70. Zhao, H.; Yang, L.; Baddour, J.; Achreja, A.; Bernard, V.; Moss, T.; Marini, J.C.; Tudawe, T.; Seviour, E.G.; San Lucas, F.A.; et al. Tumor microenvironment derived exosomes pleiotropically modulate cancer cell metabolism. *Elife* **2016**, *5*, e10250. [CrossRef]
71. Hu, T.; Hu, J. Melanoma-derived exosomes induce reprogramming fibroblasts into cancer-associated fibroblasts via Gm26809 delivery. *Cell Cycle* **2019**, *18*, 3085–3094. [CrossRef]
72. Abusamra, A.J.; Zhong, Z.; Zheng, X.; Li, M.; Ichim, T.E.; Chin, J.L.; Min, W.P. Tumor exosomes expressing Fas ligand mediate CD8+ T-cell apoptosis. *Blood Cells Mol. Dis.* **2005**, *35*, 169–173. [CrossRef]
73. Lu, H.; Bowler, N.; Harshyne, L.A.; Craig Hooper, D.; Krishn, S.R.; Kurtoglu, S.; Fedele, C.; Liu, Q.; Tang, H.Y.; Kossenkov, A.V.; et al. Exosomal αvβ6 integrin is required for monocyte M2 polarization in prostate cancer. *Matrix Biol.* **2018**, *70*, 20–35. [CrossRef]

74. Yin, C.; Han, Q.; Xu, D.; Zheng, B.; Zhao, X.; Zhang, J. SALL4-mediated upregulation of exosomal miR-146a-5p drives T-cell exhaustion by M2 tumor-associated macrophages in HCC. *Oncoimmunology* **2019**, *8*, 1601479. [CrossRef]
75. Liu, C.; Yu, S.; Zinn, K.; Wang, J.; Zhang, L.; Jia, Y.; Kappes, J.C.; Barnes, S.; Kimberly, R.P.; Grizzle, W.E.; et al. Murine Mammary Carcinoma Exosomes Promote Tumor Growth by Suppression of NK Cell Function. *J. Immunol.* **2006**, *176*, 1375–1385. [CrossRef]
76. Bobrie, A.; Krumeich, S.; Reyal, F.; Recchi, C.; Moita, L.F.; Seabra, M.C.; Ostrowski, M.; Théry, C. Rab27a supports exosome-dependent and -independent mechanisms that modify the tumor microenvironment and can promote tumor progression. *Cancer Res.* **2012**, *72*, 4920–4930. [CrossRef]
77. Maus, R.L.G.; Jakub, J.W.; Nevala, W.K.; Christensen, T.A.; Noble-Orcutt, K.; Sachs, Z.; Hieken, T.J.; Markovic, S.N. Human melanoma-derived extracellular vesicles regulate dendritic cell maturation. *Front. Immunol.* **2017**, *8*, 358. [CrossRef]
78. Wolfers, J.; Lozier, A.; Raposo, G.; Regnault, A.; Théry, C.; Masurier, C.; Flament, C.; Pouzieux, S.; Faure, F.; Tursz, T.; et al. Tumor-derived exosomes are a source of shared tumor rejection antigens for CTL cross-priming. *Nat. Med.* **2001**, *7*, 297–303. [CrossRef]
79. Theodoraki, M.N.; Yerneni, S.S.; Hoffmann, T.K.; Gooding, W.E.; Whiteside, T.L. Clinical significance of PD-L1 þ exosomes in plasma of head and neck cancer patients. *Clin. Cancer Res.* **2018**, *24*, 896–905. [CrossRef]
80. Yue, S.; Mu, W.; Erb, U.; Zöller, M. The tetraspanins CD151 and Tspan8 are essential exosome components for the crosstalk between cancer initiating cells and their surrounding. *Oncotarget* **2015**, *6*, 2366–2384. [CrossRef]
81. Yin, X.; Zheng, X.; Liu, M.; Wang, D.; Sun, H.; Qiu, Y.; Chen, J.; Shi, B. Exosomal miR-663b targets Ets2-repressor factor to promote proliferation and the epithelial–mesenchymal transition of bladder cancer cells. *Cell Biol. Int.* **2020**, *44*, 958–965. [CrossRef]
82. Li, Z.; Jiang, P.; Li, J.; Peng, M.; Zhao, X.; Zhang, X.; Chen, K.; Zhang, Y.; Liu, H.; Gan, L.; et al. Tumor-derived exosomal lnc-Sox2ot promotes EMT and stemness by acting as a ceRNA in pancreatic ductal adenocarcinoma. *Oncogene* **2018**, *37*, 3822–3838. [CrossRef]
83. Suchorska, W.M.; Lach, M.S. The role of exosomes in tumor progression and metastasis (Review). *Oncol. Rep.* **2016**, *35*, 1237–1244. [CrossRef]
84. Fedele, C.; Singh, A.; Zerlanko, B.J.; Iozzo, R.V.; Languino, L.R. The αvβ6 integrin is transferred intercellularly via exosomes. *J. Biol. Chem.* **2015**, *290*, 4545–4551. [CrossRef]
85. Lin, F.; Yin, H.B.; Li, X.Y.; Zhu, G.M.; He, W.Y.; Gou, X. Bladder cancer cell-secreted exosomal miR-21 activates the PI3K/AKT pathway in macrophages to promote cancer progression. *Int. J. Oncol.* **2020**, *56*, 151–164. [CrossRef]
86. Zheng, P.; Luo, Q.; Wang, W.; Li, J.; Wang, T.; Wang, P.; Chen, L.; Zhang, P.; Chen, H.; Liu, Y.; et al. Tumor-associated macrophages-derived exosomes promote the migration of gastric cancer cells by transfer of functional Apolipoprotein E. *Cell Death Dis.* **2018**, *9*, 434. [CrossRef]
87. Zang, X.; Gu, J.; Zhang, J.; Shi, H.; Hou, S.; Xu, X.; Chen, Y.; Zhang, Y.; Mao, F.; Qian, H.; et al. Exosome-transmitted lncRNA UFC1 promotes non-small-cell lung cancer progression by EZH2-mediated epigenetic silencing of PTEN expression. *Cell Death Dis.* **2020**, *11*, 215. [CrossRef]
88. Pan, L.; Liang, W.; Fu, M.; Huang, Z.H.; Li, X.; Zhang, W.; Zhang, P.; Qian, H.; Jiang, P.C.; Xu, W.R.; et al. Exosomes-mediated transfer of long noncoding RNA ZFAS1 promotes gastric cancer progression. *J. Cancer Res. Clin. Oncol.* **2017**, *143*, 991–1004. [CrossRef]
89. Zhang, H.; Deng, T.; Liu, R.; Bai, M.; Zhou, L.; Wang, X.; Li, S.; Wang, X.; Yang, H.; Li, J.; et al. Exosome-delivered EGFR regulates liver microenvironment to promote gastric cancer liver metastasis. *Nat. Commun.* **2017**, *8*, 15016. [CrossRef]
90. Yokoi, A.; Yoshioka, Y.; Yamamoto, Y.; Ishikawa, M.; Ikeda, S.I.; Kato, T.; Kiyono, T.; Takeshita, F.; Kajiyama, H.; Kikkawa, F.; et al. Malignant extracellular vesicles carrying MMP1 mRNA facilitate peritoneal dissemination in ovarian cancer. *Nat. Commun.* **2017**, *8*, 14470. [CrossRef]
91. Wang, D.; Wang, X.; Si, M.; Yang, J.; Sun, S.; Wu, H.; Cui, S.; Qu, X.; Yu, X. Exosome-encapsulated miRNAs contribute to CXCL12/CXCR4-induced liver metastasis of colorectal cancer by enhancing M2 polarization of macrophages. *Cancer Lett.* **2020**, *474*, 36–52. [CrossRef]
92. Sun, S.; Chen, H.; Xu, C.; Zhang, Y.; Zhang, Q.; Chen, L.; Ding, Q.; Deng, Z. Exosomal miR-106b serves as a novel marker for lung cancer and promotes cancer metastasis via targeting PTEN. *Life Sci.* **2020**, *244*, 117297. [CrossRef]
93. Liao, J.; Liu, R.; Shi, Y.J.; Yin, L.H.; Pu, Y.P. Exosome-shuttling microRNA-21 promotes cell migration and invasion-targeting PDCD4 in esophageal cancer. *Int. J. Oncol.* **2016**, *48*, 2567–2579. [CrossRef]
94. Xia, Y.; Wei, K.; Hu, L.Q.; Zhou, C.R.; Lu, Z.B.; Zhan, G.S.; Pan, X.L.; Pan, C.F.; Wang, J.; Wen, W.; et al. Exosome-mediated transfer of miR-1260b promotes cell invasion through Wnt/β–catenin signaling pathway in lung adenocarcinoma. *J. Cell. Physiol.* **2020**, *235*, 6843–6853. [CrossRef]
95. Li, Z.; Tao, Y.; Wang, X.; Jiang, P.; Li, J.; Peng, M.; Zhang, X.; Chen, K.; Liu, H.; Zhen, P.; et al. Tumor-secreted exosomal miR-222 promotes tumor progression via regulating P27 expression and re-localization in pancreatic cancer. *Cell. Physiol. Biochem.* **2018**, *51*, 610–629. [CrossRef]
96. Huang, Z.; Feng, Y. Exosomes derived from hypoxic colorectal cancer cells promote angiogenesis through Wnt4-Induced β-catenin signaling in endothelial cells. *Oncol. Res.* **2017**, *25*, 651–661. [CrossRef]
97. Treps, L.; Perret, R.; Edmond, S.; Ricard, D.; Gavard, J. Glioblastoma stem-like cells secrete the pro-angiogenic VEGF-A factor in extracellular vesicles. *J. Extracell. Vesicles* **2017**, *6*, 1359479. [CrossRef]
98. Yoshii, S.; Hayashi, Y.; Iijima, H.; Inoue, T.; Kimura, K.; Sakatani, A.; Nagai, K.; Fujinaga, T.; Hiyama, S.; Kodama, T.; et al. Exosomal microRNAs derived from colon cancer cells promote tumor progression by suppressing fibroblast TP53 expression. *Cancer Sci.* **2019**, *110*, 2396–2407. [CrossRef]

99. Zheng, P.; Chen, L.; Yuan, X.; Luo, Q.; Liu, Y.; Xie, G.; Ma, Y.; Shen, L. Exosomal transfer of tumor-associated macrophage-derived miR-21 confers cisplatin resistance in gastric cancer cells. *J. Exp. Clin. Cancer Res.* **2017**, *36*, 53. [CrossRef]
100. Yu, X.; Zhang, Q.; Zhang, X.; Han, Q.; Li, H.; Mao, Y.; Wang, X.; Guo, H.; Irwin, D.M.; Niu, G.; et al. Exosomes from macrophages exposed to apoptotic breast cancer cells promote breast cancer proliferation and metastasis. *J. Cancer* **2019**, *10*, 2892–2906. [CrossRef]
101. Li, X.; Wang, S.; Zhu, R.; Li, H.; Han, Q.; Zhao, R.C. Lung tumor exosomes induce a pro-inflammatory phenotype in mesenchymal stem cells via NFκB-TLR signaling pathway. *J. Hematol. Oncol.* **2016**, *9*, 42. [CrossRef]
102. Raimondo, S.; Saieva, L.; Corrado, C.; Fontana, S.; Flugy, A.; Rizzo, A.; De Leo, G.; Alessandro, R. Chronic myeloid leukemia-derived exosomes promote tumor growth through an autocrine mechanism. *Cell Commun. Signal.* **2015**, *13*, 8. [CrossRef]
103. Wei, Y.; Lai, X.; Yu, S.; Chen, S.; Ma, Y.; Zhang, Y.; Li, H.; Zhu, X.; Yao, L.; Zhang, J. Exosomal miR-221/222 enhances tamoxifen resistance in recipient ER-positive breast cancer cells. *Breast Cancer Res. Treat.* **2014**, *147*, 423–431. [CrossRef]
104. Qin, X.; Yu, S.; Zhou, L.; Shi, M.; Hu, Y.; Xu, X.; Shen, B.; Liu, S.; Yan, D.; Feng, J. Cisplatin-resistant lung cancer cell–derived exosomes increase cisplatin resistance of recipient cells in exosomal miR-100–5p-dependent manner. *Int. J. Nanomed.* **2017**, *12*, 3721–3733. [CrossRef]
105. Richards, K.E.; Zeleniak, A.E.; Fishel, M.L.; Wu, J.; Littlepage, L.E.; Hill, R. Cancer-associated fibroblast exosomes regulate survival and proliferation of pancreatic cancer cells. *Oncogene* **2017**, *36*, 1770–1778. [CrossRef]
106. Han, M.; Gu, Y.; Lu, P.; Li, J.; Cao, H.; Li, X.; Qian, X.; Yu, C.; Yang, Y.; Yang, X.; et al. Exosome-mediated lncRNA AFAP1-AS1 promotes trastuzumab resistance through binding with AUF1 and activating ERBB2 translation. *Mol. Cancer* **2020**, *19*, 26. [CrossRef]
107. Xu, C.G.; Yang, M.F.; Ren, Y.Q.; Wu, C.H.; Wang, L.Q. Exosomes mediated transfer of lncRNA UCA1 results in increased tamoxifen resistance in breast cancer cells. *Eur. Rev. Med. Pharmacol. Sci.* **2016**, *20*, 4362–4368.
108. Wang, J.; Lv, B.; Su, Y.; Wang, X.; Bu, J.; Yao, L. Exosome-mediated transfer of lncRNA HOTTIP promotes cisplatin resistance in gastric cancer cells by regulating HMGA1/miR-218 axis. *OncoTargets Ther.* **2019**, *12*, 11325–11338. [CrossRef]
109. Weiner-Gorzel, K.; Dempsey, E.; Milewska, M.; Mcgoldrick, A.; Toh, V.; Walsh, A.; Lindsay, S.; Gubbins, L.; Cannon, A.; Sharpe, D.; et al. Overexpression of the microRNA miR-433 promotes resistance to paclitaxel through the induction of cellular senescence in ovarian cancer cells. *Cancer Med.* **2015**, *4*, 745–758. [CrossRef]
110. Xu, H.; Han, H.; Song, S.; Yi, N.; Qian, C.; Qiu, Y.; Zhou, W.; Hong, Y.; Zhuang, W.; Li, Z.; et al. Exosome-transmitted PSMA3 and PSMA3-AS1 promote proteasome inhibitor resistance in multiple myeloma. *Clin. Cancer Res.* **2019**, *25*, 1923–1935. [CrossRef]
111. Giallombardo, M.; Taverna, S.; Alessandro, R.; Hong, D.; Rolfo, C. Exosome-mediated drug resistance in cancer: The near future is here. *Ther. Adv. Med. Oncol.* **2016**, *8*, 320–322. [CrossRef] [PubMed]
112. Zhao, K.; Wang, Z.; Li, X.; Liu, J.L.; Tian, L.; Chen, J.Q. Exosome-mediated transfer of CLIC1 contributes to the vincristine-resistance in gastric cancer. *Mol. Cell. Biochem.* **2019**, *462*, 97–105. [CrossRef] [PubMed]
113. Aung, T.; Chapuy, B.; Vogel, D.; Wenzel, D.; Oppermann, M.; Lahmann, M.; Weinhage, T.; Menck, K.; Hupfeld, T.; Koch, R.; et al. Exosomal evasion of humoral immunotherapy in aggressive B-cell lymphoma modulated by ATP-binding cassette transporter A3. *Proc. Natl. Acad. Sci. USA* **2011**, *108*, 15336–15341. [CrossRef] [PubMed]
114. Ciravolo, V.; Huber, V.; Ghedini, G.C.; Venturelli, E.; Bianchi, F.; Campiglio, M.; Morelli, D.; Villa, A.; Mina, P. Della Menard, S.; et al. Potential Role of Exosomes in Countering Trastuzumab-Based Therapy. *J. Cell. Physiol.* **2012**, *227*, 658–667. [CrossRef] [PubMed]
115. Harada, T.; Yamamoto, H.; Kishida, S.; Kishida, M.; Awada, C.; Takao, T.; Kikuchi, A. Wnt5b-associated exosomes promote cancer cell migration and proliferation. *Cancer Sci.* **2017**, *108*, 42–52. [CrossRef] [PubMed]
116. Pessolano, E.; Belvedere, R.; Bizzarro, V.; Franco, P.; De Marco, I.; Porta, A.; Tosco, A.; Parente, L.; Perretti, M.; Petrella, A. Annexin A1 may induce pancreatic cancer progression as a key player of extracellular vesicles effects as evidenced in the in vitro MIA PaCa-2 model system. *Int. J. Mol. Sci.* **2018**, *19*, 3878. [CrossRef] [PubMed]
117. Datta, A.; Kim, H.; Lal, M.; McGee, L.; Johnson, A.; Moustafa, A.A.; Jones, J.C.; Mondal, D.; Ferrer, M.; Abdel-Mageed, A.B. Manumycin A suppresses exosome biogenesis and secretion via targeted inhibition of Ras/Raf/ERK1/2 signaling and hnRNP H1 in castration-resistant prostate cancer cells. *Cancer Lett.* **2017**, *408*, 73–81. [CrossRef] [PubMed]
118. Trajkovic, K.; Hsu, C.; Chiantia, S.; Rajendran, L.; Wenzel, D.; Wieland, F.; Schwille, P.; Brügger, B.; Simons, M. Ceramide triggers budding of exosome vesicles into multivesicular endosomes. *Science* **2008**, *319*, 1244–1247. [CrossRef]
119. Yang, Y.; Li, C.W.; Chan, L.C.; Wei, Y.; Hsu, J.M.; Xia, W.; Cha, J.H.; Hou, J.; Hsu, J.L.; Sun, L.; et al. Exosomal PD-L1 harbors active defense function to suppress t cell killing of breast cancer cells and promote tumor growth. *Cell Res.* **2018**, *28*, 862–864. [CrossRef]
120. Kosaka, N.; Iguchi, H.; Hagiwara, K.; Yoshioka, Y.; Takeshita, F.; Ochiya, T. Neutral sphingomyelinase 2 (nSMase2)-dependent exosomal transfer of angiogenic micrornas regulate cancer cell metastasis. *J. Biol. Chem.* **2013**, *288*, 10849–10859. [CrossRef]
121. Roseblade, A.; Luk, F.; Ung, A.; Bebawy, M. Targeting Microparticle Biogenesis: A Novel Approach to the Circumvention of Cancer Multidrug Resistance. *Curr. Cancer Drug Targets* **2015**, *15*, 205–214. [CrossRef] [PubMed]
122. Peinado, H.; Alečković, M.; Lavotshkin, S.; Matei, I.; Costa-Silva, B.; Moreno-Bueno, G.; Hergueta-Redondo, M.; Williams, C.; García-Santos, G.; Ghajar, C.; et al. Melanoma exosomes educate bone marrow progenitor cells. *Nat. Med.* **2013**, *18*, 883–891. [CrossRef] [PubMed]
123. Guo, J.; Jayaprakash, P.; Dan, J.; Wise, P.; Jang, G.-B.; Liang, C.; Chen, M.; Woodley, D.T.; Fabbri, M.; Li, W. PRAS40 Connects Microenvironmental Stress Signaling to Exosome-Mediated Secretion. *Mol. Cell. Biol.* **2017**, *37*, e00171-17. [CrossRef] [PubMed]
124. Thyagarajan, A.; Kadam, S.M.; Liu, L.; Kelly, L.E.; Rapp, C.M.; Chen, Y.; Sahu, R.P. Gemcitabine induces microvesicle particle release in a platelet-activating factor-receptor-dependent manner via modulation of the MAPK pathway in pancreatic cancer cells. *Int. J. Mol. Sci.* **2019**, *20*, 32. [CrossRef]

125. Kosgodage, U.S.; Trindade, R.P.; Thompson, P.R.; Inal, J.M. Chloramidine / Bisindolylmaleimide-I-Mediated Inhibition of Exosome and Microvesicle Release and Enhanced Efficacy of Cancer Chemotherapy. *Int. J. Mol. Sci.* **2017**, *18*, 1007. [CrossRef]
126. Featherby, S.; Madkhali, Y.; Maraveyas, A.; Ettelaie, C. Apixaban suppresses the release of TF-positive microvesicles and restrains cancer cell proliferation through directly inhibiting TF-fVIIa activity. *Thromb. Haemost.* **2019**, *119*, 1419–1432. [CrossRef]
127. Liu, J.; Zhang, Y.; Liu, A.; Wang, J.; Li, L.; Chen, X.; Gao, X. Distinct Dasatinib-Induced Mechanisms of Apoptotic Response and Exosome Release in Imatinib-Resistant Human Chronic Myeloid Leukemia Cells. *Int. J. Mol. Sci.* **2016**, *17*, 531. [CrossRef]
128. Huang, M.B.; Gonzalez, R.R.; Lillard, J.; Bond, V.C. Secretion modification region-derived peptide blocks exosome release and mediates cell cycle arrest in breast cancer cells. *Oncotarget* **2017**, *8*, 11302–11315. [CrossRef]
129. Plebanek, M.P.; Mutharasan, R.K.; Volpert, O.; Matov, A.; Gatlin, J.C.; Thaxton, C.S. Nanoparticle targeting and cholesterol flux through scavenger receptor type B-1 inhibits cellular exosome uptake. *Sci. Rep.* **2015**, *5*, 15724. [CrossRef]
130. Bastos, N.; Ruivo, C.F.; da Silva, S.; Melo, S.A. Exosomes in cancer: Use them or target them? *Semin. Cell Dev. Biol.* **2018**, *78*, 13–21. [CrossRef]
131. Zheng, Y.; Tu, C.; Zhang, J.; Wang, J. Inhibition of multiple myeloma-derived exosomes uptake suppresses the functional response in bone marrow stromal cell. *Int. J. Oncol.* **2019**, *54*, 1061–1070. [CrossRef] [PubMed]
132. Mrowczynski, O.D.; Madhankumar, A.B.; Sundstrom, J.M.; Zhao, Y.; Kawasawa, Y.I.; Slagle-Webb, B.; Mau, C.; Payne, R.A.; Rizk, E.B.; Zacharia, B.E.; et al. Exosomes impact survival to radiation exposure in cell line models of nervous system cancer. *Oncotarget* **2018**, *9*, 36083–36101. [CrossRef] [PubMed]
133. Sampey, G.C.; Meyering, S.S.; Asad Zadeh, M.; Saifuddin, M.; Hakami, R.M.; Kashanchi, F. Exosomes and their role in CNS viral infections. *J. Neurovirol.* **2014**, *20*, 199–208. [CrossRef] [PubMed]
134. Zhang, H.G.; Kim, H.; Liu, C.; Yu, S.; Wang, J.; Grizzle, W.E.; Kimberly, R.P.; Barnes, S. Curcumin reverses breast tumor exosomes mediated immune suppression of NK cell tumor cytotoxicity. *Biochim. Biophys. Acta Mol. Cell Res.* **2007**, *1773*, 1116–1123. [CrossRef] [PubMed]
135. Pucci, F.; Garris, C.; Lai, C.P.; Newton, A.; Pfirschke, C.; Engblom, C.; Alvarez, D.; Sprachman, M.; Evavold, C.; Magnuson, A.; et al. SCS macrophages suppress melanoma by restricting tumor-derived vesicle-B cell interactions. *Science* **2016**, *352*, 242–246. [CrossRef]
136. Evander, M.; Gidlöf, O.; Olde, B.; Erlinge, D.; Laurell, T. Non-contact acoustic capture of microparticles from small plasma volumes. *Lab Chip* **2015**, *15*, 2588–2596. [CrossRef]
137. Smyth, T.; Kullberg, M.; Malik, N.; Smith-Jones, P.; Graner, M.W.; Anchordoquy, T.J. Biodistribution and delivery efficiency of unmodified tumor-derived exosomes. *J. Control. Release* **2015**, *199*, 145–155. [CrossRef]
138. Nishida-Aoki, N.; Tominaga, N.; Takeshita, F.; Sonoda, H.; Yoshioka, Y.; Ochiya, T. Disruption of Circulating Extracellular Vesicles as a Novel Therapeutic Strategy against Cancer Metastasis. *Mol. Ther.* **2017**, *25*, 181–191. [CrossRef]
139. Bttpdjbufe, F.; Gspn, T.Q.; Chalmin, F.; Ladoire, S.; Mignot, G.; Vincent, J.; Bruchard, M.; Boireau, W.; Rouleau, A.; Simon, B.; et al. Membrane-associated Hsp72 from tumor-derived exosomes mediates STAT3-dependent immunosuppressive function of mouse and human myeloid-derived suppressor cells Fanny. *J. Clin. Investig.* **2010**, *120*, 457–471. [CrossRef]
140. Yoon, J.H.; Ashktorab, H.; Smoot, D.T.; Nam, S.W.; Hur, H.; Park, W.S. Uptake and tumor-suppressive pathways of exosome-associated GKN1 protein in gastric epithelial cells. *Gastric Cancer* **2020**, *23*, 848–862. [CrossRef]
141. Zaharie, F.; Muresan, M.S.; Petrushev, B.; Berce, C.; Gafencu, G.A.; Selicean, S.; Jurj, A.; Cojocneanu-Petric, R.; Lisencu, C.I.; Pop, L.A.; et al. Exosome-carried microRNA-375 inhibits cell progression and dissemination via Bcl-2 blocking in colon cancer. *J. Gastrointest. Liver Dis.* **2015**, *24*, 435–443. [CrossRef] [PubMed]
142. Shi, H.; Li, H.; Zhen, T.; Dong, Y.; Pei, X.; Zhang, X. The Potential Therapeutic Role of Exosomal MicroRNA-520b Derived from Normal Fibroblasts in Pancreatic Cancer. *Mol. Ther. Nucleic Acids* **2020**, *20*, 373–384. [CrossRef] [PubMed]
143. Jeong, K.; Yu, Y.J.; You, J.Y.; Rhee, W.J.; Kim, J.A. Exosome-mediated microRNA-497 delivery for anti-cancer therapy in a microfluidic 3D lung cancer model. *Lab Chip* **2020**, *20*, 548–557. [CrossRef] [PubMed]
144. Chen, W.; Quan, Y.; Fan, S.; Wang, H.; Liang, J.; Huang, L.; Chen, L.; Liu, Q.; He, P.; Ye, Y. Exosome-transmitted circular RNA hsa_circ_0051443 suppresses hepatocellular carcinoma progression. *Cancer Lett.* **2020**, *475*, 119–128. [CrossRef]
145. Pakravan, K.; Babashah, S.; Sadeghizadeh, M.; Mowla, S.J.; Mossahebi-Mohammadi, M.; Ataei, F.; Dana, N.; Javan, M. MicroRNA-100 shuttled by mesenchymal stem cell-derived exosomes suppresses in vitro angiogenesis through modulating the mTOR/HIF-1α/VEGF signaling axis in breast cancer cells. *Cell. Oncol.* **2017**, *40*, 457–470. [CrossRef]
146. Simpson, R.J.; Lim, J.W.E.; Moritz, R.L.; Mathivanan, S. Exosomes: Proteomic insights and diagnostic potential. *Expert Rev. Proteomics* **2009**, *6*, 267–283. [CrossRef]
147. Hornick, N.I.; Huan, J.; Doron, B.; Goloviznina, N.A.; Lapidus, J.; Chang, B.H.; Kurre, P. Serum Exosome MicroRNA as a minimally-invasive early biomarker of AML. *Sci. Rep.* **2015**, *5*, 11295. [CrossRef]
148. Sharma, R.; Huang, X.; Brekken, R.A.; Schroit, A.J. Detection of phosphatidylserine-positive exosomes for the diagnosis of early-stage malignancies. *Br. J. Cancer* **2017**, *117*, 545–552. [CrossRef]
149. Bu, H.; He, D.; He, X.; Wang, K. Exosomes: Isolation, Analysis, and Applications in Cancer Detection and Therapy. *ChemBioChem* **2019**, *20*, 451–461. [CrossRef]
150. Boukouris, S.; Mathivanan, S. Exosomes in bodily fluids are a highly stable resource of disease biomarkers. *Proteomics Clin. Appl.* **2015**, *9*, 358–367. [CrossRef]

151. Munoz, J.L.; Bliss, S.A.; Greco, S.J.; Ramkissoon, S.H.; Ligon, K.L.; Rameshwar, P. Delivery of functional anti-miR-9 by mesenchymal stem cell-derived exosomes to glioblastoma multiforme cells conferred chemosensitivity. *Mol. Ther. Nucleic Acids* **2013**, *2*, e126. [CrossRef] [PubMed]
152. Syn, N.L.; Wang, L.; Chow, E.K.H.; Lim, C.T.; Goh, B.C. Exosomes in Cancer Nanomedicine and Immunotherapy: Prospects and Challenges. *Trends Biotechnol.* **2017**, *35*, 665–676. [CrossRef] [PubMed]
153. Viaud, S.; Terme, M.; Flament, C.; Taieb, J.; André, F.; Novault, S.; Escudier, B.; Robert, C.; Caillat-Zucman, S.; Tursz, T.; et al. Dendritic cell-derived exosomes promote natural killer cell activation and proliferation: A role for NKG2D ligands and IL-15Rα. *PLoS ONE* **2009**, *4*, e4942. [CrossRef] [PubMed]
154. Pitt, J.M.; André, F.; Amigorena, S.; Soria, J.C.; Eggermont, A.; Kroemer, G.; Zitvogel, L. Dendritic cell-derived exosomes for cancer therapy. *J. Clin. Investig.* **2016**, *126*, 1224–1232. [CrossRef]
155. Viaud, S.; Ploix, S.; Lapierre, V.; Théry, C.; Commere, P.H.; Tramalloni, D.; Gorrichon, K.; Virault-Rocroy, P.; Tursz, T.; Lantz, O.; et al. Updated technology to produce highly immunogenic dendritic cell-derived exosomes of clinical grade: A critical role of interferon-γ. *J. Immunother.* **2011**, *34*, 65–75. [CrossRef] [PubMed]
156. Vulpis, E.; Cecere, F.; Molfetta, R.; Soriani, A.; Fionda, C.; Peruzzi, G.; Caracciolo, G.; Palchetti, S.; Masuelli, L.; Simonelli, L.; et al. Genotoxic stress modulates the release of exosomes from multiple myeloma cells capable of activating NK cell cytokine production: Role of HSP70/TLR2/NF-kB axis. *Oncoimmunology* **2017**, *6*, e1279372. [CrossRef] [PubMed]
157. Xiao, W.; Dong, W.; Zhang, C.; Saren, G.; Geng, P.; Zhao, H.; Li, Q.; Zhu, J.; Li, G.; Zhang, S.; et al. Effects of the epigenetic drug MS-275 on the release and function of exosome-related immune molecules in hepatocellular carcinoma cells. *Eur. J. Med. Res.* **2013**, *18*, 61. [CrossRef] [PubMed]
158. Chen, W.; Wang, J.; Shao, C.; Liu, S.; Yu, Y.; Wang, Q.; Cao, X. Efficient induction of antitumor T cell immunity by exosomes derived from heat-shocked lymphoma cells. *Eur. J. Immunol.* **2006**, *36*, 1598–1607. [CrossRef] [PubMed]
159. Tan, A.; de la Peña, H.; Seifalian, A.M. The application of exosomes as a nanoscale cancer vaccine. *Int. J. Nanomed.* **2010**, *5*, 889–900.
160. Xie, Y.; Bai, O.; Zhang, H.; Yuan, J.; Zong, S.; Chibbar, R.; Slattery, K.; Qureshi, M.; Wei, Y.; Deng, Y.; et al. Membrane-bound HSP70-engineered myeloma cell-derived exosomes stimulate more efficient CD8+ CTL- and NK-mediated antitumour immunity than exosomes released from heat-shocked tumour cells expressing cytoplasmic HSP70. *J. Cell. Mol. Med.* **2010**, *14*, 2655–2666. [CrossRef]
161. Yang, Y.; Chen, Y.; Zhang, F.; Zhao, Q.; Zhong, H. Increased anti-tumour activity by exosomes derived from doxorubicin-treated tumour cells via heat stress. *Int. J. Hyperth.* **2015**, *31*, 498–506. [CrossRef] [PubMed]
162. Hao, S.; Bai, O.; Li, F.; Yuan, J.; Laferte, S.; Xiang, J. Mature dendritic cells pulsed with exosomes stimulate efficient cytotoxic T-lymphocyte responses and antitumour immunity. *Immunology* **2007**, *120*, 90–102. [CrossRef] [PubMed]
163. Yamashita, T.; Takahashi, Y.; Takakura, Y. Possibility of exosome-based therapeutics and challenges in production of exosomes eligible for therapeutic application. *Biol. Pharm. Bull.* **2018**, *41*, 835–842. [CrossRef] [PubMed]
164. Morishita, M.; Takahashi, Y.; Matsumoto, A.; Nishikawa, M.; Takakura, Y. Exosome-based tumor antigens–adjuvant co-delivery utilizing genetically engineered tumor cell-derived exosomes with immunostimulatory CpG DNA. *Biomaterials* **2016**, *111*, 55–65. [CrossRef] [PubMed]
165. Lu, Z.; Zuo, B.; Jing, R.; Gao, X.; Rao, Q.; Liu, Z.; Qi, H.; Guo, H.; Yin, H.F. Dendritic cell-derived exosomes elicit tumor regression in autochthonous hepatocellular carcinoma mouse models. *J. Hepatol.* **2017**, *67*, 739–748. [CrossRef]
166. Xiao, L.; Erb, U.; Zhao, K.; Hackert, T.; Zöller, M. Efficacy of vaccination with tumor-exosome loaded dendritic cells combined with cytotoxic drug treatment in pancreatic cancer. *Oncoimmunology* **2017**, *6*. [CrossRef]
167. Sedlik, C.; Vigneron, J.; Torrieri-Dramard, L.; Pitoiset, F.; Denizeau, J.; Chesneau, C.; de la Rochere, P.; Lantz, O.; Thery, C.; Bellier, B. Different immunogenicity but similar antitumor efficacy of two DNA vaccines coding for an antigen secreted in different membrane vesicle-associated forms. *J. Extracell. Vesicles* **2014**, *3*. [CrossRef]
168. Ohno, S.I.; Takanashi, M.; Sudo, K.; Ueda, S.; Ishikawa, A.; Matsuyama, N.; Fujita, K.; Mizutani, T.; Ohgi, T.; Ochiya, T.; et al. Systemically injected exosomes targeted to EGFR deliver antitumor microrna to breast cancer cells. *Mol. Ther.* **2013**, *21*, 185–191. [CrossRef]
169. Lang, F.M.; Hossain, A.; Gumin, J.; Momin, E.N.; Shimizu, Y.; Ledbetter, D.; Shahar, T.; Yamashita, S.; Parker Kerrigan, B.; Fueyo, J.; et al. Mesenchymal stem cells as natural biofactories for exosomes carrying miR-124a in the treatment of gliomas. *Neuro-Oncology* **2018**, *20*, 380–390. [CrossRef]
170. Zheng, R.; Du, M.; Wang, X.; Xu, W.; Liang, J.; Wang, W.; Lv, Q.; Qin, C.; Chu, H.; Wang, M.; et al. Exosome-transmitted long non-coding RNA PTENP1 suppresses bladder cancer progression. *Mol. Cancer* **2018**, *17*, 143. [CrossRef]
171. Shtam, T.A.; Kovalev, R.A.; Varfolomeeva, E.Y.; Makarov, E.M.; Kil, Y.V.; Filatov, M.V. Exosomes are natural carriers of exogenous siRNA to human cells in vitro. *Cell Commun. Signal.* **2013**, *11*, 88. [CrossRef] [PubMed]
172. Bellavia, D.; Raimondo, S.; Calabrese, G.; Forte, S.; Cristaldi, M.; Patinella, A.; Memeo, L.; Manno, M.; Raccosta, S.; Diana, P.; et al. Interleukin 3- receptor targeted exosomes inhibit in vitro and in vivo chronic myelogenous Leukemia cell growth. *Theranostics* **2017**, *7*, 1333–1345. [CrossRef] [PubMed]
173. Kamerkar, S.; LeBleu, V.; Sugimoto, H.; Yang, S.; Ruivo, C.; Melo, S.A.; Lee, J.; Kalluri, R. Exosomes Facilitate Therapeutic Targeting of Oncogenic Kras in Pancreatic Cancer. *Nature* **2017**, *546*, 498–503. [CrossRef] [PubMed]
174. Zhao, L.; Gu, C.; Gan, Y.; Shao, L.; Chen, H.; Zhu, H. Exosome-mediated siRNA delivery to suppress postoperative breast cancer metastasis. *J. Control. Release* **2020**, *318*, 1–15. [CrossRef] [PubMed]

175. Kim, G.; Kim, M.; Lee, Y.; Byun, J.W.; Hwang, D.W.; Lee, M. Systemic delivery of microRNA-21 antisense oligonucleotides to the brain using T7-peptide decorated exosomes. *J. Control. Release* **2020**, *317*, 273–281. [CrossRef]
176. Fatima, F.; Nawaz, M. Stem cell-derived exosomes: Roles in stromal remodeling, tumor progression, and cancer immunotherapy. *Chin. J. Cancer* **2015**, *34*, 541–553. [CrossRef]
177. Mendt, M.; Rezvani, K.; Shpall, E. Mesenchymal stem cell-derived exosomes for clinical use. *Bone Marrow Transplant.* **2019**, *54*, 789–792. [CrossRef]
178. Liang, Y.; Zhang, D.; Li, L.; Xin, T.; Zhao, Y.; Ma, R.; Du, J. Exosomal microRNA-144 from bone marrow-derived mesenchymal stem cells inhibits the progression of non-small cell lung cancer by targeting CCNE1 and CCNE2. *Stem Cell Res. Ther.* **2020**, *11*, 87. [CrossRef]
179. Xie, C.; Du, L.Y.; Guo, F.; Li, X.; Cheng, B. Exosomes derived from microRNA-101-3p-overexpressing human bone marrow mesenchymal stem cells suppress oral cancer cell proliferation, invasion, and migration. *Mol. Cell. Biochem.* **2019**, *458*, 11–26. [CrossRef]
180. Greco, K.A.; Franzen, C.A.; Foreman, K.E.; Flanigan, R.C.; Kuo, P.C.; Gupta, G.N. PLK-1 Silencing in Bladder Cancer by siRNA Delivered with Exosomes. *Urology* **2016**, *91*, 241.e1–241.e7. [CrossRef]
181. Hu, Q.; Su, H.; Li, J.; Lyon, C.; Tang, W.; Wan, M.; Hu, T.Y. Clinical applications of exosome membrane proteins. *Precis. Clin. Med.* **2020**, *3*, 54–66. [CrossRef] [PubMed]
182. Saari, H.; Lázaro-Ibáñez, E.; Viitala, T.; Vuorimaa-Laukkanen, E.; Siljander, P.; Yliperttula, M. Microvesicle- and exosome-mediated drug delivery enhances the cytotoxicity of Paclitaxel in autologous prostate cancer cells. *J. Control. Release* **2015**, *220*, 727–737. [CrossRef] [PubMed]
183. Wang, L.; Xie, Y.; Ahmed, K.A.; Ahmed, S.; Sami, A.; Chibbar, R.; Xu, Q.; Kane, S.E.; Hao, S.; Mulligan, S.J.; et al. Exosomal pMHC-I complex targets T cell-based vaccine to directly stimulate CTL responses leading to antitumor immunity in transgenic FVBneuN and HLA-A2/HER2 mice and eradicating trastuzumab-resistant tumor in athymic nude mice. *Breast Cancer Res. Treat.* **2013**, *140*, 273–284. [CrossRef] [PubMed]
184. Kim, M.S.; Haney, M.J.; Zhao, Y.; Yuan, D.; Deygen, I.; Klyachko, N.L.; Kabanov, A.V.; Batrakova, E.V. Engineering macrophage-derived exosomes for targeted paclitaxel delivery to pulmonary metastases: In vitro and in vivo evaluations. *Nanomed. Nanotechnol. Biol. Med.* **2018**, *14*, 195–204. [CrossRef] [PubMed]
185. Srivastava, A.; Amreddy, N.; Babu, A.; Panneerselvam, J.; Mehta, M.; Muralidharan, R.; Chen, A.; Zhao, Y.D.; Razaq, M.; Riedinger, N.; et al. Nanosomes carrying doxorubicin exhibit potent anticancer activity against human lung cancer cells. *Sci. Rep.* **2016**, *6*, 38541. [CrossRef]
186. Gong, C.; Tian, J.; Wang, Z.; Gao, Y.; Wu, X.; Ding, X.; Qiang, L.; Li, G.; Han, Z.; Yuan, Y.; et al. Functional exosome-mediated co-delivery of doxorubicin and hydrophobically modified microRNA 159 for triple-negative breast cancer therapy. *J. Nanobiotechnol.* **2019**, *17*, 93. [CrossRef]
187. Kim, M.S.; Haney, M.J.; Zhao, Y.; Mahajan, V.; Deygen, I.; Klyachko, N.L.; Inskoe, E.; Piroyan, A.; Sokolsky, M.; Hingtgen, S.D.; et al. Development of Exosome-encapsulated Paclitaxel to Overcome MDR in Cancer cells. *Nanomedicine* **2017**, *12*, 655–664. [CrossRef]
188. Hadla, M.; Palazzolo, S.; Corona, G.; Caligiuri, I.; Canzonieri, V.; Toffoli, G.; Rizzolio, F. Exosomes increase the therapeutic index of doxorubicin in breast and ovarian cancer mouse models. *Nanomedicine* **2016**, *11*, 2431–2441. [CrossRef]
189. Tian, Y.; Li, S.; Song, J.; Ji, T.; Zhu, M.; Anderson, G.J.; Wei, J.; Nie, G. A doxorubicin delivery platform using engineered natural membrane vesicle exosomes for targeted tumor therapy. *Biomaterials* **2014**, *35*, 2383–2390. [CrossRef]
190. Li, Y.J.; Wu, J.Y.; Wang, J.M.; Hu, X.B.; Cai, J.X.; Xiang, D.X. Gemcitabine loaded autologous exosomes for effective and safe chemotherapy of pancreatic cancer. *Acta Biomater.* **2020**, *101*, 519–530. [CrossRef]
191. Osterman, C.J.D.; Lynch, J.C.; Leaf, P.; Gonda, A.; Bennit, H.R.F.; Griffiths, D.; Wall, N.R. Curcumin modulates pancreatic adenocarcinoma cell-derived exosomal function. *PLoS ONE* **2015**, *10*, e0132845. [CrossRef] [PubMed]
192. Munagala, R.; Aqil, F.; Jeyabalan, J.; Agrawal, A.K.; Mudd, A.M.; Kyakulaga, A.H.; Singh, I.P.; Vadhanam, M.V.; Gupta, R.C. Exosomal formulation of anthocyanidins against multiple cancer types. *Cancer Lett.* **2017**, *393*, 94–102. [CrossRef] [PubMed]
193. Donoso-Quezada, J.; Guajardo-Flores, D.; González-Valdez, J. Exosomes as nanocarriers for the delivery of bioactive compounds from black bean extract with antiproliferative activity in cancer cell lines. *Mater. Today Proc.* **2019**, *13*, 362–369. [CrossRef]
194. Aqil, F.; Jeyabalan, J.; Agrawal, A.K.; Kyakulaga, A.H.; Munagala, R.; Parker, L.; Gupta, R.C. Exosomal delivery of berry anthocyanidins for the management of ovarian cancer. *Food Funct.* **2017**, *8*, 4100–4107. [CrossRef]
195. Aqil, F.; Kausar, H.; Agrawal, A.K.; Jeyabalan, J.; Kyakulaga, A.H.; Munagala, R.; Gupta, R. Exosomal formulation enhances therapeutic response of celastrol against lung cancer. *Exp. Mol. Pathol.* **2016**, *101*, 12–21. [CrossRef]
196. Bhattacharya, S.; Pal, K.; Sharma, A.K.; Dutta, S.K.; Lau, J.S.; Yan, I.K.; Wang, E.; Elkhanany, A.; Alkharfy, K.M.; Sanyal, A.; et al. GAIP interacting protein C-Terminus regulates autophagy and exosome biogenesis of pancreatic cancer through metabolic pathways. *PLoS ONE* **2014**, *9*, e114409. [CrossRef]
197. Kirave, P.; Gondaliya, P.; Kulkarni, B.; Rawal, R.; Garg, R.; Jain, A.; Kalia, K. Exosome mediated miR-155 delivery confers cisplatin chemoresistance in oral cancer cells via epithelial-mesenchymal transition. *Oncotarget* **2020**, *11*, 1157–1171. [CrossRef]
198. Kim, S.M.; Yang, Y.; Oh, S.J.; Hong, Y.; Seo, M.; Jang, M. Cancer-derived exosomes as a delivery platform of CRISPR/Cas9 confer cancer cell tropism-dependent targeting. *J. Control. Release* **2017**, *266*, 8–16. [CrossRef]
199. Zhang, Q.; Zhang, H.; Ning, T.; Liu, D.; Deng, T.; Liu, R.; Bai, M.; Zhu, K.; Li, J.; Fan, Q.; et al. Exosome-Delivered c-Met siRNA Could Reverse Chemoresistance to Cisplatin in Gastric Cancer. *Int. J. Nanomed.* **2020**, *15*, 2323–2335. [CrossRef]
200. Liu, T.; Zhang, X.; Du, L.; Wang, Y.; Liu, X.; Tian, H.; Wang, L.; Li, P.; Zhao, Y.; Duan, W.; et al. Exosome-transmitted miR-128-3p increase chemosensitivity of oxaliplatin-resistant colorectal cancer. *Mol. Cancer* **2019**, *18*, 43. [CrossRef]

201. Lou, G.; Song, X.; Yang, F.; Wu, S.; Wang, J.; Chen, Z.; Liu, Y. Exosomes derived from MIR-122-modified adipose tissue-derived MSCs increase chemosensitivity of hepatocellular carcinoma. *J. Hematol. Oncol.* **2015**, *8*, 122. [CrossRef] [PubMed]
202. Han, M.; Hu, J.; Lu, P.; Cao, H.; Yu, C.; Li, X.; Qian, X.; Yang, X.; Yang, Y.; Han, N.; et al. Exosome-transmitted miR-567 reverses trastuzumab resistance by inhibiting ATG5 in breast cancer. *Cell Death Dis.* **2020**, *11*, 43. [CrossRef] [PubMed]
203. Cui, J.; Wang, H.; Zhang, X.; Sun, X.; Zhang, J.; Ma, J. Exosomal miR-200c suppresses chemoresistance of docetaxel in tongue squamous cell carcinoma by suppressing TUBB3 and PPP2R1B. *Aging (Albany N. Y.)* **2020**, *12*, 6756–6773. [CrossRef]
204. Lou, G.; Chen, L.; Xia, C.; Wang, W.; Qi, J.; Li, A.; Zhao, L.; Chen, Z.; Zheng, M.; Liu, Y. MiR-199a-modified exosomes from adipose tissue-derived mesenchymal stem cells improve hepatocellular carcinoma chemosensitivity through mTOR pathway. *J. Exp. Clin. Cancer Res.* **2020**, *39*, 4. [CrossRef] [PubMed]
205. Besse, B.; Charrier, M.; Lapierre, V.; Dansin, E.; Lantz, O.; Planchard, D.; Le Chevalier, T.; Livartoski, A.; Barlesi, F.; Laplanche, A.; et al. Dendritic cell-derived exosomes as maintenance immunotherapy after first line chemotherapy in NSCLC. *Oncoimmunology* **2016**, *5*, 1071008. [CrossRef] [PubMed]
206. Beit-Yannai, E.; Tabak, S.; Stamer, W.D. Physical exosome:exosome interactions. *J. Cell. Mol. Med.* **2018**, *22*, 2001–2006. [CrossRef] [PubMed]
207. Lunavat, T.R.; Jang, S.C.; Nilsson, L.; Park, H.T.; Repiska, G.; Lässer, C.; Nilsson, J.A.; Gho, Y.S.; Lötvall, J. RNAi delivery by exosome-mimetic nanovesicles—Implications for targeting c-Myc in cancer. *Biomaterials* **2016**, *102*, 231–238. [CrossRef]
208. Sato, Y.T.; Umezaki, K.; Sawada, S.; Mukai, S.A.; Sasaki, Y.; Harada, N.; Shiku, H.; Akiyoshi, K. Engineering hybrid exosomes by membrane fusion with liposomes. *Sci. Rep.* **2016**, *6*, 21933. [CrossRef]

FEBS Letters

FEBS PRESS science publishing by scientists

RESEARCH ARTICLE

IL-6 mediated CD206$^+$ARG-1$^+$ tumor associated macrophage polarization induces Treg infiltration in non-responder luminal a breast cancer

Ananya Das[1], Sraddhya Roy[1], Aparajita Bairagi[1], Neyaz Alam[2] and Nabanita Chatterjee[1]

1 Department of Receptor Biology and Tumor Metastasis, Chittaranjan National Cancer Institute, Kolkata, India
2 Department of Surgical Oncology, Chittaranjan National Cancer Hospital, Kolkata, India

Correspondence
N. Chatterjee, Department of Receptor Biology and Tumor Metastasis, Chittaranjan National Cancer Institute, 37, S.P. Mukherjee Road, Kolkata 700026, India
Tel: xxxxx
E-mail: nabanita.chatterje@yahoo.com

(Received 20 September 2024, revised 2 December 2024, accepted 29 December 2024)

doi:10.1002/1873-3468.70000

Edited by Wilfried Ellmeier

Drug non-responsiveness is the major reason for the poor prognosis of hormonal receptor-positive breast cancer (ER$^+$/PR$^+$ BCa), particularly the luminal A subtype. However, the underlying mechanism of drug non-responsiveness remains unknown. Flow cytometry and t-SNE analysis followed by ELISA validation of responder and non-responder unveiled lower secretion of IFN-γ, IL-12, and higher levels of IL-6 and TGF-β in CD4$^+$ T cells ($P < 0.001$), CD8$^+$ T cells ($P < 0.001$), FOXP3$^+$ Tregs ($P < 0.001$) and CD206$^+$ TAMs ($P < 0.001$) in non-responders. Treatment of isolated CD206$^+$ TAMs with recombinant IL-6 upregulated the expression of ARG-1 (arginase-1) and subsequent increase of TGF-β$^+$ Tregs ($P < 0.001$) and IL-10$^+$ Tregs ($P < 0.001$) in luminal A BCa. Our findings showed IL-6 mediated ARG-1$^+$CD206$^+$ TAMs polarization induced FOXP3$^+$ Tregs infiltration in TME of non-responder in luminal A BCa.

Keywords: cytokines; interleukin-6; luminal A; macrophages; non-responder; T cells

Breast cancer (BCa) is the second leading cancer accounting for 11.6% of all cancer cases with around 2.3 million new cases across the world [1]. Among all the types of breast cancer (BCa), luminal A, which is both estrogen and progesterone receptor-positive, accounts for around 63.6% of all BCa cases worldwide with 25% occurrence rate in India [2,3], with 70.2% survival rate [4]. Neoadjuvant chemotherapy (NACT), has been established as a promising therapy in locally advanced BCa which results in improved survival rates for BCa patients [5]. One of the huge drawbacks of chemotherapy is the non-responsiveness of luminal A patients towards conventional chemotherapeutic drugs. The underlying mechanisms of non-responsive BCa are still under investigation. Understanding the mechanisms is crucial for developing alternate therapeutic approaches in luminal A BCa.

The innate and adaptive immune cell populations which constitute the BCa immune microenvironment (BCIM), are an important determinant of tumor progression. On the one hand, pro-inflammatory immune cells such as cytotoxic T cells (Tc), natural killer (NK) cells, NKT cells, N1 neutrophils, and M1 macrophages induce a direct cytotoxic function on tumor cells [6]. On the other hand, the immune-suppressive cell populations i.e., regulatory T cells (Tregs), Th2-skewed T helper cells (Th2), N2 neutrophils, M2 macrophages and myeloid-derived suppressor cells (MDSCs) are

Abbreviation
ARG-1, arginase 1; BCa, breast cancer; IF, immunofluorescence; IL, interleukin; MDSCs, myeloid-derived suppressor cells; NACT, neoadjuvant chemotherapy; NKT, natural killer T cells; PBMC, plasma blood mononuclear cell; PMA, phorbol 12-myristate 13-acetate; TAM, tumor-associated macrophage; Tc, cytotoxic T cell; Tconv, conventional T cells; TGF, transforming growth factor; TIL, tumor-infiltrating lymphocytes; TME, tumor microenvironment; TNF, tumor necrosis factor; Treg, regulatory T cells.

Straive™ | Journal Code: FEB2 | Article ID: 70000 / FEBSL-24-0869.R1 | WILEY | Dispatch: 29-JAN-25 | No. of Pages: 16 | CE: Ishwarya R | ME: Bhagyalakshmi

responsible for stimulating tissue remodeling, angiogenesis, disease progression and thereby these cells are correlated with poor prognosis of BCa [6]. Tregs are recruited in the TME by chemokines and cytokines secreted from tumor cells, cancer-associated fibroblasts, or immunosuppressive cells and their ability to infiltrate within tumors increases with tumor stage and correlates with poor prognosis in invasive BCa [7]. The tumor-infiltrating lymphocytes (TILs), including regulatory T (Treg) cells, have prognostic value in triple-negative breast cancers (TNBCs), their significance and correlation with luminal A BCa is less clear [8]. The crosstalk of macrophage and T cells plays an important role in T cell differentiation. In the TME, tumor-associated macrophages (TAMs) promote cancer cell survival, angiogenesis, and metastasis by inducing immune suppression in various cancers including BCa [9]. As the TME plays a significant role in tumor progression, therefore higher immune suppression in TME might result in drug non-responsiveness in BCa. Moreover, the role of TAM and Treg crosstalk in inducing drug non-responsiveness is not been studied. Therefore, a better insight into their crosstalk mechanism in non-responder luminal A BCa is crucial for the success of harnessing immunotherapeutic approaches to improve the therapeutic efficacy in patients.

Inflammation is one of the key player of the initiation and promotion of tumors, angiogenesis, and metastasis [10]. In response to oncogenic consequences including hypoxia, infiltration of tumor-infiltrating immune cells, and activation of fibroblast secretes a series of cytokines, chemokines, and growth factors to influence the tumor microenvironment [11]. Several cytokines such as Interleukin (IL)-1, IL-6, IL-10, and transforming growth factor-β (TGF-β) induce cancer cell proliferation and invasion by intracellular NF-kB signaling by accelerating tumor progression. IL-6 acts as a strong player in inducing tumorigenesis by creating a feed-forward loop with inflammation which in turn expands CSC population, and breast cancer cell survival and induces increased angiogenesis [12]. IL-6/STAT3 axis induced ARG-1^+ TAM (arginse-1^+ TAM) polarization which exerts an immune-suppressive microenvironment in BCa [13]. IL-10 and TGF-β alter the fate of innate and adaptive immune cells by maintaining an immune-suppressive environment by diminishing the functional activity of T cells i.e., Th1, Th2, and Th17 phenotype [14,15]. Tumor cells in some cases secret IL-10 and TGF-β for stimulating an immune-suppressive fate by losing MHC I, adhesion molecules like ICAM, and upregulating programmed death ligand-1 (PD-L1) in tumor niche [16]. TNF-α plays a key role in BCa including survival and proliferation of cancer cells, promoting angiogenesis, and increased infiltration of ARG-1^+ TAMs and cancer-associated fibroblasts (CAFs). Moreover, TNF-α production by peripheral T cells is positively associated with circulating tumor cells with expression of EMT markers [17]. The crosstalk of cytokines plays a major role in TME modulation of BCa. IL-10 levels enhance TGF-β secretion from Tregs and macrophages which promotes EMT. Furthermore, TGF-β together with IL-6, increases IL-10 secretion from Th-17 cells which suppresses T cell functionality in BCa [18,19]. On the other hand, IL-12 is chiefly associated with pro-inflammatory functions which include the differentiation of Th1 cells, activation of cytotoxic functionality in T and NK cells, inhibition of immunosuppressive cells, such as TAMs and MDSCs and inducing the production of IFN-γ [20–22]. IFN-γ orchestrates an anti-tumor immunity by upregulating granzyme and perforin secretion, initiating apoptosis in tumor cells, polarizing of M1 macrophages, upregulation of MHC I on both immune and non-immune cells, activation of $CD8^+$ T cells and impairment of Tregs [21,22]. Thereby, the cytokines secreted by immune cells and their interplay possess a crucial role in TME modulation of BCa; but their proper functioning in immune cells crosstalk of non-responder luminal A BCa is yet to be studied.

The underlying mechanism drug non-responsiveness of luminal A BCa has not been studied extensively. We hypothesized that the secretory cytokines induced ARG-1^+CD206$^+$TAMs polarization which further induced Tregs to build an immune-suppressive TME in non-responder Luminal A BCa. Therefore, we have analyzed the pro and anti-inflammatory cytokines profile in T cells and macrophage subsets in responder and non-responder that will help to identify the underlying mechanisms of drug non-responsiveness in luminal A BCa. The non-responder group showed a higher immune-suppressive TME compared with the responder, characterized by upregulation in IL-6, TGF-β, and IL-10 levels which induced immunosuppressive microenvironment in TME of luminal A BCa. The variation in cytokines level might provide better insight for developing new immunotherapeutic approaches for enhancing drug sensitivity in non-responder luminal A BCa.

Materials and methods

Materials

Primary tagged antibodies CD4, CD8, FOXP3, CD11b, CD68, and CD206 (Invitrogen, USA) were used for flow cytometry analysis. TAMs and Tregs were sorted using

MACS BEAD sorter (Thermo Scientific, USA) with CD45/CD11b/CD206 and CD45/CD3/CD4 lineage markers were used for biotin-tagged antibody (Invitrogen). ELISA for the respective cytokines i.e., IL-6, IL-10, TGF-β, IL-12, TNF-α, and IFN-γ was performed with ELISA Kits (R&D System, USA). $CD206^+$ TAMs were treated with human recombinant IL-6 (Pepro Tech, USA). All the details of the reagents were mentioned in Table S2.

Patients and sample

Forty patients diagnosed with luminal A BCa and treated in Chittaranjan National Cancer Hospital, Kolkata, India between January 2022 and April 2023 were included in the age group between 17 and 80 years. The attending clinician documented all the information related to clinicopathological characteristics. The study has been approved by the Institution Ethics Committee of Chittaranjan National Cancer Hospital (CNCI-IEC-75731) and written consents were collected from all participating volunteers. All of them were classified into non-responder ($N = 18$) and responder ($N = 22$) categories receiving conventional chemotherapy. During the surgery, the paired tumor and blood samples were collected from the responder and non-responder patients. BCa patients other than luminal A BCa, lactating and pregnant women, aged below 17 years and exceeding 80 years, and those patients with other comorbidities were excluded from the study. Patient clinicopathological parameters and frequency distribution are mentioned in Table S1.

All the experiments performed during the study with human participants and respective patient samples were by the ethical standards of the Ethics Committee of Chittaranjan National Cancer Hospital (CNCI-IEC-75731). All the volunteers involved in the study have given their consent to participate. The personal information regarding patients is kept confidential.

Hematoxylin and eosin staining

Paraffin-embedded tissue sections were stained with hematoxylin and eosin following the standard protocol and the sections were observed under a bright field microscope (Microscope, Bright Field DM 100, Leica Mikrosysteme Vertrieb GmbH, Germany) [25]. The procedure of TILs count was as recommended by the International TILs' Working Group 2014; by selecting the tumor area, separating the stromal and ductal region, scanning under low magnification (20×), and assessing the percentage of TILs in responder and non-responder. [26].

PBMCs isolation

Plasma blood mononuclear cells (PBMCs) were isolated from the blood samples of the respective patients. Whole blood was diluted with an equal amount of PBS (1×) to form a layer in histopaque-1077 (Sigma, USA) in 1:1 ratio. The gradient centrifugation was done at 400 ***g*** for 30 min at low acceleration. After separation of the layers, middle white cloudy layer was pipetted out carefully and washed in PBS at 4000 rpm for 5 min. The desired pellet was finally collected for further experiments.

Stimulation of PBMC

Freshly isolated PBMCs were cultured in RPMI 1640 medium containing 10% FBS and 1% penicillin–streptomycin and stimulated for 4 h with phorbol 12-myristate 13-acetate (PMA; 100 $ng{\cdot}mL^{-1}$; Sigma-Aldrich) and ionomycin (1 $\mu g{\cdot}mL^{-1}$; Sigma-Aldrich).

Single cell suspension from tumor tissue

Surgically removed tumor tissue was washed in PBS and homogenized in collagenase type IV (Sigma-Aldrich) followed by incubation for 12 h at 37 °C in a rocker (Allied Scientific Products) for uniform collagenase type IV treatment. After incubation, the homogenized mixture was strained with 40 μm strainer (40 μm, Falcon, USA) and centrifuged at 2000 rpm for 5 min for single cells.

Stimulation of single cells for activating immune cells

For analyzing intracellular cytokines, cells were stimulated with phorbol-12-myristate-13-acetate (50 $ng{\cdot}mL^{-1}$) and ionomycin (1 $\mu g{\cdot}mL^{-1}$) for 6 h at 37 °C, 5% CO_2, in the presence of 1 $mg{\cdot}mL^{-1}$ Brefeldin A (BD Biosciences, USA) in RPMI medium containing 10% FBS and 1% penicillin/streptomycin (Gibco, USA).

Intracellular cytokines staining for flow cytometry

Stimulated PBMC and activated single cells were incubated with cell surface markers against CD45, CD11b, CD80, CD206, CD3, CD4, CD8, and intracellular marker FOXP3 (Invitrogen) according to the manufacturer's protocol. Samples were then incubated with intracellular cytokine antibodies i.e., IFN-γ, TNF-α, IL-12, IL-4, IL-10, and TGF-β (Abcam, UK) in a total volume of 100 μL permeabilization buffer (eBiosciences) for 40 min in the dark at 4 °C. Then samples were incubated with goat anti-rabbit IgG (H + L) Secondary Antibody, APC/FITC (Invitrogen). Flow cytometry was performed on the BD LSRFortessa flow cytometer (BD Biosciences). Data were analyzed using FLOWJO v10.8.1.

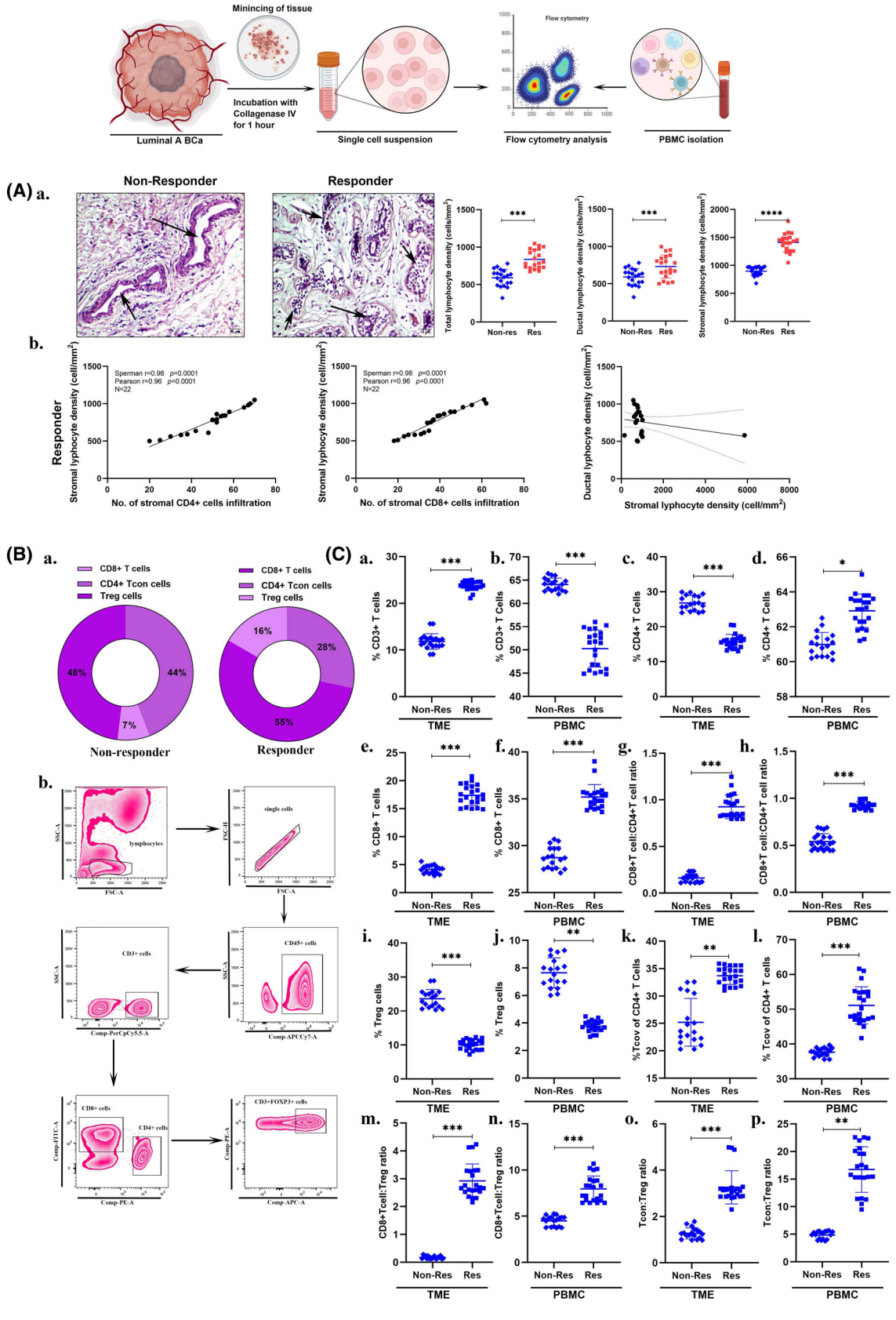
Minincing of tissue
Incubation with Collagenase IV for 1 hour
Flow cytometry
Luminal A BCa
Single cell suspension
Flow cytometry analysis
PBMC isolation
(A) a.
Non-Responder
Responder
Total lymphocyte density (cells/mm2)
Ductal lymphocyte density (cells/mm2)
Stromal lymphocyte density (cells/mm2)
Non-res Res
Non-Res Res
b.
Responder
Stromal lyphocyte density (cell/mm2)
Sperman r=0.98 p=0.0001
Pearson r=0.96 p=0.0001
N=22
No. of stromal CD4+ cells infiltration
No. of stromal CD8+ cells infiltration
Ductal lyphocyte density (cell/mm2)
Stromal lyphocyte density (cell/mm2)
(B) a.
CD8+ T cells
CD4+ Tcon cells
Treg cells
48%
44%
7%
16%
28%
55%
Non-responder
Responder
b.
lymphocytes
single cells
CD3+ cells
CD45+ cells
CD8+ cells
CD4+ cells
CD3+FOXP3+ cells
(C) a.
% CD3+ T cells
TME
b.
PBMC
c.
% CD4+ T Cells
d.
e.
% CD8+ T cells
f.
g.
CD8+T cell:CD4+T cell ratio
h.
i.
% Treg cells
j.
k.
% Tcov of CD4+ T cells
l.
m.
CD8+Tcell:Treg ratio
n.
o.
Tcon:Treg ratio
p.
Non-Res Res

Color

Fig. 1. T cell subtypes vary in responder and non-responder luminal A BCa. (Aa) Infiltration of TILs in the stromal and ductal region, (b) correlation of $CD4^+$ and $CD8^+$ T cells in ductal infiltration of responder group. (Ba) Pie chart of the differential percentage of T cell subsets, (b) Gating strategy in flow cytometry analysis. (Ca–p) Graphical expression of comparison of T cell subtypes in responder and non-responder luminal A BCa (Black arrows [→] indicating the infiltration of TILs in ductal region, yellow arrows [⟶] indicating TILs). Data shown in graphs as mean ± SD. Values of $P < 0.05$ (*), $P < 0.01$ (**), $P < 0.001$ (***), and $P < 0.0001$ (****) were considered statistically significant.

T-SNE analysis

To analyze the expression of cytokines in infiltrated T cell subsets, t-SNE analysis was performed in single cells derived from tumor tissue of responder and non-responder groups. FLOWJO v.10.8.1 was used for t-SNE analysis. First the $CD8^+$ T cells, $CD4^+$ Tconv cells, and Tregs from each sample were downsampled to 5500, 7500, and 2000 cells, respectively, with FLOWJO DOWNSAMPLE v3.3 plugin. Then the cells were concatenated for t-SNE analysis with a total of 88 000 $CD8^+$ T cells, 120 000 $CD4^+$ Tconv cells, and 32 000 Tregs based on the expression of cytokines i.e., IFN-γ, TNF-α, IL-12, IL-4, IL-10, and TGF-β with configuration of 3000 iterations, 30 perplexities, 5600 learning rate (eta), exact (vantage point tree) KNN algorithm, and Barnes-Hut gradient algorithm. Additionally, the FlowSOM clustering was performed using the FLOWJO FLOWSOM v2.6 plugin. The heat maps with the mean fluorescence intensities of cytokines for each cluster were analyzed with GRAPHPAD PRISM 8.0 [27].

ELISA

Dilution factors for serum were specific to individual markers. After dilution, samples were coated in the plates. Secretory cytokine levels were measured by ELISA (R&D Systems, USA), according to the manufacturer's instructions. The addition of TMB substrate (HiMedia, USA) resulted in the development of visible colorimetric output. The OD value was determined via a microplate reader (Tecan, infinite M200) at 450 nm [28].

Sorting of $CD11b^+CD206^+$ cells

$CD11b^+CD206^+$ TAMs were isolated by magnetic sorting from luminal A primary breast tumor and cultures in RPMI1640 media supplemented with 10% FBS and 1% Penicillin–streptomycin. The cells were incubated with human recombinant IL-6 (100 $ng{\cdot}mL^{-1}$) (Promega, USA) for 12 h before further analysis. The cells were centrifuged at 2000 rpm for 5 min and the supernatant (conditioned media) was collected for further treatment.

Sorting of $FOXP3^+$ Treg cells

$CD3^+CD4^+FOXP3^+$ Treg cells were sorted from luminal A primary breast tumor and cultured with RPMI1640 media supplemented with 10% FBS and 1% Penicillin–streptomycin. After that, the cells were incubated with condition 1 media for 12 h, and flow cytometry analysis was performed.

Statistics analysis

To compare the data, we employed the Two-tailed unpaired Student's *t*-test to assess statistical significance using GRAPHPAD PRISM 8.0. For the correlation study, both Pearson and Spearman's correlation was performed where the value of r was considered as follows; $0.0 \leq r \geq 0.2$ very weak, $0.2 \leq r \geq 0.4$ weak, $0.4 \leq r \geq 0.7$ moderate and $0.7 \leq r \geq 1.0$ strong. For every calculation value $P \leq 0.05$ was considered statistically significant. Data were shown as mean ± SD.

Software

All the Flow data was analyzed in FLOWJO V.8.1. The graphical illustrations were made with the help of BIORENDER (https://www.biorender.com/) software.

Results

Increased infiltration of T cells enhanced drug sensitivity in luminal a BCa

For evaluating the role of the tumor immune microenvironment in responder and non-responder luminal A BCa (patient details mentioned in Table S1), we have analyzed the H&E staining of the tissue. The analysis showed the total infiltration of lymphocytes was lower ($P < 0.001$) in the non-responder compared with the responder in luminal A BCa. Further evaluation revealed that both ductal ($P < 0.001$) and stromal ($P < 0.0001$) infiltration of TILs decreased in the non-responder group compared with responder (Fig. 1Aa). Pearson correlation analysis showed a positive correlation ($P < 0.0001$) between stromal infiltration of TILs and $CD8^+$ cells as well as $CD4^+$ cells in responder luminal A BCa; whereas the correlation between ductal and stromal infiltration remained non-significant (Fig. 1Ab). The data showed lower infiltration of TILs in non-responders of luminal A BCa (Fig. 1Aa).

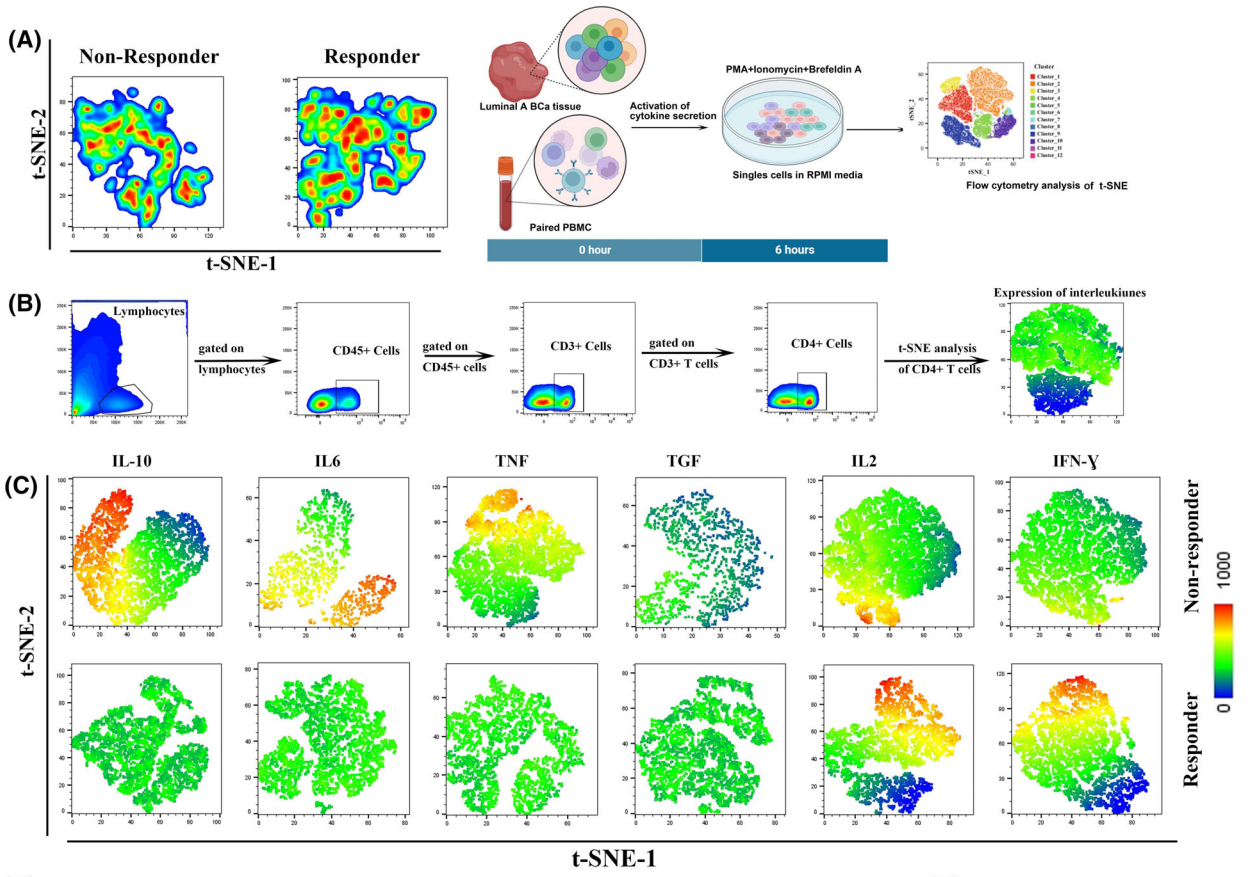
(A)
Non-Responder
Responder
t-SNE-2
t-SNE-1
Luminal A BCa tissue
Paired PBMC
Activation of cytokine secretion
PMA+Ionomycin+Brefeldin A
Singles cells in RPMI media
Flow cytometry analysis of t-SNE
0 hour
6 hours
(B)
Lymphocytes
gated on lymphocytes
CD45+ Cells
gated on CD45+ cells
CD3+ Cells
gated on CD3+ T cells
CD4+ Cells
t-SNE analysis of CD4+ T cells
Expression of interleukiunes
(C)
IL-10
IL6
TNF
TGF
IL2
IFN-Ɣ
t-SNE-2
t-SNE-1
Non-responder
Responder
1000
0
(D)
MFI of IFN-γ
MFI of IL-12
MFI of IL-10
MFI of IL-6
MFI of TGF-β
MFI of TNF-α
Non-Res
Res
ns
(E)
IFN-γ+
IL-12-
TGF-β-
IL-6-
IL-10-
TNF-α+
Non-Res
Res
600
500
400
300
(F)
TME
a. %CD3+CD4+IFN-γ+ Cells
b. %CD3+CD4+IL-12+ Cells
c. %CD3+CD4+IL-10+ Cells
d. %CD3+CD4+IL-6+ Cells
e. %CD3+CD4+TGF-β+ Cells
f. %CD3+CD4+TNF-α+ Cells
Non-Res
Res
(G)
PBMC
a. % CD3+CD4+IFN-γ+ cells
b. % CD3+CD4+IL-12+ cells
c. % CD3+CD4+IL-10+ cells
d. % CD3+CD4+IL-6+ cells
e. % CD3+CD4+TGF-β+ cells
f. %CD3+CD4+TNF-α+ Cells
Non-Res
Res
ns

Color

Fig. 2. t-SNE analysis of $CD4^+$ T cells expressing the cytokine levels. (A) graphical representation of cytokine activation of single cell suspension derived from tumor and PBMC and, (B) T cell gating strategy, (C) t-SNE analysis of pro and anti-inflammatory cytokines in $CD4^+$ T cell population of tumor derived single cells expression analysis responder and non-responder group. (D) Graphical representation of MFI of cytokines from t-SNE in responder and non-responder group. (E) Heatmap analysis of the MFI in responder and non-responder group, (Fa–f) Graphical representation of dot plot analysis of cytokine expressions in TME of $CD4^+$ T cells of luminal A BCa, Gg-l. Graphical representation of dot plot analysis of cytokine expressions in PBMC of $CD4^+$ T cells of luminal A BCa. Data shown in graphs as mean ± SD. Values of $P < 0.05$ (*), $P < 0.01$ (**), $P < 0.001$ (***), and $P < 0.0001$ (****) were considered statistically significant.

Lower infiltration of pro-inflammatory T cells correlates with non-responsiveness in luminal A BCa

After finding the increased TILs in responder luminal A BCa, we compared the percentage of T cell subsets between the responder and non-responder. For the evaluation, we performed flow cytometry analysis of single cells derived from tumors and PBMC of both responder and non-responder luminal A BCa. Flow cytometry analysis (gating strategy shown in Fig. 1Bb) showed a significant difference in T cell profile where $CD8^+$ and $CD4^+$ Tconv cells decreased significantly and Tregs increased significantly in non-responder group compared with responder (Fig. 1Ba). Both circulatory and tumor-infiltrating $CD45^+CD3^+$ T cells were lower ($P < 0.001$) in the non-responder group (Fig. 1Ca,b). We analyzed the infiltration of T cell subsets which showed $CD4^+$ T cells significantly decreased in peripheral blood ($P < 0.05$) but increased ($P < 0.001$) in TME of non-responder luminal A BCa (Fig. 1Cc,d). The infiltration of $CD8^+$ T cells significantly decreased ($P < 0.001$) in TME and peripheral blood (Fig. 1Ce,f) of the non-responder group. Moreover, the ratio of $CD8^+/CD4^+$ T cells was also significantly decreased ($P < 0.001$) in both TME and PBMC of non-responders (Fig. 1Cg,h). Whereas, the population of $CD45^+CD3^+CD4^+FOXP3^-$ Tconv cells was significantly decreased ($P < 0.001$), the $CD45^+CD3^+CD4^+FOXP3^+$ Tregs were significantly increased ($P < 0.001$) in TME as well as in peripheral blood of non-responder luminal A BCa (Fig. 1Ci–l). Together with that, the ratio of $CD8^+$/Tregs and Tconv/Tregs also decreased ($P < 0.001$) in TME and PBMC of non-responders (Fig. 1Cm–p). Non-responder luminal A TME showed a higher infiltration of Tregs and lower infiltration of $CD4^+$ Tconv and $CD8^+$ T cells which showed an immunosuppressive microenvironment in non-responder luminal A BCa.

Pro-inflammatory functional activity of $CD4^+$ T cells decreased in non-responder luminal a BCa

For further evaluating the functional activity of $CD4^+$ T cells in responder and non-responder of luminal A BCa, we analyzed the cytokine expressions in $CD4^+$ T cells. Single cell suspension and PBMC were isolated from the paired tumor and blood samples and flow cytometry was performed after cytokine activation (Fig. 2A). We have performed t-SNE analysis (Fig. 2B) of single cell suspension derived from tumor of responder and non-responder which showed an increase in pro-tumorigenic cytokine levels i.e., IL-6, IL-10, TGF-β, and TNF-α, and decrease in anti-tumorigenic cytokine levels i.e., IL-12 and IFN-γ in the non-responder group (Fig. 2C). The MFI of $CD4^+IL\text{-}6^+$ ($P < 0.001$) along with $CD4^+TGF\text{-}\beta^+$ ($P < 0.01$) and $CD4^+IL\text{-}10^+$ ($P < 0.01$) was significantly increased and decreased in $CD4^+IL\text{-}12^+$ ($P < 0.01$) and $CD4^+IFN\text{-}\gamma^+$ ($P < 0.05$) T cells in t-SNE analysis of the non-responder group (Fig. 2D). The differential expression of MFI of $CD4^+$ T cells cytokines was also represented in the heatmap (Fig. 2E). The percentage of $CD4^+IFN\text{-}\gamma^+$ and $CD4^+IL\text{-}12^+$ T cells decreased significantly in both TME ($P < 0.05$; $P < 0.001$) and PBMC ($P < 0.001$) of the non-responder group (Fig. 2Fa,b,Ga,b, Figs S1Ia and S2Ia). In TME, the percentage of tumor-infiltrating $CD4^+IL6^+$ ($P < 0.0001$), $CD4^+IL10^+$, $CD4^+TGF\text{-}\beta^+$, and $CD4^+TNF\text{-}\alpha^+$ T cells increased significantly ($P < 0.001$) in non-responder group as compared to responder (Fig. 2Fc–f). However, in PBMC, the percentage of $CD4^+TGF\text{-}\beta^+$ and $CD4^+IL6^+$ T cells significantly increased ($P < 0.001$), and the percentage changes of $CD4^+TNF\text{-}\alpha^+$ and $CD4^+IL10^+$ T cells remained non-significant in non-responder luminal A BCa (Fig. 2Gc–f, Fig. S2Ia). Therefore, the non-responder luminal A BCa group showed an immune-suppressive response in $CD4^+$ T cell population in the TME that might be correlated with the higher expression of IL-6.

Infiltration of functionally active $CD8^+$ T cells decreased in non-responder luminal a BCa

The t-SNE analysis of $CD8^+$ T cells (Fig. 3Aa) of single cell suspension derived from tumor showed an increase expression of anti-inflammatory cytokines including IL-6, IL-10, and TGF-β and lower pro-inflammatory cytokines expression of IFN-γ and IL-12

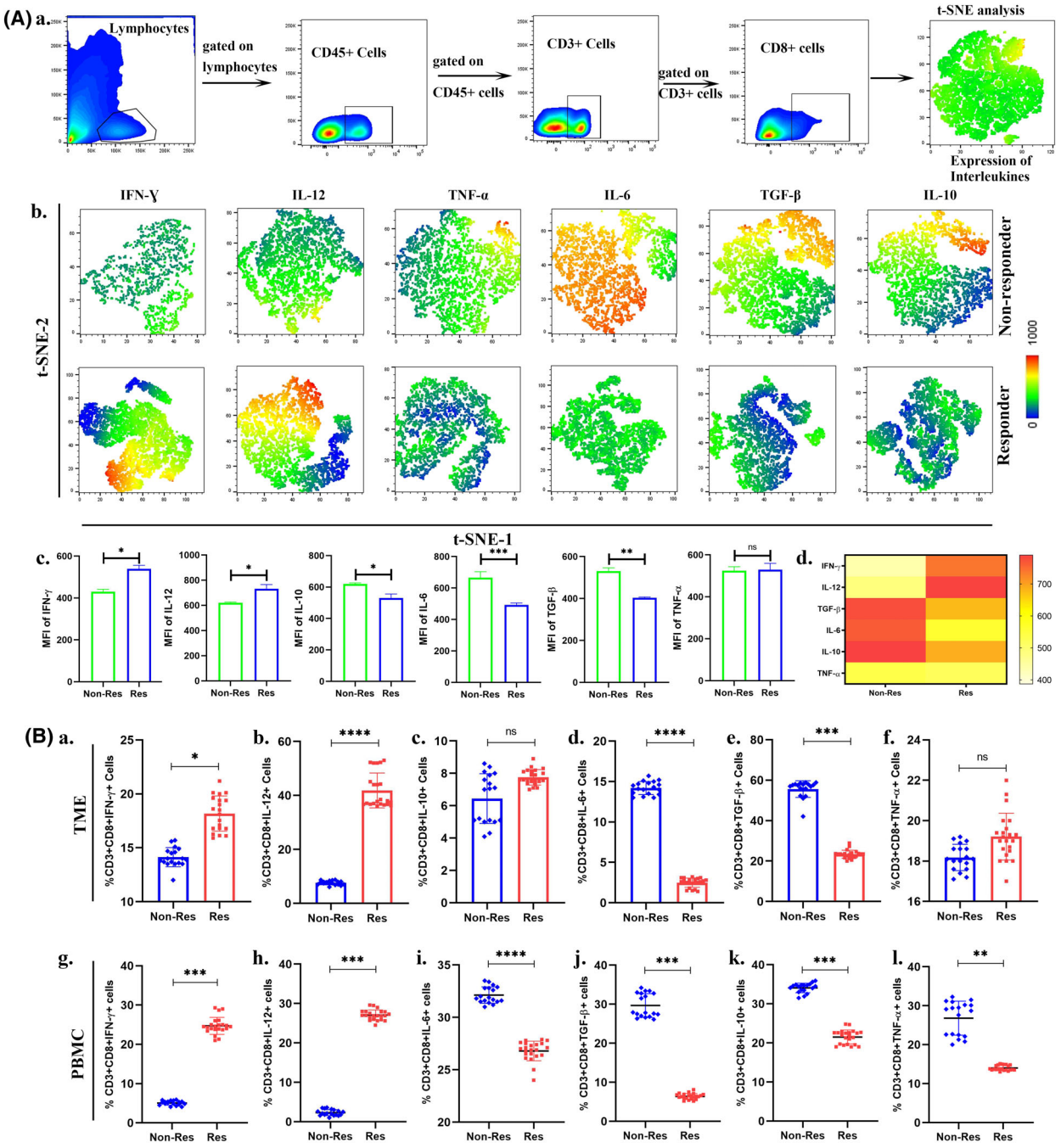

Color

Fig. 3. t-SNE analysis of CD8$^+$ T cells expressing the cytokine levels. (Aa) Gating strategy of CD8$^+$ T cells, (b) t-SNE analysis of cytokines expression (IFN-γ, IL-12, TNF-α, IL-6, TGF-β, and IL-10) in CD8$^+$ T cells population in responder and non-responder group, (c) Differential expression analysis of MFI of t-SNE of pro and anti-inflammatory cytokines in CD8$^+$ T cells of responder and non-responder group, (d) Heatmap representation of MFI of t-SNE. (Ba–f) Graphical representation of cytokine levels in TME of CD8$^+$ T cells of luminal A BCa, (Bg–l) Graphical representation of cytokine levels in PBMC of CD8$^+$ T cells of luminal A BCa. Data shown in graphs as mean ± SD. Values of $P < 0.05$ (*), $P < 0.01$ (**), $P < 0.001$ (***), and $P < 0.0001$ (****) were considered statistically significant.

in non-responder luminal A BCa (Fig. 3Ab). Although the MFI of t-SNE showed no significant difference in CD8$^+$TNF-α$^+$ population but significant increase in CD8$^+$IL-6$^+$ population ($P < 0.001$), CD8$^+$IL-10 population ($P < 0.05$) and CD8$^+$TGF-β$^+$ population ($P < 0.001$) was also observed in non-responder ones

as represented in heatmap (Fig. 3Ac,d). Dot plot analysis of PBMC and single cells derived from tumor showed that a significantly lower percentage of both the circulatory ($P < 0.001$) and tumor-infiltrating $CD8^+IFN\text{-}\gamma^+$ and $CD8^+$ $IL\text{-}12^+$ T cells ($P < 0.0001$) in non-responder luminal A BCa (Fig. 3Ba,b,g,h, Figs S1Ib and S2Ib). A higher percentage of $CD8^+IL\text{-}6^+$ T cells ($P < 0.0001$) was observed in TME and as well as in PBMC along with $CD8^+TGF\text{-}\beta^+$ T cells ($P < 0.001$) in non-responder luminal A BCa group (Fig. 3Bc–f,i,j, Fig. S1Ib). However, the percentage of $CD8^+TNF\text{-}\alpha^+$ ($P < 0.001$) and $CD8^+IL10^+$ ($P < 0.0001$) T cells were increased in PBMC (Fig. 3Bk,l, Fig. S1Ib). The data found a significantly higher infiltration of $CD8^+IL\text{-}6^+$, $CD8^+$ $TGF\text{-}\beta^+$ T cells in non-responder luminal A BCa which signify the immunosuppressive nature.

The expression of IFN-γ and IL-12 decreased in Tregs of responder luminal a BCa

Tregs associated cytokines expression was shifted towards anti-inflammatory phenotype in non-responder luminal A BCa. t-SNE analysis showed a significantly decrease in the expression of IFN-γ and IL-12 in Tregs of non-responder group (Fig. 4Aa–c). The expression of TGF-β ($P < 0.01$) and IL-10 ($P < 0.001$) increased in Tregs in the non-responder luminal A BCa (Fig. 4Aa–c). The expression of TGF-β ($P < 0.01$) and IL-10 ($P < 0.05$) was significantly higher and expression of IFN-γ ($P < 0.01$) and IL12 ($P < 0.01$) was significantly lower in $CD4^+FOXP3^+$ Tregs in the TME of non-responder group, whereas, the expression of TNF-α and IL-6 remained non-significant in TME and IL-6 and IL-10 remained non-significant in PBMC respectively (Fig. 4Ba–l, Fig. S3Ia,b). Our data showed that not only $CD4^+$ and $CD8^+$ T cells but also Tregs showed pro-tumorigenic functional activity in non-responder luminal A BCa. The consistent higher expression of IL-10 and TGF-β might induce the infiltration of $FOXP3^+$ Tregs in the TME of luminal A BCa.

The non-responder showed an increased pro-tumorigenic $CD206^+$ TAM polarization in TME of luminal a BCa

As we found the significantly higher expression of IL-6 and TGF-β in $CD4^+$ Tconv and $CD8^+$ T cells of non-responders of luminal A BCa TME, thus, we further evaluated their expression in the macrophage population. t-SNE analysis showed decreased expression of IL-12 in both $CD68^+$ M1 and $CD206^+$ TAMs and increased expression of IL-6 and TGF-β in non-responder luminal A BCa as compared to responder (Fig. 5Aa,b). MFI from t-SNE analysis showed decreased IL-12 expression with increased expression of IL-6 and TGF-β in both $CD68^+$ M1 and $CD206^+$ TAM populations of the non-responder group (Fig. 5Ac–e). Flow cytometry data showed a higher percentage of $CD206^+$ TAMs ($P < 0.001$) and a lower population of $CD68^+$ M1 macrophages ($P < 0.001$) in TME and PBMC of non-responder group (Fig. 5Ba,b, Ca,b, Fig. S4). Simultaneously, dot plot analysis also revealed that the lower infiltration of $CD68^+IL\text{-}12^+$ M1 macrophages ($P < 0.001$) and the decrease expression of $CD206^+IL\text{-}12^+$ TAM ($P < 0.001$) in TME and PBMC of non-responder group was noticed (Fig. 5Bc,f, Cc,f; Fig. S4). The infiltration of $CD68^+IL\text{-}6^+$ ($P < 0.001$) and $CD68^+TGF\text{-}\beta^+$ ($P < 0.01$) along with $CD206^+IL\text{-}6^+$ and $CD206^+TGF\text{-}\beta^+$ macrophages were increased in non-responder luminal A BCa compared with responder (Fig. 5Bd,e,g,h,Cd,e,g,h; Fig. S4). Therefore, results showed significant role of IL-6 in the immunosuppressing function of macrophages as well as T cells in non-responder luminal A BCa.

Elevated level of IL-6 correlates with immune suppression in non-responder luminal a BCa

In was established from earlier flow cytometric analysis that a significant elevated expression of IL-6, TGF-β in $CD206^+$ TAMs, $CD68^+$ M1 macrophages; $CD8^+$ T and $CD4^+$ Tconv subsets. Eventually, we evaluated the level of serum cytokines in responder and non-responder with ELISA that showed significant higher level of IL-6 ($P < 0.0001$) along with TGF-β ($P < 0.01$), IL-10 ($P < 0.01$) in non-responder group. Simultaneously, IL-12 and IFN-γ levels were significantly decreased in the same ($P < 0.01$) (Fig. 5D). Furthermore, correlation analysis revealed that IL-6 was positively correlated with $CD206^+$ TAMs and $FOXP3^+$ Tregs percentage, whereas negatively correlated with $CD4^+$ and $CD8^+$ T cells in the TME of non-responders (Fig. 5E). Therefore, elevated levels of IL-6 might play a role to induce drug non-responsiveness by increasing the polarization of $CD206^+$ TAMs which may contribute Tregs infiltration in luminal A BCa.

IL-6 induced TAM polarization and induced TAM-Treg crosstalk in luminal a BCa

To examine IL-6 induced TAM polarization in luminal A BCa, $CD11b^+$ 206^+ TAMs were sorted from luminal A primary breast tumor followed by human

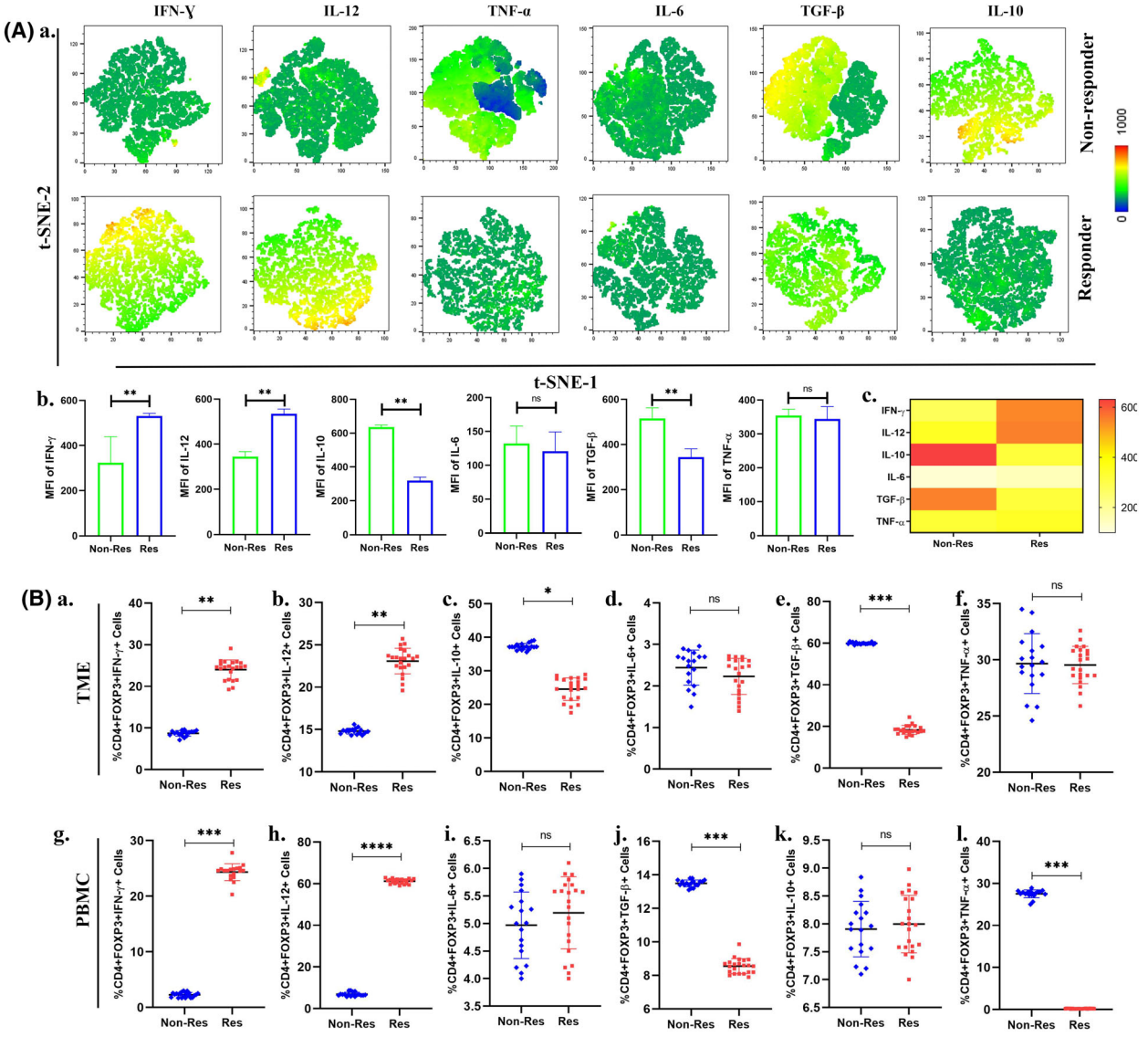

Color

Fig. 4. t-SNE analysis of $CD4^+FOXP3^+$ Treg cells expressing the cytokine levels. (Aa) t-SNE analysis of whole T cells population in responder and non-responder group, (b) Differential MFI analysis of pro and anti-inflammatory cytokines in Treg cells of responder and non-responder group, (c) Heatmap of MFI value of cytokines in Treg cells. (Ba–f) Graphical representation of cytokine levels in TME of Treg cells of luminal A BCa. (Bg–l) Graphical representation of cytokine levels in PBMC of Treg cells of luminal A BCa. Data shown in graphs as mean ± SD. Values of $P < 0.05$ (*), $P < 0.01$ (**), $P < 0.001$ (***), and $P < 0.0001$ (****) were considered statistically significant.

Color

Fig. 5. t-SNE analysis of macrophage populations expressing the cytokine levels. (Aa) Gating of macrophage population, (b) t-SNE analysis of the cytokines (IL-12, IL-6 and TGF-β) in $CD68^+$ and $CD206^+$ macrophages of responder and non-responder luminal A BCa, (c) Heatmap of MFI of t-SNE cytokine expression in responder and non-responder group, (d) MFI graph of cytokine expression in $CD68^+$ macrophages, (e) MFI graph of cytokine expression in $CD206^+$ macrophages. (Ba–h) Graphical representation of macrophage subtypes and their expressing cytokine levels in TME of responder and non-responder luminal ABCa. (Ca–h) Graphical representation of macrophage subtypes and their expressing cytokine levels in TME of responder and non-responder luminal A BCa. (Da–d) Graphical representation of cytokine levels form patients' serum of responder and non-responder luminal A BCa. (Ea–d) Correlation analysis of IL-6 with the percentage of immune cell infiltration in non-responder luminal A BCa. Data shown in graphs as mean ± SD. Values of $P < 0.05$ (*), $P < 0.01$ (**), $P < 0.001$ (***), and $P < 0.0001$ (****) were considered statistically significant.

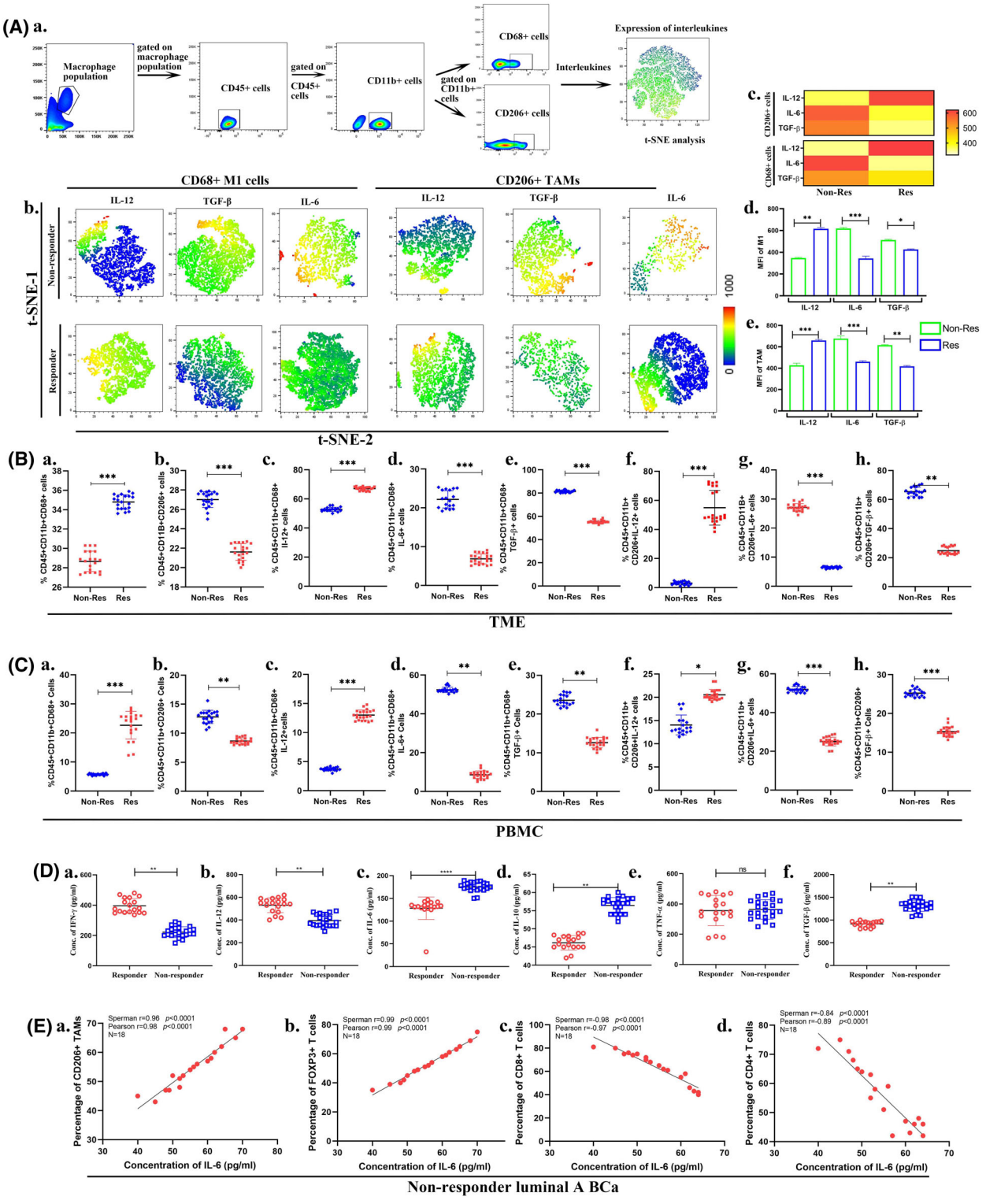

recombinant IL-6 treatment (Fig. 6Aa,b). Flow cytometry analysis showed that percentage of $CD206^{+}$ $ARG\text{-}1^{+}$ and $CD206^{+}IL\text{-}6^{+}$ TAMs significantly increased ($P < 0.01$) in the IL-6 treated group as compared to the vehicle control (Fig. 6Ac). Precisely, IL-6 induction significantly ($P < 0.01$) promoted TGF-β

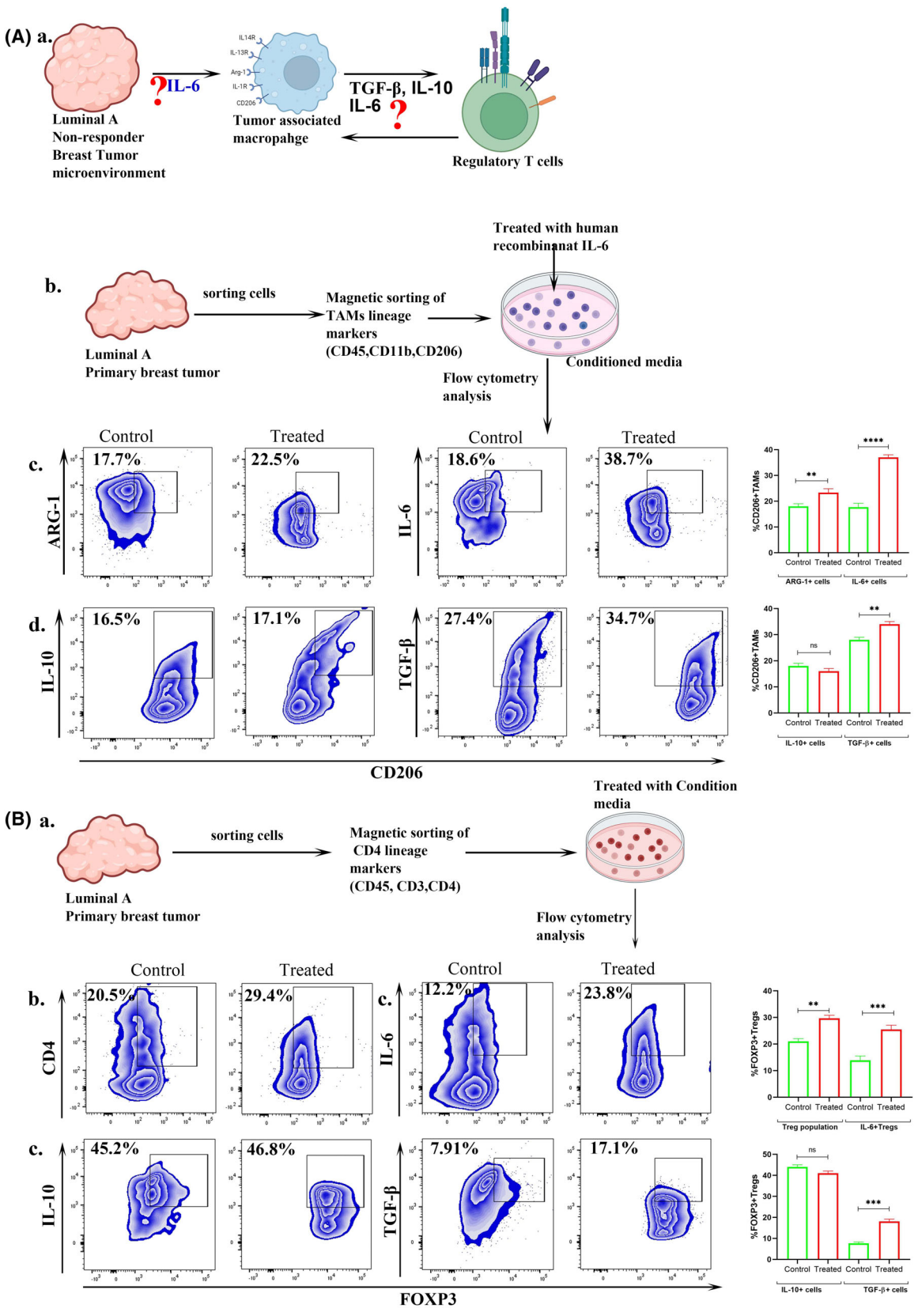
(A) a.
IL-6
Luminal A
Non-responder
Breast Tumor
microenvironment
IL14R
IL-13R
Arg-1
IL-1R
CD206
Tumor associated
macropahge
TGF-β, IL-10
IL-6
Regulatory T cells
b.
sorting cells
Luminal A
Primary breast tumor
Magnetic sorting of
TAMs lineage
markers
(CD45,CD11b,CD206)
Treated with human
recombinanat IL-6
Conditioned media
Flow cytometry
analysis
c.
Control
Treated
Control
Treated
ARG-1
17.7%
22.5%
IL-6
18.6%
38.7%
%CD206+TAMs
ARG-1+ cells
IL-6+ cells
d.
IL-10
16.5%
17.1%
TGF-β
27.4%
34.7%
IL-10+ cells
TGF-β+ cells
CD206
(B) a.
sorting cells
Luminal A
Primary breast tumor
Magnetic sorting of
CD4 lineage
markers
(CD45, CD3,CD4)
Treated with Condition
media
Flow cytometry
analysis
b.
CD4
20.5%
29.4%
c.
IL-6
12.2%
23.8%
%FOXP3+Tregs
Treg population
IL-6+Tregs
c.
IL-10
45.2%
46.8%
TGF-β
7.91%
17.1%
IL-10+ cells
TGF-β+ cells
FOXP3

Color

Fig. 6. IL-6 induced TAMs polarization and Treg infiltrating in luminal A BCa. (Aa) Diagram representation of experiment purpose, (b) Graphical representation of TAMs isolation and treatment, (c) Percentage of ARG-1$^+$ and IL-6$^+$ TAMs with graphical comparison in control and treated, (d) Percentage of \IL-10$^+$ and TGF-β$^+$ TAMs with graphical comparison in control and treated. (Ba) Experimental strategy of establishing TAM-Treg crosstalk in luminal A BCa, (b) Percentage of CD4$^+$ and IL-6$^+$ FOXP3$^+$ Tregs with graphical comparison in control and treated, (c) Percentage of IL-10$^+$ and TGF-β$^+$FOXP3$^+$ Tregs with graphical comparison in control and treated. Data shown in graphs as mean ± SD. Values of $P < 0.05$ (*), $P < 0.01$ (**), $P < 0.001$ (***), and $P < 0.0001$ (****) were considered statistically significant.

expression in CD206$^+$ TAMs, although CD206$^+$IL-10$^+$ TAMs remained non-significant (Fig. 6Ad). To find out TAM-mediated FOXP3$^+$ Tregs recruitment, we isolated CD4$^+$FOXP3$^+$ Tregs and incubated with conditioned media (CD11b$^+$CD206$^+$ TAMs culture supernatant) (Fig. 6Ba). The results established the percentage of CD4$^+$FOXP3$^+$ cells was significantly increased ($P < 0.01$) in conditioned media-treated group (Fig. 6Bb). Interestingly, the percentage of FOXP3$^+$IL-6$^+$ and FOXP3$^+$TGF-β$^+$ Tregs were significantly ($P < 0.001$) increased, although the FOXP3$^+$IL-10$^+$ Tregs did not show any significant changes under the influence of conditioned media (Fig. 6Bb,c). Therefore, the elevated IL-6 levels induced CD206$^+$ TAMs polarization and TGF-β secretion which in turn augment the infiltration of Tregs in TME in non-responder luminal A BCa.

Discussion

Tumor reprogramming, cancer cell proliferation, and chemotherapy response are primarily reliant on immune cell invasion, its activation, and production of several cytokines in TME [29]. Several cytokines i.e., IL-6, TGF-β, IL-10 and TNF-α are secreted through immunocompetent cells which induces tumor growth, cellular modification, and triggering of the receptors via intracellular signaling cascade like activation of transcriptional factors (NF-κB, STAT3) to aid in the persistence of tumor development [12,30,31]. The escalating effects of TGF-β in promoting cancer progression are indicated through the upregulation of EMT (epithelial mesenchymal transition) markers and breast cancer stem cells (BCSCs) proliferation [32,33]. Among various pro-inflammatory cytokines, IL-6 shows an aggressive phenotype in tumor cell proliferation, that regulates inducible formation and maintenance of BCSCs [12]. Serum IL-6 levels are significantly higher in BCa patients compared with healthy individuals and increased IL-6 levels that are correlated with poor survival in metastatic BCa [34]. Overexpression of IL-6 also stimulates EMT and increases invasiveness in BCa [13,35]. Therefore, cytokines are the prime regulatory factors in maintaining functional phenotype of immune cells within TME to sustain the overall patients' survival and disease progression. Thus, underlying mechanism for drug non-responsiveness of luminal A BCa on immune landscape has not been investigated yet, particularly the role of cytokines in regulating immune cells are still unclear.

Our study showed that anti-tumorigenic response was hampered in non-responder luminal A BCa, and also T cell activity differed between responders and non-responders. In comparison with responders, the non-responders showed a lower CD8$^+$ T cells infiltration, CD8/CD4 T cell and CD8/Treg ratio in TME. Microenvironment of non-responder tumor was enriched with immunosuppressive FOXP3$^+$ Tregs, also filled with increased percentage of tumor-infiltrated CD4$^+$ and CD8$^+$ T cells which highly expressed cytokines i.e., IL-6, IL-10, and TGF-β. Conversely, TME of responder group was rich with pro-inflammatory CD8$^+$ T cells and CD4$^+$ Tconv cells with higher expression of IFN-γ and IL-12. The expression of IL-10 and TGF-β was also upregulated in Tregs of non-responders. Thereby, higher infiltration of immunosuppressive T cell subsets in TME was positively correlated with non-responsiveness of luminal A BCa.

TAMs and T cells crosstalk plays a prime role in regulating TME. T cells including both Th1 and Th2 regulate the polarization of TAMs and likewise, macrophage subtypes also activate multiple T cell phenotype via antigen presentation [36]. Moreover, TAMs facilitate various tumor progressive pathways i.e., neoplastic transformation, tumor immune evasion, and the subsequent metastatic cascades. TAMs promote tumor cells as well as BCSCs survival by establishing inflammatory niche via secretion of cytokines such as IL-10, TGF-β, TNF-α, and IL-6 in various cancers including BCa [37,38]. TAMs that reside in the TME have integral functional roles in directing environmental cues for supporting angiogenesis, tumor cell migration, as well as invasion followed by distant metastasis including lung and bone, which are common sites of metastasis for BCa [39]. This study revealed non-responders TME was enriched with CD206$^+$ TAMs and showed an elevated expression of IL-6 and TGF-β on both M1 and TAMs, contrastingly the percentage of CD206$^+$IL-12$^+$, CD68$^+$IL-12$^+$, CD206$^+$IFN-γ$^+$, and CD68$^+$IFN-γ$^+$ macrophages significantly decreased. Moreover,

correlation analysis showed a positive correlation of IL-6 expression with $CD206^+ARG\text{-}1^+$ TAMs and $FOXP3^+$ Tregs in non-responders. These findings indicated that elevated levels of IL-6 induced $CD206^+$ TAMs polarization in the TME of luminal A BCa. The higher accumulation of $CD206^+ARG\text{-}1^+$ TAMs promoted the infiltration of $FOXP3^+$ Tregs in the TME and exerted an immunosuppressive microenvironment, impairing the drug effectiveness in luminal A BCa. It was noted that IL-6 also induced $CD206^+ARG\text{-}1^+$ TAMs along with enhanced secretion of IL-6, IL10 and TGF-β in the microenvironment. Interestingly, the expression of TGF-β was increased in $FOXP3^+$ Tregs in presence of conditioned media. In a nutshell, a surge was observed in $CD206^+ARG\text{-}1^+$ TAMs, $CD4^+$ $FOXP3^+$ Tregs population with diminishing level of $CD4^+$ Tconv cells, $CD8^+$ T cells, and M1 macrophages generating an immune-suppressive alcove in non-responder luminal A BCa. The elevation of IL-6 influenced an immune-suppressive environment by enhancing $CD206^+ARG\text{-}1^+$ TAMs polarization and TAM-mediated infiltration of $FOXP3^+$ Tregs, potentially impairing drug sensitivity and reduced responsiveness in luminal a BCa. Thereby, these findings pave a path towards the development of IL-6 antagonists as advanced therapeutic approaches in drug responsiveness. Thus, this may unleash a potential way for inducing drug sensitivity and developing anti-tumor therapy in non-responder luminal A BCa.

Conclusion

Our data showed significant differences in functional activity of $CD4^+$ and $CD8^+$ T cells and macrophage subtypes in the TME of responder versus non-responder luminal A BCa. Elevated level of IL-6 induced an immune-suppressive microenvironment by promoting $CD206^+ARG\text{-}1^+$ TAMs polarization and TAM-mediated $FOXP3^+$ Tregs recruitment in luminal A BCa. These findings indicated that inhibition of IL-6 might be a novel target for Chemo non-responder luminal A BCa.

Acknowledgement

The authors are grateful to the Director, Chittaranjan National Cancer Institute, Kolkata, India for providing all financial and infrastructural facilities. The authors are indebted to the Council of Scientific and Industrial Research, (09/030(0088)/2020-EMR-I) New Delhi, and the University Grants Commission for granting fellowship. The authors are thankful to the Ministry of Health and Family Welfare, Govt. of India, and Anusandhan National Research Foundation (formerly known as SERB), Core Research Grant. The authors are thankful to Mrs Shalini Upadhyay and Mr Rupankar Ghosh, Technical assistant, Central Research Instrument Facility, for the acquisition of the flow cytometry sample. We thank all the patients and healthy volunteers for participating in this study.

Author contributions

Conceptualization and designing: NC and AD, Methodology and experiments: AD, SR, AB, NC, Writing: AD and NC, Tables and figures: AD and NC; Clinicians: NA; Review, guidance, and editing: NC; Supervision and guidance: NC.

Peer review

The peer review history for this article is available at https://www.webofscience.com/api/gateway/wos/peer-review/10.1002/1873-3468.70000.

Data accessibility

Data available on request from the authors.

References

1 Ferlay J, Rebecca ME and Mph LS (2024) Global cancer statistics 2022: globocan estimates of incidence and mortality worldwide for 36 cancers in 185 countries. *CA Cancer J Clin* **74**, 1–35.
2 Kulkarni A, Stroup AM, Paddock LE, Hill SM, Plascak JJ and Llanos AAM (2019) Breast cancer incidence and mortality by molecular subtype: statewide age and racial/ethnic disparities in New Jersey. *Cancer Health Disparities* **3**, e1–e17.
3 Desai SB, Moonim MT, Gill AK, Punia RS, Naresh KN and Chinoy RF (2000) Hormone receptor status of breast cancer in India: a study of 798 tumours. *Breast* **9**, 267–270.
4 Chatterjee K, Bhaumik G and Chattopadhyay B (2018) Estrogen receptor and progesterone receptor status of breast cancer patients of eastern India: a multi-institutional study. *South Asian J Cancer* **7**, 171–174.
5 Peng JH, Zhang X, Song JL, Ran L, Luo R, Li HY and Wang YH (2019) Neoadjuvant chemotherapy reduces the expression rates of ER, PR, HER2, Ki67, and P53 of invasive ductal carcinoma. *Medicine (Baltimore)* **98**, 1–8.
6 Segovia-Mendoza M and Morales-Montor J (2019) Immune tumor microenvironment in breast cancer and

the participation of estrogens and its receptors into cancer physiopathology. *Front Immunol* **10**, 1–16.
7 Salemme V, Centonze G, Cavallo F, Defilippi P and Conti L (2021) The crosstalk between tumor cells and the immune microenvironment in breast cancer: implications for immunotherapy. *Front Oncol* **11**, 1–20.
8 Clark NM, Martinez LM, Murdock S, James T, Amy L, Effi C, Dozmorov MG and Bos PD (2020) Regulatory T cells support breast cancer progression by opposing IFN-γ-dependent functional reprogramming of myeloid cells. *Cell Rep* **33**, 108482.
9 Williams CB, Yeh ES and Soloff AC (2016) Tumor-associated macrophages: unwitting accomplices in breast cancer malignancy. *NPJ Breast Cancer* **2**, 15025.
10 Grivennikov SI, Greten FR and Karin M (2011) Immunity, inflammation, and cancer. *Cell* **140**, 883–899.
11 Esquivel-Velázquez M, Ostoa-Saloma P, Palacios-Arreola MI, Nava-Castro KE, Castro JI and Morales-Montor J (2015) The role of cytokines in breast cancer development and progression. *J Interf Cytokine Res* **35**, 1–16.
12 Korkaya H, Kim G, Davis A, Malik F, Henry NL, Quraishi AA, Tawakkol N, Angelo RD, Chung S, Luther T *et al.* (2012) Activation of an IL-6 inflammatory loop mediates trastuzumab resistance in HER2 overexpressing breast cancers by expanding the cancer stem cell population. *Mol Cell* **47**, 570–584.
13 Chen J, Wei Y, Yang W, Huang Q, Chen Y, Zeng K and Chen J (2022) IL-6: the link between inflammation, immunity and breast cancer. *Front Oncol* **12**, 1–11.
14 Jarnicki AG, Lysaght J, Todryk S and Mills KHG (2020) Suppression of antitumor immunity by IL-10 and TGF-β-producing T cells infiltrating the growing tumor: influence of tumor environment on the induction of $CD4^+$ and $CD8^+$ regulatory T cells. *J Immunol* **177**, 896–904.
15 Taylor A, Verhagen J, Blaser K, Akdis M and Akdis CA (2006) Mechanisms of immune suppression by interleukin-10 and transforming growth factor-β: the role of T regulatory cells. *Immunology* **117**, 433–442.
16 Labani-Motlagh A, Ashja-Mahdavi M and Loskog A (2020) The tumor microenvironment: a milieu hindering and obstructing antitumor immune responses. *Front Immunol* **11**, 1–22.
17 Cohen EN, Gao H, Anfossi S, Mego M, Reddy NG, Debeb B, Giordano A, Tin S, Wu Q, Garza RJ *et al.* (2015) Inflammation mediated metastasis: immune induced epithelial-to-mesenchymal transition in inflammatory breast cancer cells. *PLoS One* **10**, 1–18.
18 McGeachy MJ, Bak-Jensen KS, Chen Y, Tato CM, Blumenschein W, McClanahan T and Cua DJ (2007) TGF-β and IL-6 drive the production of IL-17 and IL-10 by T cells and restrain TH-17 cell-mediated pathology. *Nat Immunol* **8**, 1390–1397.
19 Llanes-Fernández L, Álvarez-Goyanes RI, Arango-Prado M d C, Alcocer-González JM, Mojarrieta JC, Pérez XE, López MO, Odio SF, Camacho-Rodríguez R, Guerra-Yi ME *et al.* (2006) Relationship between IL-10 and tumor markers in breast cancer patients. *Breast* **15**, 482–489.
20 Watkins SK, Egilmez NK, Suttles J and Stout RD (2013) Il-12 rapidly alters the functional profile of tumor-associated and tumor-infiltrating macrophages *in vitro* and *in vivo*. *J Immunol* **178**, 1357–1362.
21 Nguyen KG, Vrabel MR, Mantooth SM, Hopkins JJ, Wagner ES, Gabaldon TA and Zaharoff DA (2020) Localized interleukin-12 for cancer immunotherapy. *Front Immunol* **11**, 1–36.
22 Zhao J, Zhao J and Perlman S (2012) Differential effects of IL-12 on Tregs and non-Treg T cells: roles of IFN-γ, IL-2 and IL-2R. *PLoS One* **7**, e46241.
23 Jorgovanovic D, Song M, Wang L and Zhang Y (2020) Roles of IFN-γ in tumor progression and regression: a review. *Biomark Res* **8**, 1–16.
24 Kundu M, Roy A and Pahan K (2017) Selective neutralization of IL-12 p40 monomer induces death in prostate cancer cells via IL-12-IFN-γ. *Proc Natl Acad Sci USA* **114**, 11482–11487.
25 Roy S, Das A, Vernekar M, Mandal S and Chatterjee N (2022) Understanding the correlation between metabolic regulator SIRT1 and exosomes with CA-125 in ovarian cancer: a clinicopathological study. *Biomed Res Int* **2022**, 5346091.
26 Salgado R, Denkert C, Demaria S, Sirtaine N, Klauschen F, Pruneri G, Wienert S, Van den Eynden G, Baehner FL, Penault-Llorca F *et al.* (2015) The evaluation of tumor-infiltrating lymphocytes (TILs) in breast cancer: recommendations by an International TILs Working Group 2014. *Ann Oncol* **26**, 259–271.
27 Heiduk M, Plesca I, Glück J, Müller L, Digomann D, Reiche C, von Renesse J, Decker R, Kahlert C, Sommer U *et al.* (2022) Neoadjuvant chemotherapy drives intratumoral T cells toward a proinflammatory profile in pancreatic cancer. *JCI Insight* **7**, e152761.
28 Chatterjee N, Das S, Bose D, Banerjee S, Jha T and Saha KD (2014) Leishmanial lipid suppresses the bacterial endotoxin-induced inflammatory response with attenuation of tissue injury in sepsis. *J Leukoc Biol* **96**, 325–336.
29 Zhao H, Wu L, Yan G, Chen Y, Zhou M, Wu Y and Li Y (2021) Inflammation and tumor progression: signaling pathways and targeted intervention. *Signal Transduct Target Ther* **6**, 263.
30 Batlle E and Massagué J (2019) Transforming growth factor-β signaling in immunity and cancer. *Immunity* **50**, 924–940.
31 Mannino MH, Zhu Z, Xiao H, Bai Q, Wakefield MR and Fang Y (2015) The paradoxical role of IL-10 in immunity and cancer. *Cancer Lett* **367**, 103–107.

32 Woosley AN, Dalton AC, Hussey GS, Howley BV, Mohanty BK, Grelet S, Dincman T, Bloos S, Olsen SK and Howe PH (2019) TGFβ promotes breast cancer stem cell self-renewal through an ILEI/LIFR signaling axis. *Oncogene* **38**, 3794–3811.
33 Pang MF, Georgoudaki AM, Lambut L, Johansson J, Tabor V, Hagikura K, Jin Y, Jansson M, Alexander JS, Nelson CM *et al*. (2016) TGF-β1-induced EMT promotes targeted migration of breast cancer cells through the lymphatic system by the activation of CCR7/CCL21-mediated chemotaxis. *Oncogene* **35**, 748–760.
34 Bachelot T, Ray-Coquard I, Menetrier-Caux C, Rastkha M, Duc A and Blay JY (2003) Prognostic value of serum levels of interleukin 6 and of serum and plasma levels of vascular endothelial growth factor in hormone-refractory metastatic breast cancer patients. *Br J Cancer* **88**, 1721–1726.
35 Sullivan NJ, Sasser AK, Axel AE, Vesuna F, Raman V, Ramirez N, Oberyszyn TM and Hall BM (2009) Interleukin-6 induces an epithelial-mesenchymal transition phenotype in human breast cancer cells. *Oncogene* **28**, 2940–2947.
36 Li M, Jiang P, Wei S, Wang J and Li C (2023) The role of macrophages-mediated communications among cell compositions of tumor microenvironment in cancer progression. *Front Immunol* **14**, 1–23.
37 Zhang F, Li P, Liu S, Yang M, Zeng S, Deng J, Chen D, Yi Y and Liu H (2021) β-Catenin-CCL2 feedback loop mediates crosstalk between cancer cells and macrophages that regulates breast cancer stem cells. *Oncogene* **40**, 5854–5865.
38 Bose D, Banerjee S, Chatterjee N, Das S, Saha M and Das Saha K (2019) Inhibition of TGF-β induced lipid droplets switches M2 macrophages to M1 phenotype. *Toxicol In Vitro* **58**, 207–214.
39 Huang X, Cao J and Zu X (2022) Tumor-associated macrophages: an important player in breast cancer progression. *Thorac Cancer* **13**, 269–276.

Supporting information

Additional supporting information may be found online in the Supporting Information section at the end of the article.

Fig. S1. Dot Plot of flow cytometry analysis of TME of CD4+ and CD8+ T cells in responder and non-responder luminal A BCa.

Fig. S2. Dot Plot of flow cytometry analysis of PBMC of CD4+ and CD8+ T cells in responder and non-responder luminal A BCa.

Fig. S3. Dot Plot of flow cytometry analysis of Treg cells in responder and non-responder luminal A BCa.

Fig. S4. Dot Plot of flow cytometry analysis of macrophage populations in both TME and PBMC of luminal A BCa.

Table S1. Table of patient frequency and clinicopathological parameters.

Table S2. Reagent list.

Graphical Abstract

The contents of this page will be used as part of the graphical abstract of html only. It will not be published as part of main article.

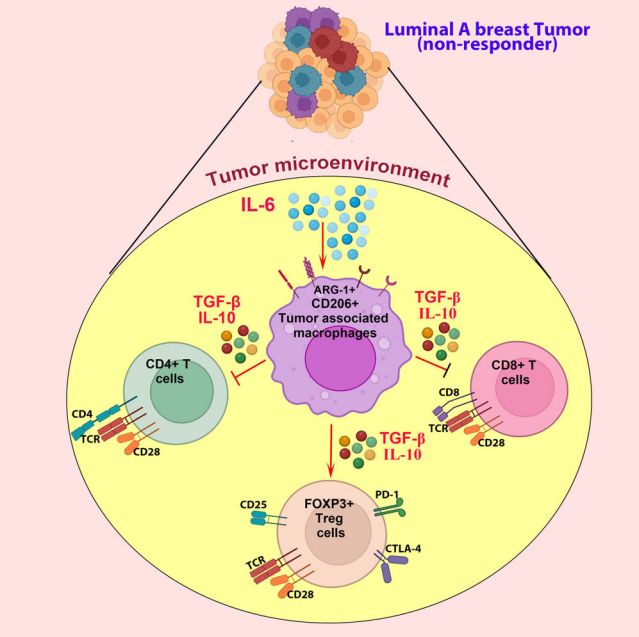

Non-responder luminal A breast cancer exhibits an immunosuppressive tumor microenvironment (TME). In this study, we show that elevated expression of IL-6 promotes infiltration of $CD206^+$ tumor-associated macrophages (TAMs), which secrete TGF-β and IL-10 and induce $FOXP3^+$ Treg cell proliferation and infiltration in the TME. Moreover, cytokines from $CD206^+$ TAMs suppress $CD4^+$ and $CD8^+$ T cell activity and foster an immunosuppressive TME in non-responder luminal A breast cancer.

NJC

ROYAL SOCIETY OF CHEMISTRY

PAPER

Cite this: *New J. Chem.*, 2024, **48**, 16189

Structure-based design to explore the anticancer efficacy of organometallic Pt(II)- and Au(III)-N-heterocyclic carbene (NHC) complexes†

Pooja Das,[a] Sraddhya Roy,[b] Chaitali Das,[a] Raju Biswas,[c] Nabanita Chaterjee*[b] and Joydev Dinda *[a]

Received 22nd June 2024,
Accepted 19th August 2024

DOI: 10.1039/d4nj02853h

rsc.li/njc

Cancer is one of the leading public health concerns globally, and therefore better drugs are required for treatment. Several strategies have been taken to improve the success of drug discovery. Our strategy is the exploration of the organometallic complexes of the platinum group metals as potential anticancer drugs. Organometallic complexes bearing N-heterocyclic carbene (NHC) ligands are getting attention for therapeutic purposes. The synthesis, structure, and anticancer activities of platinum(II)- and gold(III)-N-heterocyclic carbene complexes supported by pro-ligand 1-methyl-2-(pyridylmethyl)imidazo[1,5-a]-pyridin-4-ylium hexafluorophosphate, (**1**.HPF_6) are described. Two novel isoelectronic and isostructural complexes, *viz.* [Pt(**1**)Cl_2] (**2**) and [Au(**1**)Cl_2][$AuCl_4$] (**3**), have been synthesized and characterized using a series of spectroscopic techniques. Finally, the square planar geometry of **3** was established by single crystal X-ray diffraction studies. Interestingly, complex **3** possesses Cl–Cl interactions and this is the first organogold complex to bear the same. Molecular docking analysis revealed the highest free binding energy for complex **3** with human-DNA topoisomerase. Finally, *in vitro* anticancer studies on breast cancer cell line, MDA-MB231, revealed Au(III)–NHC complex **3** is more potent than Pt(II)–NHC complex **2**.

Introduction

Cancer is universally considered to be one of the main public health problems and it is one of the major causes of deaths in most countries.[1] The International Agency for Research on Cancer (IARC) in its survey report in 2020 state that about 19.9 million new cases of cancer were diagnosed worldwide resulting in 10 million deaths.[2] Among the available treatments for cancer, like surgery, radiotherapy, and chemotherapy,[3] chemotherapy is the most popular for cancer treatment. In the context of chemotherapy, among the many challenges that modern medicinal chemistry faces today, one of them is the development of effective anticancer drugs. Therefore, as the field of chemistry progresses the search for and design of novel compounds exhibiting anticancer activity are increasing and remain one of the main goals of chemical research.[4–9] The uses of metal complexes in medicine have gained great momentum after the discovery of the cytotoxic effect of cisplatin by Rosenberg in 1963.[10] Because of the few limitations of cisplatin and other platinum(II) drugs like carboplatin, oxaloplatin, nedaplatin, lobaplatin, and heptaplatin; other metal-based drugs, *e.g.* gold(I)-based drugs like auranofin, myocrisin and solganol; ruthenium(II)-based drugs like NAMI and KP1019 and copper(II)-based drugs like the casiopeinas are either currently in use or undergoing clinical trials.[11–16] One of the challenges that a medical practitioner faces is the ineffectiveness of drugs due to drug resistance.

Therefore, the development of new drugs with different mechanisms of action are essential to fight against resistant cancer cells. Multitarget therapy has been considered an effective strategy[17] to overcome resistance and metal complexes,[18–21] mostly those with N-heterocyclic carbene (NHC) ligands, have received great consideration.[22–28] N-Heterocyclic carbenes (NHCs) are considered cutting edge ligands in chemistry[29–31] which are highly versatile in nature and their tunable nature facilitates the balancing of their hydrophilic-lipophilic properties and renders them very stable complexes. The versatility of NHCs comes from their ability to (i) bind with most of metals of the periodic table; (ii) stabilize higher and lower oxidation

[a] *Department of Chemistry, Utkal University, Bhubaneswar 751004, Odisha, India. E-mail: joydevdinda@gmail.com*
[b] *Department of Receptor Biology and Tumor Metastasis, Chittaranjan National Cancer Institute, Kolkata 700026, West Bengal, India*
[c] *Department of Chemistry, CSIR – Indian Institute of Chemical Biology, Kolkata 700032, West Bengal, India*

† Electronic supplementary information (ESI) available. CCDC 2218852. For ESI and crystallographic data in CIF or other electronic format see DOI: https://doi.org/10.1039/d4nj02853h

states of metals (*e.g.* Au(I/III), Pd(O/I/II/III), Fe(O/II/III) *etc*); (iii) form M–NHC complexes that are stable in air, moisture; and (iv) form M–NHC complexes that are thermally stable. Moreover, most NHC backbones are either imidazoles or benzimidazoles which are biologically ubiquitous molecules; therefore, one can argue the biological importance of imidazolidenes. It is believed that synergistic effects that involve both the metal and the NHC ligand will play a crucial role in its cytotoxicity.[32,33]

The slow release of a metal is essential for it to perform as a metal-based drug, and the metal–ligand bond should be of moderate strength, *i.e.* neither very strong nor very weak, a criterion that is fulfilled by M–NHC complexes. Organometallic pharmaceutical research for cancer treatments has been primarily focused on coinage and platinum group-NHC complexes. In the literature, particularly, Ag(I)-, Au(I/III)-, Pd(II)-, Pt(II)-, Ru(II)-, and Ir(I/III)–NHC *etc.*, have shown very promising results in anticancer studies.[34] Presently, more focus is being placed on platinum- and gold-based NHC complexes. Recently, the radio-sensitizing behaviour of bimetallic (NHC)–amine–Pt(II) complexes against cancer cells through DNA damage is reported.[35] Similar types of amine–NHC–Pt(II) complexes which bind with double-stranded DNA[36] are effective against cancer cells, as reported by Marineeti. Very recently caffeine-based Pt(II)–NHC complexes have been used as multimodal anticancer agents targeting the mitochondria and inhibiting lipid, carbohydrate and nucleotide metabolic pathways.[37]

Indeed, gold complexes are considered as possible alternatives to platinum-based drugs (*e.g.* cisplatin and analogues) due to their more selective mode of action.[38] Taking the lessons of medicinal chemistry based on gold from ancient times,[39] researchers started to discover the utility of gold(I) drugs for cancer treatment. As a result, in recent times, the gold(I) drug auranofin, a successful rheumatoid arthritis treatment, has been clinically trialled for cancer treatment. Advancements in gold(I) drugs have been made by replacing a triphenylphosphine group with an electronically equivalent NHC ligand and these complexes have been successfully applied for cancer treatment. The Au(I)–NHC complexes[40] reported by Han are very potent against breast cancer cells. Panda and Ghosh also successfully synthesized an Au(I)–NHC complex that exhibited excellent efficiency against HeLa cell proliferation.[41] Filipovska *et al.* established a new approach to mitochondria-targeted antitumor agents using Au(I)-N-heterocyclic carbene compounds, where selective mitochondria targeting and selective thioredoxin reductase inhibition properties were achieved using a single molecular species.[42] Recently Ulijn reported the enhanced activity of Au(I)–NHC *via* encapsulation into a degradable peptide nanofilament.[43] A structure–activity relationship (SAR) study revealed that the inhibitory efficacy of Au(I)–NHC complexes may be enhanced if they have two chloride ligands and an NHC ligand attached rather than two NHCs.[44]

In the literature, the anticancer activities of many Au(I)–NHCs are reported, but the examples of Au(III)–NHCs are scarcer, although it is assumed that Au(III)–NHCs will still be useful compounds. As Au(III) and Pt(II) mostly exist as square planar complexes and as Au(III) is isoelectronic with Pt(II), one may expect Au(III) complexes to exhibit similar activity to Pt(II) complexes (Chart 1).[45] The promising anticancer activity of cycloaurated Au(III)-complexes were documented by Casini,[46a] and later on Bochmann demonstrated the anticancer activities of similar cycloaurated Au(III)–carbene complexes.[46c] Recently, Munro[46d] has reported anticancer activities of both Au(I)- and Au(III)–NHC complexes, which target specific biological macromolecules like DNA and proteins. Our group also reported a number of Au(III)–NHC[4b,26–28] complexes synthesized from Au(I)–NHC by a disproportionation pathway. It is observed that Au(I)–NHC complexes are more potent than Au(III)–NHCs and this may be due to the reduction of the Au(III)–NHC complexes by thiol proteins which reduces the activity.[47a] There are several *in vitro* studies that provide direct evidence of Au(III) to Au(I) reduction to achieve anticancer activity; Salassa has shown mechanistically that, during *in vivo* studies, a fraction of the Au(III)–NHC prodrug remains and that which is not immediately reduced after administration is able to reach the major organs before metabolic activation.[47b] As described earlier, Au–NHCs target the mitochondria and the driving force for the permeability of cationic Au(III) compounds in the mitochondria is due to the mitochondrial membrane potential, which generally is negative in some carcinoma cells as compared to healthy cells.[48]

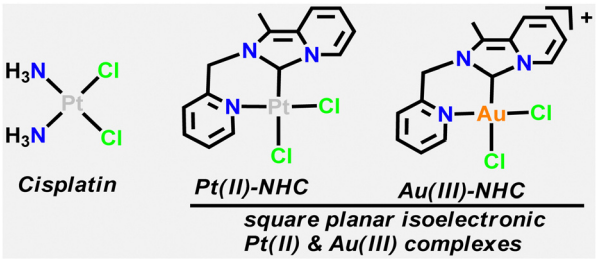

Chart 1 Cisplatin and other relevant Pt(II) and Au(III)–NHC complexes.

Breast cancer is the most common cancer among women and one of the most important causes of mortality in this group due to its increasing incidence across the globe. In 2008, 8 million deaths were recorded as a result of malignant diseases, and this figure is estimated to reach 11 million by 2030.[49] As per the World Health Organization, in 2020 there were 2.3 million women diagnosed with breast cancer and 685 000 died globally. As of the end of 2020, there were 7.8 million women diagnosed with breast cancer in the past 5 years, making it the world's most prevalent cancer. Breast cancer may occur at any age after puberty but with a higher incidence rate in the later ages. Breast cancer is a multifactorial disease,[50] where several external and internal stimuli come into participation for the onset and progression of the disease. The incidence, mortality and survival of patients differ considerably depending on lifestyle, environment, genetic factors and population structure.[51] Nearly 12% of breast cancer patients who are diagnosed with the disease go on to develop metastatic disease. There is no permanent cure for metastatic breast cancer yet, and it has a poor prognosis (5 year survival is 26%).

However, there are many treatments that can improve and lengthen the life expectancy of patients who have metastatic breast cancer.[52]

Inspired by the recent findings on the anticancer activities of Pt(II) and Au(III)–NHC complexes, we have synthesized and fully characterized Pt(II) and Au(III)–NHC complexes of picolyl functionalized C, N-donor ligands. The bidentate NHC moiety allows the synthesis of stable metallacyclic complexes and more lipophilic scaffolds may show promising anticancer activity.[53–56]

Results and discussion

Chemistry

Using previously reported procedures, the formylative cyclization reaction of the corresponding Schiff base 2-pyridylmethyl *N*-(2-acetylpyridyl)methylamine with paraformaldehyde, triethylorthoformate, and 4N HCl gives the imidazolium salt, 1-methyl-2-(pyridylmethyl)imidazo[1,5-*a*]pyridin-4-ylium hexafluorophosphate (**1**.HPF_6).[57] Using a silver(I) carbene, transition metal M–NHC complexes can be obtained readily. A silver(I) carbene complex is obtained by the reaction of **1**.HPF_6 with Ag_2O in acetonitrile at room temperature. As depicted in Scheme 1, the Pt(**1**)Cl_2 complex **2** was obtained in 73% yield from the pre-prepared Ag(**1**)$_2PF_6$ after treatment with a stoichiometric amount of K_2PtCl_4 in acetonitrile. Similarly, complex **3**, [Au(**1**)Cl_2][$AuCl_4$], was obtained in 69% yield by the reaction of Ag(**1**)$_2PF_6$ and a stoichiometric amount of $KAuCl_4$ after stirring for 2 hours in acetonitrile.

^{1}H and ^{13}C NMR as well as elemental analysis were used to characterize complexes **2** and **3**, and the results were in accordance with the expected formulations. As observed in the ^{1}H NMR spectra of complexes **2** and **3**, the imidazolium N*CH*N signal associated with **1**.HPF_6 (δ 9.77 ppm in DMSO-d_6)[31] disappeared and the downfield shift of the aromatic protons relative to **1**.HPF_6 confirms the successful formation of the complexes (as shown in ESI,† Fig. S1–S4). Compared to complex **3**, complex **2** exhibits a larger downfield shift of the resonances of most of its protons and carbon atoms. This may be because complex **3** has a less acidic Au(III) centre than the isoelectronic Pt(II) ion in complex **2**. Further evidence of the ligation of $C_{carbene}$ to Pt(II)/Au(III) arises from the downfield shifts of the $C_{carbene}$ (NCN) signals which were found at 163.43 and 161.35 ppm, respectively, for complexes **2** and **3** [free ligand 153.19 ppm]. The aryl proton signal α to the pyridine-N was shifted downfield to 8.76 and 8.68 ppm in the case of complexes **2** and **3**, respectively [free ligand 8.58 ppm].

The HR mass spectral analysis of complex **2** showed that the maximum intensity peak found at 453.0445 relates to $[Pt(NHC)(Cl)]^{1+}$; while the peak at (*m*/*z*) 494.0711 corresponds to $[Pt(NHC)(Cl)(CH_3CN)]^{1+}$. Meanwhile, complex **3** exhibits a peak at (*m*/*z*) 490.0152 corresponding to $[Au(NHC)Cl_2]^{1+}$ (shown in ESI,† Fig. S5 and S6). As we failed to obtain a single crystal of **2**, we therefore optimized the molecule and the optimized geometry is shown in Fig. 1. The bond parameters are listed in the figure caption.

The UV-Vis absorption spectra of complexes **2** and **3** were recorded in a dry CH_3CN solution at a 50 μM concentration (as shown in Fig. S7 and with the values reported in Table T1, ESI†). The high energy absorption bands were found near 280.03 and 313.30 nm in the case of ligand **1**.HPF_6. Moderately red-shifted intense absorption bands at 335.02 and 365.63 nm in complex **2** and at 313.07 nm in complex **3** were observed and are assumed to be due to intraligand charge transfer (ILCT). Weaker absorption bands at 455.60 nm and 469.70 nm were observed in the cases of complexes **2** and **3**. Based on comparable observations in other systems and the platinum-tetra-N-heterocyclic carbene complex, we hypothesize that the low energy absorption band is due to ligand-to-metal charge transfer (LMCT).[58] Furthermore, complexes **2** and **3** exhibit high energy absorptions at approximately 267.84 nm and 278 nm, which are attributed to the intraligand π–π* transitions.

Single crystals of complex **3** suitable for X-ray diffraction were obtained from the slow diffusion of diethyl ether into a saturated acetonitrile solution of complex **3**. Molecule **3** is crystallized with monoclinic symmetry in the '*P*121/*c*1' space group. The ORTEP view of the molecular structure of **3** is shown

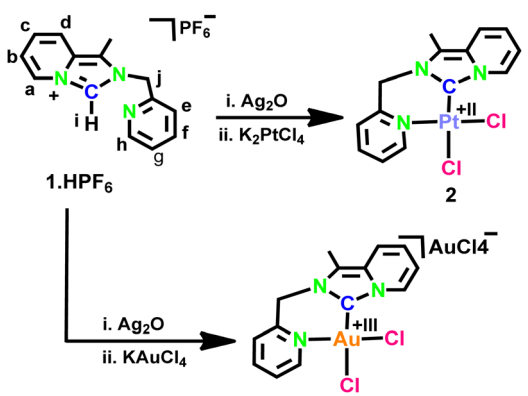

Scheme 1 Synthesis of Pt(II)- and Au(III)–NHC complexes **2** and **3**. The letters around the structure of **1**.HPF_6 refer to the NMR assignments.

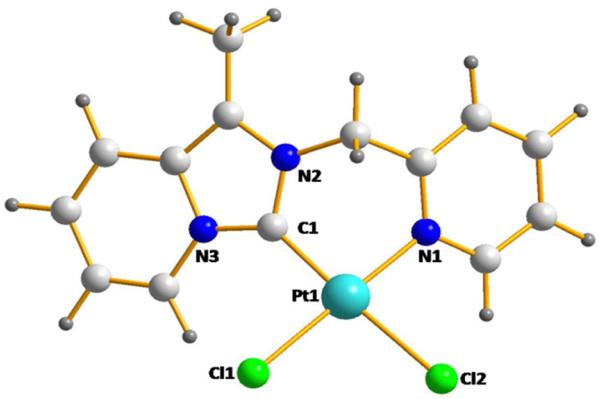

Fig. 1 Ball-stick view of the optimized geometry of **2**. Selected bond lengths (Å) and angles (°), Pt(I)–C(1) 1.968; Pt(1)–N(1) 2.043; Pt(1)–Cl(1) 2.398; Pt(1)–Cl(2) 2,450; C(1)–Pt(I)–Cl(2) 177.23; N(1)–Pt(I)–Cl(1) 178.82; C(1)–Pt(I)–Cl(1) 92.20; N(1)–Pt(I)–Cl(2) 88.65; C(1)–Pt(I)–N(1) 88.76; Cl(1)–Pt(I)–Cl(2) 90.38; N(2)–C(I)–N(3) 103.76.

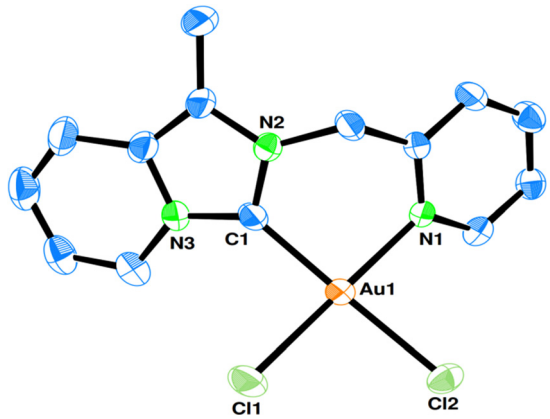

Fig. 2 ORTEP view (50% probability) of single crystal X-ray structure of **3** (the H atoms and $AuCl_4$ have been omitted for clarity).

Table 1 Selected bond lengths (Å) and angles (°) for **3**

Au(1)–C(1)	1.988(6)
Au(1)–N(1)	2.058(5)
Au(1)–Cl(1)	2.2583(16)
Au(1)–Cl(2)	2.3133(15)
C(1)–Au(1)–Cl(2)	178.43(18)
N(1)–Au(1)–Cl(1)	178.23(14)
N(1)–Au(1)–Cl(2)	90.62(13)
Cl(1)–Au(1)–Cl(2)	89.06(6)
C(1)–Au(1)–Cl(1)	92.00(17)
C(1)–Au(1)–N(1)	88.3(2)
N(2)–C(1)–N(3)	105.0(5)

in Fig. 2. Key crystallographic parameters are listed in Table T2 in the ESI† and selected bond parameters are listed in Table 1. The square planar molecular dimensions may be considered as normal, except for a few ideal bond angles at the gold atoms.

As shown in Fig. 2, the Au–$C_{carbene}$ distance *i.e.* Au(1)–C(1) = 1.988(6) Å is close to an average Au–C bond length of 2.002(12) Å, and is consistent with the values reported for other Au(III)–$C_{carbene}$ systems.[59,60] The carbene ligand and the $CAuNCl_2$ units are arranged in a non-planar fashion (dihedral angle of $CAuNCl_2$ *vs.* imidazolidene = 39.06°). A slight *trans* influence of the carbene ligand on the Au(1)–Cl(2) (2.3133(15) Å) bond is observed, making it longer than the Au(1)–Cl(1) (2.2583(16) Å) bond. The crystal packing of **3** involves short intermolecular contacts between the chlorine atoms [Cl–Cl, 3.216 Å]. Such short chlorine–chlorine contacts are a special case of 'halogen bonding'.[61] Additionally, molecule **3** possesses C–H–Cl [2.629 Å] interactions and the net effect is to form a square planar grid (Fig. 3).

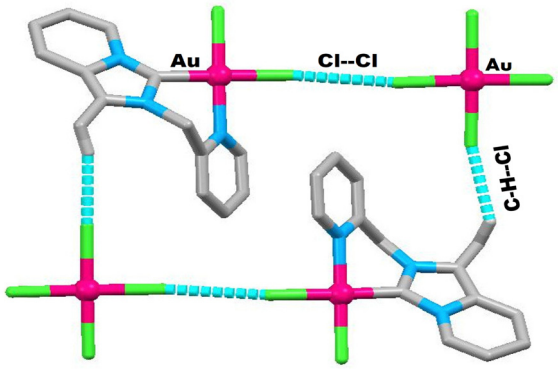

Fig. 3 Rectangular grid-like packing of **3** through Cl–Cl and C–H–Cl interactions.

Anticancer study

In this research work, we have examined the *in vitro* potency of novel compounds **2** and **3** in metastatic breast cancer cells. We have examined the EMT factors and metastatic parameters in the cancer cells after appropriate screening of the drugs. Complex **3** is very potent towards the MDA-MB-231 cell line, more so than complex **2** at a lower inhibition dose. MTT analysis of cell viability has revealed that complex **3** has a lower IC_{50} dose of 0.0084 μM than complex **2** which has an IC_{50} of 0.01613 μM (Fig. 4(A) and (B)). For cisplatin[62a] and auranofin[62b] the IC_{50} values were 25.28 and 6.00 μM against the same cell line MDA-MB-231. Therefore, the present drugs are more potent than conventional drugs cisplatin and auranofin. In both cases, the cell viability decreases with increasing concentration of the drug but the mortality rate of the cells treated with complex **3** was higher than those treated with complex **2**. The statistical difference between the two IC_{50} values of the respective compounds is shown in Fig. 4(C) and shows a significance of $P = 0.0010$.

The efficacy of complex 3 disrupts the EMT process and the stemness

Since the process of metastasis is associated with poor prognosis of the disease, we were thus inclined to check the EMT markers, namely E-cadherin (E-cad) and N-cadherin (N-cad), along with the stemness of the cancer cells. Surprisingly, we have observed that the expression of E-cad increased with the drug treatment ($P = 0.0003$) as compared to the control *i.e.* the non-treated cells (Fig. 5(A) and (B)). The drug has also shown its potency in decreasing the mesenchymal marker N-cad in comparison with the non-treated cells ($P = 0.0024$) (Fig. 5(C) and (D)). This result has provided a lead in investigating the stemness of the cancer cells and a positive result has been obtained, whereby the CD44 + CD24- co-expression in the treated cells was decreased as compared to the non-treated cells ($P = 0.0027$) (Fig. 5(E) and (F)).

The migration of the cancer cells was slowed by treatment with complex 3

On checking the migratory potential of the cancer cells by wound healing assay, we observed that the migration of the cancer cells decreased considerably in the treated cells as compared to the non-treated cells after 24 h of treatment with complex **3** (Fig. 6(A)). As shown in Fig. 6(B) and (C), respectively, the percentage of confluency in the control cells was significantly higher as compared to the treated cells ($P = 0.0083$) whereas the percentage of inhibition was higher in the treated cells as compared to the control ($P = 0.0051$).

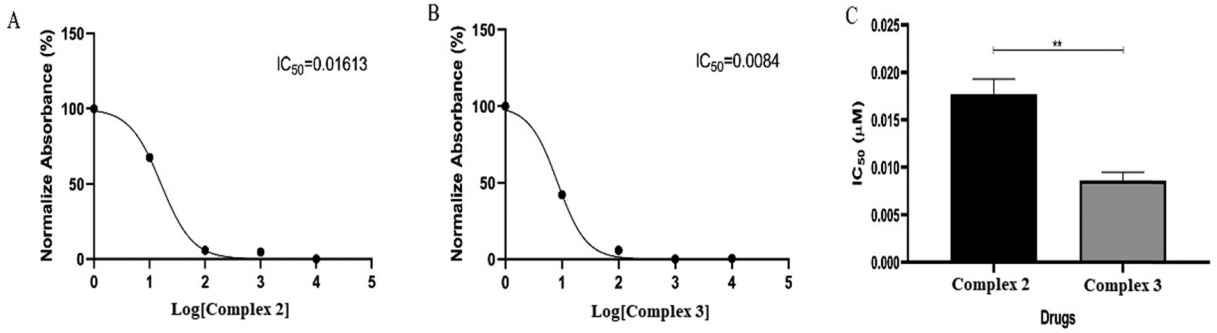

Fig. 4 MTT analysis of complexes **2** and **3** in MDA-MB231 cells: (A) and (B) IC_{50} doses of the compounds of interest. (C) Statistical analysis of the IC_{50} of the drugs by one-way ANOVA.

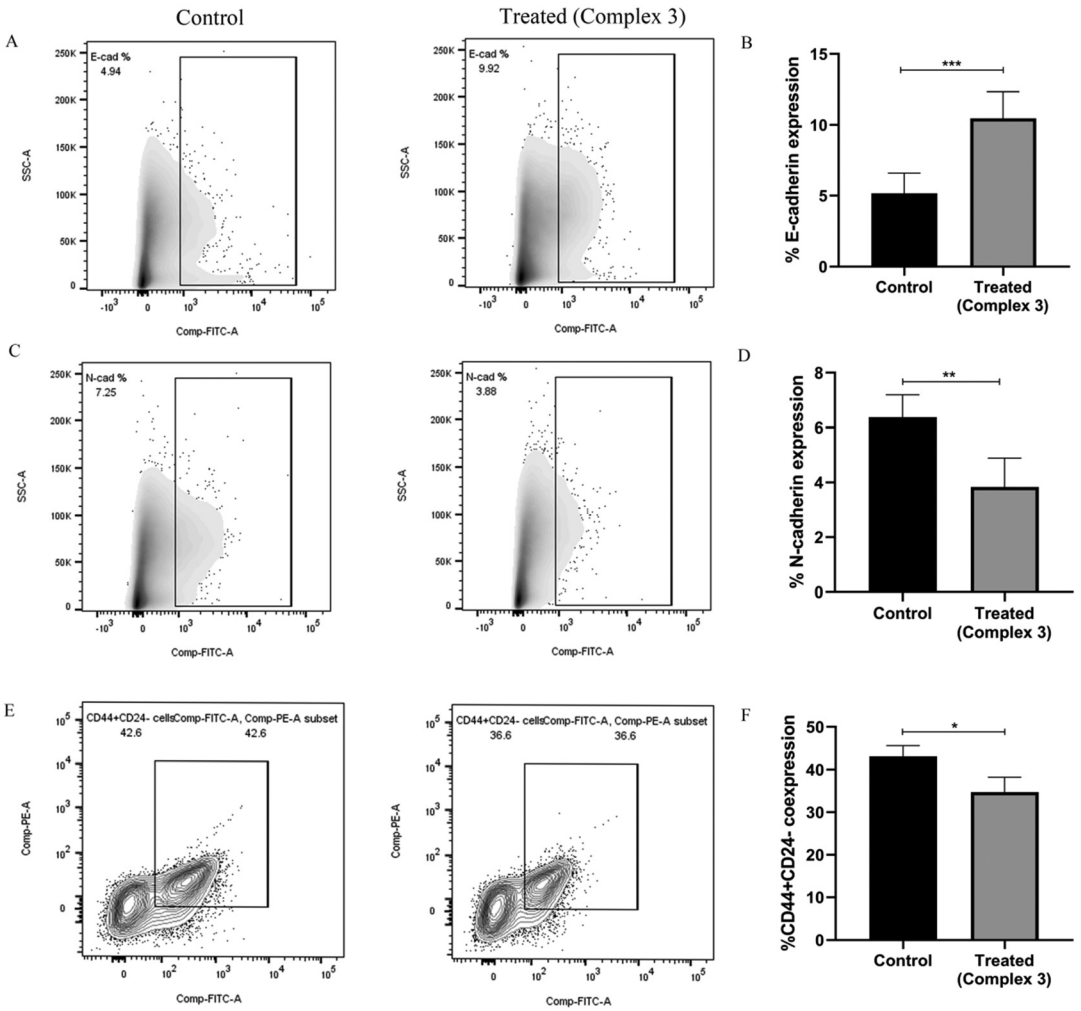

Fig. 5 Flow cytometric analysis of EMT markers: (A) estimation of the EMT marker, E-cad in control and treated MDA-MB-231 cells; (B) graphical representation of E-cad (P = 0.0003) in control and treated cells; (C) estimation of EMT marker, N-cad in control and treated MDA-MB-231 cells; (D) graphical representation of N-cad (P = 0.0024) in control and treated cells; (E) estimation of stem cells markers, CD44 + CD24-expression in control and treated MDA-MB-231 cells; and (F) graphical representation of the percentage of co-expression of CD44 + CD24-cancer cells after treatment (P = 0.0027).

The decreased migratory potential is a result of decreased expression of proliferation markers under drug treatment

Since Ki-67 and VEGF are important biomarkers and correlate with the survival of patients, we have analyzed the expression of these metastatic markers and observed that the expression of Ki-67 (Fig. 7(A) and (B)) and VEGF (Fig. 7(C) and (D)) decreased considerably under the effect of 24 h of drug treatment at significances of P = 0.0041 and P = 0.0038, respectively. Breast

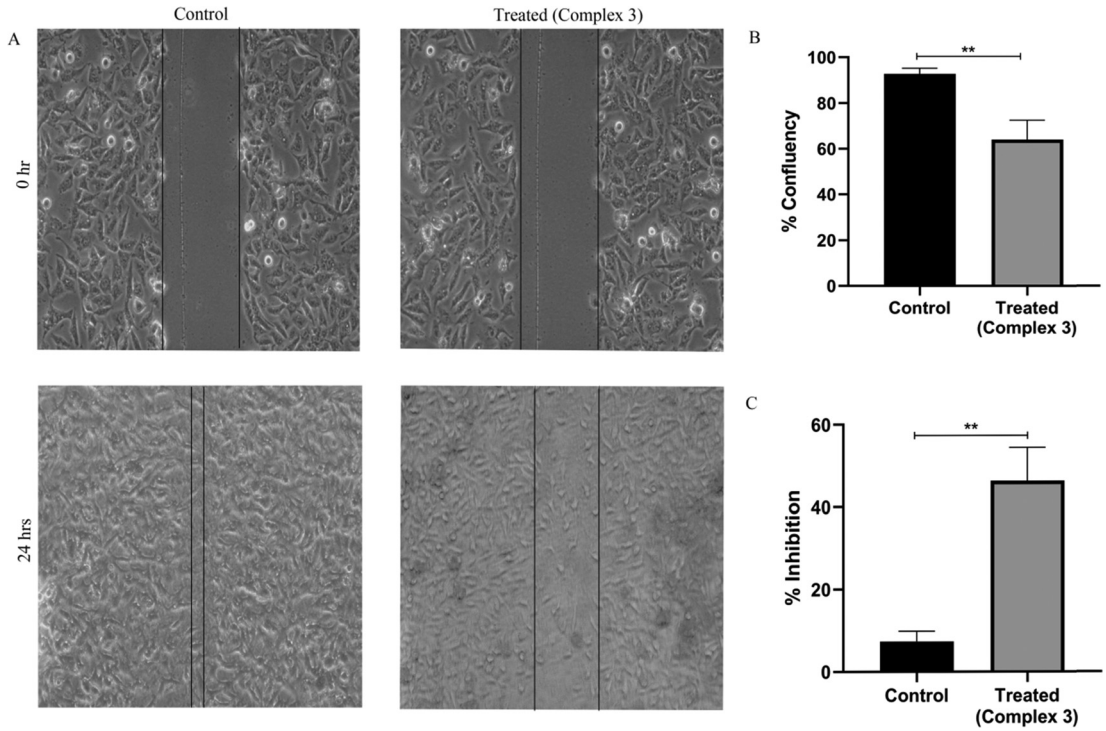

Fig. 6 Analysis of the migratory potential of MDA-MB231: (A) the migration of the cancer cells slowed after 24 h of drug treatment; (B) the percentage confluency of the cancer cells after treatment decreased significantly as compared to the control (P = 0.0083); and (C) the percentage inhibition is lower in the control cells as compared to the treated cancer cells (P = 0.0051).

cancer is characterized by a variety of tumor histologies, clinical presentations, and therapeutic responses and since the majority of breast cancer related fatalities are attributed to its metastatic form, a more comprehensive understanding of the underlying mechanisms underpinning the EMT process for breast tumors will enable the development of more effective therapeutic approaches.[52] Multiple pathways participate in the process of metastasis by regulating the EMT process, *e.g.*, TGF-β, RTK, Wnt, NF-kβ, Notch, *etc.*, which are also responsible for maintaining the balance between the self-renewal and differentiation of breast cancer stem cells.[63a] A possible mechanism of cell death is presented in Fig. 8.

Evidence suggests that EMT plays a pivotal role in fueling the migratory properties of the cancer cells thereby increasing the metastasis of the breast cancer cells by activation of GLI-mediated transcription in the neighbouring non-EMT cells.[63b] In this context, this research work studies the efficacy of the novel compound complex **3** as an anti-cancer agent and we observed that the cell viability decreased with increased concentration of the drug. This result led us to investigate the metastatic process in breast cancer cells and our results demonstrated that the epithelial marker, E-cadherin (E-cad), increased significantly under treatment and interestingly that the mesenchymal marker, N-cadherin (N-cad), decreased considerably. This result demonstrated that complex **3** has anti-metastatic properties. In parallel to this, we have also examined the co-expression of CD44 + CD24- on the cancer cells and we have observed that the stemness also decreased under drug treatment. The CD44 + CD24- subpopulation of breast cancer cells depicts the metastatic and invasive properties of the cancer cells,[64] thus the decrease in their population shows that complex **3** is capable of minimizing the upregulation of pro-invasive genes by modulating the stem cell population.

Mrouj *et al.* demonstrated that Ki-67 knockout disbalances the expression of EMT markers and suppresses the stemness of cancer cells, thus further validating our findings that complex **3** efficiently diminishes Ki-67 status, which in turn modulates the EMT markers and stemness of the breast cancer cells.[64] Further to validate the result, we aimed to study the migratory properties of the cells, and interestingly the cancer cells migrated less under the effect of the drug as compared to the non-treated cells. In addition to this, Santos *et al.* also evaluated a strong association between Ki-67 and VEGF in colorectal cancer concerning clinicopathological parameters and mortality of the patients.[65] Thus, encouraged to estimate the expression of the proliferation marker Ki-67 and metastatic marker VEGF, we surprisingly found that their expressions were also corroborated with previous results and established the anti-cancer properties of complex **3**, where the expression of Ki-67 and VEGF decreased significantly during drug treatment. Thus, the anti-cancer properties of the novel compound were established and the proliferative activity of the cancer cells can be diminished by modulating the stemness of the cancer cells which in turn modulates the EMT process in breast cancer by targeting Ki-67 and VEGF and probably by blocking the VEGFR present

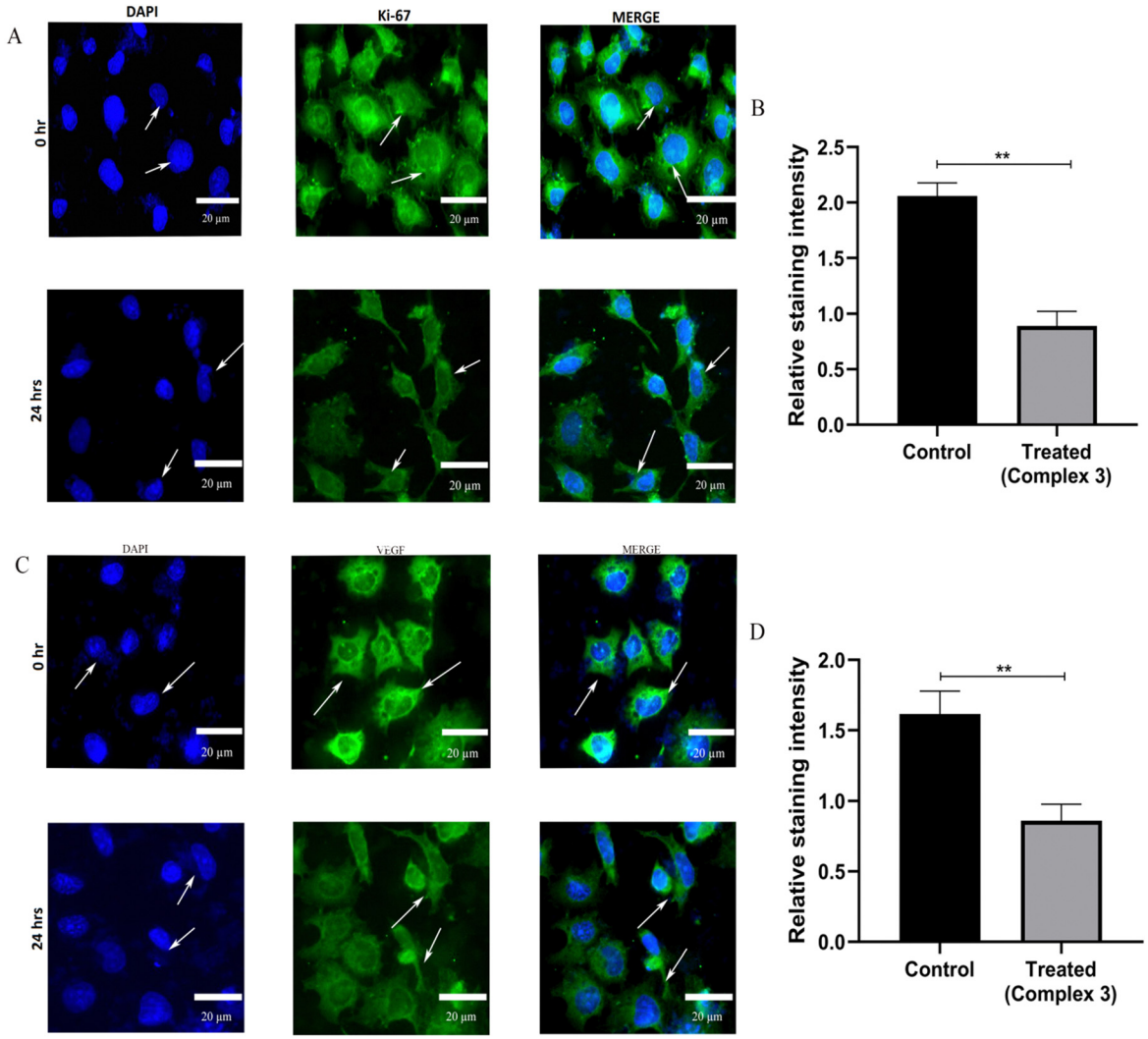

Fig. 7 Analysis of metastatic markers: (A) the expression of ki-67 is lower in the treated cells as compared to the normal cells; (B) graphical representation of the relative staining intensity of Ki-67 (P = 0.0041); (C) the expression of VEGF is lower in the treated cells as compared to the control; and (D) graphical representation of the relative staining intensity of VEGF (P = 0.0038).

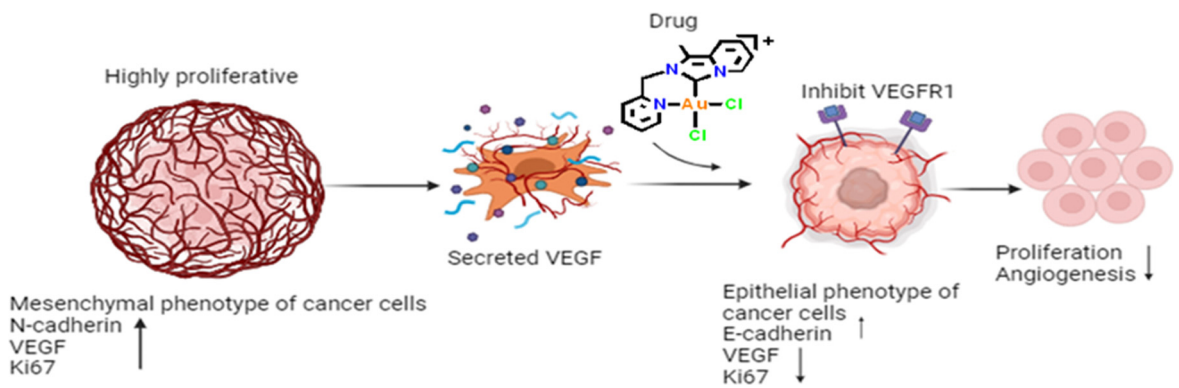

Fig. 8 Possible mechanism of the mitigation of cell proliferation and metastasis.

on the surface of the cancer cells. The blockage of VEGFR therefore mitigates the formation of new blood vessels and hinders the growth of the breast cancer cells.

Molecular docking study

Molecular docking analysis is one of the most fundamental and significant approaches to drug discovery which predicts the

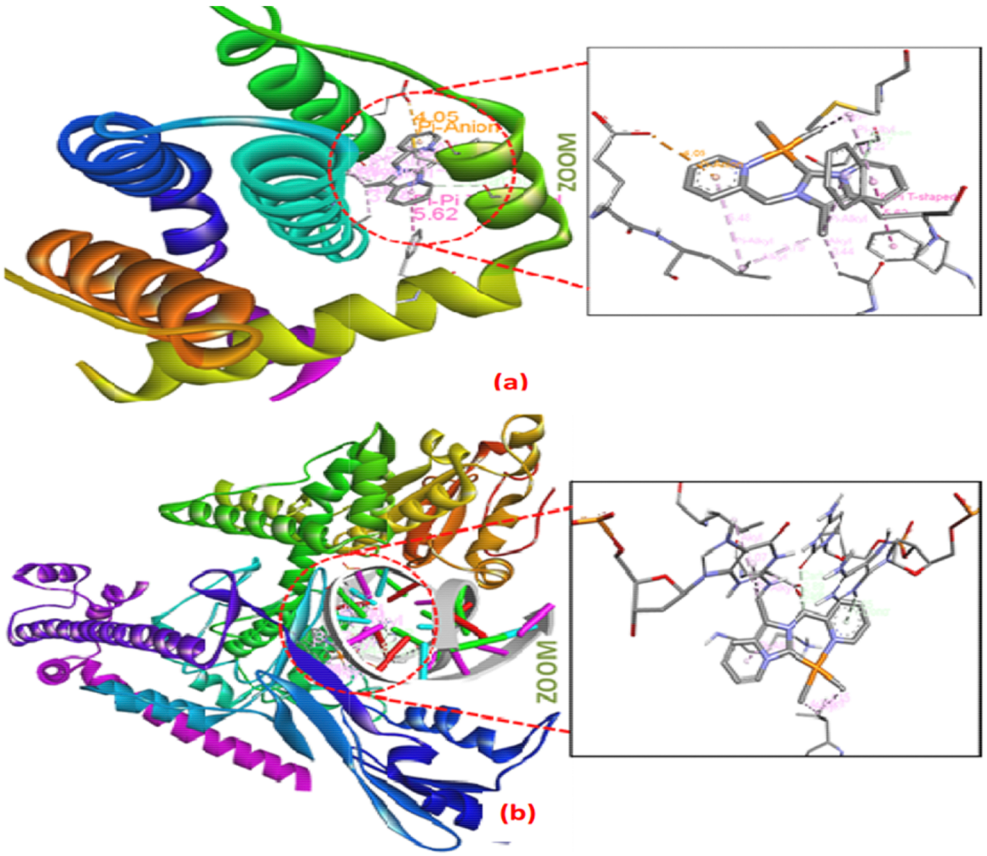

Fig. 9 Capped stick model and 2D view of the interaction mode of complex **2** with (a) BCL2 and (b) human–DNA topoisomerase.

molecular interactions that bind a protein and ligand together in the bound state. Here, the ligands in this case are complexes **2** and **3** which were found to bind at the molecular level with B-cell lymphoma 2 (BCL-2) cells as well as with human topoisomerase II (Topol II) coupled to a DNA strand, as displayed in Fig. 9 and 10. One of the most well-known cancer targets is BCL-2, which is crucial in controlling cellular apoptosis, which is managed by intricate interactions between pro- and anti-apoptotic BCL-2 family genes. Type II DNA topoisomerases are nuclear enzymes which play a crucial role in controlling the topological state of DNA and inhibiting the growth of cancer cells. When a target protein docks with a complex a more negative docking score indicates a higher binding affinity. The binding energies of complexes **2** and **3** with BCL-2 were found to be -6.24 kcal mol^{-1} and -6.48 kcal mol^{-1}, respectively, indicating that the interaction of complex **3** with BCL-2 is more efficient than that of complex **2** (as shown in Table T3, ESI†). In contrast, complex **2** exhibits a higher binding affinity (-7.45 kcal mol^{-1}) with Topol II than complex **3** (-7.27 kcal mol^{-1}). This is because complex **2** exhibits better interaction with the human topoisomerase II receptor. The alkyl/pi–alkyl interactions with A: Leu134, A: Phe150, A: Met112, and A: Ala146, the Pi–Pi T-shaped interaction with A: Phe101, and the Pi–anion with A: Glu133 were recorded in the binding of complex **2** with the BCL-2 receptor. Meanwhile, complex **3** shows an alkyl/pi–alkyl interaction with A: Met112, A: Val130, A: Ala146, A: Leu134, A: Phe101, and A: Phe150, and a Pi–Pi T-shaped interaction with A: Phe101. In the case of the binding with human topoisomerase II, alkyl/pi–alkyl (D: DG9, A: Ile856, A: Lys868, A: Leu995, and A: Leu995), and Pi-donor (C: DA8) interactions were found for complex **2**, whereas complex **3** shows alkyl/pi–alkyl (A: Met847, A: Pro716, A: Lys723, and A: Leu771), amide-Pi-stacked (A: Leu722), and Pi–Sigma (A: Asn851) interactions.

Conclusion

Breast cancer is one of the most important causes of mortality and its incidence is increasing across the globe. Current standard chemotherapy treatment with cisplatin or its derivatives, either alone or in combination with other drugs, has achieved some success. However, drug resistance has emerged as a major challenge. Therefore, an innovative therapeutic approach which will overcome the resistance problem is needed. Herein, we describe two novel complexes [Pt(**1**)Cl$_2$] (**2**) and [Au(**1**)Cl$_2$][AuCl$_4$] (**3**) based on a C, N donor N-heterocyclic carbene ligand. The square planar isoelectronic and isostructural complexes [Pt(**1**)Cl$_2$] (**2**) and [Au(**1**)Cl$_2$][AuCl$_4$] (**3**), have been synthesized and characterized using a series of spectroscopic techniques. X-ray diffraction studies established the square planar geometry of **3**. Molecular docking studies

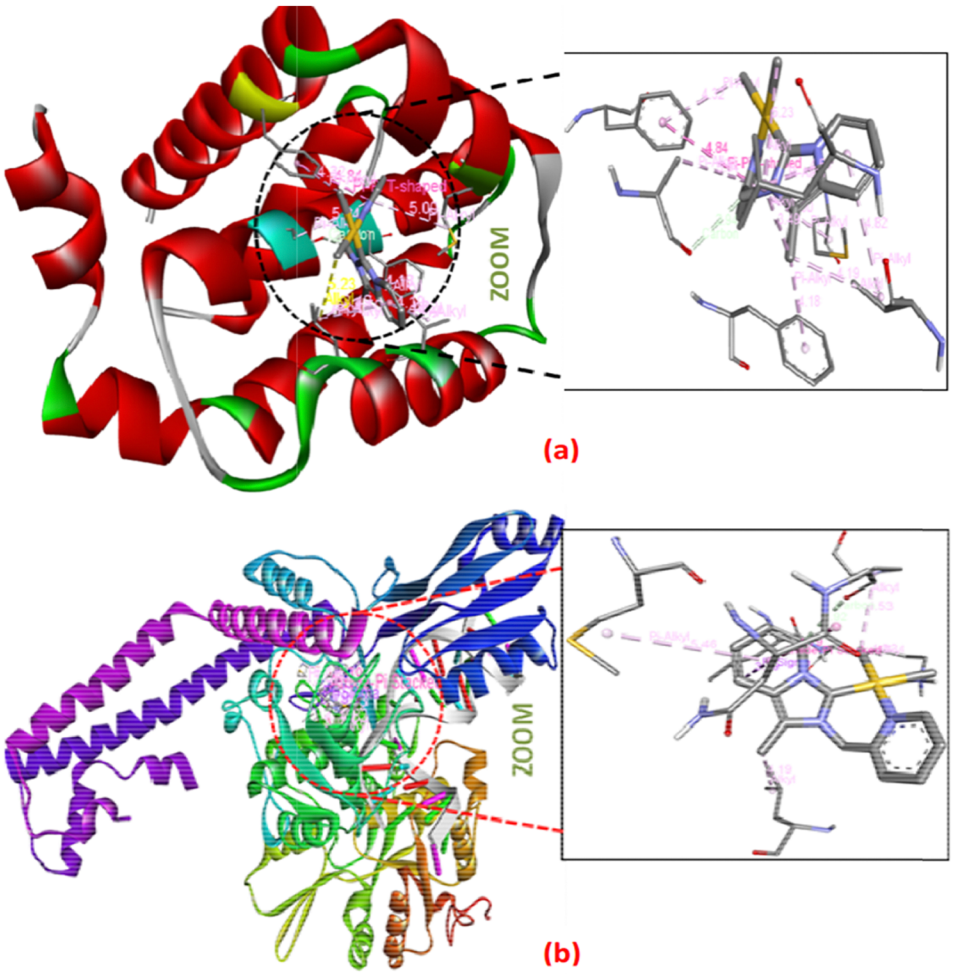

Fig. 10 Capped stick model and 2D view of the interaction mode of complex **3** with (a) BCL2 and (b) human-DNA topoisomerase.

revealed a stronger binding of complex **3** with human–DNA topoisomerase than for **2** and pro-ligand **1**.HPF_6. Finally, the compounds have been tested for their antiproliferative activity on breast cancer cell line MDA-MB231 and it was found that Au(III)–NHC complex **3** is more potent than Pt(II)–NHC complex **2**. It is observed that the expression of Ki-67 and VEGF decreased considerably under the treatment of drug **3**. Considering these points it is suggested that the $[Au(\mathbf{1})Cl_2]^+$ complex **3** could be a promising drug candidate for cancer therapy.

Experimental section

Chemistry

Reagents and solvents. The reagents silver oxide, KPF_6, 2-acetylpyridine, 2-picolylamine, paraformaldehyde, $KAuCl_4$, K_2PtCl_4, triethylorthoformate, *etc.*, were purchased from Sigma Aldrich and used without further purification. All manipulations were carried out in an open atmosphere. The NMR spectra were measured on Bruker 400 MHz spectrometers at 25 °C with tetramethylsilane as the internal standard. The absorption spectra were recorded using a Cary 100 Bio spectrophotometer.

Synthesis of $[Pt(\mathbf{1})Cl_2]$ (2). The pro-ligand **1**.HPF_6 (150 mg, 0.41 mmol) and Ag_2O (56 mg, 0.24 mmol) were suspended in 10 mL of dry acetonitrile and left to stir in the dark at room temperature for 4 h. Subsequently, the unreacted Ag_2O was then separated using a Celite plug, and the filtrate was gradually added to a stirred K_2PtCl_4 solution (170 mg, 0.41 mmol, in 5 mL of CH_3CN) in the dark at room temperature for 48 h. The resultant solution was then stirred under reflux for 2 h at 90 °C.

The color of the solution was transformed from pale yellow to colorless during this time. After a while at room temperature, the mixture was filtered using a Celite plug. To obtain a solid mass, the volume of the solution was decreased at low temperature and high pressure. Diffusion of diethyl ether into the saturated acetonitrile solution of complex **2** produced an analytically pure compound. The yield was 65% (131 mg, 0.27 mmol). ^{1}H NMR (DMSO-d_6, 25 °C, 400 MHz): δ = 8.76 (d, J = 8.0 Hz, 2H, $H^{a,h}$), 8.47 (d, J = 4.5 Hz, 1H, H^{d}), 7.91 (t, J = 7.6 Hz, 2H, $H^{c,f}$), 7.61 (d, J = 7.8 Hz, 1H, H^{e}), 7.47 (t, J = 4.2 Hz, 1H, H^{b}), 7.25 (m, J = 7.8 Hz, 1H, H^{g}), 5.90 (s, 2H, N–CH_2-py, H^{j}), 2.64 (s, 3H, –CH_3). ^{13}C NMR (DMSO-d_6, 25 °C, 100 MHz): 163.43,

150.15, 139.01, 127.19, 126.85, 124.42, 124.14, 123.43, 123.01, 122.59, 118.46, 118.09, 52.02, 8.50. Anal. calc. for $C_{14}H_{13}N_3PtCl_2$: C, 34.37; H, 2.68; N, 8.59. Found: C, 34.14; H, 2.59; N, 8.31%. ESI-MS: *m*/*z* observed at 453.0445 for $[M\text{-}Cl]^+$ and 494.0711 for $[M\text{-}Cl,CH_3CN]^+$.

Synthesis of $[Au(1)Cl_2][AuCl_4]$ (3). The pro-ligand **1**.HPF_6 (150 mg, 0.41 mmol) and Ag_2O (56 mg, 0.24 mmol) were dissolved in 10 mL of dry CH_3CN and stirred for 4 h at room temperature in the dark. After that, the unreacted Ag_2O was removed by filtration through a Celite plug. The filtrate was then gradually added to a $KAuCl_4$ solution (155 mg, 0.41 mmol, taken in 5 mL CH_3CN) while stirring at room temperature in the dark. The stirring process was continued for 2 h. As the reaction progressed, the orange-red solution became yellow in color. A solid mass was obtained by evaporating the solvent at high pressure and low temperature, after filtration through a Celite plug. By diffusing diethyl ether into the saturated solution of complex **3** in acetonitrile solution, an analytically pure compound was obtained. The yield was 45% (153 mg, 0.18 mmol). ^{1}H NMR (DMSO-d_6, 25 °C, 400 MHz): δ = 8.68 (d, J = 8.1 Hz, 2H, $H^{a,h}$), 8.56 (d, J = 4.3 Hz, 1H, H^d), 7.94 (t, J = 7.9 Hz, 2H, $H^{c,f}$), 7.58 (d, J = 7.6 Hz, 1H, H^e), 7.42 (t, J = 4.3 Hz, 1H, H^b), 7.17 (m, J = 4.2 Hz, 1H, H^g), 5.90 (s, N–CH_2-py, H^j), 2.75 (s, 3H, –CH_3). ^{13}C NMR (DMSO-d_6, 25 °C, 100 MHz): 161.35, 150.05, 138.66, 128.66, 126.96, 125.32, 124.35, 124.20, 123.45, 120.60, 118.41, 117.83, 51.93, 8.53. Anal. calc. for $C_{14}H_{13}N_3Au_2Cl_6$: C, 20.26; H, 1.58; N, 5.06. Found: C, 19.91; H, 1.27; N, 4.76%. ESI-MS: *m*/*z* observed at 490.0152 for $[MCl_2]^+$.

Single-crystal X-ray structure determination. Single crystals of complex **3** suitable for X-ray data collection were grown by slow diffusion of diethyl ether into a saturated acetonitrile solution of the respective complex. The crystal data and details of the data collected for **3** are given in Table S1 (ESI†). X-ray data were collected on a Bruker diffractometer (ImuS-Diamond source, Cu Kα radiation, λ = 1.54178 Å, Photon III detector). The structures were solved with the SHELXT[66] program and refined with the SHELXL[67] program using Olex2 as the GUI.[68]

Computational methodology. Complex **2** was optimized using the Gaussian 09 Rev D.01 software program[69] in the gas phase at the B3LYP-D3 level of theory.[70] The def2-TZVP basis set was used for the Pt center[71] whereas the carbon, hydrogen and nitrogen atoms were treated with the 6-31g**basis set.[72]

Biology

Cell culture. The breast cancer cell line MDA-MB231 was obtained from NCCS, Pune. The cell line was cultured in Dulbecco's modified Eagle medium (DMEM, Gibco) supplemented with 10% fetal bovine serum (FBS, Gibco) and 1% streptomycin/penicillin (Gibco) at 37 °C in a humidified atmosphere containing 5% CO_2. After the 6th passage, the cells were subjected to experimental analysis.[73]

MTT assay. In order to assess the viability of the cells and the cytotoxic potential of Pt-NHC complex **2** and Au–NHC complex **3**, MDA-MB231 cells were plated at a rate of 10^4 cells per well in a 96-well plate. The cells were seeded for 24 hours in 5% CO_2, followed by treatment doses of 0.1 μM, 1 μM, 10 μM, and 100 μM. The viable adherent cells were then stained with 3-dipenyl 2,5-diphenyl-tetradiatzolium bromide (MTT) (5 mg mL^{-1}) for 4 h. After 4 h, the media was removed and the formazan crystals were dissolved by the addition of 200 μL dimethyl sulfoxide (DMSO) per well. The absorbance was measured at a resolution of 540 nm. The cell viability was expressed in relative proportions to untreated controls.[74] To clarify further, we have checked the IC_{50} values of conventional drugs cisplatin and auranofin for both the complexes as reported by Wang *et al.*[62a] and Hatem *et al.*[62b]

Flow cytometry. The cells were plated in a 60-mm dish and allowed to seed for 24 h in a humified chamber. On the following day the desired dose of the drug calculated from the IC_{50} were administered to the cells and treated for 24 h. After the treatment, the cells were scrapped and centrifuged at 5000 rpm for 5 min and the cell pellet was distributed for the evaluation of the EMT markers E-cadherin and N-cadherin. Anti-E-cad and Anti-N-cad primary antibodies were added to the respective tubes followed by incubation overnight at 4 C, followed by the addition of secondary antibody APC tagged for determining their expression.[75]

Immunofluorescence. An MDA-MB-231 cell suspension was poured on a coverslip (100 μL) and allowed to settle overnight. The treatment doses were administered on the very following day and incubated for 24 h. The treated cells were then fixed with chilled methanol followed by blocking and addition of the Ki-67 and VEGF (1 : 500 dilution, Abclonal) primary antibodies individually and the cells were stored overnight at 4 °C. On the following day the cells were treated with an FITC-conjugated secondary antibody (1 : 1000 dilution) and incubated for 2 h at room temperature. Diaminidophenylindole (DAPI) was used for the nuclear staining and mounting was performed using DPX. The slides were allowed to dry and imaging was done at 40× using an Olympus fluorescence microscope.[76]

Scratch assay. The cells were plated in a 35-mm dish and allowed to seed for 24 h in a humified chamber with 5% CO_2. On the following day a scratch was drawn using a 200-μL micropipette tip and imaging was done at 0 h both for the control and treated plates under a phase contrast microscope. After the 0 h imaging, the desired treatment was added to the plates and incubated for 24 h. On the next day, images were again captured for determining the percentage closure of the scratch.[75] The percent wound confluence was calculated using $[(A - B) \times 100/A]$, where A is the width of the scratch at 0 h and B is the width upon achieving confluency.[76] The percent of inhibition was calculated using the closure rate method as reported by Bobadilla *et al.*[76b]

Statistical analysis. The statistical analysis was conducted using the unpaired student's *t*-test and the graphs of the results were prepared using GraphPad Prism software (version 8). Flow cytometry analysis was performed using FCS Express 7 software. P values of <0.001 and <0.05 were considered to be statistically significant.[77]

Molecular docking studies. Molecular docking was carried out on the AUTODOCK 4.0 software as accomplished using the graphical user interface AUTODOCK TOOLS 4.0 (AD4.1_bound.dat).

The macrocyclic receptor was chosen from the PDB and consists of a three-dimensional X-ray crystal structure of a human-DNA topoisomerase (ID: 1t8i). The graphical user interface AUTODOCK TOOLS was devoted to setting up the protein: the water molecule was deleted from the crystal of the protein and only polar hydrogen was added, the computed Gasteiger charge was calculated as 16.983 and non-polar hydrogen was merged with the carbon atom. The desired structures of the compounds were saved in the PDB format with the aid of the MERCURY program. The AUTODOCK TOOLS program was used to create a docking input file. The grid box sizes for the NHC ligand, complex **2** and complex **3** were 38 76 62; 54 64 56, and 48 46 50, respectively, with coordinates of the Central Grid Point of Maps equal to (22.477, 0.766, 30.352) and grid spacing of 1 Å. Both the receptors and the drug molecules were saved in the pdbqt format.[57] The distance-dependent functions of the dielectric constant were used for the calculation of the energetic map. Fifty runs were generated using Lamarckian genetic algorithm searches. Default settings were used with a maximum number of 2.5, 106 energy evaluations, and an initial population of 50 randomly placed individuals.[78] The final docking was run with autogrid4.exe and auto-dock4.exe functions to generate glg and dlg files, respectively. The graphical interaction pictures were found using Discovery Studio2021 visualisation software.

Data availability

The data will be available on request.

Conflicts of interest

The authors declare no conflict of interest.

Acknowledgements

JD thanks the Centre of Excellence in Advanced Materials and Applications, Utkal University for financial support.

References

1 C. P. Wild, E. Weiderpass and B. W. Stewart, *World Cancer Report: Cancer Research for Cancer Prevention*, International Agency for Research on Cancer, Lyon, France, 2020.
2 H. Sung, J. Ferlay, R. L. Siegel, M. Laversanne, I. Soerjomataram, A. Jemal and F. Bray, *CA Cancer J. Clin.*, 2021, **71**, 209–249.
3 C. Pucci, C. Martinelli and G. Ciofani, *Ecancermedicalscience*, 2019, **13**, 961–986.
4 (*a*) E. A. Martynov, T. Scattolin, E. Cavarzerani, M. Peng, K. V. Hecke, F. Rizzolio and S. P. Nolan, *Dalton Trans.*, 2022, **51**, 3462–3471; (*b*) P. K. Behera, L. Maity, S. Roy, A. Das, P. Sahu, H. K. Kisan, A. Changotra, A. A. Isab, M. B. Fettouhi, A. Bairagi, N. Chatterjee and J. Dinda, *New J. Chem.*, 2023, **47**, 18835–18848.
5 D. Varna, G. Geromichalos, D. K. Gioftsidou, D. Tzimopoulos, A. G. Hatzidimitriou, P. Dalezis, R. Papi, D. Trafalis and P. A. Angaridis, *J. Inorg. Biochem.*, 2024, **252**, 112472.
6 (*a*) S. Zhao, Z. Yang, G. Jiang, S. Huang, M. Bian, Y. Lu and W. Liu, *Coord. Chem. Rev.*, 2021, **449**, 214217; (*b*) T. Jia, O. Diane, D. Ghosh, M. Skander, G. Fontaine, P. Retailleau, J. Poupon, J. Bignon, Y. M. M. Siasia, V. Servajean, N. Hue, J.-F. Betzer, A. Marinetti and S. Bombard, *J. Med. Chem.*, 2023, **66**, 6836–6848.
7 O. A. L. Rojas, S. Cordeiro, P. V. Baptista and A. R. Fernandes, *J. Inorg. Biochem.*, 2023, **245**, 112255.
8 Z. Yang, M. Bian, L. Lv, X. Chan, Z. Wen, F. Li, Y. Lu and W. Liu, *J. Med. Chem.*, 2023, **66**, 3934–3952.
9 U. Das, B. Kar, S. Petel and P. Paira, *Dalton Trans.*, 2021, **50**, 11259–11290.
10 B. Rosenberg, L. Vancamp, J. E. Trosko and V. H. Mansour, *Nature*, 1969, **222**, 385–386.
11 N. P. Farrell, *Chem. Soc. Rev.*, 2015, **44**, 8773–8785.
12 C. G. Hartinger, S. Zorbas-Seifried, M. A. Jakupec, B. Kynast, H. Zorbas and B. K. Keppler, *J. Inorg. Biochem.*, 2006, **100**, 891–904.
13 J. Rani and S. Roy, *ChemMedChem*, 2023, **18**, e202200652.
14 C. Roder and M. J. Thomson, *Drugs R D.*, 2015, **15**, 13–20.
15 S. Leijen, S. A. Burgers, P. Baas, D. Pluim, M. Tibben, E. V. Werkhoven, E. Alessio, G. Sava, J. H. Beijnen and J. H. M. Schellens, *Invest. New Drugs*, 2015, **33**, 201–214.
16 L. Ruiz-Azuara and M. E. Bravo-Gomez, *Curr. Med. Chem.*, 2010, **17**, 3606–3615.
17 X. H. Makhoba, C. Viegas Jr., R. A. Mosa, F. P. Viegas and O. J. Pooe, *Drug Des., Dev. Ther.*, 2020, **14**, 3235–3249.
18 (*a*) J. Karges, R. W. Stokes and S. M. Cohen, *Trends Chem.*, 2021, **3**, 523–534; (*b*) J. J. Wilson and S. J. Lippard, *Chem. Rev.*, 2014, **114**, 4470–4495.
19 B. Englinger, C. Pirker, P. Heffeter, A. Terenzi, C. R. Kowol, B. K. Keppler and W. Berger, *Chem. Rev.*, 2019, **119**, 1519–1624.
20 K. M. Knopf, B. L. Murphy, S. N. MacMillan, J. M. Baskin, M. P. Barr, E. Boros and J. J. Wilson, *J. Am. Chem. Soc.*, 2017, **139**, 14302–14314.
21 C. E. Elgar, N. A. Yusoh, P. R. Tiley, N. Kolozsvári, L. G. Bennett, A. Gamble, E. V. Péan, M. L. Davies, C. J. Staples, H. Ahmad and M. R. Gill, *J. Am. Chem. Soc.*, 2023, **145**, 1236–1246.
22 W. Liu and R. Gust, *Chem. Soc. Rev.*, 2013, **42**, 755–773.
23 F. Cisnetti and A. Gautier, *Angew. Chem., Int. Ed.*, 2013, **52**, 11976–11978.
24 Q. Zhao, B. Han, C. Peng, N. Zhang, W. Huang, G. He and J.-L. Li, *Med. Res. Rev*, 2024, **44**, 2194–2235.
25 A. Gautier and F. Cisnetti, *Metallomics*, 2012, **4**, 23–32.
26 J. Dinda, A. Nandy, B. K. Rana, V. Bertolasi, K. D. Saha and C. W. Bielawskie, *RSC Adv.*, 2014, **4**, 60776–60784.
27 B. Rana, A. Nandy, V. Bertolasi, C. W. Bielawski, K. D. Saha and J. Dinda, *Organometallics*, 2014, **33**, 2544.
28 L. Jhulki, P. Dutta, M. K. Santra, M. H. Cardoso, K. G. N. Oshiro, O. L. Franco, V. Bertolasi, A. A. Isab, C. W. Bielawski and J. Dinda, *New J. Chem.*, 2018, **42**, 13948–13956.
29 F. E. Hahn and M. C. Jahnke, *Angew. Chem., Int. Ed.*, 2008, **47**, 3122–3172.

30 Z. Trávníček, J. Vančo, M. Čajan, J. Belza, I. Popa, J. Hošek, R. Lenobel and Z. Dvořák, *Appl. Organomet. Chem.*, 2024, **38**, e7401.
31 M. N. Hopkinson, C. Richter, M. Schedler and F. Glorius, *Nature*, 2014, **510**, 485–496.
32 D. C. F. Monteiro, R. M. Phillips, B. D. Crossley, J. Fielden and C. E. Willans, *Dalton Trans.*, 2012, **41**, 3720.
33 P. Padmaja, G. K. Rao, A. Indrasena, B. V. S. Reddy, N. Patel, A. B. Shaik, N. Reddy, P. K. Dubey and M. P. Bhadra, *Org. Biomol. Chem.*, 2015, **13**, 1404–1414.
34 (*a*) Y. Lu, X. Ma, X. Chang, Z. Liang, L. Lv, M. Shan, Q. Lu, Z. Wen, R. Gust and W. Liu, *Chem. Soc. Rev.*, 2022, **51**, 5518–5556; (*b*) M.-L. Teyssot, A.-S. Jarrousse, M. Manin, A. Chevry, S. Roche, F. Norre, C. Beaudoin, L. Morel, D. Boyer, R. Mahiou and A. Gautier, *Dalton Trans.*, 2009, 6894–6902.
35 T. Jia, O. Diane, D. Ghosh, M. Skander, G. Fontaine, P. Retailleau, J. Poupon, J. Bignon, Y. M. M. Siasia, V. Servajean, N. Hue, J.-F. Betzer, A. Marinetti and S. Bombard, *J. Med. Chem.*, 2023, **66**, 6836–6848.
36 M. Chtchigrovsky, L. Eloy, H. Jullien, L. Saker, E. Ségal-Bendirdjian, J. Poupon, S. Bombard, T. Cresteil, P. Retailleau and A. Marinetti, *J. Med. Chem.*, 2013, **56**, 2074–2086.
37 J.-J. Zhang, Q.-J. Xu, C. Schmidt, M. A. A. Maaty, J. Song, C. Yu, J. Zhou, K. Han, H. Sun, A. Casini, I. Ott and S. Wölfl, *J. Med. Chem.*, 2023, **66**, 3995–4008.
38 I. Ott, *Coord. Chem. Rev.*, 2009, **253**, 1670–1681.
39 R. P. Herrera and M. C. Gimeno, *Chem. Rev.*, 2021, **121**, 8311–8363.
40 Y.-F. Zhang, Y.-K. Yin, H. Zhang and Y.-F. Han, *Coord. Chem. Rev.*, 2024, **514**, 215941.
41 S. Ray, R. Mohan, J. K. Singh, M. K. Samantaray, M. M. Shaikh, D. Panda and P. Ghosh, *J. Am. Chem. Soc.*, 2007, **129**, 15042–15053.
42 J. L. Hickey, R. A. Ruhayel, P. J. Barnerd, M. V. Baker, S. J. Berners-Price and A. Filipovska, *J. Am. Chem. Soc.*, 2008, **30**, 12570–12571.
43 Y. Marciano, V. del Solar, N. Nayeem, D. Dave, J. Son, M. Contel and R. V. Ulijn, *J. Am. Chem. Soc.*, 2023, **145**, 234–246.
44 R. Rubbiani, S. Can, I. Kitanovic, H. Alborzinia, M. Stefanopoulou, M. Kokoschka, S. Mönchgesang, W. S. Sheldrick and I. Ott, *J. Med. Chem.*, 2011, **54**, 8646–8657.
45 A. Casini, C. Hartinger, C. Gabbiani, E. Mini, P. J. Dyson, B. K. Keppler and L. Messori, *J. Inorg. Biochem.*, 2008, **102**, 564–575.
46 (*a*) B. Bertrand and A. Casini, *Dalton Trans.*, 2014, **43**, 4209–4219; (*b*) M. Williams, A. I. Green, J. F.-Cestau, D. L. Hughes, M. A. O'Connell, M. Searcey, B. Bertrand and M. Bochmann, *Dalton Trans.*, 2017, **46**, 13397–13408; (*c*) M. R. M. Williams, B. Bertrand, J. F.-Cestau, Z. A. E. Waller, M. A. O'Connell, M. Searcey and M. Bochmann, *Dalton Trans.*, 2018, **47**, 13523–13534; (*d*) D. van der Westhuizen, D. I. Bezuidenhout and O. Q. Munro, *Dalton Trans.*, 2021, **50**, 17413–17437.
47 (*a*) T. Zou, C. T. Lum, S. S.-Y. Chui and C.-M. Che, *Angew. Chem., Int. Ed.*, 2013, **52**, 2930–2933; (*b*) F. Guarra, A. Terenzi, C. Pirker, R. Passannante, D. Baier, E. Zangrando, V. Gómez, T. Biver, C. Gabbiani, W. Berger, J. Llop and L. Salassa, *Angew. Chem., Int. Ed.*, 2020, **59**, 17130–17136.
48 L. B. Chen, *Annu. Rev. Cell Biol.*, 1988, **4**, 155–181.
49 J. R. Benson and I. Jatoi, *Future Oncol.*, 2012, **8**, 697–702.
50 M. Zendehdel, B. Niakan, A. Keshtkar, E. Rafiei and F. Salamat, *Iran. J. Med. Sci.*, 2018, **43**, 1–8.
51 Z. Momenimovahed and H. Salehiniya, *Breast Cancer: Targets Ther.*, 2019, **11**, 151–164.
52 Y. Wang and B. P. Zhou, *Chin. J. Cancer.*, 2011, **30**, 603–611.
53 W. K. Liu and R. Gust, *Coord. Chem. Rev.*, 2016, **329**, 191–213.
54 M. Porchia, M. Pellei, M. Marinelli, F. Tisato, F. D. Bello and C. Santini, *Eur. J. Med. Chem.*, 2018, **146**, 709–746.
55 Y.-F. Han, *Eur. J. Med. Chem.*, 2018, **146**, 709–746.
56 M.-M. Gan, J.-Q. Liu, L. Zhang, Y.-Y. Wang and F. E. Hah, *Chem. Rev.*, 2018, **118**, 9587–9641.
57 L. Maity, S. Barik, H. K. Kisan, A. Jana, A. A. Isab and J. Dinda, *New J. Chem.*, 2023, **47**, 284–296.
58 Y. Unger, A. Zeller, S. Ahrensy and T. Strassner, *Chem. Commun.*, 2008, 3263–3265.
59 L. Jhulki, P. Dutta, M. K. Santra, M. H. Cardoso, K. G. N. Oshiro, O. L. Franco, V. Bertolasi, A. A. Isab, C. W. Bielawski and J. Dinda, *New J. Chem.*, 2018, **42**, 13948–13956.
60 B. K. Rana, S. Mishra, D. Sarkar, T. K. Mondal, S. K. Seth, V. Bertolasi, K. D. Saha, C. W. Bielawski, A. A. Isab and J. Dinda, *New J. Chem.*, 2018, **42**, 10704–10711.
61 M. V. Vener, A. V. Shishkina, A. A. Rykounov and V. G. Tsirelson, *J. Phys. Chem. A*, 2013, **117**, 8459–8467.
62 (*a*) S. Wang, J. Xie, J. Li1, F. Liu, X. Wu and Z. Wang, *Am. J. Cancer Res.*, 2016, **6**, 1108–1117; (*b*) E. Hatem, N. E. Banna, A. H.-Masurel, D. Baïlle, L. Vernis, S. Riquier, M.-P. G.-Cohen, O. Guittet, C. Vallières, J.-M. Camadro, X. Qiu, N. Hildebrandt, M. Lepoivre and M.-Er Huang, *Cancers*, 2022, **14**, 4864–4881.
63 (*a*) S. Kotiyal and S. Bhattacharya, *Biochem. Biophys. Res. Commun.*, 2014, **453**, 112–116; (*b*) D. Neelakantan, H. Zhou, M. U. J. Oliphant, X. Zhang, L. M. Simon, D. M. Henke, C. A. Shaw, M.-F. Wu, S. G. Hilsenbeck, L. D. White, M. T. Lewis and H. L. Ford, *Nat. Commun.*, 2017, **8**, 15773.
64 K. Mrouj, N. Andrés-Sánchez, G. Dubra, P. Singh, M. Sobecki, D. Chahar, E. Al Ghoul, A. B. Aznar, S. Prieto, N. Pirot, F. Bernex, B. Bordignon, C. Hassen-Khodja, M. Villalba, L. Krasinska and D. Fisher, *Proc. Natl. Acad. Sci. U. S. A.*, 2021, **118**, 1–12.
65 P. M. D. dos Santos, I. S. Pereira, A. Longato and S. F. Martins, *Eurasian J. Med. Oncol.*, 2022, **6**, 258–267.
66 G. M. Sheldrick, *Acta Crystallogr., Sect. A: Found. Adv.*, 2015, **A71**, 3–8.
67 G. M. Sheldrick, *Acta Crystallogr., Sect. C: Struct. Chem.*, 2015, **C71**, 3–8.
68 O. V. Dolomanov, L. J. Bourhis, R. J. Gildea, J. A. K. Howard and H. Puschmann, *J. Appl. Cryst.*, 2009, **42**, 339–341.
69 M. J. Frisch, G. W. Trucks, H. B. Schlegel, G. E. Scuseria,M. A. Robb, J. R. Cheeseman, J. A. Montgomery

Jr., T. Vreven, K. N. Kudin,J. C. Burant, J. M. Millam, S. S. Iyengar, J. Tomasi, V. Barone, B. Mennucci, M. Cossi, G. Scalmani, N. Rega, G. A. Petersson, H. Nakatsuji, M. Hada, M. Ehara, K. Toyota, R. Fukuda, J. Hasegawa, M. Ishida, T. Nakajima, Y. Honda, O. Kitao,H. Nakai, M. Klene, X. Li,J. E. Knox, H. P. Hratchian, J. B. Cross, V. Bakken,C. Adamo, J. Jaramillo, R. Gomperts, R. E. Stratmann, O. Yazyev, A. J. Austin, R. Cammi, C. Pomelli, J. W. Ochterski, P. Y. Ayala, K. Morokuma, G. A. Voth, P. Salvador,J. J. Dannenberg, V. G. Zakrzewski, S. Dapprich, A. D. Daniels, M. C. Strain, O. Farkas, D. K. Malick, A. D. Rabuck, K. Raghavachari, J. B. Foresman, J. V. Ortiz,Q. Cui, A. G. Baboul, S. Clifford, J. Cioslowski, B. B. Stefanov, G. Liu, A. Liashenko, P. Piskorz, I. Komaromi, R. L. Martin, D. J. Fox, T. Keith, M. A. Al-Laham, C. Y. Peng, A. Nanayakkara, M. Challacombe, P. M. W. Gill, B. Johnson, W. Chen, M. W. Wong, C. Gonzalez and J. A. Pople, *Gaussian 09, Revision D.01*, Gaussian, Inc., Wallingford CT, 2013.

70 S. Grimme, J. Antony, S. Ehrlich and H. Krieg, *J. Chem. Phys.*, 2010, **132**, 154104.

71 (*a*) F. Weigend and R. Ahlrichs, *Phys. Chem. Chem. Phys.*, 2005, **7**, 3297–3305; (*b*) F. Weigend, *Phys. Chem. Chem. Phys.*, 2006, **8**, 1057–1065.

72 W. J. Hehre, R. Ditchfield and J. A. Pople, *J. Chem. Phys.*, 1972, **56**, 2257–2261.

73 S. Das, N. Chatterjee, D. Bose, S. Banerjee, T. Jha and K. D. Saha, *Tumour Biol.*, 2015, **36**, 3109–3118.

74 S. Das, N. Chatterjee, D. Bose, S. Banerjee, T. Jha and K. D. Saha, *Apoptosis*, 2015, **20**, 869–882.

75 S. K. Das, S. Roy, A. Das, A. Chowdhury, N. Chatterjee and A. Bhaumik, *Nanoscale Adv.*, 2022, **4**, 2313–2320.

76 (*a*) S. Bhattacharyya, T. Maji, D. K. Ray, A. K. Bhowmick and N. Murmu, *J. Nucl. Med. Radiat. Ther.*, 2015, **6**, 1000251; (*b*) A. V. P. Bobadilla, J. Arévalo, E. Sarró, H. M. Byrne, P. K. Maini, T. Carraro, S. Balocco, A. Meseguer and T. Alarcón, *J. R. Soc., Interface*, 2019, **16**, 20180709.

77 S. Roy, A. Das, M. Vernekar, S. Mandal and N. Chatterjee, *Biomed. Res. Int.*, 2022, **20**, 5346091.

78 J. M. Brenchley and D. C. Douek, *Method Cell Biol.*, 2004, **75**, 481–496.

ACS Biomaterials SCIENCE & ENGINEERING

pubs.acs.org/journal/abseba

Letter

Covalent Organic Frameworks as Potential Drug Carriers and Chemotherapeutic Agents for Ovarian Cancers

Atikur Hassan, Sraddhya Roy, Ananya Das, Sk Abdul Wahed, Aparajita Bairagi, Subhadip Mondal, Nabanita Chatterjee,* and Neeladri Das*

Cite This: https://doi.org/10.1021/acsbiomaterials.4c00351

Read Online

ACCESS | Metrics & More | Article Recommendations | Supporting Information

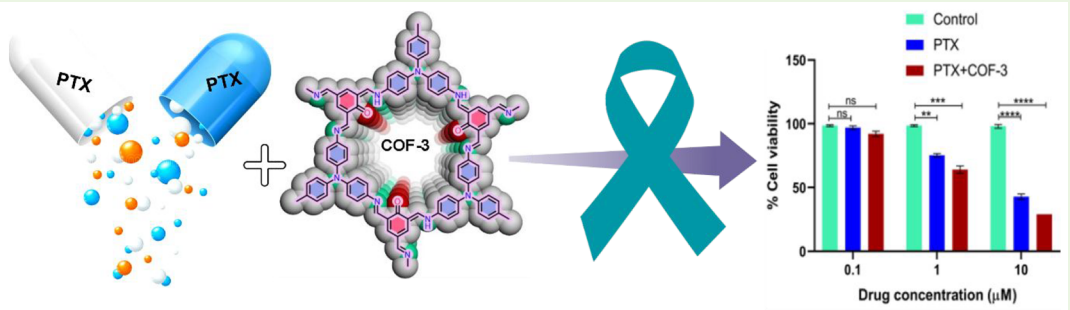

ABSTRACT: Anticancer drugs are often associated with limitations such as poor stability in aqueous solutions, limited cell membrane permeability, nonspecific targeting, and irregular drug release when taken orally. One possible solution to these problems is the use of nanocarriers of drug molecules, particularly those with targeting ability, stimuli-responsive properties, and high drug loading capacity. These nanocarriers can improve drug stability, increase cellular uptake, allow specific targeting of cancer cells, and provide controlled drug release. While improving the therapeutic efficacy of cancer drugs, contemporary researchers also aim to reduce their associated side effects, such that cancer patients are offered with a more effective and targeted treatment strategy. Herein, a set of nine porous covalent organic frameworks (COFs) were tested as drug delivery nanocarriers. Among these, paclitaxel loaded in COF-3 was most effective against the proliferation of ovarian cancer cells. This study highlights the emerging potential of COFs in the field of therapeutic drug delivery. Due to their biocompatibility, these porous COFs provide a viable substrate for controlled drug release, making them attractive candidates for improving drug delivery systems. This work also demonstrates the potential of COFs as efficient drug delivery agents, thereby opening up new opportunities in the field of sarcoma therapy.

KEYWORDS: *ovarian cancer, covalent organic frameworks, nanotherapeutics, drug delivery*

An increasing number of dangerous and complex diseases are being diagnosed worldwide as a result of variables such as population growth and changing lifestyles. Among these, cancer stands out as a major global public health problem with high morbidity and mortality.[1] Some have referred to this period as the "age of cancer" due to the increase in cancer cases.[2] In 2003, there were 6.5 million cancer deaths; by 2013, this figure rises to 12 million, and it is estimated that there will be a staggering 22 million deaths by 2030 and 35 million by 2050.[3] The common forms of this disease are breast, lung, colorectal, ovarian, prostate, cervical, and colon cancers. Ovarian cancer is the third leading cause of cancer death among women, after breast and lung cancer.[4] According to the statistics of a survey conducted by the American Cancer Society, 19,880 new cases of ovarian cancer (OvCa) and 12,810 related deaths were reported alone in the United States in 2022.[5] In OvCa, the cancer cells show high rate of proliferation and acquire chemo-resistance rather rapidly, thereby increasing the metastasizing tendency of the tumor via compression of the visceral organs of the peritoneal cavity.[6] Among four types of OvCa, epithelial ovarian cancer (EOvCa) is the most common gynecological malignancy and is therefore considered to be the most lethal with the least survival rate.[7] Generally, cases of OvCa are diagnosed at the advanced stages of metastasis and this is due to not attending nonspecific symptoms like vomiting, bloating, abdominal pain, frequent urine discharge, etc.[8,9]

Despite advancements and effectiveness in OvCa treatment processes, such as chemotherapy and debulking surgery, therapy-resistant metastasis remains a threat to patients and a major challenge to oncologists. It is quite well documented

Received: February 23, 2024
Revised: May 2, 2024
Accepted: June 3, 2024

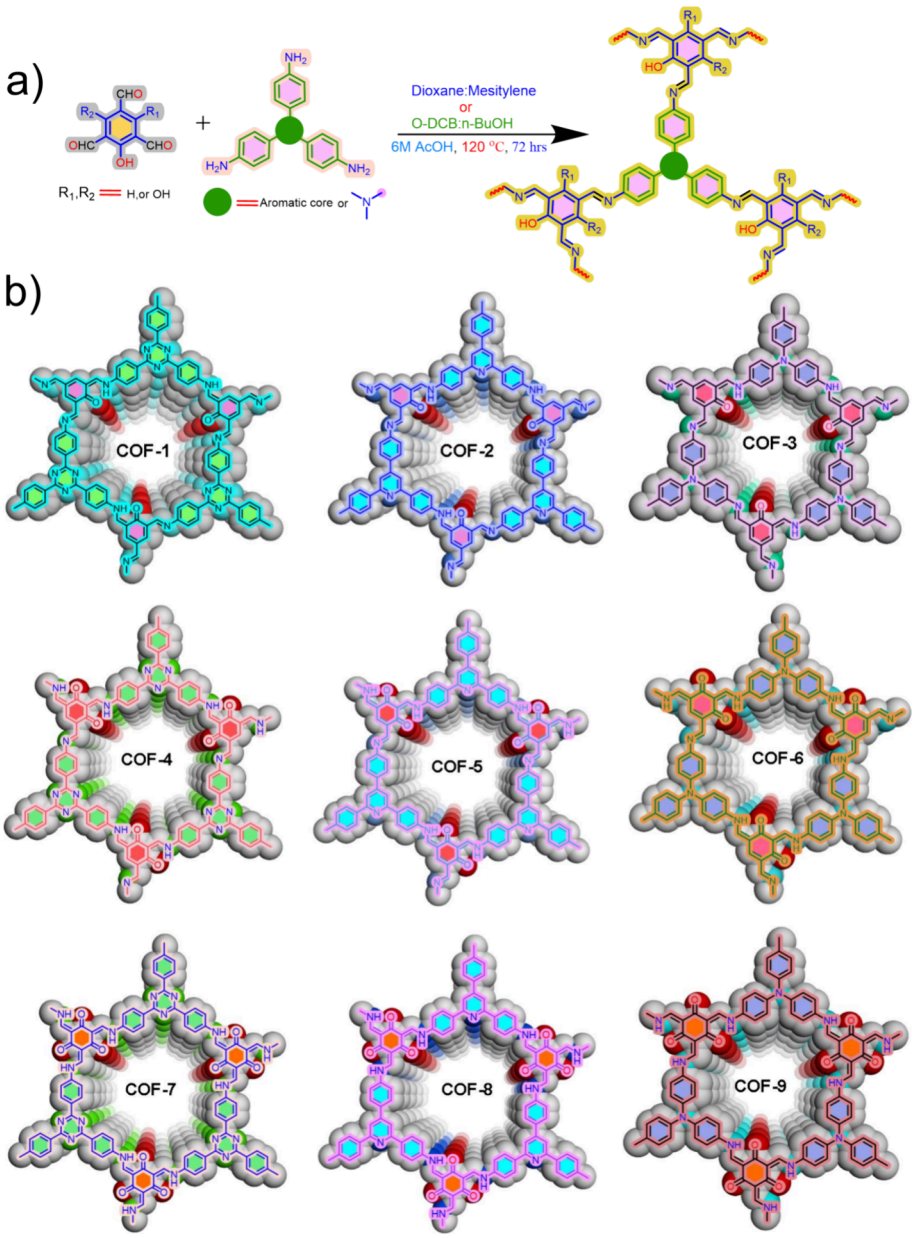

Figure 1. (a) Syntheses of COF-1 to COF-9. (b) The schematic structures of COF-1 to COF-9.

that the cancer cells move via the bloodstream in the course of metastasis, which is a highly controlled process.[10] The intense regulations in the process of metastasis begin with the interactions of the primary tumor cells with the extracellular matrix leading to aberrant dysregulations, which is often associated with metastasis.[11−13] In the epithelial−mesenchymal transition (EMT) of OvCa cells, it has been hypothesized that epithelial cancer cells of the primary tumor lose their epithelial properties like loss of the epithelial marker epithelial cadherin (E-cad) and acquire mesenchymal attributes like increase in the expression of neural cadherin (N-cad) to evade the extracellular matrix and migrate to distant sites to form a secondary tumor, resulting in metastasis of the tumor. E-cad is primarily expressed in epithelial cells, where it functions as a key molecule in cell−cell adhesion, helping to maintain the integrity and architecture of epithelial tissues. High expression of E-cadherin is typically associated with a less aggressive tumor phenotype. It helps maintain the epithelial phenotype, thus preventing epithelial cells from undergoing EMT, a process by which epithelial cells lose their cell−cell adhesion properties and gain migratory and invasive capabilities. N-cadherin, on the other hand, is commonly associated with neural and mesenchymal cells. During tumor progression, some cancer cells decrease their expression of E-cadherin and upregulate N-cadherin, a phenomenon known as the "cadherin switch". The expression of N-cadherin in tumor cells is associated with enhanced migratory and invasive capacities. This is partly because N-cadherin interacts differently with the cytoskeleton and cell signaling pathways compared to E-cadherin, promoting increased cell motility.[14] Davidson et al. reviewed multiple studies where it has been stated that higher expression of E-cad is associated with better survival of the patients whereas elevated expression of N-cad is associated with poor survival.[15] This is a gradually occurring process rather than a binary switch between epithelial and mesenchymal markers. This transition state comprises varied

https://doi.org/10.1021/acsbiomaterials.4c00351
ACS Biomater. Sci. Eng. XXXX, XXX, XXX−XXX

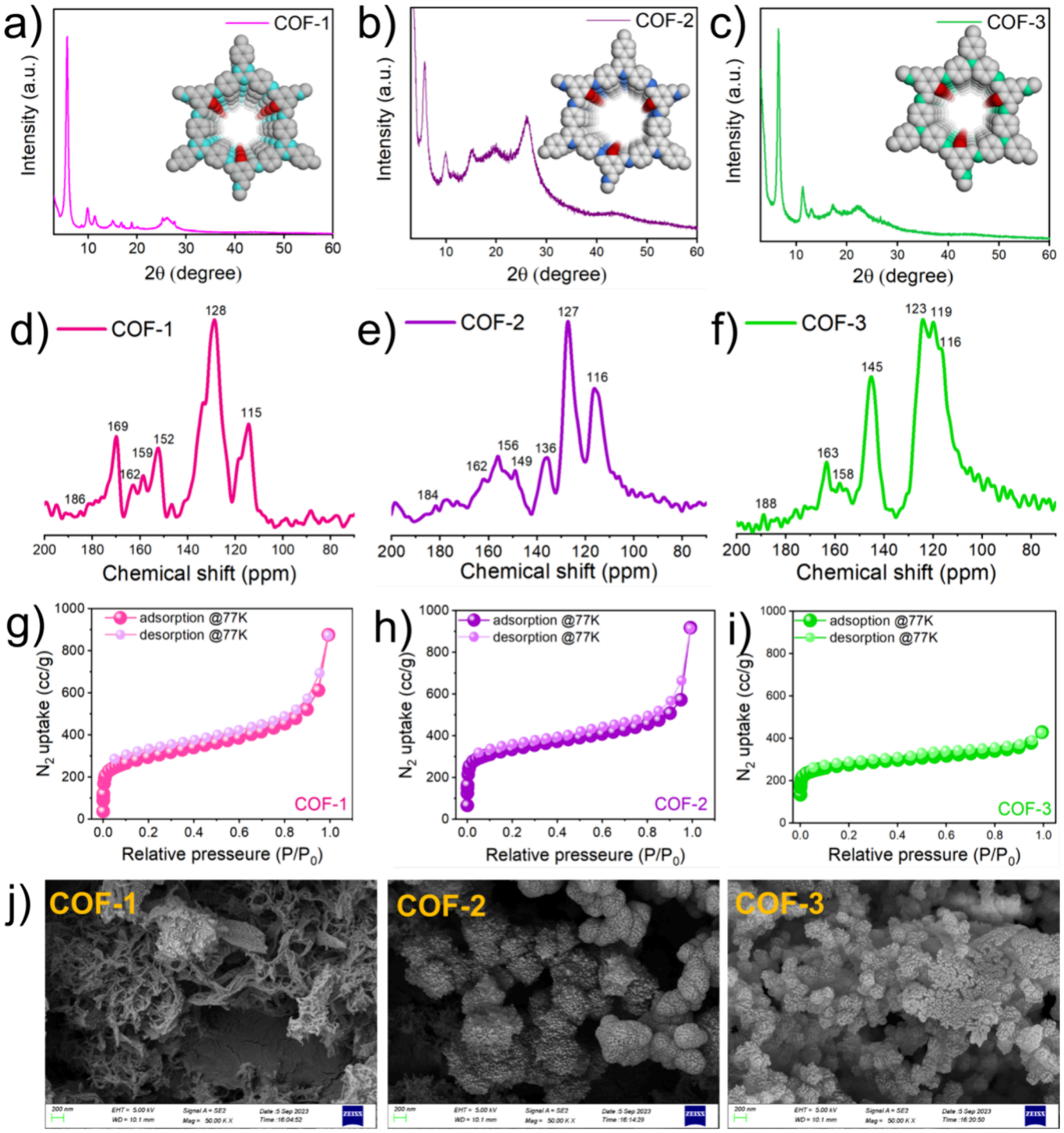

Figure 2. P-XRD plots of (a) COF-1, (b) COF-2, and (c) COF-3; solid-state ^{13}C CP-MAS NMR of (d) COF-1, (e) COF-2, and (f) COF-3; porosity analysis by low-temperature (77 K) N_2 sorption analysis of (g) COF-1, (h) COF-2, and (i) COF-3; and morphological analysis by FE-SEM in a scale bar of 200 nm of (j) COF-1, COF-2, and COF-3.

expression of EMT markers and exhibits morphological, transcriptional, and epigenetic features of the transitioning cancer cells. The intermediate stages emphasize that the transition is not just a binary switch between epithelial and mesenchymal states but rather have been described as partial EMT, incomplete EMT and hybrid EMT. Thus, the exploration of the spectrum of different characteristics is necessary to understand the process of cancer progression.[16] Marchini et al. stated that resistance to platinum drugs used in chemotherapy regimens fuels the process of EMT.[17] Thus, targeting deregulated signaling cascades in the cancer cells that are responsible for the metastasis with several small molecule inhibitors is currently being investigated in the quest to improve the conventional therapeutic approaches.[18] Das et al. also demonstrated the efficacy of cisplatin-loaded COF toward the migratory potential of breast cancer cells.[19] Simultaneously, benign drug carriers play a crucial role in reducing drug degradation and loss, thereby minimizing toxic and side effects

https://doi.org/10.1021/acsbiomaterials.4c00351
ACS Biomater. Sci. Eng. XXXX, XXX, XXX−XXX

and enhancing the overall effectiveness of medications. To date, numerous materials have been explored as drug delivery agents, including supramolecular systems, metal−organic frameworks (MOFs), covalent organic frameworks (COFs), and various other drug carrier systems.[20−23] Among these advanced materials, the COFs are rapidly emerging as promising candidates as drug carriers that have garnered significant attention of contemporary researchers.[24−26] The increasing importance of COFs in the field of biological nanomaterials is due to their amazing and unusual properties. First, COFs are quite versatile as far as their modular design is concerned.[27−31] The flexibility available in the design of COFs makes it easier to incorporate different functional components which in turn increases their suitability in different biological applications, such as fluorescence imaging and targeted tumor therapy.[32] The presence of intrinsic porosity in the COFs offers an additional advantage in the use of these materials for therapeutic interventions. In this context, encapsulation of various guest molecules and precise control of drug release are quite feasible. In addition, the use of conjugated monomers yields COFs with specific optical properties in which manipulation of topological configurations and geometric parameters often opens up new medical and imaging applications. Finally, the fact that COFs are metal-free materials ensures that these are not associated with potential biological toxicities, which are commonly known for metal-based materials, such as MOFs. The desirable properties of COFs, which include but are not limited to facile synthesis and drug loading, enhanced optical capabilities and biocompatibility, and controlled drug delivery, increase their potential as futuristic materials for sarcoma treatment.[33] In the scientific literature, there are reports of only a handful of COFs that have been explored as potential carriers of chemotherapeutic drugs such as doxorubicin (DOX), carboplatin, and cisplatin.[29,34−36] However, COFs have not been explored as a carrier for paclitaxel (PTX), a chemotherapeutic drug used for the treatment of ovarian cancer. In this regard, herein a set of nine imine or β-ketoimine linkage COFs has been synthesized for their use as drug-delivery agents for chemotherapeutic applications. Specifically, in this study we have focused on the epithelial−mesenchymal transition (EMT) of OvCa cells, a mechanism that assists cancer cells to evade the extracellular matrix and their migration to distant sites to form a secondary tumor, resulting in metastasis of the tumor. In this study, we focused on targeting the EMT with the newly synthesized COFs in combination with conventional drug paclitaxel (PTX) while observing the changes in the factors responsible for the initiation of metastasis. The detailed syntheses, characterizations, and anticancer studies of these COFs are discussed in the upcoming sections.

The development of unique porous materials with well-defined porous structures and carefully controlled porous environments is a well-investigated research domain that yields exciting two-dimensional (2D) covalent organic frameworks (COFs) for various applications.[37−42] The highly crystalline imine-functionalized COFs are associated with high chemical stability and are often projected as potential materials for various strategic applications such as gas separation, sensing, energy storage, catalysis, environmental remediation, and others.[43−46] This is due to facile synthetic protocols associated with the yield of COFs in which the ease of functionalization leads to the possibility of varying the surface and molecular properties. In recent literature, the use of imine-functionalized COFs for biomedical applications, particularly in cancer therapy, is quite limited.[47] Therefore, in this work, several imine-linked COFs (Figure 1) were obtained via Schiff base reactions between mono/di/trihydroxy-functionalized trialdehyde and triamine moieties. In particular, a set of nine two-dimensional (2D) hexagonal microporous COFs were synthesized to investigate their role as chemotherapeutic agents for ovarian cancer theranostics and study their performance as PTX drug carriers.[48]

The synthetic protocol to obtain the nine COFs is shown in Figure 1. Using the well-known Schiff base reaction, three hydroxy containing trialdehyde monomers (TFP, TFR, and TP) were reacted with three different triamino arene monomers (TZ-TA, PY@N, and TPA) to yield nine structurally different yet highly crystalline COFs (Figures 1a and 1b).

The syntheses of six monomers and the nine COFs are mentioned in Sections S1 and S2. The COFs (1−9) were characterized using multiple analytical tools, such as Fourier transform infrared (FTIR), powder X-ray diffraction (PXRD), solid-state ^{13}C NMR (^{13}C CP-MAS NMR) spectroscopy, thermogravimetric analysis (TGA), and low-temperature nitrogen (N_2) sorption measurements. The presence of ample imine linkages in these COFs (1−9) were confirmed by the appearance of a sharp band centered between 1615 to 1640 cm^{-1} in their respective FTIR spectra (Figures S1a−S1i) that was absent in the corresponding aldehyde/amine monomers. For example, in COF-3, the band at 1623 cm^{-1} is attributed to the presence of imine linkages in this material. Further, in this FTIR spectrum, the diminished intensity of characteristic peaks due to aldehyde/amine functional group bond vibrations was clear evidence to support the consumption of the monomers that led to the formation of imine-linked COF-3. Similar FTIR spectral features were also observed for other COFs reported herein.

The presence of crystallinity in these COFs (1−9) was verified from their PXRD spectra (Figures 2a−2c and Figures S2a−S2f). The molecular level characterizations of these COFs (1−9) were performed by recording their respective solid-state ^{13}C CP-MAS NMR spectrum. All these COFs (1−9) show a prominent peak between 140 to 165 ppm, which indicates the presence of imine carbons (Figures 2d−2f and Figures S3a−S3f). The peaks in the range of 110 to 140 are due to the arene carbon atoms that are present in the framework of the COFs (1−9). Peaks in the range of 165−175 ppm, observed in the ^{13}C CP-MAS NMR of COF-1, COF-4, and COF-7, are attributed to the carbon atoms present in the triazine rings. COFs 1−3 were obtained from a phenol trialdehyde (TFP), and their corresponding ^{13}C CP-MAS solid NMR spectra have very low intensity peaks for the keto functional group. It is also well-accepted in the literature that in such polymers, there exists a keto−enol tautomerism and the equilibrium is shifted toward the enol form.[49−51] Consequently, the intensity of the peak due to the keto carbon (appearing in between ∼180 to190 ppm) is relatively much lower than that of the phenol (C−OH) carbon (appearing in between ∼160 to 165 ppm) in COFs 1−3.[51] However, for COFs 4−9 that have a relatively higher number of keto groups per repeating unit, the peak due to the keto group appeared in the range of 183 to 188 ppm in the corresponding ^{13}C CP-MAS solid NMR spectrum. Overall, these observations suggest the successful reaction between the amine and aldehyde functional group containing monomers, thereby yielding COFs (1−9). The TGA thermograms show

https://doi.org/10.1021/acsbiomaterials.4c00351
ACS Biomater. Sci. Eng. XXXX, XXX, XXX−XXX

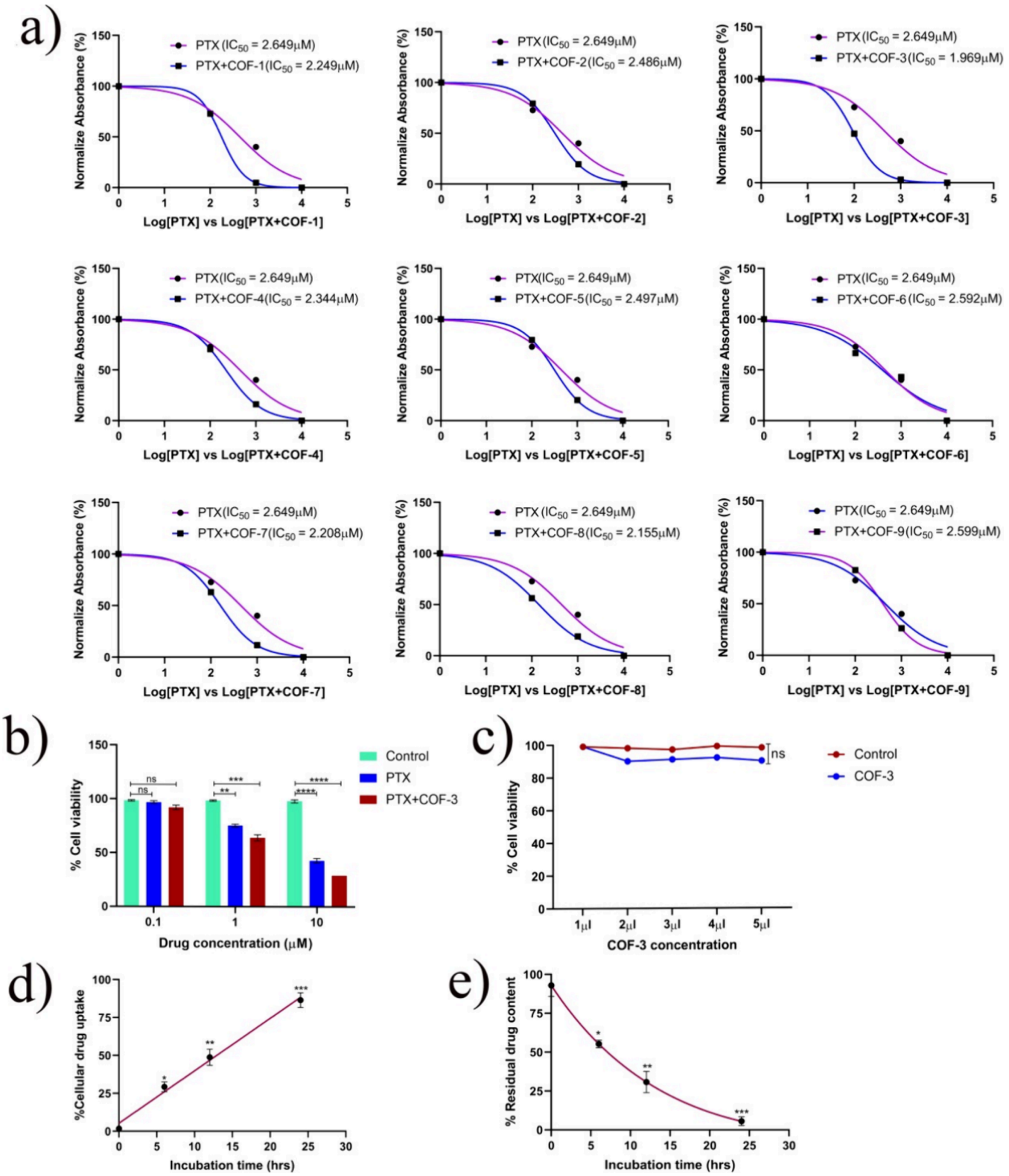

Figure 3. (a) MTT analysis of PTX in combination with carrier molecules (COF-1 to COF-9) in SKOV-3 cells. (b) Cell viability decreases considerably with increasing concentrations of PTX alone and in combination with COF-3. (c) COF-3 alone has no effect on cell viability with increasing concentration as compared to the control. (d) Drug uptake increases significantly with an increase in incubation time. (e) Residual drug content decreases with increase in incubation time.

that these materials are thermally stable in nature with T_d (10% decomposition) values greater than 350 °C in the case of most of the COFs reported herein (Figures S4a−S4i). The presence of porosity in these COFs was measured by recording N_2 sorption isotherms at 77 K (Figures 2g−2i and Figures S5a−S5o). A permanent porosity was observed for all COFs (1−9) with a maximum area up to ∼1238 m^2/g (Table S1). The pore size distribution profiles indicate that these COFs are largely

https://doi.org/10.1021/acsbiomaterials.4c00351
ACS Biomater. Sci. Eng. XXXX, XXX, XXX−XXX

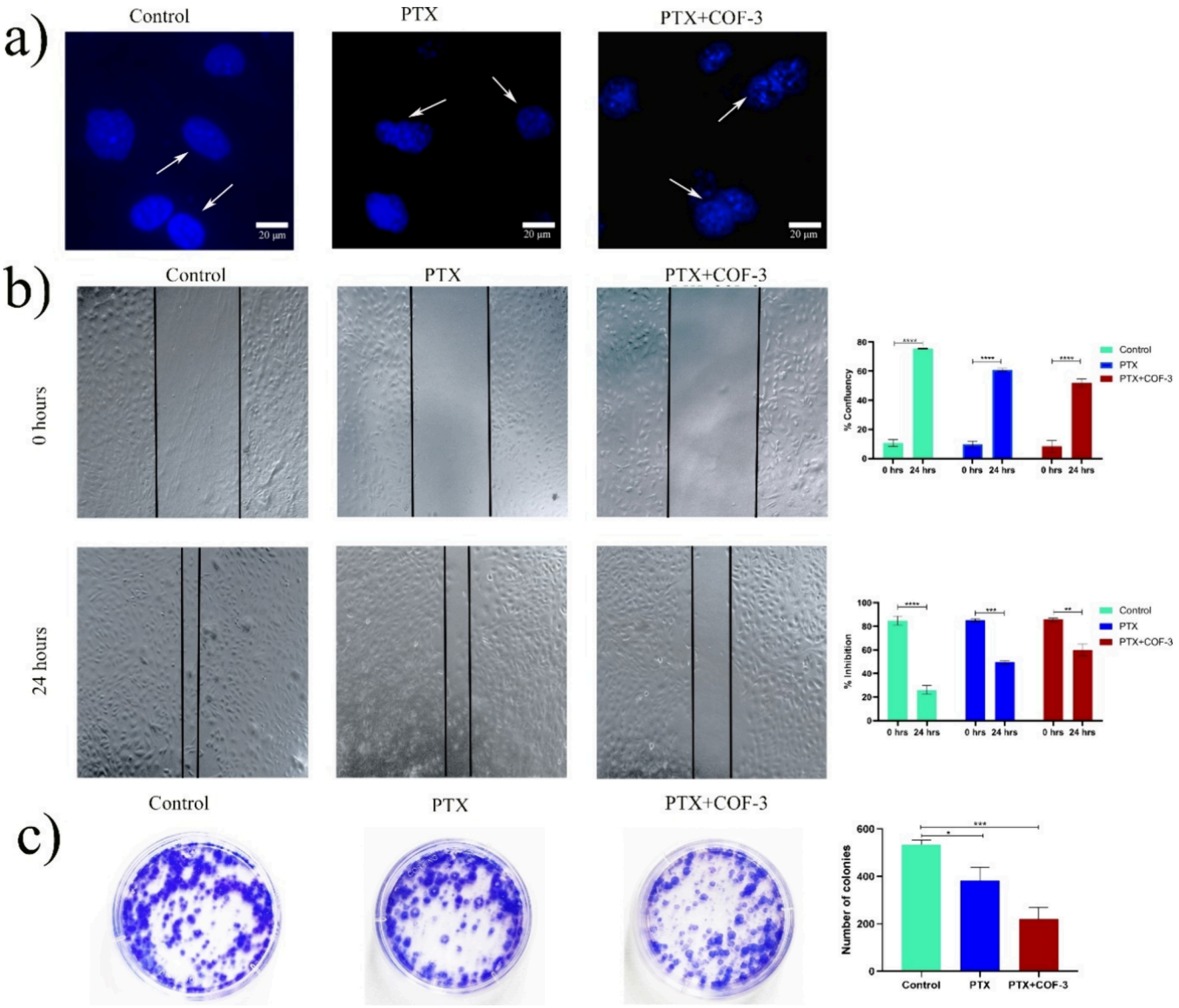

Figure 4. (a) Morphological changes with abnormal cellular morphology and fragmented nucleus observed under PTX@COF-3 treatment as compared to control and PTX treatment alone. (b) The confluency percentage after 24 h of treatment was lowest in PTX@COF-3, and the inhibition percent was maximum in PTX@COF-3. (c) The colony formation was maximum in the control and lowest in the combination dose treatment. $^{**}P < 0.005$, $^{****}P < 0.0001$.

microporous in nature. FE-SEM analysis of samples of COFs (1−9) revealed their morphological characteristics (Figure 2j and Figure S6). A thorough literature survey indicated only a few reports of imine-functionalized COFs whose biomedical applications were explored. Motivated by these reports, crystalline COFs (1−9) having ample imine linkages and high surface areas were explored as potential anticancer drug carrier agents. Specifically, the ability of COFs (1−9) to deliver paclitaxel (PTX) was studied in detail (Section S3).

In this context, PTX was chosen as the drug molecule since it is known to be effective for the treatment of various cancers including OvCa. In the process of loading COFs (1−9) with the drug, pristine samples of COFs were suspended in a solution of PTX. The cytotoxic effects of PTX-loaded samples of COFs (PTX@COFs) are presented in Figure 3a. Among the nine COFs (1−9) examined for their role in enhancing the cytotoxicity of PTX, it was observed that PTX@COF-3 was most potent in the set of all PTX@COFs with an IC_{50} value of 1.9 μM. On the other hand, under the same conditions, the IC_{50} value of PTX was higher at 2.6 μM.

The MTT assay revealed that increase in the concentration of PTX resulted in decreased cell viability, as expected. Surprisingly, the cell viability reduced to a greater extent with increasing drug concentration when cells were exposed to PTX@COF-3. The dose-dependent cell viability percentage was estimated under three conditions: (a) control, (b) PTX treated, and (c) PTX + COF-3 treated samples. These experiments revealed that there were nonsignificant differences in the percentage cell viability between PTX and PTX@COF-3 treated cells when the drug (PTX) concentration was low (0.1 μM). However, at higher concentrations of PTX loading in COF-3, a more pronounced decrease in cell viability was observed in case of PTX + COF-3 treated cells relative to the experiment in which cells were treated with only PTX (Figure 3b). The drug carrier polymer (COF-3) itself did not show any significant effect on the viability of the cells (Figure 3c). The

https://doi.org/10.1021/acsbiomaterials.4c00351
ACS Biomater. Sci. Eng. XXXX, XXX, XXX−XXX

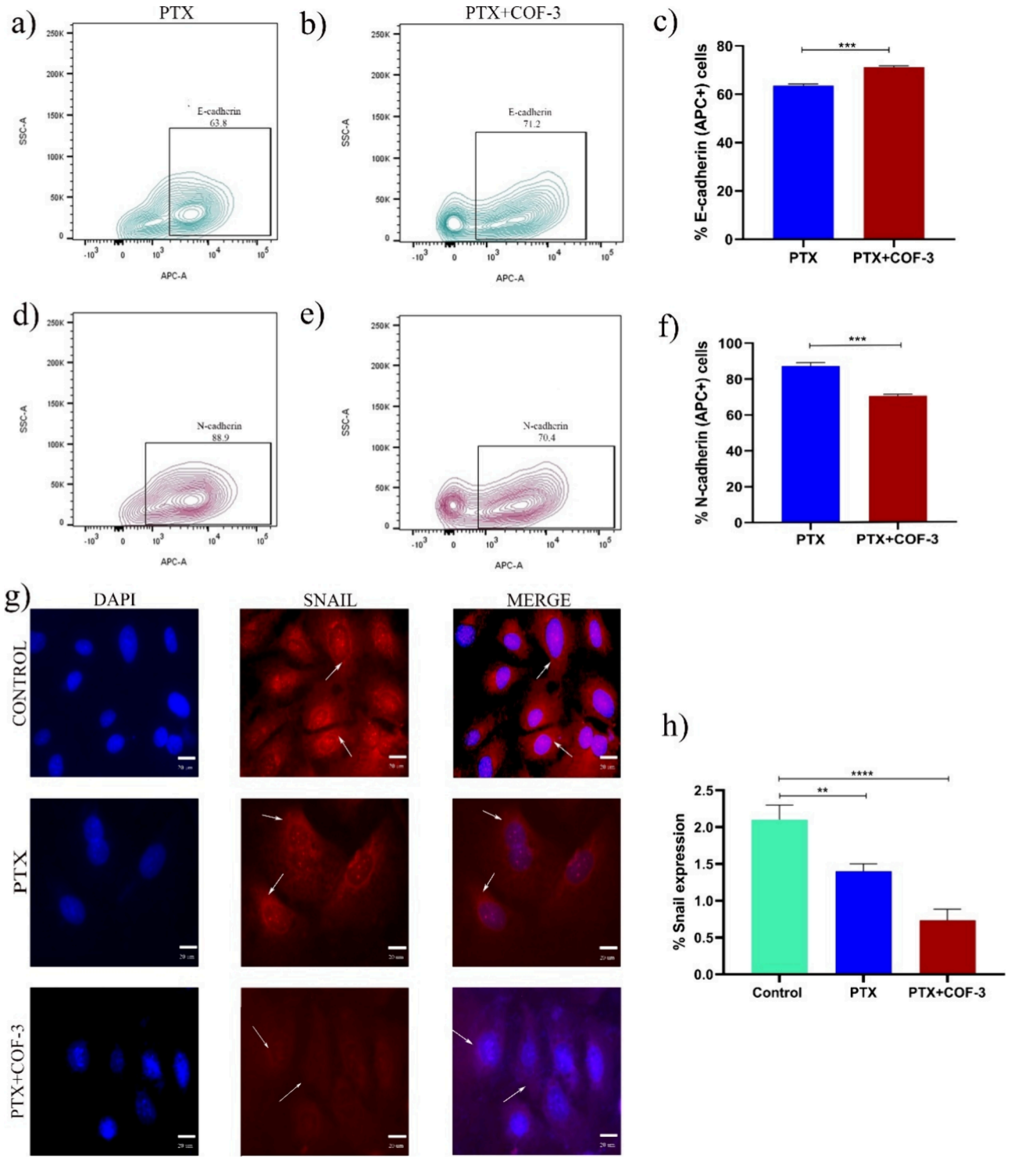

Figure 5. Expression of EMT markers and expression of transcription factor Snail. (a–c) E-cad positive cells are increased in the combination treatment. (d–f) N-cad positive cells are increased in the combination treatment. $^{**}P < 0.005$, $^{****}P < 0.0001$. (g) Cytoplasmic and nuclear localization of Snail is maximum in the control as compared to PTX alone and exhibits the least expression in the combination group. (h) Graphical representation of the expression of Snail. $^{**}P < 0.005$, $^{****}P < 0.0001$.

drug uptake analysis revealed that with an increase in incubation time, there is a significant increase in uptake of the PTX@COF-3 and a subsequent decrease in residual drug (Figures 3d and 3e). A comparison chart of different PTX-loaded COFs has been supplemented in Table S2.

Morphological analysis indicated nuclear fragmentation when cells were treated with PTX. On the other hand, appreciable distortion in the shape of the nucleus along with fragmentation was observed for the cells that were treated with PTX-loaded COF-3 (PTX@COF-3 in Figure 4a). Subsequently, the rate of cell migration was determined in the presence of PTX@COF-3. After 24 h, it was observed that the untreated (control) cells migrated fastest, followed by cells treated with PTX (only). Under the same conditions, the rate

https://doi.org/10.1021/acsbiomaterials.4c00351
ACS Biomater. Sci. Eng. XXXX, XXX, XXX−XXX

of cell migration was slowest in the case of cells treated with PTX@COF-3, as depicted in Figure 4b, wherein the % wound area was significantly higher relative to the other two experiments (untreated cells and PTX-treated cells) with $P < 0.0001$. Furthermore, much fewer colonies of SKOV-3 cells were formed under the dose treatment of PTX@COF-3 relative to those observed for cells treated with PTX and control experiments (Figure 4c). Interestingly, PTX@COF-3 did not show any cytotoxic effect against normal cells as compared with PTX (Figure S7). A comparison chart of IC_{50} values of COFs loaded with PTX has been listed in Table S1.

For evaluating the role of the drug carrier COFs on the EμT markers, flow cytometry analyses were performed. It was clearly observed that PTX-loaded COFs (PTX@COFs) displayed enhanced efficacy relative to PTX (Supplementary S1). For example, increased expression of E-cad (Figures 5a−5c) and decreased the expression of N-cad (Figures 5d−5f) were observed in case of PTX@COF-3 in comparison to PTX alone with a significance of $P = 0.0002$ and $P = 0.0001$, respectively. From these experiments, it was also concluded that the mesenchymal properties of the cells were depleted upon treatment (with PTX@COF-3 or only PTX) and the epithelial characteristics of the cells were restored. To understand the effect of the transcription factor Snail, fluorescence assays were performed to identify its expression. Surprisingly, a higher decrease in the expression of Snail was observed in case of the PTX@COF-3 treated sample ($P = 0.0007$) relative to the control PTX ($P = 0.008$) alone, both in the nucleus and the cytoplasm of the cells (Figures 5g and 5h).

Further, the MTT assay indicated that COF-3 decreased the IC_{50} value of PTX when in combination, thus increasing the cytotoxicity level of the drug. This result led us to propose that COF-3 is a potent carrier of PTX such that it delivers the anticancer drug more efficiently to the cancer cells, which in turn minimizes the tumorigenic properties of the ovarian cancer cells. Upon deriving the dose value in combination, further experiments were performed to analyze the effect of the carrier carried drug. Dose-dependent studies were performed to understand the effect of the PTX delivered by PTX@COFs. Interestingly, a retarded migration of cells was observed in the presence of PTX@COF-3 relative to experiments involving either untreated SKOV-3 or PTX treated SKOV-3 cells. These data again suggested that the COF-3 played a vital role in enhancing the potency of PTX (as a drug molecule) via a relatively higher reduction in metastasis events. It is reported in the literature that a loss of E-cad is associated with poor prognosis of the disease.[52] Therefore, the expression of E-cad was checked in the presence of PTX@COF-3. The results indicated that E-cad expression increased considerably in the PTX@COF-3 treated cells compared to the PTX treated cells. However, a reverse trend was observed in N-cad expression studies using PTX and PTX@COF-3 treated cells. Specifically, the highest decrease in N-cad expression was observed in the case of PTX@COF-3 treated cells. These experimental results motivated us to revisit the transcriptional status while analyzing the expression of Snail. It is well-known that the transcriptional factor is an important parameter that induces the process of EMT by negatively regulating E-cad and positively modulating the expression of N-cad.[53] Interestingly, our experimental results corroborated with the previously reported results since localization of Snail in both the cytosolic part as well as in the nucleus of the cancer cells decreased to the highest extent upon treatment with PTX@COF-3. Generally, cytoplasmic Snail has a short half-life, as it is a target for ubiquitin-mediated proteasome degradation by GSK-3β-induced phosphorylation. Thus, these translocate to the nucleus to exert its function.[54] Based on these facts, it can be proposed that the treatment of cells with PTX@COF-3 increases the phosphorylation of Snail, which in turn decreases its half-life and mitigates the translocation of Snail to the nucleus to perform its activity of regulating the EMT markers. Our results also confirmed that Snail transcriptionally regulates the EMT markers, and upon treatment of cancer cells with PTX@COF-3, the initiation of metastasis is strongly inhibited. Thus, PTX@COF-3 can be considered a potential candidate for sarcoma therapy via inhibition of metastasis.

Herein, facile synthesis (metal-free) and characterization of a set of nine covalent organic frameworks (COFs 1−9) have been described. The obtained COFs (1−9) have a well-defined nanoporous structure, which makes these materials suitable for hosting guest molecules. For the first time, this article describes the loading of COFs with paclitaxel, a chemotherapeutic agent suitable for the treatment of various cancers. Detailed studies indicate that a paclitaxel (PTX)-loaded COF (PTX@COF-3) is much more effective than the drug (PTX) itself in inhibiting metastasis. This work demonstrates the potential of COFs as efficient drug delivery agents, thereby opening up new opportunities in the field of sarcoma therapy. The effective demonstration of the biological applicability of COFs attempts to cover a significant gap and encourages others to further explore the applicability of COFs for the treatment of cancer.

■ ASSOCIATED CONTENT

Supporting Information

The Supporting Information is available free of charge at https://pubs.acs.org/doi/10.1021/acsbiomaterials.4c00351.

Materials, instruments, and methods; detailed synthetic procedures to obtain precursors and COFs; characterization data of monomers and COFs; and cell viability of HaCaT cells and references (PDF)

■ AUTHOR INFORMATION

Corresponding Authors

Nabanita Chatterjee − *Receptor Biology and Tumor Metastasis, Chittaranjan National Cancer Institute, Kolkata 700 026, India*; Email: nabanita.chatterje@yahoo.com

Neeladri Das − *Department of Chemistry, Indian Institute of Technology Patna, Patna 801106 Bihar, India*; orcid.org/0000-0003-3476-1097; Email: neeladri@iitp.ac.in, neeladri2002@yahoo.co.in

Authors

Atikur Hassan − *Department of Chemistry, Indian Institute of Technology Patna, Patna 801106 Bihar, India; Functional Materials Group, Gulf University for Science and Technology, Mubarak Al-Abdullah 32093, Kuwait*; orcid.org/0000-0002-4048-6952

Sraddhya Roy − *Receptor Biology and Tumor Metastasis, Chittaranjan National Cancer Institute, Kolkata 700 026, India*

Ananya Das − *Receptor Biology and Tumor Metastasis, Chittaranjan National Cancer Institute, Kolkata 700 026, India*

https://doi.org/10.1021/acsbiomaterials.4c00351
ACS Biomater. Sci. Eng. XXXX, XXX, XXX−XXX

Sk Abdul Wahed − *Department of Chemistry, Indian Institute of Technology Patna, Patna 801106 Bihar, India;* orcid.org/0009-0009-3200-566X

Aparajita Bairagi − *Receptor Biology and Tumor Metastasis, Chittaranjan National Cancer Institute, Kolkata 700 026, India*

Subhadip Mondal − *Department of Chemistry, Indian Institute of Technology Patna, Patna 801106 Bihar, India;* orcid.org/0009-0002-1730-4847

Complete contact information is available at: https://pubs.acs.org/10.1021/acsbiomaterials.4c00351

Notes

The authors declare no competing financial interest.

■ ACKNOWLEDGMENTS

N.D. and S.M. thank IIT Patna for providing research infrastructure and facilities. A.H. and S.A.W. thank IIT Patna for an Institute Research Fellowship. The authors acknowledge SAIF-IIT Patna for providing access to the solid-state NMR facility. N.C., S.R., A.D., and A.B. thank Chittaranjan National Cancer Institute for providing research facilities.

■ REFERENCES

(1) Lujambio, A.; Lowe, S. W. The microcosmos of cancer. *Nature* **2012**, *482* (7385), 347−355.

(2) Armitage, P.; Doll, R. The age distribution of cancer and a multi-stage theory of carcinogenesis. *Br. J. Cancer* **2004**, *91* (12), 1983−1989.

(3) Tulchinsky, T. H.; Varavikova, E. A. Chapter 16 - Global Health. In *The New Public Health*, 3rd ed.; Tulchinsky, T. H., Varavikova, E. A. Eds.; Academic Press, 2014; pp 821−866.

(4) Torre, L. A.; Trabert, B.; DeSantis, C. E.; Miller, K. D.; Samimi, G.; Runowicz, C. D.; Gaudet, M. M.; Jemal, A.; Siegel, R. L. Ovarian cancer statistics, 2018. *CA: A Cancer Journal for Clinicians* **2018**, *68* (4), 284−296.

(5) Meng, C.; Sun, Y.; Liu, G. Establishment of a prognostic model for ovarian cancer based on mitochondrial metabolism-related genes. *Frontiers in Oncology* **2023**, *13*, 1144430.

(6) Lengyel, E. Ovarian Cancer Development and Metastasis. *American Journal of Pathology* **2010**, *177* (3), 1053−1064.

(7) Lheureux, S.; Gourley, C.; Vergote, I.; Oza, A. Epithelial ovarian cancer. *The Lancet* **2019**, *393* (10177), 1240−1253.

(8) Siegel, R. L.; Miller, K. D.; Jemal, A. Cancer statistics, 2019. *CA: a cancer journal for clinicians* **2019**, *69* (1), 7−34.

(9) Penny, S. M. Ovarian cancer: an overview. *Radiologic technology* **2020**, *91* (6), 561−575.

(10) Yeung, T.-L.; Leung, C. S.; Yip, K.-P.; Au Yeung, C. L.; Wong, S. T.; Mok, S. C. Cellular and molecular processes in ovarian cancer metastasis. A review in the theme: cell and molecular processes in cancer metastasis. *American Journal of Physiology-Cell. Physiology* **2015**, *309* (7), C444−C456.

(11) Cho, A.; Howell, V. M.; Colvin, E. K. The extracellular matrix in epithelial ovarian cancer−a piece of a puzzle. *Frontiers in oncology* **2015**, *5*, 245.

(12) Hynes, R. O.; Naba, A. Overview of the matrisome—an inventory of extracellular matrix constituents and functions. *Cold Spring Harbor perspectives in biology* **2012**, *4* (1), No. a004903.

(13) Bonnans, C.; Chou, J.; Werb, Z. Remodelling the extracellular matrix in development and disease. *Nat. Rev. Mol. Cell Biol.* **2014**, *15* (12), 786−801.

(14) Yu, W.; Yang, L.; Li, T.; Zhang, Y. Cadherin Signaling in Cancer: Its Functions and Role as a Therapeutic Target. *Frontiers in Oncology* **2019**, *9*, 989.

(15) Davidson, B.; Trope, C. G.; Reich, R. Epithelial−Mesenchymal Transition in Ovarian Carcinoma. *Frontiers in Oncology* **2012**, *2*, n/a.

(16) Pastushenko, I.; Blanpain, C. EMT Transition States during Tumor Progression and Metastasis. *Trends in Cell Biology* **2019**, *29* (3), 212−226.

(17) Marchini, S.; Fruscio, R.; Clivio, L.; Beltrame, L.; Porcu, L.; Nerini, I. F.; Cavalieri, D.; Chiorino, G.; Cattoretti, G.; Mangioni, C.; et al. Resistance to platinum-based chemotherapy is associated with epithelial to mesenchymal transition in epithelial ovarian cancer. *Eur. J. Cancer* **2013**, *49* (2), 520−530.

(18) Teeuwssen, M.; Fodde, R. Wnt Signaling in Ovarian Cancer Stemness, EMT, and Therapy Resistance. *Journal of Clinical Medicine* **2019**, *8* (10), 1658.

(19) Das, S. K.; Roy, S.; Das, A.; Chowdhury, A.; Chatterjee, N.; Bhaumik, A. A conjugated 2D covalent organic framework as a drug delivery vehicle towards triple negative breast cancer malignancy. *Nanoscale Advances* **2022**, *4* (10), 2313−2320.

(20) Scicluna, M. C.; Vella-Zarb, L. Evolution of Nanocarrier Drug-Delivery Systems and Recent Advancements in Covalent Organic Framework−Drug Systems. *ACS Applied Nano Materials* **2020**, *3* (4), 3097−3115.

(21) Zhang, L.; Yang, L.-L.; Wan, S.-C.; Yang, Q.-C.; Xiao, Y.; Deng, H.; Sun, Z.-J. Three-Dimensional Covalent Organic Frameworks with Cross-Linked Pores for Efficient Cancer Immunotherapy. *Nano Lett.* **2021**, *21* (19), 7979−7988.

(22) Khan, N.; Slathia, G.; Kaliya, K.; Saneja, A. Recent progress in covalent organic frameworks for cancer therapy. *Drug Discovery Today* **2023**, *28* (6), 103602.

(23) Hu, L.; Lv, Y. Covalent organic framework-based nanoplatforms with tunable mechanical properties for drug delivery and cancer therapy. *Mechanobiology in Medicine* **2023**, *1* (2), No. 100024.

(24) Singh, N.; Son, S.; An, J.; Kim, I.; Choi, M.; Kong, N.; Tao, W.; Kim, J. S. Nanoscale porous organic polymers for drug delivery and advanced cancer theranostics. *Chem. Soc. Rev.* **2021**, *50* (23), 12883−12896.

(25) Shao, Y.; Liu, B.; Di, Z.; Zhang, G.; Sun, L.-D.; Li, L.; Yan, C.-H. Engineering of Upconverted Metal−Organic Frameworks for Near-Infrared Light-Triggered Combinational Photodynamic/Chemo-/Immunotherapy against Hypoxic Tumors. *J. Am. Chem. Soc.* **2020**, *142* (8), 3939−3946.

(26) Singh, N.; Won, M.; Xu, Y.; Yoon, C.; Yoo, J.; Li, M.; Kang, H.; Kim, J. S. Covalent organic framework nanoparticles: Overcoming the challenges of hypoxia in cancer therapy. *Coord. Chem. Rev.* **2024**, *499*, 215481.

(27) Huang, N.; Wang, P.; Jiang, D. Covalent organic frameworks: a materials platform for structural and functional designs. *Nature Reviews Materials* **2016**, *1* (10), 16068.

(28) Mitra, S.; Kandambeth, S.; Biswal, B. P.; Khayum, M. A.; Choudhury, C. K.; Mehta, M.; Kaur, G.; Banerjee, S.; Prabhune, A.; Verma, S.; et al. Self-Exfoliated Guanidinium-Based Ionic Covalent Organic Nanosheets (iCONs). *J. Am. Chem. Soc.* **2016**, *138* (8), 2823−2828.

(29) Mitra, S.; Sasmal, H. S.; Kundu, T.; Kandambeth, S.; Illath, K.; Díaz Díaz, D.; Banerjee, R. Targeted Drug Delivery in Covalent Organic Nanosheets (CONs) via Sequential Postsynthetic Modification. *J. Am. Chem. Soc.* **2017**, *139* (12), 4513−4520.

(30) Kumar Mahato, A.; Pal, S.; Dey, K.; Reja, A.; Paul, S.; Shelke, A.; Ajithkumar, T. G.; Das, D.; Banerjee, R. Covalent Organic Framework Cladding on Peptide-Amphiphile-Based Biomimetic Catalysts. *J. Am. Chem. Soc.* **2023**, *145* (23), 12793−12801.

(31) Paul, S.; Gupta, M.; Kumar Mahato, A.; Karak, S.; Basak, A.; Datta, S.; Banerjee, R. Covalent Organic Frameworks for the Purification of Recombinant Enzymes and Heterogeneous Biocatalysis. *J. Am. Chem. Soc.* **2024**, *146* (1), 858−867.

(32) Guiyang, Z. Applications of Covalent Organic Frameworks (COFs) in Oncotherapy. In *Covalent Organic Frameworks*; Yanan, G., Fei, L. Eds.; IntechOpen, 2022.

(33) Shi, Y.; Yang, J.; Gao, F.; Zhang, Q. Covalent Organic Frameworks: Recent Progress in Biomedical Applications. *ACS Nano* **2023**, *17* (3), 1879−1905.

(34) Mehvari, F.; Ramezanzade, V.; Asadi, P.; Singh, N.; Kim, J.; Dinari, M.; Kim, J. S. A panoramic perspective of recent progress in 2D and 3D covalent organic frameworks for drug delivery. *Aggregate* **2024**, *5* (2), No. e480.
(35) Ge, L.; Qiao, C.; Tang, Y.; Zhang, X.; Jiang, X. Light-Activated Hypoxia-Sensitive Covalent Organic Framework for Tandem-Responsive Drug Delivery. *Nano Lett.* **2021**, *21* (7), 3218−3224.
(36) Bai, L.; Phua, S. Z. F.; Lim, W. Q.; Jana, A.; Luo, Z.; Tham, H. P.; Zhao, L.; Gao, Q.; Zhao, Y. Nanoscale covalent organic frameworks as smart carriers for drug delivery. *Chem. Commun.* **2016**, *52* (22), 4128−4131.
(37) Waller, P. J.; Gándara, F.; Yaghi, O. M. Chemistry of Covalent Organic Frameworks. *Acc. Chem. Res.* **2015**, *48* (12), 3053−3063.
(38) Sasmal, H. S.; Aiyappa, H. B.; Bhange, S. N.; Karak, S.; Halder, A.; Kurungot, S.; Banerjee, R. Superprotonic Conductivity in Flexible Porous Covalent Organic Framework Membranes. *Angew. Chem., Int. Ed.* **2018**, *57* (34), 10894−10898.
(39) Khayum, M. A.; Vijayakumar, V.; Karak, S.; Kandambeth, S.; Bhadra, M.; Suresh, K.; Acharambath, N.; Kurungot, S.; Banerjee, R. Convergent Covalent Organic Framework Thin Sheets as Flexible Supercapacitor Electrodes. *ACS Appl. Mater. Interfaces* **2018**, *10* (33), 28139−28146.
(40) Karak, S.; Dey, K.; Torris, A.; Halder, A.; Bera, S.; Kanheerampockil, F.; Banerjee, R. Inducing Disorder in Order: Hierarchically Porous Covalent Organic Framework Nanostructures for Rapid Removal of Persistent Organic Pollutants. *J. Am. Chem. Soc.* **2019**, *141* (18), 7572−7581.
(41) Hassan, A.; Mollah, M. M. R.; Das, S.; Das, N. Rapid and selective removal of toxic and radioactive anionic pollutants using an ionic covalent organic framework (iCOF-2). *Journal of Materials Chemistry A* **2023**, *11* (32), 17226−17236.
(42) Nayak, S.; Hassan, A.; Das, N.; Das, P. Carbon dot-based superhydrophobic modification of a covalent organic framework for oil-in-water emulsion separation. *Chem. Commun.* **2023**, *59* (55), 8548−8551.
(43) Ding, S.-Y.; Wang, W. Covalent organic frameworks (COFs): from design to applications. *Chem. Soc. Rev.* **2013**, *42* (2), 548−568.
(44) Geng, K.; He, T.; Liu, R.; Dalapati, S.; Tan, K. T.; Li, Z.; Tao, S.; Gong, Y.; Jiang, Q.; Jiang, D. Covalent Organic Frameworks: Design, Synthesis, and Functions. *Chem. Rev.* **2020**, *120* (16), 8814−8933.
(45) Kandambeth, S.; Dey, K.; Banerjee, R. Covalent Organic Frameworks: Chemistry beyond the Structure. *J. Am. Chem. Soc.* **2019**, *141* (5), 1807−1822.
(46) Alam, A.; Kumbhakar, B.; Chakraborty, A.; Mishra, B.; Ghosh, S.; Thomas, A.; Pachfule, P. Covalent Organic Frameworks for Photocatalytic Hydrogen Peroxide Generation. *ACS Materials Letters* **2024**, *6*, 2007−2049.
(47) Rathi, P.; Chowdhury, S.; Das, P. P.; Keshri, A. K.; Chaudhary, A.; Siril, P. F. Pore-interface engineering improves doxorubicin loading to triazine-based covalent organic framework. *Materials Advances* **2024**, *5* (1), 136−142.
(48) Pramanik, M.; Chatterjee, N.; Das, S.; Saha, K. D.; Bhaumik, A. Anthracene-bisphosphonate based novel fluorescent organic nanoparticles explored as apoptosis inducers of cancer cells. *Chem. Commun.* **2013**, *49* (82), 9461−9463.
(49) Ning, G.-H.; Chen, Z.; Gao, Q.; Tang, W.; Chen, Z.; Liu, C.; Tian, B.; Li, X.; Loh, K. P. Salicylideneanilines-Based Covalent Organic Frameworks as Chemoselective Molecular Sieves. *J. Am. Chem. Soc.* **2017**, *139* (26), 8897−8904.
(50) Chen, Y.; Luo, X.; Zhang, J.; Hu, L.; Xu, T.; Li, W.; Chen, L.; Shen, M.; Ren, S.-B.; Han, D.-M.; et al. Bandgap engineering of covalent organic frameworks for boosting photocatalytic hydrogen evolution from water. *Journal of Materials Chemistry A* **2022**, *10* (46), 24620−24627.
(51) Li, X.; Gao, Q.; Aneesh, J.; Xu, H.-S.; Chen, Z.; Tang, W.; Liu, C.; Shi, X.; Adarsh, K. V.; Lu, Y.; et al. Molecular Engineering of Bandgaps in Covalent Organic Frameworks. *Chem. Mater.* **2018**, *30* (16), 5743−5749.
(52) Faleiro-Rodrigues, C.; Macedo-Pinto, I.; Pereira, D.; Lopes, C. Prognostic value of E-cadherin immunoexpression in patients with primary ovarian carcinomas. *Annals of oncology* **2004**, *15* (10), 1535−1542.
(53) Hao, L.; Ha, J.; Kuzel, P.; Garcia, E.; Persad, S. Cadherin switch from E-to N-cadherin in melanoma progression is regulated by the PI3K/PTEN pathway through Twist and Snail. *British Journal of Dermatology* **2012**, *166* (6), 1184−1197.
(54) Yang, Z.; Rayala, S.; Nguyen, D.; Vadlamudi, R. K.; Chen, S.; Kumar, R. Pak1 phosphorylation of snail, a master regulator of epithelial-to-mesenchyme transition, modulates snail's subcellular localization and functions. *Cancer research* **2005**, *65* (8), 3179−3184.

https://doi.org/10.1021/acsbiomaterials.4c00351
ACS Biomater. Sci. Eng. XXXX, XXX, XXX−XXX

NJC

ROYAL SOCIETY OF CHEMISTRY

PAPER

View Article Online
View Journal | View Issue

Cite this: *New J. Chem.*, 2023, **47**, 18835

Therapeutic potential of Ag(I)–, Au(I)–, and Au(III)–NHC complexes of 3-pyridyl wingtip N-heterocyclic carbenes (NHCs) against lung cancer†

Prafulla K Behera,[a] Lakshmikanta Maity,[a] Sraddhya Roy,[b] Ananya Das,[b] Priyanka Sahu,[a] Hemanta K. Kisan,[ac] Avtar Changotra,[d] Anvarhusein A. Isab,[e] Mohammed Benyounes Fettouhi,[e] Aparajita Bairagi,[b] Nabanita Chatterjee*[b] and Joydev Dinda*[a]

Received 22nd June 2023,
Accepted 18th September 2023

DOI: 10.1039/d3nj02882h

rsc.li/njc

Herein, we report the easy synthetic approaches, structural features, theoretical studies, and extensive bioactivity of $[Ag(1)_2][PF_6]$ (**2**), $[Au(1)_2][PF_6]$ (**3**), and $[Au(1)Cl_3]$ (**4**) compounds prepared from the NHC precursor 3-[(pyridin-3-yl)]imidazo[1,5-*a*]pyridin-4-ylium hexafluorophosphate (**1**·HPF_6). All the compounds were prepared and characterized by employing various spectroscopic techniques. The geometry of Au(I) complex, **3**, was further confirmed using single-crystal X-ray diffraction (SCXRD) studies. DFT studies were performed to optimize the geometry and gain insights into the structure. The new compounds were implicated in studying their anti-oncogenic role in the most prevalent lung cancer. Anti-proliferative properties and very outstanding cytotoxicity were observed against various cancer cell lines but high potency towards lung cancer cells (A549) was observed. An MTT (3-[4,5-dimethylthiazol-2-yl]-2,5-diphenyl tetrazolium bromide) assay of the drugs revealed their cytotoxicity and further study revealed that the drug plays a pivotal role in the mitochondrial reactive oxygen species (ROS)-dependent intrinsic apoptotic pathway. These studies widened the array of bioactive organometallics and revealed the remarkable efficacy of such compounds in solving therapeutic challenges.

Introduction

N-Heterocyclic carbenes (NHCs) have gained research interest owing to their unique properties[1] as compared to the conventional phosphine- and nitrogen-based ligands. NHCs are powerful σ-donors, and hence, these M–NHC complexes are more stable towards atmosphere and heat[2] than the previously widely used phosphine complexes. Nowadays, research is focused on NHCs containing various wingtip moieties called weak donor-functionalized NHCs. Indeed, various wingtips, such as pyridine,[3] pyrimidines,[4] pyrazoles,[5] and phenanthroline[6] moieties, can be smoothly blended with the NHC systems to process bischelating,[7] pincer,[8] tripodal,[9] or bridging NHC ligands,[10] which show superior catalytic,[11] photophysical,[12] and biomedical activities[13] to non-wingtip NHC ligands.[14] The study of coinage M–NHC complexes is now a promising research area owing to their various applications. Among them, Ag(I)–NHC is mainly used in (a) the preparation of other M–NHC complexes *via* transmetallation pathway, (b) catalysis-like ring-opening polymerization (ROP) reaction, (c) biomedical field, *e.g.* antimicrobial, antibacterial, and anticancer activity, and (d) preparation of Ag nanomaterials.[15] The dissociation energy study of the coinage M–NHC complex shows strong M–NHC bonds in the order of gold(I) > copper(I) > silver(I).[16] This study also proved the utilization of Ag(I)–NHCs for the synthesis of other coinage M–NHC complexes. Recent studies have revealed silver(I)–NHC complexes to be very effective against various drug-resistant pathogens.[17] Youngs and others have reported that silver(I)–NHCs are good candidates in anticancer and antibacterial applications.[17] Biver reported the anticancer activities of

[a] *Department of Chemistry, Utkal University, Bhubaneswar-751004, Odisha, India. E-mail: joydevdinda@utkaluniversity.ac.in, joydevdinda@gmail.com*
[b] *Department of Receptor Biology and Tumor Metastasis, Chittaranjan National Cancer Institute, Kolkata-700026, West Bengal, India. E-mail: nabanita.chatterje@yahoo.com*
[c] *Department of Chemistry, Indian Institute of Technology Bhilai, Raipur-492015, (C.G.), India*
[d] *School of Science, Department of Chemistry, Cluster University of Jammu, Jammu-180001, India*
[e] *Department of Chemistry, King Fahd University of Petroleum and Minerals, Dhahran 31261, Saudi Arabia*

† Electronic supplementary information (ESI) available. Crystallographic data for complexes **1**·HPF_6 (CCDC no. 1898678) and **3** (CCDC no. 1897575). For ESI and crystallographic data in CIF or other electronic format see DOI: https://doi.org/10.1039/d3nj02882h

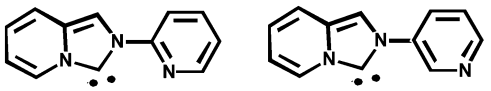

Chart 1 Advancement of 2-pyridyl to 3-pyridyl wingtip NHCs.

Cu(I), Ag(I), Au(I), and Au(III)–NHC complexes comprising mono- and bis-carbenes.[15b] Eloy *et al.* reported a panel of Ag(I)–NHCs that are very potent against various cancer cell lines.[15c] Recent studies by Youngs and others have shown that Ag-NHCs are useful in antibacterial and anticancer applications.[15d] Many silver(I) complexes show a common working principle *via* the extrication of Ag^+ ions that go through the cell membranes and destroy their functions. Unfortunately, the rapid delivery of silver ions is an ongoing challenge that reduces the effectiveness of silver(I)-based drugs. However, this restriction may be overcome by the application of N-heterocyclic carbenes, as they bind strongly to metals[18] and slowly release the metal (Chart 1).

Not only silver but other invaluable metals have also been used in the biomedical field in recent times. Gold is an eminent illustration, which is used for centuries in various Chinese medicines. For example, auranofin (Ridaura), sodium aurothiomalate (Myocrisin), and aurothioglucose (Solganal) are economically accessible and clinically assayed.[19a] The gold(I)–phosphine compound, auranofin, was primarily created as an anti-rheumatic candidate, but later it was used as an anticancer agent. Berners-Price and Barnard obtained excellent results against mouse cancer cells using an Au(I)–NHC complex.[19b] Panda and Ghosh also successfully developed an Au(I)–NHC complex that exhibited excellent efficiency against HeLa cell proliferation.[19c] Gold(I)–NHCs show better antibacterial activity than silver(I)–NHCs, due to their higher electron density at the gold(I) center.

The widespread use of gold and gold(I) complexes is reported in the literature[20] but only a few analogous gold(III) complexes are explained. It is assumed that high electrophilicity in the gold(III) compounds may pursue biological functionalities under similar environments.[17] Gold(III) is isoelectronic with platinum(II), both possessing square planar geometries in most of the cases, hence like cisplatin, we can also predict the biological efficiency of gold(III)–NHCs. Furthermore, the problems frequently faced by cisplatin, like nephrotoxicity and others, may be decreased by the utilization of properly schemed gold(III)–NHC drugs.[21]

Lung cancer is a vital reason for cancer-associated deaths globally. Approximately 1.8 million deaths in 2020 were caused by lung cancer, which accounts for 18%, *i.e.* one in five of most cancer-related deaths[22a] with only a 10–20% 5 year survival rate.[22b] Lung cancer has been sub-classed into two broad categories: non-small cell lung cancer (NSCLC) and small cell lung cancer (SCLC), where NSCLCs constitute 85% of the lung cancer prevalence.[23] NSCLCs have been further classified into squamous-cell carcinoma (25–30%), adenocarcinoma (40%), and large-cell carcinoma (5–10%), where adenocarcinoma is the most common type creating havoc among the affected individuals.[23] The incredibly high metastatic nature of lung cancer accounts for the poor prognosis of the disease. Moreover, the appearance of clinical symptoms at an advanced stage contributes to the unfavourable outcome of the disease where there exists a high risk of developing resistance to the conventional drugs being used for treating the disease.[24] Chemotherapy and radiation resistance can be caused in part by faulty apoptotic signaling.[25] One of the important factors associated with the lung cancer progression is the programmed cell death mechanism, apoptosis. Plasma membrane blebbing, cell shrinkage, chromatin condensation/fragmentation, and cell break down into apoptotic bodies are the outcomes of apoptosis, which occur due to the pivotal roles played by caspases, a group of cystein–aspartate enzymes. Caspases are categorized into 2 groups: initiator caspases (caspase-2, -8, -9, and -10 in human cells), which cleave and activate the second group, and the effector caspases (caspase-3, -6, and -7 in human cells), which subsequently undertake selective proteolysis.[26] Many anticancer drugs currently used show high toxicity against both the cancer cells and the normal cells, thus adding on ailments to the patients. Under these conditions, there exists an urge towards the development of drugs that are less toxic to the adjacent normal cells by the aid of chemical synthesis as well as derivatives from natural compounds. Thus, in this work, we evaluated the anti-cancer attributes of novel chemically synthesized compounds *in vitro* by exploring their roles in the apoptosis of lung cancer cells and the underlying mechanisms responsible for apoptosis.

Keeping in mind the biological application of various metal–NHC complexes, in this work we synthesized imidazo[1,5-*a*] pyridine-based NHC ligands. This type of NHC ligand is already established as a valuable class of ligand for various coinage metals, which are potent anticancer drugs,[27] and the activities of related compounds are shown in Fig. S0 (ESI†). On account of these studies, here we formulated 3-[(pyridin-3-yl)]imidazo [1,5-*a*]pyridin-4-ylium hexafluorophosphate (**1**·HPF_6), a proligand of NHC, containing a 3-pyridyl wingtip. We successfully prepared silver(I)–NHC, gold(I)–NHC, and gold(III)–NHCs. In order to test the oncogenic properties of these newly synthesized compounds, we evaluated the activities of all these compounds in three different cancer cells *in vitro* and analyzed their inhibition property. Depending on this analysis, we selected one compound, which lowers IC_{50}, and depending on the viability, we proceeded with the cancer cell that reflects viability at a minimum drug dose.

Results and discussion

Synthesis and spectroscopic characterization

The precursor 3-[(pyridin-3-yl)]imidazo[1,5-*a*]pyridin-4-ylium hexafluorophosphate, **1**·HPF_6, was prepared using the Schiff base 3-pyridyl-*N*-(2 pyridyl)methylamine, as described by our group.[28]

The silver(I)–NHC complex **2** was synthesized when the mixture of proligand **1**·HPF_6 and Ag_2O was stirred in an acetonitrile solvent in the dark for 4 h, as shown in Scheme 1. Excess

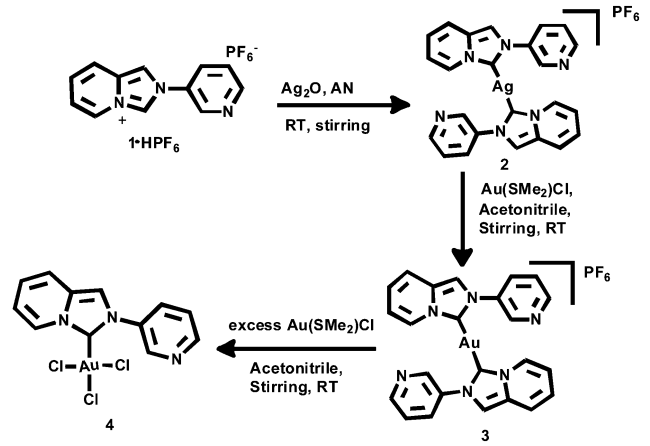

Scheme 1 Strategy of preparation of silver(I)–, gold(I)–, and gold(III)–NHC complexes 2, 3, and 4.

Ag_2O was eliminated through a plug of Celite. The solvent was collected and the solid was recrystallized from CH_3CN/Et_2O, and complex **2** obtained an 87% yield. The confirmation of complex **2** formation was ascertained as the dissipation of diagnostic imidazolium NC*H*N singlet signal corresponding to the imidazopyridine (10.38 ppm for **1**·HPF_6) in ^{1}H NMR spectroscopy (Fig. S1, ESI†). Additionally, a downfield shift of the corresponding carbene carbon N*C*N signal (171.9 ppm, shown in Fig. S2, ESI†) of complex **2** was observed compared to proligand **1**·HPF_6 (151.84 ppm) in the ^{13}C NMR spectroscopy, and a signal was recorded at *m*/*z* 498.27 assigned to binuclear species $[Ag(\mathbf{1})_2]^+$ (shown in Fig. S3, ESI†), confirming the formation of silver(I)–NHCs.

The conversion of this imidazolium salt-derived precursors to other groups of d^{10} metal complexes can easily be accomplished *via* the silver(I) carbene transmetallation process. Gold(I)–NHC complex, **3**, was obtained by a similar approach, as summarized in Scheme 1. Proligand **1**·HPF_6 and an excess amount of Ag_2O were stirred in a CH_3CN solvent in the darkness for 4 h. After that, unreacted Ag_2O was separated by filtration through a pack of Celite. Then, an acetonitrile solution of $[Au(Me_2S)Cl]$ was added dropwise to the filtrate and further stirred for 2 h. After that, the solution was filtered through a plug of Celite, concentrated, and then recrystallized from CH_3CN/Et_2O. Complex **3** was obtained in 80% yield. Similar to complex **2**, the formation of complex **3** was evidenced by the disappearance of the diagnostic imidazolium NC*H*N proton signal of imidazopyridine in the ^{1}H NMR spectrum (shown in Fig. S4, ESI†), in addition to the downfield shift of the N*C*N signal (172.5 ppm, shown in Fig. S5, ESI†) in the ^{13}C NMR spectrum (free ligand 151.84 ppm). In the case of gold(I)–NHC complex **3**, the carbene carbon N*C*N signal was shifted more downward than that of silver(I)–NHC complex **2**. Complex **3** was further characterized by mass spectroscopy. In complex **3**, a signal was reported at *m*/*z* 587.132, attributed to the binuclear species $[Au(\mathbf{1})_2]^+$ (shown in Fig. S6, ESI†). Following the established disproportionation process presented by our group,[29] the gold(III)–NHC complex **4** was prepared. When a clear colorless acetonitrile solution of gold(I)–NHC complex **3** was stirred with excess $Au(SMe_2)Cl$ in the darkness at room temperature for 6 h, affording the orange Au(III)–NHC complex **4** and a yellow precipitate of Au(0). The yellow precipitate of Au was isolated and reconverted into $Au(SMe_2)Cl$. The confirmation of complex **4** formation was indicated by the upfield shift of the carbenic carbon N*C*N signal (δ = 162.14 ppm) with respect to complex **3** in the ^{13}C NMR spectrum although the pattern of ^{1}H NMR spectrum was similar to that of complex **3** (shown in Fig. S7, ESI†). A similar up-field shift of the carbenic nucleus of the gold(III)–NHC complex (as presented in Fig. S8, ESI†) with respect to the gold(I)–NHC complex was observed previously.[29] This observation may be due to the greater Lewis acid nature of gold(III) compared to gold(I), as explained.[30] Proligand **1**·HPF_6 and complex **3** were also characterized by SCXRD. The X-ray diffraction standard single crystals were procured from the slow diffusion of diethyl ether into the saturated acetonitrile solution of respective compounds.

X-ray crystal structure description of proligand 1·HPF_6

The ORTEP view of the solid-state structure of proligand **1**·HPF_6 is presented in Fig. 1. The crystallographic parameters are presented in Table S1 (ESI†), and the selected bond distances and bond angles are given in Fig. 1. Proligand **1**·HPF_6 exhibited a monoclinic symmetry with the space group of *C*2/*c*. The mean C–N distance in the imidazolidine moiety of the NHC proligand is 1.36 Å and the imidazolidine N–C–N angle is 107.4°. In the crystal unit, the whole unit of proligand **1**·HPF_6 is not planar; the plane containing an annelated imidazole moiety of the NHC ligand makes an angle of 33.71° with the plane containing a 3-pyridyl wingtip moiety.

Structural description of complexes 2, 3, and 4

As we were unsuccessful in getting a single crystal of **2**, the configuration was established theoretically by DFT, which is presented in Fig. 2. The calculated Ag(1)–$C_{carbene}$ distance of 2.0983 Å, and the $C_{carbene}$–Ag(1)–$C_{carbene}$ angle of 180°, confirmed the linear geometry of **2**. The calculated carbenic angle N(1)–C(1)–N(2) is 103.7°, which is closer to the experimentally obtained value in co-sister complex 103.2(6)°.[31] Moreover, the

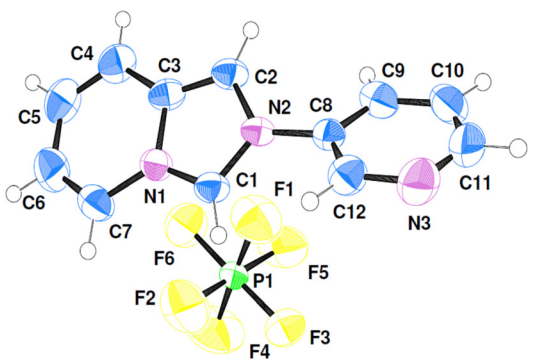

Fig. 1 ORTEP view of the single-crystal X-ray structure of proligand **1**·HPF_6 with 50% probability. C(1)–N(1), 1.329 Å; C(1)–N(2), 1.334 Å, C(3)–N(1), 1.396 Å; C(2)–N(2), (1.367 Å); N(1)–C(1)–N(2), 107.42°.

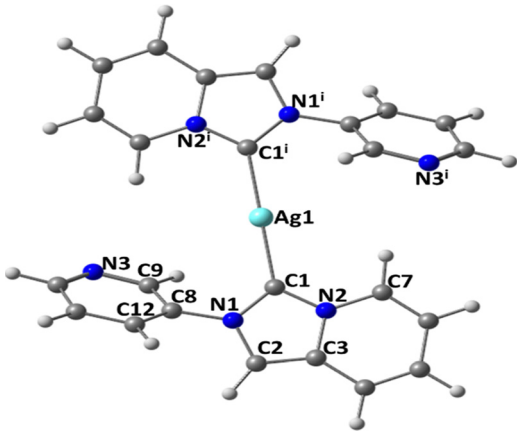

Fig. 2 Optimized geometry of Ag(I) complex 2; anion PF_6 was omitted for clarity.

measured Ag(I)–$C_{carbene}$ bond distances and $C_{carbene}$–Ag(1)–$C_{carbene}$ angles in the linear d^{10} complexes were consistent (shown in Tables 1 and 2) with those experimentally measured values of other silver(I)–NHC complexes,[32] also analogous to the aggregate of the covalent radii of the silver and carbon nuclei (2.111 Å).

The ORTEP presentation of the solid-state structure of complex **3** is presented in Fig. 3. The crystallographic findings are summarized in Table S1 (ESI†), and the selected bond distances and bond angles are tabulated in Tables 1 and 2. The molecule crystallized with a monoclinic symmetry with the *P*21/*n* space group with one cation and the hexafluorophosphate anion in the asymmetric unit. The two gold(I)–$C_{carbene}$ bond lengths in linear bis-carbene gold(I) are similar having Au(1)–C(1) = 2.028(4) Å, which are analogous with other known gold(I)–NHC bis-NHC compounds.[31,33] The two gold(I)–$C_{carbene}$ is within the sum of van der Waals radii of gold and carbon atoms [Au–C = 2.108 Å]. The geometry around gold(I) is perfectly linear, possessing a 180.0° bond angle of C(1)–Au(1)–C(1^i). It is concluded that the experimental bond parameters of complex **3** are comparable to other gold(I)–NHC annelated complexes designed by our group.[27]

The mean C–N bond length in the imidazolidine moiety of two NHC ligands of complex **3** is 1.37 Å, and imidazolidine N–C–N angles (103.6°) are very close to those earlier reported[27] and with other pointed Au(I)–NHC complexes.[33] In complex **3**, the annelated imidazole moiety of bis carbene and Au(I) ions make a plane, which makes an angle of 47.7° with the plane containing a 3-pyridyl wingtip moiety. Complex **3** possesses

Table 1 Selected bond lengths (Å) of complexes **2** and **3**

	2	3	
Bond	Theo	Exp.	Theo
M–$C_{carbene}$	2.0983	2.028(4)	2.0475
N(1)–C(2)	1.3831	1.372(5)	1.3822
N(1)–C(1)	1.3649	1.355(5)	1.3648
N(2)–C(1)	1.3662	1.362(5)	1.3673
N(2)–C(3)	1.4139	1.401(5)	1.4128

Table 2 Selected bond angles (°) of complexes **2** and **3**

	2	3	
Angles	Theo	Exp.	Theo
C(1)–M(1)–C(1′)	180.0	180.0(3)	180.0
N(1)–C(1)–N(2)	103.7	103.6(3)	104.1
C(1)–N(1)–C(2)	112.6	112.5(3)	112.3
C(1)–N(2)–C(3)	111.6	111.5(3)	111.2
C(1)–N(1)–C(8)	122.8	122.9(3)	123.4
C(1)–N(2)–C(7)	127.3	127.6(4)	127.5
N(1)–C(8)–C(9)	120.1	119.8(4)	120.3
N(1)–C(8)–C(12)	120.5	120.0(3)	120.3

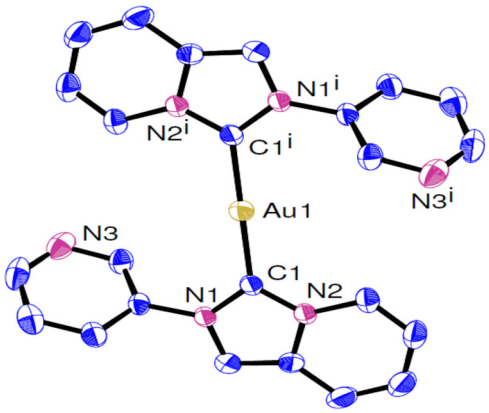

Fig. 3 ORTEP view of the single-crystal X-ray structure of 3 with 50% probability (H atom and anion PF_6 have been omitted for clarity).

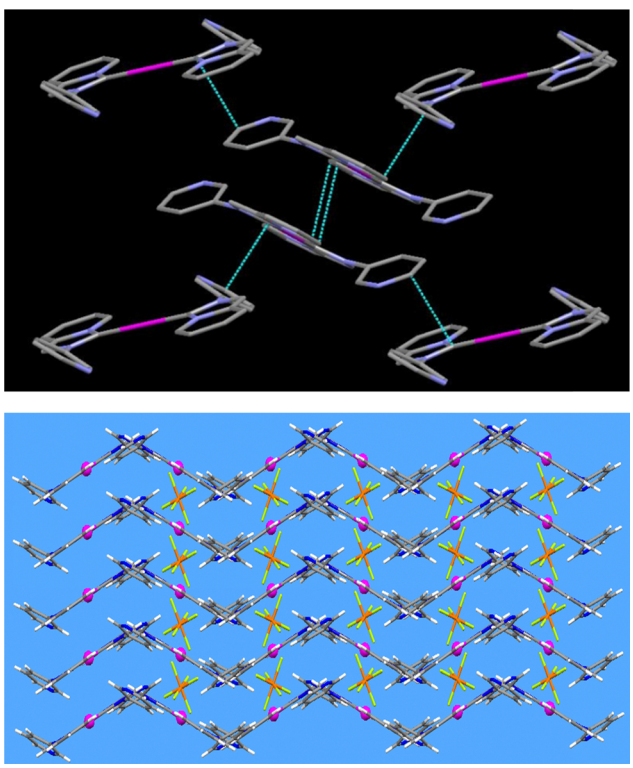

Fig. 4 (above) Packing view and various π–π, C–H–π interactions present in the solid-state structure of **3**; (below) 2D layer formed by packing of **3**.

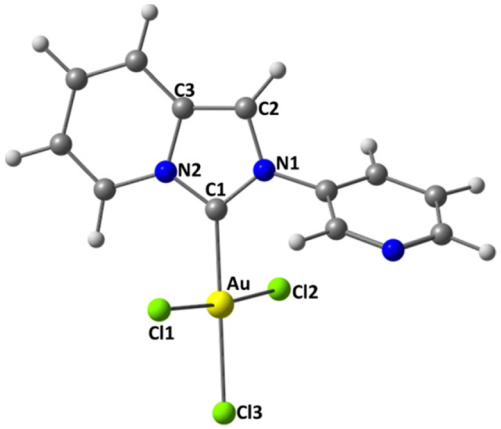

Fig. 5 Optimized geometry of Au(III)–NHC complex, **4**.

several types of non-covalent interactions in its crystal packing view. The molecule forms a 2D layer in a zig-zag fashion by these various intermolecular interactions, namely, C–H···F($d_{(C–H···F)}$ = 2.407–2.667 Å), C–H...π ($d_{(C–H···π)}$ = 3.478 Å), and aromatic stacking π···π ($d_{(π···π)}$ = 3.627 Å, between two imidazopyridines; $d_{(π···π)}$ = 3.631 Å, between imidazopyridine and 3-pyridyl wingtip) interactions are shown in Fig. 4. This type of 2D layer forms a 3D structure by various C–H···F, π···π, and C–H···π interactions. Complex **3** does not possess short aurophilic interactions, and the observed short Au···Au interaction in the complex is 8.699 Å.

The optimized geometry of **4** is shown in Fig. 5, and the calculated bond parameters are summarized in Table 3. The calculated gold(III)–$C_{carbene}$ distance (2.0345 Å) is lower than the sum of van der Waals radii of gold and carbon atoms [Au–C = 2.108 Å] and is very close to other gold(III)–$C_{carbene}$ bond distances pointed by our group.[27,31] The calculated gold(III)–Cl bond distances are very close to the experimental values of known NHC–Au–Cl_3 complexes.[27,29] The calculated bond angles C(1)–Au(III)–Cl(3) (179.8°), Cl(1)–Au(III)–Cl(2) (174.7°), C(1)–Au(III)–Cl(1)(87.3°) and C(1)–Au(III)–Cl(2)(87.5°) support the square planar arrangement around gold(III) ions. The calculated carbenic angle N(1)–C(1)–N(2) is 105.5°, which is less than the observed value in the co-sister complex, 106.8°.[31]

Density functional theory studies of complexes 2–4

We performed DFT and TDDFT studies to have a clear picture of the intrinsic structure and bonding parameters of the synthesized complexes **2–4**, and the measured data are presented in Tables 1–,3. Natural bond orbital (NBO) studies[34,35] were implemented to get the electronic structures of all these complexes. The Wiberg bond index (WBI) computation obtained from natural bond orbital (NBO) studies (bond order) is shown in Table 4.

Table 3 Selected calculated bond parameters of complex **4**

Bond lengths (Å)		Bond angles (°)	
	Theo		Theo
Au(III)–$C_{carbene}$	2.0345	C(1)–Au(III)–Cl(3)	179.8
N(1)–C(2)	1.3839	Cl(1)–Au(III)–Cl(2)	174.7
N(1)–C(1)	1.3512	C(1)–Au(III)–Cl(1)	87.3
N(2)–C(1)	1.3582	C(1)–Au(III)–Cl(2)	87.5
N(2)–C(3)	1.4150	N(1)–C(1)–N(2)	105.5
Au(III)–Cl(1)	2.3426		
Au(III)–Cl(2)	2.3387		
Au(III)–Cl(3)	2.3249		

Table 4 Bond order: Wiberg bond index coming from NBO analysis and chemical hardness

Complex	WBI (bond order)	Chemical hardness
Complex **2**	WBI [Ag(1)–C(1)]: 0.5004 WBI [C(1)–N(1)]: 1.2492 WBI [C(1)–N(2)]: 1.2207 WBI [N(1)–C(2)]: 1.1311 WBI [N(2)–C(3)]: 1.0479	2.075
Complex **3**	WBI [Au(1)–C(1)]: 0.5960 WBI [C(1)–N(1)]: 1.2439 WBI [C(1)–N(2)]: 1.2127 WBI [N(1)–C(2)]: 1.1345 WBI [N(2)–C(3)]: 1.0499	2.0138
Complex **4**	WBI [Au–C(1)]: 0.5545 WBI [C(1)–N(1)]: 1.2647 WBI [C(1)–N(2)]: 1.2158 WBI [N(1)–C(2)]: 1.1281 WBI [N(2)–C(3)]: 1.0418 WBI [Au–Cl(3)]: 0.6604 WBI [Au–Cl(2)]: 0.6458 WBI [Au–Cl(1)]: 0.6344	1.3456

The calculated WBI values for the silver(I)–$C_{carbene}$ bond of complex **2** is 0.5004, whereas 0.5960 for the gold(I)–$C_{carbene}$ bond of complex **3** and 0.5545 for the gold(III)–$C_{carbene}$ bond of complex **4**. These values assist the shorter Au–C bond length than the comparable Ag–C bond lengths. The Wiberg bond indices (WBI) measured for the gold(I)–NHC complex (**3**) are slightly higher than that of the Au(III)–NHC congener. It is shown that the oxidation of gold(I) → gold(III) carrying identical ligands did not alter the gold(I)/gold(III)–$C_{carbene}$ bond length.[29] Similarly, here we observed gold(I)–$C_{carbene}$ bond distances to be nearly equal to the calculated gold(III)–$C_{carbene}$ bond distance. In addition, we can contrast the bond length and bond order of all the corresponding bonds of complexes **2–4**.

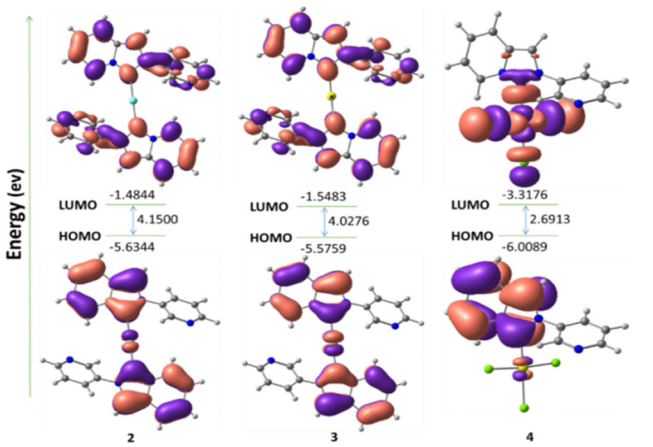

Fig. 6 Contour plots of the selected molecular orbitals of complex **2–4**.

Table 5 Binding energy, type of interaction, and amino acids involved in the interaction of BCL2 and topoisomerase proteins with complex **2**, **3**, and **4**

Protein–ligand	Binding energy (kcal mol^{-1})	Interactions amino acids with different atoms;
BCL2-complex **2**	−7.17	Asp108, Met112, Glu133, Leu134, Gly142, Arg143, Ala146, Val153
BCL2-complex **3**	−7.24	Ala97, Asp100, Phe101, Gly142, Arg143, Val145, Phe195, Leu198
BCL2-complex **4**	−5.88	Asp108, Met112, Val130, Val153
Topoisomerase-complex **2**	−8.23	Pro593,Arg672,Glu682, Asp683,Leu685, Lys701, Leu705
Topoisomerase-complex **3**	−8.02	Pro593, Leu685, Phe668, Arg672, Glu682, Lys701, Leu705
Topoisomerase-complex **4**	−6.91	Leu685, Leu705, Glu702

Fig. 6 shows the contour plots of selected molecular orbitals of complexes **2–4**. The DFT calculations on complex **2** revealed that HOMO (E_0 = −5.6344 eV) is primarily coupled to the annelated imidazolidine part with a little assistance from silver metal ions, whereas in LUMO (E_0 = −1.4844 eV), the electron is concentrated on the whole NHC ligand only. Therefore, in complex **2**, HOMO → LUMO charge transfer is supposed to be mixed MLCT/ILCT. Similarly, theoretical studies on complex **3** imply that the HOMO (E_0 = −5.5759 eV) is primarily coupled to the annelated imidazolidine part with the lowest assistance from gold(I) ions, whereas in LUMO (E_0 = −1.5483 eV), the electron is concentrated on the whole NHC ligand only. Therefore, in complex **3**, HOMO → LUMO charge transfer also seemed as mixed MLCT/ILCT. Unlike complex **2** and **3**, a parallel analysis on complex **4** displayed that the HOMO (E_0 = −6.0089 eV) is primarily coupled to the imidazoline part of the NHC ligand, with the smallest assistance from gold(III) ions, whereas LUMO (E_0 = −3.3176 eV) is essentially centered on $C_{carbene}$–gold(III)–Cl_3. Therefore, in complex **4**, the HOMO → LUMO charge transfer is taken as mixed ILCT/LMCT. Based on the chemical hardness, complex **4** is potentially more reactive than **2** and **3**, which are in line with the HOMO–LUMO energy gap, generally more the energy gap, more is the stability.

Molecular docking analysis

Molecular docking analyses have played a significant role in the interpretation of the molecular-level interaction of ligands (small molecules) with receptors by placing the ligand in the binding site of the receptor. Here we consider BCL-2 and human DNA topoisomerase II as receptors for the docking analysis. BCL-2 is an establishing constituent of the BCL family of proteins that regulates cell death (apoptosis). Human DNA topoisomerase(II) is an essential enzyme that modulates different fundamental processes of DNA like DNA topology and chromosome organization.[36] The binding energies corresponding to the interaction of complex **2**, **3**, and **4** with BCL-2 and topoisomerase II are tabulated in Table 5, from which it is clear that the complex shows maximum affinity towards topoisomerase II protein between the two chosen receptors. Complex **2** interacts with the BCL-2 receptor *via* the amino acid residues Asp108, Met112, Glu133, Leu134, Gly142, Arg143, Ala146, and Val153. Similarly, Complex **2** interacts with the topoisomerase II receptor through the amino acid residues Pro593, Arg672, Glu682, Asp683, Leu685, Lys701, and Leu705. The energetically most favorable conformations of complex **2**, **3**, and **4** with BCL-2 and topoisomerase II are shown in Fig. 7.

Complex **3** interacts with the BCL2 receptor through the amino acid residues Ala97, Asp100, Phe101, Gly142, Arg143, Val145, Phe195, and Leu198. Similarly, complex **3** interacts with the topoisomerase II receptor through the amino acid residues Pro593, Leu685, Phe668, Arg672, Glu682, Lys701, and Leu705. Complex **4** interacts with the BCL2 receptor through the amino acid residues Asp108, Met112, Val130, and Val153. Similarly, Complex **4** interacts with the topoisomerase II receptor through the amino acid residues Leu685, Leu705, and Glu702. From the binding energy point of view, complexes **2** and **3** show similar

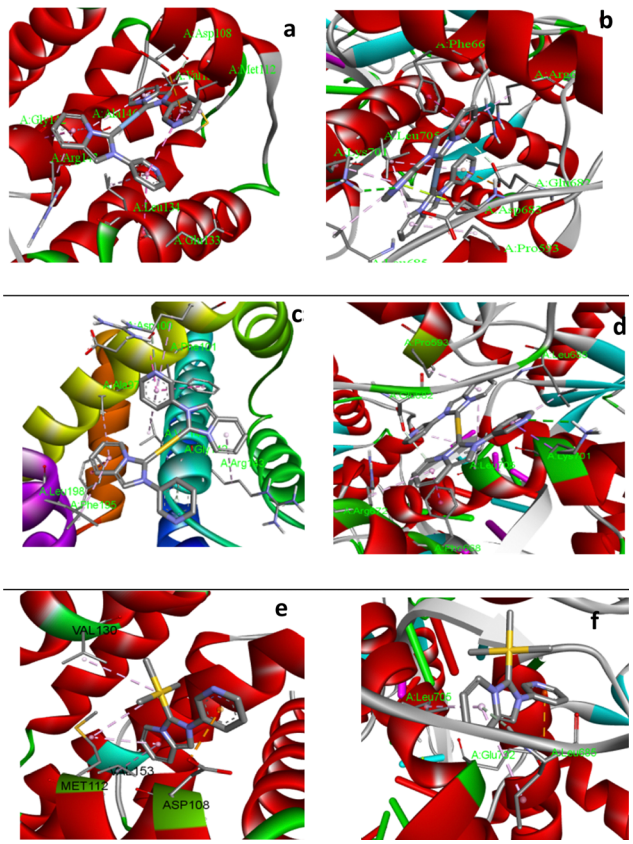

Fig. 7 (a) Capped stick model view of the interaction of complex **2** with BCL2 (PDB ID: 4lvt). (b) Capped stick model view of the interaction of complex **2** with human DNA topoisomerase II (PDB ID: 4fm9). (c) Capped stick model view of the interaction of complex **3** with BCL2 (PDB ID: 4lvt). (d) Capped stick model view of the interaction of complex **3** with human DNA topoisomerase II (PDB ID: 4fm9). (e) Capped stick model view of the interaction of complex **4** with BCL2 (PDB ID: 4lvt). (f) Capped stick model view of the interaction of complex **4** with human DNA topoisomerase II (PDB ID: 4fm9).

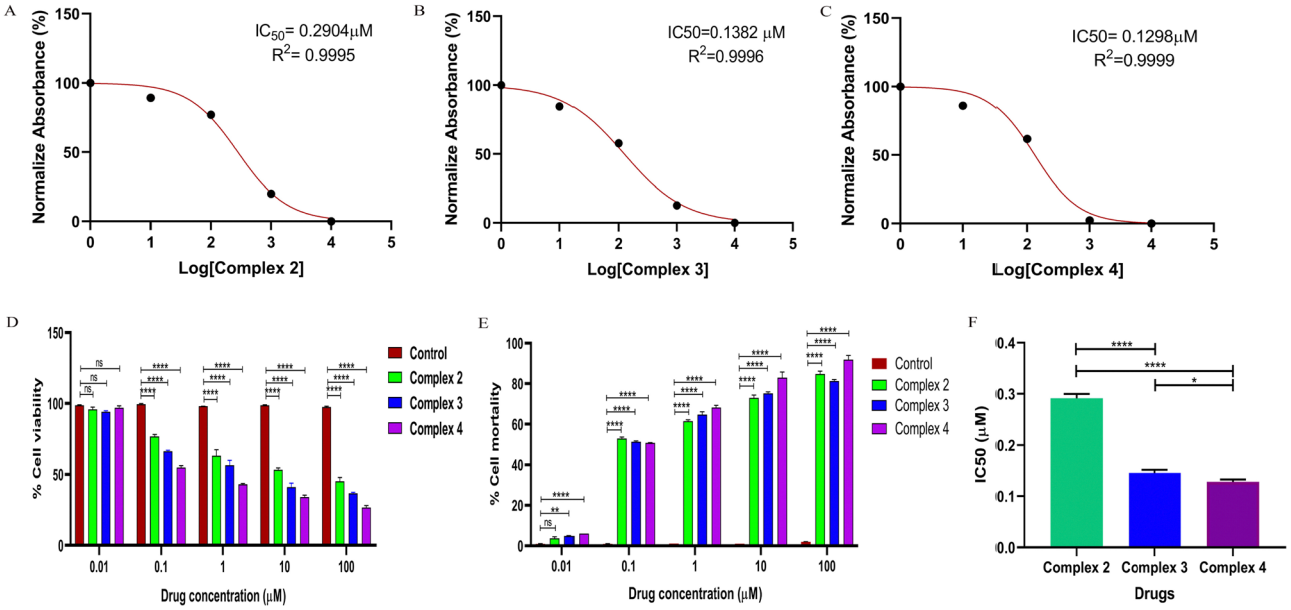

Fig. 8 MTT analysis of complex **2**, **3**, and **4** in A549 cells: (A)–(C) IC_{50} doses of the compounds of interest; (D) percentage of cell viability representation under the effect of the compounds at different concentrations; (E) percentage of cell mortality representation under the effect of the compounds at different concentrations; and (F) statistical analysis of IC_{50} of the drugs by one-way ANOVA.

activities toward BCL-2 and topoisomerase II; at the same time, complex 4 has less affinity than **2** and **3**.

Biological evaluation

Comparative analysis of cell viability reveals a new compound with lower dose inhibition

The MTT evaluation of three complexes **2**, **3**, and **4** revealed that among the three drugs, Au(III)–NHC **4** was more potent with a large inhibitory tendency with a lower IC_{50} value of 0.1298 μM (Fig. 8A–C). The cell viability representation in Fig. 8D reveals that the viability of the cells reduced with the increase in concentration of the drugs, whereas cell mortality (Fig. 8E) depicts a similar result in parity with cell viability. Fig. 8F reveals a remarkable difference in the IC_{50} values of the drugs of interest, where the IC_{50} value of complex **4** is significantly higher than that of complex **2** at a significance of $P < 0.0001$, whereas lesser significance has been obtained in comparison with complex **3** at a significance of $P = 0.0431$. It is needless to mention that present gold(I) and gold(III) complex **3** and **4** are much more potent than gold(I) and gold(III)–NHC complex of sister 2-pyridyl wingtip imidazopyridine through different cell lines.[31] IC_{50} doses of complex **2**, complex **3**, and complex **4** on SKOV3 and MDA-MB-231 are presented in Table 6. We studied the anticancer activities of complex **2**, **3**, and **4** against A549, SKOV3, and MDA-MB-231 at different concentrations 0.1 μM, 0.01 μM, 1 μM, and 100 μM over a period of 24 h (Fig. S9, ESI†). It is found that the drugs are very cell-specific, they show better potency against A549, and therefore, we studied details against the A549 cell line.

Table 6 Summary of IC_{50} values (μM) against A549, SKOV3 and MDA-MB-231 cell lines

Cell line	Complex, **2**	Complex, **3**	Complex, **4**
A549	0.2904 ± 0.5	0.1382 ± 0.5	0.1298 ± 0.5
SKOV3	0.2707 ± 0.5	0.2022 ± 0.5	0.1604 ± 0.5
MDA-MB-231	0.2561 ± 0.5	0.5706 ± 0.5	0.2105 ± 0.5

Morphological differences depict the efficacy of complex 4

The A549 cells under the treatment of the compound show a distorted shape with a round morphology of uneven boundary, as shown in Fig. 9. Moreover, the detection of the nucleus of the treated cells reveals the fragmentation of the nucleus in comparison with non-treated cells.

Drug treatment induces apoptosis in A549 cells by the intrinsic pathway

Examining the assertion of the pro-apoptotic marker Bax and anti-apoptotic marker BCL-2 by flow cytometry has depicted that there is an increase in Bax in the treated cells as compared to the non-treated control cells ($P = 0.0025$) (Fig. 10). Concurrently, there is a fall in the BCL-2 proteins between the two groups ($P = 0.0002$). Upon further investigation of the caspases involved in the intrinsic and extrinsic pathways of apoptosis induction, it has been observed that caspase 9 that regulates the intrinsic pathway was significantly higher in comparison to caspase 8, which drives the extrinsic pathway in the treated cells ($P < 0.0001$). Furthermore, caspase 9 and caspase 3 hold a significant correlation ($P < 0.0001$) but caspase 8 and caspase 3 share a non-significant relation. The result of Annexin V/PI staining has also corroborated with the analysis of apoptotic marker expression, which strongly validates the findings.

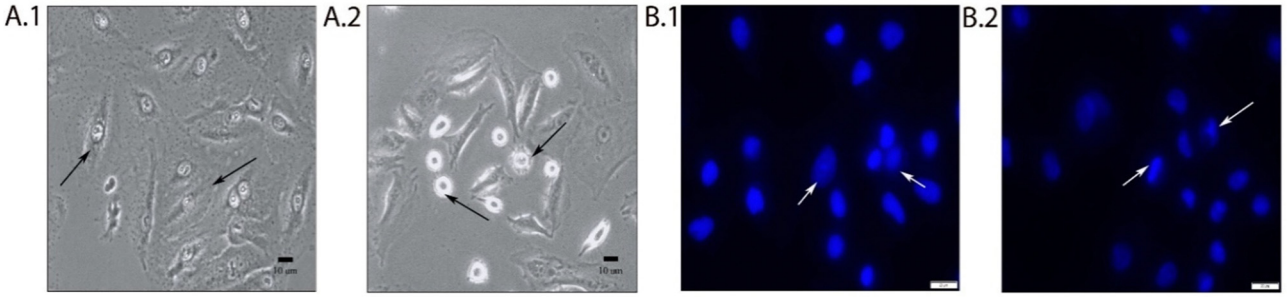

Fig. 9 Morphological analysis of A549 cells: (A.1) healthy morphology of the non-treated cells at 10× and (A.2) distorted morphology of the treated cells at 10×. (B.1) Intact nucleus of the non-treated cells at 100× and (B.2) fragmented nucleus of the treated cells at 100×.

Increased level of cytochrome (Cyt) *c* directs the elevated generation of ROS inducing depolarization of mitochondrial membrane under treatment

To evaluate the signalling cascade directing the apoptotic pathway under the effect of the drug, we explored mitochondrial protein Cyt *c*, ROS generation, and mitochondrial membrane potential (Fig. 11). Our study depicts that Cyt *c* levels have increased in the treated cells as compared to the control cells at a significance of $P = 0.0092$. The generation of ROS has also increased in the treated cells, $P = 0.0018$, but interestingly depolarization of the mitochondrial membrane decreased considerably upon treatment, where a significant increase was observed between the treated and non-treated control cells ($P = 0.0002$).

Discussion in support of anticancer activities

The programmed cell death mechanism, apoptosis, plays a crucial role in deciding the fate of cancer cells during the oncogenic transformation till metastasis. The inhibition or dysregulation of the apoptotic pathway by some endogenous or exogenous stimuli facilitates the cancer cells to proliferate and progress. Thus, apoptotic cell death stands out to be the main effector function of many anti-cancer therapies. Previously, the mitochondria had been reported to appear normal during apoptotic events;[37] however, the first clue that directed that the mitochondria may also be related to apoptosis during the localization of the BCL-2 protein in the outer membrane of the mitochondria.[38] In addition to this, the reduction in the BCL-2 inhibition on apoptotic cells due to the lack of the C-terminal *trans*-membrane domain also provided a hint regarding the involvement of the mitochondria in apoptotic mechanisms.[39,40] These facts were further supported by the fact that the mitochondrial membrane potential was found to be related to ROS generation and Cyt *c* was necessary for the activation of caspase proteins, which, in turn, are important regulatory factors for both intrinsic and extrinsic apoptotic pathways.[41–43] The secretion of Cyt *c* from the mitochondria is a prime location for regulating BCL-2 in apoptosis.[44,45] Under this scenario, we analyzed the inhibitory effect of complex **4** on A549 cells, where there was a significant decrease in the anti-apoptotic protein BCL-2 with an upsurge in Bax and pro-apoptotic protein expression, indicating that the drug has the potency to induce apoptotic cell death. Furthermore, for checking whether the signalling pathway undertaken is intrinsic or extrinsic, the expression level of caspase 3, caspase 8, and caspase 9 was evaluated, where the expression level of caspase 9 was significantly higher than that of caspase 8, which, in turn, depicted that the apoptotic signal is in the intrinsic mode. To validate the involvement of mitochondrial regulatory mechanisms responsible for apoptosis, we analyzed the ROS generation, the secretary level of Cyt *c*, and depolarization of mitochondrial membrane in both the treated and non-treated A549 cells. Surprisingly, the mitochondrial membrane potential ($\Delta\psi_m$) decreased in treated cells, illustrating that the deformed mitochondria fuel the release of mitochondrial Cyt *c*; however, the levels of Cyt *c* and ROS were larger in the treated group than those in the non-treated group. The above-mentioned findings are summarised in Fig. 12 to describe the possible pathway of cell death through apoptosis. Thus, these findings have opened a new arena for the investigation of cancer biology, stating that this new compound has the potency to combat lung cancer progression by inducing an intrinsic apoptotic pathway in a mitochondrial ROS-dependent manner. We studied the anticancer activities of similar silver(I), gold(I), and gold(III)–NHC complexes of sister ligand 2-pyridyl-imidazolidine,[31] and it was observed that presently reported 3-pyridyl-imidazolidine is more potent (in terms of IC_{50} values), though in two cases, the cancer cells are different. Present complex **2**, **3** and **4** is more potent against cancer cell A459 in comparison to similar Ag(I), Au(I) and Au(III)–NHC complexes of 1-methyl-2-(phenyl)imidazo[1,5-*a*]pyridine-2-ylidene.[36] It is expected that pyridyl-N in the 3-position helps better to bind with DNA than pyridyl-N in the 2-position. In the present case, the Au(III)–NHC complex, *i.e.* complex **4** is slightly more potent than silver(I)–NHC, **2** and gold(I)–NHC, **3**. ADMET analysis was also performed (see ESI,† Fig. S10), from the radar plot, as shown in Fig. S10 (ESI†); it is observed that five parameters are in the physicochemical range (represented as pink area) in case of complexes **2** and **4**, whereas only four parameters are in the physicochemical range in case of complex **3**. Overall, ADMET analysis supports the scope of complex **2**, **3** and **4** as potent drugs, as also supported by other studies.

Conclusions

In summary, very potent bioactive silver(I), gold(I)– and gold(III)–NHC complexes have been synthesized and fully

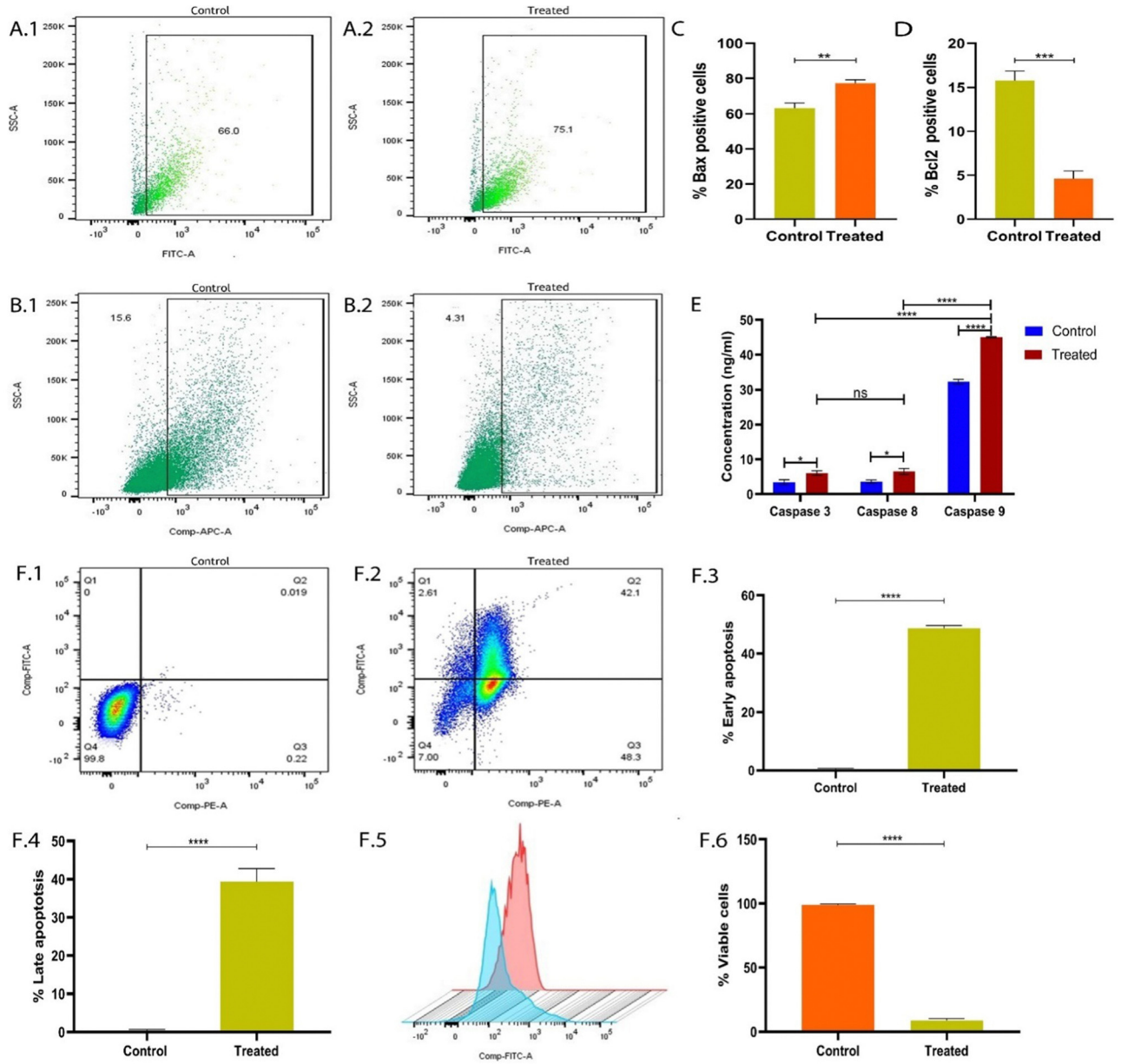

Fig. 10 Flow cytometric analysis of apoptotic markers: (A.1) and (A.2) estimation of pro-apoptotic marker Bax in control and treated A549 cells; (B.1) and (B.2): estimation of anti-apoptotic marker Bcl2 in control and treated A549 cells; (C) and (D) graphical representation of Bax (P = 0.0025) and Bcl2 (P = 0.0002) in control and treated cells; (E) ELISA analysis of caspase proteins in A549 cells. Caspase 3 secreted by A549 cells under control and treated conditions (P = 0.0427), caspase 8 secreted by A549 cells under control and treated conditions (P = 0.0276); caspase 9 secreted by A549 cells under control and treated conditions ($P < 0.0001$), caspase 3 and caspase 8 has non-significant relation (ns) under treated conditions, caspase 3 and caspase 8 both has significant relation with caspase 9 ($P < 0.0001$); (F.1) and (F.2) Annexin-PI analysis for the viability of control and treated cells ($P < 0.0001$); (F.3) graphical representation of the percentage of early apoptotic cells after treatment ($P < 0.0001$); (F.4) graphical representation of the percentage of late apoptotic cells after treatment ($P < 0.0001$); (F.5) graphical representation of live and dead cells, and (F.6) graphical representation of the percentage of viable cells ($P < 0.0001$).

characterized by several spectroscopic methods. A linear configuration of gold(I)–NHC complex **3** has been supported by single-crystal X-ray diffraction analyses. Spectroscopic and DFT studies support a linear geometry of silver(I)–NHC complex **2** and a square planar geometry of gold(III)–NHC complex **4**. The potential of cytotoxic silver(I), gold(I), and gold(III)–NHCs as anticancer agents and apoptosis have been extensively demonstrated. The apoptosis pathway of death of cancer cells has been established by several techniques along with protein expression and ROS production. The mitochondrial membrane potential depolarization, production of ROS, and caspase cascade eventually lead to apoptosis, thereby accelerating the extent of Bax and reducing the extent of BCL-2. Cell apoptosis was accomplished *via* mitochondria-moderated routes. The silver(I), gold(I), and gold(III)–NHC drugs are cell specific. The highest activity is displayed in the case of gold(III)–NHC, **4**. Weak donor-functionalized NHC-based gold(I) derivatives will impart remarkable importance in the future because of

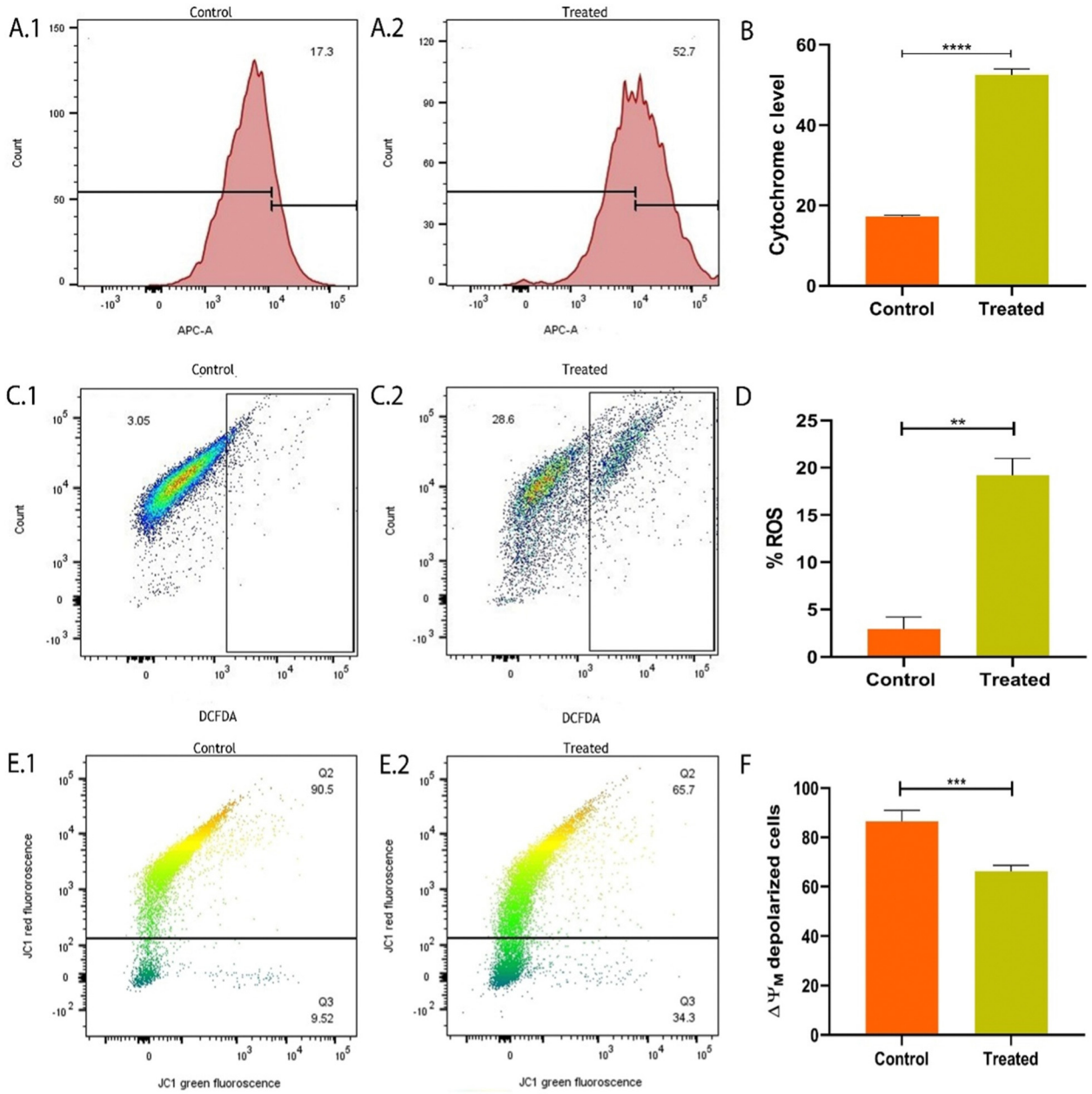

Fig. 11 Flow cytometric analysis of Cyt *c*, ROS production and mitochondrial membrane potential in A549 cells: (A.1) and (A.2) estimation of the secretion of cytochrome *c* in control (17.3%) and treated (52.7%) A549 cells; (B) graphical representation of A549 cells Cyt *c* under control and treated conditions ($P < 0.0001$); (C.1) and (C.2) estimation of the ROS level in control (3.05%) and treated (28.6%) A549 cells; (D) graphical representation of the ROS level in control and treated cells ($P = 0.0072$); (E.1) and (E.2) estimation of the percentage of depolarized control (90.5%) and treated (65.7%) A549 cells; and (F) graphical representation of A549 depolarized control and treated cells ($P = 0.0002$).

their noteworthy efficiency toward tumor cells along with much lower toxicity against normal cells.

Experimental section

Materials and methods

All the reagents from Sigma Aldrich such as silver oxide, potassium hexafluorophosphate, 2-pyridinecarboxaldehyde, 3-aminopyridine, paraformaldehyde, and triethyl orthoformate were used without further purification. Chloro(dimethylsulfide)gold(I) was synthesized according to the procedure.[36] A Bruker 400 MHz NMR spectrometer was used for spectroscopic characterization at 25 °C using tetramethylsilane as an internal standard.

Synthesis of $[Ag(1)_2][PF_6]$, (2)

The proligand **1**·HPF_6, (500 mg, 1.46 mmol) and silver oxide (180 mg, 0.78 mmol) were taken in a round-bottom flask and stirred in 15 mL dry acetonitrile in the darkness at room

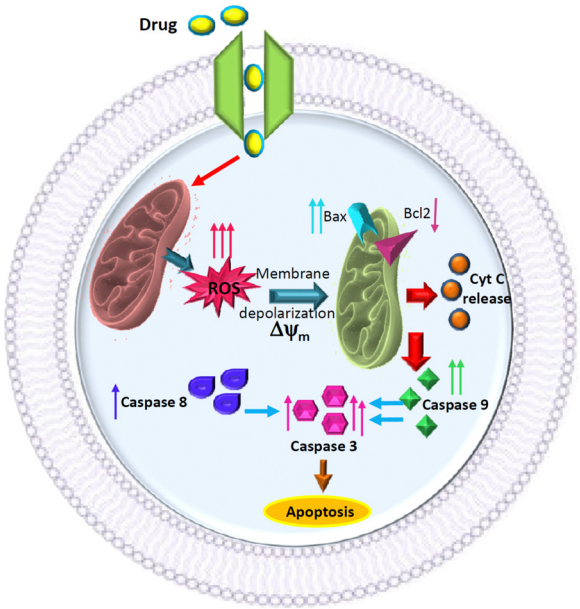

Fig. 12 Possible mechanism of cell death through apoptosis.

temperature. After 4 h, the unreacted silver oxide was removed by filtration through a pack of Celite. The solvent was evaporated at a low temperature and a high pressure. The compound was recrystallized by slow diffusion of Et_2O into a saturated acetonitrile solution of complex **2**. The analytically pure compound was obtained in 87% yield (412 mg, 0.64 mmol). ^{1}H NMR (DMSO-d_6) δ = 9.10 (s, 1H, H^e), 8.76 (d, J = 4.0 Hz, 1H, H^a), 8.73 (d, J = 8 Hz, 1H, H^d), 8.38 (s, 1H, H^i), 8.28 (d, J = 4 Hz, 1H, H^h), 7.71 (d, J = 8.0 Hz, 1H, H^f), 7.63 (m, 1H, H^c), 7.13 (t, J = 8.0 Hz, 1H, H^b), 6.97 (t, J = 8.0 Hz, 1H, H^g). ^{13}C NMR (DMSO-d_6) δ = 171.9 (N*C*N), 150.5, 145.6, 136.9,132.9, 131.3, 128.7, 124.6, 123.9, 118.0, 115.2, 113.3. Anal. calcd for $C_{24}H_{18}N_6AgPF_6$: C, 44.79; H, 2.79; N, 13.06%. Found: C, 44.68; H, 2.76; N, 12.97%.

Synthesis of [Au(1)$_2$][PF$_6$], (3)

The proligand **1**·HPF$_6$, (125 mg, 0.37 mmol) and silver oxide (45 mg, 0.19 mmol) were stirred in 10 mL dry acetonitrile in the darkness at room temperature. After 4 h, the solution was filtered through a plug of Celite. An acetonitrile solution of prepared Au(SMe$_2$)Cl (54 mg, 0.19 mmol) was added dropwise to the filtrate with stirring at room temperature, and an immediate white precipitate was observed. After 1 h of stirring, the solution was filtered through a plug of Celite to obtain a clear solution. The solvent was evaporated at a low temperature and a high pressure to get solid mass. The compound was recrystallized by slow diffusion of Et_2O into the saturated acetonitrile solution of complex **3**. The analytically pure compound was obtained in 80% yield (107 mg, 0.15 mmol). ^{1}H NMR (DMSO-d_6) δ = 9.13 (s, 1H, H^e), 8.76 (d, J = 4.0 Hz, 1H, H^a), 8.72 (d, J = 8 Hz, 1H, H^d), 8.37 (s, 1H, H^i), 8.29 (d, J = 8 Hz, 1H, H^h), 7.68 (m, 2H, $H^{c,b}$), 7.14 (d, J = 8.0 Hz, 1H, H^f), 6.97 (t, J = 8.0 Hz, 1H, H^g). ^{13}C NMR (DMSO-d_6) δ = 172.5 (N*C*N), 150.8, 146.0, 137.3, 133.1, 131.7, 129.2, 124.9, 124.4, 118.5, 115.6, 113.8. Anal. Calcd for $C_{24}H_{18}N_6AuPF_6$: C, 39.34; H, 2.46; N, 11.48%. Found: C, 39.28; H, 2.42; N, 11.40%.

Synthesis of [Au(1)Cl$_3$], (4)

To a 10 mL acetonitrile solution of **3** (200 mg, 0.45 mmol), a dichloromethane solution of Au(SMe$_2$)Cl (235.9 mg, 0.91 mmol) was added at room temperature, and the resulting mixture was stirred for further 5–6 h. After that, a little amount of precipitate was observed and the colorless solution turned yellow. To collect the metallic gold, the solution was filtered and the collected gold was further utilized to synthesize Au(SMe$_2$)Cl. The solvent was removed at a low temperature and a high pressure to get a reddish solid mass. The crude product was recrystallized by slow diffusion of Et_2O into an acetonitrile solution of complex **4**. The analytically pure compound was obtained in 33% yield (76.1 mg, 0.15 mmol). ^{1}H NMR (DMSO-d_6) δ = 9.17 (s, 1H, H^e), 8.84 (d, J = 4.0 Hz, 1H, H^a), 8.73 (d, J = 8 Hz, 1H, H^d), 8.43 (s, 1H, H^i), 8.33 (d, J = 4 Hz, 1H, H^h), 7.73 (d, J = 8.0 Hz, 1H, H^f), 7.64 (m, 1H, H^c), 7.19 (t, J = 8.0 Hz, 1H, H^b), 7.01 (t, J = 8.0 Hz, 1H, H^g). ^{13}C NMR (DMSO-d_6) δ = 162.1 (N*C*N), 149.4, 144.8, 137.3, 133.3, 131.5, 129.1, 124.8, 124.2, 118.7, 115.4, 113.6. Anal. calc. for $C_{12}H_9N_3AuCl_3$: C, 28.89; H, 1.81; N, 8.43%. Found: C, 28.72; H, 1.76; N, 8.14%.

Biological studies

Cell culture

A549 (human non-small lung carcinoma), SKOV3 (human ovarian cancer), and MDA-MB-231 (human breast cancer) cells were obtained from the National Centre for Cell Science, Pune, India. The cell lines were maintained in RPMI media supplemented with 10% FBS and 1% antibiotic (PSN) and incubated at 37 °C in a humidified chamber containing 5% CO_2. At the confluence level of approx. 75–80%, the cells were trypsinized with 0.025% of trypsin and 0.52 mM EDTA in a buffer and seeded for regrowth to initiate the pre-designed experiments.

Cell viability assay

A549, SKOV3, and MDA-MB-231 cells were seeded at a density of 5 × 10^3 cells into a 96-well flat-bottom transparent plate followed by overnight growth at 37 °C in an atmosphere containing 5% CO_2. On the following day, the cells were treated with the new drugs of interest, namely, complex 2, 3, and 4 at four different concentrations, *i.e.*, 0.1 μM, 0.01 μM, 1 μM, and 100 μM over a period of 24 hours. After the incubation period, 20 μL 3-(4,5-dimethylthiazol-2-yl)-2,5 diphenyltetrazolium bromide (MTT) was prepared and added to each well. The plate was further incubated for 3 hours at 37 °C and 150 μL dimethyl sulphoxide (DMSO) was added; the OD values were recorded using a microplate plate reader at 570 nm.[37]

Morphological analysis

The cells were seeded at a density of 5 × 10^5 cells on a 22 mm glass coverslip kept in a 35 mm Petri dish and upon seeding, treatment of 0.08 μM dose of Complex 4 was given to the cells

for 24 hours and both bright field and fluorescence microscopies were performed. For fluorescence microscopy, the treated cells were fixed in 2% paraformaldehyde and then stained with 4′,6′-diamidino-2 phenylindole (DAPI) for the detection of chromatin condensation and DNA fragmentations for 2 min in the darkness followed by DPX mounting and image capturing using an OLYMPUS fluorescence microscope.[38]

Detection of apoptosis-associated mitochondrial proteins

For the determination of the status of anti-apoptotic and pro-apoptotic proteins in the A549 cells upon the treatment of interest, the cells were treated in the same way as discussed earlier and a primary antibody for apoptosis-associated mitochondrial proteins, *i.e.* pro-apoptotic marker (Bax), anti-apoptotic marker (Bcl2) and mitochondrial Cyt *c*, was added at a dilution of 1 : 500 and kept at 4 °C for 2 hours, followed by tagged secondary antibody incubation at a dilution of 1 : 1000 for 1 h. The expression levels of Bax, Bcl2 and Cyt *c* in control and treated cells were then recorded by flow cytometry.[39]

Analysis of caspase proteins

The cell culture supernatant that was collected from both the control and treated cells was then implemented for estimating caspase 3, caspase 8, and caspase 9. The experiments were executed using three distinct ELISA kits, namely, Human Active Caspase-3 Immunoassay (RnD Systems, Catalog Number KM300), Human CASP 9 (Caspase 9) ELISA Kit (Assay Genie, Catalog Number HUES01822), and Human Caspase 8 ELISA Kit (Invitrogen, Catalog Number BMS2024).

Annexin V/FITC apoptosis assay

The cells were seeded in a 60 mm Petri dish at a density of 2×10^5 cells per well and incubated with a 0.08 μM complex 4 for 24 hours. A549 cells were stained with 5 μL Annexin V-FITC and 10 μL PI at room temperature for 10–20 minutes according to the instructions in the Annexin V-FITC/PI Apoptosis Kit, centrifuged, and analyzed by flow cytometry.[43]

Analysis of ROS generation

For the detection of intracellular ROS levels, 2×10^5 A549 cells were seeded in a 60 mm Petri dish, and on the following day, the cells were treated with 0.08 μM dose of complex 4 for a period of 24 hours. After the treatment tenure, the cells were scrapped off and washed in 1× PBS by centrifugation at 5000 rpm for 5 min. The cells were then treated with dichlorodihydrofluorescein diacetate (DCFDA) in the darkness at 37 °C for 30 min, followed by washing with 1× PBS. The cell suspensions, both control and treated, were transferred to a flow cytometer for recording data.[44]

Analysis of the mitochondrial membrane potential ($\Delta\psi_m$)

For determining the alteration in the mitochondrial membrane potential (MMP) in A549 cells, a 60 mm Petri dish was used for cell seeding followed by treatment with 0.08 μM dose of complex 4 and incubated for 24 hours. After the treatment, the cell culture supernatant was collected and stored for further experiments and the cells, both control (non-treated) and treated, were incubated with 5,5′,6,6′-tetrachloro-1,1′,3,3′-tetraethylbenzimidazolyl carbo-cyanine iodide (JC-1), Sigma working solution, at 37 °C for 20 min. The supernatant was discarded, and the cells were washed twice with a 1× JC-1 staining buffer and the mitochondrial membrane transition was detected using a flow cytometer.[43,45]

Statistical analysis

The statistical analysis and graphs of the results were prepared using the Graph Pad Prism software (version 8) by one-way and two-way analysis of variance (ANOVA) and unpaired t-test, wherever applicable. Flow cytometry analysis was performed using the FlowJo software. P values < 0.001 and < 0.05 were considered to be statistically significant.[46]

Crystal structure determinations

The crystals of proligand **1**·HPF_6 and complex **3** appropriate for X-ray data collection were developed by slow diffusion of diethyl ether into a saturated acetonitrile solution of the respective complexes. The crystal data and details of the collected data are given in Table 1. X-ray data were collected using a Bruker diffractometer (ImuS-Diamondsource, Cu Kα radiation, λ = 1.54178 Å, Photon III detector). The structures were solved using SHELXT[47] and refined using the SHELXL[48] programs with Olex2 as GUI.[49]

Computational methodology

The complexes **2–4** were optimized by the DFT, TD-DFT/CPCM(acetonitrile)/B3LYP-D3/6-31G**, def2TZVP, 6-31G** (C, H, N) level of theory.[50] All DFT/B3LYP calculations were performed using the GAUSSIAN16 package program.[50] During optimization, metal was considered by def2TZVP the triple-ζvalence basis set[51] while the other elements were considered with the 6-31G(d,p) basis set.[52] Gauss Sum 2.1 was used to calculate the fractional contributions.

Author contributions

Prafulla K. Behera: conceptualization; data analysis. Lakshmikanta Maity: data analysis. Sraddhya Roy: anticancer studies. Ananya Das: anticancer data analysis. Priyanka Sahu: formal writing the paper and docking studies. Hemanta K. Kisan: theoretical data analysis. Avtar Changotra: theoretical data collection. Anvarhusein A. Isab: correction of the manuscript. Mohammed Benyounes Fettouhi: SCXRD data collection of 3. AparajitaBairagi: cancer cell analysis. Nabanita Chatterjee: supervised anticancer studies. Joydev Dinda: project designing, conceptualization, writing the paper, and coordinating between several collaborators.

Conflicts of interest

The authors declare no competing financial interest.

Acknowledgements

JD is grateful to Utkal University for the start of the grand WBOHPEE project (FY 2021-22). N. C. is sincerely grateful to Dr Jayanta Chakraborty, Director, Chittaranjan National Cancer Institute for the entire in-vitro work and instrument facilities like microscope and flow Cytometer facility. A. D. and A. B. sincerely extend their gratitude to the University Grants Commission, The Council of Scientific & Industrial Research, and the Chittaranjan National Cancer Institute JRF Fellowship respectively for providing support for the implementation of the research idea.

Notes and references

1 (*a*) A. J. Arduengo III, R. L. Harlow and M. A. Kline, *J. Am. Chem. Soc.*, 1991, **113**, 361–363; (*b*) V. A. Voloshkin, N. V. Tzouras and S. P. Nolan, *Dalton Trans.*, 2021, **50**, 12058–12068; (*c*) T. Tu, W. Assenmacher, H. Peterlik, G. Schnakenburg and K. H. Dotz, *Angew. Chem., Int. Ed.*, 2008, **47**, 7127–7131; (*d*) Z. Lei, M. Endo, H. Ube, T. Shiraogawa, P. Zhao, K. Nagata, X.-L. Pei, T. Eguchi, T. Kamachi, M. Ehara, T. Ozawa and M. Shionoya, *Nat. Commun.*, 2022, **13**, 4288.

2 J. D. Egbert, A. Chartoire, A. M. Z. Slawin and S. P. Nolan, *Organometallics*, 2011, **30**, 4494–4496.

3 X. Liu and W. Chen, *Dalton Trans.*, 2012, **41**, 599–608.

4 D. Meyer, M. A. Taige, A. Zeller, K. Hohlfeld, S. Ahrens and T. Strassner, *Organometallics*, 2009, **28**, 2142–2149.

5 C. Chen, H. Qiu and W. Chen, *Inorg. Chem.*, 2011, **50**, 8671–8678.

6 S. Gu, B. Liu, J. Chen, H. Wu and W. Chen, *Dalton Trans.*, 2012, **41**, 962–970.

7 A. Azua, S. Sanz and E. Peris, *Chem. – Eur. J.*, 2011, **17**, 3963–3967.

8 C. S. Lee, R. R. Zhuang, S. Sabiah, J. C. Wang, W. S. Hwang and I. J. B. Lin, *Organometallics*, 2011, **30**, 3897–3900.

9 A. Rit, T. Pape and F. E. Hahn, *J. Am. Chem. Soc.*, 2010, **132**, 4572–4573.

10 F. M. Conrady, R. Fröhlich, C. S. Brink, T. Pape and F. E. Hahn, *J. Am. Chem. Soc.*, 2011, **133**, 11496–11499.

11 M. M. Hansmann, M. Rudolph, F. Rominger and A. S. K. Hashmi, *Angew. Chem., Int. Ed.*, 2013, **52**, 2593–2598.

12 M. C. Gimeno, A. Laguna and R. Visbal, *Organometallics*, 2012, **31**, 7146–7157.

13 W. Liu and R. Gust, *Chem. Soc. Rev.*, 2013, **42**, 755–773.

14 V. J. Catalano and A. O. Etogo, *Inorg. Chem.*, 2007, **46**, 5608–5615.

15 (*a*) K. M. Hindi, T. J. Siciliano, S. Durmus, M. J. Panzner, D. A. Medvetz, D. V. Reddy, L. A. Hogue, C. E. Hovis, J. K. Hilliard, R. Mallet, C. A. Tessier, C. L. Cannon and W. J. Youngs, *J. Med. Chem.*, 2008, **51**, 1577–1583; (*b*) F. Guarra, A. Pratesi, C. Gabbiani and T. Biver, *J. Inorg. Biochem.*, 2021, **217**, 111355–111373; (*c*) L. Eloy, A. S. Jarrousse, M. L. Teyssot, A. Gautier, L. Morel, C. Jolivalt, T. Cresteil and S. Roland, *ChemMedChem*, 2012, **7**, 805–814; (*d*) A. Kascatan-Nebioglu, M. J. Panzner, C. A. Tessier, C. L. Cannon and W. J. Youngs, *Coord. Chem. Rev.*, 2007, **251**, 884–895.

16 C. Boehme and G. Frenking, *Organometallics*, 1998, **17**, 5801–5809.

17 (*a*) G. Roymahapatra, S. M. Mandal, W. F. Porto, T. Samanta, S. Giri, J. Dinda, O. L. Franco and P. K. Chattaraj, *Curr. Med. Chem.*, 2012, **19**, 4184–4193; (*b*) D. van der Westhuizen, D. I. Bezuidenhout and O. Q. Munro, *Dalton Trans.*, 2021, **50**, 17413–17437.

18 J. Dinda, B. K. Rana, A. Nandy, V. Bertolasi, K. D. Saha and C. W. Bielawski, *RSC Adv.*, 2014, **4**, 60776–60784.

19 (*a*) L. Messori and G. Marcon, *Met. Ions Biol. Syst.*, 2004, **41**, 279–304; (*b*) P. J. Barnard and S. J. Berners-Price, *Coord. Chem. Rev.*, 2007, **2519**, 1889–1902; (*c*) S. Ray, R. Mohan, J. K. Singh, M. K. Samantaray, M. M. Shaikh, D. Panda and P. Ghosh, *J. Am. Chem. Soc.*, 2007, **129**, 15042–15053.

20 (*a*) Z. Yang, M. Bian, L. Lv, X. Chang, Z. Wen, F. Li, Y. Lu and W. Liu, *J. Med. Chem.*, 2023, **66**, 3934–3952; (*b*) P. Kapitza, A. l Scherfler, S. Sopper, M. Cziferszky, K. Wurst and R. Gust, *J. Med. Chem.*, 2023, **66**, 8238–8250.

21 L. Oehninger, R. Rubbiani and O. Ingo, *Dalton Trans.*, 2013, **42**, 3269–3284.

22 (*a*) F. Bray, J. Ferlay, I. Soerjomataram, R. L. Siegel, L. A. Torre and A. Jemal, *CA Cancer J. Clin.*, 2018, **68**, 394–424; (*b*) C. Allemani, H. K. Weir, H. Carreira, R. Harewood, D. Spika and X. S. Wang, *Lancet*, 2015, **385**, 977–1010.

23 C. Zappa and S. A. Mousa, *Transl. Lung Cancer Res.*, 2016, **5**, 288–300.

24 D. R. Camidge, W. Pao and L. V. Sequist, *Nat. Rev. Clin. Oncol.*, 2014, **11**, 473–481.

25 R. W. Johnstone, A. A. Ruefli and S. W. Lowe, *Cell*, 2002, **108**, 153–164.

26 D. W. Nicholson, *Cell Death Differ.*, 1999, **6**, 1028–1042.

27 (*a*) B. K. Rana, A. Nandy, V. Bertolasi, C. W. Bielawski, K. D. Saha and J. Dinda, *Organometallics*, 2014, **33**, 2544–2548; (*b*) T. Samanta, R. N. Munda, G. Roymahapatra, A. Nandy, K. D. Saha, S. S. Al-Deyab and J. Dinda, *J. Organometal. Chem.*, 2015, **791**, 183–191.

28 L. Maity, S. Barik, R. Biswas, R. Natarajan and J. Dinda, *Appl. Organomet. Chem.*, 2022, **36**, e6854.

29 J. Dinda, S. D. Adhikary, S. K. Seth and A. Mahapatra, *New J. Chem.*, 2013, **37**, 431–438.

30 S. Gaillard, M. Z. Slawin, A. T. Bonura, E. D. Stevens and S. P. Nolan, *Organometallics*, 2010, **29**, 394–402.

31 J. Dinda, T. Samanta, A. Nandy, K. Das Saha, S. K. Seth, S. K. Chattopadhyay and C. W. Bielawski, *New J. Chem.*, 2014, **38**, 1218–1224.

32 T. H. Hsu, J. J. Naidu, B. J. Yang, M. Y. Jang and I. J. Lin, *Inorg. Chem.*, 2012, **51**, 98–108.

33 F. Hackenberg, H. Muller-Bunz, R. Smith, W. Streciwilk, X. Zhu and M. Tacke, *Organometallics*, 2013, **32**, 5551–5560.

34 (*a*) S. D. Adhikary, A. Mondal, H. K. Kisan, C. W. Bielawski and J. Dinda, *Appl. Organometal. Chem.*, 2019, e5335; (*b*) V. Rani, H. B. Singh and R. J. Butcher, *Organometallics*, 2017, **36**, 4741–4752.

35 (*a*) A. E. Reed, L. A. Curtiss and F. Weinhold, *Chem. Rev.*, 1988, **88**, 899–926; (*b*) E. D. Glendening, A. E. Reed, J. E. Carpenter and F. Weinhold, *NBO Version 3.1*.

36 L. Jhulki, P. Dutta, M. K. Santra, M. H. Cardoso, K. G. N. Oshiro, O. L. Franco, V. Bertolasi, A. A. Isab, C. W. Bielawski and J. Dinda, *New J. Chem.*, 2018, **42**, 13948–13956.

37 S. K. Das, S. Roy, A. Das, A. Chowdhury, N. Chatterjee and A. Bhaumik, *Nanoscale Adv.*, 2022, **4**, 2313–2320.

38 N. B. Ghate, B. Hazra, R. Sarkar, D. Chaudhuri and N. Mandal, *In Vitro Cell. Dev. Biol. – Animal*, 2014, **50**, 527–537.

39 B. Gillissen, A. Richter, A. Richter, R. Preissner, K. Schulze-Osthoff, F. Essmann and P. T. Daniel, *J. Biol. Chem.*, 2017, **292**, 6478–6492.

40 J. F. R. Kerr, A. H. Wyllie and A. R. Currie, *Br. J. Cancer*, 1972, **26**, 239–257.

41 D. Hockenbery, G. Nuñez and C. Milliman, *Nature*, 1990, **348**, 334–336.

42 D. M. Hockenbery, Z. N. Oltvai, X. Yin, C. L. Milliman and S. J. Korsmeyer, *Cell*, 1993, **75**, 241–251.

43 (*a*) S. Das, N. Chatterjee, D. Bose, S. Banerjee, T. Jha and K. D. Saha, *Tumour Biol.*, 2015, **36**, 3109–3118; (*b*) T. R. Figueira, D. R. Melo, A. E. Vercesi and R. F. Castilho, *Mitochondrial Bioenergetics*, 2012, **810**, 103–117.

44 (*a*) X. M. Lin, S. B. Liu S, Y. H. Luo, W. T. Xu, Y. Zhang and T. Zhang, *BioMed Res. Int.*, 2020, 3042636; (*b*) X. Liu, C. N. Kim, J. Yang, R. Jemmerson and X. Wang, *Cell*, 1996, **86**, 147–157.

45 J. Yang, X. Liu, K. Bhalla, C. N. Kim, A. M. Ibrado, J. Cai, T. Peng, D. P. Jones and X. Wang, *Science*, 1997, **275**, 1129–1132.

46 (*a*) S. Roy, A. Das, M. Vernekar, S. Mandal and N. Chatterjee, *BioMed Res. Int.*, 2022, 5346091; (*b*) N. Chatterjee, S. Das, D. Bose, S. Banerjee, T. Jha and K. D. Saha, *PLoS One*, 2015, **10**, e0120509.

47 G. M. Sheldrick, *Acta Crystallogr., Sect. A: Found. Adv.*, 2015, **71**, 3–8.

48 G. M. Sheldrick, *Acta Crystallogr., Sect. C: Struct. Chem.*, 2015, **71**, 3–8.

49 O. V. Dolomanov, L. J. Bourhis, R. J. Gildea, J. A. K. Howard and H. Puschmann, *J. Appl. Crystallogr.*, 2009, **42**, 339.

50 (*a*) S. Grimme, J. Antony, S. Ehrlich and H. Krieg, *J. Chem. Phys.*, 2010, **132**, 154104–1541022; (*b*) F. Weigend and R. Ahlrichs, *Phys. Chem. Chem. Phys.*, 2005, **7**, 3297–3305; (*c*) M. J. Frisch, G. W. Trucks, H. B. Schlegel, G. E. Scuseria, M. A. Robb, J. R. Cheeseman, G. Scalmani, V. Barone, G. A. Petersson, H. Nakatsuji, X. Li, M. Caricato, A. V. Marenich,J. Bloino, B. G. Janesko, R. Gomperts, B. Mennucci, H. P. Hratchian, J. V. Ortiz, A. F. Izmaylov, J. L. Sonnenberg, D. Williams-Young, F. Ding, F. Lipparini, F. Egidi, J. Goings, B. Peng, A. Petrone,T. Henderson, D. Ranasinghe, V. G. Zakrzewski, J. Gao, N. Rega, G. Zheng, W. Liang, M. Hada, M. Ehara, K. Toyota, R. Fukuda, J. Hasegawa, M. Ishida, T. Nakajima, Y. Honda, O. Kitao, H. Nakai, T. Vreven, K. Throssell, J. A. Montgomery, Jr., J. E. Peralta, F. Ogliaro, M. J. Bearpark, J. J. Heyd, E. N. Brothers, K. N. Kudin, V. N. Staroverov, T. A. Keith, R. Kobayashi, J. Normand, K. Raghavachari, A. P. Rendell, J. C. Burant, S. S. Iyengar, J. Tomasi, M. Cossi, J. M. Millam, M. Klene, C. Adamo, R. Cammi, J. W. Ochterski, R. L. Martin, K. Morokuma, O. Farkas, J. B. Foresman and D. J. Fox, Gaussian, Inc., Wallingford CT, 2016.

51 (*a*) F. Weigend and R. Ahlrichs, *Phys. Chem. Chem. Phys.*, 2005, **7**, 3297–3305; (*b*) F. Weigend, *Phys. Chem. Chem. Phys.*, 2006, **8**, 1057–1065.

52 (*a*) W. J. Hehre, R. Ditchfield and J. A. Pople, *J. Chem. Phys.*, 1972, **56**, 2257–2261; (*b*) P. C. Hariharan and J. A. Pople, *Theor. Chim. Acta*, 1973, **28**, 213–222.

Nanoscale Advances

ROYAL SOCIETY OF CHEMISTRY

PAPER

Cite this: *Nanoscale Adv.*, 2022, **4**, 2313

A conjugated 2D covalent organic framework as a drug delivery vehicle towards triple negative breast cancer malignancy†

Sabuj Kanti Das,[a] Sraddhya Roy,[b] Ananya Das,[b] Avik Chowdhury,[a] Nabanita Chatterjee*[b] and Asim Bhaumik*[a]

Cancer, one of the deadliest diseases for both sexes, has always demanded updated treatment strategies with time. Breast cancer is responsible for the highest mortality rate among females worldwide and requires treatment with advanced regimens due to the higher probability of breast cancer cells to develop drug cytotoxicity followed by resistance. Covalent organic framework (COF) materials with ordered nanoscale porosity can serve as drug delivery vehicles due to their biocompatible nature and large internal void spaces. In this research work, we have employed a novel biocompatible COF, TRIPTA, as a drug delivery carrier towards breast cancer cells. It served as a drug delivery vehicle for cisplatin in triple negative breast cancer (TNBC) cells. We have checked the potency of TRIPTA in combating the proliferation of metastatic TNBC cells. Our results revealed that cisplatin loaded over TRIPTA-COF exhibited a greater impact on the $CD44^{+}/CD24^{-}$ cancer stem cell niche of breast cancer. Retarded migration of cancer cells has also been observed with the dual treatment of TRIPTA and cisplatin compared to that of cisplatin alone. Epithelial–mesenchymal transition (EMT) has also been minimized by the combinatorial treatment of cisplatin carried by the carrier material in comparison to cisplatin alone. The epithelial marker E-cadherin is significantly increased in cells treated with cisplatin together with the carrier COF, and the expression of mesenchymal markers such as N-cadherin is lower. The transcriptional factor Snail has been observed under the same treatment. The carrier material is also internalized by the cancer cells in a time-dependent manner, suggesting that the organic carrier can serve as a specific drug delivery vehicle. Our experimental results suggested that TRIPTA-COF can serve as a potent nanocarrier for cisplatin, showing higher detrimental effects on the proliferation and migration of TNBC cells by increasing the cytotoxicity of cisplatin.

Received 14th February 2022
Accepted 1st April 2022

DOI: 10.1039/d2na00103a

rsc.li/nanoscale-advances

1. Introduction

Among the various disease states, cancer shows high mortality and poor survival. Breast cancer is the most common heterogeneous malignancy among females across the world and represents around 30% of all the malignancies occurring in females.[1] It is categorized into three subtypes depending on the expression of hormone receptors, namely the estrogen receptor (ESR1), progesterone receptor (PGR), and HER2 epidermal growth factor receptor (ERBB2). The absence of expression of all three of these receptors is recognized as triple negative breast cancer (TNBC),[2] which shows more metastasis and a more aggressive disease state. Based on the gene expression patterns, 79% of TNBC belongs to the basal-like subtype,[3] one of the six stratified intrinsic molecular subtypes, the others of which are luminal subtype A, luminal subtype B, luminal subtype C, normal breast-like and ERBB2+. The absence of three receptors confines the treatment strategy towards TNBC; thus, chemotherapy is regarded as the sole standard for treating TNBC. Altered *BRCA*1 gene expression due to promoter methylation and p53 frameshift or nonsense mutations has been correlated with good response to chemotherapeutic regimens using cisplatin, a platinum-based drug, towards TNBC;[4] however, several factors account for the development of chemoresistance in cancer cells, such as accumulation of the drug in cells either by suppression of uptake or increased efflux, detoxification of the drug by redox mechanisms, altered regulation of the apoptotic pathway or impairment of DNA repair mechanisms.[5–8] Moreover, recent data by Hill *et al.* stated that there exist multiple mechanisms by which TNBC can acquire the property of cisplatin resistance.[9]

[a]*School of Materials Sciences, Indian Association for the Cultivation of Science, 2A & 2B Raja S. C. Mullick Road, Jadavpur, Kolkata 700032, India. E-mail: msab@iacs.res.in*

[b]*Receptor Biology and Tumor Metastasis, Chittaranjan National Cancer Institute, 37, S P Mukherjee Road, Kolkata-700 026, India. E-mail: nabanita.chatterje@gmail.com*

† Electronic supplementary information (ESI) available: FTIR, HRTEM, EMT with the involvement of TRIPTA COF cisplatin, drug binding assay, Cytotoxicity study. See https://doi.org/10.1039/d2na00103a

Thus, keeping this background in mind, here, we have checked the anticancer property of cisplatin in TNBC cells, MDA-MB-231, in combination with a novel nanoporous carrier material. For drug carriers, drug delivery vehicles or potential drugs, different organic, inorganic, and organic–inorganic hybrid molecules or nanomaterials are widely used.[10–13] Due to the advantages of cell viability, high surface area, and nanoscale porosity together with high void space and reactive surface functional groups, porous nanomaterials play significant roles as drug delivery vehicles.[14–16] Silica-based mesoporous materials, MOFs, COFs and porous polymeric materials have drawn significant attention due to their drug delivery capability.[17–20] Chemical stability and metal leaching are the serious drawbacks of MOF materials for bio-medicinal applications. Covalently bonded highly crystalline COF materials with metal-free framework structures can overcome those drawbacks. Easy tailoring of the structural and functional moieties of COF materials through pre and post synthesis modification[21,22] provides diverse opportunities in several potential applications, such as adsorption,[23] separation,[24] sensing,[25] electrochemical studies,[26,27] and biomedical applications.[28,29] Thus, here, we have loaded cisplatin over a 2D crystalline COF material, TRIPTA,[30,31] and used the resulting nanocomposite as a drug delivery vehicle towards metastatic breast cancer cells (Scheme 1). In order to determine whether this novel carrier material increases the efficacy of cisplatin, this study has been conducted; usage of TRIPTA may prove to be beneficial as a novel therapeutic approach towards the cisplatin treatment of TNBC cells.

2. Experimental

2.1. Chemicals

Phloroglucinol was obtained from Sigma-Aldrich and used for the synthesis of 1,3,5-triformylphloroglucinol (TFP).[27] 4-Aminobenzonitrile and trifluoromethanesulfonic acid were purchased from Sigma-Aldrich and used for the synthesis of 1,3,5-tris-(4-aminophenyl)-triazine (TAPT).[19] Anhydrous *N*,*N*-dimethylformamide, hexamine, trifluoroacetic acid and hydrochloric acid were obtained from Merck, India, and all were used without further purification.

2.2. Material characterization techniques

A Bruker AXS D-8 Advance SWAX diffractometer was used to obtain the powder X-ray diffraction pattern of TRIPTA, where the radiation source was Cu-Kα ($\lambda = 1.5406$ Å). High-resolution transmission electron microscopy (TEM) images of the COF material were collected from a HR-TEM system (JEOL JEM 2100) operated with a 200 kV electron source. For the HRTEM analysis of TRIPTA, a sonicated ethanolic dilute solution of the carrier was dropped over a carbon-coated copper grid and then dried under high vacuum for 12 h. A Quantachrome Autosorb-iQ surface area analyzer (USA) was used for surface area and porosity analysis at 77 K. From the N_2 adsorption/desorption isotherms, we calculated the Brunauer–Emmett–Teller (BET) surface area and pore size distribution plot using non-local density functional theory (NLDFT), taking N_2 sorption at 77 K on carbon with the slit pore model as a reference. The powder sample of TRIPTA-COF was Soxhlet extracted for 72 h using anhydrous MeOH : THF (1 : 1) followed by drying under vacuum at 160 °C for 24 h. A Mettler Toledo TGA/DTA 851e TA-SDT Q-600 instrument was used for the thermal stability analysis. The FTIR spectrum of TRIPTA was recorded using a PerkinElmer spectrum 100 spectrophotometer. The amount of cisplatin loading in the drug-loaded TRIPTA was analyzed by measuring the total Pt content with the help of ICP-OES analysis by using a PerkinElmer Optima 2100 DV optical emission spectrometer.

2.3. Synthesis of TRIPTA

TRIPTA was synthesized through a solvothermal Schiff base polycondensation reaction using a Pyrex sealed tube.[30] 141.2 mg TAPT (0.4 mmol) and 84 mg TFP (0.4 mmol) were taken in the dry Pyrex tube, followed by the addition of 6 ml 1 : 1 mesitylene and 1,4-dioxane along with 0.5 ml 6 N acetic acid. Sonication was performed for 20 min to afford a homogeneously dispersed reaction mixture. The as-prepared mixture was degassed three times with a freeze–pump–thaw cycle. After that, the Pyrex tube was flame sealed, and the solvothermal reaction was allowed to proceed for 4 days. Finally, the deep orange-red fine powder material was filtered off and washed with ethanol followed by THF to remove unreacted starting monomers. Finally, the guest-free porous COF material was obtained by Soxhlet extraction with THF : methanol (1 : 1) for 48 h and dried under vacuum at 150 °C overnight. The isolated yield of the COF material was 81 wt%.

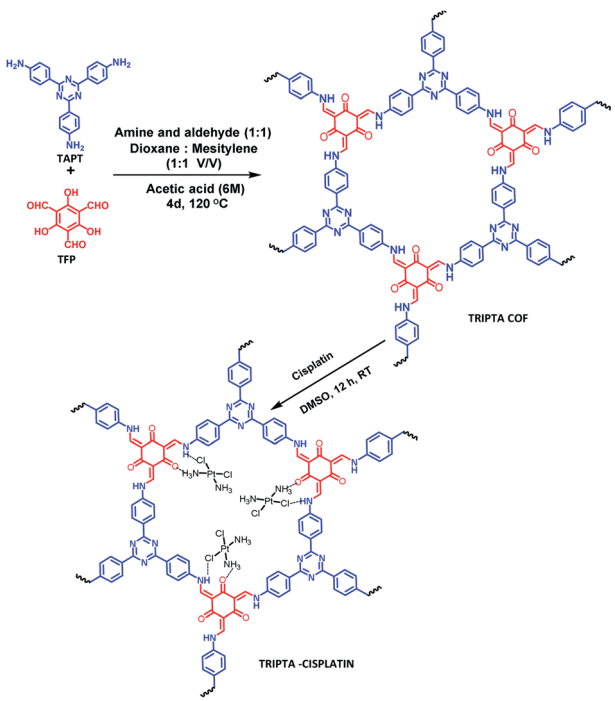

Scheme 1 Synthesis of the TRIPTA-COF and cisplatin-loaded TRIPTA-CISPLATIN.

2.4. Synthesis of TRIPTA-CISPLATIN

Cisplatin was impregnated into the void spaces of the COF through overnight stirring of TRIPTA and cisplatin in a round bottom flask using DMSO as a solvent. The desired product was collected through a filtration process followed by washing with DI water several times and drying at room temperature under vacuum. After loading of the drug into the COF material, we performed the quantitative drug loading assay using gravimetric as well as ICP-OES techniques (detailed calculations are provided in the ESI, Section S1†). The obtained cisplatin loading efficiency was 31.19%. From the ICP-OES analysis, considering the amount of Pt, the calculated ratio of cisplatin and COF was found to be 2 : 1, *i.e.*, two cisplatin molecules per hexagonal unit.

2.5. Cell culture

MDA-MB-231 triple negative breast cancer cells were grown in DMEM:F12 media supplemented with 10% heat-inactivated fetal bovine serum (FBS) and 1% antibiotic (PSN) at 37 °C in a humidified atmosphere under 5% CO_2. After 75–80% confluency, the cells were harvested with 0.025% trypsin and 0.52 mM EDTA in phosphate buffered saline (PBS) and seeded at the desired density to allow them to re-equilibrate a day before the start of the experiment.

2.6. Cell viability assays

To define the cell viability, an MTT assay was performed. Cells were plated at a count of 5×10^3 cells in a 96-well flat-bottom transparent plate and allowed to seed overnight at 37 °C in 5% CO_2.[32] After their adhesion, the cells were treated under different conditions, with only cisplatin, only carrier, and a combination of cisplatin and carrier. Treatments were given at specific time intervals of 0, 24, 48 and 72 h. Following treatment with the drug and carrier, 20 μl 3-(4,5-dimethylthiazol-2-yl)-2,5 diphenyltetrazolium bromide (MTT) tetrazolium dissolved in PBS were added to each well and incubated for 3 h at 37 °C. After incubation, 150 μl dimethyl sulphoxide (DMSO) was added to each well. The plates were analyzed in a microplate plate reader at 595 nm.[33]

2.7. Scratch wound assay

For the scratch assay, MDA-MB-231 cells were seeded in three 35 mm plates ($n = 6$) with a cell population density of 0.025×10^6 cells per well followed by incubation for 24 h for their growth. After obtaining confluent monolayers of cells, a scratch wound was created as a straight line with a 200 μl sterile pipette tip, and the time was designated as 0 h. One plate was the control, and the other two plates were treated with only 100 μl cisplatin and 10 μl TRIPTA-COF of interest. Images were captured at 0 h and after 48 h. The percent wound confluence was calculated using $[(A - B) \times 100/A]$, where A is the width of the scratch at 0 h and B is the width upon achieving confluency after 48 h.[34]

2.8. Cellular uptake

After 12 h of incubation, the cellular uptake study revealed that TRIPTA-COF was internalized by the cell membrane, leading to a cytosolic portion of cells with a maximum uptake of more than 60%.[35] To check the uptake of carrier molecules within the cells, the carrier molecule was administered in a six-well plate seeded with MDA-MB-231 cells. In the control wells, no carrier molecule was added, while carrier molecules were added to the other wells at 0, 0.5, 1, 3 and 12 h intervals in order to check their uptake at specific time intervals. Data were collected using a spectrophotometer at 510 nm.[36]

2.9. Stemness assay

For the flow cytometry analysis, MDA-MB-231 cells in the logarithmic growth phase were digested with 0.25% trypsin and washed with PBS three times, followed by being re-suspended in 100 μl PBS; then, they were stained with anti-CD44-FITC and anti-CD24-PE or stained with their isotype control at room temperature for 40 min. The samples were then washed with PBS three times and finally re-suspended in 200 μl PBS. Flow cytometry analysis was performed on a BD FACSverse Flow Cytometer (BD Bioscience). The expression ratio of CD44 and CD24 ($CD44^+/CD24^-$) in the breast cancer cell line was calculated from the percentage of CD44-positive and CD24-negative sub-populations in the flow cytometry analysis.

2.10. Analysis of protein expression

After treatment with cisplatin, the resulting TRIPTA-CISPLATIN fixation in cells was conducted in 4% paraformaldehyde in PBS (pH 7.4) for 20 min at room temperature. 0.1% TritonX-100 in PBS was used for permeabilization with 0.1% FBS for 5 min. After washing twice with PBS with 3% FBS, the permeabilized cells were incubated with the primary antibody on ice for 2 h and washed with PBS. Then, the cells were incubated with FITC-conjugated goat anti-rabbit IgG as the secondary antibody for 2 h on ice and washed twice with PBS. The stained cells were acquired and analyzed using a BD FACSverse Flow Cytometer (San Jose, CA, USA) with the FlowJo software.

2.11. Statistical analysis

All values are expressed as mean ± SD. Statistical significance was compared between various treatment groups and controls using one-way analysis of variance (ANOVA). Data were considered statistically significant when P values were <0.01.

3. Results and discussion

3.1. PXRD and spectroscopic analysis

The formation of the crystalline organic framework of TRIPTA was confirmed from the PXRD analysis. The PXRD pattern of the COF in the 2θ value range from 4 to 60° is shown in Fig. 1A, where the peaks at 5.6°, 9.8°, 15.2° and 26.4° can be assigned to the crystal planes of 100, 110, 210 and 001, respectively. The PXRD pattern is very similar to that of TRIPTA previously synthesized by our group.[30] To investigate the incorporation of cisplatin into the COF, a PXRD study was performed with a powder sample of cisplatin-loaded TRIPTA-COF (Fig. 1B). The PXRD peaks at 5.74° (100 plane) and 26.3° (001 plane) remain almost identical, which indicates the structural integrity of

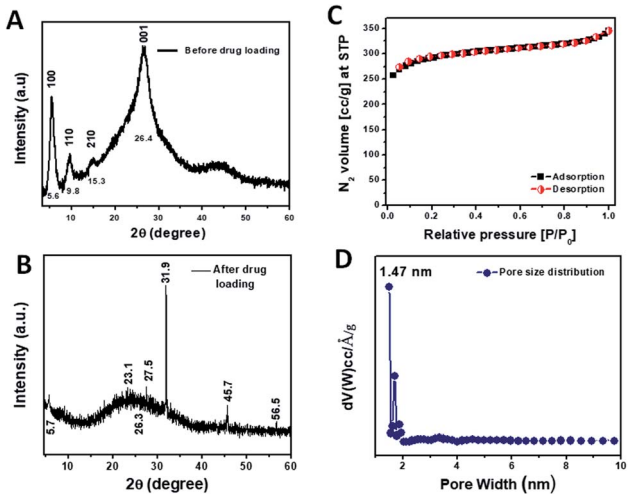

Fig. 1 PXRD patterns of TRIFTA-COF (A) and TRIPTA-CISPLATIN (B); N_2 adsorption/desorption isotherms (C) along with the pore size distribution plot (D).

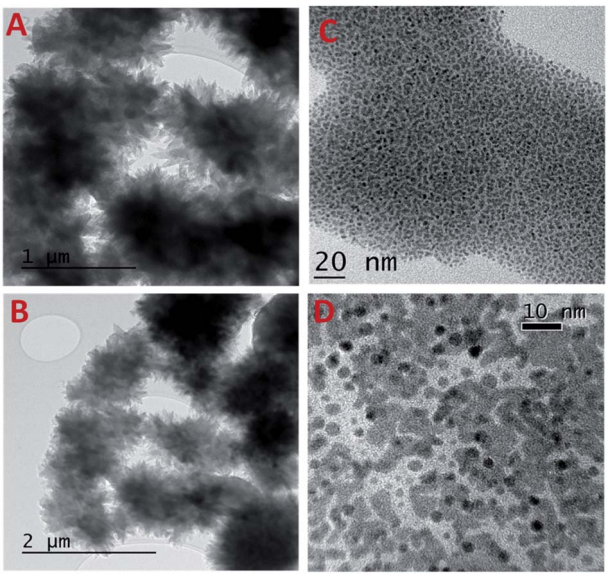

Fig. 2 HRTEM images of TRIPTA (A and B) and TRIPTA-CISPLATIN (C and D) at different resolutions.

TRIPTA-COF. Very slight shifting of the PXRD peaks may have arisen from the loading of cisplatin into the porous network. Additional peaks that appeared at 23.1°, 27.6°, 31.9°, 45.7° and 56.5° indicate the incorporation of cisplatin in the COF matrix.[37] FTIR data (Fig. S1†) were collected using a powder sample of TRIPTA-COF in the range of 400 to 4000 cm^{-1}, where the characteristic peaks appeared at 1623, 1575 and 1256 cm^{-1}. These peaks are assigned to the >C=O (α,β-unsaturation), >C=C< and >C–NH– (keto-enamine) groups, respectively.[30] Thus, the FTIR analysis confirms the formation of TRIPTA as well as the presence of different bonding connectivities in the porous polymer framework.

3.2. Surface area and porosity analysis

Specific surface area and pore size distribution analyses were carried out using the N_2 adsorption/desorption isotherms (Fig. 1C) taken at 77 K. The N_2 adsorption/desorption isotherms of TRIPTA could be classified as typical Type I, indicating the microporous nature of the material.[38] The specific surface area calculated from the isotherms was 1074 $m^2\ g^{-1}$. The pore size distribution plot (Fig. 1D) was obtained from the N_2 adsorption/desorption isotherms by employing the NLDFT model; the pore sizes appeared in the microporous region, with a peak pore size distribution at *ca.* 1.47 nm.

3.3. Morphological analysis

HRTEM analysis was carried out to understand the morphology of the COF carrier TRIPTA and cisplatin-loaded COF, which are shown in Fig. 2. HRTEM images confirm the flower-like particle morphology of the COF (Fig. 2A and B). Further, the images of samples treated with different acids, 7.4 pH buffer and neutral pH are shown in Fig. S2.† It can be seen from these images that the morphology of the COF remained unchanged under different conditions. This result suggests the high structural integrity of TRIPTA. TRIPTA-COF has been successfully utilized as a drug delivery vehicle to deliver cisplatin towards triple negative breast cancer malignancy. TRIPTA-CISPLATIN showed enhancement of the *in vitro* anticancer activity of cisplatin against breast cancer cells. HRTEM images of the cisplatin-loaded COF are shown in Fig. 2C, D and S3,† where the actual sizes of the COF and cisplatin are electronically visualized at different magnifications (100, 20, 10 and 5 nm) with an average particle size of less than 10 nm. Materials or nanoparticles with particle sizes less than 50 nm are highly efficient for cellular uptake. Zhao *et al.* summarized the intercellular uptake of different kinds of materials with wide particle size ranges through endocytosis.[39]

3.4. The COF increases the cytotoxicity of cisplatin while decreasing the viability of MDA-MB-231 cells

When checking the percentage viability of breast cancer cells, MTT analysis revealed that the percentage viability decreased gradually with increasing concentration of cisplatin and carrier. Decreased viability was observed under individual treatment of cisplatin and carrier; however, the rate of decreased viability with increasing concentration was considerably lower than that of cisplatin and TRIPTA-CISPLATIN. The cell viability under cisplatin and carrier treatment decreased to zero at 100 μM concentration and was recorded to be maximum in the control, followed by only carrier treatment and only cisplatin treatment, as per Fig. 3A and C. The IC50 values of cisplatin and TRIPTA-CISPLATIN were calculated to be 20 μM and 2.5 μM, respectively.

3.5. The carrier molecule enhances the activity of cisplatin in decreasing the population of $CD44^+/CD24^-$ stemness in MDA-MB-231 cells

Cancer stem cells are a highly tumorigenic population of cells that are endowed with self-renewal ability and are often

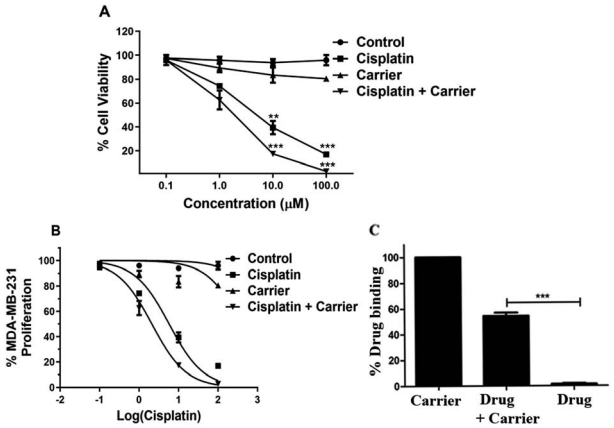

Fig. 3 Cells were treated with TRIPTA-COF along with cisplatin in the concentration range of 0–100 μM of cisplatin and TRIPTA-COF for 48 h. A significant result was found with TRIPTA-COF and cisplatin as compared to cisplatin alone, where (A) cell viability, (B) % MDA-MB-231 proliferation and (C) % drug binding were assayed by flow cytometric analyses with cisplatin, carrier and cisplatin + carrier. The data are represented as mean ± standard deviation (SD) from triplicate independent experiments (*$P \leq 0.05$, ***$P \leq 0.001$).

associated with drugs.[40] We compared the expression of $CD44^+/CD24^-$ in cisplatin and cisplatin with carrier-treated cells, as shown in Fig. 4A. We found significant changes in the $CD44^+/CD24^-$ stem cell population among the control, cisplatin and cisplatin with carrier groups. As shown in Fig. 4B and C, the $CD44^+/CD24^-$ stem cell population decreased in the cisplatin with carrier molecule group compared with the only cisplatin group and control group. The control group has the highest population of $CD44^+/CD24^-$ stem cells, which eventually decreased with the treatment of cisplatin and cisplatin with the carrier molecule. We found a significant difference in the $CD44^+/CD24^-$ stem cell population of the control and cisplatin groups as well as in the cisplatin and cisplatin and carrier molecule groups.

The uptake of a carrier molecule increases with incubation time. In order to check the potency and efficacy of the carrier molecule, a cellular uptake assay was performed. The uptake of the carrier molecules was observed to be maximum under 12 h of treatment, where the uptake percentage was above 60% and decreased gradually with decreasing treatment time; the lowest percentage was obtained at 0 h, as per Fig. 4D. The uptake at 12 h and 24 h was significantly high compared to that of the control. As shown in Fig. S4,† we performed a drug binding assay where we checked the drug (cisplatin), carrier (TRIPTA-COF) and covalent organic framework (TRIPTA-CISPLATIN) by flow cytometry analysis and drug release (Fig. S5†).

3.6. TRIPTA-CISPLATIN is more potent in inhibiting the migration of breast cancer cells

The control group did not receive any dosage of treatment, and after 48 h, the scratch created was filled with migrating breast cancer cells with 80% confluency. However, it was noted that treatment of MDA-MB-231 cells with cisplatin (2.5 μM) had a retarding effect on the migration of the cells and had approximately 60% confluency in the scratch. This migration retarding effect on the cancer cells was further enhanced in the cell plate treated with cisplatin and the carrier of interest, where the confluency was reduced to below 40% (Fig. 5A–C). Thus, it could be concluded that although cisplatin has an inhibiting effect on cancer cells, its inhibitory activity can be increased when administered in combination with the carrier.

The carrier COF with cisplatin attenuates EMT (epithelial–mesenchymal transition) in MDA-MB-231 cells. EMT, in which cancer cells lose their epithelial property and adopt mesenchymal features, is one of the important mechanisms involved in stemness, metastasis and the recurrence of breast cancer. We investigated the role of the carrier molecule in the EMT of TGF-

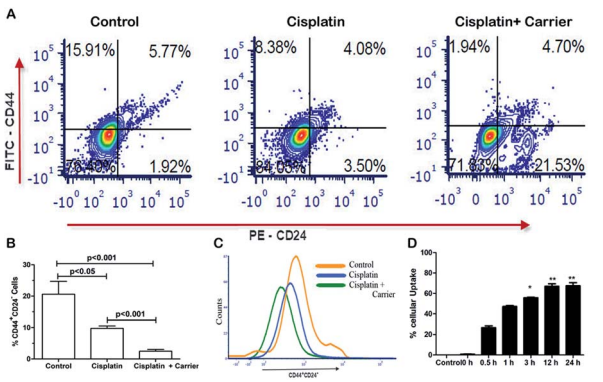

Fig. 4 Cells were pretreated with TGF-β to induce EMT and treated with TRIPTA-COF along with cisplatin. After 12 h of treatment, the cells stained with anti-FITC-CD44 and anti-PE-CD24 were compensated and analyzed with flow cytometry. (A) Flow cytometry data (control, cisplatin, control + cisplatin as TRIPTA-CISPLATIN) with anti-CD44 and anti-CD24, (B) percentages of $CD44^+/CD24^-$ cells, (C) histogram positive events ($CD44^+/CD24^-$ cells), and (D) percentages of cellular uptake of TRIPTA-COF in a time-dependent manner by spectrometry. The data are represented as mean ± standard deviation (SD) from triplicate independent experiments.

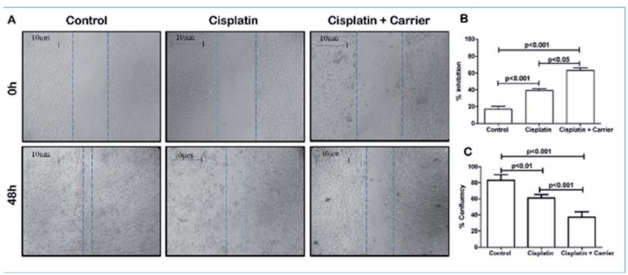

Fig. 5 Effect of cisplatin + carrier as TRIPTA-CISPLATIN on cell migration in MDA-MB-231 cells. (A) Analysis of MDA-MB-231 cell migration by scratch assay. (B) Percentages of inhibition and quantitative representation of the percentages of cell migration into the wound scratch after TRIPTA-CISPLATIN treatment for 24 h. (C) Percentages of confluency-quantitative representation of the percentages of cell migration into the wound scratch after TRIPTA-CISPLATIN treatment for 24 h. Representative images of wound healing at 0 and 24 h following scratch induction and TRIPTA-CISPLATIN treatment. The data are represented as mean ± standard deviation (SD) from triplicate independent experiments.

β-induced MDA-MB-231 cells, as shown in Fig. 6. We observed that the carrier material itself does not attenuate EMT; however, together with cisplatin, it decreases mesenchymal markers and increases the expression of epithelial markers (Fig. S6†). The carrier material enhances the cellular uptake of cisplatin and thus enhances its functional activity. We found significant changes in the expression of E-cadherin and N-cadherin between the carrier and the carrier with cisplatin groups, as shown in Fig. 6A–D. The expression of the epithelial marker E-cadherin (E-Cad) increased significantly in the carrier with cisplatin group compared with that in the carrier group, and the expression of the mesenchymal markers N-cadherin (N-Cad) and Snail decreased significantly.

The transcriptional factor Snail promotes and regulates the expression of EMT proteins such as E-Cad and N-Cad. Under treatment with the carrier molecule along with cisplatin, we found reduced expression of Snail in the flow cytometry analysis (Fig. 7), which in turn may be the underlying reason for the greater expression of E-Cad as compared to N-Cad.

3.7. Discussion

More metastatic and aggressive breast cancer cells, MDA-MB-231, are more prone to developing cisplatin resistance, with lower response to this platinum-derived agent compared to other mammary carcinoma cells. In this study, we have investigated the cytotoxicity of cisplatin in MDA-MB-231 in the presence of a novel porous carrier material, TRIPTA-COF, in order to check whether there is any increment in the efficiency of the drug to decrease the proliferation of cells and increase their sensitivity to the drug *via* regulating the stemness (Fig. S6†).

The proliferation and migration of cancer cells are intrinsic properties that depict the growth and metastasizing capability of cancer cells. Targeting cell proliferation can minimize the probability of metastasis. In this study, when the carrier molecule was administered with cisplatin, positive results with minimal migration were observed as compared to that with cisplatin alone. This suggests that the carrier molecules and cisplatin together have a detrimental effect on cell division, thereby minimizing the mobility of cancer cells. Furthermore, this novel carrier molecule has a high tendency to be internalized by cancer cells in a time-dependent manner, indicating that it can efficiently transfer cisplatin to cancer cells, which may increase the cytotoxicity of cisplatin. We have investigated the role of the carrier COF material in $CD44^{+}/CD24^{-}$ stem cell populations and the EMT of the MDA-MB-231 cell line. It has been observed that the carrier molecule together with cisplatin significantly decreases the population of $CD44^{+}/CD24^{-}$ in MDA-MB-231 cells, indicating that the stemness of the cancer cells in turn is a probable reason for retarded migration.

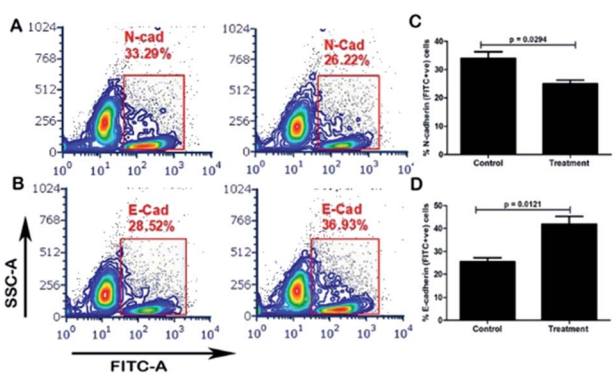

Fig. 6 Evaluation of the expression of E-cadherin and N-cadherin by flow cytometry. After treatment with cisplatin + carrier as TRIPTA-CISPLATIN along with only cisplatin and followed by TGF-β induction, we evaluated the (A) N-cadherin (N-Cad) expression; (C) quantitative analysis of the % N-Cad positive cells; (B) E-cadherin (E-Cad) expression; and (D) quantitative analysis of the % E-Cad positive cells. The data are represented as mean ± standard deviation (SD) from triplicate independent experiments.

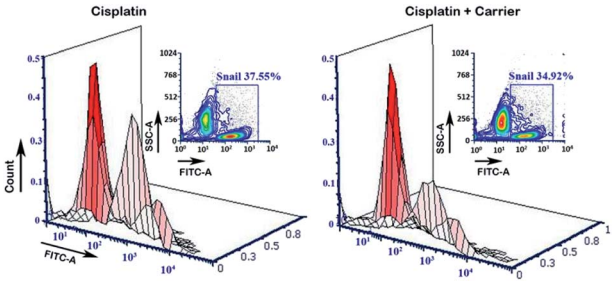

Fig. 7 Estimation of the expression of Snail by flow cytometry analysis. After treatment with cisplatin + carrier as TRIPTA-CISPLATIN along with only cisplatin and followed by TGF-β induction, the Snail expression with 3D analysis was evaluated. The data are represented as triplicate experiments.

MDA-MB-231 cells are prone to undergo EMT associated with breast cancer metastasis by transforming themselves from the polarized epithelial state to the non-polarized mesenchymal state to initiate the process of cancer progression.[41] Recently, Wang *et al.* reported that cisplatin in combination with paclitaxel is capable of retarding TGF-β-induced EMT in breast cancer cells.[42] To enhance the cytotoxicity of cisplatin towards TNBC cells, we attempted to administer cisplatin *via* the TRIPTA-COF carrier material (Fig. S7†). We have studied the role of the carrier molecule in enhancing the functional activity of cisplatin on EMT. The carrier COF was unable to change the expression of EMT markers; however, together with cisplatin, it was able to significantly decrease the expression of the mesenchymal marker N-cadherin and the transcription factor Snail and increase the expression of the epithelial marker E-cadherin. The carrier material also plays a role in enhancing the activity of cisplatin in EMT; however, TRIPTA-COF alone has not shown any effect on the EMT process.

4. Conclusion

We have immobilized cisplatin on the surface of TRIPTA-COF, and the resulting nanocomposite material has been utilized for triple negative breast cancer cell destruction. The anticancer activity of cisplatin itself is significantly lower than that of cisplatin-loaded TRIPTA-COF. As the COF material alone did

not play any significant role in the EMT process, it may act by precisely delivering cisplatin towards breast cancer cells for enhancement of the anticancer activity of cisplatin. Thus, the efficacy of cisplatin can be enhanced when it is encapsulated in the novel porous drug delivery carrier material, TRIPTA. Hence, our experimental results of utilizing TRIPTA-COF as a transporter of an anticancer drug reported herein will open up new opportunities in biomedical research in the future.

Conflicts of interest

There are no conflicts to declare.

Acknowledgements

SKD would like to thank IACS Kolkata and UGC, New Delhi, for Senior Research Fellowships. SR would like to thank University Grant Commission: for a Junior Research Fellowship. AB would like to thank IGSTC, New Delhi, for the Indo-German project research grant (Project no. IGSTC/Call 2018/CO2BioFeed/15/2019-20/). Cells and other biological samples used in this work were gifted by Dr A. K. Srivastava, Scientist, CSIR-Indian Institute of Chemical Biology.

Notes and references

1 S. D. Cosimo and J. Baselga, *Nat. Rev. Clin. Oncol.*, 2010, **7**, 139–147.
2 J. R. Jhan and E. R. Andrechek, *Pharmacogenomics*, 2017, **18**, 1595–1609.
3 A. Prat, B. Adamo, M. C. U. Cheang, C. K. Anders, L. A. Carey and C. M. Perou, *Oncologist*, 2013, **18**, 123–133.
4 D. P. Silver, A. L. Richardson, A. C. Eklund, Z. C. Wang, Z. Szallasi, Q. Li, N. Juul, C. O. Leong, D. Calogrias, A. Buraimoh, A. Fatima, R. S. Gelman, P. D. Ryan, N. M. Tung, A. D. Nicolo, S. Ganesan, A. Miron, C. Colin, D. C. Sgroi, L. W. Ellisen, E. P. Winer and J. E. Garber, *J. Clin. Oncol.*, 2010, **28**, 1145–1153.
5 C. A. Rabik, E. B. Maryon, K. Kasza, J. T. Shafer, C. M. Bartnik and M. E. D. Cara, *Cancer Chemother. Pharmacol.*, 2009, **64**, 133–142.
6 Z. Zhu, S. Du, Y. Du, J. Ren, G. Ying and Z. Yan, *J. Neurochem.*, 2018, **144**, 93–104.
7 L. Galluzzi, L. Senovilla, I. Vitale, J. Michels, I. Martins, O. Kepp, M. Castedo and G. Kroemer, *Oncogene*, 2012, **31**, 1869–1883.
8 M. Parhizkar, P. J. T. Reardon, A. H. Harker, R. J. Browning, E. Stride, R. B. Pedley, J. C. Knowles and M. Edirisinghe, *Nanoscale Adv.*, 2020, **2**, 1177–1186.
9 D. P. Hill, A. Harper, J. Malcolm, M. S. McAndrews, S. M. Mockus, S. E. Patterson, T. Reynolds, E. J. Baker, C. J. Bult, E. J. Chesler and J. A. Blake, *BMC Cancer*, 2019, **19**, 1039.
10 J. K. Patra, G. Das, L. F. Fraceto, E. V. R. Campos, M. P. R. Torres, L. S. A. Torres, L. A. D. Torres, R. Grillo, M. K. Swamy, S. Sharma, S. Habtemariam and H.-S. Shin, *J. Nanobiotechnol.*, 2018, **16**, 71.
11 L. Fu, H. Q. Gao, M. Yan, S. Z. Li, X. Y. Li, Z. F. Dai and S. Q. Liu, *Small*, 2015, **11**, 2938–2945.
12 L. Bai, S. Z. F. Phua, W. Q. Lim, A. Jana, Z. Luo, H. P. Tham, L. Zhao, Q. Gao and Y. Zhao, *Chem. Commun.*, 2016, **52**, 4128–4131.
13 Z. Shi, Y. Zhou, T. Fan, Y. Lin, H. Zhang and L. Mei, *Smart Mater. Med.*, 2020, **1**, 32–47.
14 C. Chen, W. Tang, D. W. Jiang, G. L. Yang, X. L. Wang, L. N. Zhou, W. A. Zhang and P. Wang, *Nanoscale*, 2019, **11**, 11012–11024.
15 P. Kumar, K. H. Kim, A. Saneja, B. Wang and M. Kukkar, *J. Porous Mater.*, 2019, **26**, 655–675.
16 L. C. C. Fonseca, M. de Sousa, D. L. S. Maia, V. L. de Luna and O. L. L. Alves, *Nanoscale Adv.*, 2020, **2**, 1290–1300.
17 C. Bharti, U. Nagaich, A. K. Pal and N. Gulati, *J. Pharm. Invest.*, 2015, **5**, 124–133.
18 M. Liu, L. Wang, X. H. Zheng, S. Liu and Z. Xie, *ACS Appl. Mater. Interfaces*, 2018, **10**, 24638–24647.
19 S. K. Das, S. Mishra, K. Manna, U. Kayal, S. Mahapatra, K. Das Saha, S. Dalapati, G. P. Das, A. A. Mostafa and A. Bhaumik, *Chem. Commun.*, 2018, **54**, 11475–11478.
20 L. L. Feng, C. Qian and Y. L. Zhao, *ACS Mater. Lett.*, 2020, **2**, 1074–1092.
21 V. Valtchev, G. Majano, S. Mintova and J. Perez-Ramirez, *Chem. Soc. Rev.*, 2013, **42**, 263–290.
22 S. Das, P. Heasman, T. Ben and S. Qiu, *Chem. Rev.*, 2017, **117**, 1515–1563.
23 H. Wei, S. Chai, N. Hu, Z. Yang, L. Wei and L. Wang, *Chem. Commun.*, 2015, **51**, 12178–12181.
24 B. P. Biswal, H. P. Chaudhari, R. Banerjee and U. K. Kharul, *Chem. – Eur. J.*, 2016, **22**, 4695–4699.
25 S. H. Zhang, Q. Yang, X. T. Xu, X. H. Liu, Q. Li, J. R. Guo, N. L. Torad, S. M. Alshehri, T. Ahamad, M. S. A. Hossain, Y. V. Kaneti and Y. Yamauchi, *Nanoscale*, 2020, **12**, 15611–15619.
26 X. Zhao, P. Pachfule and A. Thomas, *Chem. Soc. Rev.*, 2021, **50**, 6871–6913.
27 S. K. Das, K. Bhunia, A. Mallick, A. Pradhan, D. Pradhan and A. Bhaumik, *Microporous Mesoporous Mater.*, 2018, **266**, 109–116.
28 Q. Guan, G. B. Wang, L. L. Zhou, W. Y. Li and Y. B. Dong, *Nanoscale Adv.*, 2020, **2**, 3656–3733.
29 S. Bhunia, K. A. Deo and A. K. Gaharwar, *Adv. Funct. Mater.*, 2020, **30**, 2002046.
30 R. Gomes and A. Bhaumik, *RSC Adv.*, 2016, **6**, 28047–28054.
31 S. K. Das, B. K. Chandra, R. A. Molla, M. Sengupta, S. M. Islam, A. Majee and A. Bhaumik, *Mol. Catal.*, 2020, **480**, 110650.
32 C. Germain, N. Niknejad, L. Ma, K. Garbui, T. Hai and J. Dimitroulakos, *Neoplasia*, 2010, **12**, 527–538.
33 N. Chatterjee, S. Das, D. Bose, S. Banerjee, T. Jha and K. Das Saha, *PLoS One*, 2015, **10**, e0120509.
34 P. Buachan, L. Chularojmontri and S. K. Wattanapitayakul, *Nutrients*, 2014, **6**, 1618–1634.
35 F. Zhao, Y. Zhao, Y. Liu, X. Chang, C. Chen and Y. Zhao, *Small*, 2011, **7**, 1322–1337.

36 M. Pramanik, N. Chatterjee, S. Das, K. Das Saha and A. Bhaumik, *Chem. Commun.*, 2013, **49**, 9461–9463.
37 A. C. Jayasuriya and A. J. Darr, *J. Biomed. Sci. Eng.*, 2013, **6**, 586–592.
38 S. K. Das, S. Chatterjee, S. Mondal and A. Bhaumik, *Mol. Catal.*, 2019, **475**, 110483.
39 F. Zhao, Y. Zhao, Y. Liu, X. Chang, C. Chen and Y. Zhao, *Small*, 2011, **7**, 1322–1337.
40 W. Li, H. Ma, J. Zhang, L. Zhu, C. Wang and Y. L. Yang, *Sci. Rep.*, 2017, **7**, 13856.
41 Z. Huang, P. Yu and J. Tang, *OncoTargets Ther.*, 2020, **13**, 5395–5405.
42 H. Wang, S. Guo, S. J. Kim, F. Shao, J. W. Kei Ho, K. U. Wong, Z. Miao, D. Hao, M. Zhao, J. Xu, J. Zeng, K. H. Wong, L. Di, A. H. H. Wong, X. Xu and C. X. Deng, *Theranostics*, 2021, **11**, 2442–2459.

Clinical Immunology 231 (2021) 108804

Contents lists available at ScienceDirect

Clinical Immunology

journal homepage: www.elsevier.com/locate/yclim

Review Article

Understanding the immunological aspects of SARS-CoV-2 causing COVID-19 pandemic: A therapeutic approach

Ananya Das [a], Sraddhya Roy [a], Snehasikta Swarnakar [b,**], Nabanita Chatterjee [a,*]

[a] Department of Receptor Biology and Tumor Metastasis, Chittaranjan National Cancer Institute, Kolkata, India
[b] Department of Infectious Diseases and Immunology, CSIR-Indian Institute of Chemical Biology, Kolkata, India

ARTICLE INFO

Keywords:
SARS-CoV-2
Immune response
COVID-19 therapy

ABSTRACT

In December 2019, Severe Acute Respiratory Syndrome Coronavirus 2 (SARS-CoV-2), a novel variant of coronavirus has emerged from Wuhan in China and has created havoc impulses across the world with a larger number of fatalities. At the same time, studies are on roll to discover potent vaccine against it or repurposing of approved drugs which are widely adopted are under trial to eradicate the SARS-CoV-2 causing COVID-19 pandemic. Reports have also shown that there are asymptomatic carriers of COVID-19 disease who can transmit the disease to others too. However, the first line defense of the viral attack is body's strong and well-coordinated immune response producing excessive inflammatory innate reaction, thus impaired adaptive host immune defense which lead to death upon the malfunctioning. Considerable works are going on to establish the relation between immune parameters and viral replication that, might alter both the innate and adaptive immune system of COVID-19 patient by up riding a massive cytokines and chemokines secretion. This review mainly gives an account on how SARS-CoV-2 interacts with our immune system and how does our immune system responds to it, along with that drugs which are being used or can be used in fighting COVID-19 disease. The curative therapies as treatment for it have also been addressed in the perspective of adaptive immunity of the patients.

Abbreviations: ACE, angiotensin converting enzyme; Agn, angiotensin; AMs, alveolar macrophages; APCs, antigen presenting cells; ARDS, acute respiratory distress syndrome; ASCs, antigen secreting cells; AT2, alveolar type 2; BAL, bronchoalveolar lavage; CD, cluster of differentiation; cDCs, conventional dendritic cells; CCL, C-C motif chemokine ligand; CDHR3, cadherin related family member 3; CLpro, chymotrypsin-like protease; Covid-19, coronavirus disease, 2019; CTL, cytotoxic T lymphocyte; CTLA, cytotoxic T lymphocyte associated antigen; CXCL, C-X-C motif chemokine ligand; CXCR, C-X-C motif chemokine receptor; DMVs, double membrane vesicles; DPP4, dipeptidyl peptidase 4; dsDNA, double stranded DNA; dsRNA, double stranded RNA; E, envelope; FGF, fibroblast growth factor; G-CSF, granulocyte colony stimulating factor; GM-CSF, granulocyte-monocyte colony stimulating factor; GZMA, granzyme; HCoV, human coronavirus; H, hydrogen; HLA, human leucocyte antigen; ICIs, immune checkpoint inhibitors; IFN, interferon; Ig, immunoglobulin; IL, interleukin; IMs, inflammatory monocytes; IMMs, inflammatory monocyte-macrophages; IP-10, inducible protein 10; IRF, interferon regulatory factor; ISG, interferon stimulated gene; LAG3, lymphocyte activation gene 3; M, membrane; mABs, monoclonal antibodies; MBL, mannose binding lectin; MCP1, membrane cofactor protein 1; MERS, middle east respiratory syndrome; MHC, major histocompatibility complex; MIP, macrophage inflammatory protein; moDCs, monocytes-derived dendritic cells; MSCs, mesenchymal stem cells; MYD88, myeloid differentiation primary response 88; N, nucleocapsid; nABs, neutralizing antibodies; NGS, of next generation sequencing; NK cells, natural killer cells; NKG2A, NK group 2 member 2A; Nsps, non-structural proteins; ORFs, open reading frames; PAMPs, pathogen associated molecular patterns; PCR, polymerase chain reaction; PD1, programmed cell death protein 1; PD-L1, programmed cell death protein ligand 1; PDGF, platelet derived growth factor; PLpro, papain like protease; Pp, polypeptides; PRRs, pattern recognition receptors; RA, rheumatoid arthritis; RBD, receptor binding domain; RBM, receptor binding motif; RLRs, RIG-I like receptors; RTC, replication transcription complex; S, spike; SARS-CoV-2, severe acute respiratory syndrome-coronavirus-2; scRNAseq, single cell RNA sequencing; SLE, systemic lupus erythematosus; ssRNA, single stranded RNA; STAT, signal transducer and activator of transcription; TIGIT, T cell immunoreceptor with Ig and ITIM domains; TIM 3, T cell immunoglobulin and mucin domain 3; TLRs, Toll like receptors; TMPRSS2, transmembrane protease serine 2; TNF, tumor necrosis factor; VEGF A, vascular endothelial growth factor A.

* Correspondence to: N. Chatterjee, Department of Receptor Biology and Tumor Metastasis, Chittaranjan National Cancer Institute, Kolkata 700026, India.
** Correspondence to: S. Swarnakar, Department of Infectious Diseases and Immunology, CSIR-Indian Institute of Chemical Biology, 4 Raja S.C. Mullick Road, Jadavpur, Kolkata 700032, India.
E-mail addresses: sikta@iicb.res.in (S. Swarnakar), nabanita.chatterje@yahoo.com (N. Chatterjee).

https://doi.org/10.1016/j.clim.2021.108804
Received 1 February 2021; Received in revised form 3 May 2021; Accepted 20 July 2021
Available online 23 July 2021
1521-6616/

1. Introduction

Evidences from the history focuses a spotlight on the incidences where coronavirus was found to be the reason for the outbreak of disease and recently a new strain of coronavirus, named Severe Acute Respiratory Syndrome-Coronavirus-2 (SARS-CoV-2), has been reported from Wuhan city, China. The disease is called Coronavirus disease, 2019 (COVID-19), named by WHO on Feb 11, 2020, that has first emerged in December 2019. As per the data, among the three outbreaks Middle East respiratory syndrome CoV (MERS-CoV) was the fatal most with a mortality rate of 34.77% while SARS-CoV stands out to be 10.87% of fatality and the SARS-CoV-2 has been reported to be 2.08%, although it is increasing with time. Meanwhile the mortality rate in SARS-CoV-2 infection is lower than the previously reported two pandemics but its transmission rate is quite higher in comparison to the earlier ones [1]. WHO reported that in September 4, 2020, there are 26,171,112 confirmed COVID-19 cases and death of 865,154 patients recorded [2]. Samples from the lower respiratory tract upon sequencing have depicted a novel coronavirus known to infect humans. The severe acute respiratory syndrome coronavirus 2 (SARS-CoV-2) is reported to be highly contagious [3]. The prime transmission route of COVID-19 is droplets formation of aerosols including all other possible modes of direct contact. SARS-CoV-2 incubation period is approximately 5–14 days or 24 days in some cases as per the retrospective pandemic report identified [4]. Most of the patients suspected for COVID-19 positive require supportive care, isolation to avoid the transmission chances and stronger immune power for recovery. Though the actual mechanism is still unclear, few anti-viral drugs such as remdesivir, lopinavir, ritonavir are being used for treatment [5]. The SARS-CoV-2 infection in lungs with adverse symptoms namely acute respiratory distress syndrome (ARDS) leads to severe lung injury mediated by host immune system [6]. The SARS-CoV-2 positive lung biopsy reports revealed that the content bilateral diffuse damage of alveoli, proliferation of fibroblasts and activated circulating $CD4^+/CD8^+$ lymphocytes [7]. Due to the rapid SARS-CoV-2 transmission globally, much more investigations are needed for the development of effective immunotherapy. In view of this context, addressing of the immunological aspects of SARS-CoV-2 spreading COVID-19 has become a major focus.

2. SARS-CoV background

According to WHO, SARS-CoV-2 is from the beta lineage of the coronavirus family of group 2B with 70% genetic similarities with SARS-CoV [8]. There are four genera classification of family namely *Alphacoronavirus, Betacoronavirus, Deltacoronavirus and Gammacoronavirus* [9]. Cryo-electron tomography and cryo-electron microscopy gives an idea about the morphology of SARS-CoV. HCoV-229E and HCoV-OC43 were the two human coronavirus that were responsible for causing mild respiratory dysfunctions in humans prior to the rise of SARS-CoV infection in 2002, thereafter emergence of two new human coronavirus, HCoV-NL63 in 2004 and HCoV-HKU1 in 2005 has occurred, where HCoV-229E and HCoV-NL63 are found in bats [10]. Genome sequencing of SARS-CoV-2 revealed more or less 79% similarity with SARS-CoV and 50% similarity MERS-CoV. According to genome sequencing, the strain of virus infecting the bat species underwent a series of genetic mutations and recombinations which enabled them to infect the human hosts [11]. In the present scenario, the life risk situation that is prevailing all over the world because of SARS-CoV-2, raises a question forward regarding the origin of the virus. The most probable origin that has been brought to light is the zoonotic transfer of the virus from the illegally imported Malayan pangolins (*Manis javanica*) as genetic and evolutionary evidences suggest that the SARS-CoV harbored by these pangolins is 91.02% similar to the SARS-CoV-2 [12]. While angiotensin converting enzyme 2 (ACE2) host receptor sequence in bats (*Rhinolophus sinicus*), pangolins and human were taken under consideration, it revealed that the ACE2 sequence similarity between human and bats was 80.60% which is less similar than between human and pangolins i.e. 84.76%, indicating that pangolins can be the original host or intermediate host of SARS-CoV-2 and therefore can promote transmission of the virus [13]. However, the genetic analysis of SARS-CoV-2 shows greater than 80% similarity compared with SARS-CoV and also more or less 50% similarity compared with MERS-CoV, both of them have a common origin i.e. bat [11]. According to phylogenetic analysis suggests that COVID-19, seventh member of the family of beta-coronavirus, is classified as a member of the ortho-coronavirinae subfamily and can be counted within the clade of the subgenus sarbecovirus [14]. Relating to the previous epidemiological investigations we can figure out that the emergence of the new coronavirus may be of zoonotic origin, keeping in mind the food habits of the Chinese people [15]. According to the present literatures, it is assumed that bats and pangolins are the original

Table 1
Various mutations found in SARS-CoV-2.

Mutations	Features	Outcomes	Ref.
SpikeD614G	A missense mutation in S protein encoding gene, where an amino acid (aa) change from aspartate to glycine at 614 position was found. With this mutation this strain contains 3 other mutations as follow: 1. C-to-T mutation at the 5′ untranslated region (UTR) at position 241, 2. C-to-T mutation at position 3037, 3. a nonsynonymous C-to-T mutation at position 14,408 within the RNA-dependent RNA polymerase gene.	D614G substitution was a rare mutation at the beginning of the COVID-19 spread before March 2020, found as predominant in Europe, but later it occurred about 74% in all published sequences in June 2020 and spread worldwide. This mutation enhances the viral replication in the upper respiratory tract and also has higher susceptible to neutralization by monoclonal antibodies.	[21,22]
NSP2 and NSP3	SARS-CoV-2 contains a polar aa instead of nonpolar aa unlike bat SARS at position 321 and glycine is replaced by serine in NSP3 at position of 543.	This may affect the mechanisms involved in viral entry and replication and increases the contagiousness of the virus.	[23]
SARS-CoV-2 VUI 202012/01	This new variant of SARS-CoV-2 has 29 aa substitution from the original Wuhan strain with a mutation N501Y which is located in the receptor binding region.	It is first reported in UK. According to till now revealed reports this new strain possesses a high transmissible rate than the original strain.	[24]
Mutations in Rdrp	A mutation was found in the RNA dependent RNA polymerase at the position of 14,408.	It might result in drug resistant viral phenotype.	[25]
Mutations in ORF region	According to the present studies there are mutations in ORF region as follow: 1. C > T in ORF1ab gene at position 8782, 2. T > C in ORF8 gene at position 28,144.	Better studies needed to understand the role of this mutation in virulence of the virus.	[26]
Δ382 variant	This variant has 382 nucleotide deletion in ORF8.	This variant, seen during the early epidemic in Wuhan, is mild infectious with lower concentration of proinflammatory cytokines.	[27]
SARS-CoV-2 AZ-ASU2923	This variant has a deletion of 81 nucleotide in the ORF7a region found in Arizona.	Pathogenic consequences are yet to be studied.	[28]

source of human SARS-CoV-2 and from them it is transmitted to humans but the actual intermediate host and the nature of emergence is yet to be explored [16–19].

Being RNA virus, SARS-COV-2 has a high mutation rate that may involve in increasing virulence and pathogenicity of the infection in patients. Mutations in the surface proteins could change the tropism of the virus and increase its adaptability in new host with greater pathogenicity. Accumulation of mutations in SARS-CoV-2 may result in higher potency of pathogenicity. According to studies, high levels of mutations have been found in NSP and S proteins (Table 1). Current scenarios of COVID cases with 61.8 M (million) cases and over 1.4 M deaths globally, reported by WHO on 1st December 2020, shows a gradual increase in the COVID cases [20]. High level of mutations in S proteins may indicate a second wave of COVID-19 with greater severity if essential steps are not taken.

3. Host pathogen interactions

The first five reported cases of COVID-19 in December, 2019 were hospitalized with ARDS out of which one deceased. Among all human associated CoVs, four patients were having mild respiratory symptoms, while two among them, with the infection of SARS-CoV and MERS-CoV were having severe respiratory diseases, [29] which mainly had been transmitted from animals to humans via an intermediate mammalian host [30]. The results of next generation sequencing (NGS) or Real-time polymerase chain reaction (RT-PCR) of patient's sputum targeted for the envelope gene of CoV confirmed the positive infection for COVID-19 [31] and SARS-CoV-19 shares almost 80% genome similarity with SARS-CoV [4]. Patients with positive infection of SARS-CoV-2, an enveloped single stranded RNA (ssRNA) virus with positive-sense RNA, show clinical manifestations [32]. In a nutshell, the pathogenesis of COVID-19 can be categorized as systemic disorders that include fever, dry cough, headache, fatigue, high sputum production, acute cardiac injury, dysponea, lymphopenia, cytokine storm and respiratory disorders that include sore throat, sneezing, rhinorrhoea, severe pneumonia, ground-glass opacities, RNAaemia and ARDS. As per improvised current clinical symptoms, loss of smell and taste has become a new and confirmatory symptom for COVID-19 along with the others. A very recent study has shown that a higher expression of ACE2 and Type 2 transmembrane serine protease (TMPRSS2) on olfactory cells are highly affected by SARS-CoV-2 resulting in the impairment of olfactory cells [33].

SARS-CoV-2, sourcing from symptomatic along with asymptomatic patients, after infecting a healthy person, has an incubation time of 4–14 days (average 3–7 days). Respiratory droplets from affected individual infect the healthy people to transmit the disease whereas it could also be transmitted through fecal-oral route because viral nucleic acid has been detected in the faeces and urine of COVID-19 patients [34,35]. Along with the disease-causing comorbidities (cardiovascular, cerebrovascular, diabetes) and people of age more than 55 has shown more susceptibility to the COVID-19 infection and also the cancer patients under chemotherapy and surgery treatment are more susceptible to SARS-CoV-2 [34] [36,37]. On contrary, the patients who are receiving immunotherapy using immune checkpoint inhibitors (ICIs) like anti-cytotoxic T lymphocyte associated antigen (CTLA) 4 or anti-PD-1/PD-L1 are comparatively less prone to the COVID-19 disease [38].

4. Molecular mechanisms of COVID-19 as pathogen

Based on the published literatures and the observations of the COVID-19 patients, the entry of the virus occurs via nasal and larynx mucosal membranes and reaches to the lungs via respiratory tract. S (spike) protein imparts virulence by binding to the host cell ACE2 receptor followed by their entry through clathrin-mediated endocytosis [39]. Different strains of coronavirus can recognize different host cell receptors e.g. the receptor for SARS-CoV is ACE2 which affects the pneumatocytes (Type II) and ciliated bronchial epithelial cells [40,41], the receptor for HCoV-229E is aminopeptidase N or CD13, the receptors for MERS-CoV is DPP4 (dipeptidyl peptidase4) or CD26 [41]. Based on the genetic sequence analysis, difference lies between SARS-CoV-2 and SARS-CoV-1 and thus emerged as an absolute new betacorona virus of the novel coronavirus i.e. nCOVID-19. Overall structural analysis of S protein between the two SARS-CoVs showed similarity of approximately 50–53% for the RBM (receptor binding motif), around 75% for the receptor binding domain (RBD) along with 76 to 78% whole protein [42]. Assumption of using same receptors for binding comes from amino acid sequence analysis that revealed a high similarity in binding domain of ACE2 receptor in SARS-CoV [42,43]. In addition, ACE2 is an integral member of glycoprotein which is highly expressed in the lung, kidney, heart and epithelial cells as well as endothelial cells of small intestine. [44]. The main function of ACE2 is the degradation of angiotensin (Ang)-II into Ang 1–7 [44]. Pulmonary ACE2 maintains the balance between the circulating AngII /Ang1–7 levels. AngII, in response to hypoxia, induces pulmonary vasoconstriction and hunts lung injury in victims and thus pneumonia is prevented [45].

In ARDS, ACE causes disease prognosis by increasing AngII levels but ACE2 protects lungs from failure by degrading AngII. Experimental evidences show that mice model where ACE2 is knockdown, drastic symptoms of ARDS is more prominent than wildtype while overexpression seems to be protective [46]. An increase of $CD14^{+}HLA{-}DR^{low}$ inflammatory monocytes (IMs) and Ficolin-1^{+} monocyte-derived macrophages has been detected by single cell RNA sequencing (scRNAseq) of pulmonary tissues of COVID-19 patients. In addition, the activation of interferon (IFN) signaling and monocytes recruitment decreases the alveolar potency and aids ARDS progression [47]. S protein on SARS-CoV-2 binds with greater affinity to host ACE2 receptors in comparison to SARS-CoV-1 [48]. Apart from $ACE2^{+}$ cells, another study has focused on TMPRSS2, a cellular protease, which is required by the virus for entering into the cell as it helps the S protein on the virus surface to bind to the host ACE2 receptor, specially to alveolar type-2 cells (AT2 cells) which express TMPRSS2 in large amounts [49,50]. Whereas, the affinity towards the cadherin related family member 3 (CDHR3) which serve as a receptor for a rhinovirus-C of ciliated epithelial cells in the upper airway, is still not clear [51,52]. COVID-19 infection results into the inflammation in the lung tissues due to less frequent exchange between oxygen and carbondioxide upon decrease in haemoglobin. This occurs due to the role of open reading frames (ORF1ab, ORF3a, ORF10), which breaks the 1-beta chain of haemoglobin into porphyrin where surface glycoproteins attach. This mechanism can be treated with drugs like chloroquine, favipiravir [53]. Transcriptomic study revealed that the genome of the virus is highly complicated and undergoes innumerable transcription events that in turn contribute to the production of unknown ORFs harboring mutations and undergoes recombination events. Rapid evolution of the virus, aids the virus to be drug resistant along with frequently altered host specificity, thereby contributing to the virulence of the virus [54].

5. COVID-19 affecting immune system

5.1. Antigen presentation

Whenever a pathogen enters into our body, it is recognized as antigen and presented through antigen presenting cells (APCs) via major histocompatibility complex (MHC) molecules present on their surface. The exact mechanism of presentation of coronavirus is not fully known. According to the researches on SARS-CoV, MHC I molecule mediates the antigen presentation of the virus [55] and sometimes MHC II also participates in the process [56]. Human leukocyte antigen (HLA) gene plays an important role in viral antigen presentation pathway and is also associated with viral susceptibility and disease severity. While HLA-DR of MHC II is involved in the antigen presentation to Th (T helper cells) whereas HLA-A, -B and –C of MHC I molecule present antigen to Tc

Table 2
The structural proteins involved in immunopathology.

Name of the structural protein	Structure	Function on immunological aspects		
		SARS-CoV-1	MERS	SARS-CoV-2
Nonstructural protein (Nsp)1 [71–73]	It is a leader protein, cleaved chain of ORF1b.	Antagonizes IFN-β production by decreasing the phosphorylation level of STAT1.	Helps in viral replication.	Detailed functions are still not known.
Nsp 15 [74–78]	Nidoviral RNA uridylate specific endoribonuclease (NendoU) that belongs to EndoU family. 34 KDa, around 345 amino acids, with three domains: N- terminal, middle and C-terminal domain.	Cleaves polyuridine (polyU) sequences from PUN RNAs and limits the formation of a PAMP and thus impedes the ability of activation the innate immune response to infection by MDA5.	Prevents activation of dsRNA sensors in host cell for evading immune system.	Inhibits the nuclear localization of IFR3 and antagonize the production of IFN and also target RNF41 (also known as NRDP1) to regulate innate immune system.
Nsp 9 and Nsp 10 [78–80]	The crystalline structure of Nsp9 of SARS-CoV revealed that the molecule forms two distinct types of dimers where the core of the protein is an open 6-stranded β-barrel that in turn comprises of two antiparallel β sheets packed orthogon.	Nsp10 regulates the activity of the 2′-O-Methyltransferase (2′-O- MTase) that prevents virus detection by cell innate immunity mechanisms and viral translation inhibition by the interferon-stimulated IFIT-1 protein.	According to available data Nsp9 helps in viral replication.	Interacts with NF-κB repressor, NKRF and activates IL-8/IL-6 mediated chemotaxis of neutrophils that results in inflammatory response in patients.
Nsp 13 [77,78,81]	It is a helicase of superfamily 1 and helps in viral RNA replication via unwinding of duplex RNA and DNA leaving a 5′ single-stranded tail in a 5′ to 3′ direction.	It acts as a helicase and helps in unfold the RNA-DNA hybrid.	Nsp13 attenuates the viral replication.	Targets TBK1 and TBKBP1 to inhibit interferon pathway to regulate innate immune response in host cell.
N (Nucleocapsid) protein [82]	N protein of SARS-CoV-2 is 29.9 kb in length, similar to 27.9 kb SARS-CoV and 30.1 kb MERS-CoV genome.	Generation of IFN is retarded upon crosstalk between the SPRY domain of TRIM25 and C terminus of the N protein as it blocks RIG-I ubiquitination by TRIM25.	Interacts with TRIM25 and interfere the IFN production in host cell.	Detailed functions are not clearly known.
ORF (open reading frame) 9b [83,84]	ORF-9b possesses a long hydrophobic lipid binding tunnel formed due to interwined dimer with an amphipathic outer surface	ORF-9b manipulates host cell mitochondrial function by disable MAVS signaling that results in reducing NLRP3 inflammasome activity, thus evading innate immune system.	Function in immune system is not known.	ORF9b in association with Tom70 interacts with a signaling adaptor MAVS indirectly
ORF6 [76,77]	SARS-CoV-1 and SARS-CoV-2 share only 69% amino acid similarity	It prevents primary production of interferon.	Helps in viral assembly and viral release and can act as a potential B cell epitope.	It prevents interferon production by various signaling molecules MDA5, MAVS, TBK1 and IRF3-5D, which is a phospho-mimic of the activated form of IRF3.
ORF3 [85–87]	Accessory protein formed by the cleavage of ORF1 and ORF1b.	ORF3a is responsible for activation of the NLRP3 inflammasome by secreting IL-1β.	Prevents interferon production and prevents inflammation.	The hypothesis is that ORF3a of SARS-CoV-2 may be less efficient in inflammasome activation.

IFIT, interferon-induced protein with tetratricopeptide repeats; IFN, interferon; IRF, interferon regulatory factor; MTase, methyltransferase; N, nucleocapsid; NendoU, nidoviral RNA uridylate specific endoribonuclease; NF-κB, nuclear factor **kappa**-light-chain-enhancer of activated B cells; NLRP3, NLR family pyrin domain containing 3; NRDP1, neuregulin receptor degradation protein 1; Nsps, non-structural proteins; ORFs, open reading frames; PAMP, pathogen associated molecular patterns; PolyU, poluuridine; RNF41, ring finger protein 41; SPRY, sprouty RTK signaling antagonist; STAT, signal transducer and activator of transcription; TBK1, TANK binding kinase 1; TBKBP1, TANK binding kinase-1, binding protein 1; TRIM25, tripartite motif containing 25.

(cytotoxic T cells) [57,58]. The polymorphism in HLA gene is associated with differential antigen presentation which leads to differential disease susceptibility in case of SARS-CoV-2 infection [59]. HLA genes present small pathogen derived peptides to T cells and the polymorphism in HLA influences the binding strength with pathogen peptides. According to the studies, the HLA allele frequencies of healthy ones did not match with the COVID-19 infected patients, clearly depicting a link between the HLA polymorphism and viral susceptibility. Evidences have shown that various HLA polymorphisms are related to strong susceptibility of SARS-CoV-2 infection whereas some are protective against the infection. According to various data, a variety of polymorphisms such as human HLA-DR, B1*1202, HLA-B*4601, HLA-B*0703a and HLA-Cw*0801 correlates to the infection susceptibility of SARS virus [56,60]. Especially, HLA-B*4601 has the lowest binding with peptides of SARS-CoV-2. Patients with this polymorphism are highly vulnerable to SARS-CoV-2 infection or have correlated with severe condition during COVID-19 infection [61]. On the other hand, HLA-B*1503 has the ability to present highly conserved SARS-CoV-2 peptides [61]. According to the study, HLA-Cw1502 and HLA-DR0301 may be involved in playing a protective role in SARS-CoV infection by facilitating the viral antigen presentation and thereby enhancing the functional activity of $CD4^+$ T cells, $CD8^+$ T cells and NK cells [62]. Polymorphisms like HLA-DRB1*11:01 and HLA-DQB1*02:0 in MHC II molecules elevate the risk for developing MERS-CoV infection. Moreover, mannose binding lectin (MBL) also presents SARS-CoV to the immune cells. According to the present literatures, other than HLA, alleles associated with low MBL production are a susceptible-factors for SARS infection and also those who are associated with greater production of CCL2 protein are more susceptible to SARS infection. The correlation of MBL and CCL2 with SARS-CoV-2 infection susceptibility is yet to be studied. [63].

5.2. Immune evasion

In SARS-CoV-2, pattern recognition receptors (PRRs) activate the innate immune responses via extracellular and endosomal Toll- like receptors (TLRs) in concert with cytosolic RIG-I like receptors (RLRs) [64]. Following the activation of PRRs, downstream signaling cascades stimulate the cytokine production like Type I/III IFNs as defense against virus, tumor necrosis factor alpha (TNF-α), interleukins (IL-1, IL-6, IL-18) and other proinflammatory cytokines [65]. The complex signaling pathways involving myeloid differentiation primary response 88 (MYD88) produce Type I IFNs and activate the transcription factor NF-κB which in turn induces the transcription and production of pro-inflammatory cytokines [66]. Type-I IFNs activate the downstream signal transducer and activator of transcription (STAT) proteins that catalyze generation of interferon stimulated genes (ISGs) coded antiviral proteins like IFN-induced protein with tetratricopeptide repeats-1. This phenomenon retards the replication of the virus in both neighboring and infected cells by activating an immune response against the virus. So, how does COVID-19 cause severe infection in patients? What are the

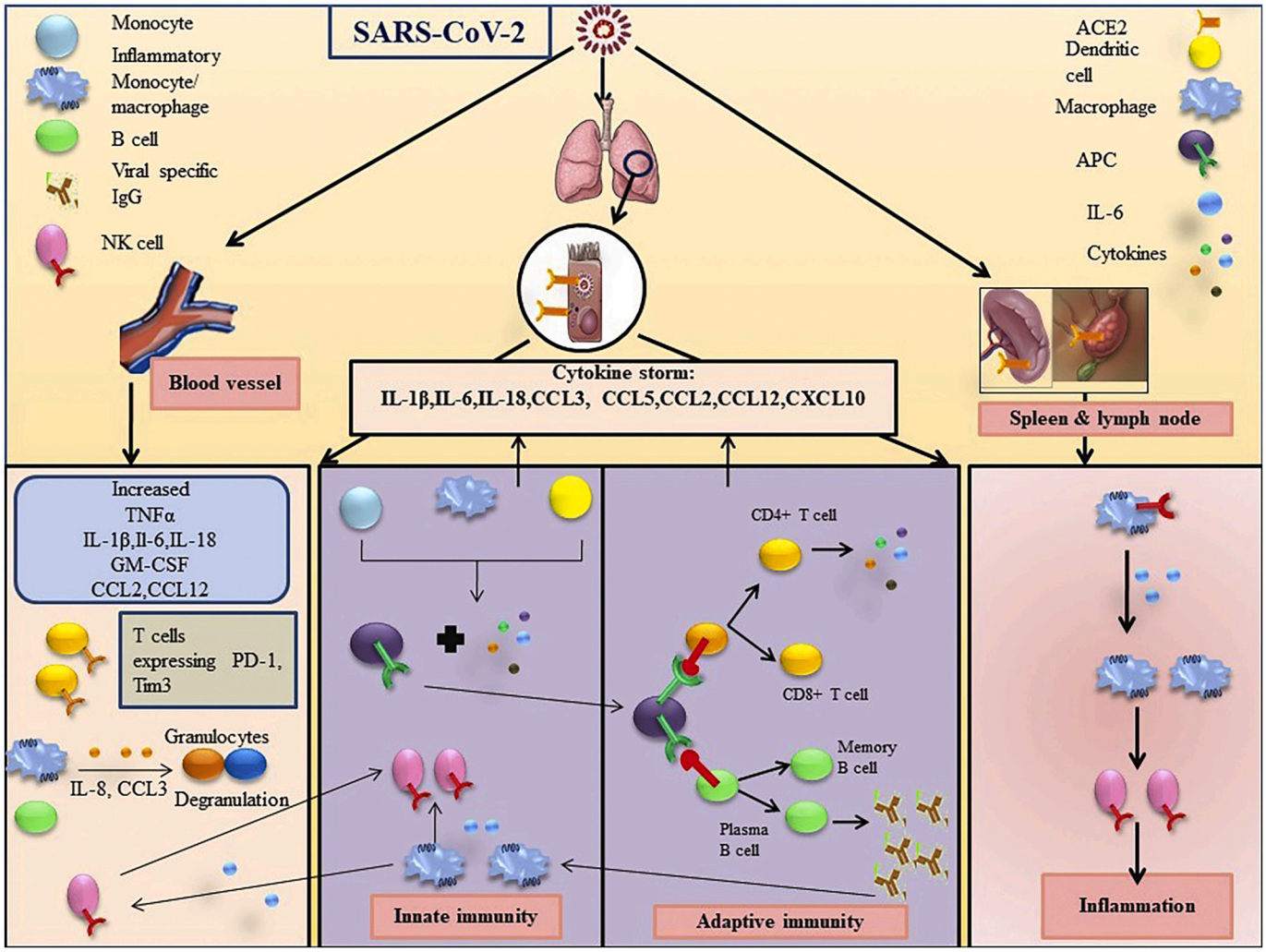

Fig. 1. Immune response following SARS-CoV-2 infection. SARS-CoV-2 mostly affects the lungs because of higher expression of angiotensin converting enzyme 2 (ACE2) receptor. Upon binding with ACE2 receptor, SARS-CoV-2 enters into cells and elicits immune responses. Dendritic cells, monocytes, macrophages act as antigen presenting cells (APCs) that interact with $CD4^+$ and $CD8^+$ T cells to induce the proliferation of virus specific T cells and facilitate secretion of various cytokines in the lungs. APCs also induce the release of viral specific antibodies, which recruit natural killer (NK) cells from peripheral blood to the lungs, B cells in the lungs and ultimately results in cytokine storm by increasing the secretions of various interleukins (ILs) including IL-6, IL-6, IL-β, TNF-α, C-C motif chemokine ligand (CCL)3, CCL5, CCL2, CCL12, C-X-C motif chemokine ligand (CXCL)10, granulocyte-monocyte colony stimulating factor (GM-CSF). On the other hand, in peripheral blood, in response to virus entry in concert with the high expression of exhaustion markers such as T cell immunoglobulin and mucin domain 3 (Tim3), programmed death-1 (PD-1) in T cells, the expressions of IL-1β, IL-6, IL-18, TNF-α, GM-CSF, CCL2, CCL12 are also elevated. Inflammatory monocytes (IMs) induce the degranulation of granulocytes by secreting CCL3 and IL-8. Due to the expression of ACE2 receptor, SARS-CoV-2 affects spleen along with lymph nodes to the same extent. Virus entry also induces IMs to secret IL-6 and recruits NK cells in tissue microenvironment.

immune escape strategies that are being adapted by the deadly virus?

Evidences suggest that, not only SARS-CoV but MERS-CoV too produces double-membrane vesicles (DMVs) and avoid detection of their double stranded RNA (dsRNA) by host [67]. The nonspecific proteins 1 (Nsp1) of SARS-CoV represses the activation of IFN regulatory factor 3 (IRF3) and IRF7 and together with nsp3, nsp1 also inhibit activation of IFN-β promoter which is viral dependent [68]. The induction of IFN is blocked by accessory protein 4a of MERS-CoV upon interaction with double stranded DNA (dsDNA) directly [69]. Furthermore, studies have shown that in MERS-CoV infection ORF4a, ORF4b, ORF5 and membrane (M) proteins block the transport of IRF3 into the nucleus and also activate IFNβ promoter [70]. The gene expressions for antigen presentation are also downregulated after MERs-CoV infection. Thus, SARS-CoV and MERS-CoV has modified themselves to escape from host immune surveillance. Efficient data is not available to support the theory that SARS-CoV-2 also uses the same mechanism to avoid immune surveillance or not. Table 2 provides a comparative study on the immunological functions played by structural proteins of the virus.

5.3. Innate immune system and SARS-CoV-2

First line of defense comes from the cells of innate immune system that include residential macrophages, conventional dendritic cells (cDCs), monocytes-derived dendritic cells (moDCs), granulocytes and natural killer cells [88]. In any viral infection, the innate immune system relies on Type I interferon (IFN) responses whose downstream cascade regulate the viral replication and induce adaptive immune responses. However, nCOVID-19 may dampen the IFN Type-1 response to terminate the anti-viral response. According to studies, SARS-CoV directly affect macrophages and T cells [89]. Recent research has shown that SARS-CoV-2 induces $CD169^+$ tissue-resident macrophages to produce IL-6 which results into lymphocyte apoptosis via upregulation of Fas in human spleen and lymph nodes [90]. According to the data of scRNAseq of COVID patients, there was expansion of $CD14^+IL\text{-}1\beta^+$ monocytes

[91], IMs, Ficolin-1$^+$ monocyte-derived macrophages and tissue-resident reparative alveolar macrophages (AMs) and elevated level of IL-β associated inflammation in peripheral blood of COVID-19 patients with severe condition [92,93]. In severe infection, lung macrophages express high levels of IL-1β, IL-6, TNF-α and chemokines like C-C motif chemokine ligand 2 (CCL2), CCL3, CCL4 and CCL7, C-X-C motif chemokine ligand (CXCL) 9, CXCL10, CXCL11 but CXCL16, whose binding receptor C-X-C motif chemokine receptor (CXCR) 6 was more highly expressed in patients with moderate infection [93]. Moreover, lung macrophages in patients with severe COVID-19 infection may recruit IMs and neutrophils though CCR1 and CXCR2 [93]. According to earlier data, SARS-CoV-1 infection resulted in an diverging phenotype of AM phenotype which limits the trafficking of DCs and activation of T cells [94] and YM1$^+$ FIZZ1$^+$ alternatively activated macrophages increased hypersensitivity in airway, thus worsening the fibrosis caused by SARS-infection [95]. These mechanisms, in SARS-CoV-2, need more research focus. Recent research revealed that ACE2 and SARS-CoV-2 N protein is also present on CD169$^+$ macrophages of spleen and lymph node of SARS-CoV-2 patients that are involved in production of IL-6 [96]. As mentioned earlier, SARS-CoV-2 undergoes the process of causing infection via ACE2 receptors but very low macrophages percentage in lungs express ACE2 receptors. So, the question arises is that whether there any other receptor present through which SARS-CoV-2 is infecting the immune cells? Evidences revealed reduced number of natural killer (NK) cells, in peripheral blood are positively correlated with COVID severity [97–99]. In influenza infection, CXCR3 mediated NK cells infiltration [100]. *In vitro* study has shown there is increased levels of CXCR3 ligand (CXCL9–11) in SARS-CoV-2 infected tissues of human lungs along with expanded monocytes level stimulated by CXCR3 ligands in SARS-CoV-2 infection [47]. These studies suggest that the CXCR3 pathway recruits NK cells in SARS-CoV-2 infected patients towards the lungs from the peripheral blood. Recent studies have shown that peripheral blood NK cells of SARS-CoV-2 patients have deceased expression of enzymes such as granzyme B, granulysin and also reduced surface markers CD107a, Ksp37 along with impaired chemokine production of TNF-α and IFN-ɣ that suggest an impaired cytotoxicity [98,101]. Moreover, SARS-CoV-2 infection has shown less number of CD16$^+$KIR$^+$ peripheral blood NK cells [102]. The expression of immune checkpoint NK group 2 member 2A (NKG2A) is increased with the upregulation of genes encoding inhibitory receptors lymphocyte activation gene 3 (LAG3) and T cells immunoglobulin and mucin domain 3 (TIM3) on NK cells of COVID patients [98,101]. Thus SARS-CoV-2 impairs the activity of NK cells. The impaired immune response stimulated by SARS-CoV-2 has been summarized in Fig. 1.

5.4. Adaptive immune system and SARS-CoV-2

Antigen presentation by APCs to other immune cells subsequently activates pathogen (virus) specific B cells and T cells. Similarly in SARS-CoV, viral infection a typical pattern of IgG and IgM has been observed where the IgM antibodies disappear in the 12th week but the IgGs which are viral S-specific and N-specific, last for a longer period [103]. The near-universal presence of IgGs, IgM, IgAs and neutralizing IgGs antibodies (nABs) in COVID patients indicates a humoral immune response mediated by increased B cells. COVID-19 patients show higher levels of antigen secreting cells (ASCs) derived from precursor naïve B cells. These B cells are regarded as double negative2 (DN2) as they lack naïve IgD, memory CD27 markers, CXCR5 and CD21 markers. The ASCs express high levels of CD11c and T-bet molecular markers and respond to TLR7 [104]. Patients in early stages with high levels of ACEs provide a protective function against eradication of virus whereas in later stages high levels ACE show poor outcomes. The circulating ACE2 enzymes protect virus-induced lung injury in influenza (H7N9) infection [105]. In COVID-19 infection, the higher level of circulating ACE2 might provide a protective function towards severe lung injury. According to studies, estrogen facilitates the upregulation of ACE2 which might explain the protectiveness of female vs male and also increases protection in children as they have higher level of circulating ACE2 than adults [106]. SARS-CoV-2 specific IgG of S protein was found in the serum of patients even after 60 days of symptoms onset, which decreased within 8 weeks of onset of post symptoms period [65]. Further studies are needed on the existence of viral specific IgG$^+$ memory cells in recovered COVID-19 patients.

Latest data has shown that in COVID-19 patients the peripheral count of CD4$^+$ and CD8$^+$ T cells have been greatly reduced but they were hyperactive in functional status as evidenced by i) a higher proportion of HLA-DR (CD4 3·47%) and CD38 (CD8 39·4%) double-positive fractions, ii) a hike in highly proinflammatory CCR4$^+$CCR6$^+$ CD4$^+$ T cells (Th17 cells) producing IL-17 and granulysin expressing Tc cells were observed in patients with severe immune injury and iii) the cytotoxic Tc cells (CD8$^+$ T cells) harbor greater concentration of cytotoxic granules e.g. 31.6% cells were perforin positive, 64.2% cells were granulysin positive and 30.5% cells were double positive for both perforin and granulysin [107]. These results implicate that the hyperactive function of Th17 and CD8$^+$ T cells are responsible for severe immune inflammation in patients and produce low IFN-γ and TNF-α in CD4$^+$ T cells and high granzyme B and perforin in CD8$^+$ T cells in COVID-19 infected patients [108]. It has been reported that CD8$^+$ T cells, developed during SARS-CoV infection, are specifically produced for the antigen S, M, E and N proteins. In SARS-CoV infection, CD8$^+$ T cells have been observed to differentiate into CD45RO$^-$CCR7$^-$CD62L$^-$ effector memory cells while CD4$^+$ T cells express CD45$^+$CCR7$^+$CD62L$^-$ central memory T cells [109]. Th1 cells which were hyperactivated release granulocyte-monocyte colony stimulating factors (GM-CSF) and IFNγ. This recruited increased numbers of CD14$^+$CD16$^+$ monocytes that are inflammatory, stimulated by IL-6 [110]. In moderately infected lung, macrophages produce increased chemokines, that will attract T cells, via the engagement of CXCR3 and CXCR6 [47]. So, innate and adaptive immune cells interact with each other and are involved in a positive loopback in expressing higher inflammation in COVID-19 infection. CD8$^+$ T cells expressing high level cytotoxic genes such as *granzyme K, A, B* (*GZMK, GZMA, GZMB)* and *XCL1* along with *KLRC1* which remained high in mild symptoms, have been detected in bronchoalveolar lavage (BAL) of COVID patients [111]. Moreover, experimental analysis suggests that these memory cells lasts for 3–4 years after the infection has been cured and slowly diminishes in the absence of antigen after 4 years [109]. Moreover, all the subtypes of T cells found in SARS-CoV-2 infection, show higher expression of negative immune checkpoint markers and exhaustion markers that is correlated with severe immune pathogenicity. The study of 10 patients group revealed increased levels of PD-1 in CD8$^+$ T cells and Tim-3 in CD4$^+$ T cells were observed in three patients of both prodromal and symptomatic stages of SARS-CoV-2 infection [112]. Furthermore, several other investigations reported increase in the expression of both co-stimulatory and inhibitory molecules such as OX-40 and CD137 [110], CTLA-4 and T cell immunoreceptor with Ig and ITIM domains (TIGIT) [108] and NKG2A [98], were found in T cells which suppressed the cytotoxic activity. Till now there is no potent evidence of any memory cells developed in cured COVID-19 patients against SARS-CoV-2.

5.5. Cytokine storm and SARS-CoV-2

Till now according to the reports, the main cause of death due to COVID-19 is severe pneumonia and ARDS. The key cause behind the occurrence of ARDS is the severe “cytokine storm” in infected patients that resulted in pneumonia, respiratory failure and other organs failure. A high cytokine storm occurring in COVID-19 patients include IL1-β, IL-17RA, IL-7, IL-9, IL-10, basic-fibroblast growth factor 2 (FGF2), granulocyte colony stimulating factor (G-CSF), GM-CSF, IFNγ, inducible protein (IP)10, membrane cofactor protein 1 (MCP1), macrophage inflammatory protein 1α (MIP1α), MIP1-β, platelet derived growth factor B (PDGF-B), TNFα, and vascular endothelial growth factor A (VEGFA)

Table 3
Drugs and their combinations are currently used in the treatment.

Name of drug	Description	Function
Chloroquine and hydroxyl chloroquine [119–121]	These drugs are basically used in malaria treatment and some extent to Systemic Lupus Erythematosous (SLE) and rheumatoid arthritis (RA) treatment.	Chloroquine and hydroxychloroquine inhibits viral entry into cells. The glycosylation of host receptors, endosomal acidification and proteolytic processing are inhibited. These agents also affect immunopathology via inhibition of cytokines production for lysosomal activity and autophagy of immune cells.
Lopinavir/ ritonavir [122]	Lopinavir and ritonavir are approved by US Food and Drug Administration (FDA) and in treatment of HIV.	No published data are available but invitro studies show that they act by inhibiting 3-chymotrypsin-like protease.
Remdesivir [123]	Remdesivir, also called GS-5734, is a monophosphate prodrug that forms an active C-adenosine nucleoside triphosphate analogue undergoing metabolism.	The drug was designed against microbes with activity also against RNA viruses. Remdesivir targets the RNA dependent RNA polymerase and hamper the replication cycle of RNA viruses. Remdesivir first used for the treatment of Ebola.
Umifenovir [124]	Umifenovir or Arbid, an antiviral drug.	It inhibits S protein/ACE2 interaction via blocking the fusion of membrane with the viral envelope. Arbid is used for the treatment of influenza in Russia and China and is recently in the interest for treating COVID-19.

ACE2, angiotensin converting enzyme 2; HIV, human immunodeficiency virus; RA, rheumatoid arthritis; S, spike; SLE, systemic lupus erythematosus; FDA, food and drug administration.

[31,113]. The ICU patients show high levels of pro-inflammatory cytokines such as IL-2, IL-7, IL-10, G-CSF, IP-10, MCP-1, MIP-1α, and TNFα, which are positively correlated with disease severity [31]. In a report from Wuhan where 99 cases had been studied, an increase in total neutrophils, decrease in total lymphocytes and increased in serum IL-6 has been observed. A delayed IFN-I signaling was observed which accumulate inflammatory monocyte-macrophages (IMMs). This resulted in high levels of cytokines and chemokines in lungs, vascular leakage and impaired the response of viral-specific T cells [114]. In SARS infected patients, an elevated level of IL-6, IL-8 and IP-10 has been found in lung tissues [115]. Increased level of pro-inflammatory cytokines is mainly responsible for severe lung injury, leading to demise of COVID-19 victims [107]. High levels of IP-10 has been related with immune mediated severe lung injury and apoptosis of lymphocytes in SARS [115]. Together with the cytokines, certain chemokines such as CXCL10, IP10, CCL2, CCL3, CCL5, CXCL8, CXCL9 support the impaired systemic inflammatory response in SARS-CoV-2 [116]. In comparison with SARS-CoV, SARS-CoV-2 upregulated five chemokines namely CXCL1, CXCL5, CXCL10, CCL2 and IL-6 [117]. SARS-CoV-2 patients with more severe pneumonia and pulmonary syndrome showed correlated higher expression of GM-CSF^{+} and IL-6^{+}CD4^{+} T cells, higher co-expression of IFN-γ and GM-CSF in pathogenic Th1 cells, much higher expression of CD14^{+}CD16^{+} monocytes [110]. In a nutshell, high infiltration of all types of immune cells such as T cells, monocytes, macrophages, NK cells, DCs and secretion of their proinflammatory cytokines into lungs cause severe ARDS leading to death of the patients.

6. Ongoing therapies

Currently there are not potent antiviral vaccine for the treating SARS-CoV-2. All patients are treated with supportive treatment strategies targeted to culminate the patients' symptoms (like pneumonia, fever, breathing problems) and often supported with combination of drugs. However, these strategies cannot be implemented for a long time. Being RNA virus, SARS-CoV-2 can be inhibited by repurposing drugs used for other RNA viruses such as the Human Immunodeficiency Virus (HIV). Clinical trials are currently undergoing with combinational drugs mainly ritonavir and lopinavir. Several other drugs are under clinical trials such as Kevzara, a rheumatoid arthritis (RA) drug that decreases lung complications. Kevzara has been successfully tested in COVID-19 patients. As per data, there are 11 phase 4, 36 phase 2 and 4 phase 1 trails [118]. Table 3 encloses a list of commonly used combinational drugs for the treatment of COVID-19.

As it has been an absolute outbreak and pandemic disease declared by WHO, a specific cure has to be found out to cure the disease completely. According to the genomic and structural analysis of SARS-CoV-2, there are a number of therapeutic targets which are under clinical trials in different laboratories across the whole world.

6.1. Viral targets

The Washington Department of Health Administration has first introduced remdesivir which inhibit RNA dependent RNA polymerase activity intravenously and found that it has a potential to protect from SARS-CoV-2 infection. The combination of remdesivir and choloroquine has shown to prevent SARS-CoV-2 infection *invitro*. Therefore, other nucleotide analogue such as favipiravir, ribavirin can also be administered as potential inhibitors. There are certain proteases such as 3 chymotrypsin-like protease (CLpro) along with papain like protease (PLpro) that cleaves viral polyproteins, can be the noble drug targets for the treatment. These also affect the replication of virus and antagonize IFN, IL-6. As SARS-CoV-2 binds with the ACE2 receptors of host cells, therefore targeting the S protein on the surface of the virus or the binding of the S protein and ACE2 can be a potential therapeutic target to combat COVID-19 infection. Fig. 2 points out the role of various drugs in distinctive stages of SARS-CoV-2 replication process.

6.2. Antibody and plasma therapy

According to studies the development of recombinant monoclonal antibody (mAb) can be a noble way to neutralize SARS-CoV-2. For example, CR3022, a SARS specific human mAb, can bind with the RBD of SARS-CoV-2 and can be used as candidate vaccine for SARS-CoV-2. Other mAbs, such as m396, CR3014, can be an alternative against SARS-CoV-2. Recently, a recombinant mAb named tocilizumab has come into application that can bind to IL-6 receptors, thereby terminating its signal transduction but its efficiency is still under study [38]. In addition to it, virus neutralizing antibody isolated from convalescent serum of COVID-19 patients, who has recovered from the infection, has also been administered in susceptible individuals as it had proved to be promising treatment approach during the previous corona outbreaks. It can impose immediate immune response in the unaffected susceptible individuals [125]. The generation of antibodies against the S proteins of the virus is being followed by Moderna Inc., MA, USA. There is also hope for development of new mAbs, which might take less time to be available to the doctors due to their speedy trials and their high specificity.

6.3. Development of vaccine

In this pandemic situation, approved vaccines against SARS-CoV-2 are essentially required as soon as possible for decreasing disease severity together with reduced shedding and transmission of virus. In the world full of darkness, a keen ray of light has been illuminated by the recent development of a vaccine mRNA1273 by The National Institute of Allergy and Infectious Diseases (NIAID), part of the National Institutes of Health (NIH). Various vaccination platforms are now being considered

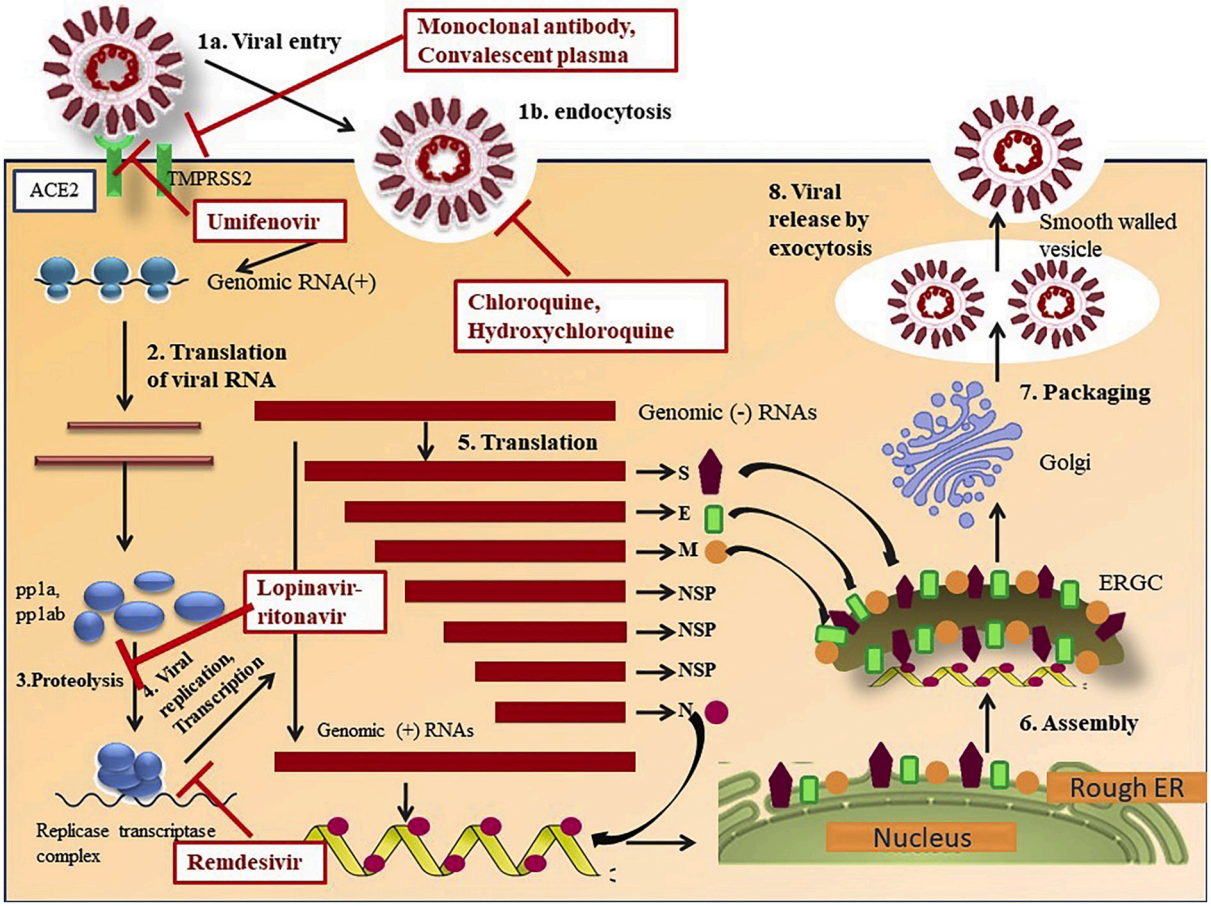

Fig. 2. Molecular mechanism of relevant drugs and therapies for the infection of SARS-CoV-2. SARS-CoV-2 enters into the host cell via angiotensin converting enzyme 2(ACE2) receptor by endocytosis with the release of its RNA contents into the recipient cell to replicate. Monoclonal antibody or convalescent plasma therapy inhibits the ACE2 receptor or interferes with transmembrane serine protease 2 (TMPRSS2) function to affect the viral binding with the host cell. Chloroquine and hydroxychloroquine interfere with the entry of virus via endocytosis. Umifenovir targets spike (S) protein/ACE2 interaction and inhibits membrane fusion of the viral envelope. After the shedding of viral RNA, it translates into polypeptide (pp)1b, pp1ab leading to the formation of double membrane vesicles (DMVs) and establishment of the replication-transcription complex (RTC). This stage is followed by generation of intermediate negative strand RNA from which more numbers of positive strand RNA and mRNAs are generated. Lopinavir/ritonavir inhibits protease to prevent proteolysis, a mechanism that establishes RTC. Remdesivir targets the RNA dependent RNA polymerase and hamper the replication cycle of RNA viruses. Structural nucleocapsid (N) proteins are generated from the translation of nucleocapsid (N) mRNA, which in turn encapsulates the newly generated positive RNA strands. However, other structural proteins, envelope (E) proteins and membrane (M) proteins are formed via the translation in endoplasmic reticulum (ER) and gather in endoplasmic reticulum golgi intermediate complex (ERGIC) and cis-Golgi. In addition to the structural proteins some non-structural proteins (Nsps) are also generated. The assembly of the viral components begins when the accumulated proteins exit from the golgi apparatus and eventually fuse with the cell membrane, resulting in the release of new virus particles.

to eradicate SARS-CoV-2 by developing passive immunization namely live attenuated vaccine (whole virus), sub-unit vaccine, viral-vector based vaccine, RNA vaccines, DNA vaccines. Although each of them has their own discrete benefits and disadvantages [126]. NVX-CoV2373 (Novavax, Inc.| Emergent BioSolutions), Triple Antigen Vaccine (Premas Biotech, India), Coroflu (University of Wisconsin-Madison | FluGen | Bharat Biotech), Ad5-nCoV (CanSino Biologics Inc. | Beijing Institute of Biotechnology), BNT162b1 (BioNTech| FosunPharma| Pfizer), DelNS1-SARS-CoV-2-RBD (University of Hong Kong) etc. are some of the vaccines that are being developed under the vaccination platforms [126]. Despite of the immense struggle of the researchers towards development of the vaccines, the mutant strains that are developing these days has compelled the research platforms to rethink and implement budding strategies for developing new vaccination formulas. A number of vaccines have been developed and some others are under development. Among them Covaxin and Covishield has shown promising ways in terms of immunization, especially in India as most of the populations are vaccinated with either of them. Although the approved vaccines that are currently available in the market have given promising effect, but their roles against the new mutant strains need to be studied.

6.4. *Epitope mapping*

Significant studies have been focused on identifying various target epitopes mapping on SARS-CoV-2 for development of targeted vaccines. Apart from antibodies targeting RBD of S proteins, studies have been undertaken to identify additional viral fragments (epitopes). This investigation has utilized the data on genetic differences and similarities among the three strains of coronavirus by utilizing bioinformatics analysis [127,128]. By implementing immune informatics scientists discovered five cytotoxic T lymphocytes (CTLs) epitopes and eight B-cell epitopes in the viral surface glycoproteins. Among the B cell epitopes three are sequential and rest five are discontinuous. Furthermore, CTL epitopes which are activated as judged by molecular dynamicity that the interaction between the CTL epitopes and HLA chains of MHC-I complexes are mediated by hydrogen (H) bonds and salt bridges, indicating their efficacy to confer immune responses [128]. Another study has identified five linear and two conformational B cell epitopes of SARS-CoV-2 surface proteins [129].

Table 4
List of drugs and vaccines that are on clinical trials.

Candidate drug	Mode of action and dose	Existing disease approval	Trial sponsor	Location	Expected result	Phase trial
Hydroxycholoroquine (ID: NCT04329611) [131]	Hydroxychloroquine inhibits acidification of endosomes, deglycosylates receptors of recipient cells, prevents proteolytic processing thus retards entry of virus. Inhibition of cytokine production modulates the host immune system. It also inhibits in host autophagy and lysosomal functionality **Dose:** Hydroxychloroquine dose of 400 mg po bid on day 1 followed by 200 mg po which will be given twice daily for 4 days	Malaria, rheumatoid arthritis (RA), lupus	Dr. Michael Hill	University of Calgary	Preliminary trials indicated that it is a potential and safe drug against COVID-19 pneumonia and shorten the disease course about 50%. Later it was found that both these drugs have side effects like allergic reactions, hypoglycemia, cardiomyopathy. On April, 2020 in Brazil 11 patients died due to irregular heart rates.	Phase III
Remdesivir (ID: NCT04292899 and NCT04292730) [132–134]	Antiviral **Dose:** RDV 200 mg on first Day followed by RDV 100 mg for next 4 days together with standard therapy.	–	Gilead, WHO, INSERM	China, japan	According to US NIAID, remdesivir shows faster recover from COVID-19 in 11 days compared to other drugs. A clinical trial in china, reported on 29thApril several adverse effect of remdesivir in treated patients.	In April 2020, there was 9 phase III clinical trials across the world.
Duvelisib (ID: NCT04372602) [135]	Target PI3K and control hyperactivation of innate immune system by affecting macrophage polarization, reducing inflammation in pulmonary and limit the persistence of viral load. **Dose:** 25 mg twice daily for 10 days, orally	–	Washington University School of Medicine.	Washington University School of Medicine, Saint Luis, Missouri, United Sates	Current primary outcome reported on 30th April overall survival	Phase II
Deferoxamine (ID: NCT04333550) [136,137]	It is a natural product which is isolated from *Streptomyces pilosus*. It helps in the formation of iron complexes and its mesylate form perform as chelating agent,	–	Kermanshah University of Medical Science	Regenerative Medicine Research Center, Kermanshah University of Medical Science, Iran, kemanshah.	Trial ongoing	Phase I Phase II
Favipiravir (ID: NCT04336904) [138]	It targets RNA-dependent RNA polymerase (RdRp) enzymes, which are necessary for the transcription and replication of viral genomes. **Dose:** Day 1:1800 mg, BID is given at 1800 mg on day 1 and day 2 followed by TID dose at 600 mg for 14 days. Thereafter: 600 mg, TID, for a maximum of 14 days.	Used before against Ebola virus and lassa virus.	Giuliano Rizzardini Asst Fatebenefratelli Sacco, Milan Ilaty		the normalization of pyrexia, normal respiratory rate and relief from cough is maintained for at least 72 h.	Phase III
Tocilizumab (ID: NCT04345445) [139]	Human monoclonal antibody against IL-6 receptor. **Dose:** Intravenously administered with a concentration of 8 mg/kg (body weight) once, within 60 min.	This drug has been used against immune suppression and in RA.	Genentech-hoffmann La Roche	Multiple countries	As per 8-point WHO scale, improvement of more than 2 point is observed.	Phase II
Sarilumab (ID: NCT04327388) [140]	Human monoclonal antibody against IL-6 receptor. **Dose:** Sarilumab Dose 1 given intravenously one time on Day 1	RA	Regeneron-Sanofi	Multiple countries	Patients improvement in oxygenation.	Phase II/ Phase III
Dapagliflozin (ID: NCT04350593) [141,142]	It acts as a sodium glucose cotransporter inhibitor. **Dose:** Dapagliflozin 10 mg daily	Hypoglycemia	Saint Luke's Mid America Heart Institute, Astrazeneca	Multiple countries	No detoriation in functionality of organs are observed in	Phase III

(*continued on next page*)

Table 4 (*continued*)

Candidate drug	Mode of action and dose	Existing disease approval	Trial sponsor	Location	Expected result	Phase trial
					hospitalized patients at 30th day.	
Recombinant human angiotensin-converting enzyme 2 (rhACE2) (ID: NCT04287686) [143]	It is a monocarboxy-peptidase that metabolizes several peptides, including the degradation of angiotensin II, and contributes to cardiovascular effect. **Dose:** Together with standard treatment0.4 mg/kg IV BID given for 7 days.	–	Hospital of Guangzhou Medical University	Guangdong, China	24–48 h of Pulmonary imaging showed that progression of the lesions are more than 50% and the patients were managed as severe	Phase II
Clevudine with combination hydroxychloroquine (ID:NCT04347915) [144]	Clevudine is an antiviral drug used against hepatitis B. **Dose:** Clevudine 120 mg once daily for 14 days (Hydroxychloroquine 200 mg twice daily for 14 days.	Hepatitis B	Bukwang Pharmaceutical		Trial ongoing	Phase II
Drug: FT516 (ID: NCT04363346) [145]	FT516 is a cryopreserved NK cell product of an iPSC that was transduced with ADAM17 non-cleavable CD16 (Fc receptor). **Dose:** Firstly, FT516 is administered at 9 x10^7 cells/dose in low concentration Secondly, FT516 is first given at low dose (9 x10^7 cells/dose) additionally at Day 4 it is provided in medium dose at (3 x 10^8 cells/dose) Thirdly, along with the low and medium doses, a higher dose of drug is given at day 7 (9 x 10^8 cells/dose)	Cancer	Masonic Cancer Center, University of Minnesota	Minneapolis, Minnesota, United States.	Trial ongoing	Phase I
DAS181 (ID: NCT04324489) [146]	Enzymatically cleaves viral receptors on host cells **Dose:** From day 1 to 10, once or twice a day, for 10 consecutive days, a total of 9 mg (7 mL)	Parainfluenza and other flu viruses including resistant strains	Renmin Hospital of Wuhan University	China	Better clinical outcomes	Completed
Losartan (ID: NCT04335123) [147]	– **Dose:** 25 mg for first 3 days folllowed by 50 mg QD till study completion	–	University of Kansas Medical Center	Kansas City, United States.	Trial ongoing	Phase I
Ivermectin with Nitazoxanide (ID: NCT04360356) [148–150]	Antiviral drug that affects the viral RNA and DNA replication in a broad spectrum. **Dose:** Ivermectin 200 mcg/kg once orally on empty stomach plus Nitazoxanide 500 mg twice daily orally with meal for 6 days	–	Tanta University	–	Trial ongoing	Phase II
Transfusion of SARS-CoV-2 Convalescent Plasma. (ID:NCT04372979) [151,152]	Convalescent plasma contains antibody against SARS-CoV-2. **Dose:** Intravenous	–	Direction Centrale du Service de Santé des Armées	France	Trial ongoing	Phase III
Isotretinoin (ID: NCT04361422) [153]	Inhibitors of PLpro, a protein encoded by SARS-CoV-2 **Dose:** Orally	Used to decrease virema in HIV+ patients	Tanta University	–	Clinical clearance Change in COVID-19 virus load	Phase III
Colchicine (ID: NCT04375202) [154]	Non-selective inhibition of NLRP3, a pathophysiologic component of SARS-CoV **Dose:** 0.5 mg every 8 h for 30 days, orally (Tablet)	Cardiovascular disease	University of Perugia	Italy	Trial ongoing	Phase II
Ruxolitinib (ID: NCT04355793, NCT04338958) [155–157]	Treat the cytokine storm and hyperinflammation in COVID-19 patients **Dose:** 5 mg orally twice daily	Treat bone marrow disorders like myelofibrosis	Incyte corporation University of Jena	USA	Reduce 25% hyperinflammation caused due to the cytokine storm	Phase II

(*continued on next page*)

Table 4 (*continued*)

Candidate drug	Mode of action and dose	Existing disease approval	Trial sponsor	Location	Expected result	Phase trial
Sildenafil (ID: NCT04304313) [158]	Relaxes the muscles of the lungs by increasing the potency of nitric oxide gas to widen the blood vessels resulting in more oxygen inhalation **Dose:** 0.1 g daily for 14 days, orally	Erectile dysfunction	Tongji hospital	China	Respiratory symptom remission Decrease in fever C-reactive protein recovery	Phase III
Sirolimus (ID: NCT04341675) [159]	mTOR inhibitor, immune suppressor **Dose:** 6 mg on first Day then 2 mg daily for next 13 days.	Used for preventing organ transplant rejection and lymphangioleiomyomatosis (LAM)	University of Cincinnati	USA	Trail ongoing	Phase II
Peginterferon Lambda-1a (ID:NCT04331899) [160]	Reduces viral shedding of SARS-CoV-2 **Dose:** One subcutaneous injection of 180 ug	Hepatitis B Virus infection Hepatitis C virus infection	Stanford University	USA	Trial ongoing	Phase II
Rintatolimod and IFN Alpha-2b (ID: NCT04379518) [161]	Rintatolimod is a dsRNA designed to mimic viral infection by activating immune pathways and IFN Alpha-2b activate immune responses and both participate in limiting viral replication and shedding **Dose:** IV rintatolimod for 2.5–3 h together with IV of recombinant interferon alpha-2b over 20 min on days 1, 3, 5, and 8 if there will be the disease progression or no unacceptable toxicity treatment will be followed up at 14th day and 28th day	Viral infections	Roswell Park Center Cancer Institute	USA	Trial ongoing	Phase I/ IIa
L-ascorbic acid (ID: NCT04357782) [162]	Reduce inflammation, ARDS, reduce supplement oxygenation, reduce risk respiratory failure which intubation **Dose:** 50 mg/kg IV given every 6 h for 4 days (16 total doses),	Sepsis	Hunter Holmes Mcguire Veteran Affairs Medical Center	Virginia, USA	Trial ongoing	Phase I/ II
mRNA1273 (ID: NCT04283461) [163,164]	A lipid nanoparticle (LNP) encapsulated with mRNA encoding full length S protein of SARS-CoV-2. **Dose:** 10/25/50/100/250 mcg mRNA1273 with .05 mL intramuscular injection in deltoid muscle.	–	National Institute of Allergy and Infectious Disease (NIAID)	–	Trial ongoing	Phase I
INO-4880 (ID: NCT04336410) [165]	It is a DNA vaccine against whole- length S protein of SARS-CoV-2. **Dose:** intradermal injection of 1.0 mg of INO-4800	–	Inovio Pharmaceuticals	–	Trial ongoing	Phase I
ChAdOx1 nCoV-19 COVID-19 (ID: NCT04324606) [166,167]	Adenovirus encoding full-length S protein **Dose:** One dose of 5 x 10^10vp	–	University of Oxford	UK	Trial ongoing	Phase II
COVID-19 LV- SMENP-DC (ID:NCT04276896) [168]	Lentivirus infected dendritic cells with SMENP minigenes that express COVID-19 antigens and activated CTLs.	–	Shenzhen Geno-Immune Medical Institute	China	Trial ongoing	Phase II
SARS-Cov-2 (ID: NCT04368988) [169]	Nanoparticle vaccine of spike (S) protein of SARS-CoV-2	–	Novavax	–	Trial ongoing	Phase I
BNT162a1, b1, b2, c2 (ID: NCT04368728) [170]	It is a LNP encapsulated mRNA vaccines with mRNA targets for both larger S sequence and RBD. **Dose:**0.5 mL intramuscular injection.	–	BioNTech SE and Pfizer, Inc.	–	Trial ongoing	Phase I
Recombinant Novel Coronavirus Vaccine	Adenovirus type 5 encoded with full length S protein	–	CanSino Biologics, Inc.	China	The vaccine is tolerable and immunogenic at	Phase I

(*continued on next page*)

Table 4 (*continued*)

Candidate drug	Mode of action and dose	Existing disease approval	Trial sponsor	Location	Expected result	Phase trial
(Adenovirus Type 5 Vector) (ID: NCT04313127) [72]					28 days post-vaccination in healthy adults, and rapid specific T-cell responses were noted from day 14 post-vaccination.	
bacTRL-Spike-1 (ID: NCT04334980) [171]	Live *Bifidobacteriumlongum*, engineered for the delivery of plasmids containing synthetic DNA encoding spike protein from SARS-CoV-2.	–	Symvivo Corporation		Trail ongoing	Phase I
Mrna-1273 vaccine (ID: NCT04470427) [164]	Neutralizing activity against recombinant vesicular stomatitis virus (rVSV)–based SARS-CoV-2 (a pseudovirus-based model) in serum samples of new variants of the virus. **Dose:** Participants will receive 1 intramuscular (IM) injection of 100 microgram (ug) mRNA-1273 on Day 1 and on Day 29.	–	ModernaTX, Inc.		Efficacy, safety, and immunogenicity of mRNA-1273 to prevent COVID-19 for up to 2 years after the second dose of mRNA-1273.	Phase III
Decitabine for Coronavirus (COVID-19) Pneumonia - Acute Respiratory Distress Syndrome (ARDS) Treatment (ID: NCT04482621) [172]	Works as hypomethylating agents, affecting replication **Dose:** 10 mg/mˆ2/day IV day x 5 days (1 cycle only) intravenously	Myelodysplastic syndrome (MDS)	Johns Hopkins University	USA	Recruiting	Phase II
Xuanfei Baidu granules (XFBD), Traditional Chinese medicine (TCM) (ID: NCT04810689) [173]	Acts as anti-coagulant agent which dissolves blood clots, relieves shortness of breath by relaxing the tracheal muscles. **Dose:** Orally twice daily for 14 days, 1 h after food in the morning and at night with at least 8 h in between doses	Used for fever recovery and suppress of cough by clearing phlegm	Darcy Spicer, University of Southern California	USA	Recruiting	Phase II
STI-5656 (Abivertinib Maleate) (ID: NCT04528667) [174]	Third-generation EGFR tyrosine kinase inhibitor and BTK inhibitor. **Dose:** Subjects receive either 100 mg of STI-5656 or placebo daily for 7 days	Advanced non-small cell lung carcinoma	Sorrento Therapeutics, Inc.	Brazil	Recruiting	Phase II
Desferal (ID: NCT04333550) [136,175]	Acts as chelating agent **Dose:** Intravenous injection	Patients with acute or chronic iron and aluminium toxicity	Kermanshah University of Medical Sciences	Iran	Recruiting	Phase I/II
Pulmozyme/ Recombinant human deoxyribonuclease (rhDNase) (ID: NCT04445285) [176]	Reduces sputum viscoelasticity. **Dose:** 2.5 mg Pulmozyme/ Recombinant human deoxyribonuclease (rh-DNase) aerosolized treatment once every 24 h for five (5) consecutive days; a total of five (5) doses	Cystic fibrosis	Jon Simmons, University of South Alabama	USA	Recruiting	Phase II
COVID-19 vaccine (COVAXIN) (BBV152) (ID: NCT04641481 [177]	The vaccine is used along with immune stimulants, commonly known as vaccine adjuvants (Alhydroxiquim-II), to improve immune response and longer-lasting immunity **Dose:** 0.5 mL per dose	–	Bharat Biotech International Limited	India	Active, not recruiting	Phase III
Dornase Alpha (Pulmozyme) (ID: NCT04432987) [178]	It helps in clearing the NETs created by neutrophils in the lungs **Dose:** Drug will be administered at a dose of	Cystic fibrosis	Acibadem University	Istanbul, Tutkey	Recruiting	Phase II

(*continued on next page*)

Table 4 (*continued*)

Candidate drug	Mode of action and dose	Existing disease approval	Trial sponsor	Location	Expected result	Phase trial
	2.5 mg/2 times per day for 7 days					
AZD7442 (A combination of AZD8895 and AZD1061) (ID: NCT04723394) [179]	mABs affects the RBD of viral S protein. Amino acid substitutions have been introduced into the antibodies to both extend their half-lives, which can prolong their potential prophylactic benefit, and minimize Fc effector function. **Dose:** Single dose (× 2 separate IM injections) of 600 mg of AZD7442.	–	AstraZeneca	England, UK	Recruiting	Phase III
Emricasan (ID: NCT04803227) [180]	Peripheral blood lymphocytes of COVID-19 patients overexpress caspase-1. Caspase-1 plays a role in a form of cell death called pyroptosis. EMR inhibits pyroptosis, thus it serves as a pan caspase inhibitor **Dose:** 25 mg BID (days 1–14). Oral (capsule) administration.	–	Histogen	SUNY Downstate Health Sciences University Brooklyn, New York, United States	Recruiting	Phase I
Sirolimus (ID: NCT04461340) [181]	Inhibits IL-2 and other cytokine receptor-dependent signal transduction mechanisms **Dose:** Oral dose of 6 mg on day1 followed by 2 mg daily for 9 days	Head and Neck Lymphatic Malformations	Alexandria University	Egypt	Recruiting	Phase II
Sitagliptin (ID: NCT04382794) [182]	Inhibits the action of dipeptilpeptidase-4 expressed at parenchyma and lung interstitium level	Type -II diabetes	University of Milan	Italy	Lessens the activity of proinflammatory cytokines, growth factors and vasoactive peptides	Completed
Rivaroxaba (ID: NCT04757857) [183]	Acts as anticoagulants **Dose:** 1st to the 14th day, a dose of 10 mg of rivaroxaban - OA (Oral Administration).	Thrombosis and pulmonary embolism	Alemão Oswaldo Cruz	Brazil	Recruiting	Phase IV
Dendritic Cell Vaccine (ID: NCT04685603) [184]	–	Cancer	Indonesia-MoH	Indonesia	Recruiting	Phase I
AZD1222 (ID: NCT04516746) [185]	Recombinant replication-defective chimpanzee adenovirus expressing the SARS-CoV-2-5 surface glycoprotein. **Dose:** 0.5 mL of 2 dose on day 1 and day 29.	–	AstraZeneca	United States	Active, not recruiting	Phase III
SII-ChAdOx1 nCoV-19 [186]	Recombinant replication-defective chimpanzee adenovirus expressing the SARS-CoV-2- Spike protein. **Dose:** 0.5 ml of 2 dose on day 1 and day 29.	–	Serum Institute of India	India	–	Phase III

ADAM 17, a disintegrin and metalloproteinase 17; CTLs, cytotoxic T lymphocytes; dsRNA, double stranded RNA; EGFR, epidermal growth factor receptor; IFN, interferon; LAM, lymphangioleiomyomatosis; LNP, lipid nanoparticle; mTOR, mammalian target of rapamycin; NETs, neutrophils extracellular traps; NK, natural killer; NLRP 3, NLR family pyrin domain containing 3; PI3K, phosphatidylinositol 3 kinase; RBD, receptor binding domain; RA, rheumatoid arthritis; RdRp, RNA dependent RNA polymerase; S, spike; SARS-CoV-2, severe acute respiratory syndrome coronavirus.

6.5. Stem cell therapy

This noble therapeutic approach was not undertaken into study until two distinct studies conducted by China and detected that stem cell therapy can be a new aspect in the treatment of COVID-19. Intravenous infusion of mesenchymal stem cells (MSCs) can play a vital role in curing the dysfunctions of the lung i.e. complications like pulmonary edema, dysfunction of air-exchange, ARDS, acute cardiac injury which are the results increased inflammation due to the account of the virally triggered cytokine storm caused damage to lung tissues [50,130]. These MSCs, depending on their properties of modulating the immune system and regeneration or differentiating capability can counteract the increased release of cytokines and their repairing capacity thus restored the damaged tissues, followed by curing the disease. Moreover, RNA-sequencing of transplanted MSCs has revealed the presence of undifferentiated transfused MSCs and remained to ACE2 negative thus there

exist no chance for the virus to affect these cells [130].

7. Ongoing interventional studies

A landmark initiative to put forward the development of vaccines and their potential is undertaken across the world on observing the severity of COVID-19. From the increasing number of fatalities and affected individuals reported across the world, it is clear that COVID-19 is escaping the treatment strategies undertaken to eradicate it. Due to the immense capability of SARS-CoV-2 to mutate very rapidly, a challenge has been thrown to the scientists to develop a potent vaccine that can destroy it all. Keeping pace with the above-mentioned treatment strategies, several drugs which were used for treating other diseases, are now under clinical trials to find a solution to the menace of COVID-19. A list of interventional drugs and vaccines under trial has been illustrated in the Table 4.

Another concept of controlling the rapid spread of the virus is to develop herd immunity which is defined as decrease in population of susceptible individuals below the threshold value required for transmission. The contagious state of SARS-CoV-2 (R_0) varies between 2%–3%. So, for acquiring herd immunity the threshold value is 67% for this virus.

8. Conclusion

The current scenario of rapidly spreading and unpredicted infectious nature of SARS-CoV-2 demands an urgency to focus on basic science and clinical research. Though there are a few resemblances of immunopathogenesis of SARS-CoV-2 with SARS-CoV-1 and MERS but the differences are prominent enough to focus on new therapeutic targets for developing vaccines. Within short time there is significant knowledge about the immunology of SARS-CoV-2 infection which can aid in potent vaccine development. The emerging cases of asymptomatic situations is demanding a better and deep evaluation about the mechanisms of immune response following SARS-CoV-2 infection to develop a promising therapeutic approach. Recently new variants of COVID-19 virus are being reported across the world and targeting these mutated forms of virus has thrown a challenge to the researchers these days. Furthermore, food habits of the communities need to be checked and considered by food authorities to avoid the inevitable menace caused by the zoonotic origin of the virus. The SARS-CoV-2 pandemic is just another example of the emergence of new virus types due to a straight forward link between humans and animals via food chain. In this background, this review comprises of some recent literatures that interrogate the viral entry, invasion, immune escape and immune mechanisms, the dysfunctions of various immune cells like T cells, NK cells, monocytes lineages with a brief view on the memory cells. We have also addressed monoclonal antibody therapy and plasma therapy as well as vaccine development against SARS-CoV-2. Further studies are needed to explain the immune response varying in victims encompassing both symptomatic and asymptomatic ones. Existing clinical trials of SARS-CoV-2 may give an appropriate idea to accomplish the unmet needs. From the reported evidences, it is clear that the immune system is highly affected by this infection and it is critically important to discover efficient drugs to reduce the mortality rate and gain the normal situation as before. Furthermore, some vaccines like Covaxin, Covishield have already undergone the trial phase and is now commercially available for implementation but the question rises on the efficiency of the vaccines against the new evolving strains of the virus. Finally, concluding remarks can be made on the initiatives taken by the respective Government authorities to combat the spread. Personal hygiene, maintaining proper nutritional value, hydration has to be kept in mind to avoid being affected by the virus and for boosting the immune system to fight the virus until a proper and effective treatment strategy towards all the deadly strains of the SARS-CoV-2.

Author contributions

A.D and S.R wrote the manuscript. S.S. and N.C. reviewed and corrected the manuscript.

Funding

This research did not receive any specific grant from funding agencies in the public, commercial, or not-for-profit sectors.

Declaration of Competing Interest

Authors do not have any conflict of interest.

Acknowledgement

We are thankful to our Director, CNCI, Kolkata for his continuous support and encouragement to complete this scientific input.

References

[1] S.A. Meo, A.M. Alhowikan, T. Al-Khlaiwi, I.M. Meo, D.M. Halepoto, M. Iqbal, A. M. Usmani, W. Hajjar, N. Ahmed, Novel coronavirus 2019-nCoV: prevalence, biological and clinical characteristics comparison with SARS-CoV and MERS-CoV, Eur. Rev. Med. Pharmacol. Sci. 24 (2020) 2012–2019, https://doi.org/10.26355/eurrev_202002_20379.

[2] WHO Coronavirus Disease (COVID-19) Dashboard, WHO Coronavirus Disease (COVID-19) Dashboard, 2021.

[3] A.E. Gorbalenya, S.C. Baker, R.S. Baric, R.J. de Groot, C. Drosten, A.A. Gulyaeva, B.L. Haagmans, C. Lauber, A.M. Leontovich, B.W. Neuman, D. Penzar, S. Perlman, L.L.M. Poon, D.V. Samborskiy, I.A. Sidorov, I. Sola, J. Ziebuhr, The species Severe acute respiratory syndrome-related coronavirus: classifying 2019-nCoV and naming it SARS-CoV-2, Nat. Microbiol. 5 (2020) 536–544, https://doi.org/10.1038/s41564-020-0695-z.

[4] R. Lu, X. Zhao, J. Li, P. Niu, B. Yang, H. Wu, W. Wang, H. Song, B. Huang, N. Zhu, Y. Bi, X. Ma, F. Zhan, L. Wang, T. Hu, H. Zhou, Z. Hu, W. Zhou, L. Zhao, J. Chen, Y. Meng, J. Wang, Y. Lin, J. Yuan, Z. Xie, J. Ma, W.J. Liu, D. Wang, W. Xu, E. C. Holmes, G.F. Gao, G. Wu, W. Chen, W. Shi, W. Tan, Genomic characterisation and epidemiology of 2019 novel coronavirus: implications for virus origins and receptor binding, Lancet. 395 (2020) 565–574, https://doi.org/10.1016/S0140-6736(20)30251-8.

[5] T. Pillaiyar, S. Meenakshisundaram, M. Manickam, Recent discovery and development of inhibitors targeting coronaviruses, Drug Discov. Today 25 (2020) 668–688, https://doi.org/10.1016/j.drudis.2020.01.015.

[6] M. Zhou, X. Zhang, J. Qu, Coronavirus disease 2019 (COVID-19): a clinical update, Front. Med. 14 (2020) 126–135, https://doi.org/10.1007/s11684-020-0767-8.

[7] S. Tian, Y. Xiong, H. Liu, L. Niu, J. Guo, M. Liao, S.-Y. Xiao, Pathological study of the 2019 novel coronavirus disease (COVID-19) through postmortem core biopsies, Mod. Pathol. 33 (2020) 1007–1014, https://doi.org/10.1038/s41379-020-0536-x.

[8] D.S. Hui, E.I. Azhar, T.A. Madani, F. Ntoumi, R. Kock, O. Dar, G. Ippolito, T. D. Mchugh, Z.A. Memish, C. Drosten, A. Zumla, E. Petersen, The continuing 2019-nCoV epidemic threat of novel coronaviruses to global health — The latest 2019 novel coronavirus outbreak in Wuhan, China, Int. J. Infect. Dis. 91 (2020) 264–266, https://doi.org/10.1016/j.ijid.2020.01.009.

[9] S. Perlman, J. Netland, Coronaviruses post-SARS: Update on replication and pathogenesis, Nat. Rev. Microbiol. 7 (2009) 439–450, https://doi.org/10.1038/nrmicro2147.

[10] T.S. Fung, D.X. Liu, Human Coronavirus: host-pathogen interaction, Annu. Rev. Microbiol. 73 (2019) 529–557, https://doi.org/10.1146/annurev-micro-020518-115759.

[11] J. Cui, F. Li, Z.L. Shi, Origin and evolution of pathogenic coronaviruses, Nat. Rev. Microbiol. 17 (2019) 181–192, https://doi.org/10.1038/s41579-018-0118-9.

[12] T. Zhang, Q. Wu, Z. Zhang, Probable pangolin origin of SARS-CoV-2 associated with the COVID-19 outbreak, Curr. Biol. 30 (2020) 1346–1351, e2, https://doi.org/10.1016/j.cub.2020.03.022.

[13] P.H. Guzzi, D. Mercatelli, C. Ceraolo, F.M. Giorgi, Master regulator analysis of the SARS-CoV-2/human interactome, J. Clin. Med. 9 (2020) 982, https://doi.org/10.3390/jcm9040982.

[14] N. Zhu, D. Zhang, W. Wang, X. Li, B. Yang, J. Song, X. Zhao, B. Huang, W. Shi, R. Lu, P. Niu, F. Zhan, X. Ma, D. Wang, W. Xu, G. Wu, G.F. Gao, W. Tan, A novel coronavirus from patients with pneumonia in China, 2019, N. Engl. J. Med. 382 (2020) 727–733, https://doi.org/10.1056/NEJMoa2001017.

[15] Z.W. Ye, S. Yuan, K.S. Yuen, S.Y. Fung, C.P. Chan, D.Y. Jin, Zoonotic origins of human coronaviruses, Int. J. Biol. Sci. 16 (2020) 1686–1697, https://doi.org/10.7150/ijbs.45472.

[16] T. Leitner, S. Kumar, Where did SARS-CoV-2 come from? Mol. Biol. Evol. 37 (2020) 2463–2464, https://doi.org/10.1093/molbev/msaa162.

[17] A. Banerjee, A.C. Doxey, K. Mossman, A.T. Irving, Unraveling the zoonotic origin and transmission of SARS-CoV-2, Trends Ecol. Evol. 36 (2020) 180–184, https://doi.org/10.1016/j.tree.2020.12.002.

[18] R. Tiwari, K. Dhama, K. Sharun, M. Iqbal Yatoo, Y.S. Malik, R. Singh, I. Michalak, R. Sah, D.K. Bonilla-Aldana, A.J. Rodriguez-Morales, COVID-19: animals, veterinary and zoonotic links, Vet. Q. 40 (2020) 169–182, https://doi.org/10.1080/01652176.2020.1766725.

[19] H.S. Yoo, D. Yoo, COVID-19 and veterinarians for one health, zoonotic- and reverse-zoonotic transmissions, J. Vet. Sci. 21 (2020), e51, https://doi.org/10.4142/jvs.2020.21.e51.

[20] World Health Organisaton, COVID-19 Weekly Epidemiological Update Global summary, 2020, pp. 1–22.

[21] J.A. Plante, Y. Liu, J. Liu, H. Xia, B.A. Johnson, K.G. Lokugamage, X. Zhang, A. E. Muruato, J. Zou, C.R. Fontes-Garfias, D. Mirchandani, D. Scharton, J.P. Bilello, Z. Ku, Z. An, B. Kalveram, A.N. Freiberg, V.D. Menachery, X. Xie, K.S. Plante, S. C. Weaver, P.Y. Shi, Spike mutation D614G alters SARS-CoV-2 fitness, Nature (2020), https://doi.org/10.1038/s41586-020-2895-3.

[22] S. Isabel, L. Graña-Miraglia, J.M. Gutierrez, C. Bundalovic-Torma, H.E. Groves, M. R. Isabel, A.R. Eshaghi, S.N. Patel, J.B. Gubbay, T. Poutanen, D.S. Guttman, S. M. Poutanen, Evolutionary and structural analyses of SARS-CoV-2 D614G spike protein mutation now documented worldwide, Sci. Rep. 10 (2020) 1–9, https://doi.org/10.1038/s41598-020-70827-z.

[23] S. Angeletti, D. Benvenuto, M. Bianchi, M. Giovanetti, S. Pascarella, M. Ciccozzi, COVID-2019: the role of the nsp2 and nsp3 in its pathogenesis, J. Med. Virol. 92 (2020) 584–588, https://doi.org/10.1002/jmv.25719.

[24] European Centre for Disease Prevention and Control, Rapid increase of a SARS-CoV-2 variant with multiple spike protein mutations observed in the United Kingdom. http://covid19-country-overviews.ecdc.europa.eu/#34_United_Kingdom, 2020.

[25] M. Pachetti, B. Marini, F. Benedetti, F. Giudici, E. Mauro, P. Storici, C. Masciovecchio, S. Angeletti, M. Ciccozzi, R.C. Gallo, D. Zella, R. Ippodrino, Emerging SARS-CoV-2 mutation hot spots include a novel RNA-dependent-RNA polymerase variant, J. Transl. Med. 18 (2020) 1–9, https://doi.org/10.1186/s12967-020-02344-6.

[26] R.A. Khailany, M. Safdar, M. Ozaslan, Since January 2020 Elsevier has created a COVID-19 resource centre with free information in English and Mandarin on the novel coronavirus COVID- 19. The COVID-19 resource centre is hosted on Elsevier Connect, the company' s public news and information, Gene Reports. 19 (2020) 1–6.

[27] B.E. Young, S.W. Fong, Y.H. Chan, T.M. Mak, L.W. Ang, D.E. Anderson, C.Y. P. Lee, S.N. Amrun, B. Lee, Y.S. Goh, Y.C.F. Su, W.E. Wei, S. Kalimuddin, L.Y. A. Chai, S. Pada, S.Y. Tan, L. Sun, P. Parthasarathy, Y.Y.C. Chen, T. Barkham, R.T. P. Lin, S. Maurer-Stroh, Y.S. Leo, L.F. Wang, L. Renia, V.J. Lee, G.J.D. Smith, D. C. Lye, L.F.P. Ng, Effects of a major deletion in the SARS-CoV-2 genome on the severity of infection and the inflammatory response: an observational cohort study, Lancet 396 (2020) 603–611, https://doi.org/10.1016/S0140-6736(20)31757-8.

[28] L.A. Holland, E.A. Kaelin, R. Maqsood, B. Estifanos, L.I. Wu, A. Varsani, R. U. Halden, B.G. Hogue, M. Scotch, E.S. Lim, An 81-nucleotide deletion in SARS-CoV-2 ORF7a identified from sentinel surveillance in Arizona (January to March 2020), J. Virol. 94 (2020), https://doi.org/10.1128/jvi.00711-20.

[29] V.M. Corman, J. Lienau, M. Witzenrath, Coronaviren als Ursache respiratorischer Infektionen, Internist (Berl). 60 (2019) 1136–1145, https://doi.org/10.1007/s00108-019-00671-5.

[30] T.P. Sheahan, A.C. Sims, R.L. Graham, V.D. Menachery, L.E. Gralinski, J.B. Case, S.R. Leist, K. Pyrc, J.Y. Feng, I. Trantcheva, R. Bannister, Y. Park, D. Babusis, M. O. Clarke, R.L. Mackman, J.E. Spahn, C.A. Palmiotti, D. Siegel, A.S. Ray, T. Cihlar, R. Jordan, M.R. Denison, R.S. Baric, Broad-spectrum antiviral GS-5734 inhibits both epidemic and zoonotic coronaviruses, Sci. Transl. Med. 9 (2017), eaal3653, https://doi.org/10.1126/scitranslmed.aal3653.

[31] C. Huang, Y. Wang, X. Li, L. Ren, J. Zhao, Y. Hu, L. Zhang, G. Fan, J. Xu, X. Gu, Z. Cheng, T. Yu, J. Xia, Y. Wei, W. Wu, X. Xie, W. Yin, H. Li, M. Liu, Y. Xiao, H. Gao, L. Guo, J. Xie, G. Wang, R. Jiang, Z. Gao, Q. Jin, J. Wang, B. Cao, Clinical features of patients infected with 2019 novel coronavirus in Wuhan, China, Lancet. 395 (2020) 497–506, https://doi.org/10.1016/S0140-6736(20)30183-5.

[32] H.A. Rothan, S.N. Byrareddy, The epidemiology and pathogenesis of coronavirus disease (COVID-19) outbreak, J. Autoimmun. 102433 (2020), https://doi.org/10.1016/j.jaut.2020.102433.

[33] K. Bilinska, P. Jakubowska, C.S. Von Bartheld, R. Butowt, Expression of the SARS-CoV-2 entry proteins, ACE2 and TMPRSS2, in cells of the olfactory epithelium: identification of cell types and trends with age, ACS Chem. Neurosci. 11 (2020) 1555–1562, https://doi.org/10.1021/acschemneuro.0c00210.

[34] M. Guo, W. Tao, R.A. Flavell, S. Zhu, Potential intestinal infection and faecal–oral transmission of SARS-CoV-2, Nat. Rev. Gastroenterol. Hepatol. 18 (2021), https://doi.org/10.1038/s41575-021-00416-6.

[35] M. Arslan, B. Xu, M.G. El-din, Since January 2020 Elsevier has created a COVID-19 resource centre with free information in English and Mandarin on the novel coronavirus COVID- 19. The COVID-19 resource centre is hosted on Elsevier Connect, the company's public news and information, 2020.

[36] A. Sanyaolu, C. Okorie, A. Marinkovic, R. Patidar, K. Younis, P. Desai, Z. Hosein, I. Padda, J. Mangat, M. Altaf, Comorbidity and its impact on patients with COVID-19, SN Compr. Clin. Med. 2 (2020) 1069–1076, https://doi.org/10.1007/s42399-020-00363-4.

[37] S. Erener, Diabetes, infection risk and COVID-19, Mol. Metab. 39 (2020) 101044, https://doi.org/10.1016/j.molmet.2020.101044.

[38] M. Bersanelli, Controversies about COVID-19 and anticancer treatment with immune checkpoint inhibitors, Immunotherapy. 12 (2020) 269–273, https://doi.org/10.2217/imt-2020-0067.

[39] H. Wang, P. Yang, K. Liu, F. Guo, Y. Zhang, G. Zhang, C. Jiang, SARS coronavirus entry into host cells through a novel clathrin- and caveolae-independent endocytic pathway, Cell Res. 18 (2008) 290–301, https://doi.org/10.1038/cr.2008.15.

[40] W. Li, M.J. Moore, N. Vasilieva, J. Sui, Angiotensin-converting enzyme 2 is a functional receptor for the SARS coronavirus, Nature. 426 (2003) 450–454, https://doi.org/10.1038/nature02145.

[41] G. Lu, Y. Hu, Q. Wang, J. Qi, F. Gao, Y. Li, Y. Zhang, W. Zhang, Y. Yuan, J. Bao, B. Zhang, Y. Shi, J. Yan, G.F. Gao, Molecular basis of binding between novel human coronavirus MERS-CoV and its receptor CD26, Nature. 500 (2013) 227–231, https://doi.org/10.1038/nature12328.

[42] Y. Wan, J. Shang, R. Graham, R.S. Baric, F. Li, Receptor recognition by the novel Coronavirus from Wuhan: an analysis based on decade-long structural studies of sARS Coronavirus, J. Virol. 94 (2020) e00127-20, https://doi.org/10.1128/jvi.00127-20.

[43] P. Zhou, X. Lou Yang, X.G. Wang, B. Hu, L. Zhang, W. Zhang, H.R. Si, Y. Zhu, B. Li, C.L. Huang, H.D. Chen, J. Chen, Y. Luo, H. Guo, R. Di Jiang, M.Q. Liu, Y. Chen, X.R. Shen, X. Wang, X.S. Zheng, K. Zhao, Q.J. Chen, F. Deng, L.L. Liu, B. Yan, F.X. Zhan, Y.Y. Wang, G.F. Xiao, Z.L. Shi, A pneumonia outbreak associated with a new coronavirus of probable bat origin, Nature. 579 (2020) 270–273, https://doi.org/10.1038/s41586-020-2012-7.

[44] C. Tikellis, M.C. Thomas, Angiotensin-converting enzyme 2 (ACE2) is a key modulator of the renin angiotensin system in health and disease, Int. J. Pept. 2012 (2012) 256294, https://doi.org/10.1155/2012/256294.

[45] D.G. Kiely, R.I. Cargill, N.M. Wheeldon, W.J. Coutie, B.J. Lipworth, Haemodynamic and endocrine effects of type 1 angiotensin II receptor blockade in patients with hypoxaemic cor pulmonale, Cardiovasc. Res. 33 (1997) 201–208, https://doi.org/10.1016/s0008-6363(96)00180-0.

[46] Y. Imai, K. Kuba, S. Rao, Y. Huan, F. Guo, B. Guan, P. Yang, R. Sarao, T. Wada, H. Leong-poi, M.A. Crackower, A. Fukamizu, C. Hui, L. Hein, S. Uhlig, A. S. Slutsky, C. Jiang, J.M. Penninger, Angiotensin-converting enzyme 2 protects from severe acute lung failure, Nature. 436 (2005) 112–116, https://doi.org/10.1038/nature03712.

[47] M. Liao, Y. Liu, J. Yuan, Y. Wen, G. Xu, J. Zhao, L. Cheng, J. Li, X. Wang, F. Wang, L. Liu, I. Amit, S. Zhang, Z. Zhang, Single-cell landscape of bronchoalveolar immune cells in patients with COVID-19, Nat. Med. 26 (2020) 842–844, https://doi.org/10.1038/s41591-020-0901-9.

[48] K. Kuba, Y. Imai, S. Rao, H. Gao, F. Guo, B. Guan, Y. Huan, P. Yang, Y. Zhang, W. Deng, L. Bao, B. Zhang, G. Liu, Z. Wang, M. Chappell, Y. Liu, D. Zheng, A. Leibbrandt, T. Wada, A.S. Slutsky, D. Liu, C. Qin, C. Jiang, J.M. Penninger, A crucial role of angiotensin converting enzyme 2 (ACE2) in SARS coronavirus – induced lung injury, Nat. Med. 11 (2005) 875–879, https://doi.org/10.1038/nm1267.

[49] L. Mousavizadeh, S. Ghasemi, Genotype and phenotype of COVID-19: their roles in pathogenesis, J. Microbiol. Immunol. Infect. (2020), https://doi.org/10.1016/j.jmii.2020.03.022.

[50] A.A. Ali Golchin, E. Seyedjafari, Mesenchymal stem cell therapy for COVID-19: present or future, Stem Cell Rev. Rep. 16 (2020) 427–433, https://doi.org/10.1007/s12015-020-09973-w.

[51] T.F. Griggs, Y.A. Bochkov, S. Basnet, T.R. Pasic, R.A. Brockman-Schneider, A. C. Palmenberg, J.E. Gern, Rhinovirus C targets ciliated airway epithelial cells, Respir. Res. 18 (2017) 84, https://doi.org/10.1186/s12931-017-0567-0.

[52] J.L. Everman, S. Sajuthi, B. Saef, C. Rios, A.M. Stoner, M. Numata, D. Hu, C. Eng, S. Oh, J. Rodriguez-Santana, E.K. Vladar, D.R. Voelker, E.G. Burchard, M. A. Seibold, Functional genomics of CDHR3 confirms its role in HRV-C infection and childhood asthma exacerbations, J. Allergy Clin. Immunol. 144 (2019) 962–971, https://doi.org/10.1016/j.jaci.2019.01.052.

[53] W. Liu, H. Li, COVID-19: attacks the 1-beta chain of hemoglobin and captures the porphyrin to inhibit human heme metabolism, ChemRxiv. Preprint (2020), https://doi.org/10.26434/chemrxiv.11938173.v5.

[54] D. Kim, J. Lee, J. Yang, J.W. Kim, V.N. Kim, H. Chang, The architecture of SARS-CoV-2 transcriptome, 2020, pp. 1–29.

[55] J. Liu, P. Wu, F. Gao, J. Qi, A. Kawana-tachikawa, J. Xie, C.J. Vavricka, A. Iwamoto, T. Li, G.F. Gao, Novel immunodominant peptide presentation strategy: a featured HLA-A * 2402-restricted cytotoxic T-lymphocyte epitope stabilized by intrachain hydrogen bonds from severe acute respiratory syndrome coronavirus nucleocapsid protein, J. Virol. 84 (2010) 11849–11857, https://doi.org/10.1128/JVI.01464-10.

[56] N. Keicho, S. Itoyama, K. Kashiwase, N. Chi, H. Thuy, Association of human leukocyte antigen class II alleles with severe acute respiratory syndrome in the Vietnamese population, HIM. 70 (2009) 527–531, https://doi.org/10.1016/j.humimm.2009.05.006.

[57] M. Jendro, J.J. Goronzy, C.M. Weyand, Structural and functional characterization of hla-dr molecules circulating in the serum, Autoimmunity. 8 (1991) 289–296, https://doi.org/10.3109/08916939109007636.

[58] A.R.R.A. Levy, A. Rojas-villarraga, R.A. Levy, Cancer and Autoimmunity (2000), https://doi.org/10.1016/b978-0-444-50331-2.x5000-0.

[59] M.H.L. Ng, K.M. Lau, L. Li, S.H. Cheng, W.Y. Chan, P.K. Hui, B. Zee, C.B. Leung, J. J.Y. Sung, Association of human-leukocyte-antigen class I (B*0703) and class II (DRB1*0301) genotypes with susceptibility and resistance to the development of severe acute respiratory syndrome, J. Infect. Dis. 190 (2004) 515–518, https://doi.org/10.1086/421523.

[60] Y.M. Chen, S.Y. Liang, Y.P. Shih, C.Y. Chen, Y.M. Lee, L. Chang, S.Y. Jung, M. S. Ho, K.Y. Liang, H.Y. Chen, Y.J. Chan, D.C. Chu, Epidemiological and genetic correlates of severe acute respiratory syndrome coronavirus infection in the hospital with the highest nosocomial infection rate in Taiwan in 2003, J. Clin. Microbiol. 44 (2006) 359–365, https://doi.org/10.1128/JCM.44.2.359.

[61] A. Nguyen, J.K. David, S.K. Maden, M.A. Wood, B.R. Weeder, A. Nellore, R. F. Thompson, Human leukocyte antigen susceptibility map for SARS-CoV-2, MedRxiv. 94 (2020) 1–12, https://doi.org/10.1101/2020.03.22.20040600.

[62] S.S. Infection, S. Wang, K. Chen, M. Chen, W. Li, Y. Chen, Human-leukocyte antigen class I Cw 1502 and class II DR 0301 genotypes are associated with resistance to severe acute respiratory, Viral Immunol. 24 (2011) 421–426, https://doi.org/10.1089/vim.2011.0024.

[63] X. Tu, W. Po, Y. Zhai, Functional polymorphisms of the CCL2 and MBL genes cumulatively increase susceptibility to severe acute respiratory syndrome coronavirus infection, J. Inf. Secur. 71 (2015) 101–109, https://doi.org/10.1016/j.jinf.2015.03.006.

[64] M. Kikkert, Innate immune evasion by human respiratory RNA viruses, J. Innate Immun. 12 (2020) 4–20, https://doi.org/10.1159/000503030.

[65] N. Vabret, G.J. Britton, C. Gruber, S. Hegde, J. Kim, M. Kuksin, R. Levantovsky, L. Malle, A. Moreira, M.D. Park, L. Pia, E. Risson, M. Saffern, B. Salomé, M. Esai Selvan, M.P. Spindler, J. Tan, V. van der Heide, J.K. Gregory, K. Alexandropoulos, N. Bhardwaj, B.D. Brown, B. Greenbaum, Z.H. Gümüş, D. Homann, A. Horowitz, A.O. Kamphorst, M.A. Curotto de Lafaille, S. Mehandru, M. Merad, R.M. Samstein, M. Agrawal, M. Aleynick, M. Belabed, M. Brown, M. Casanova-Acebes, J. Catalan, M. Centa, A. Charap, A. Chan, S.T. Chen, J. Chung, C.C. Bozkus, E. Cody, F. Cossarini, E. Dalla, N. Fernandez, J. Grout, D. F. Ruan, P. Hamon, E. Humblin, D. Jha, J. Kodysh, A. Leader, M. Lin, K. Lindblad, D. Lozano-Ojalvo, G. Lubitz, A. Magen, Z. Mahmood, G. Martinez-Delgado, J. Mateus-Tique, E. Meritt, C. Moon, J. Noel, T. O'Donnell, M. Ota, T. Plitt, V. Pothula, J. Redes, I. Reyes Torres, M. Roberto, A.R. Sanchez-Paulete, J. Shang, A.S. Schanoski, M. Suprun, M. Tran, N. Vaninov, C.M. Wilk, J. Aguirre-Ghiso, D. Bogunovic, J. Cho, J. Faith, E. Grasset, P. Heeger, E. Kenigsberg, F. Krammer, U. Laserson, Immunology of COVID-19: current state of the science, Immunity 52 (2020) 910–941, https://doi.org/10.1016/j.immuni.2020.05.002.

[66] E. De Wit, N. Van Doremalen, D. Falzarano, V.J. Munster, SARS and MERS: recent insights into emerging coronaviruses, Nat. Rev. Microbiol. 14 (2016) 523–534, https://doi.org/10.1038/nrmicro.2016.81.

[67] E.J. Snijder, Y. van der Meer, J. Zevenhoven-Dobbe, J.J.M. Onderwater, J. van der Meulen, H.K. Koerten, A.M. Mommaas, Ultrastructure and origin of membrane vesicles associated with the severe acute respiratory syndrome coronavirus replication complex, J. Virol. 80 (2006) 5927–5940, https://doi.org/10.1128/jvi.02501-05.

[68] M.G. Wathelet, M. Orr, M.B. Frieman, R.S. Baric, Severe acute respiratory syndrome coronavirus evades antiviral signaling: role of nsp1 and rational design of an attenuated strain, J. Virol. 81 (2007) 11620–11633, https://doi.org/10.1128/jvi.00702-07.

[69] D. Niemeyer, T. Zillinger, D. Muth, F. Zielecki, G. Horvath, T. Suliman, W. Barchet, F. Weber, C. Drosten, M.A. Muller, Middle east respiratory syndrome coronavirus accessory protein 4a is a type I interferon antagonist, J. Virol. 87 (2013) 12489–12495, https://doi.org/10.1128/jvi.01845-13.

[70] Y. Yang, L. Zhang, H. Geng, Y. Deng, B. Huang, Y. Guo, Z. Zhao, W. Tan, The structural and accessory proteins M, ORF 4a, ORF 4b, and ORF 5 of Middle East respiratory syndrome coronavirus (MERS-CoV) are potent interferon antagonists, Protein Cell. 4 (2013) 951–961, https://doi.org/10.1007/s13238-013-3096-8.

[71] S. Dong, J. Sun, Z. Mao, L. Wang, Y.L. Lu, J. Li, A guideline for homology modeling of the proteins from newly discovered betacoronavirus, 2019 novel coronavirus (2019-nCoV), J. Med. Virol. (2020), https://doi.org/10.1002/jmv.25768.

[72] F.C. Zhu, Y.H. Li, X.H. Guan, L.H. Hou, W.J. Wang, J.X. Li, S.P. Wu, B. Sen Wang, Z. Wang, L. Wang, S.Y. Jia, H.D. Jiang, L. Wang, T. Jiang, Y. Hu, J.B. Gou, S.B. Xu, J.J. Xu, X.W. Wang, W. Wang, W. Chen, Safety, tolerability, and immunogenicity of a recombinant adenovirus type-5 vectored COVID-19 vaccine: a dose-escalation, open-label, non-randomised, first-in-human trial, Lancet (2020), https://doi.org/10.1016/S0140-6736(20)31208-3.

[73] R. Zhang, Y. Li, T.J. Cowley, A.D. Steinbrenner, J.M. Phillips, B.L. Yount, R. S. Baric, S.R. Weiss, The nsp1, nsp13, and M proteins contribute to the hepatotropism of murine coronavirus JHM.WU, J. Virol. 89 (2015) 3598–3609, https://doi.org/10.1128/jvi.03535-14.

[74] M. Hackbart, X. Deng, S.C. Baker, Coronavirus endoribonuclease targets viral polyuridine sequences to evade activating host sensors, Proc. Natl. Acad. Sci. U. S. A. 117 (2020) 8094–8103, https://doi.org/10.1073/pnas.1921485117.

[75] M.N.I. Kim Young, J. Robert, Crystal structure of Nsp15 endoribonuclease NendoU from SARS-CoV-2, Protein Sci. Publ. Protein Soc. 29 (2019) 1596–1605.

[76] C.K. Yuen, J.Y. Lam, W.M. Wong, L.F. Mak, X. Wang, H. Chu, J.P. Cai, D.Y. Jin, K. K.W. To, J.F.W. Chan, K.Y. Yuen, K.H. Kok, SARS-CoV-2 nsp13, nsp14, nsp15 and orf6 function as potent interferon antagonists, Emerg. Microbes Infect. 9 (2020) 1418–1428, https://doi.org/10.1080/22221751.2020.1780953.

[77] Y.H. Li, C.Y. Hu, N.P. Wu, H.P. Yao, L.J. Li, Molecular characteristics, functions, and related pathogenicity of MERS-CoV proteins, Engineering. 5 (2019) 940–947, https://doi.org/10.1016/j.eng.2018.11.035.

[78] Q. Liang, J. Li, M. Guo, X. Tian, C. Liu, X. Wang, X. Yang, P. Wu, Z. Xiao, Y. Qu, Y. Yin, J. Fu, Z. Zhu, Z. Liu, C. Peng, T. Zhu, Virus-host interactome and proteomic survey of PMBCs from COVID-19 patients reveal potential virulence factors influencing SARS-CoV-2 pathogenesis, BioRxiv (2020), https://doi.org/10.1101/2020.03.31.019216.

[79] W. Aouadi, A. Blanjoie, J. Vasseur, B. Canard, E. Decroly, Crossm binding of the methyl donor 91, 2017, pp. 1–18.

[80] G. Sutton, E. Fry, L. Carter, S. Sainsbury, T. Walter, J. Nettleship, N. Berrow, R. Owens, R. Gilbert, A. Davidson, S. Siddell, L.L.M. Poon, J. Diprose, D. Alderton, M. Walsh, J.M. Grimes, D.I. Stuart, The nsp9 replicase protein of SARS-coronavirus, structure and functional insights, Structure. 12 (2004) 341–353, https://doi.org/10.1016/j.str.2004.01.016.

[81] K.J. Jang, S. Jeong, D.Y. Kang, N. Sp, Y.M. Yang, D.E. Kim, A high ATP concentration enhances the cooperative translocation of the SARS coronavirus helicase nsP13 in the unwinding of duplex RNA, Sci. Rep. 10 (2020) 1–13, https://doi.org/10.1038/s41598-020-61432-1.

[82] S. Kang, M. Yang, Z. Hong, L. Zhang, Z. Huang, X. Chen, S. He, Z. Zhou, Z. Zhou, Q. Chen, Y. Yan, C. Zhang, H. Shan, S. Chen, Crystal structure of SARS-CoV-2 nucleocapsid protein RNA binding domain reveals potential unique drug targeting sites, Acta Pharm. Sin. B (2020), https://doi.org/10.1016/j.apsb.2020.04.009.

[83] C.-S. Shi, H.-Y. Qi, C. Boularan, N.-N. Huang, M. Abu-Asab, J.H. Shelhamer, J. H. Kehrl, SARS-coronavirus open reading frame-9b suppresses innate immunity by targeting mitochondria and the MAVS/TRAF3/TRAF6 signalosome, J. Immunol. 193 (2014) 3080–3089, https://doi.org/10.4049/jimmunol.1303196.

[84] D.E. Gordon, G.M. Jang, M. Bouhaddou, J. Xu, K. Obernier, K.M. White, M. J. O'Meara, V.V. Rezelj, J.Z. Guo, D.L. Swaney, T.A. Tummino, R. Huettenhain, R. M. Kaake, A.L. Richards, B. Tutuncuoglu, H. Foussard, J. Batra, K. Haas, M. Modak, M. Kim, P. Haas, B.J. Polacco, H. Braberg, J.M. Fabius, M. Eckhardt, M. Soucheray, M.J. Bennett, M. Cakir, M.J. McGregor, Q. Li, B. Meyer, F. Roesch, T. Vallet, A. Mac Kain, L. Miorin, E. Moreno, Z.Z.C. Naing, Y. Zhou, S. Peng, Y. Shi, Z. Zhang, W. Shen, I.T. Kirby, J.E. Melnyk, J.S. Chorba, K. Lou, S.A. Dai, I. Barrio-Hernandez, D. Memon, C. Hernandez-Armenta, J. Lyu, C.J.P. Mathy, T. Perica, K.B. Pilla, S.J. Ganesan, D.J. Saltzberg, R. Rakesh, X. Liu, S. B. Rosenthal, L. Calviello, S. Venkataramanan, J. Liboy-Lugo, Y. Lin, X.P. Huang, Y.F. Liu, S.A. Wankowicz, M. Bohn, M. Safari, F.S. Ugur, C. Koh, N.S. Savar, Q. D. Tran, D. Shengjuler, S.J. Fletcher, M.C. O'Neal, Y. Cai, J.C.J. Chang, D. J. Broadhurst, S. Klippsten, P.P. Sharp, N.A. Wenzell, D. Kuzuoglu, H.Y. Wang, R. Trenker, J.M. Young, D.A. Cavero, J. Hiatt, T.L. Roth, U. Rathore, A. Subramanian, J. Noack, M. Hubert, R.M. Stroud, A.D. Frankel, O.S. Rosenberg, K.A. Verba, D.A. Agard, M. Ott, M. Emerman, N. Jura, M. von Zastrow, E. Verdin, A. Ashworth, O. Schwartz, C. d'Enfert, S. Mukherjee, M. Jacobson, H.S. Malik, D. G. Fujimori, T. Ideker, C.S. Craik, S.N. Floor, J.S. Fraser, J.D. Gross, A. Sali, B. L. Roth, D. Ruggero, J. Taunton, T. Kortemme, P. Beltrao, M. Vignuzzi, A. García-Sastre, K.M. Shokat, B.K. Shoichet, N.J. Krogan, A SARS-CoV-2 protein interaction map reveals targets for drug repurposing, Nature 583 (2020), https://doi.org/10.1038/s41586-020-2286-9.

[85] K.S. Yuen, Z.W. Ye, S.Y. Fung, C.P. Chan, D.Y. Jin, SARS-CoV-2 and COVID-19: the most important research questions, Cell Biosci. 10 (2020) 1–5, https://doi.org/10.1186/s13578-020-00404-4.

[86] V.D. Menachery, H.D. Mitchell, A.S. Cockrell, L.E. Gralinski, B.L. Yount, R. L. Graham, E.T. McAnarney, M.G. Douglas, T. Scobey, A. Beall, K. Dinnon, J. F. Kocher, A.E. Hale, K.G. Stratton, K.M. Waters, R.S. Baric, MERS-CoV accessory orfs play key role for infection and pathogenesis, MBio. 8 (2017) 1–14, https://doi.org/10.1128/mBio.00665-17.

[87] I.Y. Chen, M. Moriyama, M.F. Chang, T. Ichinohe, Severe acute respiratory syndrome coronavirus viroporin 3a activates the NLRP3 inflammasome, Front. Microbiol. 10 (2019) 1–9, https://doi.org/10.3389/fmicb.2019.00050.

[88] M. Guilliams, B.N. Lambrecht, H. Hammad, Division of labor between lung dendritic cells and macrophages in the defense against pulmonary infections, Mucosal Immunol. 6 (2013) 464–473, https://doi.org/10.1038/mi.2013.14.

[89] S. Perlman, A.A. Dandekar, Immunopathogenesis of coronavirus infections: implications for SARS, Nat. Rev. Immunol. 5 (2005) 917–927, https://doi.org/10.1038/nri1732.

[90] B. Diao, Z. Feng, C. Wang, H. Wang, L. Liu, C. Wang, R. Wang, Y. Liu, Y. Liu, G. Wang, Z. Yuan, Y. Wu, Y. Chen, Human kidney is a target for novel severe acute respiratory syndrome coronavirus 2 (SARS-CoV-2) infection, MedRxiv 2 (2020), https://doi.org/10.1101/2020.03.04.20031120.

[91] W. Wen, W. Su, H. Tang, W. Le, X. Zhang, Y. Zheng, X. Liu, L. Xie, J. Li, J. Ye, L. Dong, X. Cui, Y. Miao, D. Wang, J. Dong, C. Xiao, W. Chen, H. Wang, Immune cell pro fi ling of COVID-19 patients in the recovery stage by single-cell sequencing, Cell Discov. 6 (2020) 31, https://doi.org/10.1038/s41421-020-0168-9.

[92] E.Z. Ong, Y. Fu, Z. Chan, W.Y. Leong, A. Bertoletti, E.E. Ooi, E.Z. Ong, Y. Fu, Z. Chan, W.Y. Leong, N. Mei, Y. Lee, S. Kalimuddin, Brief report. A dynamic immune response shapes COVID-19 progression, Cell Host Microbe 27 (2020) 879–882, e2, https://doi.org/10.1016/j.chom.2020.03.021.

[93] M. Liao, Y. Liu, J. Yuan, Y. Wen, G. Xu, J. Zhao, L. Chen, J. Li, X. Wang, F. Wang, L. Liu, S. Zhang, Z. Zhang, The landscape of lung bronchoalveolar immune cells in COVID-19 revealed by single-cell RNA sequencing, MedRxiv (2020), https://doi.org/10.1101/2020.02.23.20026690, 2020.02.23.20026690.

[94] J. Zhao, J. Zhao, N. Van Rooijen, S. Perlman, Evasion by stealth: inefficient immune activation underlies poor T cell response and severe disease in SARS-CoV-infected mice, PLoS Pathog. 5 (2009), e1000636, https://doi.org/10.1371/journal.ppat.1000636.

[95] C. Page, L. Goicochea, K. Matthews, Y. Zhang, P. Klover, M.J. Holtzman, L. Hennighausen, M. Frieman, Induction of alternatively activated macrophages enhances pathogenesis during severe acute respiratory syndrome coronavirus, J. Virol. 86 (2012) 13334–13349, https://doi.org/10.1128/JVI.01689-12.

[96] Z. Feng, B. Diao, R. Wang, G. Wang, C. Wang, Y. Tan, C. Wang, Y. Liu, Y. Liu, Z. Yuan, L. Ren, Y. Wu, The novel severe acute respiratory syndrome coronavirus 2 (SARS-CoV-2) directly decimates human spleens and lymph nodes running title: SARS-CoV-2 infects human spleens and lymph nodes, MedRxiv. 2 (2020) 1–18.

[97] J.H. Wenjun, L. Xiaoqing, W. Sipei, L. Puyi, H. Liyan, L. Yimin, C. Linling, C. Sibei, N. Lingbo, L. Yongping, The definition and risks of cytokine release syndrome-like in 11 COVID-19-infected pneumonia critically ill patients: disease characteristics and retrospective analysis, MedRxiv (2020), https://doi.org/10.1101/2020.02.26.20026989.

[98] M. Zheng, Y. Gao, G. Wang, G. Song, S. Liu, D. Sun, Y. Xu, Z. Tian, Functional exhaustion of antiviral lymphocytes in COVID-19 patients, Cell. Mol. Immunol. 17 (2020) 533–535, https://doi.org/10.1038/s41423-020-0402-2.

[99] C.-Y. Song, J. Xu, J.-Q. He, Y.-Q. Lu, COVID-19 early warning score: a multi-parameter screening tool to identify highly suspected patients, MedRxiv (2020), https://doi.org/10.1101/2020.03.05.20031906.

[100] L.E. Carlin, E.A. Hemann, Z.R. Zacharias, J.W. Heusel, K.L. Legge, Natural killer cell recruitment to the lung during influenza A virus infection is dependent on CXCR3, CCR5, and virus exposure dose, Front. Immunol. 9 (2018) 781, https://doi.org/10.3389/fimmu.2018.00781.

[101] M. Liao, Y. Liu, J. Yuan, Y. Wen, G. Xu, J. Zhao, L. Cheng, J. Li, X. Wang, F. Wang, L. Liu, I. Amit, S. Zhang, Z. Zhang, Single-cell landscape of bronchoalveolar immune cells in patients with COVID-19, Nat. Med. 26 (2020) 842–844, https://doi.org/10.1038/s41591-020-0901-9.

[102] F. Wang, J. Nie, H. Wang, Q. Zhao, Y. Xiong, L. Deng, S. Song, Z. Ma, P. Mo, Y. Zhang, Characteristics of peripheral lymphocyte subset alteration in COVID-19 pneumonia, J. Infect. Dis. 221 (2020) 1762–1769, https://doi.org/10.1093/infdis/jiaa150.

[103] G. Li, X. Chen, A. Xu, Profile of specific antibodies to the SARS-associated coronavirus, N. Engl. J. Med. 349 (2003) 508–509, https://doi.org/10.1056/NEJM200307313490520.

[104] D.L. Thomas, COVID - 19 progression linked to B cell activation, 2020.

[105] P. Yang, H. Gu, Z. Zhao, W. Wang, B. Cao, C. Lai, X. Yang, L.Y. Zhang, Y. Duan, S. Zhang, W. Chen, W. Zhen, M. Cai, J.M. Penninger, C. Jiang, X. Wang, Angiotensin-converting enzyme 2 (ACE2) mediates influenza H7N9 virus-induced acute lung injury, Sci. Rep. 4 (2014) 7027, https://doi.org/10.1038/srep07027.

[106] E. Ciaglia, C. Vecchione, A.A. Puca, COVID-19 infection and circulating ACE2 levels: protective role in women and children, Front. Pediatr. 8 (2020) 11–13, https://doi.org/10.3389/fped.2020.00206.

[107] Z. Xu, L. Shi, Y. Wang, J. Zhang, L. Huang, C. Zhang, S. Liu, P. Zhao, H. Liu, L. Zhu, Y. Tai, C. Bai, T. Gao, J. Song, P. Xia, J. Dong, J. Zhao, F.S. Wang, Pathological findings of COVID-19 associated with acute respiratory distress syndrome, Lancet Respir. Med. 8 (2020) 420–422, https://doi.org/10.1016/S2213-2600(20)30076-X.

[108] H. Zheng, M. Zhang, C. Yang, N. Zhang, X. Wang, X. Yang, X. Dong, Y. Zheng, Elevated exhaustion levels and reduced functional diversity of T cells in peripheral blood may predict severe progression in COVID-19 patients, Cell. Mol. Immunol. 17 (2020) 541–543, https://doi.org/10.1038/s41423-020-0401-3.

[109] Y.Y. Fan, Z.T. Huang, L. Li, M.H. Wu, T. Yu, R.A. Koup, R.T. Bailer, C.Y. Wu, Characterization of SARS-CoV-specific memory T cells from recovered individuals 4 years after infection, Arch. Virol. 154 (2009) 1093–1099, https://doi.org/10.1007/s00705-009-0409-6.

[110] Y. Zhou, B. Fu, X. Zheng, D. Wang, C. Zhao, Y. Qi, R. Sun, Z. Tian, X. Xu, H. Wei, Pathogenic T-cells and inflammatory monocytes incite inflammatory storms in severe COVID-19 patients, Natl. Sci. Rev. 7 (2020) 998–1002, https://doi.org/10.1093/nsr/nwaa041.

[111] M. Liao, Y. Liu, J. Yuan, Y. Wen, G. Xu, J. Zhao, L. Chen, J. Li, X. Wang, F. Wang, L. Liu, S. Zhang, Z. Zhang, The landscape of lung bronchoalveolar immune cells in COVID-19 revealed by single-cell RNA sequencing, Br. Med. J. 26 (2020) 842–844, https://doi.org/10.1101/2020.02.23.20026690.

[112] B. Diao, C. Wang, Y. Tan, X. Chen, Y. Liu, L. Ning, L. Chen, M. Li, Y. Liu, G. Wang, Z. Yuan, Z. Feng, Y. Zhang, Y. Wu, Y. Chen, Reduction and functional exhaustion of T cells in patients with coronavirus disease 2019 (COVID-19), Front. Immunol. 11 (2020) 827, https://doi.org/10.3389/fimmu.2020.00827.

[113] C.K. Wong, C.W.K. Lam, A.K.L. Wu, W.K. Ip, N.L.S. Lee, I.H.S. Chan, L.C.W. Lit, D. S.C. Hui, M.H.M. Chan, S.S.C. Chung, J.J.Y. Sung, Plasma inflammatory cytokines and chemokines in severe acute respiratory syndrome, Clin. Exp. Immunol. 136 (2004) 95–103, https://doi.org/10.1111/j.1365-2249.2004.02415.x.

[114] R. Channappanavar, A.R. Fehr, R. Vijay, M. Mack, J. Zhao, D.K. Meyerholz, S. Perlman, Dysregulated type I interferon and inflammatory monocyte-macrophage responses cause lethal pneumonia in SARS-CoV-infected mice, Cell Host Microbe 19 (2016) 181–193, https://doi.org/10.1016/j.chom.2016.01.007.

[115] Y. Jiang, J. Xu, C. Zhou, Z. Wu, S. Zhong, J. Liu, W. Luo, T. Chen, Q. Qin, P. Deng, Characterization of cytokine/chemokine profiles of severe acute respiratory syndrome, Am. J. Respir. Crit. Care Med. 171 (2005) 850–857, https://doi.org/10.1164/rccm.200407-857OC.

[116] F. Coperchini, L. Chiovato, L. Croce, F. Magri, M. Rotondi, The cytokine storm in COVID-19: an overview of the involvement of the chemokine/chemokine-receptor system, Cytokine Growth Factor Rev. 53 (2020) 25–32, https://doi.org/10.1016/j.cytogfr.2020.05.003.

[117] X. Li, M. Geng, Y. Peng, L. Meng, S. Lu, Molecular immune pathogenesis and diagnosis of COVID-19, J. Pharm. Anal. 10 (2020) 102–108, https://doi.org/10.1016/j.jpha.2020.03.001.

[118] J.M. Sanders, M.L. Monogue, T.Z. Jodlowski, J.B. Cutrell, Pharmacologic treatments for coronavirus disease 2019 (COVID-19). A review, JAMA. 323 (2020) 1824–1836, https://doi.org/10.1001/jama.2020.6019.

[119] C.A. Devaux, J.-M. Rolain, P. Colson, D. Raoult, New insights on the antiviral effects of chloroquine against coronavirus: what to expect for COVID-19? Int. J. Antimicrob. Agents 105938 (2020) https://doi.org/10.1016/j.ijantimicag.2020.105938.

[120] P. Colson, J.M. Rolain, J.C. Lagier, P. Brouqui, D. Raoult, Chloroquine and hydroxychloroquine as available weapons to fight COVID-19, Int. J. Antimicrob. Agents 55 (2020) 105932, https://doi.org/10.1016/j.ijantimicag.2020.105932.

[121] D. Zhou, S.-M. Dai, Q. Tong, COVID-19: a recommendation to examine the effect of hydroxychloroquine in preventing infection and progression, J. Antimicrob. Chemother. 75 (2020) 1667–1670, https://doi.org/10.1093/jac/dkaa114.

[122] B. Cao, Y. Wang, D. Wen, W. Liu, J. Wang, G. Fan, L. Ruan, B. Song, Y. Cai, M. Wei, X. Li, J. Xia, N. Chen, J. Xiang, T. Yu, T. Bai, X. Xie, L. Zhang, C. Li, Y. Yuan, H. Chen, H. Li, H. Huang, S. Tu, F. Gong, Y. Liu, Y. Wei, C. Dong, F. Zhou, X. Gu, J. Xu, Z. Liu, Y. Zhang, H. Li, L. Shang, K. Wang, K. Li, X. Zhou, X. Dong, Z. Qu, S. Lu, X. Hu, S. Ruan, S. Luo, J. Wu, L. Peng, F. Cheng, L. Pan, J. Zou, C. Jia, J. Wang, X. Liu, S. Wang, X. Wu, Q. Ge, J. He, H. Zhan, F. Qiu, L. Guo, C. Huang, T. Jaki, F.G. Hayden, P.W. Horby, D. Zhang, C. Wang, A trial of lopinavir-ritonavir in adults hospitalized with severe covid-19, N. Engl. J. Med. 382 (2020) 1787–1799, https://doi.org/10.1056/NEJMoa2001282.

[123] J.A. Al-Tawfiq, A.H. Al-Homoud, Z.A. Memish, Remdesivir as a possible therapeutic option for the COVID-19, Travel Med. Infect. Dis. 34 (2020) 101615, https://doi.org/10.1016/j.tmaid.2020.101615.

[124] R.U. Kadam, I.A. Wilson, Structural basis of influenza virus fusion inhibition by the antiviral drug Arbidol, Proc. Natl. Acad. Sci. U. S. A. 114 (2017) 206–214, https://doi.org/10.1073/pnas.1617020114.

[125] A. Casadevall, L. Pirofski, The convalescent sera option for containing COVID-19, J. Clin. Invest. 130 (2020) 1545–1548, https://doi.org/10.1172/jci138003.

[126] S.P. Kaur, V. Gupta, COVID-19 vaccine: a comprehensive status report, Virus Res. 288 (2020) 198114, https://doi.org/10.1016/j.virusres.2020.198114.

[127] M. Yuan, N.C. Wu, X. Zhu, C.C.D. Lee, R.T.Y. So, H. Lv, C.K.P. Mok, I.A. Wilson, A highly conserved cryptic epitope in the receptor binding domains of SARS-CoV-2 and SARS-CoV, Science (80-.) 368 (2020) 630–633, https://doi.org/10.1126/science.abb7269.

[128] V. Baruah, S. Bose, Immunoinformatics-aided identification of T cell and B cell epitopes in the surface glycoprotein of 2019-nCoV, J. Med. Virol. 92 (2020) 495–500, https://doi.org/10.1002/jmv.25698.

[129] J.R. Lon, Y. Bai, B. Zhong, F. Cai, H. Du, Prediction and evolution of B cell epitopes of surface protein in SARS-CoV-2, BioRxiv (2020), https://doi.org/10.1101/2020.04.03.022723.

[130] S.M. Metcalfe, Mesenchymal stem cells and management of COVID-19 pneumonia, Med. Drug Discov. 5 (2020) 100019, https://doi.org/10.1016/j.medidd.2020.100019.

[131] ALBERTA HOPE, COVID-19 for the Prevention of Severe COVID19 Disease - Full Text View. ClinicalTrials.gov, 2021.

[132] Study to Evaluate the Safety and Antiviral Activity of Remdesivir (GS-5734™) in Participants With Severe Coronavirus Disease (COVID-19) - Full Text View. ClinicalTrials.gov, 2021.

[133] J.D. Goldman, D.C.B. Lye, D.S. Hui, K.M. Marks, R. Bruno, R. Montejano, C. D. Spinner, M. Galli, M.-Y. Ahn, R.G. Nahass, Y.-S. Chen, D. SenGupta, R. H. Hyland, A.O. Osinusi, H. Cao, C. Blair, X. Wei, A. Gaggar, D.M. Brainard, W. J. Towner, J. Muñoz, K.M. Mullane, F.M. Marty, K.T. Tashima, G. Diaz, A. Subramanian, Remdesivir for 5 or 10 Days in Patients with Severe Covid-19, N. Engl. J. Med. (2020), https://doi.org/10.1056/nejmoa2015301.

[134] C.D. Spinner, R.L. Gottlieb, G.J. Criner, J.R. Arribas López, A.M. Cattelan, A. Soriano Viladomiu, O. Ogbuagu, P. Malhotra, K.M. Mullane, A. Castagna, L.Y. A. Chai, M. Roestenberg, O.T.Y. Tsang, E. Bernasconi, P. Le Turnier, S.-C. Chang, D. SenGupta, R.H. Hyland, A.O. Osinusi, H. Cao, C. Blair, H. Wang, A. Gaggar, D. M. Brainard, M.J. McPhail, S. Bhagani, M.Y. Ahn, A.J. Sanyal, G. Huhn, F. M. Marty, Effect of remdesivir vs standard care on clinical status at 11 days in patients with moderate COVID-19, JAMA (2020), https://doi.org/10.1001/jama.2020.16349.

[135] Duvelisib to Combat COVID-19 - Full Text View. ClinicalTrials.gov, 2021.

[136] Application of Desferal to Treat COVID-19 - Full Text View. ClinicalTrials.gov, 2021.

[137] H. Wang, Z. Li, J. Niu, Y. Xu, L. Ma, A. Lu, X. Wang, Z. Qian, Z. Huang, X. Jin, Q. Leng, J. Wang, J. Zhong, B. Sun, G. Meng, Antiviral effects of ferric ammonium citrate, Cell Discov. 4 (2018) 14, https://doi.org/10.1038/s41421-018-0013-6.

[138] Clinical Study To Evaluate The Performance And Safety Of Favipiravir in COVID-19 - Full Text View. ClinicalTrials.gov, 2021.

[139] Study to Evaluate the Efficacy and Safety of Tocilizumab Versus Corticosteroids in Hospitalised COVID-19 Patients With High Risk of Progression - Full Text View. ClinicalTrials.gov, 2021.

[140] Sarilumab COVID-19 - Full Text View. ClinicalTrials.gov, 2021.

[141] J.J.V. McMurray, S.D. Solomon, S.E. Inzucchi, L. Kober, M.N. Kosiborod, F. A. Martinez, P. Ponikowski, M.S. Sabatine, I.S. Anand, J.B. Lohlavek, M. Bohm, C. E. Chiang, V.K. Chopra, R.A. De Boer, A.S. Desai, M. Diez, J. Drozdz, A. Dukat, J. Ge, J.G. Howlett, T. Katova, M. Kitakaze, C.E.A. Ljungman, B. Merkely, J. C. Nicolau, E. O'Meara, M.C. Petrie, P.N. Vinh, M. Schou, S. Tereshchenko, S. Verma, C. Held, D.L. DeMets, K.F. Docherty, P.S. Jhund, O. Bengtsson, M. Sjostrand, A.M. Langkilde, Dapagliflozin in patients with heart failure and reduced ejection fraction, N. Engl. J. Med. 381 (2019) 1995–2008, https://doi.org/10.1056/NEJMoa1911303.

[142] Dapagliflozin in Respiratory Failure in Patients With COVID-19 - Full Text View. ClinicalTrials.gov, 2021.

[143] Recombinant Human Angiotensin-converting Enzyme 2 (rhACE2) as a Treatment for Patients With COVID-19 - Full Text View. ClinicalTrials.gov, 2021.

[144] The Phase 2 Study to Evaluate the Safety and Efficacy of Clevudine in Patients With Moderate COVID-19 - Full Text View. ClinicalTrials.gov, 2021.
[145] Study of FT516 for the Treatment of COVID-19 in Hospitalized Patients With Hypoxia - Full Text View. ClinicalTrials.gov, 2021.
[146] DAS181 for Severe COVID-19: Compassionate Use - Full Text View. ClinicalTrials.gov, 2021.
[147] Study of Open Label Losartan in COVID-19 - Full Text View. ClinicalTrials.gov, 2021.
[148] C. Lv, W. Liu, B. Wang, R. Dang, L. Qiu, J. Ren, C. Yan, Z. Yang, X. Wang, Ivermectin inhibits DNA polymerase UL42 of pseudorabies virus entrance into the nucleus and proliferation of the virus in vitro and vivo, Antivir. Res. 159 (2018) 55–62, https://doi.org/10.1016/j.antiviral.2018.09.010.
[149] S.K. Hong, H.J. Kim, C.S. Song, I.S. Choi, J.B. Lee, S.Y. Park, Nitazoxanide suppresses IL-6 production in LPS-stimulated mouse macrophages and TG-injected mice, Int. Immunopharmacol. 13 (2012) 23–27, https://doi.org/10.1016/j.intimp.2012.03.002.
[150] Ivermectin and Nitazoxanide Combination Therapy for COVID-19 - Full Text View. ClinicalTrials.gov, 2021.
[151] C. Shen, Z. Wang, F. Zhao, Y. Yang, J. Li, J. Yuan, F. Wang, D. Li, M. Yang, L. Xing, J. Wei, H. Xiao, Y. Yang, J. Qu, L. Qing, L. Chen, Z. Xu, L. Peng, Y. Li, H. Zheng, F. Chen, K. Huang, Y. Jiang, D. Liu, Z. Zhang, Y. Liu, L. Liu, Treatment of 5 critically ill patients with COVID-19 with convalescent plasma, JAMA - J. Am. Med. Assoc. 323 (2020) 1582–1589, https://doi.org/10.1001/jama.2020.4783.
[152] Efficacy of Convalescent Plasma Therapy in the Early Care of COVID-19 Patients. - Full Text View. ClinicalTrials.gov, 2021.
[153] Isotretinoin in Treatment of COVID-19 - Full Text View. ClinicalTrials.gov, 2021.
[154] Colchicine in COVID-19: a Pilot Study - Full Text View. ClinicalTrials.gov, 2021.
[155] Ruxolitinib in Covid-19 Patients With Defined Hyperinflammation - Full Text View. ClinicalTrials.gov, 2021.
[156] Expanded Access Program of Ruxolitinib for the Emergency Treatment of Cytokine Storm From COVID-19 Infection - Full Text View. ClinicalTrials.gov, 2021.
[157] F. La Rosée, H.C. Bremer, I. Gehrke, A. Kehr, A. Hochhaus, S. Birndt, M. Fellhauer, M. Henkes, B. Kumle, S.G. Russo, P. La Rosée, The Janus kinase 1/2 inhibitor ruxolitinib in COVID-19 with severe systemic hyperinflammation, Leukemia. 34 (2020) 1805–1815, https://doi.org/10.1038/s41375-020-0891-0.
[158] A Pilot Study of Sildenafil in COVID-19 - Full Text View. ClinicalTrials.gov, 2021.
[159] Sirolimus Treatment in Hospitalized Patients With COVID-19 Pneumonia - Full Text View. ClinicalTrials.gov, 2021.
[160] Single-Blind Study of a Single Dose of Peginterferon Lambda-1a Compared With Placebo in Outpatients With Mild COVID-19 - Full Text View. ClinicalTrials.gov, 2021.
[161] Rintatolimod and IFN Alpha-2b for the Treatment of Mild or Moderate COVID-19 Infection in Cancer Patients - Full Text View. ClinicalTrials.gov, 2021.
[162] Administration of Intravenous Vitamin C in Novel Coronavirus Infection (COVID-19) and Decreased Oxygenation - Full Text View. ClinicalTrials.gov, 2021.
[163] Safety and Immunogenicity Study of 2019-nCoV Vaccine (mRNA-1273) for Prophylaxis of SARS-CoV-2 Infection (COVID-19) - Full Text View. ClinicalTrials.gov, 2021.
[164] L.A. Jackson, E.J. Anderson, N.G. Rouphael, P.C. Roberts, M. Makhene, R. N. Coler, M.P. McCullough, J.D. Chappell, M.R. Denison, L.J. Stevens, A. J. Pruijssers, A. McDermott, B. Flach, N.A. Doria-Rose, K.S. Corbett, K. M. Morabito, S. O'Dell, S.D. Schmidt, P.A. Swanson, M. Padilla, J.R. Mascola, K. M. Neuzil, H. Bennett, W. Sun, E. Peters, M. Makowski, J. Albert, K. Cross, W. Buchanan, R. Pikaart-Tautges, J.E. Ledgerwood, B.S. Graham, J.H. Beigel, An mRNA vaccine against SARS-CoV-2 — Preliminary report, N. Engl. J. Med. (2020), https://doi.org/10.1056/nejmoa2022483.
[165] Safety, Tolerability and Immunogenicity of INO-4800 for COVID-19 in Healthy Volunteers - Full Text View. ClinicalTrials.gov, 2021.
[166] P.M. Folegatti, K.J. Ewer, P.K. Aley, B. Angus, S. Becker, S. Belij-Rammerstorfer, D. Bellamy, S. Bibi, M. Bittaye, E.A. Clutterbuck, C. Dold, S.N. Faust, A. Finn, A. L. Flaxman, B. Hallis, P. Heath, D. Jenkin, R. Lazarus, R. Makinson, A. M. Minassian, K.M. Pollock, M. Ramasamy, H. Robinson, M. Snape, R. Tarrant, M. Voysey, C. Green, A.D. Douglas, A.V.S. Hill, T. Lambe, S.C. Gilbert, A. J. Pollard, J. Aboagye, K. Adams, A. Ali, E. Allen, J.L. Allison, R. Anslow, E. H. Arbe-Barnes, G. Babbage, K. Baillie, M. Baker, N. Baker, P. Baker, I. Baleanu, J. Ballaminut, E. Barnes, J. Barrett, L. Bates, A. Batten, K. Beadon, R. Beckley, E. Berrie, L. Berry, A. Beveridge, K.R. Bewley, E.M. Bijker, T. Bingham, L. Blackwell, C.L. Blundell, E. Bolam, E. Boland, N. Borthwick, T. Bower, A. Boyd, T. Brenner, P.D. Bright, C. Brown-O'Sullivan, E. Brunt, J. Burbage, S. Burge, K. R. Buttigieg, N. Byard, I. Cabera Puig, A. Calvert, S. Camara, M. Cao, F. Cappuccini, M. Carr, M.W. Carroll, V. Carter, K. Cathie, R.J. Challis, S. Charlton, I. Chelysheva, J.S. Cho, P. Cicconi, L. Cifuentes, H. Clark, E. Clark, T. Cole, R. Colin-Jones, C.P. Conlon, A. Cook, N.S. Coombes, R. Cooper, C. A. Cosgrove, K. Coy, W.E.M. Crocker, C.J. Cunningham, B.E. Damratoski, L. Dando, M.S. Datoo, H. Davies, H. De Graaf, T. Demissie, C. Di Maso, I. Dietrich, T. Dong, F.R. Donnellan, N. Douglas, C. Downing, J. Drake, R. Drake-Brockman, R.E. Drury, S.J. Dunachie, N.J. Edwards, F.D.L. Edwards, C.J. Edwards, S.C. Elias, M.J. Elmore, K.R.W. Emary, M.R. English, S. Fagerbrink, S. Felle, S. Feng, S. Field, C. Fixmer, C. Fletcher, K.J. Ford, J. Fowler, P. Fox, E. Francis, J. Frater, J. Furze, M. Fuskova, E. Galiza, D. Gbesemete, C. Gilbride, K. Godwin, G. Gorini, L. Goulston, C. Grabau, L. Gracie, Z. Gray, L.B. Guthrie, M. Hackett, S. Halwe, E. Hamilton, J. Hamlyn, B. Hanumunthadu, I. Harding, S.A. Harris, A. Harris, D. Harrison, C. Harrison, T.C. Hart, L. Haskell, S. Hawkins, I. Head, J.A. Henry, J. Hill, S.H.C. Hodgson, M.M. Hou, E. Howe, N. Howell, C. Hutlin, S. Ikram, C. Isitt, P. Iveson, S. Jackson, F. Jackson, S.W. James, M. Jenkins, E. Jones, K. Jones, C.E. Jones, B. Jones, R. Kailath, K. Karampatsas, J. Keen, S. Kelly, D. Kelly, D. Kerr, S. Kerridge, L. Khan, U. Khan, A. Killen, J. Kinch, T.B. King, L. King, J. King, L. Kingham-Page, P. Klenerman, F. Knapper, J.C. Knight, D. Knott, S. Koleva, A. Kupke, C.W. Larkworthy, J.P.J. Larwood, A. Laskey, A. M. Lawrie, A. Lee, K.Y. Ngan Lee, E.A. Lees, H. Legge, A. Lelliott, N.M. Lemm, A. M. Lias, A. Linder, S. Lipworth, X. Liu, S. Liu, R. Lopez Ramon, M. Lwin, F. Mabesa, M. Madhavan, G. Mallett, K. Mansatta, I. Marcal, S. Marinou, E. Marlow, J.L. Marshall, J. Martin, J. McEwan, L. McInroy, G. Meddaugh, A. J. Mentzer, N. Mirtorabi, M. Moore, E. Moran, E. Morey, V. Morgan, S.J. Morris, H. Morrison, G. Morshead, R. Morter, Y.F. Mujadidi, J. Muller, T. Munera-Huertas, C. Munro, A. Munro, S. Murphy, V.J. Munster, P. Mweu, A. Noé, F. L. Nugent, E. Nuthall, K. O'Brien, D. O'Connor, B. Oguti, J.L. Oliver, C. Oliveira, P.J. O'Reilly, M. Osborn, P. Osborne, C. Owen, D. Owens, N. Owino, M. Pacurar, K. Parker, H. Parracho, M. Patrick-Smith, V. Payne, J. Pearce, Y. Peng, M. P. Peralta Alvarez, J. Perring, K. Pfafferott, D. Pipini, E. Plested, H. Pluess-Hall, K. Pollock, I. Poulton, L. Presland, S. Provstgaard-Morys, D. Pulido, K. Radia, F. Ramos Lopez, J. Rand, H. Ratcliffe, T. Rawlinson, S. Rhead, A. Riddell, A. J. Ritchie, H. Roberts, J. Robson, S. Roche, C. Rohde, C.S. Rollier, R. Romani, I. Rudiansyah, S. Saich, S. Sajjad, S. Salvador, L. Sanchez Riera, H. Sanders, K. Sanders, S. Sapaun, C. Sayce, E. Schofield, G. Screaton, B. Selby, C. Semple, H. R. Sharpe, I. Shaik, A. Shea, H. Shelton, S. Silk, L. Silva-Reyes, D.T. Skelly, H. Smee, C.C. Smith, D.J. Smith, R. Song, A.J. Spencer, E. Stafford, A. Steele, E. Stefanova, L. Stockdale, A. Szigeti, A. Tahiri-Alaoui, M. Tait, H. Talbot, R. Tanner, I.J. Taylor, V. Taylor, R. Te Water Naude, N. Thakur, Y. Themistocleous, A. Themistocleous, M. Thomas, T.M. Thomas, A. Thompson, S. Thomson-Hill, J. Tomlins, S. Tonks, J. Towner, N. Tran, J.A. Tree, A. Truby, K. Turkentine, C. Turner, N. Turner, S. Turner, T. Tuthill, M. Ulaszewska, R. Varughese, N. Van Doremalen, K. Veighey, M.K. Verheul, I. Vichos, E. Vitale, L. Walker, M.E.E. Watson, B. Welham, J. Wheat, C. White, R. White, A.T. Worth, D. Wright, S. Wright, X.L. Yao, Y. Yau, Safety and immunogenicity of the ChAdOx1 nCoV-19 vaccine against SARS-CoV-2: a preliminary report of a phase 1/2, single-blind, randomised controlled trial, Lancet 396 (2020) 467–478, https://doi.org/10.1016/S0140-6736(20)31604-4.
[167] A Study of a Candidate COVID-19 Vaccine (COV001) - Full Text View. ClinicalTrials.gov, 2021.
[168] Immunity and Safety of Covid-19 Synthetic Minigene Vaccine - Full Text View. ClinicalTrials.gov, 2021.
[169] Evaluation of the Safety and Immunogenicity of a SARS-CoV-2 rS (COVID-19) Nanoparticle Vaccine With/Without Matrix-M Adjuvant - Full Text View. ClinicalTrials.gov, 2021.
[170] Study to Describe the Safety, Tolerability, Immunogenicity, and Potential Efficacy of RNA Vaccine Candidates Against COVID-19 in Healthy Adults - Full Text View. ClinicalTrials.gov, 2021.
[171] Evaluating the Safety, Tolerability and Immunogenicity of bacTRL-Spike Vaccine for Prevention of COVID-19 - Full Text View. ClinicalTrials.gov, 2021.
[172] NCT04482621, Decitabine for Coronavirus (COVID-19) Pneumonia- Acute Respiratory Distress Syndrome (ARDS) Treatment: DART Trial. https://Clinicaltrials.Gov/Show/NCT04482621, 2021.
[173] Pilot Trial of XFBD, a TCM, in Persons With COVID-19 - Full Text View. ClinicalTrials.gov, 2021.
[174] Study of the Safety and Efficacy of STI-5656 (Abivertinib Maleate) in Subjects Hospitalized Due to COVID-19 - Full Text View. ClinicalTrials.gov, 2021.
[175] Deferoxamine - StatPearls - NCBI Bookshelf, 2021.
[176] Phase 2 Trial Using rhDNase to Reduce Mortality in COVID-19 Patients With Respiratory Failure - Full Text View. ClinicalTrials.gov, 2021.
[177] An Efficacy and Safety Clinical Trial of an Investigational COVID-19 Vaccine (BBV152) in Adult Volunteers - Full Text View. ClinicalTrials.gov, 2021.
[178] Dornase Alpha for the Treatment of COVID-19 - Full Text View. ClinicalTrials.gov, 2021.
[179] NCT04723394, Phase III Study of AZD7442 for Treatment of COVID-19 in Outpatient Adults. https://Clinicaltrials.Gov/Show/NCT04723394, 2021.
[180] Safety and Tolerability of Etanercept in Alzheimer's Disease - Full Text View. ClinicalTrials.gov, 2021.
[181] Efficacy and Safety of Sirolimus in COVID-19 Infection - Full Text View. ClinicalTrials.gov, 2021.
[182] Sitagliptin Treatment in Diabetic COVID-19 Positive Patients - Full Text View. ClinicalTrials.gov, 2021.
[183] COVID-19 Antithrombotic Rivaroxaban Evaluation - Full Text View. ClinicalTrials.gov, 2021.
[184] Dendritic Cell Vaccine to Prevent COVID-19 - Full Text View. ClinicalTrials.gov, 2021.
[185] Nct, Phase III Double-blind, Placebo-controlled Study of AZD1222 for the Prevention of COVID-19 in Adults. https://Clinicaltrials.Gov/Show/NCT04516746, 2020.
[186] AstraZeneca, ChAdOx1-S/nCoV-19 [recombinant], COVID-19 vaccine, 2021.

CHAPTER 12

Role of Mitochondrial-mediated Pathways in Breast Cancer: An Overview

Nabanita Chatterjee[*], **Debangshi Das, Ashna Jha** and **Sraddhya Roy**

Chittaranjan National Cancer Institute, 37, Shyama Prasad Mukherjee Road, Kolkata-700026, India

Abstract: The powerhouse of the cell, mitochondria play several cellular functions, and it also regulates the physiological adjustment of the body. The deregulation of any of the key factors in the regulation pathway of energy production or cellular metabolism leads to disease conditions and, sometimes even cancer. Several studies emphasize the fact that the alteration in metabolic pathways, generate or evoke cancer susceptibility including breast cancer. Among the several cancers, breast cancer is a major concern in the female population. Thus, the alteration of any mitochondrial factors or metabolites associated with the mitochondrial energy cycle, the changes in breast cancer development or progression of metastasis is high. Mitochondrial regulation could be a promising therapeutic approach in the treatment of breast cancer.

Keywords: Breast cancer, Metabolic pathway, Mitochondria, mtDNA, Reactive oxygen species, Warburg effect.

INTRODUCTION

The Powerful Cellular Organelle: Mitochondria

Mitochondria is a membrane-bound organelle found in the cytoplasm of almost all eukaryotic organisms [1]. The role of mitochondria is the production of the ATP which is known as the energy currency of the cell *via* respiration. It helps in the regulation of cellular metabolism. It is also known as the 'powerhouse' of the cell [2]. Citric acid cycle and Krebs's cycle are involved in the production of ATP molecules [3, 4]. Signaling, cell growth, maintaining cell cycle and cell death are several other functions performed by the mitochondria.

It is also involved in various human disorders such as cardiac dysfunction, mitochondrial disorders, autism, and heart failure [5 - 10].

[*] **Corresponding Author Dr. Nabanita Chatterjee**: Chittaranjan National Cancer Institute, 37, Shyama Prasad Mukherjee Road, Kolkata -700026, India; E-mails: nabanita.chatterje@yahoo.com/nabanitachatterjee@cnci.org.in

Shankar Suman, Garima Suman and Sanjay Mishra (Eds.)

The number of mitochondria varies in the cell, depending on the organism, cells, and type of tissues. For instance, the liver has around 2000 mitochondria whereas RBCs do not contain any mitochondria. These organelles consist of compartments that include the outer membrane, inner membrane, cristae, matrix and the intermembrane space that individually performs specialized functions [11]. The genome of mitochondria shows similarity to bacterial genomes. In addition, mitochondrial proteins differ widely based on tissues and species type.

Mitochondrial Energy

The primary function of mitochondria is ATP production. The oxidization mainly does energy conversion. In the cytosol, the main compound is glucose, which gets converted to pyruvate, NADH and this process is known as aerobic respiration, which is an oxygen-dependent process during oxidation. Sometimes, the process is oxygen-independent when the oxygen supply is limited, and it starts anaerobic fermentation [12]. In this process, the ATP production is 13-times higher in aerobic respiration than fermentation [13]. The release of ATP occurs through the outer membrane channel porin from the inner membrane with the help of several other proteins.

The Process of ATP Production: Pyruvate and Citric Acid Cycle

In the process of glycolysis, the out product is pyruvate, which is actively transported to the matrix. After that, it gets oxidized and followed by the combination with co-enzyme A and its associates, leading to form acetyl CoA or decarboxylated to oxaloacetate. The second reaction, denoted with it, is the citric acid cycle, where all the intermediates like citrate, alpha-keto-glutarate, and succinate oxaloacetate again turn into the cycle whenever it needs the regeneration of cycles. That cycle could produce citric acid in a combination of excess or low mount of oxaloacetate with reacting acetyl-CoA that might be referred to as anaplerotic or cataplerotic effect. Thus, the amount of ATP production is directly or indirectly regulated by mitochondria. After this reaction of oxidative reaction, the acetate portion of acetyl-CoA gets oxidized to carbon dioxide, water, and ATP. More importantly, acetyl-CoA is the only compound that enters the TCA cycle either from pyruvate oxidation or β-oxidation of fatty acids. This also affects several disease conditions including cancer [14]. Few more parameters of oxidation also influence the interaction process like the gluconeogenic pathway [15].

Pyruvate and the TCA Cycle

Pyruvate molecules produced *via* the glycolysis pathway are carried across the inner membrane of mitochondria and into the matrix where pyruvate molecules

get oxidized and combine with coenzyme-A forming CO_2, acetyl-CoA, and NADH. It can be carboxylated by pyruvate carboxylase that forms oxaloacetate [16]. This results in an increase in the amount of oxaloacetate in the TCA cycle which in [17] turn increases the cycle's capacity to metabolize acetyl Co-A to form citric acid. Thus, the increase or decrease in the rate of ATP production is regulated by the mitochondria. All the intermediates (*e.g.*, citrate, iso-citrate, alpha-ketoglutarate, succinate, fumarate, *etc*.) are generated during each turn of the TCA cycle. Acetyl CoA is the only combustible fuel that enters the citric acid or TCA cycle derived from pyruvate oxidation or β-oxidation of the fatty acids [18], and it is consumed for each of the molecules of oxaloacetate which is present in the mitochondrial matrix. CO_2, water, and energy are produced by the oxidation of acetate protein of acetyl CoA captured in the form of ATP [14, 19].

In the liver, the cytosolic pyruvate is carboxylated into oxaloacetate in gluconeogenic pathway, which under the influence of an increased level of glucan in the blood converts lactate and as well as de-aminated alanine into the glucose. Most of the enzymes of the TCA cycle are located in the mitochondrial matrix, but succinate dehydrogenase is bound to the inner mitochondrial membrane as a part of complex II [20]. Oxidization of acetyl-CoA to CO_2 by the citric acid cycle or TCA cycle produces reduced cofactors that include three molecules of NADH and one molecule of FADH2. These reduced cofactors are a source of electrons for electron transport chain [21].

Electron Transport Chain [NADH and FADH2]

Through the electron transport chain, redox energy from NADH and FADH2 is transferred to oxygen [22]. NADH and FADH2 molecules are produced *via* the TCA cycle within the matrix and through the process of glycolysis in the cytoplasm. Using the glycerol phosphate shuttle or the malate-aspartate shuttle system, the reducing equivalents from the cytoplasm can be imported. NADH dehydrogenase, cytochrome c reductase, cytochrome c oxidase in the inner membrane performs the transfer process, and the energy released is used for pumping protons into the intermembrane space. This process can lead to mitochondrial dysfunction associated with aging and oxidative stress [23, 24].

Heat Production

The process by which protons can enter the mitochondrial matrix without the synthesis of ATP is known as Proton leak or mitochondrial uncoupling [11]. This process takes place due to the facilitated diffusion of protons resulting in the release of electrochemical gradient energy in the form of heat mediated by a proton channel called thermogenin or UCP1 [25].

Storage of Calcium Ions

Many reactions can be regulated by the concentration of free calcium in the cell which is significant for signal transduction in the cell. Calcium is stored in mitochondria that contribute to the cell's homeostasis of calcium. Mitochondria can also help in the take-up and release of calcium ions [26].

A series of second messenger system proteins are activated by the release of calcium, which coordinates the process such as the release of hormones in endocrine cells and release of neurotransmitters in nerve cells [27]. Mitochondria play a central role in many other metabolic tasks, such as signaling through mitochondrial reactive oxygen species, regulating membrane potential, apoptosis, calcium signaling (including calcium-evoked apoptosis), regulating of cellular metabolism, certain heme synthesis reactions, steroid synthesis, and hormonal imbalance *etc.* [28, 29].

Cancer: Breast Cancer

Cancer that specifically develops from breast and its associate ductal parts occurs mainly in females. Lack of physical exercise, obesity, early age at first menstruation, having children late, family history of breast cancer, drinking alcohol, *etc*., are the risk factors concerned with developing breast cancer. Around 5-10% of breast cancer occurs due to genes inherited from parents, including BRCA1 and BRCA2 [30]. It commonly occurs in the lining of milk ducts and the lobules. Cancers developed from the lining of duct are called ductal carcinomas, whereas ones developed from lobules known as lobular carcinomas. Ductal carcinomas are developed from pre-invasive lesions. Breast cancer is determined by performing a biopsy of concerning lump [31]. After the diagnosis, more tests are performed in order to determine if carcinoma cells have spread beyond the breast [32].

Triple-negative Breast Cancer

Triple-negative breast cancer (TNBC) is a type of breast cancer that tests negative for estrogen receptors, progesterone receptors and excess HER2 protein. The hormone receptors inside and on the surface of the healthy breast cells receive a message from estrogen and progesterone. The hormones attach to these receptors thereby provide instructions to the cells to grow and function properly. However, triple-negative breast cancer does not have these receptors. On the other hand, TNBC has about 20% of the excess HER2 protein. When the breast cancer cells have an excessive amount of HER2 protein, they grow, divide quickly and develop metastasis. Among others, about 10-20% of cancer of breast cancers are found as TNBC [33, 34]. They are unlikely to respond to medicines that target

HER2 protein, such as Herceptin [chemical name: Trastuzumab], Kadcyla (chemical name: T-DMA or ado-Trastuzumabemtansine), Nerlynx (chemical name: neratinib), Perjeta (chemical name: Pertuzumab), or Tykerb (chemical name: Lapatinib) [35].

Common Features of TNBC [36]:

• TNBC is considered aggressive, having a poorer prognosis than any other breast cancer types.

• It tends to be higher in grade.

• It is the "basal-like" cell type.

TNBC is commonly found in younger people, African-American and Hispanic women, and people with BRCA1 mutation [37].

Treatment for TNBC: Triple-negative breast cancer is treated with a combination of surgery, radiation therapy, and chemotherapy [38].

Some of them are listed below:

• Neo-adjuvant chemotherapy- Triple negative breast cancer treated with chemotherapy before surgery is called neo-adjuvant chemotherapy. This type of treatment makes disease-free survival and other survival better [39].

• PARP inhibitor- PARP inhibitor, such as Lynparza (chemical name: olaparib), Talzenna (chemical name: talazoparib) are used to treat advanced-stage HER2-negative breast cancer in people with BRCA1 or BRCA2 mutation. This helps in preventing poly ADP-ribose polymerase (PARP) enzyme from fixing DNA damage in breast cancer cells [40].

• Immunotherapy- The immunotherapy medicines, Tecentriq and Abraxane, is used for treating unresectable locally advanced or metastatic triple-negative, PD-L1 positive breast cancer. Tecentriq is an immune checkpoint inhibitor medicine that targets a specific protein inhibiting PD-L1 protein expression. By doing so, it allows the immune system cells to recognize cancer cells and kill them [41].

Alterations in Cancer Cells

Normal cell growth and development requires the optimal function of regulatory signaling pathways, which resist or tolerate in response to external or internal stimuli. Deregulation of these signaling pathways can lead to the occurrence of various diseases, such as diabetes, a neurodegenerative disorder, developmental

defects and cancer [42]. Defects in the cellular growth and apoptotic pathway can lead to carcinogenesis and metastatic tumor progression. However, defects in apoptosis are observed as the primary cellular malfunction in tumor growth and metastatic progression. Cancer cells exhibit strong metabolic faults in the mitochondrial apoptotic process which includes increased fatty acid synthesis, boosting glutamine metabolism and dependence on aerobic glycolysis for gaining energy. All these metabolic adaptations take place due to the defects in normal mitochondria function, thereby developing resistance towards cancer treatments and apoptotic evasion, which leads to an increase in cancer growth and progression [43, 44].

Therefore, targeting and restoring mitochondrial steady state is considered to be a useful strategy for cancer control and management. Metabolic inhibitors, such as 2-deoxy-D-glucose (2DG), dichloroacetate (DCA), hexokinase inhibitors, and lactate dehydrogenase inhibitors, have commonly been used to inhibit aerobic glycolysis pathway and restore steady-state oxidative phosphorylation in mitochondria [45]. These have been effective against various cancer cells [46].

MITOCHONDRIAL INVOLVEMENT: BETWEEN NORMAL AND CANCER CELLS IN RESPECT OF METABOLISM

Cancer cells vary from normal cells in separate metabolic aspects. Differential cellular metabolisms of cells are a fully dependent anaerobic glycolytic pathway, glutaminolysis and fatty acid synthesis that helps in cellular proliferation, development, survival, and growth. Oxidization of glucose by normal cells through the TCA cycle generates 30 ATP per molecule of glucose in the mitochondria to fulfill their cellular requirements [47]. Cancer cells also depend on glycolysis for generating 2 ATP per glucose molecule in the cytoplasm. Therefore, cancer cells help in the up-regulation of glucose transporter extending the uptake of glucose to meet their energy needs [47, 48]. Glucose oxidation through TCA in the mitochondrial cell prevents respiratory dysfunction in cancer cells. An increase in glycolysis provides substance for gluconeogenesis, lipid metabolism and the pentose phosphate pathway for macromolecules required in anabolic reaction and to generate NADH. This distinguished alteration in the bioenergetics metabolic process stipulates a new era of cancer research in the therapy of cancer treatment [49].

Metabolic Pathway and its Resistance in Cancer

Apoptosis resistance in cancer cells develops due to altered metabolism and active glycolytic processes. Upregulation and activation of hexokinase in cancer cells, translocates it into the mitochondria and inhibits mitochondria-mediated apoptosis. Phosphate and tensin homolog (PTEN), oncogenic activation and

hypoxic conditions are the events that help in the modulation of glycolytic factors and act as resistant to carcinoma cells. Inhibition of cellular respiration is due to hexokinase 2 expression and PDH inactivation by PDK. PDK-PDH circuit plays a very significant role in the regulation of energy metabolism between oxidative phosphorylation and glucose. The role of PDK is to phosphorylate and inhibits PDH activity with the help of ATP. PDH Phosphatase causes dephosphorylation of PDH thus restoring its activity. This PDH activation helps in the conversion of pyruvate to acetyl CoA leading to the entry of pyruvate molecules in mitochondria. Glucose is converted into lactate through the glycolysis pathway when PDH is deactivated and PDK activity is enhanced.

Similarly, in the presence of activated PDH and inhibited PDK, glucose oxidation through the TCA cycle occurs in the mitochondria. In cancer cells, overexpression of PDK3 enhances glycolysis which in turn increases the chances of cancer recurrence and drug resistance. Hence, a hyperactive glycolytic pathway leads to the inhibition of the apoptotic pathway in cancer cells. Thus, the PDK–PDH signaling circuit is considered a very significant target in cancer therapy, expecting better treatments in cancer patients [50, 51].

Regulation of Tumorigenesis in Mitochondria

The formation of a mass of cells is known as a tumor and the process involved is called tumorigenesis. It may not be cancerous, the mass of cells can be either malignant or benign [52]. Mitochondria has a central role in most eukaryotic cells, ranging from regulation of apoptosis to energy production. Energy metabolism plays a vital role in carcinogenesis. Mitochondria modulate Reactive Oxygen Species (ROS) production, Ca^{+2} homeostasis and apoptosis, which are necessary for normal cellular homeostasis. Mitochondria possess the capability of sensing the overall level of cellular physiological stress and synchronize the liberation of various apoptosis initiating factors, that lead to caspase activation and cell death [53]. The flaw in the mitochondrial system including mtDNA mutations, deletions and alternations in nuclear-coded proteins are pivotal for mitochondrial function leading to the formation of cancer cells. mtDNA mutations are found to affect the functions of mitochondrial physiology, also considering oxidative phosphorylation complexes, ROS-producing potential, Ca^{+2} homeostasis and apoptosis-initiating potential, that gets serious by a high rate of glycolytic pathway or by the oxidative phosphorylation activity [54].

Mitochondria metabolism varies from their normal counterparts in cancer cells. ROS accumulation, aerobic glycolysis, hypoxia, anti-apoptotic signals are the important characteristics of mitochondria in cancer cells. Mutations in mtDNA lead to the deregulation of enzymes. This trait is interlinked which in turn

accelerates tumorigenesis in cancer cells by reductive carboxylation of glutamine. Behind the activation of hypoxia-inducible factors (HIFs), mutations in TCA cycle enzymes encoding genes have a vital role [55].

As we know, mitochondria regulate programmed cell death, and apoptotic inducing factors are generally preserved inside mitochondria, which upon the opening of the MTP (mito-transition pores) are released into the cytosol to initiate cell death. Increased ROS and mitochondrial depolarization modulate the opening of MTPs, ROS production and redox state which are determined by the flux of electrons in ETC (electron transport chain). Production of NADH and FADH2 electron donors from the TCA cycle decide the redox state [56].

The accession of a glycolytic phenotype and halting of pyruvate entry into the mitochondria suppresses acetyl-CoA formation, thus reducing the effect both Krebs's cycle and ETC, which leads to MTP closure and reduction in apoptosis [57]. Mitochondria are also involved in programmed cell death *via* other mechanisms, which include intracellular Ca^{+2} uptake and H_2O_2 production by dismutation of mitochondrial superoxide by manganese superoxide dismutase. Reversing signaling from mitochondria to the nucleus modulates cell death initiation and energy metabolism. Retrograde signaling of mitochondria and Ca^{+2} signaling regulates genetic and epigenetic changes that assist cellular metabolism favoring tumorigenesis [58].

The altered regulation in mitochondrial functions could promote transformational changes, which leads to malignancies [59]. There are few important factors moderate the consequences of healthy cells including (i) alteration in reactive oxygen species, (ii) abundance of metabolic factors (succinate, fumarate, 2-hydrxyglutarate), denoted as oncometabolite, (iii) mitochondrial outer membrane potential permeabilization/mitochondrial permeability transition increases resistances due to oncogenic driven [60].

The pivotal metabolic process glycolysis regulates energy production in mitochondria and anabolic growth in cancer cells. Cancer cells mainly required an amount of ATP, which induces the growth of malignant cells. According to the 'Warburg phenotype' high amount of glucose uptake during the high-level glycolytic activity, the pyruvate is produced by mitochondrial metabolism (Fig. **1**). MAPK pathway is the oncogenic signaling pathway, which increases the glucose uptake and reroutes the mitochondrial metabolism into glycolysis and provides the cell the energy for proliferation. The cancer cell mitochondria are involved in ATP biosynthesis and macromolecular biosynthesis mitochondrial metabolism plays a key role in cancer cell development and growth [61].

Warburg Effect on Cancer Cells

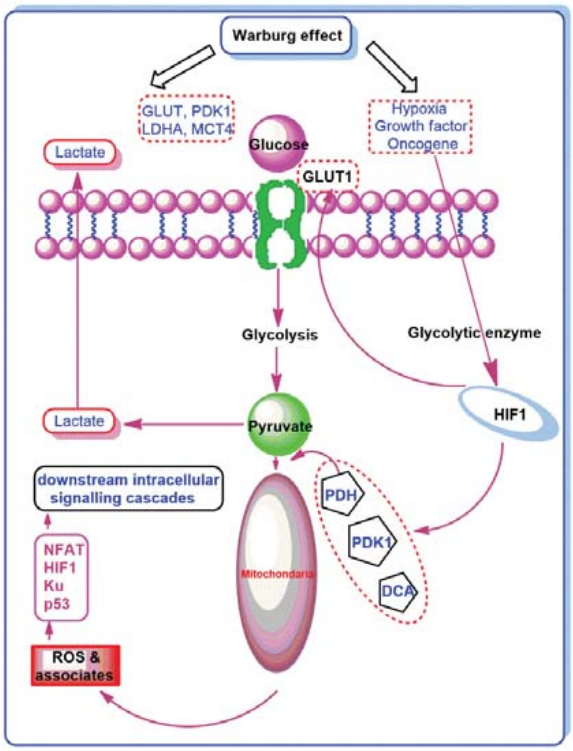

Fig. (1). As per the Warburg effect, hypoxia-inducible factor 1 alpha is upregulated during aerobic glycolysis that regulates glucose metabolism. H1F1-alpha also regulated the glucose transporter GLUT1 that increases the demand for glucose by cancer cells. The process glycolysis is upregulated *via* glycolytic enzymes whereas PDK inhibits several conversations. HIF1alpha induces the lactate production and simultaneously, ROS and αKG regulate several cellular functions in cellular physiology.

MITOCHONDRIAL METABOLISM IN BREAST CANCER PROGRESSION

The key features altered in tumor progression due to the involvement of mitochondria are:

I. Building blocks for anabolism.

II. Generation of ROS.

III. Regulation in RCD signaling.

Proliferation

During glycolysis, cancer cells can obtain enough ATP under optimal growth conditions. Mitochondria acts in the proliferation process while enough amounts of pyruvate and uridine are provided exogenously to compensate for aspartate and pyrimidine biosynthesis. In response to fluctuating conditions regarding the microenvironment, they can use glycolysis, oxidative phosphorylation and fatty acid oxidation interchangeably as the source of energy. For proliferation at optimal rates, cancer cells require an enzyme that can convert citrate into acetyl-Co A, such as ATP citrate lyase. In breast cancers, which are highly proliferating, cytosolic malic enzyme 1 induces a function that leads to the production of NADPH from glutamate. Aceto-acetate is derived from Acetyl-CoA which can support the cancer cells to proliferate by activating and boosting the BRAF-kinase and MAPK signaling consequently. By stabilizing HIF1A or by inactivating the tumor suppressors like phosphate and tensin homolog, minutely increased level of ROS can stimulate proliferation [62].

Alteration in RCD

Some tumors are specified by an increased level of mitochondrial transmembrane potential which is linked to the high rates of glycolysis and gained resistance towards RCD. Unfavorable micro-environmental conditions (such as low nutrient availability, hypoxia, GF withdrawal, *etc*.) are encountered with the progressing neoplasms, for which mitochondrial RCD is derived normally *via* MPT or MOMP. However, for irreversible permeabilization (beyond overexpression of BCL2 family members), several alterations are acquired by the malignant cells which increase the mitochondrial threshold. So, with the help of the chemical PDK1 inhibitors, the restoration of pyruvate generation is sufficient for causing RCD and as well as inhibiting tumor growth *in vivo*. Similarly, in malignant cells, the detachment of hexokinase 2 or hexokinase 1 from mitochondria causes MOMP [63].

Metastatic Modification

Metastatic modification occurs by dissemination, a multistep process where the malignant cells can acquire the ability for colonization and at distant sites macroscopic lesions are formed. This process requires oxidative phosphorylation and optimal mitochondrial biogenesis. By favoring the overproduction of mild ROS, metastatic dissemination is also promoted by mitophagy defects. There are many signal transduction cascades like SRC and protein tyrosine kinase 2 beta, which are associated with this process and ROS activates these signal transduction cascades. If there is an imbalance in mitochondrial dynamics, a little bit overproduction of ROS and as well as consequent metastatic dissemination can

occur as a result [64]. Conversely, ROS can inhibit metastatic dissemination in the presence of high oxidative stress, probably as a direct consequence of RCD and reduced fitness or cellular senescence [65].

Mitochondrial Metabolism in Breast Cancer and its Therapeutic Approaches

Mitochondrial metabolism in response to the treatments and the several metabolic characteristics are involved in the therapeutic responses. All forms of treatments such as chemotherapy, radiation therapy and immune therapy inactivate malignant cells *via* cellular senescence and regulating cell death. Mitochondria control the therapy driven RCD in cancer cells, which alters the molecular mechanism in mitochondria. As a result, MOMP (mitochondrial outer membrane permeabilization) and MPT (Mitochondrial permeability transition) as a major resistance source. The mitochondrial metabolic enzyme, IDH2, is used for the development of anticancer agents. FDA approved agent venetoclax for killing the transform cells or can be used for treatment by MOMP or MPT. $BRAF^{V600E}$ inhibits this FDA approved agent. As a result, the malignant cells can switch from glycolysis to OXPHOS (oxidative phosphorylation), which is required for melanoma cells to resist the treatments. Malignant cells utilize the OXPHOS for the ATP production which resists the treatment *via* cancer cell-intrinsic and extrinsic pathways. Mitochondrial ATP has several pumps that activate the various transporter of ATP binding cassettes family hence support the chemoresistance. Finally, malignant cells can switch between glycolysis and OXPHOS plays a major role in the resistance of oncogenic development [66].

Mitochondrial Metabolism in Breast Cancer and Immunosurveillance

In breast cancer, both intrinsic and extrinsic cancer cells have influenced the mitochondria, and it produces the dangerous signals which are released from cancer cells and the consequence of activating the tumor-targeting immune response. Mitochondrial products such as ATP, operate the extracellularly dangerous signals and intracellularly signals operate from ROS and mtDNA. Mitochondrial components are participating in immune functions *via* metabolic pathways such as the TCA cycle, OXPHOS, and fatty acid oxidation are important for T cell differentiation. ROS is required not only for TCR signaling but also for activating various transcription factors necessary for T cell activation. OXPHOS gives metabolic support to the memory T cell, as a result, it involves mitochondrial elongation and inhibits the mTOR (mechanistic target of rapamycin complex 1) for autophagy activation. Mitochondrial metabolism influences macrophage polarization. M1 macrophage activity is inhibited by the ETC to promote the tumoricidal and pro-inflammatory state, which displays the predominantly glycolytic metabolism in mitochondria. OXPHOS is a source of

ATP and it is the differentiation of immunosuppressive cells, including M2 macrophages, $CD4^+$, $CD25^+$, FOX, $P3^+$ regulatory T (Treg) cells and myeloid-derived suppressor cells (MDSCs), CTL (cytotoxic T lymphocyte) [67, 68]. Mitochondria acts as a target for the development of noble anticancer agents because they underlie their phenotypic and metabolic plasticity and resist the malignant cells by RCD induction treatments [69].

Role of the Mitochondrial Metabolism in Malignant Transformation

Malignant transformation is the process by which the cells acquire the properties of cancer in the case of breast cancer, specially. Mitochondria are involved in the malignant transformation by three key mechanisms:

1. The reactive oxygen species or ROS support to increase the potentially oncogenic DNA defects.

2. The abnormal accumulation of specific mitochondrial metabolites such as fumarate, succinate, 2-hydroxyglutarate (2-HG), has significant transforming effects.

3. Functional deficits in mitochondrial permeable transitions (MPT) are generally required for the endurance of neo-formed malignant transformed malignant transformation [70].

The mitophagy should maintain mitochondrial fitness and it also removes the ROS (Reactive Oxygen Species). The different group has shown the knockout and knockdown of the autophagy-related gene Atg7 and Atg5 which are essential for which promotes the oncogenesis. ROS are genotoxins, mtDNA mutations that affect various components of Electron Transport Chain (ETC) and they increase the ROS production to form breast associated tumors. ROS activates many signaling cascades that are Mitogen-activated protein kinase (MAPK), Hypoxia Inducible Factor 1α (HIF-1) and Epidermal Growth Factor Receptor (EGFR) signaling. The produced ROS activate MAPK for breast cancer and increased the cytotoxic level for breast cancer by using GSH inhibitors [71]. The role of the ROS in cancer progression by alteration in redox balance deregulated the redox signaling [72].

What are the Potential Mitochondrial Targets on Breast Cancer?

Mitochondria are the membrane-bound organelles that are found in eukaryotic cells. They are responsible for mobilizing cellular energy production. They have a central role in the maintenance of life and they also serve as the gatekeepers of cell death, as per Fig. (**2**) [73, 74].

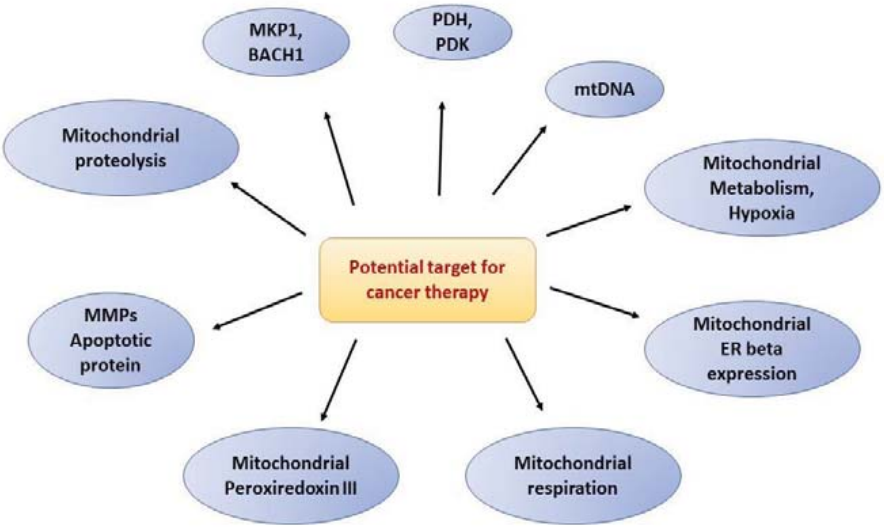

Fig. (2). Different mitochondrial targets for breast cancer therapy.

Targeting the Apoptotic Proteins

Mitochondria are having a normal homeostasis and cell death initiation when the cell experiences stress responses [73]. Induction of apoptosis cell death necessitates Mitochondrial Membrane Permeabilization (MMP). Agents are responsible for regulating MMP affect the outer MMP, the inner MMP or both of them. Evolutionarily conserved B-cell lymphoma 2 (Bcl-2) family proteins are responsible for the modulation of the coherence of the outer mitochondrial membrane [75].

In humans, BCL-2 is encoded by the BCL-2 gene, which is the initiating member of the BCL-2 family of regulator proteins that are responsible for modulating cell death [apoptosis], by either inhibiting (anti-apoptotic) or inducing (pro-apoptotic) apoptosis [76].

Proteins like BCL-2 and BCL-XL block the emancipation of apoptogenic factors from mitochondria. On the other hand, BCL-2 associated x protein (Bax) and BCL-2 antagonist (Bak), which are proapoptotic BCL-2 members induce outer MMP, allowing the liberation of proapoptotic factors from MMP [60]. Therefore a balance competition between these two processes decides the death and the survival of the cell.

Targeting mtDNA Regulation

mtDNA encodes crucial oxidative phosphorylation proteins, the modulation of mtDNA copy number can be embarked for cancer therapy and mtDNA has a significant role in diagnosing the sensitivity of cancer cells in reciprocation to multiple chemotherapeutic agents. In mammalian cells, many agents are accountable for causing depletion of mtDNA like 4-quinolone drugs such as ciprofloxacin which inhibits TOP2β in mtDNA, resulting in the accumulation of positively supercoiled mtDNA, along with the cessation of mitochondrial transcription and the initiation of replication that leads to the depletion of mtDNA copy number. This leads to the disruption of the function of mitochondria. There are also other agents such as cisplatin, resveratrol, *etc*. So, it can be suggested that mtDNA is involved in regulating cancer cell death as it is observed that cancer agents have the ability to bind with mtDNA. On the other hand, anti-cancer agents can also deplete DNA. Oxidative phosphorylation can be another mitochondrial target in the treatment of cancer. In cancer cells, cell death is generally initiated by the activation of oxidative phosphorylation with the initiation of apoptosis *via* the production of ROS [74]. By subduing the activity of oxidative phosphorylation and inhibiting the glycolytic pathway results in reduction of cell death in the extremely proliferative tumor cells [77]. On low-level glucose conditions, the activity of mitochondria is stimulated by forskolin, generally growing cancer cells are comparatively more sensitive to the very low level of oxidative phosphorylation inhibitors and cell death. Due to defective mitochondrial functions, cancer cells have the ability to resist treatment strategies. DCA can restore the oxidative phosphorylation function which in turn initiates the ROS production with apoptotic cell death [78].

Targeting Pyruvate Dehydrogenase and Pyruvate Dehydrogenase Kinase (PDH-PDK) and Associates in Breast Cancer

Managing and controlling cancer cells are essential by restoring mitochondrial function in the therapy of breast cancer. Mitochondria are hyperpolarized in breast cancer cells, causing an increase in intracellular calcium ion, activation of the nuclear factor activated T cells, increase in aerobic glycolysis, reduction of ROS level, upregulation of antiapoptotic Bcl-2 [67]. The rate of glycolysis increases in the cancer cell formation, and as a result of the hexokinase level also increases, for which mitochondria are translocated, and it leads to apoptosis inhibition & hyperpolarization of mitochondria. In cancer cells, all these events lead towards apoptosis and induce cell proliferation, enhance the survival rate, terminate cell senescence. So, if the mitochondrial functions are reactivated, then it will reverse these events and lead to suppressing the aerobic glycolysis process & apoptosis. The decision either to undergo glucose oxidation or to follow aerobic glycolysis,

depends on the overall LBH and PDH-PDK regulatory circuit interactions. Both suppress LDH and activates PDH by inhibiting PDK that can increase the pumping of pyruvate into mitochondria. Thus in oxidative phosphorylation, ETC is reactivated, leading to ROS production, calcium ions flux into the mitochondria as well as induction of apoptosis [79, 80].

Agents such as DCA can increase the rate of oxidation of glucose by pumping pyruvate to the citric acid cycle reactive oxidative phosphorylation and it can induce the ROS production, which leads to apoptotic cell death of the tumor cells. Against the metastatic cells of breast cancer, potential anticancer effects are offered by DCA. Against the T cell lymphoma, the antitumor effects of DCA are associated with the alterations in pH homeostasis and the metabolism of glucose, which leads to suppression in the survival rate of the tumor cells in breast cancer.

There is an increased rate of delivery of pyruvate into the mitochondria due to PDH is activated by DCA, which is followed by an increased level of glucose oxidation, which will lead to the restoration of the mitochondrial function [81]. By producing ROS and activating NFAT, the apoptosis inducing effects are mediated by DCA which leads to the release of Cytochrome C and apoptosis-inducing factors into the cytosol from mitochondria. DCA disrupts HIF-1α dependent adaptive response in tumors under hypoxia. For killing the hypoxic tumor cells, the effectiveness of chemotherapy is gradually increasing [82] (Table **1**).

Table 1. Signalling pathways involved in the activation and regulation of HIF in breast cancer [82].

Increase In HIFs Regulation		
Hypoxia	Increase in reactive oxygen species (ROS) formation	NF-kB
RTK	Notch	IL6/IL6R
TGF-â/ TGF-âR	TNF-á	PI3K
Akt/mTOR	STAT3	MAPK

CONCLUDING REMARKS AND FUTURE PERSPECTIVES

Mitochondria have been considered as the target for developing novel anti-cancer agents in breast cancer. It has a major impact on processes linked to oncogenesis, encompassing malignant transformation, tumor progression, response to treatment and anticancer immune-surveillance, dying of cancer cell, metastatic cancer cell, MOMP, MPT, reactive oxygen species, and tumor microenvironment [83, 84] (Table **2**). Regulation of aerobic glycolysis and mitochondrial dysfunction are linked to cancer survival, apoptotic invasion and resistance to cancer therapies.

All these may be associated with the sequestration of proapoptotic proteins or the nonapoptotic function of various proapoptotic proteins in mitochondria leading to the inhibition of cancer cell apoptosis. Hexokinase and PDK activation inhibits the function of proapoptotic Bax and Bak. Thus the PDK inhibition may activate these pro-apoptotic proteins, causing cytochrome c release and enhancing cancer cell apoptosis.

Table. 2 Signalling factors and factors promoted by an increase in HIFs regulation in breast cancer [83,84]:

Increase in HIFs regulation causing to				
Oct-3/4, Nanog, SOX-2 increase	GLUT-1/2 hexokinase 2, aldolase A, PGK1, PKM, CAIX, MCT4 increase	TGF-á, EGFR, CXCL4, snail, twist, lox, lox2, MMPs increase	VEGF increase	BCL-2, survivin, BCL-xl, MUG-1, Pgp, ABCG2 increase
Stemnessself-renewal	Glycolysis pH regulation	EMT metastatic spread	Angiogenesis	Resistance to CT/RT survival Antiapoptotic effect
Causing tumor growth, metastasizing, resistance to therapy				

On the other hand, HSP folding machinery plays an important role in proper mitochondrial function. A defect in this machinery causes cells to grow and divide uncontrollably, forming tumors. Thus, targeting the downregulation of pre-cancerous HSPs or upregulation of anti-cancerous HSPs can be an important approach in controlling tumorigenesis. Also, restoration of mitochondrial OXPHOS and inhibition of the glycolytic pathway can be another approach in treating cancer patients.

Besides, there are various challenges to establish potent anticancer agents. DCA regulation contains strong anticancer agents. Its higher dose may be essential in therapeutic approaches, but it can be toxic to normal tissues. Thus, the synthesis of DCA analogs proved to have a better efficacy that selectively targets tumor cells. Hence, future researchers are focusing on DCA analog synthesis alone or with nanoparticle encapsulation or in combination with other anticancer agents to develop more efficient anticancer agents that can effectively kill the cancer cells. Thus, the function of mitochondria provides building blocks for tumor anabolism, controlling of redox and calcium signaling, participate in transcriptional regulation and cell death. The promising contribution of this powerful cellular organelle develops constant focus as the novel target in regards to anti-metastatic drug development. By altering cellular metabolism, it also regulates the drug resistance, especially in the tumor micro-environment. The altered strategies in mitochondrial regulation allow the selected cell populations to devise for the

therapeutic potential of mitochondria-targeting agents in clinics. More preclinical and clinical approaches are required to achieve this ambitious and useful objective.

ABBREVIATIONS

AIF:	Apoptosis inducing factor
BCL-2:	B cell lymphoma-2
BCL-XL:	B cell lymphoma-extra-large
BCRPs:	Breast cancer resistance proteins
CAFs:	Cancer associated fibroblast
CAIX:	Carbonic Anhydrase
CT:	Chemotherapy
CXCL 4:	Chemokine ligands 4
EGFR:	Epidermal Growth factor Receptor
EMT:	Epithelial to mesenchymal transition
GLUT:	Glucose Transporter
HIFs:	Hypoxia Inducible Factors
IL-6/IL-6R:	Interleukin 6/ Interleukin 6 Receptor
MAPK:	Mitogen-activated Protein kinase
MCT-4:	Monocarboxylate transporter 4
MIC-1:	Macrophage inhibitory cytokine-1
MMPs:	Metalloproteinases
MOMP:	Mitochondrial Outer Membrane Permeabilization
MPT:	Mitochondrial Permeability Transition
mTOR:	Molecular target of rapamycin
MUC-1:	Mucin-1
NF-KB:	Nuclear Factor KB
Oct-3/4:	Octamer binding transcriptional Factor 3/4
P13K:	Phosphatidyl inositol-3-kinase
PGK-1:	Phosphogylcerate kinase-1
Pgp:	P Glycoprotein
PKM:	Pyruvate kinase M
RCD:	Regulated cell death Signaling
ROS:	Reactive Oxygen Species
RT:	Radiotherapy
RTK:	Receptor tyrosine kinase
SOX-2:	Sex Determining Region Y
STAT 3:	Signal transducer activator of transcription 3
TGF-β/TGFR:	Transforming growth factor-β/Transforming growth factor-β Receptor
TNF-α:	Tumor necrosis factor-α

VEGF: Vascular endothelial growth factor

CONSENT FOR PUBLICATION

Not applicable.

CONFLICT OF INTEREST

The authors confirm that the contents of this chapter have no conflict of interest.

ACKNOWLEDGEMENT

We acknowledge the Director of CNCI, Kolkata, for providing the research environment and continuous support.

REFERENCES

[1] Henze K, Martin W. Evolutionary biology: essence of mitochondria. Nature 2003; 426(6963): 127-8. [http://dx.doi.org/10.1038/426127a] [PMID: 14614484]

[2] Birceanu O. Mitochondria are too hot to handle! J Exp Biol. 2018; 221(9): 1-4. [http://dx.doi.org/10.1242/jeb.170027]

[3] Campbell NA, Williamson B, Heyden RJ. Pearson/Prentice Hallexploring life. 0--13--250882-6 Boston, Massachusetts: Pearson Prentice Hall 2006.

[4] McBride HM, Neuspiel M, Wasiak S. Mitochondria: more than just a powerhouse. Curr Biol 2006; 16(14): R551-60. [http://dx.doi.org/10.1016/j.cub.2006.06.054] [PMID: 16860735]

[5] Valero T. Mitochondrial biogenesis: pharmacological approaches. Curr Pharm Des 2014; 20(35): 5507-9. [http://dx.doi.org/10.2174/1381612820351409111421118] [PMID: 24606795]

[6] Sanchis-Gomar F, Garcia-Gimenez J, Gomez-Cabrera M, Pallardo F. Mitochondrial biogenesis in health and disease. Molecular and therapeutic approaches. Curr Pharm Des 2014; 20(35): 5619-33.

[7] Gardner A, Boles R. Is a "mitochondrial psychiatry" in the future? A review. Curr Psychiatry Rev 2005. [http://dx.doi.org/10.2174/157340005774575064]

[8] Lesnefsky EJ, Moghaddas S, Tandler B, Kerner J, Hoppel CL. Mitochondrial dysfunction in cardiac disease: ischemia--reperfusion, aging, and heart failure. J Mol Cell Cardiol 2001; 33(6): 1065-89. [http://dx.doi.org/10.1006/jmcc.2001.1378] [PMID: 11444914]

[9] Dorn GW II, Vega RB, Kelly DP. Mitochondrial biogenesis and dynamics in the developing and diseased heart. Genes Dev 2015; 29(19): 1981-91. [http://dx.doi.org/10.1101/gad.269894.115] [PMID: 26443844]

[10] Griffiths KK, Levy RJ. Evidence of mitochondrial dysfunction in autism: Biochemical links, genetic-based associations, and non-energy-related mechanisms. Oxid Med Cell Longev 2017; 2017: 4314025. [http://dx.doi.org/10.1155/2017/4314025] [PMID: 28630658]

[11] Andersson SGE, Karlberg O, Kurland CG. On the origin of mitochondria : a genomics perspective. 2003; (December 2002): 165-79. [http://dx.doi.org/10.1098/rstb.2002.1193]

[12] Rich PR. The molecular machinery of Keilin's respiratory chain. Biochem Soc Trans 2003; 31(Pt 6):

1095-105.
[http://dx.doi.org/10.1042/bst0311095] [PMID: 14641005]

[13] Stoimenova M, Igamberdiev AU, Gupta KJ, Hill RD. Nitrite-driven anaerobic ATP synthesis in barley and rice root mitochondria. Planta 2007; 226(2): 465-74.
[http://dx.doi.org/10.1007/s00425-007-0496-0] [PMID: 17333252]

[14] King A, Selak MA, Gottlieb E. Succinate dehydrogenase and fumarate hydratase: linking mitochondrial dysfunction and cancer. Oncogene 2006; 25(34): 4675-82.
[http://dx.doi.org/10.1038/sj.onc.1209594] [PMID: 16892081]

[15] Berg J, Tymoczko J, Stryer L. Biochemistry. 5th edition. New York: W H Freeman; 2002. Section 24.2, Amino Acids Are Made from Intermediates of the Citric Acid Cycle and Other Major Pathways. Available from: https://www.ncbi.nlm.nih.gov/books/NBK22459/.

[16] Akram M. Citric acid cycle and role of its intermediates in metabolism. Cell Biochem Biophys 2014; 68(3): 475-8.
[http://dx.doi.org/10.1007/s12013-013-9750-1] [PMID: 24068518]

[17] Mailloux RJ, Bériault R, Lemire J, *et al.* The tricarboxylic acid cycle, an ancient metabolic network with a novel twist. PLoS One 2007; 2(8): e690.
[http://dx.doi.org/10.1371/journal.pone.0000690] [PMID: 17668068]

[18] Hui S, Ghergurovich JM, Morscher RJ, *et al.* Glucose feeds the TCA cycle *via* circulating lactate. Nature 2017; 551(7678): 115-8.
[http://dx.doi.org/10.1038/nature24057] [PMID: 29045397]

[19] Ramakrishna R, Edwards JS, McCulloch A, Palsson BO. Flux-balance analysis of mitochondrial energy metabolism: Consequences of systemic stoichiometric constraints. Am J Physiol - Regul Integr Comp Physiol 2001; 280(349-3): 695-704.
[http://dx.doi.org/10.1152/ajpregu.2001.280.3.r695]

[20] Cortassa S, Aon MA, O'Rourke B, Winslow RL. Metabolic control analysis applied to mitochondrial networks. Proc Annu Int Conf IEEE Eng Med Biol Soc EMBS 2011; 4673-6.
[http://dx.doi.org/10.1109/IEMBS.2011.6091157]

[21] Nazaret C, Heiske M, Thurley K, Mazat JP. Mitochondrial energetic metabolism: a simplified model of TCA cycle with ATP production. J Theor Biol 2009; 258(3): 455-64.
[http://dx.doi.org/10.1016/j.jtbi.2008.09.037] [PMID: 19007794]

[22] Silverstein TP. An exploration of how the thermodynamic efficiency of bioenergetic membrane systems varies with c-subunit stoichiometry of F_1F_0 ATP synthases. J Bioenerg Biomembr 2014; 46(3): 229-41.
[http://dx.doi.org/10.1007/s10863-014-9547-y] [PMID: 24706236]

[23] Durieux J, Wolff S, Dillin A. The cell-non-autonomous nature of electron transport chain-mediated longevity. Cell 2011; 144(1): 79-91.
[http://dx.doi.org/10.1016/j.cell.2010.12.016] [PMID: 21215371]

[24] Huang H, Manton KG. The role of oxidative damage in mitochondria during aging: a review. Front Biosci 2004; 9: 1100-17.
[http://dx.doi.org/10.2741/1298] [PMID: 14977532]

[25] Mozo J, Emre Y, Bouillaud F, Ricquier D, Criscuolo F. Thermoregulation: what role for UCPs in mammals and birds? Biosci Rep 2005; 25(3-4): 227-49.
[http://dx.doi.org/10.1007/s10540-005-2887-4] [PMID: 16283555]

[26] Denton RM. Regulation of mitochondrial dehydrogenases by calcium ions. Biochim Biophys Acta - Bioenerg 2009; 1787(11): 1309-16.
[http://dx.doi.org/10.1016/j.bbabio.2009.01.005]

[27] Kirichok Y, Krapivinsky G, Clapham DE. The mitochondrial calcium uniporter is a highly selective ion channel. Nature 2004; 427(6972): 360-4.

[http://dx.doi.org/10.1038/nature02246] [PMID: 14737170]

[28] Pinto MCX, Kihara AH, Goulart VAM, *et al.* Calcium signaling and cell proliferation. Cell Signal 2015; 27(11): 2139-49.
[http://dx.doi.org/10.1016/j.cellsig.2015.08.006] [PMID: 26275497]

[29] Collins S, Meyer T. Cell biology: A sensor for calcium uptake. Nature 2010; 467(7313): 283.
[http://dx.doi.org/10.1038/467283a] [PMID: 20844529]

[30] Carriers M. Cancer Risks in BRCA2 Mutation Carriers. 1999; 91 (15).

[31] Stephens PJ, Tarpey PS, Davies H, *et al.* Oslo Breast Cancer Consortium (OSBREAC). The landscape of cancer genes and mutational processes in breast cancer. Nature 2012; 486(7403): 400-4.
[http://dx.doi.org/10.1038/nature11017] [PMID: 22722201]

[32] Marcom PK. Breast Cancer. Elsevier Inc.; 2017.
[http://dx.doi.org/10.1016/B978-0-12-800685-6.00010-2]

[33] Dent R, Trudeau M, Pritchard KI, *et al.* Triple-negative breast cancer: clinical features and patterns of recurrence. Clin Cancer Res 2007; 13(15 Pt 1): 4429-34.
[http://dx.doi.org/10.1158/1078-0432.CCR-06-3045] [PMID: 17671126]

[34] Schneider BP, Winer EP, Foulkes WD, *et al.* Triple-negative breast cancer: risk factors to potential targets. Clin Cancer Res 2008; 14(24): 8010-8.
[http://dx.doi.org/10.1158/1078-0432.CCR-08-1208] [PMID: 19088017]

[35] Oakman C, Viale G, Di Leo A. Management of triple negative breast cancer. Breast 2010; 19(5): 312-21.
[http://dx.doi.org/10.1016/j.breast.2010.03.026] [PMID: 20382530]

[36] Chavez KJ, Garimella SV, Lipkowitz S. Triple negative breast cancer cell lines: one tool in the search for better treatment of triple negative breast cancer. Breast Dis 2010; 32(1-2): 35-48.
[http://dx.doi.org/10.3233/BD-2010-0307] [PMID: 21778573]

[37] Atchley DP, Albarracin CT, Lopez A, *et al.* Clinical and pathologic characteristics of patients with BRCA-positive and BRCA-negative breast cancer. J Clin Oncol 2008; 26(26): 4282-8.
[http://dx.doi.org/10.1200/JCO.2008.16.6231] [PMID: 18779615]

[38] Telli ML. Triple-negative breast cancer In: Badve S., Gökmen-Polar Y. (eds). Mol Path of Breast Cancer. Springer, Cham 2016; pp 71-80.
[http://dx.doi.org/10.1007/978-3-319-41761-5_6]

[39] Liu SV, Melstrom L, Yao K, Russell CA, Sener SF. Neoadjuvant therapy for breast cancer. J Surg Oncol 2010; 101(4): 283-91.
[http://dx.doi.org/10.1002/jso.21446] [PMID: 20187061]

[40] Lin KY, Kraus WL. PARP Inhibitors for Cancer Therapy. Cell 2017; 169(2): 183.
[http://dx.doi.org/10.1016/j.cell.2017.03.034] [PMID: 28388401]

[41] Nathan MR, Schmid P. The emerging world of breast cancer immunotherapy. Breast 2018; 37: 200-6.
[http://dx.doi.org/10.1016/j.breast.2017.05.013] [PMID: 28583398]

[42] Hanahan D, Weinberg RA. The hallmarks of cancer. Cell 2000; 100(1): 57-70.
[http://dx.doi.org/10.1016/S0092-8674(00)81683-9] [PMID: 10647931]

[43] Cairns RA, Harris IS, Mak TW. Regulation of cancer cell metabolism. Nat Rev Cancer 2011; 11(2): 85-95.
[http://dx.doi.org/10.1038/nrc2981] [PMID: 21258394]

[44] DeBerardinis RJ, Chandel NS. Fundamentals of cancer metabolism. Sci Adv 2016; 2(5): e1600200.
[http://dx.doi.org/10.1126/sciadv.1600200] [PMID: 27386546]

[45] Pelicano H, Martin DS, Xu RH, Huang P. Glycolysis inhibition for anticancer treatment. Oncogene 2006; 25(34): 4633-46.

[http://dx.doi.org/10.1038/sj.onc.1209597] [PMID: 16892078]

[46] Muñoz-Pinedo C, El Mjiyad N, Ricci JE. Cancer metabolism: current perspectives and future directions. Cell Death Dis 2012; 3: e248.
[http://dx.doi.org/10.1038/cddis.2011.123] [PMID: 22237205]

[47] Szent-Gyorgyi A. Metabolism and cancer. *Int J Quantum Chem.* 1985;28(12 S):257-261.
[http://dx.doi.org/10.1002/qua.560280725]

[48] Seyfried TN, Shelton LM. Cancer as a metabolic disease. Nutr Metab (Lond) 2010; 7: 7.
[http://dx.doi.org/10.1186/1743-7075-7-7] [PMID: 20181022]

[49] Cantor JR, Sabatini DM. Cancer cell metabolism: one hallmark, many faces. Cancer Discov 2012; 2(10): 881-98.
[http://dx.doi.org/10.1158/2159-8290.CD-12-0345] [PMID: 23009760]

[50] Jain M, Nilsson R, Sharma S, *et al.* Metabolite profiling identifies a key role for glycine in rapid cancer cell proliferation. Science (80-) 2012; 336(6084): 1040-4.
[http://dx.doi.org/10.1126/science.1218595]

[51] Dagogo-Jack I, Shaw AT. Tumour heterogeneity and resistance to cancer therapies. Nat Rev Clin Oncol 2018; 15(2): 81-94.
[http://dx.doi.org/10.1038/nrclinonc.2017.166] [PMID: 29115304]

[52] Vyas S, Zaganjor E, Haigis MC. Mitochondria and cancer. Cell 2016; 166(3): 555-66.
[http://dx.doi.org/10.1016/j.cell.2016.07.002] [PMID: 27471965]

[53] Idelchik MDPS, Begley U, Begley TJ, Melendez JA. Mitochondrial ROS control of cancer. Semin Cancer Biol 2017; 47: 57-66.
[http://dx.doi.org/10.1016/j.semcancer.2017.04.005] [PMID: 28445781]

[54] Tubbs A, Nussenzweig A. Endogenous DNA damage as a source of genomic instability in cancer. Cell 2017; 168(4): 644-56.
[http://dx.doi.org/10.1016/j.cell.2017.01.002] [PMID: 28187286]

[55] Calabrese C, Iommarini L, Kurelac I, *et al.* Respiratory complex I is essential to induce a Warburg profile in mitochondria-defective tumor cells. Cancer Metab 2013; 1(1): 11.
[http://dx.doi.org/10.1186/2049-3002-1-11] [PMID: 24280190]

[56] Cherian MG, Jayasurya A, Bay BH. Metallothioneins in human tumors and potential roles in carcinogenesis. Mutat Res 2003; 533(1-2): 201-9.
[http://dx.doi.org/10.1016/j.mrfmmm.2003.07.013] [PMID: 14643421]

[57] Lapuente-Brun E, Moreno-Loshuertos R, Aciń-Pérez R, *et al.* Supercomplex assembly determines electron flux in the mitochondrial electron transport chain. Science (80-) 2013; 340(6140): 1567-70.
[http://dx.doi.org/10.1126/science.1230381]

[58] Turrens JF. Mitochondrial formation of reactive oxygen species. J Physiol 2003; 552(Pt 2): 335-44.
[http://dx.doi.org/10.1113/jphysiol.2003.049478] [PMID: 14561818]

[59] Schmitt S, Zischka H, Hygiene E. Targeting Mitochondria for Cancer Therapy The Role of Mitochondria in Programmed Cell Death Apoptosis as Cancer Therapy. 2018. German Journal of Oncology 2018; 50: 124-130.
[http://dx.doi.org/10.1055/a-0657-4437]

[60] Yang M, Brackenbury WJ. Membrane potential and cancer progression. Front Physiol 2013; 4: 185.
[http://dx.doi.org/10.3389/fphys.2013.00185] [PMID: 23882223]

[61] Xie J, Wu H, Dai C, *et al.* Beyond Warburg effect--dual metabolic nature of cancer cells. Sci Rep 2014; 4: 4927.
[http://dx.doi.org/10.1038/srep04927] [PMID: 24820099]

[62] Shaw RJ. Glucose metabolism and cancer. Curr Opin Cell Biol 2006; 18(6): 598-608.
[http://dx.doi.org/10.1016/j.ceb.2006.10.005] [PMID: 17046224]

[63] Zhong H, De Marzo AM, Laughner E, *et al.* Overexpression of hypoxia-inducible factor 1α in common human cancers and their metastases. Cancer Res 1999; 59(22): 5830-5.
[PMID: 10582706]

[64] Liou GY, Storz P. Reactive oxygen species in cancer. Free Radic Res 2010; 44(5): 479-96.
[http://dx.doi.org/10.3109/10715761003667554] [PMID: 20370557]

[65] Kim JW, Tchernyshyov I, Semenza GL, Dang CV. HIF-1-mediated expression of pyruvate dehydrogenase kinase: a metabolic switch required for cellular adaptation to hypoxia. Cell Metab 2006; 3(3): 177-85.
[http://dx.doi.org/10.1016/j.cmet.2006.02.002] [PMID: 16517405]

[66] Weinberg SE, Chandel NS. Targeting mitochondria metabolism for cancer therapy. Nat Chem Biol 2015; 11(1): 9-15.
[http://dx.doi.org/10.1038/nchembio.1712] [PMID: 25517383]

[67] Scharping NE, Menk AV, Moreci RS, *et al.* The tumor microenvironment represses T cell mitochondrial biogenesis to drive intratumoral T Cell metabolic insufficiency and dysfunction. Immunity 2017; 45(2): 374-88.
[http://dx.doi.org/10.1016/j.immuni.2016.08.009]

[68] Wang JB, Erickson JW, Fuji R, *et al.* Targeting mitochondrial glutaminase activity inhibits oncogenic transformation. Cancer Cell 2010; 18(3): 207-19.
[http://dx.doi.org/10.1016/j.ccr.2010.08.009] [PMID: 20832749]

[69] Sotgia F, Whitaker-Menezes D, Martinez-Outschoorn UE, *et al.* Mitochondria "fuel" breast cancer metabolism: fifteen markers of mitochondrial biogenesis label epithelial cancer cells, but are excluded from adjacent stromal cells. Cell Cycle 2012; 11(23): 4390-401.
[http://dx.doi.org/10.4161/cc.22777] [PMID: 23172368]

[70] Glunde K, Bhujwalla ZM, Ronen SM. Choline metabolism in malignant transformation. Nat Rev Cancer 2011; 11(12): 835-48.
[http://dx.doi.org/10.1038/nrc3162] [PMID: 22089420]

[71] Sabharwal SS, Schumacker PT. Mitochondrial ROS in cancer: initiators, amplifiers or an Achilles' heel? Nat Rev Cancer 2014; 14(11): 709-21.
[http://dx.doi.org/10.1038/nrc3803] [PMID: 25342630]

[72] Frezza C, Gottlieb E. Mitochondria in cancer: not just innocent bystanders. Semin Cancer Biol 2009; 19(1): 4-11.
[http://dx.doi.org/10.1016/j.semcancer.2008.11.008] [PMID: 19101633]

[73] Galluzzi L, Kepp O, Vander Heiden MG, Kroemer G. Metabolic targets for cancer therapy. Nat Rev Drug Discov 2013; 12(11): 829-46.
[http://dx.doi.org/10.1038/nrd4145] [PMID: 24113830]

[74] Gogvadze V, Orrenius S, Zhivotovsky B. Mitochondria in cancer cells: what is so special about them? Trends Cell Biol 2008; 18(4): 165-73.
[http://dx.doi.org/10.1016/j.tcb.2008.01.006] [PMID: 18296052]

[75] Panieri E, Santoro MM. ROS homeostasis and metabolism: a dangerous liason in cancer cells. Cell Death Dis 2016; 7(6): e2253.
[http://dx.doi.org/10.1038/cddis.2016.105] [PMID: 27277675]

[76] Jin Z, El-Deiry WS. Overview of cell death signaling pathways. Cancer Biol Ther 2005; 4(2): 139-63.
[http://dx.doi.org/10.4161/cbt.4.2.1508] [PMID: 15725726]

[77] Vander Heiden MG, Locasale JW, Swanson KD, *et al.* Evidence for an alternative glycolytic pathway in rapidly proliferating cells. Science 2010; 329(5998): 1492-9.
[http://dx.doi.org/10.1126/science.1188015]

[78] Harrison H, Farnie G, Howell SJ, *et al.* Regulation of breast cancer stem cell activity by signaling

through the Notch4 receptor. Cancer Res 2010; 70(2): 709-18.
[http://dx.doi.org/10.1158/0008-5472.CAN-09-1681] [PMID: 20068161]

[79] Liu AM, Wang W, Luk JM. Liu A.M., Wang W., Luk J.M. (2013) Targeting Cancer Metabolisms. In: Lee N., Cheng C., Luk J. (eds) New Advances on Disease Biomarkers and Molecular Targets in Biomedicine. Humana Press, Totowa,NJ.
[http://dx.doi.org/10.1007/978-1-62703-456-2_9]

[80] Zhao Y, Butler EB, Tan M. Targeting cellular metabolism to improve cancer therapeutics. Cell Death Dis 2013; 4: e532.
[http://dx.doi.org/10.1038/cddis.2013.60] [PMID: 23470539]

[81] Hitosugi T, Fan J, Chung TW, *et al*. Tyrosine phosphorylation of mitochondrial pyruvate dehydrogenase kinase 1 is important for cancer metabolism. Mol Cell 2011; 44(6): 864-77.
[http://dx.doi.org/10.1016/j.molcel.2011.10.015] [PMID: 22195962]

[82] Kim JW, Gao P, Liu Y-C, Semenza GL, Dang CV. Hypoxia-inducible factor 1 and dysregulated c-Myc cooperatively induce vascular endothelial growth factor and metabolic switches hexokinase 2 and pyruvate dehydrogenase kinase 1. Mol Cell Biol 2007; 27(21): 7381-93.
[http://dx.doi.org/10.1128/MCB.00440-07] [PMID: 17785433]